TID-7652

Proceedings of the Symposium on the

Protection Against Radiation Hazards in Space

held in
Gatlinburg, Tennessee
November 5-7, 1962

BOOK 1

UNITED STATES ATOMIC ENERGY COMMISSION

TID-7652
PHYSICS

PROCEEDINGS OF THE SYMPOSIUM ON THE

PROTECTION AGAINST RADIATION HAZARDS IN SPACE

Gatlinburg, Tennessee

November 5-7, 1962

BOOK 1: Radiation Environment in Space
Effects of Space Radiation on Radiosensitive Objects
Biological Effects of Space Radiation

BOOK 2 : Shielding Against Space Radiations

Sponsored by:

Oak Ridge National Laboratory

Manned Spacecraft Center, NASA

American Nuclear Society

FOREWORD

The realization in recent years that outer space is traversed by high-energy radiations has caused man to reevaluate the feasibility of manned or even instrumented exploration outside our atmosphere. Fortunately, it is possible to determine the nature and intensities of these radiations and to produce similar radiations on earth by means of accelerators. Thus we can learn how to attenuate them and to design capsules which afford protection against them. Of course this protection carries a weight penalty so that there is a premium on optimizing the shield design. Many groups in the United States are engaged in research to this end, and it was the purpose of this symposium to bring these groups together so that they could exchange information. To make the meeting more comprehensive, sessions on the nature of the radiations and their effects on people and things were included. However, the major part of the meeting was devoted to discussions on shielding research, comprising theoretical calculations and experiments carried out mainly with high-energy accelerators. The symposium committee feels that the aims of the symposium were met and that progress in space research program was greatly accelerated thereby.

Symposium Committee

Committee Members

E. P. Blizard, Chairman
Oak Ridge National Laboratory

C. D. Zerby
Oak Ridge National Laboratory

Wright Langham
Los Alamos Scientific Laboratory

Wilmot N. Hess
Goddard Space Flight Center

W. L. Gill
Manned Spacecraft Center
National Aeronautics and Space Administration

J. Warren Keller
National Aeronautics and Space Administration
Washington

Fred C. Maienscheim
Oak Ridge National Laboratory

PROGRAM AND CONTENTS

BOOK 1

Session C

BIOLOGICAL EFFECTS OF SPACE RADIATIONS

Robley D. Evans -- Chairman
Massachusetts Institute of Technology

BOOK 2

Session D

SHIELDING AGAINST SPACE RADIATIONS

Clayton D. Zerby -- Chairman
Oak Ridge National Laboratory

Session E

SHIELDING AGAINST SPACE RADIATIONS (continued)

H. J. Schaefer -- Chairman
U. S. Naval School of Aviation Medicine

Session F

SHIELDING AGAINST SPACE RADIATIONS (continued)

T. F. Foelsche -- Chairman
Langley Field, NASA

THE MISSION OF MAN IN SPACE

Homer E. Newell
Director, Office of Space Sciences
National Aeronautics and Space Administration

Introduction

This meeting on Protection Against Radiation Hazards in Space is a timely one. It comes at a time when world-wide attention has been drawn to the subject by the striking effects of artificial radiation belts on some unmanned satellites. It takes place against a background of growing programs and far-reaching plans for scientific research, practical applications, and manned flight and exploration in space.

The first years of the Space Age have demonstrated clearly that unmanned spacecraft can play a significant role in man's quest for knowledge and human advancement. On the scientific side, Explorers, Pioneers, Mariner, Ranger, Sputniks, and Luniks have already yielded a wealth of knowledge, answering many important scientific questions. The future is bright for these electromechanical extensions of man's presence beyond the earth, especially when increased payload capacity permits us to launch Surveyors to the moon and Voyagers to the planets.

TIROS, Telstar, and Transit have shown how effective unmanned satellites can be in weather surveillance, for long range communications, and as navigational aids. The outstanding success of the TIROS research satellite gives full assurance that the Nimbus and Aeros operational satellites to come will advance weather surveillance, forecasting, and research far beyond their previous status. Telstar, a private venture of AT&T, speaks for itself, and it, too, presages a bright future for the application of satellite technology to human advancement.

All these, and other examples of the effectiveness and usefulness of unmanned satellites and deep space probes, testify to their worth. It follows as a corollary that the matter of providing these inanimate servants of mankind with protection against radiation hazards of the space in which they must operate is worthy of careful attention. Protection, through shielding, overdesign (or perhaps under the circumstances one should say "adequate design"), modified demands on components or systems, substitution of suitable components for unsuitable ones, or avoidance of hazardous regions or times, must be worked out in theory and in practice to make most effective use of the space opportunities that lie before us. And this is a part of the subject of the present meeting.

But what about protection for man, himself? If he would just stay at home on earth where some people think he belongs, the problem would be solved. You recall the old chestnut about the man with the broken leg. His pal, rushing into the doctor's office, in his excitement could hardly tell the doctor what the trouble was. Finally, breathlessly, he managed to get out with, "Doctor, what do you do about a man who has broken his leg in two places?" To which the doctor replies, "Tell him to stay out of those places!"

Well, the easiest way to protect a man from the radiations in space is to keep him out of space. And, indeed, there are many who insist that that would be the best all-around course of action. They say that we don't need man in space; that everything we wish to accomplish out there can be done with unmanned vehicles and equipments; and that in fact it would be cheaper to do it without man.

I don't agree. No matter how you design and build, you won't be able to put man's discernment, judgment, versatility, and adaptability in space except by putting the man himself there. The more complex the mission, and the farther from the earth it must be carried out, the greater will be the need for that human versatility and insight and adaptability. At some point in complexity and distance from the earth, it will actually become cheaper to use the man than to build the mechanical substitute. Some, who have studied the matter, assert that the switchover occurs between the moon and the nearest planet.

At any rate, this is no longer an open question. Man has already gone out into space. He is going to go out again, and then again. This nation is committed in dead seriousness to placing a man on the moon in the present decade, and thousands of people are tackling this most difficult of all mankind's ventures with a determination to bring it about.

It is quite to the point, therefore, to ask what will he do out there? What is there for him to do in space anyway? With your permission I should like to explore with you now, this very question, and to review the lengthy list of reasons why man should go out into space, thereby requiring the protection that you are gathered here to discuss.

Scientific Exploration

First a few general statements. It is clear that the very first thing that man will do in space, on the moon, and on the planets, will be to explore. Whether systematized or not, whether planned or incidental, every look he takes, every glance will be exploration. And if he is an accurate observer, all of it will be science. Each bit of information, each observation, each new phenomenon or object noted, will be listened to and seized upon avidly by the scientific community.

Following this initial scientific exploration, based on the first-look results, specific investigations will be designed and carried out. Later, although right now many, indeed most, of them cannot be foreseen, there will be many practical applications, both civilian and military, of the new space knowledge and technology, and of the human ability to move about in space.

Man in Orbit

Man in orbit acquires a perspective in which to view the earth that cannot be achieved on the ground or from the lower atmosphere. Already small beginnings have been made by the Mercury pilots in the area of scientific observations from orbit. In these early days when the principal concern is with the struggle to fly at all in space and return safely, the scientific exploration necessarily received little attention. But as confidence and ability develops, the man in an earth-orbiting satellite will be able to devote more and more attention to such matters as observations of weather patterns, the airglow, the aurora, the zodiacal light, the Gegenschein, the sun's corona, and other astronomical objects.

At some time in the development of the space program, it will be important to send aloft scientists to do their own observing. It is important, therefore, that the scientific community begin to give careful thought not only to the scientific tasks to be done in orbit, but also to how they are to be done, and by whom. If scientists themselves are to go into orbit to do science there in person, these scientists must receive appropriate training for survival, for performance of their duties as members of the spacecraft crew, as well as in how to carry out their scientific investigations under the unusual conditions of space and space flight. At some appropriate time such scientists must be introduced into the NASA astronaut training program.

Actually more thought seems to have gone into the research that a man might do in person on the moon, than in a satellite orbiting about the earth. This is due in part to President Kennedy's commitment of the nation to the landing of a man on the moon within the present decade. It is due also in part to the fact that the moon is clearly an explorable body in the same sense as the earth is. One can easily see in the mind's eye men walking around, looking, poking here and there in search of interesting and important finds, picking up specimens for later study in the laboratory, taking pictures, making field tests, drilling holes, implanting instruments and automatic observing stations, and in general doing the many things that an exploration geophysicist might do on earth. It is also due in part to the fact that many of the questions of current scientific interest concerning the earth, its atmosphere, the sun, and astronomical problems are already being attacked with vigor and promise by means of unmanned satellites and probes.

But there are enough valuable scientific observations for a scientist in orbit to make, that are already apparent, that it behooves the sceintific community to pursue the subject further with vigor. We have mentioned a little earlier some of the geophysical and astronomical

observations that a man in a satellite might make. In addition, man himself, in orbit, is an important subject of scientific study. Indeed, when large orbiting laboratories can be put into operation there will be opportunity to conduct, under the same conditions of careful control and with same close personal attention that one gives in the laboratory on the ground, biological experiments on the effects of weightlessness, radiation, new periodicities, and other conditions strange to terrestrial life. In such a laboratory, fundamental and applied research, and perhaps even some of the development, of closed ecological systems can be carried out under the very conditions under which they will be required to operate. For example, those systems to be used on manned planetary missions, will have to operate for years without failure. In an orbiting laboratory such a system could be given a life test that would be fully meaningful and in which one could place some confidence.

When man has learned to move about freely in space, especially when he is able to move around outside the spacecraft or space station that serves as his home base in space, there will be many activities that he can pursue. One of these will be engineering and construction in space. At the present time, space engineering is carried out on the ground. The engineered object, if it is a space vehicle or a spacecraft, is placed in orbit after the engineering has been accomplished. In this approach, man stays on the ground, and sends his engineered object out into space. Much has been accomplished by this approach, in the form of scientific satellites and space probes, weather satellites, communications satellites, navigation satellites, and military applications of space technology, and even manned satellites.

But one day man will do some of his engineering and building right out in space. A lot of this activity may perhaps be more properly referred to as construction and maintenance, but the novelty of the problems and the environment to be faced will be such that for a long time to come the constructors and the maintainers will actually have to be engineers in the true sense of the word.

One can foresee the need to assemble in space large laboratories, huge antenna systems, stations to serve as staging areas for interplanetary flight, and even space vehicles for making flights to the planets and into deep space.

It may be necessary to form the reflecting surfaces for astronomical telescopes under the conditions of weightlessness under which they are to operate so as to eliminate distortions that would be introduced by forming them on the ground under 1 g and then launching them into orbit.

Considering the tremendous expense that one must anticipate for the construction of huge observatories and laboratories of the future, it may well prove to be far cheaper to provide human maintenance and repair, than to rebuild and launch a new satellite every time an old one has ceased to function. In fact, in many cases it may not be just a matter of maintenance and repair. By replacement of instruments in an orbiting observatory it may be possible to update at relatively low cost a basically expensive facility.

This newly developed ability to engineer, inspect, build, maintain, renovate, and carry out complex logistics operations in space, will also have military value. In the matter of military applications of space, informed thought appears to have gone full circle. At first, years ago, although opinions varied, the general thought was that space provided an overwhelming military potential, and that he who dominated space would dominate the world. This was followed by a reaction period, during which the general thought swung to the opinion that perhaps there was very little of military value in space. At the present time, there are few who would deny that space does offer possibilities for many important military applications. I would venture to predict that in time engineering in space will form an important segment of the sum total of manned operations in space for military purposes.

Man on the Moon

One of the most important reasons for placing a man on the moon is to carry out a scientific investigation of that body. The moon is of especial interest to the scientist for a number of reasons.

We know that the solar system was formed about 4.5 billion years ago, but we do not know how it was formed, and this problem has been the subject of much speculation and thought for centuries. The investigation of the origin of the solar system is a project of the greatest scientific interest, one to which the exploration of the moon can contribute significantly.

The moon will play a special role in this investigation because it is a body whose surface has preserved the record of its history for a much longer period than the earth, and probably much longer than Mars and Venus as well. On the earth, the atmosphere and the oceans wear away surface features in 10 to 50 million years. Mountain-building activity turns over large areas of the surface in about the same time. There is little left on the surface of the earth of the features that existed several hundred million years ago. The same is probably true of Mars and Venus. But on the moon there exist no oceans and very little atmosphere to destroy the surface. Also, inspection of the moon's surface in a telescope shows few signs of the mountain-building activity which distorts and defaces the surface of the earth so rapidly.

Thus the moon's surface will carry us back very far into the early history of the solar system, perhaps not back to the birth of the sun and planets, but certainly billions of years back --- much longer than the 10 to 20 million years to which we are limited on the earth.

Not only the lunar surface, but also the internal structure of the moon may provide a clue to the early history of the solar system and the birth of the planets.

One of the theories for the creation of the planets, popular until recent times, held that the solar system was created during a near collision between our sun and another star, in which the gravitational forces between these two massive bodies tore huge streams of flaming gas out of each. As the intruding star receded, the masses of gas which happened to be near the sun were captured by it into orbits in which they eventually cooled and solidified to form the planets. If such a collision was the manner of formation of the solar system, then the moon and planets must have been molten at an earlier stage in their histories. In that event, the iron in their interiors would melt and run to the center to form a dense core.

Another theory holds that the planets were formed out of pockets of condensation in the du t surrounding our sun during the early stages of its lifetime. We know that stars themselves are almost certainly formed in this way, by condensation of pockets of interstellar gas and dust which happened to be somewhat denser than their surroundings. It seems likely that additional subcondensations could have developed in the tenuous matter surrounding the sun before the central condensation had proceeded to its final stages; and that the moon and planets were eventually formed from these subcondensations.

Large bodies like the earth have enough radioactive uranium inside them to produce melting of iron simply through the heat generated in nuclear decays. Therefore, the existence of a dense core of iron in the interior of the earth does not prove the validity of the collision theory, or disprove the theory of condensation. However, the moon is smaller and colder, and will provide a much better indication than the earth, as to which of the two theories on the origin of the solar system is correct.

The necessary observations and measurements obviously cannot all be made just by man's standing on the moon and looking around. But a giant step will have been taken when the first scientist on the moon does look around and begins to zero in on the most likely answers, and more importantly, can determine the most promising courses to follow for obtaining the answers. Before that time some data will have been obtained by means of unmanned spacecraft, Rangers and Surveyors, but the full power of the lunar science effort will not be brought to bear until man and instrument together tackle the problems to be solved.

This subject was discussed at length at the Space Science Summer Study conducted at the State University of Iowa, under NASA sponsorship, this past summer. Most of the participants felt that the first scientist-astronaut to be landed on the moon should be a geologist. His first job should be to look -- and think. There was considerable discussion about the qualifications of this first scientist on the moon. The thought was brought out that this man should be a top notch, first rate scientist. As an illustration, it was pointed out that it took a Darwin to make the voyage of the Beagle the historic success that it was. If one wants to be quantitative about it, one might say that the difference between sending

a run-of-the-mill scientist, or a non-scientist given special supplementary training in science, to the moon to look around, and sending a Darwin there is a matter of many many orders of magnitude in what returns are realized from the venture. Of course, the problem is to find a Darwin who can also become an astronaut, and is willing to.

The question of how man will do science on the moon is one that is worthy of much thought. One approach is that already mentioned, namely, to send scientists to the moon. Another is to train the astronauts to look for anticipated objects and phenomena and to try to be alert to the unanticipated ones and report them accurately. Still a third might be to have an astronaut-scientist team in which the astronaut on the moon is linked with the scientist on the earth by means of radio and television. In two-way conversation, the astronaut receives guidance from the scientist who sees through the television what the astronaut sees. By questioning the astronaut, the scientist can get additional details from the man on the moon about objects that appear to be of special significance.

At any rate, the scientific observer on the moon will have plenty to keep him busy. As mentioned, the first thing he should do is look and think. He should examine the surface, note the various geologic formations, select appropriate samples to bring back to earth, and take pictures. Eventually, although very likely not on the first trip, he should conduct measurements of surface properties, radioactivity, temperature and heat flow, seismic activity, etc., bringing with him the necessary instruments to accomplish these tasks. At some time, he will begin to use the moon as a base for a variety of observations, some of them not necessarily of the moon itself. Studies of the librations of the moon can give a great deal of information about the internal construction of the moon, but other astronomical investigations may well concern the sun and stars. For example, the other side of the moon has been pointed to as ideal for setting up a radio astronomy observatory. Also there may be great value in observations of the earth, particularly atmospheric phenomena, from the moon.

At first this observing from the moon as a base may well be done with automatic or semi-automatic equipment emplaced on the moon by the men who go there, supplementing other such observatories that were landed on the moon by unmanned spacecraft. Eventually, however, manned bases, including scientific observatories, will probably be established.

We have already said that the first scientist to land on the moon should probably be a geologist. Because of the construction work that will in time take place on the moon, it is also desirable that among the early lunar explorers there be a civil engineer. His job also will be to look and think, and collect data for the day when construction of supply depots, radiation shelters, roads, landing areas, large bases, and observatories will take place.

Already it is certain that when man does do engineering and building on the moon, he will do it under conditions far different from those encountered on the earth. The gravity will be only one-sixth of that met with on earth while the lack of an atmosphere, bombardment by meteoritic particles, the constant presence of the interplanetary radiations, the

tremendous range of temperatures, the possible presence of dust that may be more than just a nuisance, unusual conditions of electrostatic charging, etc., will confront him with problems that will tax his ingenuity and skill to the utmost.

When manned lunar bases or observatories go into operation, it will be necessary to have worked out a plan for maintaining the supply lines to them. The required logistics and operatiónal support to the endeavor will make an Antartic expedition look like a grade school exercise in comparison.

All of this will require, of course, that an adequate scheme for protecting the men involved from the radiations of space will have been worked out, and put into use.

Man Around the Moon

Doubtless man will circumnavigate the moon, even go into orbit around it, before making a landing. At any rate, this is the present U. S. plan. During such maneuvers, prior to landing, man can make preliminary observations. Such observations will be needed to support the ultimate landing on the lunar surface, particularly those that reveal the character of the surface and permit one to select suitable landing sites. They will also be of scientific value. Of especial importance will be pictures that can be taken from the circumnavigating or orbiting spacecraft.

After man has landed and established a base on the moon, a lunar orbiting space station carrying one or more human observers can be used in conjunction with the observatory on the ground for further scientific exploration of the moon. For some time to come, the lunar satellite approach may be easier than lunar surface transportation for a global survey of the moon.

Interplanetary Space

On the way to the moon or the planets, man must traverse the space between earth and them. Although much of the investigation of these regions will doubtless best be done by intrumented space probes, nevertheless man will again have the opportunity to look about and search for the unexpected. Most of his observational opportunities will be astronomical in character. The zodiacal light, the Gegenschein, the sun's corona, the atmospheres of the planets, new views of the bodies of the solar system, can come under new scrutiny. In addition, man can continue observations on himself, under conditions of isolation not producible in any other fashion.

Man on the Planets

The investigation of the moon and planets by satellites, deep space probes, and manned exploration, serves to broaden the horizons of the geophysicst tremendously. A little thought will show that the techniques and experience that must be called upon in investigating these bodies must be those of the geophysicist. Moreover, as one goes forward with these lunar and planetary investigations, the student of the earth should find the broadened perspective provided by increased knowledge about the moon and planets a powerful lever to use in prying loose some of the secrets of the earth itself. Indeed, it is in recognition of these facts that the American Geophysical Union just recently voted to establish a new Section on Planetary Science.

The experience gained in manned exploration of the moon will no doubt serve as a basis for beginning the manned exploration of the planets. There will be many similarities, and many differences. Among the latter are the considerably greater distances that must be traversed, the longer times that man must spend out in the lonely voids of space, and the existence of atmospheres on the planets.

The ability to send measuring instruments to the moon and planets, and eventually to visit them in person, permits man to study directly more than one sample of the material of which the universe is composed, and more than one sample of the bodies of the universe. It is possible that the scientist may also have the opportunity to study more than one sample of physical life in the universe.

Certainly one of the most exciting possibilities in space exploration is that indigenous life may be found there. The most likely candidate, as you know, is Mars, where balloon observations in the infrared have detected emissions characteristic of the carbon-hydrogen bond. While this does not prove the existence of life on Mars, it is most certainly highly provocative. For this reason, preparations are going forward with various types of instruments to search for living forms on the Red Planet. These will be carried in fly-bys and landers as soon as we are able to provide the necessary transportation.

All the data available at present would indicate that there is little likelihood of life on Venus. Various radioastronomical observations of the planet indicate that the surface temperatures are in the vicinity of 600°K., well over the boiling point of water. These temperatures are in themselves discouraging enough, but when taken in conjunction with probably very high pressures existing on Venus (exceeding 20 atmospheres at the surface) it seems most likely that the entire planetary surface is bathed in a searing atmosphere, and that there is no chance of life there. The biologists insist, however, that there may yet be life on Venus, existing in the cooler upper atmosphere. Balloon samplings are being made of the earth's upper atmosphere to search for organisms that

might be living there. Results from these investigations may shed additional light on how much of a point the biologists have in connection with Venus.

It does not appear likely that there are living forms on the surface of the moon, because of the lack of an atmosphere, the lack of any observable water, and the extreme temperature ranges to which the lunar surface is subjected. Some believe, however, that there might be living forms existing at some distance below the hostile lunar surface. But even if there are no living forms on the moon, other biologists point out that the moon is still of interest in that it may carry the residue of previously living forms or possibly material that is in the nature of precursors to life. Controversy rages on this issue, with some scientists categorizing this reasoning on the part of the biologists as absolute nonsense. But the biologists can counter with the observation that if they should be right, walking all over the moon with dirty feet, or plastering it with dirty material, can destroy a once-in-forever opportunity to make exobiological studies that may have great bearing on our understanding of terrestrial life.

At any rate it seems clear that we must be careful about what we do in the case of Mars. A suggestion was made at the SUI Space Science Summer Study that Mars be made an ecological preserve, where steps are taken to protect the planet from undesirable contamination. According to the suggestion, Mars would be investigated in such a manner as to protect the interests and needs of the biologists who wish to search for and study any living forms or traces of life that might exist there. This proposal also included the suggestion that, although Venus and the moon not be considered as ecological preserves, care be taken to minimize their contamination.

Of course, if Mars is to be maintained as an ecological preserve, this can be done only by international cooperation, specifically, at the present time between the U. S. and the U.S.S.R.

One might mention in passing, that those who are concerned about possible contamination of our neighbors in space through the introduction of terrestrial organisms, also point to the possible danger of back contamination of the earth by the introduction of extraterrestrial organisms. Careful thought must be given to this problem, and in due time appropriate steps taken to remove any risks that are judged unacceptable.

When man reaches out toward the planets, who can say where it will all end? Your imaginations can explore this question as well as mine. Manned bases, observatories, landings on the satellites of planets, such as those of Jupiter or Saturn, artificial orbiting observatories about the different planets, and many other such things are in the realm of possibilities that the far distant future holds out to man. One even hears mention of the possibility of modifying the atmosphere of Mars to

make it less hostile or even almost habitable. This might be accomplished by the introduction of suitable biological agents to the planet, after the initial search for and investigations of indigenous life have been made.

But these speculations can serve us no real good here except to indicate that the field of space is wide open as far into the future as we can now see, and that the path to the planets leads farther than man can peer from his present position on the earth, at this point in time.

Conclusion

I am sure that I haven't made any startling revelations to you, or carried our subject any further in thought than you could have done, or perhaps have already done. But, hopefully, this little review of the things that man can look forward to doing in space, will serve the good purpose of showing clearly that it is indeed desirable to find ways of protecting man against the radiation hazards of space, so that he may go out into space in pursuit of his destiny.

Paper A-1

Brief Note on the Radiation Belts of the Earth

by

J. A. Van Allen
State University of Iowa

There are many different aspects to the radiation belts of the earth which may engage one's interest. This note is intended to present a brief graphical summary of one of these aspects, namely, the positional dependence of the absolute intensity of several selected components of the trapped particle population.

One of the earliest findings was that there are two distinct "belts" of trapped particles in the geomagnetic field -- an inner belt whose outer boundary is approximately the "magnetic shell" which crosses the equator at 1.6 earth radii from the center of the earth; and an outer belt which lies between this shell and one which crosses the equator at approximately 12 earth radii [Van Allen and Frank, 1959a]. The properties of the radiation in the respective

belts were found to be quite different [Van Allen and Frank, 1959b] [Van Allen, Ludwig, and McIlwain, 1959].

In subsequent work of a more comprehensive nature, using a variety of instruments carried by satellites, rockets, and space probes, it has become clear that the structure of the trapping region is quite complex and in fact that there are as many different structure functions as they are components of the trapped radiation to be considered. The concept of a two-belt structure has persisted, though it has now assumed a rather different significance than the original one. The distinctive general characteristic of the inner belt is now regarded as its relative time-stability whereas the distinctive general characteristic of the outer belt is its large and rapid time-variability. (Orders of magnitude change in intensity of selected components within times of the order of days and even of hours.) The magnetic shell which crosses the equator at 1.8 earth radii continues to represent the approximate interface between inner and outer zones. Despite the great time variability of particle populations and energy spectra in the outer zone, there has been observed during the past four years a remarkable tendency for it to relax back to a more or less standard state during prolonged periods of geomagnetically quiet conditions. The accompanying figures represent an effort to depict four sample structure functions

which are moderately well known and which give an abridged view of present knowledge. Each of these figures is a geomagnetic-meridian cross-section of the earth and of its near-astronomical environment. The semicircle at the left is the cross-section of the solid earth and the linear scale is in units of earth radii (6371 km). The contours are labeled by the value of omnidirectional intensity of the component specified in the caption. The distribution of particles in three dimensions is understood to be obtained by the rotation of the structure function shown about the vertical axis.

Figure 1 is considered to have a good level of reliability. It is based primarily on data from Explorer IV and from Pioneers III and IV (see references cited above). The omnidirectional intensity of protons having $E > 30$ MeV has its peak value at 1.4 earth radii on the equator and is about $3 \times 10^4/cm^2$ sec; beyond 2 earth radii it is less than $10/cm^2$ sec and may be much less than this beyond 4 earth radii.

Figure 2 is based in large part on the data from Pioneers III and IV (cited above), from Explorer VI [Arnoldy, Hoffman, and Winckler, 1960] [Fan, Meyer, and Simpson, 1961] [Rosen and Farley, 1961], and from Explorer XII [O'Brien, Van Allen, Laughlin, and Frank, 1962]. Values as high as 10^5 to $10^6/cm^2$ sec are sometimes found in the

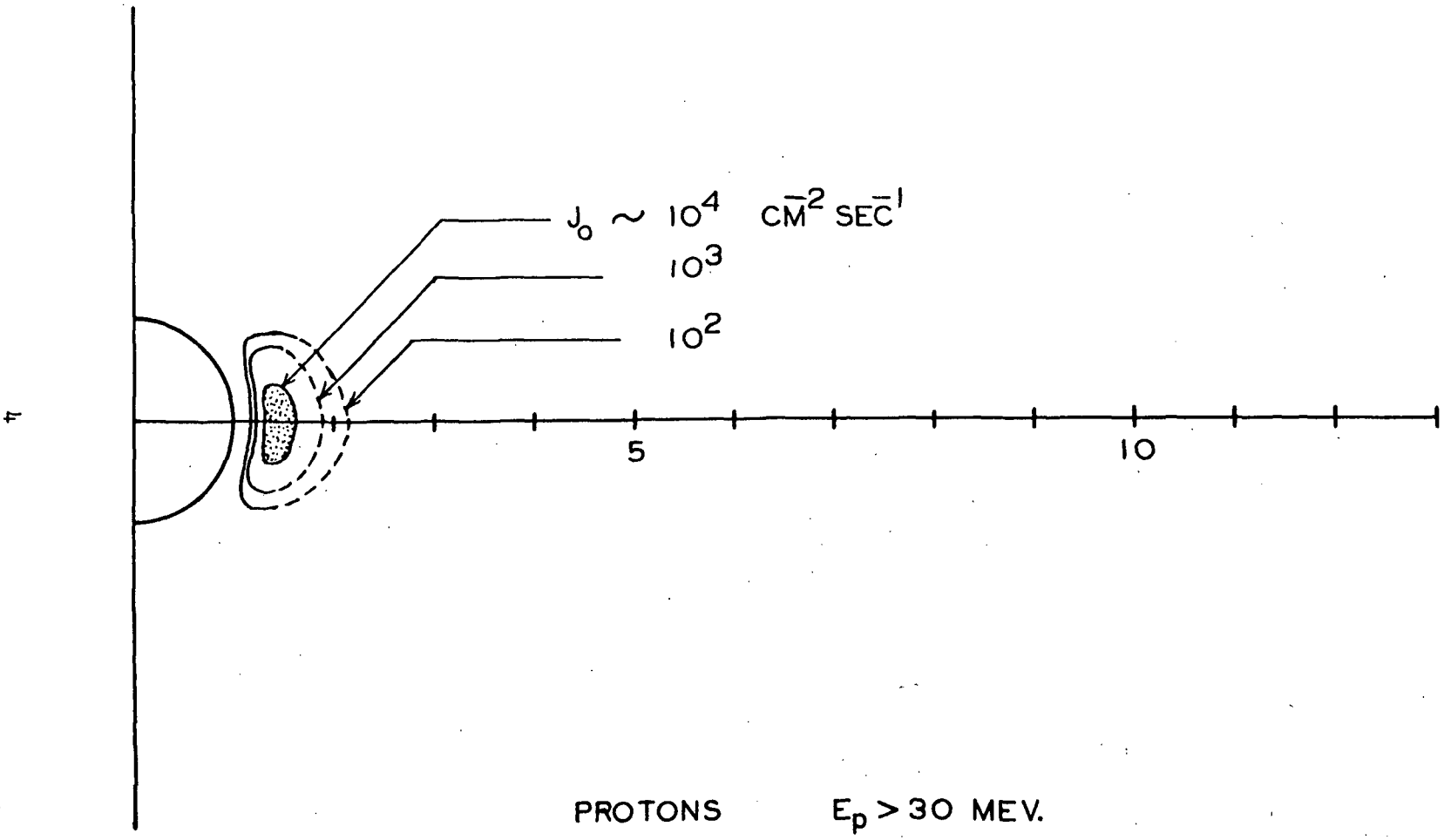

Fig. 1

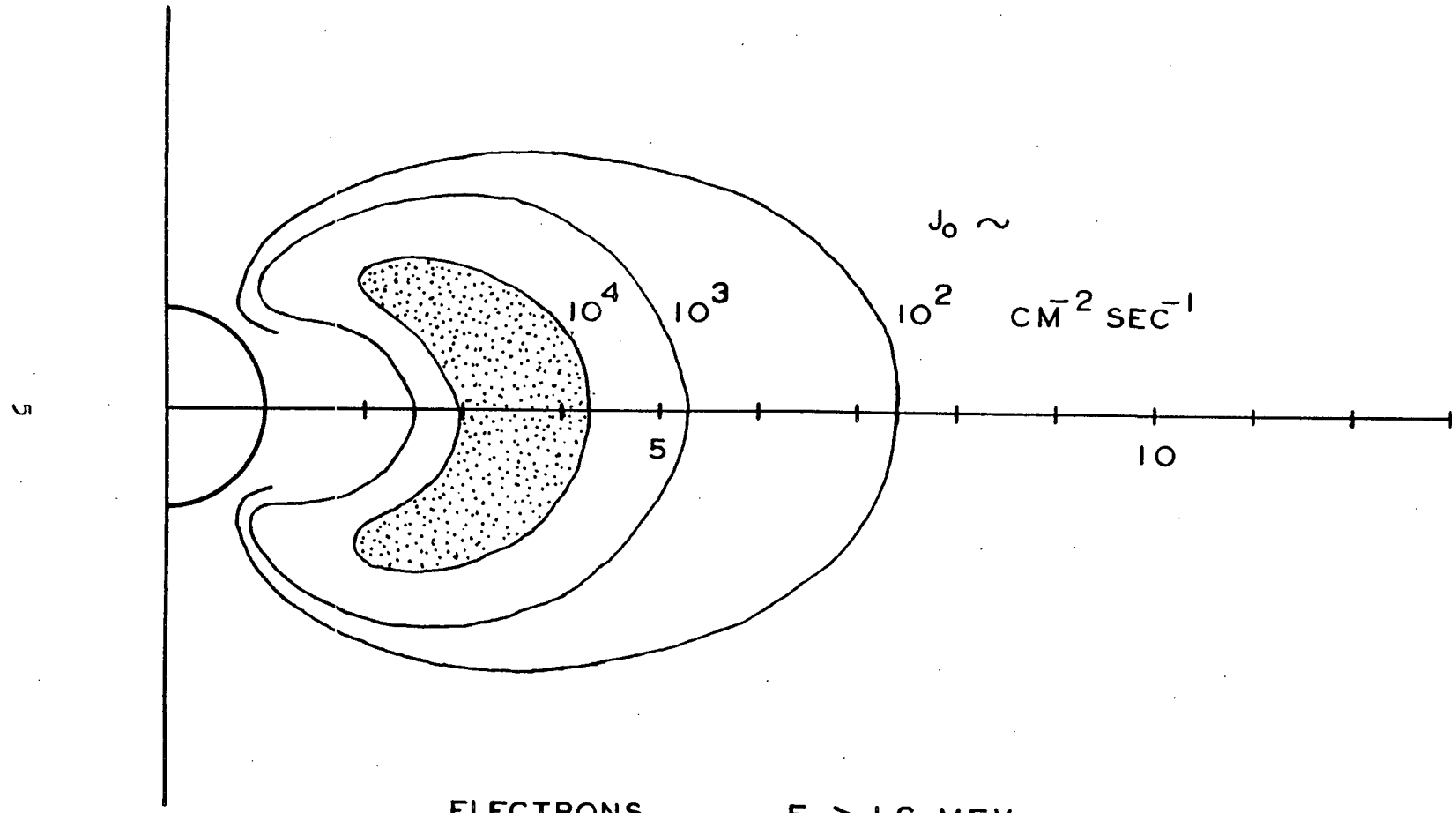

ELECTRONS $E_e > 1.6$ MEV.

Fig. 2

vicinity of 4 earth radii. On other occations, the intensity of electrons of $E > 1.6$ MeV drops below the plotted values by as much as two orders of magnitude. The values shown in Figure 2 are intended to be representative of quiet conditions. The maximum intensity near 3.5 earth radii under such conditions is of the order of $10^5/cm^2$ sec. A comprehensive survey is currently underway with Explorer XIV [Van Allen and Frank, 1962], whose apogee is at 16.4 earth radii and whose perigee is at an altitude of about 400 km.

The structure function of Figure 3 for protons of energy $0.1 < E < 5$ MeV is an attempt on the part of the present author to represent the observations of Bame, Conner, Hill, and Holly [1961], Naugle and Kniffen [1962], and most importantly those of Davis and Williamson [1962], the latter with Explorer XII. Further extensive surveys are currently underway with Explorer XIV and Explorer XV.

Figure 4 synthesizes low altitude observations with Injun I [O'Brien, Laughlin, Van Allen, and Frank, 1962] and extensive observations with Explorer XII in a highly eccentric orbit [O'Brien, Van Allen, Laughlin, and Frank, 1962] [Rosser, O'Brien, Van Allen, Frank, and Laughlin, 1962]. Again there are marked time variations. Current observations with Explorer XIV are confirming the general character of Figure 4 and are contributing definitive new knowledge

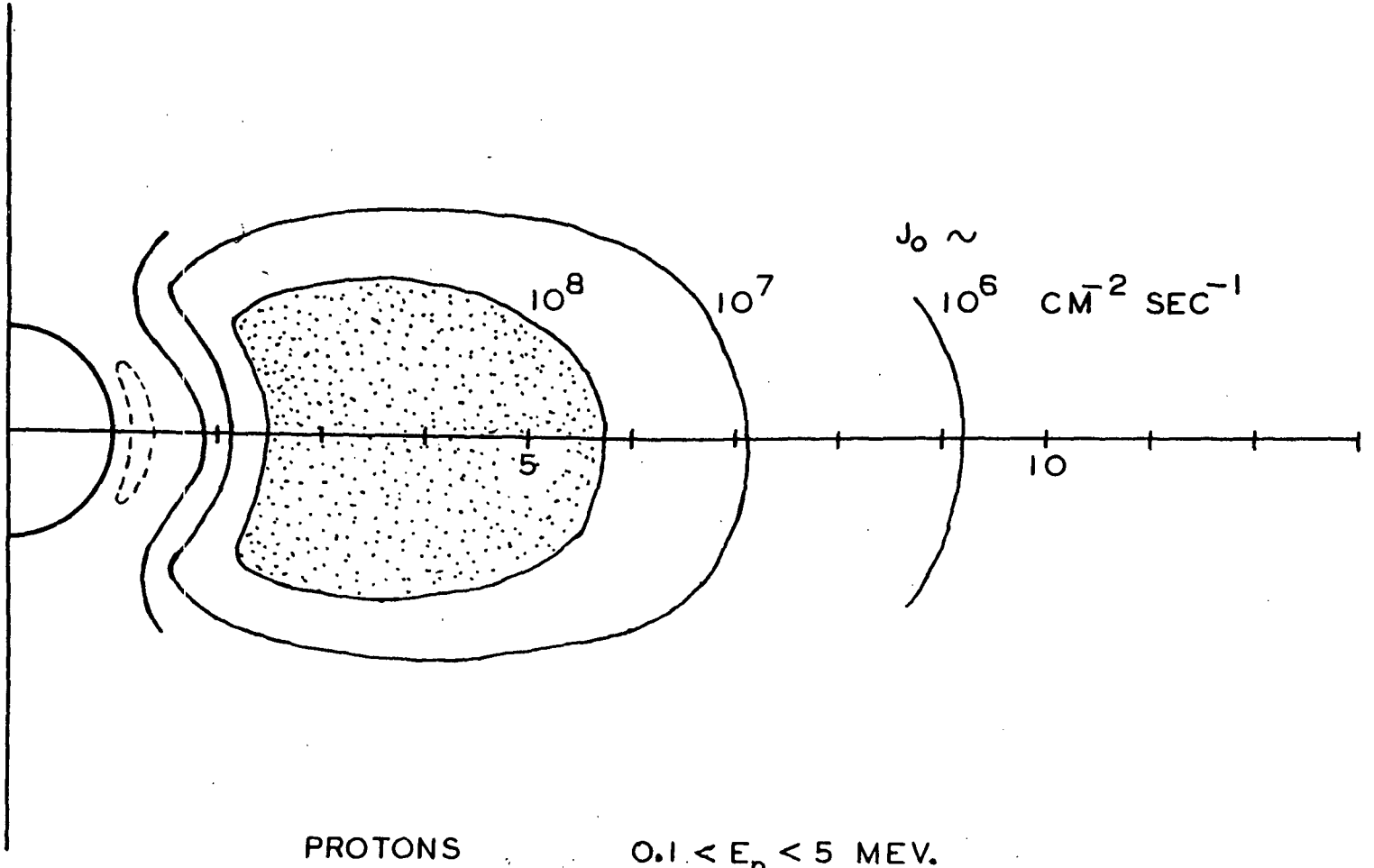

Fig. 3

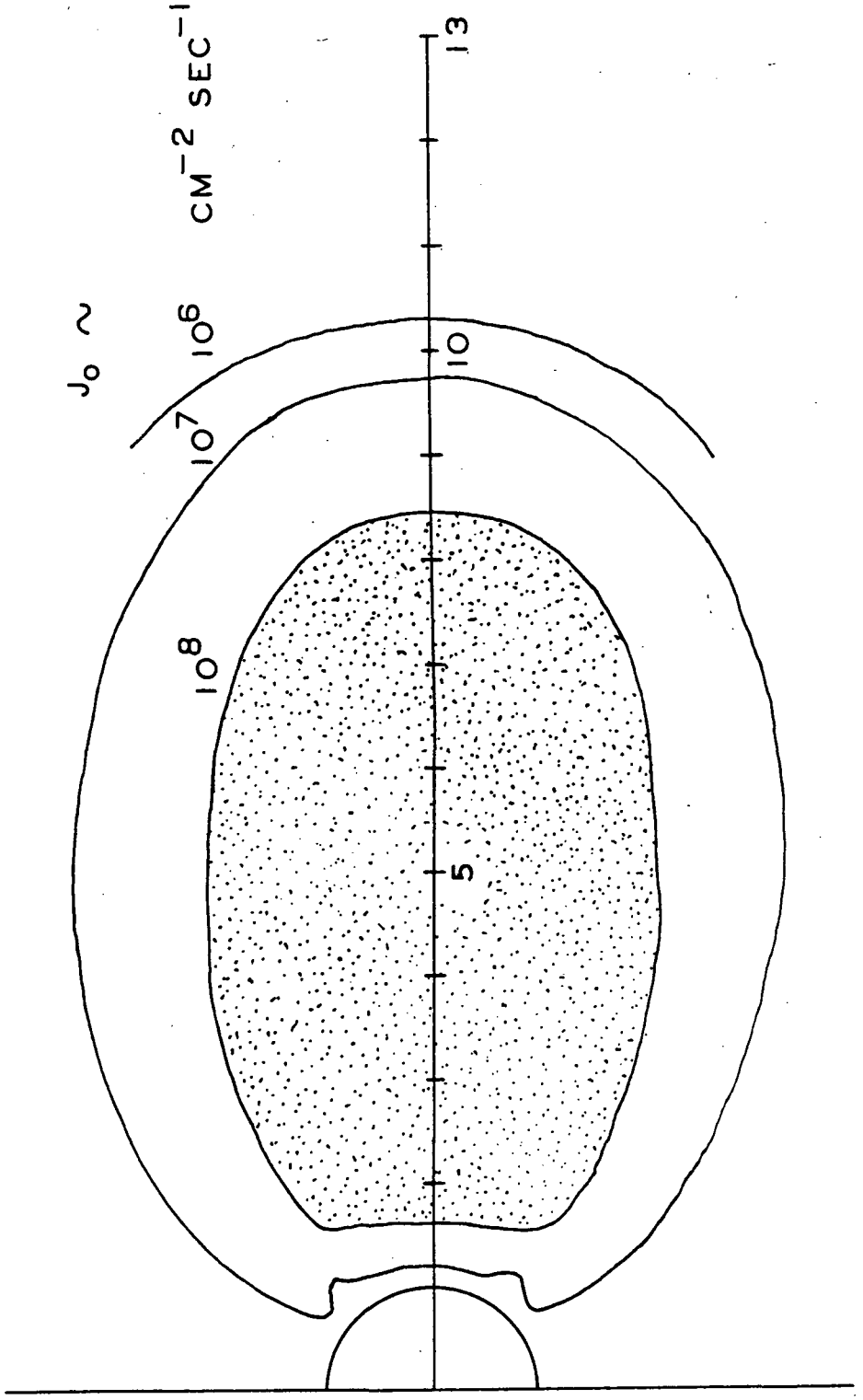

ELECTRONS $E_e > 40$ KEV.

Fig. 4

on the omnidirectional intensity of electrons having $E > 40$ keV as well as those having $E > 250$ keV and those having $E > 1.6$ MeV [Van Allen and Frank, 1962].

For an earlier review of a more comprehensive character, the reader is referred to a paper in the Proceedings of the International Astronomical Union [Van Allen, 1962]

REFERENCES

Arnoldy, R. L., R. A. Hoffman, and J. R. Winckler, "Observations of the Van Allen Radiation Regions during August and September 1959, Part 1", J. Geophys. Research 65, 1361-1375 (1960).

Bame, S. J., J. P. Conner, H. H. Hill, and F. E. Holly, "Protons in the Outer Van Allen Belt", J. Geophys. Research 67, 1628 (Abstract) (1962).

Davis, L. R. and J. M. Williamson, "Low-Energy Trapped Protons", Third International Space Science Symposium and COSPAR Plenary Meeting, Washington, D. C., April 30-May 9, 1962.

Fan, C. Y., P. Meyer, and J. A. Simpson, "Dynamics and Structure of the Outer Radiation Belt", J. Geophys. Research 66, 2607-2640 (1961).

Naugle, J. E. and D. A. Kniffen, "The Flux and Energy Spectra of the Protons in the Inner Van Allen Belt", Journal of the Physical Society of Japan Vol. 17 Supplement A-II, 1962, International Conference on Cosmic Rays and the Earth Storm Part II, pp. 118-122.

O'Brien, B. J., C. D. Laughlin, J. A. Van Allen, and L. A. Frank, "Measurements of the Intensity and Spectrum of Electrons at 1000-Kilometer Altitude and High Latitudes", J. Geophys. Research 67, 1209-1225 (1962).

O'Brien, B. J., J. A. Van Allen, C. D. Laughlin, and L. A. Frank, "Absolute Electron Intensities in the Heart of the Earth's Outer Radiation Zone", J. Geophys. Research 67, 397-403 (1962).

REFERENCES (continued)

Rosen, A. and T. A. Farley, "Characteristics of the Van Allen Radiation Zones as Measured by the Scintillation Counter on Explorer VI", J. Geophys. Research 66, 2013-2028 (1961).

Rosser, W. G. V., B. J. O'Brien, J. A. Van Allen, L. A. Frank, and C. D. Laughlin, "Electrons in the Earth's Outer Radiation Zone", J. Geophys. Research 67 (in press).

Van Allen, J. A., "Dynamics, Composition and Origin of the Geomagnetically-Trapped Corpuscular Radiation", Proceedings, International Astronomical Union, 1962 (in press).

Van Allen, J. A. and L. A. Frank, "Radiation Around the Earth to a Radial Distance of 107,400 Kilometers", Nature (London) 183, 430-434 (1959).

Van Allen, J. A. and L. A. Frank, "Radiation Measurements to 658,300 Km with Pioneer IV", Nature (London) 184, 219-224 (1959).

Van Allen, J. A. and L. A. Frank (Private Communication, 1962).

Van Allen, J. A., C. E. McIlwain, and G. H. Ludwig, "Radiation Observations with Satellite 1958 Epsilon", J. Geophys. Research 64, 271-286 (1959).

Paper A-2

An Evaluation of the Radiation Hazard Due to Solar Cosmic Rays

by
W. R. Webber and P. S. Freier*

Introduction

Although the characteristics of the galactic cosmic radiation have been recognized and investigated in detail for many years, the ability of the sun to produce large bursts of energetic particles was discovered only in 1946 (Reference 1) and the arrival of this solar cosmic radiation at the earth has been studied in detail only since 1956. In the ten years preceding the solar cosmic ray event of February 23, 1956, there were only four cases of an increase of cosmic ray intensity at the earth (as measured at ground-level by ionization-type detectors) that could be related to solar activity. Therefore the idea became widespread that these events were quite rare.

The introduction of the neutron monitor in 1949 (Reference 2) somewhat improved the sensitivity of the ground-level measurements, but the real breakthrough came recently with particle counters and emulsions flown in balloons, satellites, and space probes. In addition, it has been found that the solar particle bursts may be detected indirectly through their effects on the absorption of VHF cosmic noise in the ionospheric D-layer over the polar caps - called polar cap absorption (PCA).

From the studies of solar particle bursts over the last few years by this wide variety of techniques, a reasonably complete picture of these events is beginning to emerge (Reference 3). The cosmic ray particles ejected from the sun are known to be primarily protons with typically steep energy spectra and

*University of Minnesota

in energy
ranging/from less than 10 Mev to a few Bev. Such cosmic ray particles may be present near the earth in detectable numbers a significant fraction of the time (5 - 10 percent), exceeding the normal galactic cosmic ray intensity for a much smaller period of time (~ 1 percent) and occasionally for intervals of one or two days, reaching intensities many thousands of times greater than the galactic cosmic ray intensity.

The intensity-time, directional, spectral, and charge characteristics of the solar cosmic rays differ considerably from event to event. For example, some events may contain a relatively large fraction of high-energy particles, thus producing a rare effect in a sea-level detector; but, on the other hand contain few low energy particles, thus giving a small integrated particle intensity. The latter characteristic causes the event to be classified as a relatively small one. Other important dissimilarities exist from event to event, and for this reason we shall catalog some of the more important ones individually. However, we may define certain general characteristics - common to all events - which may aid in understanding these events.

The Intensity-Time Profile

A typical event will have a set of intensity-time profiles, one for each energy, such as those shown in Figure 1 . Certain times characterize each profile:

1. The onset-delay time is defined as the time from the maximum of the visual flare intensity to the arrival of the first particles at the earth. This time is variable from event to event and is strongly energy-dependent, the higher energies arriving first. Onset-delay times may vary from a few

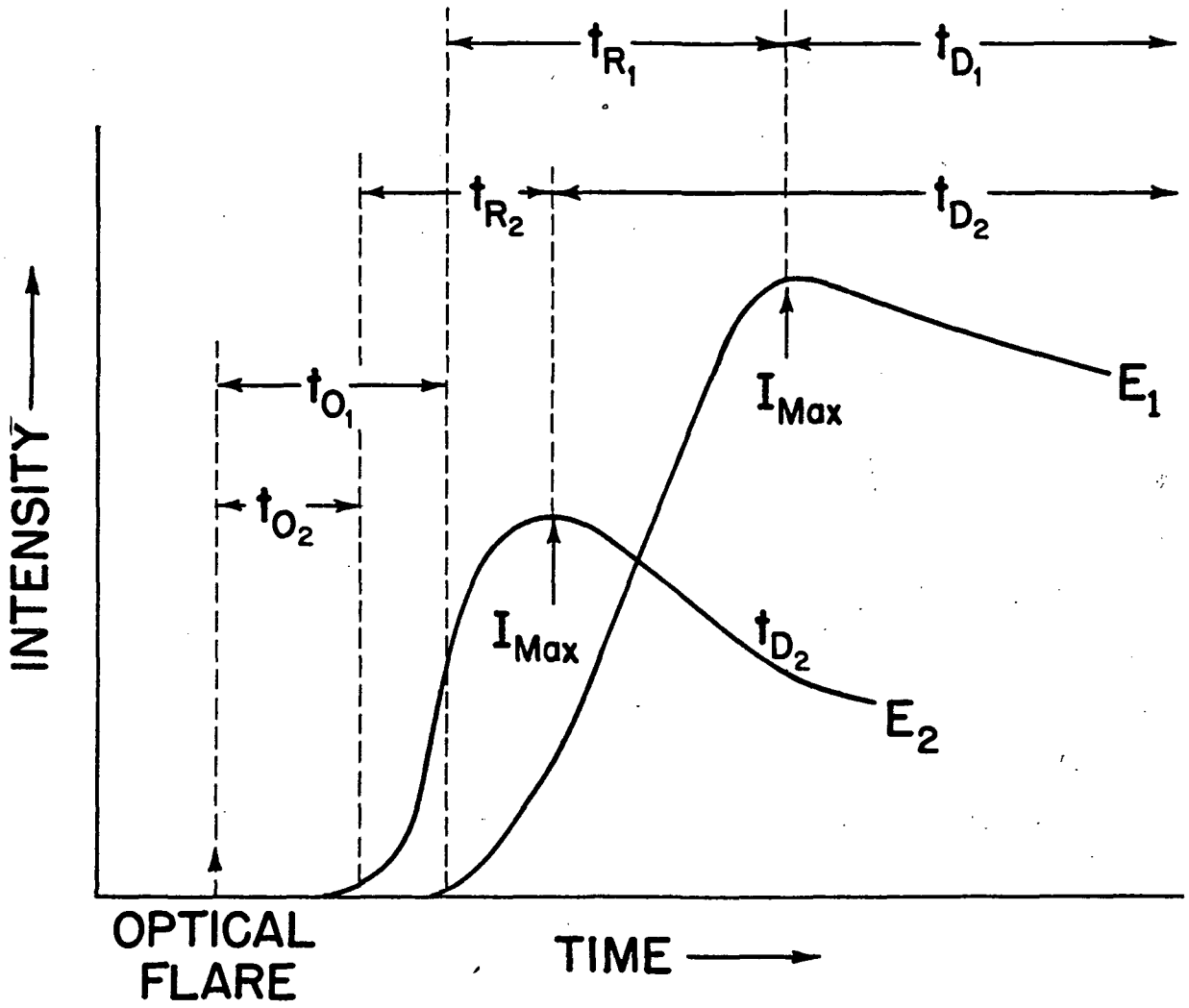

Figure 1 - Intensity-time profiles for a typical event. Curve E_2 represents the arrival of particles of energies that are high in comparison with the energies of the particles represented by curve E_1. T_{O_1} and T_{O_2} are onset-delay times; T_{R_1} and T_{R_2}, rise times; and T_{D_1} and T_{D_2}, decay times.

minutes for high energy particles in some events to many hours for low energy particles in other events.

2. The rise time is defined as the time interval from the first arrival at the earth of particles of a particular energy to the time at which maximum intensity of these particles is attained. This time also varies from event to event and is strongly energy-dependent, the higher energies reaching maximum intensity first. These times are usually related to the onset times in a particular event, and may range from a few minutes for high energy particles in some events to many hours for low energy particles in other events.

3. A growing body of evidence indicates that the decay of the intensity of the particles above a particular energy is exponential at most times and over a wide range of energies (Reference 3). Thus we may define a characteristic decay time t_D and write the following equation for the intensity of flare particles with energies greater than some energy E at some time t after the maximum intensity $I_{Max}(E)$ attained:

$$I = I_{Max}(E)\ e^{-t/t_D}.$$

The time t_D itself is a function of energy being smaller for higher energies and is variable from event to event. It may be changed during the course of an event by the arrival at the earth of a changed interplanetary field configuration, such as might be evidenced by a magnetic storm or other magnetic activity. The decay time may range from 3-4 hours for high energy particles in some events to 2-3 days for low energy particles in other events.

Anisotropies in the Flare Particles

For the most part the solar flare particles arrive at the earth very

nearly isotropically (within $\pm$ 5-10 percent) and the aforementioned intensity-time characteristics refer to this isotropic radiation. Frequently, however, significant anisotropies exist in the direction of arrival of solar flare particles in the earth's vicinity. In particular, the particles appear to arrive from a highly preferred and fairly narrow direction in space. Such directional radiation is usually of short duration compared to the isotropic part; however, unusually high intensities may occur in the preferred direction for periods of a few minutes. It is also possible to define onset-delay, rise, and decay times for this directional radiation.

The Energy Spectrum of the Flare Particles

It is obvious from the foregoing discussion on the intensity-time characteristics of the flare particles and from the energy-dependence of each of the parameters involved that there is no unique energy spectrum for any one event. The spectrum measured in a single event will depend upon the specific time in the event at which the measurements are made. The problem of determining a useful and meaningful representation of the solar flare particle spectrum has been one of the most difficult connected with the study of the flare particles. Usually the differential number spectrum of the flare particles has been expressed either as a power law energy spectrum eg $\frac{dJ}{dE} = \frac{K_1}{E^{n_1}}$ or as a power law rigidity spectrum eg $\frac{dJ}{dP} = \frac{K_2}{P^{n_2}}$ (the rigidity of a particle $\equiv P = \frac{pC}{Ze}$ where p is the particle momentum, C the velocity of light, e the unit charge, and Z the charge number of the particle). When either of these representations is used n_1 (or n_2) is a function of both energy (or rigidity) and time (eg n_1 or n_2 is usually smaller for lower energies or rigidities causing a bending over of the spectrum - also n_1 or n_2 increase with time after

the onset of an event thus resulting in a steepening of the particle spectrum with time).

Because the energy or rigidity interval viewed in any one measurement is usually quite narrow, it is possible to represent reasonably well the number spectrum of solar flare particles as a power law energy or rigidity spectrum with a constant n over the interval of measurement. This does not prove to be a useful representation over the entire range of rigidities involved in the solar outburst, however.

After a careful examination of the data from a large number of events which were difficult to interpret if the solar particle spectrum were considered to be power laws in either energy or rigidity we have reached the conclusion that a one parameter system best defines the spectra of the solar flare particles (Reference 4). This one parameter system is an exponential rigidity spectrum of the form $\frac{dJ}{dP} = \left(\frac{dJ}{dP}\right)_o e^{-P/Po(t)}$. $P_o(t)$ is a characteristic rigidity which in a single event is a function of time only - decreasing as the event progresses. Its value and time dependence may vary from event to event, however. Such spectra apply to all rigidities providing the time is a few times the normal delay time for particles of a particular energy arriving from the sun.

The above conclusion is reached only after a considerable modification of our interpretation of solar particle spectra from measurements made during balloon ascents and particularly after a considerable reinterpretation of the intensities and spectra of low energy solar flare particle from riometer measurements. The grounds for these modifications are discussed in detail in reference 4.

With such spectra it is not necessary to "artificially" bend over the power law spectra at lower energies - the effect of an exponential spectrum

is the same as a "bent over" power law. A comparison of the time development of a typical solar cosmic ray spectrum during an event using the two representations is shown in Figure 2. Typical initial values of the "characteristic" rigidity may range from ~ 300 MV in events with very flat spectra containing many high energy particles to ~ 50 MV in events with very steep spectra containing many low energy particles and producing strong radiowave absorption.

Charge Composition of the Flare Particles

The particles emitted in a solar flare burst are predominantly protons, but in each event, to a greater or lesser degree, particles heavier than protons appear to be present - predominantly alpha particles but including nuclei in the CNO group at least (references 5 and 6). To date these heavier particles have actually been observed during six solar cosmic ray events, by only one or two spot measurements during each event. In addition these measurements may represent intensity integrals of solar particles over several hours. It is useful, however, to define a characteristic ratio of the protons to the heavier nuclei present in a particular event eg P/a = proton-alpha particle ratio. This characteristic ratio apparently varies from event to event. The P/a ratio may be from as high as 40 to as low as 1 in different events, and the P/CNO ratio may vary from 10^2 to 10^3. This ratio appears to be constant as a function of rigidity since both the alpha particles and heavier nuclei seem to also be best represented by an exponential rigidity spectrum. As far as total particle numbers are concerned, the heavier nuclei in solar flares are probably, on the average, relatively less abundant than the heavier nuclei in the galactic radiation.

Specific Features of Important Solar Cosmic Ray Events and Related Solar Flares

During the period 1956-1961 nearly 50 solar cosmic ray outbursts have been recorded at the earth by a wide variety of techniques. These events display

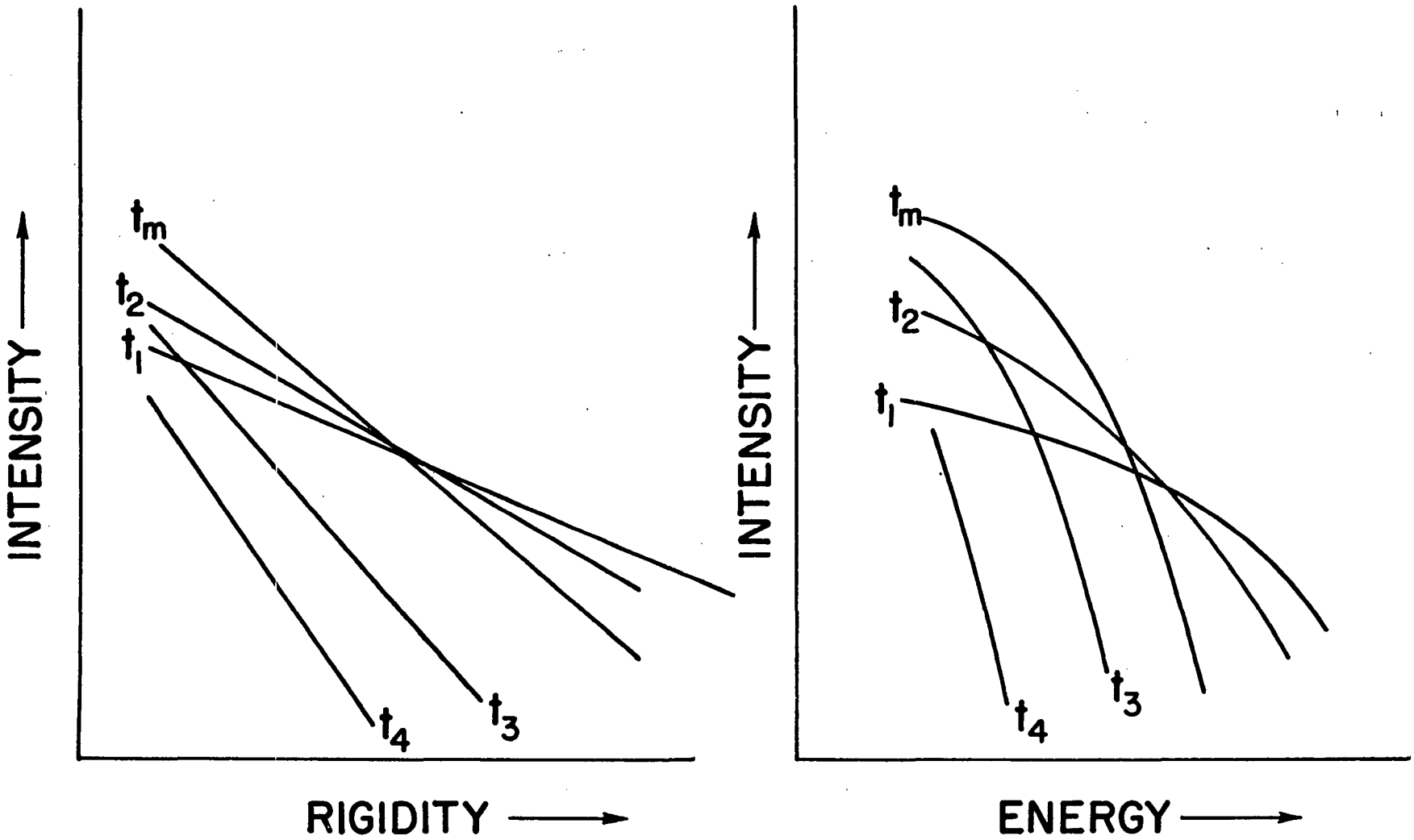

Figure 2 - Typical power law energy and exponential rigidity spectra obtained at different times (T_1 T_2 T_m T_3 T_4) during a single event.

an enormous variation (10^4 - 10^5) of integrated particle intensities for the duration of the outbursts. Of these events, approximately 30 of the largest - those with minimum integrated intensity of 10^{-6} particles/cm^2 at energies greater than 30 Mev observed at the earth - have been selected for discussion here. These events are comparable to the integrated intensity of galactic radiation for one week; the smaller events obviously do not contribute appreciably to the enhancement of the cosmic ray intensity near the earth. Prior to 1956 it was not possible to make a size estimate on any of the solar cosmic ray events; therefore, these events are not included, although undoubtedly many important ones occurred. The identification of a solar cosmic ray event by radiowave absorption (riometer) data alone is not regarded as sufficient to make a specific size estimate. In fact, size estimates based on the relative radiowave absorption may be grossly misleading, since the absorption may in many instances be produced by solar cosmic rays of much lower energy than the 30 Mev lower limit selected, or by auroral electron effects. (The chosen lower energy limit represents a penetration of about 1 gm/cm^2.)

Rough size estimates have been made when direct measurements of solar cosmic ray intensities at the top of the atmosphere or in space near the earth were available at one time during the event. Detailed estimates of intensity-time characteristics, spectral distribution, and size have been made only when a number of direct measurements of solar cosmic ray intensities and/or spectra exist at the top of the atmosphere or in space near the earth for a particular event.

By referring to Table I, we may elaborate more critically on some features of specific solar flares and related cosmic ray events. First we note that although 30 separate events are cataloged over the six-year period, they occur in only 16 different active centers. During the last three years (1959-1961) this tendency is even more pronounced, for 18 separate events have been associated with only 5 different active centers. The active centers associated with these flares were usually already well developed when they appeared at the east limb of the sun. Only once did the same active center continue to produce large cosmic ray events during its subsequent appearance on the visible hemisphere of the sun. From four of these active centers (McMath Plage Numbers 3400, 5269, 5925 and 6171) have come over 90 percent of all of the solar cosmic rays with energy >30 Mev observed at the earth in the last six years.

From Table 1, we note that, of the 30 events listed, 22 have been from flares in the sun's western hemisphere and 8 from the eastern. Of the 10 largest events, 6 have come from flares in the western hemisphere and 4 from flares in the eastern. Finally, from the 5 active regions that have produced 18 of the cosmic ray flares in the last three years, 11 of the flares have occurred while the active center was in the western hemisphere; and 7 in the eastern. Of these five active regions, the four major ones have been in the northern hemisphere and the remaining one in the southern.

From the above statistics we can say that for cosmic-ray-producing flares as a whole, there is a greater likelihood of observing cosmic rays at the earth when the flare is in the sun's western hemisphere. This situation suggests that on the average a greater fraction of the particles produced are received at the earth when the flare is nearest the west limb of the sun. A large,

Table I

Solar Flare and Cosmic Ray Data Relating to the Major Solar Cosmic Ray Outbursts Occurring During the Years 1956-1961

	Date	Solar Flare Data: Importance	Solar Flare Data: Heliographic Position (degrees)	Solar Flare Data: Time of Optical Maximum	Solar Flare Data: Maximum RF Emission*	Cosmic Ray Data: Onset and Rise Time (hours) >30 Mev	Onset and Rise Time (hours) >100 Mev	Decay Time (hours) >30 Mev	Decay Time (hours) >100 Mev	Peak Intensity** >30 Mev	Peak Intensity** >100 Mev	Characteristic Po (MV)	Integrated Intensity >30 Mev	Integrated Intensity >100 Mev	Integrated Skin dose*** >30 Mev	Integrated Skin dose*** >100 Mev
1956	Feb 23	3+	N22 W74	0340	20,000 at 0341	6-8	3-4	30	16	6,200	5,000	325	6.5×10^{8}	3.2×10^{8}	120	28
1956	Aug 31	3	N16 E16	1241		No detailed estimate possible							3×10^{7}		10	
1957	Jan 20	3+	S25 W30	1120						2,000-3,000	100-200		3×10^{8}	10^{7}	60	1.2
1957	Jul 03	3+	N14 W40	0740		No detailed estimate possible							1×10^{7}		3	
1957	Aug 29 to 31	(uncertain flare, possibly two events)								200-300	~10		5×10^{6}		15	
1957	Oct 20	3+	S26 W45	1642		No detailed estimate possible							1×10^{7}		3	
1958	Feb 09	2+	S12 W14	2142		No detailed estimate possible							5×10^{6}		1.5	
1958	Mar 23	3+	S14 E78	1005	10,000 at 1004			(40)	(20)	1200-1500	~50		2×10^{8}	5×10^{6}	50	0.7
1958	Jul 07	3+	N25 W08	0115	2,000 at 0112			32	16-20	1500-2000	~80		3×10^{8}	7×10^{6}	80	1.0
1958	Aug 16	3+	S14 W50	0440	6,200 at 0442	10		18		200			2×10^{7}		4	
1958	Aug 22	3	N18 W10	1448		10-12	3-4	20	8-12	500	20		5×10^{7}	1×10^{6}	20	0.15
1958	Aug 26	3	N20 W54	0027	6,700 at 0025	~9		(12)		1,100			5.3×10^{7}		17	

1959	May 10	3+	N23 E47	2118	~10,000	18-22	12-18	22	10-14	6,000-8,000	1,000	60	7×10^{8}	7.5×10^{7}	170	10
	Jul 10	3+	N22 E70	0222	15,000 at 0224	30-40	18-20	40	20	4,000	1,200	90	8.8×10^{8}	1.0×10^{8}	148	11
	Jul 14	3+	N16 E07	0349	6,300 at 0352	16-20	12-16	18	9-12	10,000-12,000	1,200	70	1.1×10^{9}	6.3×10^{7}	177	7.4
	Jul 16	3+	N08 W26	2145	6,500 at 2200	12-14	4-5	30	18	6,000-8,000	1,500	110	8.1×10^{8}	1.3×10^{8}	125	19
1960	Apr 01	3	N12 W10	0859		2-3	<1	12	4-6	50	6		2.7×10^{6}	1.5×10^{5}	0.6	0.001
	Apr 05	2+	N10 W61	0245	~8,000 at 0203			12		40			2×10^{6}		0.7	
	Apr 28	3	S05 E34	0130		8-10	3-4	18 24	8	300	20		2.5×10^{7}	7×10^{5}	6	0.08
	May 04	3+	N14 W90	1020		2-3	<1	8	4	200	40	300	7×10^{6}	7×10^{5}	16	0.07
	May 06		uncertain flare							50-100			5×10^{6}		1.5	
	Sep 03	3	N18 E88	0110	12,000 at 0108	12-16	7-9	32	26	240	60		4×10^{7}	7×10^{6}	4	0.6
	Nov 12	3+	N27 W02	1329	10,000 at 1329	12-16	8-10	18-24	14-18	12,000	2,500	145	1.4×10^{9}	3.5×10^{8}	205	33
	Nov 15	3+	N30 W32	0221	14,000 at 0227	10-16	3-5	16-20	8-12	6,000	2,400	135	5.2×10^{8}	1.2×10^{8}	100	12
	Nov 20	3	N28 W113	2020		3-4	~1	10-16	4-6	1,000	4,000		6×10^{7}	6×10^{6}	15	0.7
1961	Jul 11	3	S06 E32	1700	2,500	8-18	4	22-26	18	20	3		2×10^{6}	3×10^{3}	0.5	0.03
	Jul 12	3+	S07 E22	1030	7,500	8-12	6	16-20	12	120	15	50	1.0×10^{8}	1.6×10^{6}	10.5	.29
	Jul 18	3+	S06 W60	1010	5,000	6-10	2-3	24	12	2,500	600	135	2.1×10^{8}	4.8×10^{7}	27	3
	Jul 20	3+	S07 W90	(1600)	2,500	4-6	1.5	6-8	3	300	70		9×10^{6}	1.2×10^{5}	2.5	0.2
	Sep 28	3	N14 E30	2223								250	2.2×10^{5}	9.7×10^{4}	0.5	0.15

*Max Emission in range 3,000-10,000 Mc in units of 10^{-22} w/(m^2-cps)
**In units of particles/(cm^2/sec) or particles/cm^2 in free space (1m) x integrated intensities
***In units of rad (1 rad = 3.2×10^{7} (particles/cm^2) x average specific ionization in units of 1.6 Mev)

important cosmic-ray event is almost equally likely to arise from a flare in the western or eastern hemisphere. However, a distinct northern hemisphere preference is noted.

The correlation between the peak RF emission in the frequency range between 3,000 and 10,000 Mc/s during the flares, and the size of the cosmic ray event at the earth is sufficiently good that we can use the values of this peak RF emission to make fairly useful statements regarding the integrated size of the cosmic ray event. If the peak RF emission in this range exceeds $10{,}000 \times 10^{-22}$ w/m^2-cps, about 50 times normal, the integrated intensity of solar cosmic rays at energies above 30 Mev at the earth will generally exceed 10^8 particles/cm^2 (i.e., exceed the average yearly integrated intensity of galactic cosmic rays). If the peak RF emission in this range exceeds $3{,}000 \times 10^{-22}$ w/m^2-cps, the cosmic ray event will still be important and the integrated intensity of particles at energies greater than 30 Mev at the earth will usually exceed 10^7 particles/cm^2. If the peak emission in this range is less than 1,000 to 2,000 $\times 10^{-22}$ w/m^2-cps, the cosmic ray event is usually not a major one.

Turning now to the characteristic intensity-time profiles of the solar cosmic rays as observed in the earth's vicinity, we see that the average initial delay from the time of the peak optical (and radio) emission until the first arrival of the isotropic component of solar particles at the earth (for particle energies above 100 Mev) is about 1/2 hour for flares in the western hemisphere and about 1-1/2 hours in the eastern. The average rise times for the particles with energies $>$100 Mev are 2-3 hours and 6-8 hours for the western and eastern hemispheres respectively. The onset and rise times

for the isotropic component of particles with energies above 30 Mev are longer by a factor of 2 in each event, but otherwise show the same characteristics.

A detailed examination of the rise-time characteristics for particles with energies above 100 Mev during a number of events reveals that this increase in solar particle intensity may be closely approximated by

$$I = I_{Max}(E)\, e^{-t/t_R},$$

where t_R is the characteristic rise time and t is measured from the time of peak intensity $I_{Max}(E)$ back to the time of the flare. In view of our previous statements t_R will be a function of the energy of the particles and also of the position of the flare on the sun.

The decay of intensity of the solar flare particles near the earth, like the onset characteristics, appears to be related in some lesser degree to the position of the flare on the sun. Thus, the time scales of the decays will be related to the time scales of the onsets just discussed, although there is not a strict one-to-one correspondence between these features. A detailed examination of the decay characteristics of a number of events reveals that the decay may be closely approximated by

$$I = I_{Max}(E)e^{-t/t_D},$$

where t_D is the characteristic decay time which depends on the energy and probably to some extent also on the flare's location; and t is measured from the time of the peak intensity $I_{Max}(E)$ to later times in the event. For particle energies greater than 100 Mev, t_D ranges from 10 to 20 hours in 15 of the 18 events in which it was possible to determine a characteristic decay time. There is some tendency for the longest characteristic decays to be associated with flares near the sun's east limb; and the three shortest decays, with

characteristic times less than 10 hours, are all associated with flares occurring near the west limb (and in active centers which had previously produced cosmic rays). Consequently, there is the aforementioned relation between t_R and t_D. The average for the 18 events, considering particle energies greater than 100 Mev, is $t_D/t_R = 4$ with extremes from 1.5 to 6. The characteristic decay times for particles with energies exceeding 30 Mev are about twice as long as for particles with energies exceeding 100 Mev. A similar ratio for t_D/t_R also exists for the lower energy particles, since t_R for the latter is also twice t_R for particles with energies greater than 100 Mev.

The utilization of the characteristically similar intensity-time behavior for events having widely differing peak intensities and occurring at different locations on the sun permits a fairly simple estimate of the total integrated intensities of particles with energies greater than 30 Mev and those with energies greater than 100 Mev in space near the earth. Thus for J, the total integrated intensity in an event, we have

$$J\ (>E) = \int_{-\infty}^{0} I_{Max}\ (>E)\ e^{-t/t_R}\ dt + \int_{0}^{\infty} I_{Max}\ (>E)\ e^{-t/t_D}\ dt$$

$$= (t_R + t_D)\ I_{Max}\ (>E),$$

The appropriate $J_{Max}(>E)$ is determined from the measured spectra in each event and a study of the variation of Jo and the characteristic rigidity Po with time during the event.. This data may be found in reference 4. We should point out that the $I_{Max}(>E)$ derived here are considerably lower than previous estimates, particularly at the lower energies. This is due to a number of

reasons - the main ones being - (1) the adaption of the exponential rigidity spectrum for the solar particles (2) the use of ionospheric parameters that predict a larger radiowave absorption for a given solar particle intensity - or conversely a lower solar particle intensity for a given (measured) radiowave absorption (reference 7) (3) the modification of the solar particle spectra deduced from balloon ascent measurements.

The total skin or free-space doses evaluated for each event depend only on the total integrated particle intensity/cm^2 and the average specific ionization (relative to the minimum ionization) of each particle. Meanwhile, the average specific ionization per particle depends on the characteristic rigidity describing the spectrum of the radiation. As we have noted, this characteristic rigidity varies over the course of a single event, being largest at earlier times and smallest at later times. However, an average value over the course of an event has been deduced and we use this value to obtain the average specific ionization per particle of the radiation. For I_{Max}(>30Mev), this specific ionization ranges from about 8 times minimum for characteristic rigidity $\sim$ 50 MV to about 3 times minimum for characteristic rigidity $\sim$ 300 MV, assuming the incident radiation to be composed of protons only. For I_{Max} (>100 Mev) these values are $\sim$ 4 times minimum and 2 times minimum respectively. (The minimum ionization is 1.6 Mev/gm-cm^2 in air or 2.6 x 10^{-6}erg/gm-cm^2. Since one roentgen equals 83.7 ergs/gm of air, an integrated intensity of 3.2 x 10^7 particles/$cm^2$of minimum ionization produces a dose of one roentgen.)

The total skin or free space doses evaluated for each event are presented in Table I along the peak particle intensities >30 Mev and 100 Mev and the total integrated particle intensities over the entire event above these energies.

Summary of Solar Cosmic Ray Events in Relation to Dose Rates Obtained in Space

The main objective of this summary of solar cosmic ray events is, of course, to attempt an evaluation in general terms of the radiation hazard in space presented by these events. It seems reasonable to evaluate the hazard in terms of the integrated dose of galactic radiation, for this radiation forms an almost constant background in space - and one so penetrating that reasonable shielding considerations have little effect on the intensity of the radiation. The free-space galactic particle intensity varies from 1.5 particles/cm^2-sec near sunspot maximum to about 4 particles/cm^2-sec near sunspot minimum. The integrated weekly rates are thus roughly 1×10^6 and 2.5×10^6 particles/cm^2 respectively; the yearly rates range from 5×10^7 to 1.2×10^8 particles/cm^2. (Assuming an average specific ionization about 3 times minimum for these galactic particles, the integrated weekly dose ranges from 0.1 to 0.25 rad and yearly dose from 5 to 12 rad.)

In Table 2 the yearly integrated intensities of solar particles above 30 and 100 Mev are compared with the total integrated intensity of galactic particles for the years 1956-1961. Over this six-year period the integrated intensity of solar cosmic rays with energies greater than 100 Mev and greater than 30 Mev are respectively, about 2.5 and about 15 times the total integrated galactic intensity. Most of the solar cosmic ray intensity occurs during the three particular years 1956, 1959, and 1960. In fact, most of the solar cosmic ray intensity comes from the solar events associated with only three active centers; McMath Plage 3400 for the February, 1956 event; 5269 for July, 1959; and 5925 for November, 1960. The remaining events during this six year period contribute only 0.2 and 2 times the integrated galactic cosmic ray intensity above 100 Mev

Table 2

Yearly Integrated Intensities of Solar Cosmic Rays with Energies Above 30 and 100 Mev and of Galactic Cosmic Rays

Year	Number of Events	Solar Cosmic Rays Integrated Intensity (particles/cm^2)		Galactic Cosmic Rays Integrated Intensity (particles/cm^2)
		30 Mev	100 Mev	
1956	2	7×10^8	3.2×10^8	1×10^8
1957	4 or 5	4×10^8	1.0×10^7	7×10^7
1958	6	7×10^8	1.0×10^7	6×10^7
1959	4	3.6×10^9	3.4×10^8	6×10^7
1960	8	2×10^9	5.0×10^8	8×10^7
1961	5	3.2×10^8	6.0×10^7	1×10^8
TOTAL	30	7.2×10^9	1.2×10^9	4.7×10^8

and 30 Mev respectively. A study of the smaller events not individually listed here reveals that, even if the frequency of these events is 20 to 30 a year, the integrated yearly intensity of solar cosmic rays with energies greater than 30 Mev from these events is not likely to exceed that from galactic cosmic rays. Thus we can state that during a time scale of one year - neglecting the three largest events - the integrated intensities of solar cosmic rays with energies above 30 Mev and of galactic cosmic rays are comparable; and with a reasonable minimum shielding of only 2 to 3 gm/cm^2 the yearly average dose from solar cosmic rays is less than that from galactic cosmic rays (i.e., less than 12 rad).

Thus, the problem of radiation exposure from solar cosmic ray outbursts would reduce to the problem of such exposure from the few largest events. The total integrated dose from these events may present a problem, the seriousness of which depends on the amount of shielding - as can be seen from the doses due to particles with energies above 30 and 100 Mev (Table 1). The two largest sequence of events, those of July 1959 or November 1960 produced integrated skin doses from particles with energy >30 Mev of ~ 450 rad and 300 rad respectively. Such would be the doses under slightly more than 1 g/cm^2 of shielding. For 10 g/cm^2 shielding corresponding to particles 100 Mev the doses would have been ~ 40 rad and 45 rad respectively for these "most dangerous" events.

The statistics relating to the frequency of occurrence of the largest events are, of course, very limited - 6 events in 6 years, or an average of one event every year producing a dose >100 rad (or 3 events producing a dose >200 rad) during six years from particles >30 Mev. Only one of these events would have been observable by the techniques used prior to 1950, when four events were recorded in about 10 years of observation. If we assume then that the techniques in operation during this period could detect one out of three events of truly major importance, about 12 such events may have occurred during the 10 year period. These considerations are undoubtedly crude but they are the best available at present. Combined with the recent, more definitive data, they suggest that on the average of once every year an active region appears that will ultimately emit one or more major cosmic ray bursts. Although dozens of smaller events may occur during such a period, they are relatively unimportant in consideration of the overall integrated solar cosmic ray intensity.

It is quite certain that the appearance of active regions producing major cosmic ray bursts is not strongly correlated with the maximum in the eleven-year cycle of solar activity. During the recent maximum, 1957-58, no such major cosmic ray bursts were recorded, and the yearly integrated solar cosmic ray intensities at energies greater than 30 and 100 Mev were lower than for adjacent years of lower solar activity. From the limited number of large events available for study it appears that they are most frequent during periods of increasing and, particularly, decreasing solar activity, with the periods near maximum and minimum relatively free from such events. In other words, in periods of increasing or decreasing solar activity the frequency of potentially dangerous cosmic ray outbursts may be greater than one per year and, in periods near maximum or minimum, less than one per year.

REFERENCES

1. Forbush, S. E., "Three Unusual Cosmic-Ray Increases Possibly Due to Charged Particles from the Sun," Phys. Rev. 70(9 and 10):771-772, November 1 and 15, 1946.

2. Adams, N., "A Temporary Increase in the Neutron Component of Cosmic Rays," Phil. Mag. 41:503-505, May 1950.

3. Webber, W. R., "Time Variations of Low Energy Cosmic Rays during the Recent Solar Cycle," in: Progress in Elementary Particle and Cosmic Ray Physics, ed. by J. G. Wilson and S. A. Wouthuysen, Amsterdam: North-Holland Publ. Co., Vol. 6, 1962 (In Press).

4. Freier, P. S. and Webber, W. R., "Exponential Rigidity Spectra for Solar Flare Cosmic Rays," J. Geophys. Res. (in press).

5. Fichtel, C. E. and Guss, D. E., "Heavy Nuclei in Solar Cosmic Rays," Phys. Rev. Letters 6 (9):495-497, May 1, 1961.

6. Biswas, S., Freier, P. S., and Stein, W., "Solar Protons and α Particles from the September 3, 1960 Flares," J. Geophys. Res. 67(1):13-24, January 1962.

7. Webber, W. R. "The Production of Free Electrons in the Ionospheric D Layer by Solar and Galactic Cosmic Rays and the Resultant Absorption of Radio Waves," J. Geophys. Res. 67(12):3991-4006, 1962.

Paper A-3

COMPOSITION OF SOLAR COSMIC RAYS

C. E. Fichtel
Goddard Space Flight Center
Greenbelt, Maryland

Introduction

Having Dr. Webber's previous paper as an excellent summary of the general properties of solar cosmic rays, this report can begin at once with the treatment of one particular aspect of these solar particles, namely their composition.

The energetic solar particles arriving at the earth after some major disturbances on the sun are known to consist primarily of hydrogen nuclei. There are, however, smaller quantities of other nuclei which appear to be present in every event, since every time an observation has been made in the appropriate energy range they have been seen when the general intensity of the event was sufficiently high to expect to be able to detect them on the basis of their abundances in other events. In addition, there is also some relatively limited knowledge on electrons and γ radiation. Within the scope of the present incomplete knowledge, then, the relative abundances of these less plentiful components, namely helium nuclei, heavier nuclei, electrons, and γ-rays, will be given.

Helium Nuclei

Beginning with helium, the second most abundanent nuclear species, it is realized at once that care must be taken in how the helium to proton ratio is defined. Firstly, since these two nuclear species have different charge to mass ratios, they will not have the same rigidity[1] if they have

[1]Rigidity, R, is defined by the equation $\frac{cP}{Z}$, where c is the velocity of light, P is the total momentum, and z is the charge in units of the proton charge.

the same velocity. For example, a helium nucleus with a total kinetic energy of 200 MeV. has the same energy per nucleon as a proton of 50 MeV., but the same rigidity as a proton of 187 MeV. Further, an examination of the particle spectra as a function of energy per nucleon, rigidity, or possibly other variables must be made to determine whether or not they have the same or different spectra.

Because protons and helium nuclei that are in the same energy per nucleon interval, or equivalently the same velocity interval, also are in the same particle range interval, it seems worthwhile to look at the energy per nucleon spectra first since for shielding purposes range is the most significant parameter. In general, the helium nuclei spectrum has a steeper slope than that of the protons. This feature has been seen on several occasions [2,3,4], every time a measurement was possible. Typical examples[3] are shown in figs. 1 and 2. On the other hand when the spectra are plotted in terms of rigidity, R, they are always found to be similar.[2,3,4,5] A typical example of similar rigidity spectra[3] is shown in figure 3. Webber and Freier[5] have shown that proton spectra can be represented very

---

[2]S. Biswas, P. S. Freier, and W. Stein, J. of Geophys. Research 67, 13 (1962)

[3]S. Biswas, C. E. Fichtel, and D. E. Guss, "A Study of Hydrogen, Helium, and Heavy Nuclei in the November 12, 1960 Solar Cosmic Ray Event", to be published in the Physical Review.

[4]S. Biswas, C. E. Fichtel, D. E. Guss, and C. J. Waddington, private communication.

[5]Drs. Biswas, Freier, Ney, and Stein have made many measurements which are summarized in P. S. Freier and W. R. Webber, "Exponential Rigidity Spectra for Solar Flare Cosmic Rays", submitted to J. of Geophys. Research

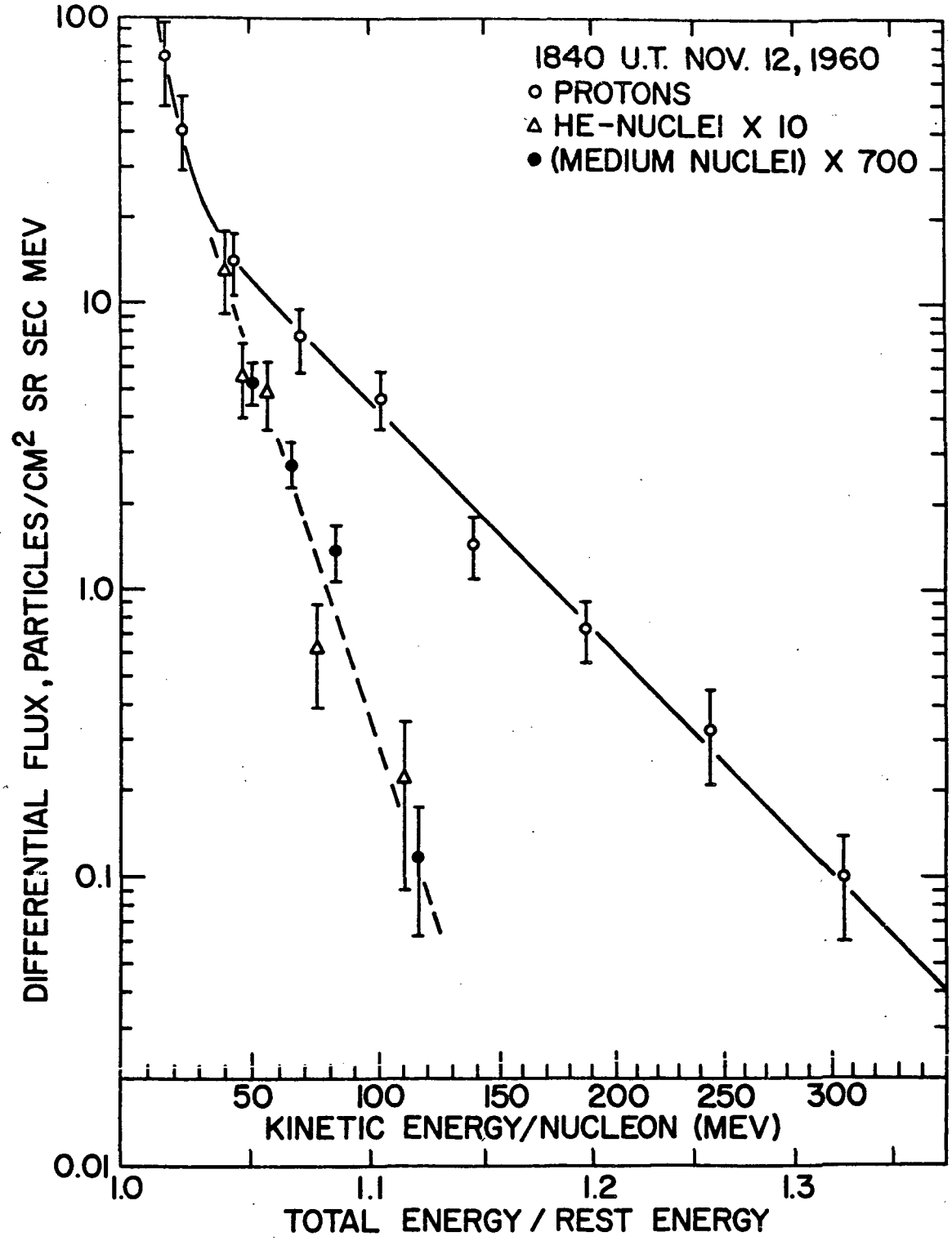

FIG. 1: Energy spectra for solar particles at 1840 U.T., NOV. 12, 1960.[3]

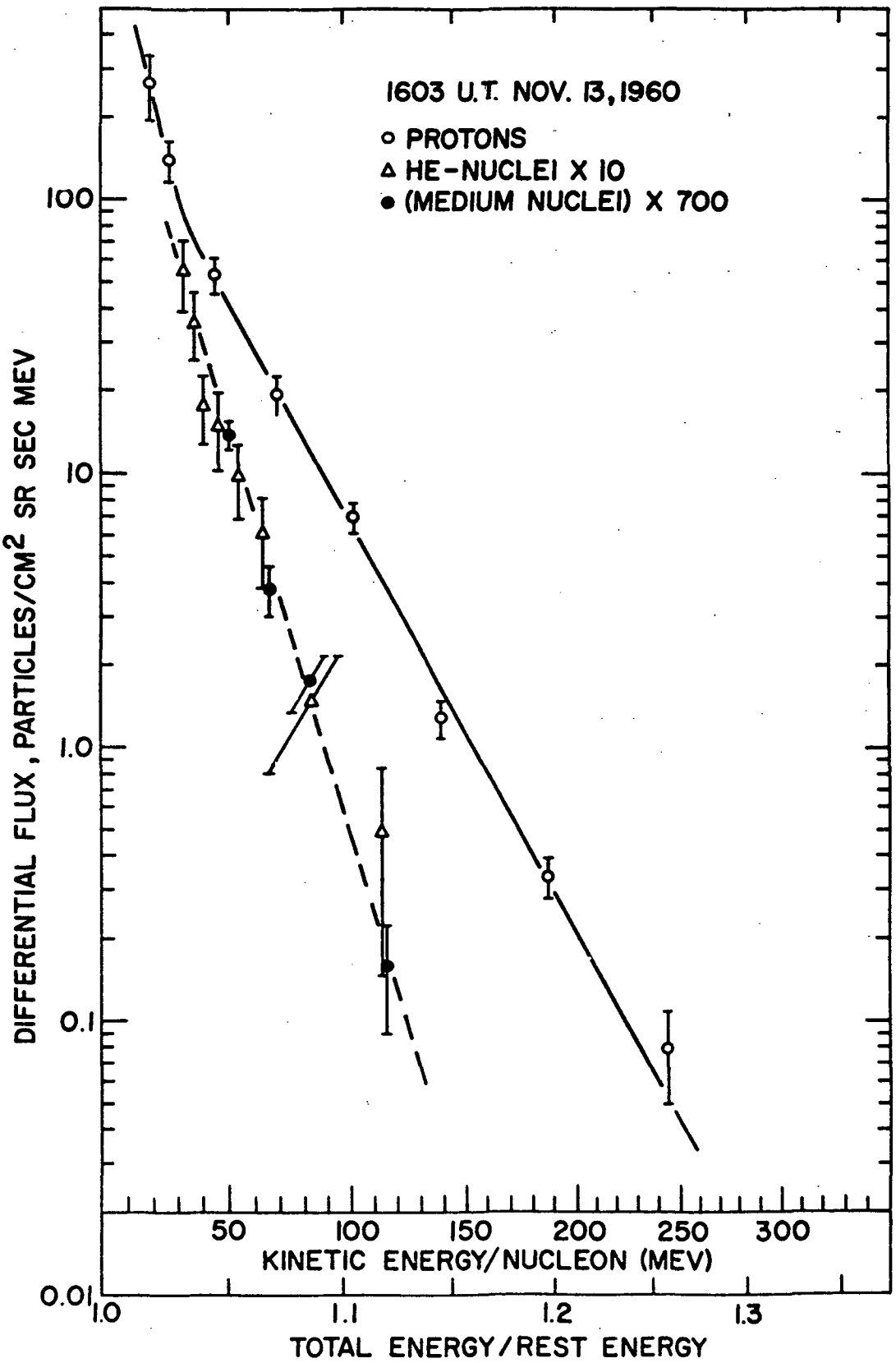

FIG. 2: ENERGY SPECTRA FOR SOLAR PARTICLES AT 1603 U.T., NOV. 12, 1960.[3]

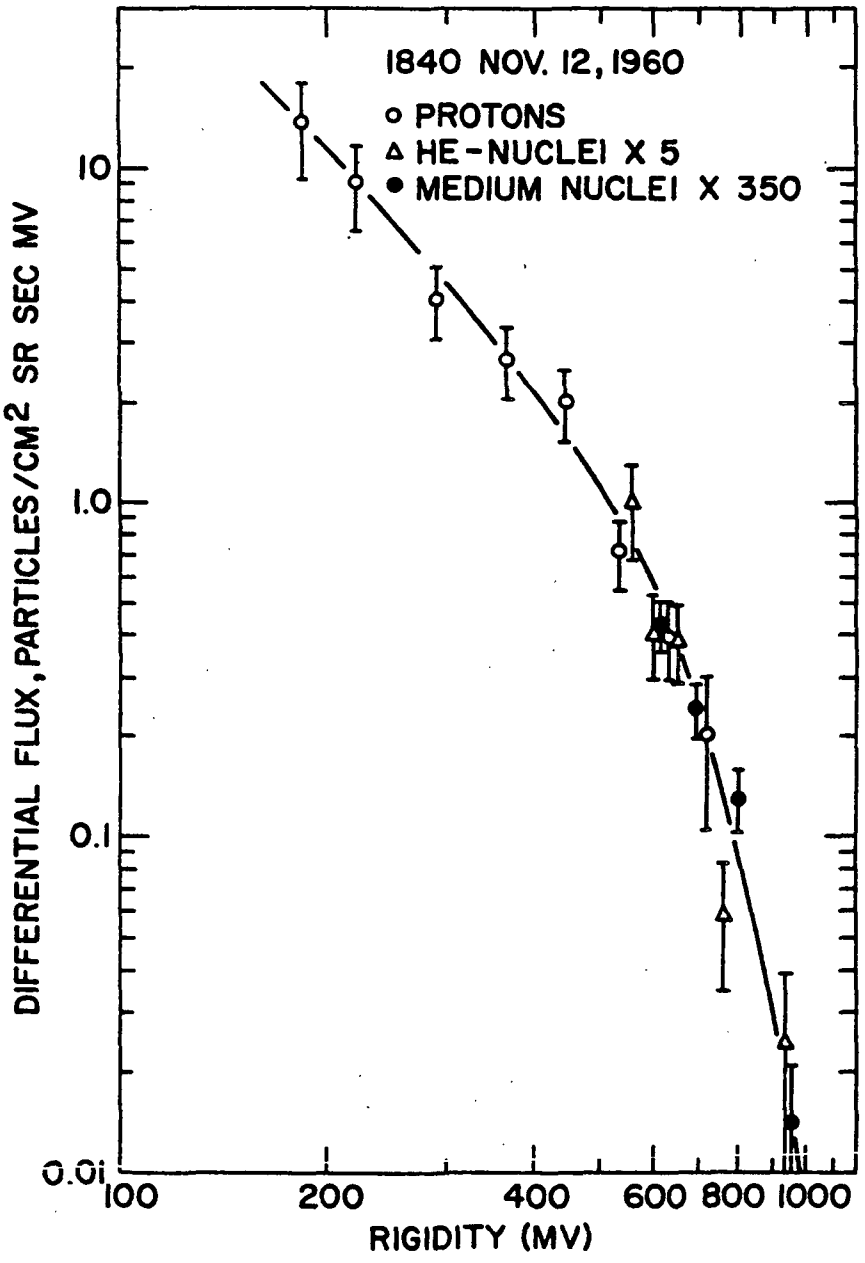

FIG. 3: RIGIDITY SPECTRA FOR SOLAR PARTICLES AT 1840 U.T., NOV. 12, 1960.[3]

well in general by an expression of the form

$$dJ/dR = J_o \exp(-R/R_o) \qquad (1)$$

where dJ/dR is the differential rigidity flux and J_o and R_o are constants. Further, since the helium nuclei have the same shape this expansion will also represent the helium nuclei with the same R_o, but a different J_o.

When proton to helium ratios are compared, however, it is found that, although the helium and hydrogen nuclei seem to have the same rigidity spectrum, the ratio of the two components in the same rigidity interval varies greatly from one event to another and at different times in one event. For example, at approximately MV rigidity, the proton to helium ratio has varied from $\geq$ 50:1 to 1:1. A list of some of the ratios that have been observed by Biswas, Freier, Ney, Stein[2,5], Fichtel, Guss[3], and Waddington[4] is given in Table I. A more complete list can be found in the indicated references. It should perhaps be noted that not all of the data in Table I correspond to the same rigidity interval; however, since the rigidity spectra are the same, it seems justified to compare all of the ratios listed, especially since the rigidity intervals are not very different.

On the other hand, there is now some evidence to indicate that for a given velocity interval the proton to helium ratio is similar in each event, although not exactly the same. In this case, however, the interval must be specified since the ratio of the hydrogen to helium nuclei varies with energy per nucleon. The proton to helium ratio is typically bound

to vary from about twenty at 40 MeV./nucleon to a few hundred at 120 MeV./nucleon. These ratios are not exactly the same from one event to another or even with time in an event, but the limited data available does seem to indicate that they are typical.

Heavy Nuclei

Turning now to the heavy nuclei, that is those with a nuclear charge greater than three, present evidence indicates that the energy per nucleon spectra of the various multiply charged nuclei are the same[3,4]. Further, since all of the multiply charged nuclei of interest have essentially the same charge to mass ratio, if their energy per nucleon spectra are the same their rigidity spectra will be also. These features are shown for typical cases in figures 1, 2, and 3. The relative abundances among the heavy nuclei taken in the same energy per nucleon intervals have been found to be the same each time a measurement was made, namely five times in two events. The helium to medium nuclei ($6 \leq Z \leq 9$) ratio has been measured in three events and found to be the same each time within uncertainties[3,4]. The composition for the same energy per nucleon intervals is given in table II below with a base of ten having been chosen for oxygen. It is seen that the medium nuclei are the most abundant among the heavy group and are about one-sixtieth as abundant as helium. Notice also in table II that the abundances are similar to those in the sun and different from those of galactic cosmic rays.

Although the heavy nuclei are easily stopped because they are of very low energy and high charge, they should perhaps not be completely ignored

TABLE I

PROTON TO HELIUM RATIOS IN THE SAME RIGIDITY INTERVALS

~ 1200 U.T., July 11, 1959[5]	1.4 ± 0.2
~ 1800 U.T., July 12, 1959[5]	5.0 ± 0.8
~ 2130 U.T., May 5, 1960[5]	≥ 50
~ 1400 U.T., Sept. 3, 1960[2]	31
~ 2000 U.T., Sept. 4, 1960[2]	19
1840 U.T., Nov. 12, 1960[3]	5 ± 1
1603 U.T., Nov. 13, 1960[3]	1 ± 0.2
1951 U.T., Nov. 16, 1960[4]	1.7 ± 0.5
0339 U.T., Nov. 18, 1960[4]	1.7 ± 0.5
~ 1630 U.T., July 18, 1961[5]	6 ± 1

TABLE II

RELATIVE ABUNDANCES WITH A BASE OF 10 FOR OXYGEN

Nuclei	He	Li,Be,B	C	N	O	F	Ne	$11 \leq Z \leq 18$
Solar Cosmic Rays*	1100	< 0.2	6	$\lesssim 2$	10	< 0.3	1.5	1.3
Sun +	?	< 0.01	6	1	10	< 0.01	?	1
Galactic Cosmic Rays*	360	11	18	$\lesssim 8$	10	$\lesssim 1$	3	9

*The uncertainty in the values in this line varies from 10% to about 30%

+The uncertainty in the values in this line is of the order of a factor of 1.5 to 2.

if relatively thin shields will be used. For example, the flux of medium nuclei that would penetrate 2 gm/cm^2 of aluminum was nearly 10^2 particles/(m^2.sr.sec.) for more than a day in the Nov. 12, 1960 event, and all of them would be of the low energy, or "ending", variety.

At a few times for periods of the order of ten to twenty minutes, Kurnosova et al[8] have seen increases in the counting rate of the higher dE/dx channels of their Cirenkov detectors flown on satellites which they interpret as short term increases of relativistic heavy nuclei associated with solar disturbances. These increases, however, represent an integral particle flux which is quite small compared to the daily average of relativistic heavy nuclei in the same charge region, and, therefore, they do not need to be considered as an additional hazard.

Electrons

We come now to the next component, electrons. The abundance of very energetic electrons is expected to be small due to the high rate of energy loss by synchtrotron radiation at large relativistic energies; so, even if there were large numbers of these energetic electrons initially, they would soon lose their energy.

Although the flux of very energetic solar electrons is known to be relatively small, appreciably less than the proton component, positive

---

[8] Kurnosova, L. V., L. A. Razorenov, and M. I. Fradkin, "Short-Term Increases of the Cosmic Ray Intensity Associated with the Solar Activity", Journal of the Physical Society of Japan 17, Supplement A-II, 315 (1962); Iskusstvennye Sputnik: Zeml: No. 6, 132 (1961); Iskusstvennye Sputnik: Zeml: No. 12, 31 (1962)

evidence for electrons does exist for at least one event.[7] In this case, the flux of electrons greater than 100 MeV. was only 0.04 el./ (cm^2 sr sec), or a few percent of the proton flux in the same kinetic energy region.

Relatively large fluxes of low energy electrons, kinetic energy < 1 MeV., have also been seen on occasions. Hoffman et al[8] saw 3×10^6 el/ (cm^2 sr sec) between 10 and 35 KeV. for about ten minutes on Sept. 30, 1961, associated approximately with the arrival of the sudden commencement. Except for that period the flux was less than the detectable limit of 2×10^5 el/(cm^2 sr sec).

γ-Rays

At the present time, the information on high energy electromagnetic radiation is very limited. There have been at least two events observed in which the energy flux was estimated to be of the order of 10^7 ev/ (cm^2 sec) for less than five minutes, with the average kinetic energy in the range of 20 to 500 KeV.[9,10] Several other events with a smaller total

---

[7] P. Meyer and R. Vogt, Phys. Rev. Letters 8, 387 (1962)

[8] R. A. Hoffman, L. R. Davis, and J. M. Williamson, "0.1 to 5 MeV. Protons and 20 KeV. Electrons at 12 Earth Radii during Sudden Commencement on 30 September 1961," submitted to the J. of Geophys. Research.

[9] L. E. Peterson and J. R. Winckler, J. of Geophys. Research 64, 697 (1959)

[10] J. R. Winckler, T. C. May, and A. J. Mosley, J. of Geophys. Research, 66, 316 (1961)

energy flux above 20 KeV have also been observed.[11,12] All of the events seem to be of short duration, although in some cases the period of observation was not long enough to permit a determination of the length of the event. The shape of the energy spectrum seems to vary appreciably from one event to the next. There have also been several negative results, that is cases where γ-rays were not detected although a rather large flare was seen on the sun.

[11]K. A. Anderson and J. R. Winckler, J. of Geophys. Research 67, 4103 (1962)

[12]T. A. Chubb, H. Friedman, and R. W. Kreplin, J. of Geophys. Research 65, 1831 (1960)

Paper A-4

DETAILS OF INDIVIDUAL SOLAR PARTICLE EVENTS*

by
Carl E. Fichtel, Donald E. Guss, and K. W. Ogilvie

INTRODUCTION

This paper attempts to present a time history of the intensities and energies of solar cosmic ray particles detected at or near the earth. Ideally it would be desirable to show the complete energy spectrum of the proton component in these events as a function of time. Upon consideration of the incomplete information and uncertainties involved in the measurements, however, we see that this can only be done approximately. Regions of time and energy which have not been adequately surveyed can be described only by interpolation and, to some extent, by extrapolation. The goal is to remain within a factor of 2 of the real intensity at all times. Frequently the accuracy attained is very much better.

This survey begins with the event on February 23, 1956 – the first one for which there is an estimate of both the low and high energy flux components. All of the largest events from that date to the present and some of the smaller ones for which particularly complete data are available have been selected for examination. All events for which there was a riometer reading in excess of 10 db (indicating a particle flux greater than about 600 particles/cm^2-ster-sec for particles with energies above 20 Mev) have been included. Also any event with a high energy component sufficiently large to be detected on the neutron monitor has been studied. Events for which less than 10 db of absorption was detected on the riometer and no detectable neutron monitor increase was observed have, in general, been included only if there were other data from detectors flown on balloons and satellites.

The description of the various detectors used to study the solar particles will be followed by a discussion of the individual events in order to emphasize the interesting features and the variety of geophysical effects occurring from time to time. The descriptions will be followed by diagrams giving the integral flux as a function of time above specified energies and energy spectra at various times during the event. Finally, an imaginary event will be presented which is just large enough to include all the types of events observed.

* Reprinted from Goddard Space Flight Center External Document Number X-611-62-122

DETECTORS

The Riometer

The riometer measures the signal strength of extraterrestrial radio noise (References 15 and 16). During solar particle events the bombardment of the earth by energetic charged particles increases the electron density in the upper atmosphere causing absorption of the extraterrestrial noise and a consequent decrease in the signal measured at the ground (Reference 17). The particles primarily responsible for this absorption are protons in the 20-200 Mev kinetic energy range. Owing to the earth's magnetic field these particles can enter only at high latitudes; hence, this phenomenon is termed polar cap absorption (PCA). Thus at high latitudes, a riometer permits continuous monitoring of the intensity of protons in this energy range.

Magneto-ionic theory shows that, if the riometer observation frequency, ω, is much greater than both the critical frequency of the ionosphere and the longitudinal component of the magnetic gyrofrequency, the absorption for a vertically incident plane wave is found by integrating the following equation over the height of the ionosphere:

$$A = 0.46 \int \frac{N\nu}{\nu^2 + \omega^2} \, dh \, , \tag{2-1}$$

where A is the absorption in decibels, N the electron density, ν the electron collision frequency, and h the altitude in centimeters. The electron density at any height is related to the electron production rate q by the equation

$$N = q^{1/2} \left[(1 + \lambda) \alpha_e \right]^{-1/2} \, , \tag{2-2}$$

where α_e is the effective recombination rate for electrons and λ is the negative-ion to electron ratio. By substitution of Equation 2-2 into Equation 2-1, we then get the following equation.

$$A = 0.46 \int q^{1/2} \left[\nu \left(\nu^2 - \omega^2 \right)^{-1} (1 + \lambda)^{-1/2} \alpha_e^{-1/2} \right] dh \, . \tag{2-3}$$

During a PCA event, the electron production rate at any altitude is directly proportional to the total rate of energy loss by ionization of solar protons at that altitude. Equation 2-3, then, is a relation between the absorption measured by a riometer and the intensity and energy spectrum of the particles causing the PCA. For spectra of the same shape Equation 2-3 also predicts that the absorption in decibels is directly proportional to the square root of the particle intensity, provided the quantity in the brackets is independent of q.

During the daytime this is indeed the case to a high degree of accuracy, but there is a somewhat important dependence of λ on q during times of darkness.

Because of the photo-detachment effect of sunlight on the ionosphere, the absorption during a PCA is much stronger during the day than at night. A calculation by Reid (Reference 18), based on currently accepted values for the atmospheric parameters, yields a value of about 3 for the ratio of day to night absorption at an observing frequency of 30 Mc for a particular spectrum shape. Observations indicate that the average ratio is about 4, but that it can vary considerably and is sometimes as large as 10 or 12. The riometer provides its most useful information during the daylight hours and conversion of nighttime absorption readings to effective daytime absorption readings must be approached with some caution.

By the nature of its response, the riometer absorption is a function of geomagnetic latitude. However, the riometer records from College, Alaska; Churchill, Canada; and Thule, Greenland, generally show approximately the same absorption, though the cutoff energies for protons calculated by Quenby and Webber (Reference 19) are 113, 6.4, and approximately 0 Mev., respectively. Here it was assumed that the absorption from these stations was equivalent, and absorption values from stations other than Churchill were used when needed.

In order to calculate the expected absorption during a PCA the particle spectrum, intensity, and directionality must be known. The radiation causing the PCA is generally assumed to be isotropic over the upper hemisphere; and this is a good approximation a few hours after the flare causing the event. The electron production rate must be determined from the spectrum shape and intensity, and Equation 3 integrated. This has been done by a number of authors (References 17, 18, and 20) for specific times in specific events where some spectral details have been determined experimentally.

To find the spectral shape and intensities of solar particles from the observed absorption is a more ambiguous process, and several assumptions must be made. A calculation by Brown and Weir (Reference 20) shows that for protons with energies greater than 100 Mev, the predicted absorption is very insensitive to the shape of the energy spectrum and depends primarily upon the particle intensity. A similar calculation by Bailey (Reference 17) indicates that the same is true for particles in the energy range between 20 and 100 Mev. For protons with energies at the top of the atmosphere less than about 20 Mev the effectiveness for producing absorption is a rapidly decreasing function of energy, because protons of these energies ionize primarily at altitudes where the electron collision frequency is small.

From a series of rocket shots during PCA's in the fall of 1960 the energy spectra and intensities of protons were obtained down to energies below 20 Mev for a variety of riometer absorption intensities (References 21 and 22). The results indicated that for these events, the shape of the energy spectrum does not remain constant to very low energies. If the shape

of the energy spectrum is expressed by means of a power law

$$dN(E) = CE^{-\gamma}dE \,, \qquad (2\text{-}4)$$

then the exponent γ is a decreasing function of energy. Because of this and the fact that protons with energies below 20 Mev are less effective in producing absorption, it was assumed that the absorption at the times of the rocket shots was determined by the intensity of particles with energies greater than 20 Mev. The proton intensity at energies greater than 20 Mev is plotted against the observed absorption on the 30 Mc riometer at Churchill in Figure 2-1. This curve was subsequently used to obtain the PCA-determined particle intensities for the other events studied here. The extremum lines shown in Figure 2-1 indicate the uncertainty in the riometer readings alone and do not reflect the uncertainty in the resulting particle intensities, which is estimated to be about a factor of 2.

The shape of the energy spectrum for most solar particle events shows that the primary contribution to the absorption is from protons in the energy range below 100 Mev, since the

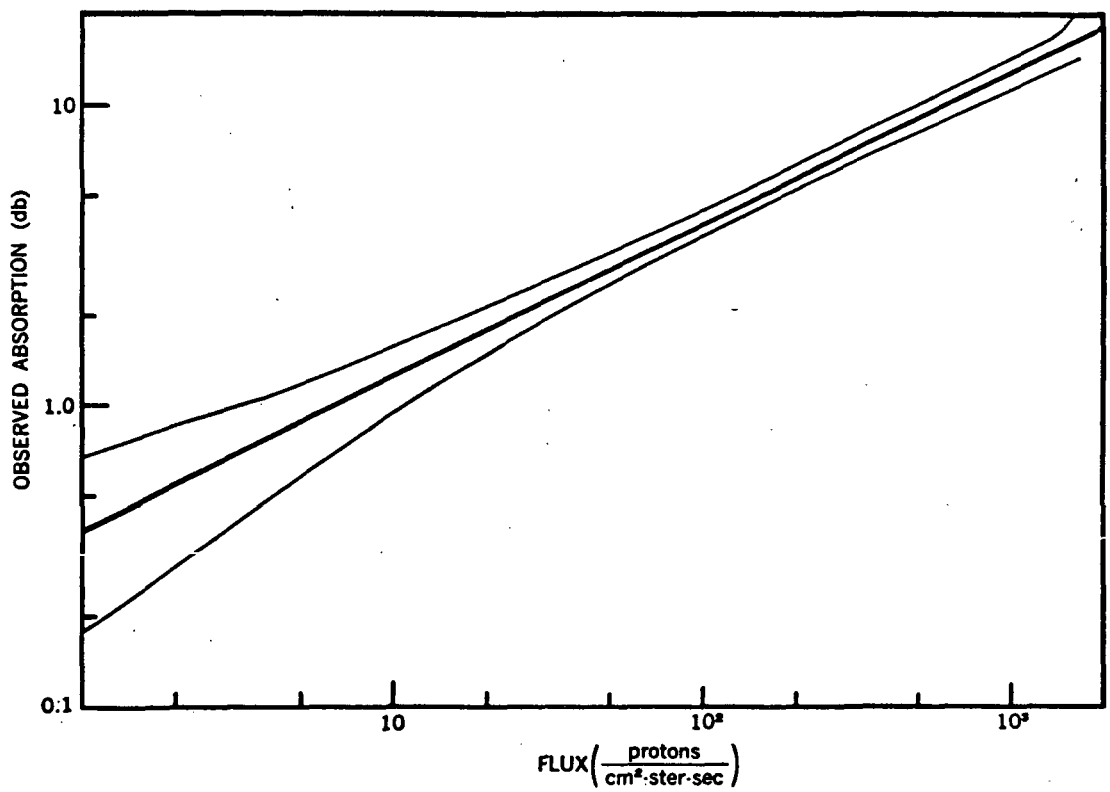

Figure 2-1—Proton flux versus riometer absorption

particle intensity above this energy is negligible by comparison, except for times early in the events. If the energy spectrum at higher energies is known, a knowledge of the absorption data makes it possible to show something of the nature of the spectrum as well as the intensity below 100 Mev. For example, the proton flux was measured during the daylight hours of July 13, 1961 by nuclear emulsions on a balloon flight at Churchill. The intensity with energies above 78 Mev was 1.6 P/cm^2-ster-sec, and between 78 and 230 Mev $\gamma = 5.5 \pm 0.3$. Extrapolating this spectrum back to 20 Mev would result in an intensity $7.9 \times 10^{+2} P/cm^2$-ster-sec which, from Figure 3, corresponds to an absorption of 11 db. However, the observed absorption on the 30 Mc polar riometer at Churchill was equal to or greater than 15 db during the entire flight, while that on the 27.6 Mc riometer at College varied from 14.5 to 17.5 db. This indicates that the shape of the spectrum did not change appreciably down to energies below 20 Mev. It must be noted that, although particles below 20 Mev become increasingly less effective at producing absorption, there would be 16 times as many particles between 20 and 10 Mev as there are above 20 Mev if γ did not decrease with energy.

The interpretation of riometer absorption in terms of particle intensities is complicated by two other problems: the superposition of auroral absorption upon the PCA; and the occurence of anomalous but real changes in absorption.

At stations within the auroral zone riometers show auroral absorption as well as the PCA. College lies near the maximum of the auroral absorption zone, and Churchill at the northern edge. Usually the auroral absorption can be at least partially eliminated since it appears as absorption spikes superposed upon the generally smoothly varying PCA. Leinbach and Reid (Reference 23) suggested that the PCA is best represented by the minimum absorption recorded over a period of several hours when auroral absorption is present.

During a number of PCA events anomalous decreases of absorption have been observed immediately following a sudden commencement. These have been discussed by J. Ortner, et al. (Reference 24). Leinbach (Reference 25) has also noted the occurrence, on some occasions, of *mid-day recoveries* at College, and on at least one occasion this phenomenon was observed at Churchill. These seem best attributed to local changes in the geomagnetic cutoff or local changes of the characteristics of the absorption layer rather than to a change in the intensity of the particles causing the event.

Increases in absorption have also been observed near the time of a sudden commencement (Reference 24). Recently, it was found that the sudden increase in absorption immediately preceding a sudden commencement following the flare of September 28, 1961 was coincident with an increase in the intensity of very low energy particles as observed by the satellites Explorer XII (Reference 27) and Injun I (Reference 3) (1961 υ and 1961 $o2$, respectively).

In general, it is assumed herein that the PCA is a smoothly varying function of time, although a sustained increase in absorption following a sudden commencement is interpreted

as an increase in particle intensity. "Spikes" are generally interpreted to be auroral absorption or due to local manipulation of the ionization causing the absorption rather than actual fluctuations in particle intensity.

In calculating particle intensities, the daytime values of absorption from the 30 Mc riometer at Churchill were used whenever possible. During periods of particular interest a factor of 4 was used to convert nighttime absorption to effective daytime absorption unless this procedure seemed unreasonable. At several periods of importance the absorption records from College, Barrow, and Thule were used. These riometers record a higher absorption before saturating than does that at Churchill. In all cases it was assumed that there was no effective cutoff operating at any of these stations.

Webber (Reference 3) has also calculated particle intensities from riometer records for several events. The absorption for a 30 Mc riometer and for a differential rigidity* spectrum of the form

$$dN(R) = CR^{-6}dR \qquad (2\text{-}5)$$

was calculated in a manner similar to that of Bailey (Reference 17) but with the more recent values for the atmospheric constants. He then used these curves to calculate the particle intensities as a function of time for a number of PCA events. In Figure 2-1, the transformation from db to particle intensities agrees quite well with the values obtained by Webber and the differences in particle intensity are results of differences in interpretation of the absorption. The most notable difference occurs for the event of February 23, 1956. Before the sudden commencement Webber assumed a proton cutoff of 113 Mev at College, Alaska. In this paper, we assume that there is no effective cutoff at College and that the absorption increase following the sudden commencement is attributable to an increase in very low energy particles similar to that observed on September 28, 1961.

The Neutron Monitor

The neutron monitor (Reference 28) consists of an extensive structure in which BF_3 neutron proportional counters are surrounded by an arrangement of lead and paraffin blocks. A high energy proton or neutron passing through this lead has a high probability of undergoing an interaction similar to a *star* in a nuclear emulsion; and some of the reaction products will be neutrons. These neutrons are slowed down in the paraffin by collisions with hydrogen nuclei, which are then detected by the counters. Thus the detected particles are, for the most part, secondaries to the nucleonic component of the cosmic radiation at sea level. Consequently, the neutron monitor is more sensitive to primary particles of rigidity in the range 1 to 2 Bv than any other sea level monitor. The neutron method of detecting cosmic ray intensity

*Rigidity is defined by the equation R = pc/z, where R is the particle rigidity, p its momentum, z its charge, and c the velocity of light.

changes also has the advantage that the necessary corrections for meteorological effects can be made accurately, as cannot be done, for instance, with a meson detector.

We can write (Reference 29), the following relation between the counting rate of a monitor and the primary spectrum:

$$N(R,x,t_0) = \int_{R_0}^{\infty} S(p,x) \frac{dJ(R,t)}{dR} dR \ . \qquad (2\text{-}6)$$

Here the counting rate – a function of rigidity, time, and the depth of the detector in the atmosphere – is obtained from the primary differential spectrum J by multiplying dJ for a rigidity interval dR by a function S(p,x), and integrating over a range of rigidity from R_0 to infinity. The quantity S, called the specific yield function, gives the number of secondary particles detected in a neutron monitor at any given atmospheric depth as a function of primary particle rigidity. It depends upon the composition of the primary radiation, and henceforth we shall assume that this remains constant. R_0, the lowest primary rigidity incident at the top of the atmosphere, is a function of the geomagnetic coordinates of the detector. Atmospheric absorption causes S to go to zero for R less than about 1 Bv independently of the influence of the earth's magnetic field. In Figure 2-2 S is plotted in terms of R.

Thus, if particles in the rigidity range from about 1 Bv upwards are isotropically incident upon the earth, a network of neutron monitors set up at points with known R_0 permits something to be learned about their energy spectrum, since S is known. This situation is complicated by at least two effects. If the source of the particles is localized in space in a region surrounding the sun, for example, we cannot assume in general that the particles are incident isotropically. In fact, anisotropic incidence usually occurs early in the solar event; later isotropy can usually be assumed. An intense magnetic storm can change the magnetic threshold rigidity R_0 and this must also sometimes be taken into account.

The motion of particles toward the earth from the sun has been studied by many authors (References 30 and 31), and we now have a fair knowledge of the effects which occur. These are discussed in detail in Chapter 3.

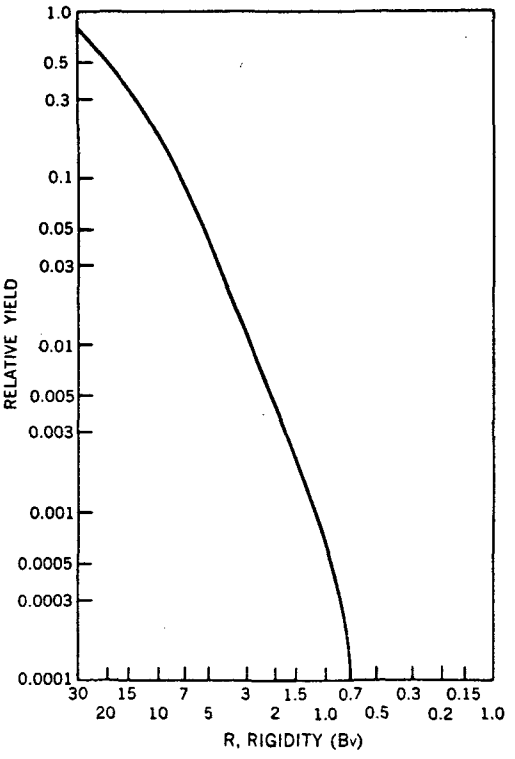

Figure 2-2—The specific yield function

In Figure 2-3 the times of these events are superimposed upon a plot of smoothed sunspot numbers (Reference 32). Even making allowance for the increase in the number of detecting stations during the past solar cycle it seems, in contrast to the PCA, that there is a definite tendency for flares producing a large flux of particles in the Bv rigidity range to occur during the increase and decrease of sunspot activity rather than during the maximum. At present there is no explanation for this tendency.

Using the neutron monitor record we can determine easily the percentage increase in the rate at any time during an event. The background rate is caused by the galactic cosmic rays which are always incident upon the earth. If we use the known spectrum of these particles and the specific yield functions*, we can obtain from Equation 2-6 a quantity proportional to the rate due to particles having rigidities above R_0. A similar calculation made with various assumed or measured spectra for the flare particles gives a quantity proportional to the additional rate due to flare particles. A difficulty arises in that the primary spectrum varies with time over the solar activity cycle (References 33 and 34) but an approximate correction can be made for this. Various relevant assumed spectra and threshold rigidities have been employed in Table 2-1 to show the intensity increase required above rigidity R_0 (in units of the normal cosmic ray background above R_0) to double the counting rate of a neutron monitor. We shall use these figures and the primary spectrum variations to deduce intensities in the rigidity range from the observed counting rate increases. By using the figures in the second column for interpreting rate increases of neutron monitors situated at points where the

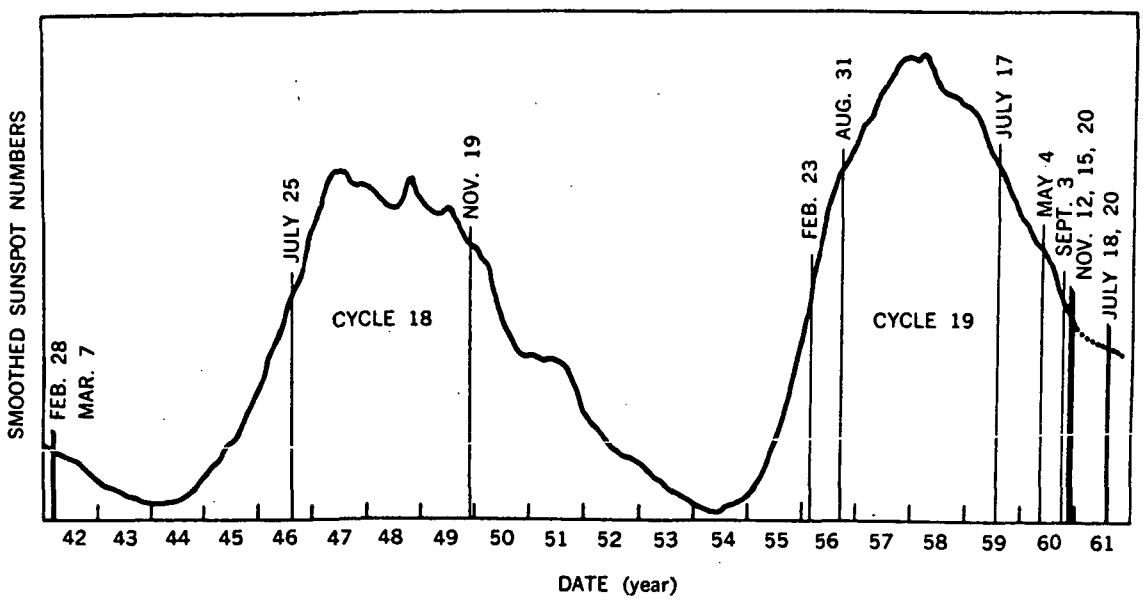

Figure 2-3—Distribution of cosmic ray events detected at sea level as a function of the solar cycle

*Obtained by using the revised specific yield function s' /n in Figure 2-2.

Table 2-1

The Radiation Increase Required above Rigidity R_0 (in Units of Normal Cosmic Ray Background above R_0) to Double the Counting Rate of the Neutron Monitor

Differential Spectral Exponent	Intensity Increase			
	R_0 = 1 Bv	R_0 = 2 Bv	R_0 = 3 Bv	R_0 = 5 Bv
4	10	17	24	40
5	12	31	62	160
6	13	45	130	–

cutoff rigidity is less than 1 Bv, we make the assumption that they are not affected by the additional particles present. Thus a 5 percent increase in the rate of a high latitude neutron monitor(R_0 = 1 Bv) indicates, if the incident spectrum is $1\text{-}p^6$, an incident flux of $0.05 \times 13 \times J_0 = 0.05 \times 13 \times 0.23$ (in February 1956) = 0.150/cm^2-ster-sec, in addition to the background above 1 Bv. The minimum increase that can be detected with certainty is less than 5 percent, and probably about 2 percent. This figure depends to some extent on the monitor involved and upon geophysical conditions. For example a confusing situation might arise if the increase in flux occurs during a Forbush decrease. At such times the diurnal variation in rate becomes large and irregular in phase and might conceivably obscure a slow change due to solar emitted particles.

The procedure outlined above for determining the intensity of particles away from the earth, requires two approximations. First, there is the question of the primary spectrum referred to above; and second, the specific yield function has been extrapolated from 2 Bv to 1 Bv – a region of critical importance with steep spectra. In deducing the spectra the assumption is made that the intensity of the radiation in the asymptotic cones of acceptance is the same; this is difficult to check, but probably true. It seems likely that the intensities given here are accurate to at least a factor of 2. The largest contribution to the error arises from the uncertainty in the knowledge of the spectral exponent.

Direct Primary Particle Detectors

Some information on solar cosmic rays has been obtained directly from particle detectors flown on balloons, sounding rockets, and satellites. Balloon borne experiments have provided valuable information on the intermediate energy interval (between approximately 80 and 500 Mev) for protons. The lower limit of the energy interval is determined by the air cutoff – usually of the order of 6 gm/cm^2. The upper energy limit is set by the difficulty of obtaining anything but an integral flux above that energy with the detectors used and the fluxes observed.

The detectors used on these flights can be divided into three very broad groups: nuclear emulsions; simple omnidirectional or wide-angle counters; and complex electronic systems including both a small solid angle and fine energy discrimination. Nuclear emulsions have the advantage of yielding an excellent energy spectrum and permitting one to determine the charge composition, but have the disadvantage of not providing time variation information throughout a flight. Simple counters do provide time resolution, when other factors such as balloon altitude variations are not present; but it is difficult to deduce good quantitative flux values because of the absorber variation as a function of solid angle and, in some cases, the lack of sufficient knowledge about the energy spectrum. However, an estimate of the energy spectrum can sometimes be obtained by observing the counting rate as a function of altitude during ascent and by using atmospheric absorption information. In addition, for some flights, nuclear emulsion data exist for a time interval included in the counter record and may therefore be used as an absolute flux calibration for the counting rates. Unfortunately, there have been only a few balloon flights with electronic experiments capable of energy resolution, so information from this source is limited.

For balloons flown where the geomagnetic particle rigidity cutoff is normally greater than that caused by the residual atmosphere, there is the additional problem of time dependent magnetic field effects, which permit varying percentages of the total particle flux to reach the detector. At the present, it is not possible to construct a model, based upon existing data, which gives the actual percentages of transparency as a function of energy and time in the event. In practice, fortunately, at Minneapolis, where many of the measurements were made, the cutoff often seems either to be the same as during geomagnetically quiet times or not to exist for energies greater than the air cutoff. However, this difficulty has limited the degree to which the proton energy spectra of solar cosmic ray events can be described in quantitative detail.

Sounding rockets with recoverable payloads provide a means of studying these events above the earth's atmosphere with both electronic counters and nuclear emulsion techniques. Data from these payloads provide information on the proton energy spectrum down to a fraction of an Mev, and detailed charge composition measurements exist for three of the events to be included in the present analysis. This method provides only a sampling of the radiation at a few times during the event; however, it does help to calibrate those instruments which do record time variations, such as the riometer.

Finally, electronic experiments in satellites outside the Van Allen belts can give a detailed time history of the energy spectrum down to very low energies. However, not until Explorer XII was launched on August 15, 1961 did such a system exist; and at present, data giving the detailed history of the proton energy spectra are available only for the September 28, 1961 event. Previous satellites have provided integral fluxes above an energy cutoff, determined from the counting rate of a single detector under a known amount of material. These results have been used in developing the history of several of the events discussed in this report.

From several of the previously mentioned sources, it has been determined that protons are by far the most abundant nuclei in these events. In the same energy/nucleon interval (and hence the same range interval), helium nuclei are less abundant than hydrogen nuclei by a factor of 20 or more. Nuclei with a charge greater than 3 are more scarce than protons in the same energy/nucleon interval by a factor of a few thousand at low energies (40-100 Mev) and probably by a larger factor at higher energies.

HISTORY AND ENERGY SPECTRA OF EVENTS

In the diagrams of spectra presented here a solid curve indicates that the detailed energy spectrum has been obtained directly. A dashed curve indicates an interpolation between these data and the integral flux at 20 Mev deduced from PCA measurements*. In the time variation curves a solid line represents the particle intensity greater than 20 Mev; a dotted portion of the curve represents an extrapolation, and a blank space represents a portion for which a reasonable interpolation could not be made. This time variation curve normally was obtained from riometer results which were generally in agreement with satellite data at those times when a valid comparison could be made. The only exception is the latter portion of the May 4, 1960 event, for which information from a satellite-borne counter was available, but no riometer data. A dashed curve represents neutron monitor results, and a dot-and-dash curve represents the variation of intensity above 100 Mev. The zero of time represents the time of the beginning of the flare, and it should be noted that there is a change of scale at 12 hours.

0331 UT February 23, 1956

The February 23, 1956 flare produced the largest intensity of particles yet observed in the Bv range. However, the riometer observations show that the intensity of low energy particles was an order of magnitude smaller than in many other solar particle events (Figure 2-4). There is only a single counter measurement (Reference 35) indicating an intensity at Minneapolis (threshold 0.81 Bv) 4-5 times normal at 2030 UT on the 23rd.

A great deal of work has been done on the neutron monitor observations of this event, and we shall summarize these with a view to finding the intensity, the spectrum, and their variation with time. The spectrum of particles at various times has been derived by examination of the latitude effect (Table 2-2).

Pronounced impact zone effects were seen during the first 10 minutes of the event (References 37 and 38) but isotropy may be safely assumed for much later times after 0400, at least in space close to the earth. The first spectrum refers to the direct radiation; that is to say radiation received in the primary impact zone, which covered most of

*It must be remembered that a very high intensity of particles with energy below 20 Mev can appreciably increase the riometer absorption. In such cases the particle intensity as deduced from Figure 2-1, if interpreted as an integral intensity above 20 Mev must be considered as an upper limit. The events of April 29, 1960 and May 6, 1960 are probably examples of this effect.

Table 2-2

February 23, 1956 High Energy Observations

Source	Energy Threshold	Time from Flare	Diff. Rigidity Spectrum
Pfotzer	1 Bv	20 min.	p^{-4}
Simpson	1.6 Bv	2 hr. 20 min.	p^{-6}
		20 hr.	p^{-7}

*Reference 36
†Reference 37

Europe at the time. The storage region was not filled up at that time, but the steeper spectra observed later refer to radiation stored in that region. If we now apply our results to these observations, we arrive at the data given in Table 2-3. Thus an expression for the integral rigidity spectrum containing the best available information for the period from 0400 UT to 1000 UT is $150/p^5\ t^{-3/2}$ with R in Bv above 1 Bv, and t in hours from 0400 UT. Simpson (Reference 37) has established that the neutron monitor rate at Chicago and other stations decayed according to a $t^{-3/2}$ law between 0430 and 1000 UT (t = 0 at 0350 UT), and exponentially thereafter with a decay constant of about 8 hours.

Table 2-3

February 23, 1956 High Energy Intensities

Time from Flare (min.)	Station	Threshold (Bv)	Diff. Spectrum	Integral Intensity above Threshold $\left(\frac{\text{particles}}{\text{cm}^2\text{-ster-sec}}\right)$
20	Leeds	1.77	$1/p^4$	150
40	Chicago	1.6	$1/p^6$	160
50	Ottawa	1.05	$1/p^6$	90*
150	Chicago	1.6	$1/p^7$	34

*The inconsistency between Ottawa and Chicago may be due to the late arrival of particles at low energies.

The peak intensity for particles with energies greater than 20 Mev, as deduced from the riometer observations at College (Reference 15) by using the curve of Figure 2-1, is radically different from the value at 30 Mev determined by Webber and Malitson†; the

†Chapter 1.

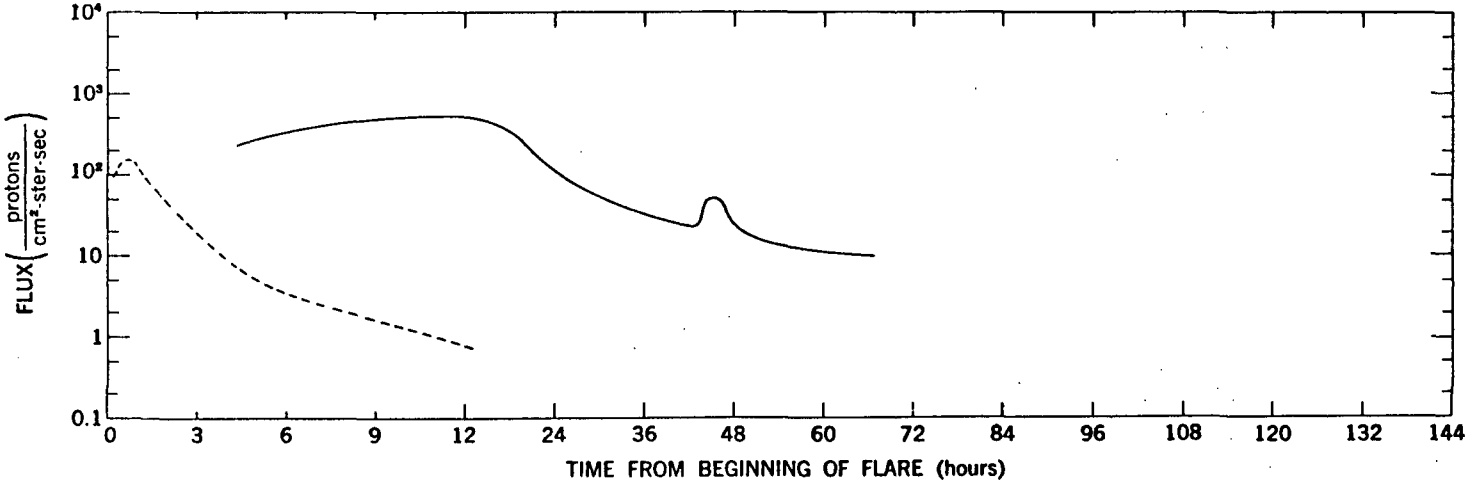

(a) Time history

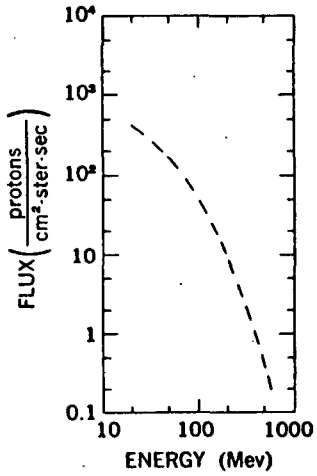

(b) Energy spectrum at 2030 UT (+17 hours)

Figure 2-4—The February 23, 1956 event

difference results from a difference in interpretation. Here it is assumed that the geomagnetic cutoff at College is not appreciably different from that at Churchill. This, indeed, seems to be the case during all other events for which comparisons are available. The interpretation here is that the event was large at high energy and small at low energy — similar to that of September 3, 1960 or July 18, 1961.

A small increase in absorption preceded the sudden commencement on February 25th and this was interpreted as an increase in particle intensity similar to that of the Explorer XII observations (Reference 26).

1030 UT August 29, 1957

In the August 29, 1957 event (Figure 2-5) a PCA lasted for 49 hours, reaching a maximum of 8 db at Churchill (Reference 39). There was no neutron monitor increase and also no increase detected at balloon altitudes between 1400 UT (Reference 40) on the 29th, an hour after the start of the PCA, and 0600 UT on the 30th. Such a detector could have found an increase of 10 percent, and from this fact it can be shown that the exponent γ of a spectrum $N = N_0 E^{-\gamma}$ must have been of the order of 6 or more and that this spectrum must have persisted down to at least 20 Mev.

0947 UT March 23, 1958

The PCA began within a few hours after the flare (Reference 41). At the time of the sudden commencement, 1540 UT on the 25th, there was a rapid increase in the PCA to about 12 db. This was probably a consequence of an intensity increase at low energies of the type observed by Bryant et al. (Reference 26) with instruments flown in Explorer XII on September 28, 1961. There was no detectable neutron monitor increase, but at 0700 UT on March 26th a lower limit of 0.07 ± 0.01 particle/cm^2-ster-sec (between 120 and 180 Mev), was determined by balloon measurements at Minneapolis (Reference 42). Probable variations of

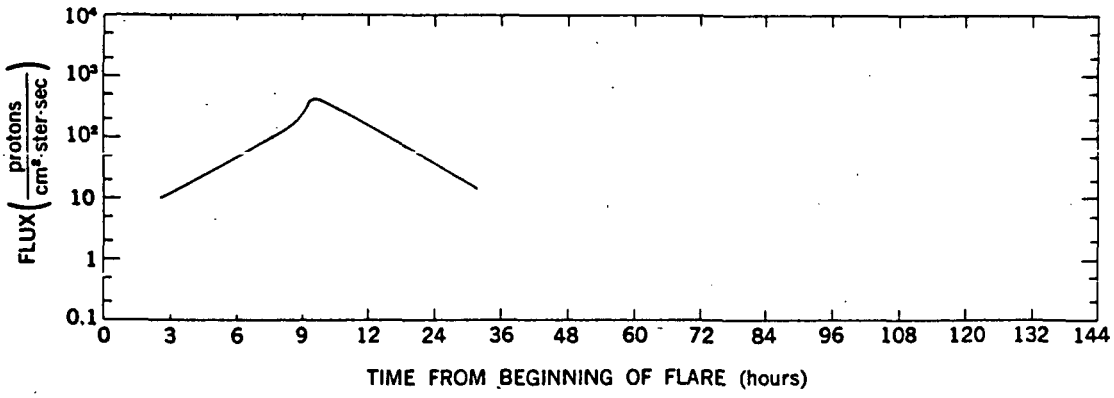

Figure 2-5—The time history for August 29, 1957 event

the magnetic threshold during the flight prevent anything more than the determination of a lower limit to the flux or an upper limit of 4 to the exponent of the integral energy spectrum in the 20-200 Mev interval.

0020 UT July 7, 1958

The flare produced a PCA reaching as much as 17 db at Kiruna (Reference 43) at 0400 UT on July 8th. No neutron monitor increase was observed, but balloon measurements were made by Russian workers at Kiruna (References 44 and 45). At an atmospheric depth of 10 gm/cm^2 the intensity was 4 times normal at 1000 UT on July 8th, when the riometer absorption was 18 db, and returned to normal by 1500 UT when the riometer absorption was 13 db (Figure 2-6). In this instance it is hard to reconcile the balloon and riometer results, but it is evidence for a very steep spectrum. It is possible that the energy spectrum was so steep that, if the second balloon were under a few gm/cm^2 more atmosphere than the first, the difference in counting rate could be caused by the differences in the cut-off energy determined by the air above the balloon.

0433 UT August 16, 1958

For this event only riometer data, showing a maximum absorption greater than 15 db, are available. Because an energy spectrum cannot be constructed from riometer data alone, no figure is presented for this event.

1428 UT August 22, 1958

This event is characterized by a steep spectrum and no detectable neutron monitor increase (Figure 2-7). The solar particles were observed by means of balloons (Reference 46) and by the Explorer IV (1958ϵ) satellite (Reference 47). At Churchill, after only 1 hour, the intensity of protons with kinetic energies above 100 Mev was 20 times normal; and the subsequent rapid fluctuations until 1900 UT were probably due to fluctuations in particle emission. The spectra exhibited are derived from the balloon and satellite observations. A direct determination at 0500 UT on August 23rd gives an approximate integral energy spectrum proportional to $1/E^{3.5}$ above 100 Mev; and the satellite results support the validity of extrapolating this energy spectrum to 30 Mev. Measurements made on Explorer IV (References 47 and 48) give integral fluxes, above 30 and 40 Mev, at three times during the event, which are consistent with the riometer observations (Reference 39).

0005 UT August 26, 1958

For this event only riometer data showing a maximum absorption greater than 15 db, are available*. Because an energy spectrum cannot be constructed from riometer data alone, no figure is presented for this event.

*Chapter 1.

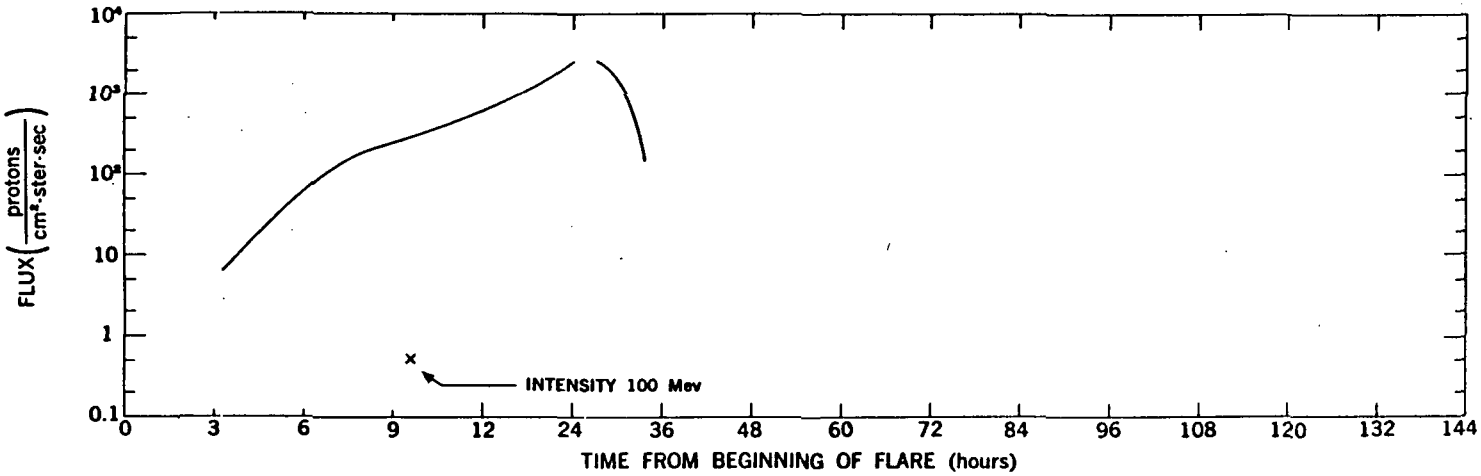

(a) Time history

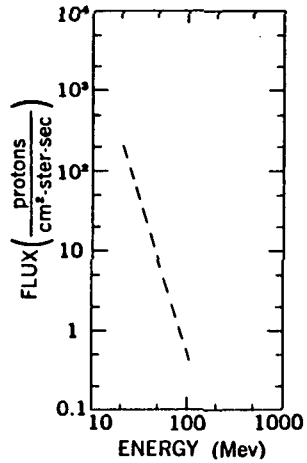

(b) Energy spectrum at 1000 UT
(+9-2/3 hours)

Figure 2-6—The July 7, 1958 event

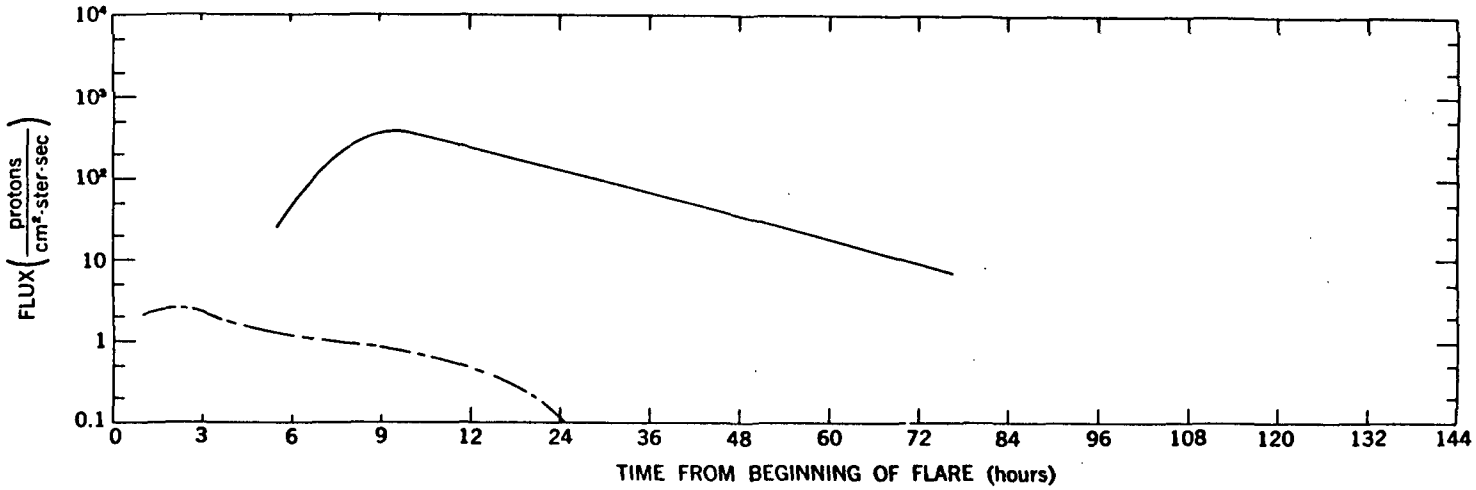

(a) Time history

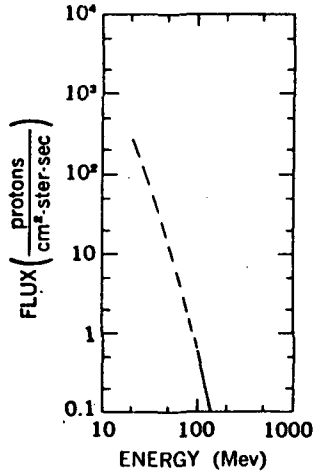

(b) Energy spectrum at 0430 UT (+14 hours)

Figure 2-7—The August 22, 1958 event

2101 UT May 10, 1959

Energy spectra were obtained at balloon altitudes during the period of 0400 to 1600 UT on May 12, 1959 at Minneapolis, by the University of Minnesota (References 49, 51, and 51). However, balloon observations by Charakhch'yan, et al. (Reference 44) show that during the latter portion of this time only a fraction of the total particle flux reached Minneapolis, so that only the energy spectrum at 0640 UT has been shown (Figure 2-8). The PCA began about 5 hours after the flare, reached an absorption maximum in excess of 12 db at Longyearbyen, and recovered over a period of several days (Reference 52).

The July 1959 Events

The complex series of events occurring during July 1959 are the subject of a monograph published by UGGI (Reference 53). In brief, a series of three great solar flares, occurring before 0210 UT July 10th, at 0319 UT July 14th, and at 2118 UT July 16th, caused a series of three large solar cosmic ray events (Figures 2-9, 2-10 and 2-11). The last of the flares also produced particles in a range of energies and in a quantity detectable by neutron monitors. The absorption showed increases to greater than 20 db for all three of the events, as recorded by the 27.6 Mc riometer at College (Reference 23); the riometers at Barrow (Reference 23), Thule (Reference 23), and Churchill (Reference 54), are in general agreement with these maximum values.

The neutron monitor increase has been discussed by McCracken and Palmeira (Reference 14) who point out the very slow rate of rise, and the isotropic nature of the flux at the energies detected by the neutron monitors. High latitude monitors detected an increase at about 0300 UT on the 17th and, between 0800 UT and 1200 UT, recorded an increase of about 6 percent for particles above 1 Bv. If we take a differential spectrum (Reference 53) of the form $1/p^6$, a particle intensity of $0.06 \times 13 \times 0.09 = 0.07$ particles/cm^2-ster-sec ($P > 1$ Bv) is implied. This is consistent with the fact that stations with thresholds above 1.2 Bv did not see an increase.

The neutron monitor records show no additional particles–even at the highest latitudes–after about 1800 UT on the 17th. If we assume a steepening of the spectrum of $1/p^6$, and that a 1 percent increase would have been detected, the intensity above 1 Bv was less than $0.01 \times 13 \times 0.09 = 0.0012$ particles/cm^2-ster-sec.

A number of balloon flights provided particle data in the intermediate energy range. Information from Freier (Reference 49), Winckler, et al. (Reference 55), Webber (Reference 56), Brown and D'Arcy (Reference 57), and Anderson and Enemark (Reference 40), have been combined to give energy spectra at four times during the July 10th event and twice during each of the other two, as well as relatively complete histories of the integral flux above 100 Mev.

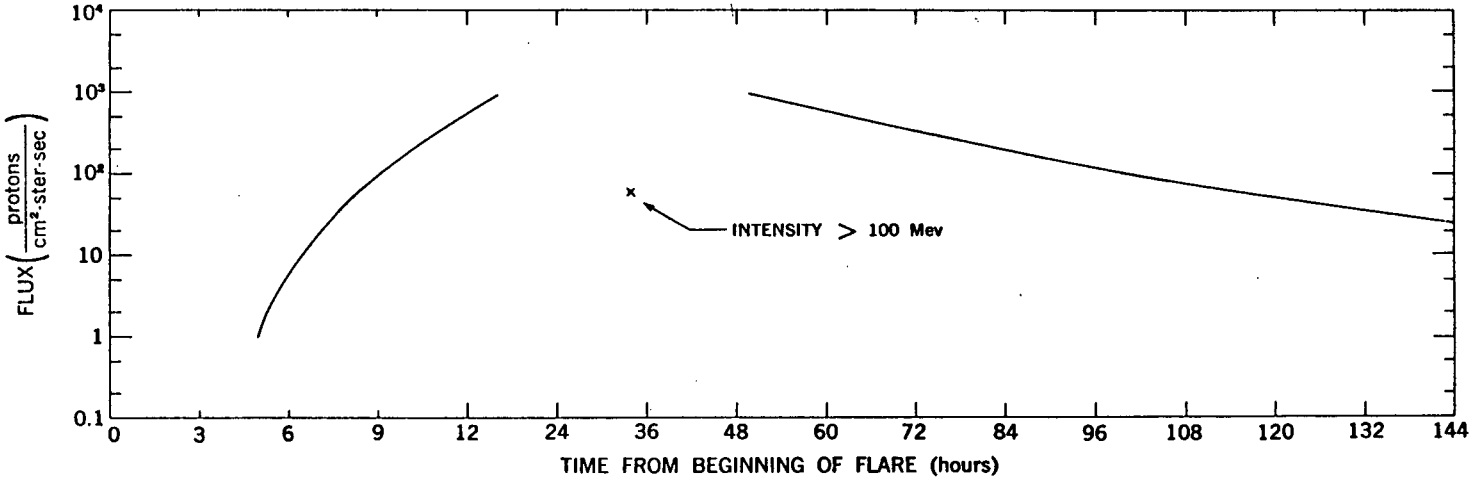

(a) Time history

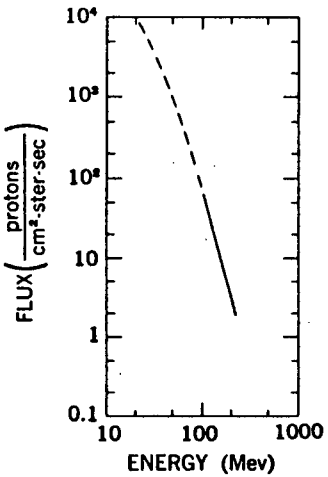

(b) Energy spectrum at 0640 UT (+34 hours)

Figure 2-8—The May 10, 1959 event

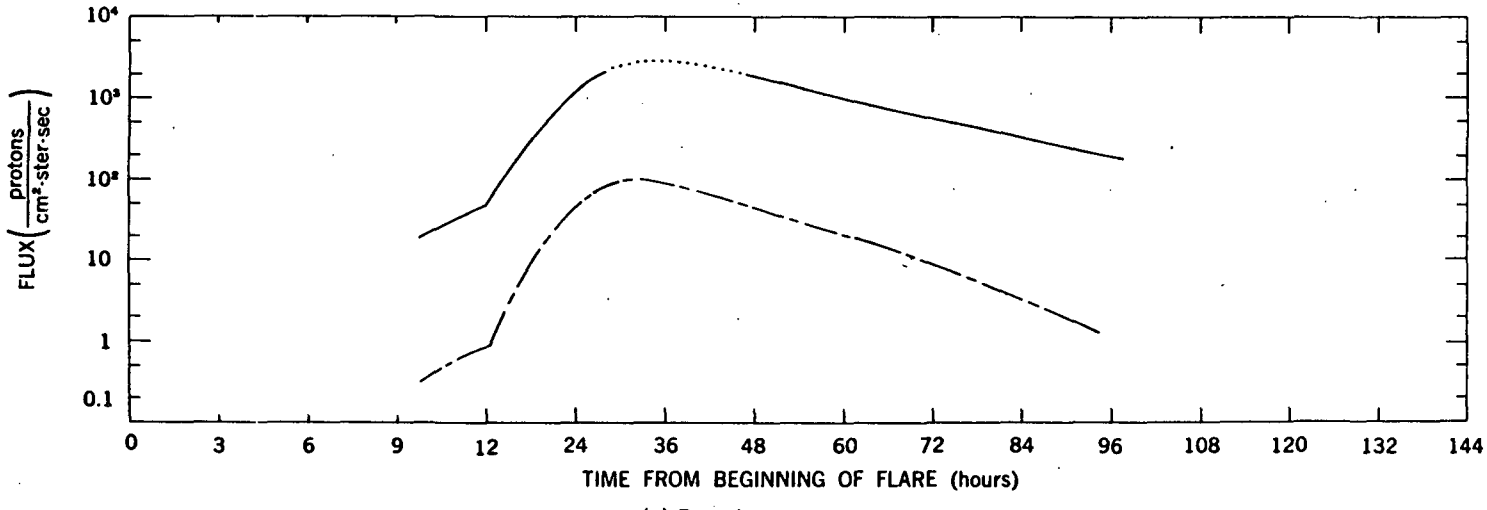

(a) Time history

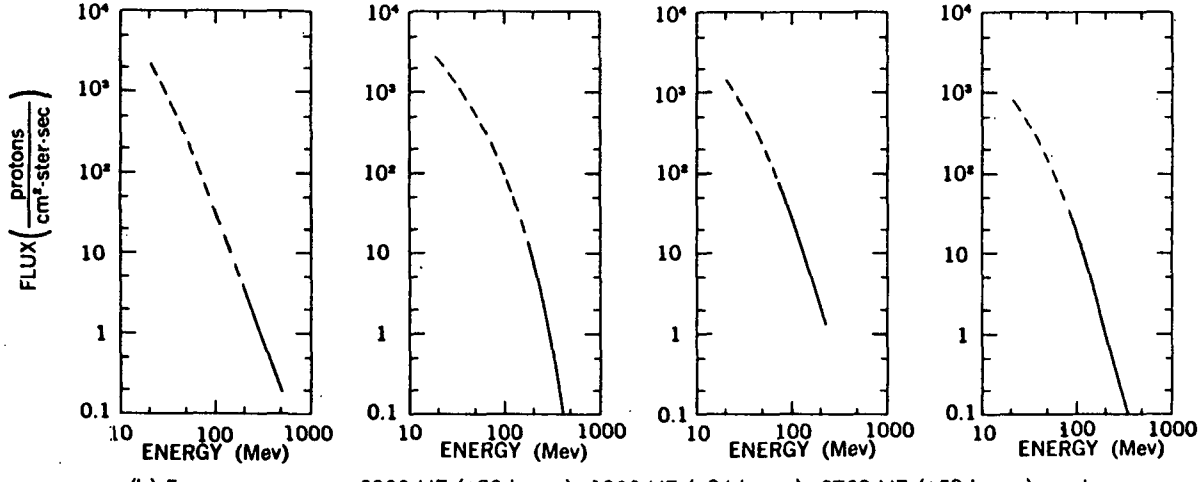

(b) Energy spectra at 0800 UT (+30 hours); 1200 UT (+34 hours); 0700 UT (+53 hours); and 1800 UT (+64 hours)

Figure 2-9—The July 10, 1959 event

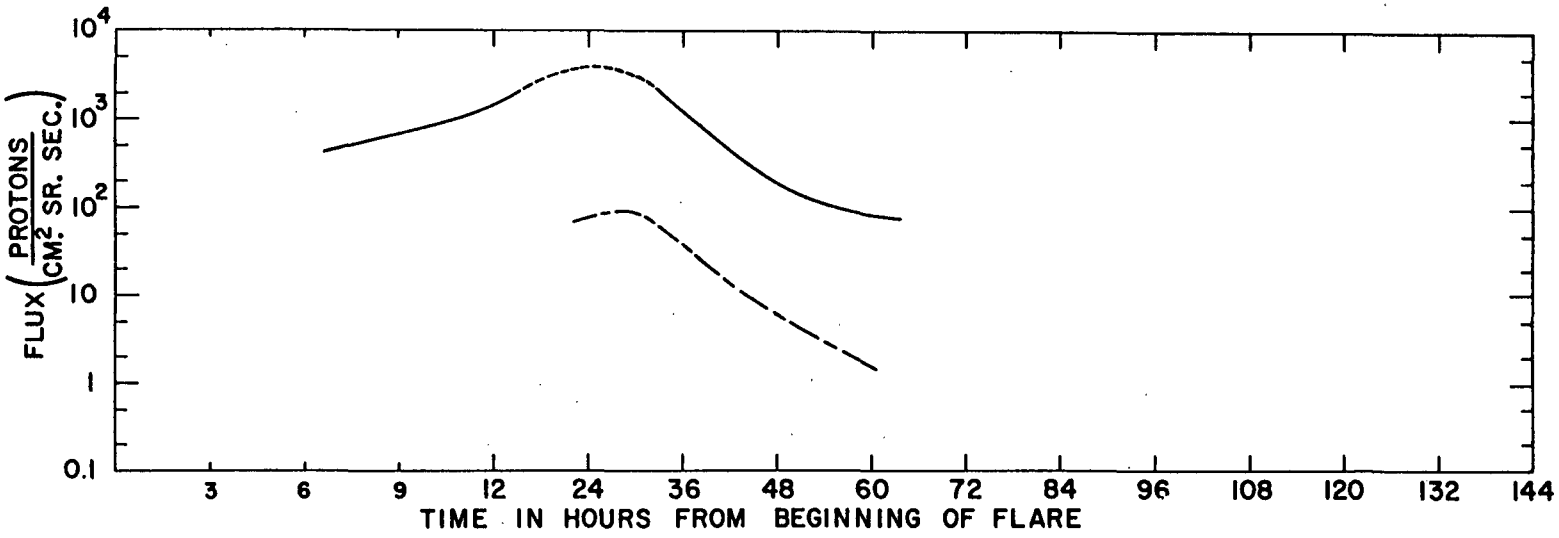

(a) Time history

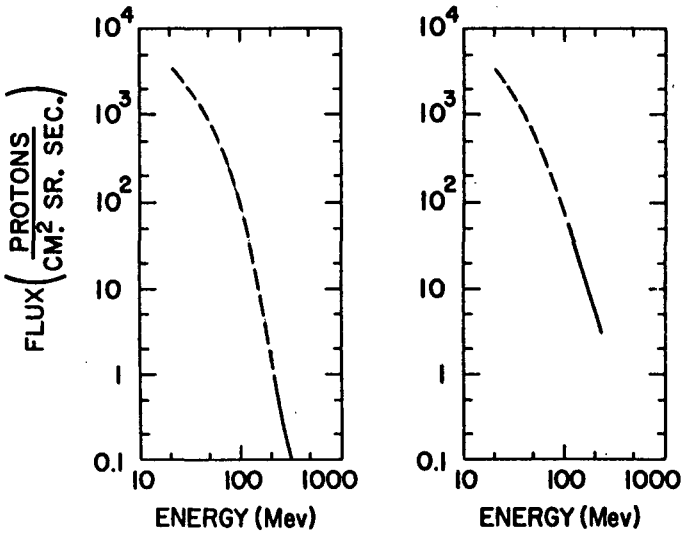

(b) Energy spectra at 0500 UT (+25-1/2 hours) and 1042 UT (+31 hours)

FIGURE 2—10 — THE JULY 14, 1959 EVENT

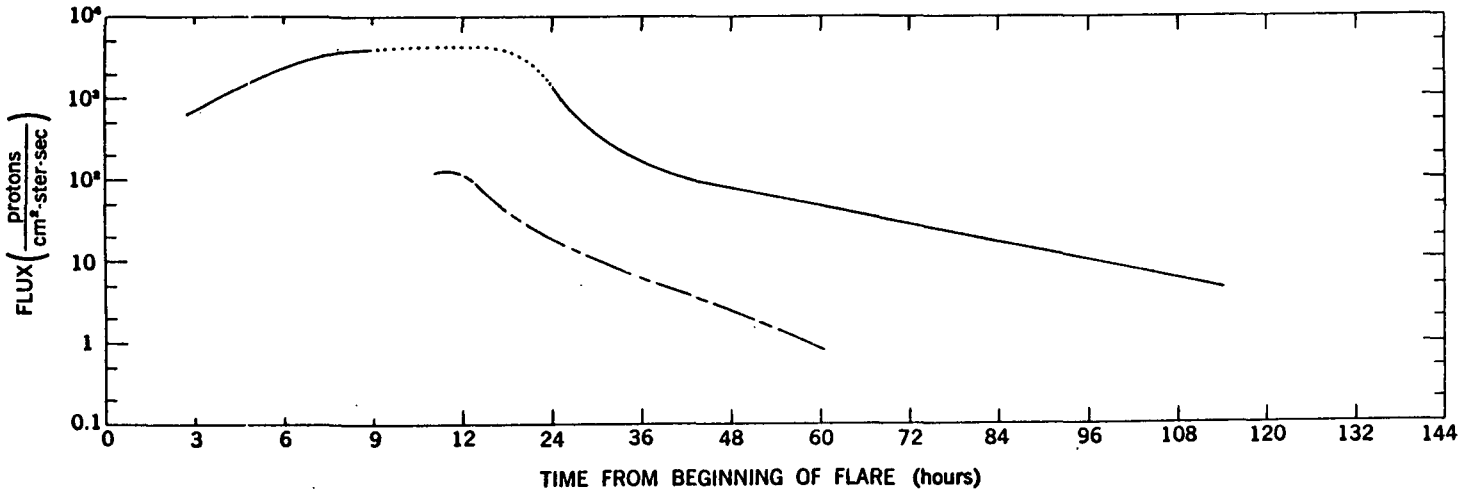

(a) Time history

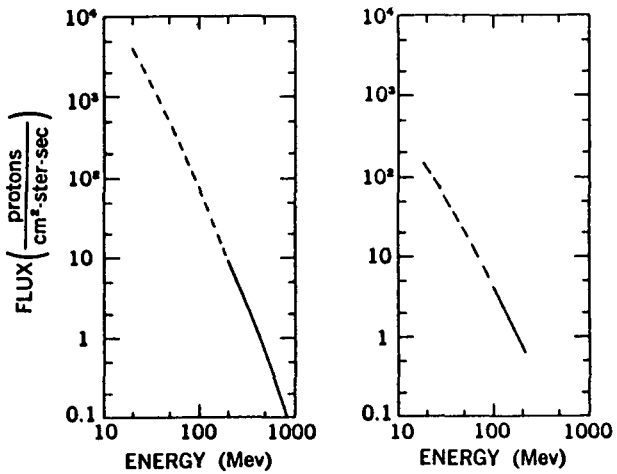

(b) Energy spectra at 1200 UT (+14-3/4 hours) and 1510 UT (+42 hours)

Figure 2-11—The July 16, 1959 event

0138 UT April 29, 1960

The riometers at College (Reference 41), Thule (Reference 41), and Churchill (Reference 54) were in essential agreement during this event and showed a maximum absorption of about 13 db on April 30th at about 0600 UT (Figure 2-12). Several readings from the Explorer VII (1959, 1) (Reference 58) counters during the period 1800 UT April 29th through 0100 UT April 30th at L values* where the full intensity was often seen in other events indicated flux values more than an order of magnitude lower than those inferred from the riometer data. This shows that either the satellite was situated in a position where the minimum energy observable due to geomagnetic effects was larger than the nominal threshold energy of the detectors (18 and 30 Mev) or that there was a large component at energies below 18 Mev.

1000 UT May 4, 1960

This event, observed at sea level by neutron monitors, falls into the category of *rapid risers* and shows pronounced impact zone effects. The intensity in the impact zones started to rise at 1030 ±1 UT, and reached maximum at 1040 ±2 UT, with a differential spectrum of about p^{-4} (Figure 2-13). Outside the impact zones the intensity began to rise at 1035 UT and reached maximum at 1048 ±2 UT, with a differential spectrum varying approximately as p^{-5}. The neutron monitor at Deep River detected particles arriving directly and observed an increase of 3.5 times at maximum, which implies an intensity of $3.5 \times 12 \times 0.1 = 4.5$ particles/cm^2-ster-sec above 1 Bv. This quantity checks within a factor of 2 with the increase recorded at the Jungfraugoch where the threshold is 3.6 Bv; the agreement provides some confidence in the spectrum. The decay above 1 Bv can be approximated by an expression of the

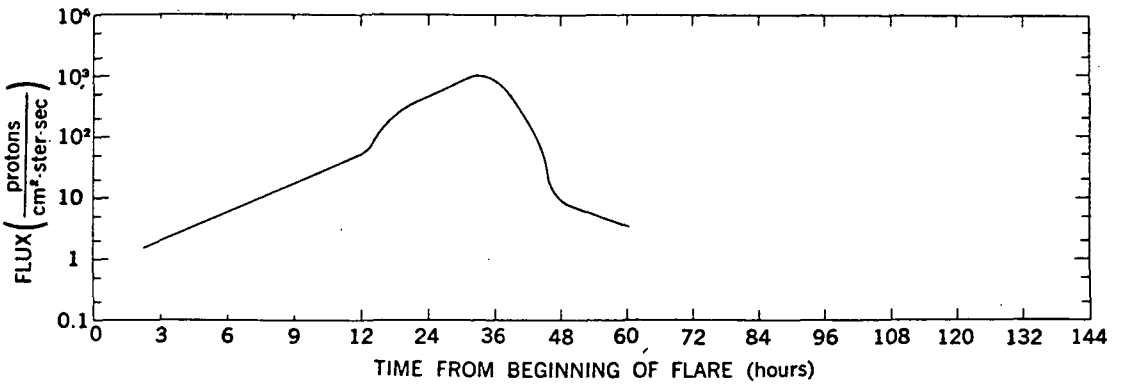

Figure 2-12—The time history of the April 29, 1960 event

*The distance called the "L value" is the radius (in earth radii) at which the magnetic line of force to which it refers crosses the equatorial plane.

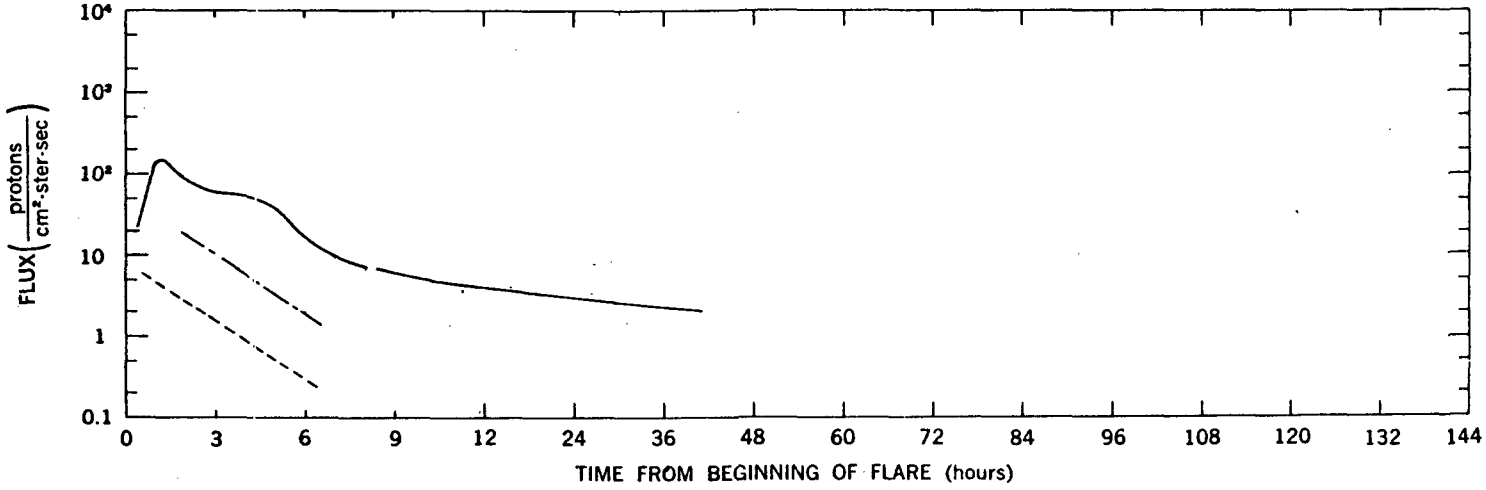

(a) Time history

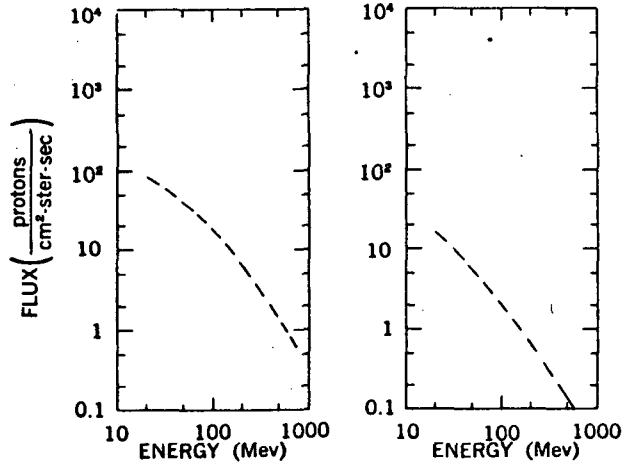

(b) Energy spectra at 1220 UT (+2 hours) and 1630 UT (+6 hours)

Figure 2-13—The May 4, 1960 event

form $N = N_0 e^{-t/t_0}$ with t_0 = 2 hours. J. R. Winckler et al. (Reference 59), at 1630 UT on May 4th, found a flux above 1 Bv with detectors flown on balloons, which is in excellent agreement with the flux inferred by neutron monitor data.

The riometer data from Thule (Reference 41) showed a rapid increase to a maximum absorption of about 5 db two hours after the start of the flare. The riometers at College (Reference 41) and Churchill (Reference 54) were in darkness at that time. Following the maximum, the three riometers were in agreement, and the inferred particle intensity agreed with the State University of Iowa (SUI) Explorer VII data (Reference 58) obtained from 10 to 32 hours after the flare.

1404 UT May 6, 1960

The riometers at College (Reference 41), Churchill (Reference 54), and Thule (Reference 40) showed agreement for this event, with a maximum absorption of about 13 db, forty hours after the flare (Figure 2-14). Again there is disagreement with the SUI Explorer VII data (Reference 54), probably for the same reasons discussed in connection with the event of April 29, 1960.

0037 UT September 3, 1960

In this interesting event the solar emission, due to a class 3 flare at 17°N 87°E on the sun, occurred during the transit to the earth of distrubances from two previous flares. A slowly rising isotropic flux was detected, which caused an increase of about 2 percent in the neutron monitor rate at Deep River at 0900 UT (Reference 32). Rockets launched from Churchill at 1400 UT and 1700 UT measured a spectrum steepening towards high energies (Reference 21), which could be approximated in differential form $1/p^{3.3}$ between 0.15 and 0.7 Bv (Figure 2-15). If we assume that $1/p^6$ is appropriate above 1 Bv, then the intensity at the time of maximum was about 0.05 particles/cm^2-ster-sec. Winckler (References 55, 60, and 61) deduced an integral spectrum $2 \times 10^7 E^{-3.1}$ (E in Mev) from balloon

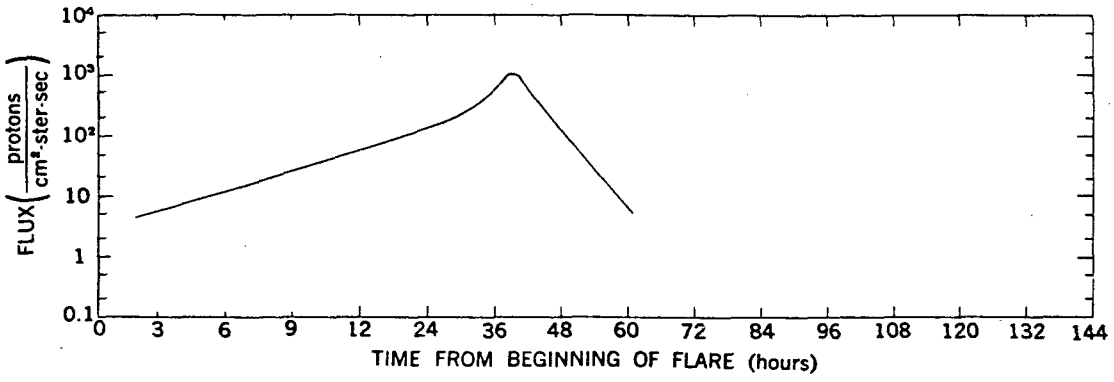

Figure 2-14—The time history of the May 6, 1960 event

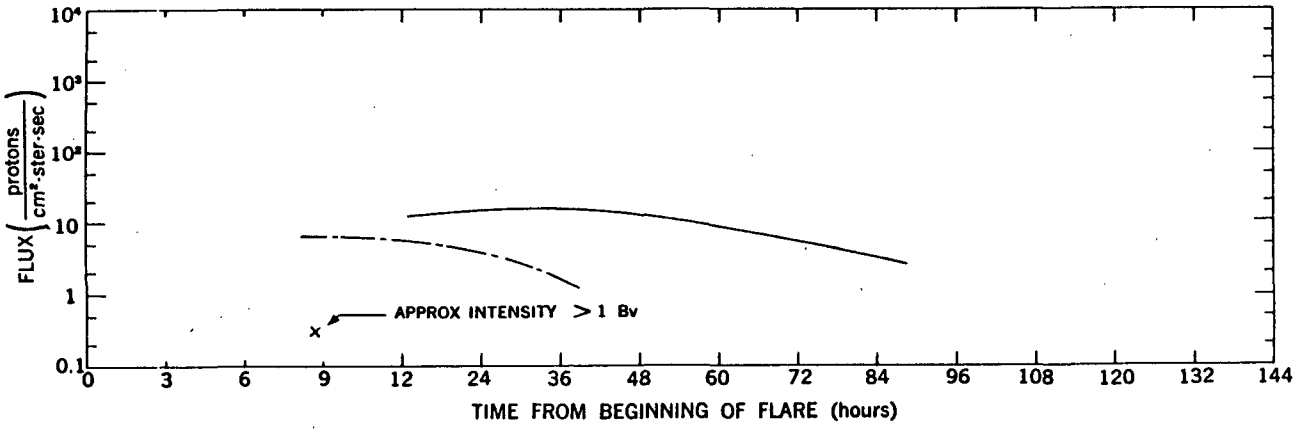

(a) Time history

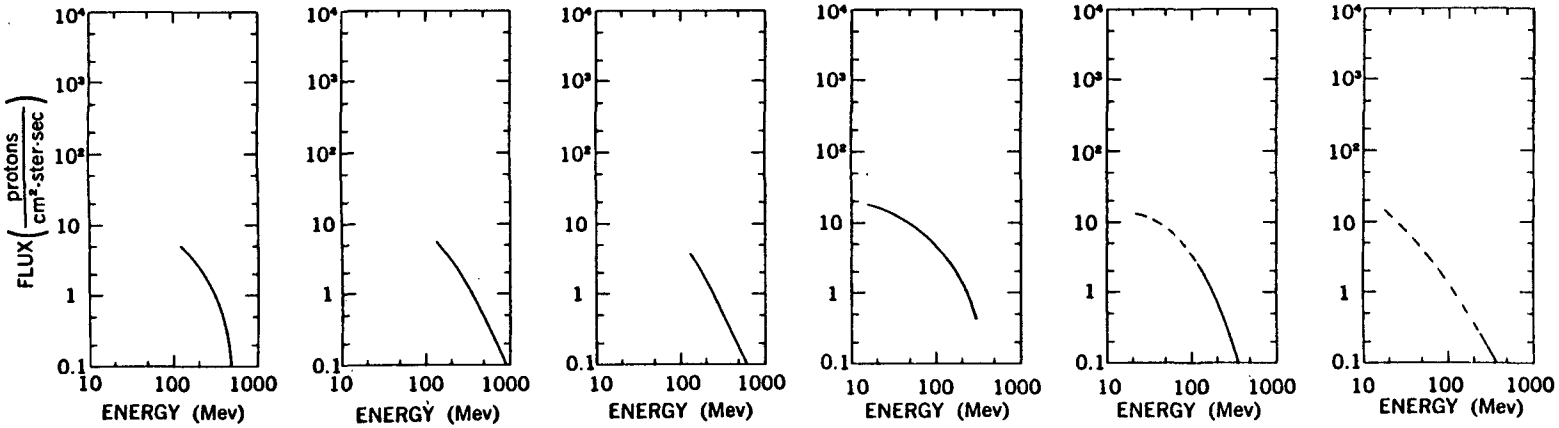

(b) Energy spectra at 0900 UT (+8 hours); 1000 UT (+9 hours); approximately 1230 UT (+12 hours); 1408 UT (+13-1/2 hours); 0000 UT (+23 hours), and 1615 UT (+39-1/2 hours)

Figure 2-15—The September 3, 1960 event

measurements at Minneapolis and Churchill at about 1730 UT. This is in fair agreement with the intensity value given above, as are the results of Biswas et al. (Reference 5). In the energy region from 22 to 67 Mev the intensity remained the same between 1400 and 1700 UT. We know from the behavior of the low energy particles producing the cosmic noise absorption that the decay of the event at these energies was very slow; and examination of the emulsion measurements at 1 Bv at Minneapolis showed that the high energy flux decayed by a factor of almost 10 in about 30 hours.

The PCA observations indicated a very flat spectrum, consistent with that found by the rocket emulsion measurements. In addition the measurements of Explorer VII (Reference 58) are in agreement with the intensities inferred from riometer absorption.

1322 UT November 12, 1960

This event was a complicated one in which two separate maxima are displayed at high latitudes by the neutron monitor records. Figure 2-16 shows the records of the Deep River neutron monitor for the month of November 1960 showing the coordinates of the important flares. It has been postulated (References 62 and 63), that the flares occurring on the 10th and 11th produced plasma fronts, and these were in transit towards the earth when the flare on the 12th produced an injection of high energy particles. Thus, detectors on the earth sampled the intensity of solar particles for six hours before and several hours after the passage of a front which generated a large magnetic storm and a very rapid Forbush decrease. In addition to the neutron monitor and riometer data, detailed energy spectra were

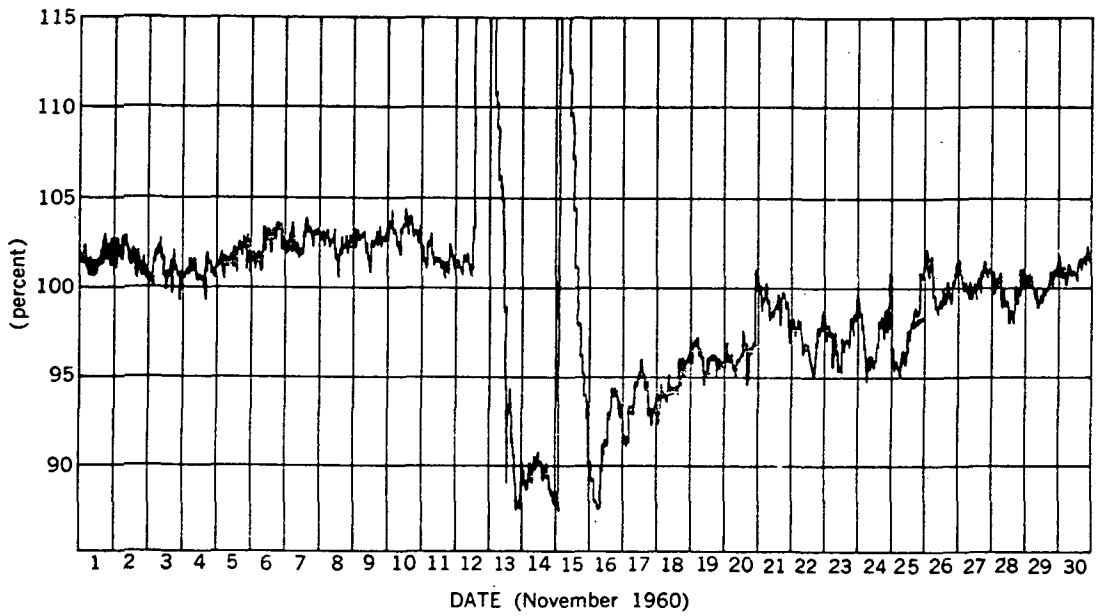

Figure 2-16—November, 1960 neutron monitor data from Deep River

obtained at three times during this event by the reduction of data from sounding rockets fired from Churchill (References 63 and 64). These spectra for the November 12 event are shown in Figure 2-17. The low energy component between 20 and 80 Mev was seen to increase markedly between 1840 and 2330 UT in agreement with the riometer data. Between 2330 UT on November 12 and 1603 UT on November 13, the high energy component continued to decline as indicated by the curve deduced from neutron monitor data between about 2000 UT on November 12 and 0400 UT on November 13.

For this event Lockwood and Shea (Reference 65) have performed calculations similar to those reported here; and this permits a check on our procedure for finding the flux above the atmosphere corresponding to a given neutron excess. Lockwood and Shea find a spectrum of the form p^{-6} between 1600 and 1630 UT on November 12, and deduce a differential spectrum for protons which corresponds to 2.9 particles/cm^2-ster-sec above 1.25 Bv. Our calculation leads to $0.85 \times 21 \times 0.11 = 2.0$ particles/cm^2-ster-sec above 1.25 Bv.

Further confirmation can be found from the results of the measurements made at 1840 UT by a NASA rocket launched from Churchill just before the earth entered the trapping region (Reference 65). From the emulsion measurements, Fichtel and Guss found an intensity above 680 Mv of 24 particles/cm^2-ster-sec, and a slope of about -6 for the integral rigidity spectrum. Assuming this slope to continue, the intensity above 1 Bv would be 3.5 particles/cm^2-ster-sec. It is difficult to obtain a rate of decrease with time which has much meaning over a wide rigidity range. After 1900 UT Manzano et al. (Reference 66) found a decrease proportional to $t^{-2.3}$ and a sudden increase in the decay rate at 1000 on November 13th.

0200 UT November 15, 1960

After the first hour, during which particles were incident principally from a direction about 50° west of the earth-sun line and the intensity rose rapidly, a regular decline set in at high energies. The maximum of the neutron monitor increase at high latitudes indicates an intensity of approximately 3 particles/cm^2-ster-sec above 1.25 Bv, assuming a $1/p^6$ differential rigidity spectrum. Lockwood and Shea deduced a differential rigidity spectrum of $10^2 p^{-6}$ for P in the range 1-7 Bv. This leads to an intensity above 1.25 Bv of 6.5 particles/cm^2-ster-sec at the time of the maximum, which is in fair agreement with the calculation made here.

The riometer data indicate that the maximum flux of particles above 20 Mev occurred about twenty hours after the flare (Reference 41), and was almost 10^4 particles/cm^2-ster-sec (Figure 2-18). Detailed energy spectra were available early in the event from balloon borne equipment (Reference 6) and later in the event from sounding rockets (References and). The Explorer VII (Reference 58) data agree with the other data obtained to within a factor of 2. A relatively fast decline is observed late in the event, with the decay following a law of the form $1/T^n$, with T = 0 at the time of the flare and n perhaps as large as 3 (Reference 67).

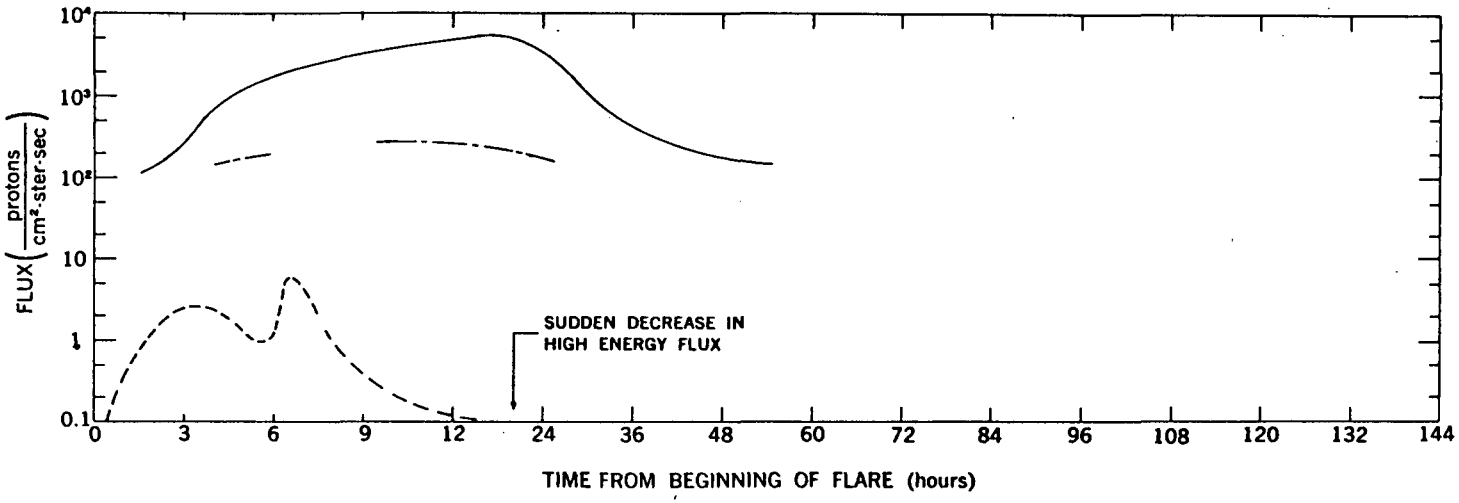

(a) Time history

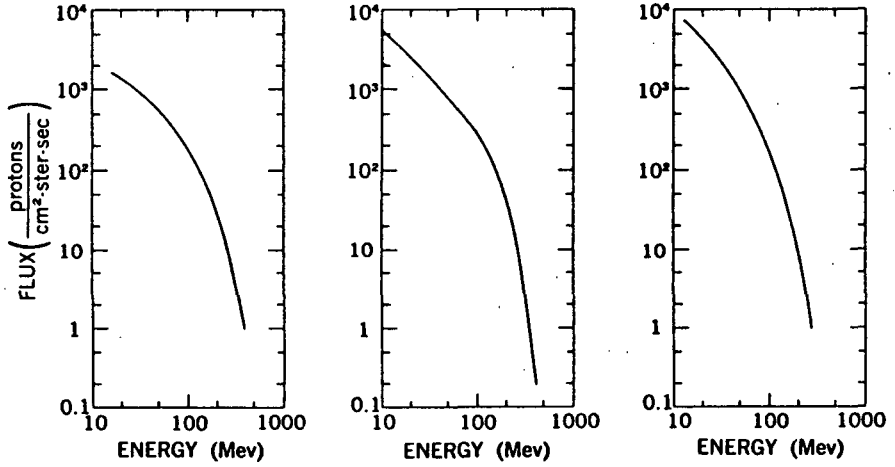

(b) Energy spectra at 1840 UT (+5 hours); 2330 UT (+10 hours); and 1603 UT (+26-1/2 hours)

Figure 2-17—The November 12, 1960 event

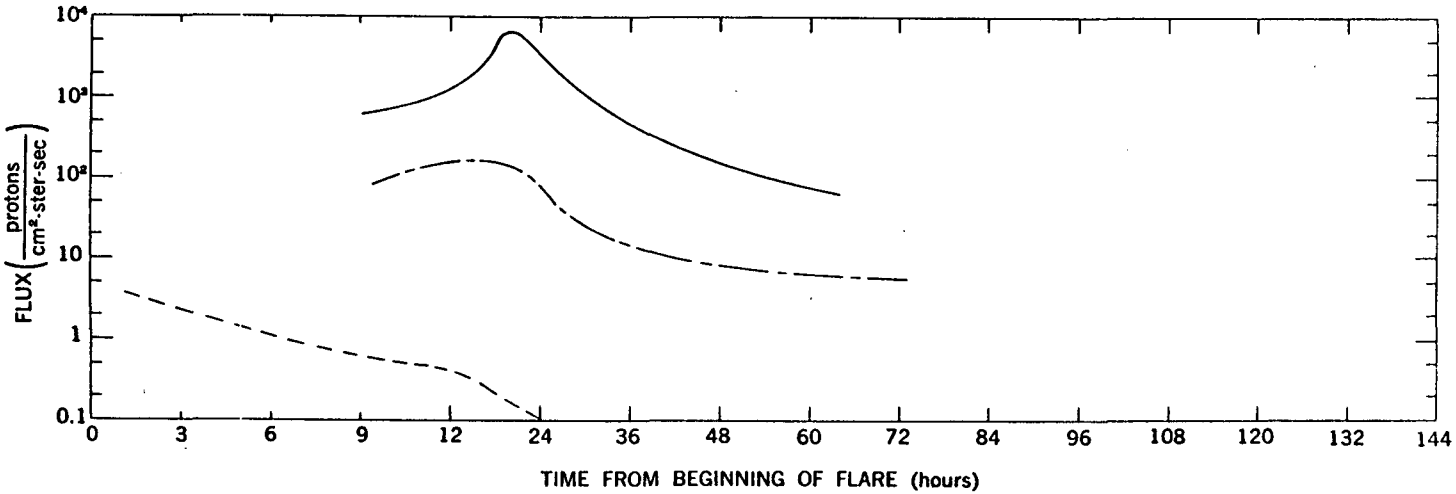

(a) Time history

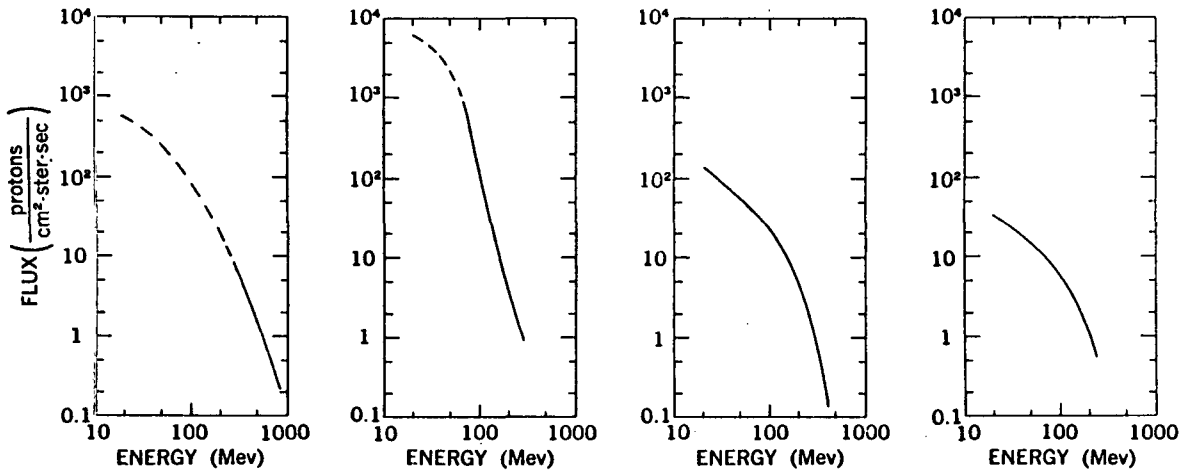

(b) Energy spectra at 1130 UT (+9-1/2 hours); 2200 UT (+20 hours); 1600 UT (+38 hours); and 0340 UT (+74 hours)

Figure 2-18—The November 15, 1960 event

November 20, 1960

On November 20th there was another solar event; the flare was from the same region as the flares associated with the November 12th and 15th events which, by then, was just around the western limb of the sun. The increase at neutron monitor energies was small and took about one hour to reach its maximum value, 5 percent above background, at Deep River (Reference 20). An increase of the order of 1/2 to 1 percent occurred at points with a threshold rigidity of 3 Bv, indicating a very flat spectrum. The riometer increase was also relatively small, indicating that the integral intensity of particles above 20 Mev did not exceed 100 particles/cm^2-ster-sec.

July 12, 1961

The integral flux of particles greater than 20 Mev, as determined by the absorption detected on the riometer (References 41 and 54), increased relatively slowly early in the July 12, 1961 event and reached a maximum shortly after the sudden commencement – 24 hours after the flare (Figure 2-19). From nuclear emulsions flown on a balloon near Churchill, Guss and Waddington (Reference 68) obtained an energy spectrum averaged over a 10 hour period centered about 26-1/2 hours after the flare*, when the intensity was greatest. From Figure 2-19, we see that the integral proton energy spectrum is very steep at this time, of the order of $1/E^{4.5}$, in the energy range from 78 to 140 Mev. Based on the riometer data, we conclude that it must have remained approximately that steep to energies below 20 Mev. From geiger counter observations on another balloon at a slightly lower altitude (Reference 69) and the riometer data, it is known that the energy spectrum was at least this steep during the entire period around maximum intensity.

0930 UT July 18, 1961

This event is presumed to be associated with the 3+ flare at 0930 UT on July 18, 1961 because of the relatively rapid flux increase shortly thereafter as detected by neutron monitors and the riometers at various northern stations. There were, however, two major flares shortly before this time, a class 3 flare at 0505 UT and a class 2 flare at 0805 UT, which may have contributed particles to the event. Unlike the previous event on July 12, the riometer absorption for this event shows a rapid rise almost to the maximum value within about two hours (Figure 2-20). In addition, there was a detectable particle flux in excess of about 450 Mev as shown by the neutron monitor increase. There was a balloon in the air from 1305 to 1918 UT on July 18th carrying nuclear emulsion (Reference 71). A combination of this, the riometer, and the neutron monitor data permits the determination of an energy spectrum early in the event. On the basis of the neutron monitor and riometer records, as well as the behavior of other events, it is reasonable to assume that the energy spectrum

*Data obtained from the Injun satellite (Reference 70) is in general agreement with this interpretation.

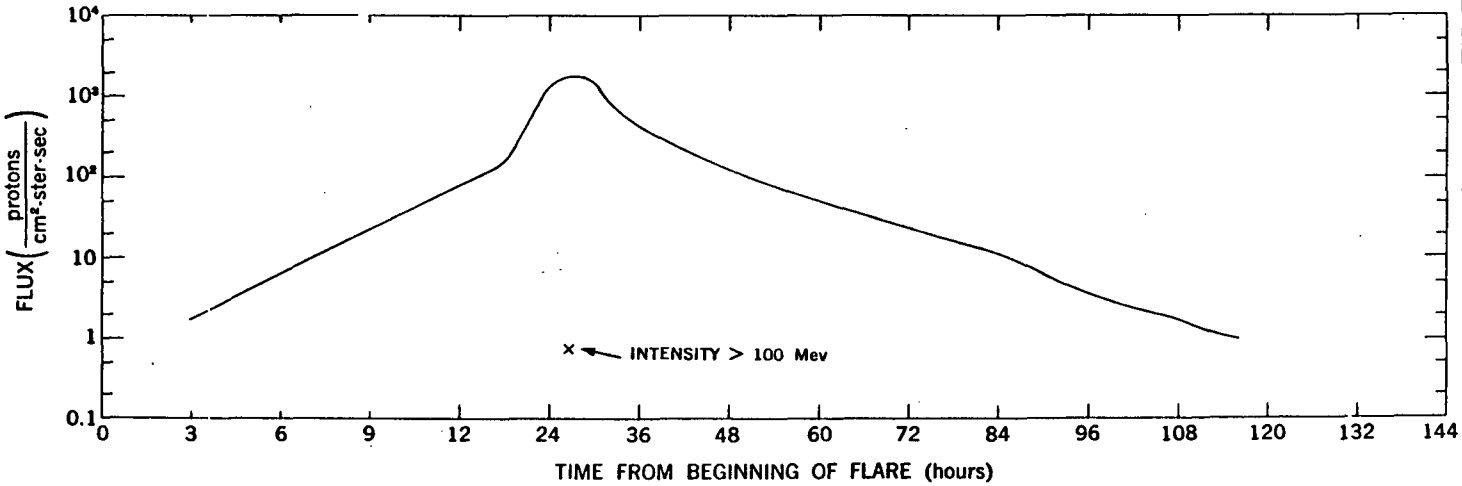

(a) Time history

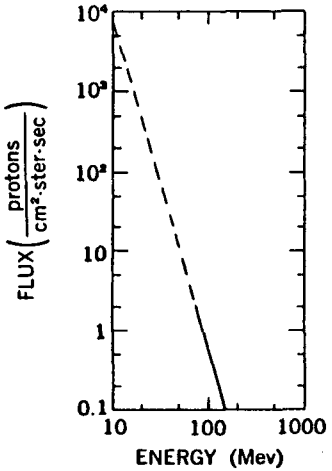

(b) Energy spectrum at 1300 UT (+27 hours)

Figure 2-19—The July 12, 1961 event

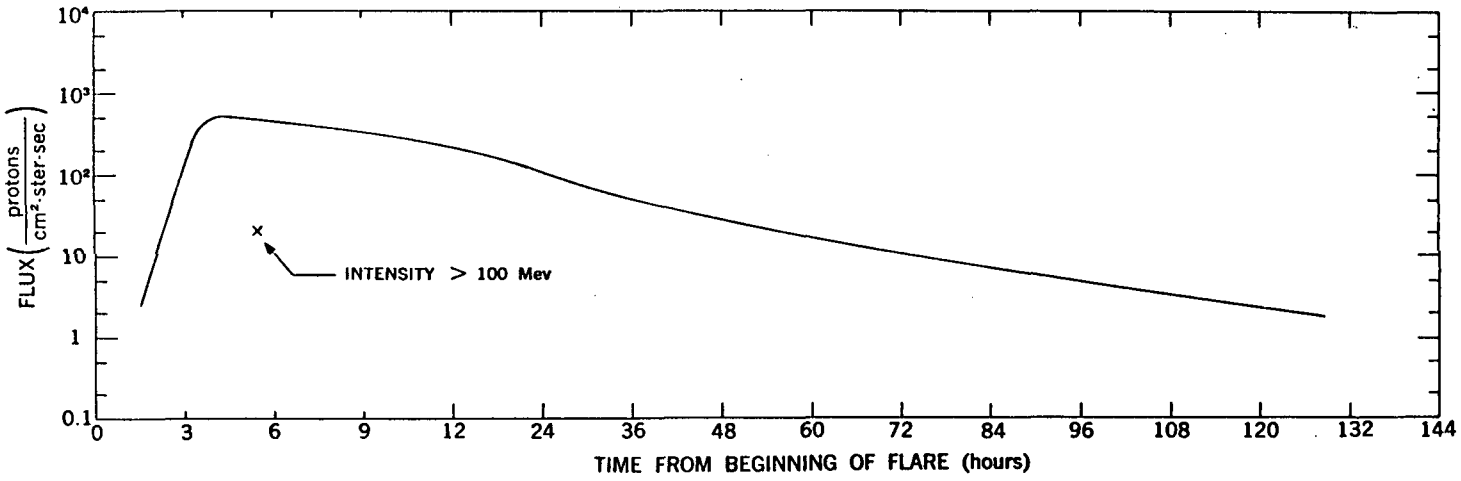

(a) Time history

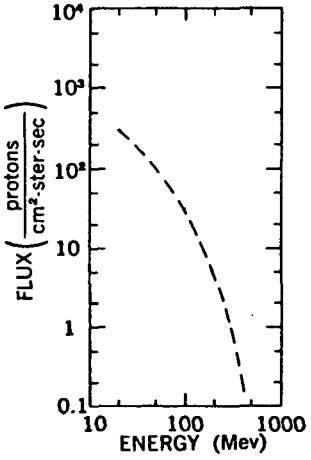

(b) Energy spectrum at 1600 UT (+6-1/2 hours)

Figure 2-20—The July 18, 1961 event

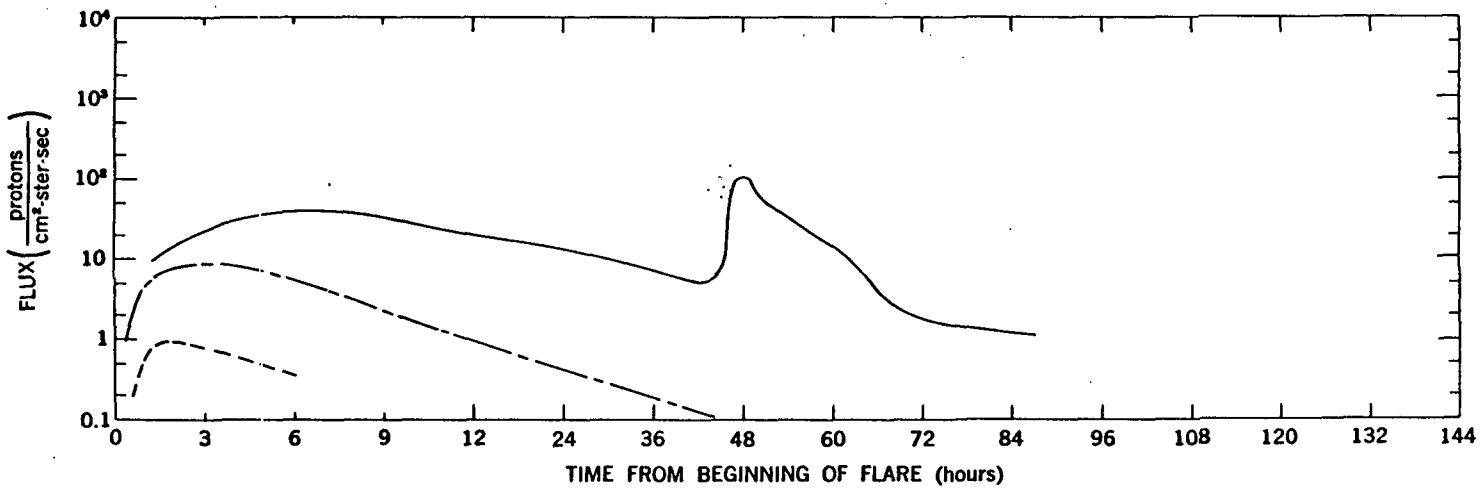

(a) Time history

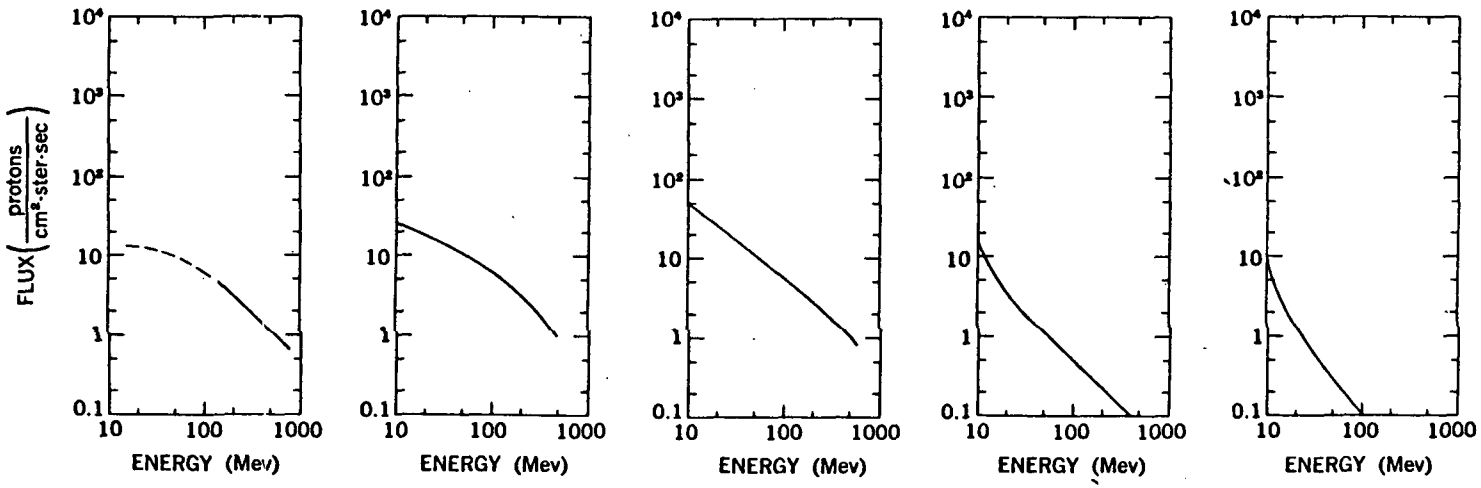

(b) Energy spectra at 2330 UT (+2-1/2 hours); 0140 UT (+4-1/2 hours; 0410 UT (+7 hours); 1730 UT (+20 hours); and 1902 UT (+46 hours)

Figure 2-21—The September 28, 1961 event

steepened with time for the first twelve or more hours of the event. The integral flux above 20 Mev had already begun to decline six hours after the event began.

2115 UT September 28, 1961

The September 28, 1961 event is the first for which there is a detailed energy spectrum, as a function of time from 10-1000 Mev, for a large fraction of the event (Figure 2-21). The data was obtained from instruments flown on Explorer XII by D. A. Bryant et al. (Reference 26). The flare presumed to be associated with the event began at approximately 2215 UT, September 28 and reached its maximum intensity at about 2230 UT. The slope of the integral energy spectrum progressively increased with time in the low energy region until it was approximately as steep as that at high energies. Then there was a general decay with relatively little change in spectral shape above about 30 Mev. In the energy region from 1.5-30 Mev the flux was seen to increase markedly around the time of the sudden commencement and remain at a high level for several hours (References 26 and 72). The fluxes obtained by D. A. Bryant et al. (Reference 26) and O'Brien et al. (Reference 72) in the low energy region are found to be in agreement, within expected uncertainties, with each other and with the fluxes deduced from the riometer absorption curve.

Imaginary Envelope Event

In Figure 2-22 the curves of proton flux as a function of time were drawn so that the integral flux above the indicated energy level would be just slightly larger than in any event ever observed at the corresponding time from the beginning of the flare. Although this imaginary event is based on the best available data, there is, of course, the strong possibility that some past events have been bigger. Also, some future solar outbursts may very well have larger effects.

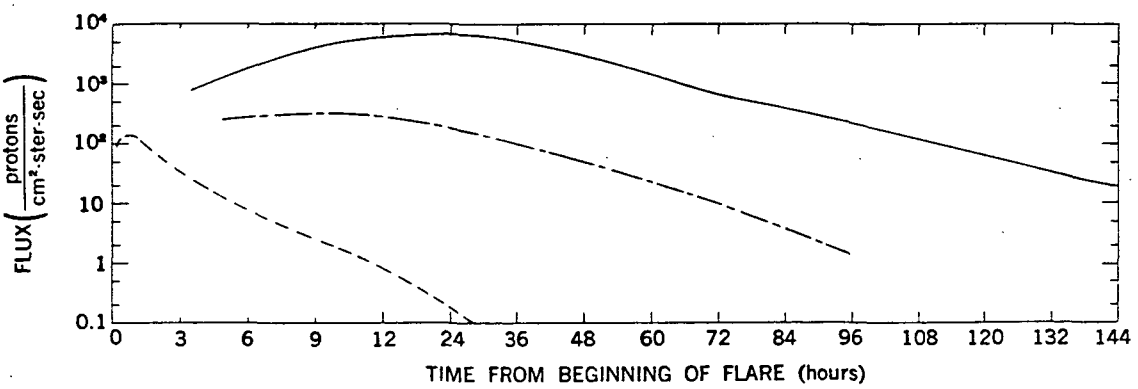

Figure 2-22—The time history of an imaginary envelope event which includes all the types of events observed

ACKNOWLEDGMENTS

The authors are happy to acknowledge the contributions of the following people, many of whom were kind enough to permit the inclusion of unpublished data: P. D. Bhavsar; S. Biswas; D. A. Bryant; L. L. Cline; U. Desai; P. S. Freier; T. R. Hartz; H. Leinbach; W. C. Lin; F. B. McDonald; E. P. Ney; B. J. O'Brien; G. C. Reid; W. Stein; J. A. Van Allen; E. L. Vogan; W. R. Webber; J. R. Winckler.

REFERENCES

1. Forbush, S. E., "Three Unusual Cosmic-Ray Increases Possibly Due to Charged Particles from the Sun," *Phys. Rev.* 70(9 and 10):771-772, November 1 and 15, 1946.

2. Adams, N., "A Temporary Increase in the Neutron Component of Cosmic Rays," *Phil. Mag.* 41:503-505, May 1950.

3. Webber, W. R., "Time Variations of Low Energy Cosmic Rays during the Recent Solar Cycle," in: *Progress in Elementary Particle and Cosmic Ray Physics*, ed. by J. G. Wilson and S. A. Wouthuysen, Amsterdam: North-Holland Publ. Co., Vol. 6, 1962 (In Press).

4. Fichtel, C. E. and Guss, D. E., "Heavy Nuclei in Solar Cosmic Rays," *Phys. Rev. Letters* 6(9):495-497, May 1, 1961.

5. Biswas, S., Freier, P. S., and Stein, W., "Solar Protons and α Particles from the September 3, 1960 Flares," *J. Geophys. Res.* 67(1):13-24, January 1962.

6. Ney, E. P. and Stein, W., "Solar Protons in November 1960," in: *Proc. Internat. Conf. on Cosmic Rays and the Earth Storm, Kyoto, September 1961. II. Joint Sessions*, Tokyo: Physical Society of Japan, 1962, pp. 345-353.

7. Dodson, H. W., "Observation of Loop-Type Prominences in Projection Against the Disk at the Time of Certain Solar Flares," *Proc. Nat. Acad. Sci.* 47(7):901-905, July 15, 1961.

8. Kundu, M. R. and Haddock, F. T., "A Relation Between Solar Radio Emission and Polar Cap Absorption of Cosmic Noise," *Nature* 186(4725):610-613, May 21, 1960.

9. Hachenberg, O. and Krüger, A., "The Correlation of Bursts of Solar Radio Emission in the Centimetre Range with Flares and Sudden Ionospheric Disturbances," *J. Atmos. Terrest. Phys.* 17(1/2):20-33, December 1959.

10. Bachelet, F., Conforto, A. M., and Iucci, N., "Solar Flares with Type IV Radioburst and Transient Phenomena of Cosmic Rays," in: *Space Research, Proc. 1st Internat. Space Sci. Sympos., Nice, January 1960*, Amsterdam: North-Holland Publ. Co., 1960, pp. 662-664.

11. Thompson, A. R. and Maxwell, A., "Solar Radio Bursts and Low-Energy Cosmic-Rays," *Nature* 185(4706):89-90, January 9, 1960.

12. Boischot, A. and Denisse, J.-F., "Les Émissions de Type IV et l'Origine des Rayons Cosmiques Associés aux Éruptions Chromosphériques," *Comptes Rendus, Academie des Sciences* (Paris) 245(25):2194-2197, December 16, 1957.

13. Peterson, L. E. and Winckler, J. R., "Gamma-Ray Burst From a Solar Flare," *J. Geophys. Res.* 64(7):697-707, July 1959.

14. McCracken, K. G. and Palmeira, R. A. R., "Comparison of Solar Cosmic Ray Injections Including July 17, 1959, and May 4, 1960," *J. Geophys. Res.* 65(9):2673-2683, September 1960.

15. Little, C. G. and Leinback, H., "Some Measurements of High-Latitude Ionospheric Absorption Using Extraterrestrial Radio Waves," *Proc. IRE* 46(1):334-348, January 1958.

16. Little, C. G. and Leinback, H., "The Riometer — A Device for the Continuous Measurement of Ionospheric Absorption," *Proc. IRE* 47(2):315-320, February 1959.

17. Bailey, D. K., "Abnormal Ionization in the Lower Ionosphere Associated with Cosmic-Ray Flux Enhancements," *Proc. IRE* 47(2):255-266, February 1959.

18. Reid, G. C., "A Study of the Enhanced Ionization Produced by Solar Protons during a Polar Cap Absorption Event," *J. Geophys. Res.* 66(12):4071-4085, December 1961.

19. Quenby, J. J. and Webber, W. R., "Cosmic Ray Cut-Off Rigidities and the Earth's Magnetic Field," *Phil. Mag.* 4(37):90-113, January 1959.

20. Brown, R. R. and Weir, R. A., "Ionospheric Effects of Solar Protons," *Arkiv för Geofysik* 3:523-529, 1961.

21. Davis, L. R., Fichtel, C. E., et al., "Rocket Observations of Solar Protons on September 3, 1960," *Phys. Rev. Letters* 6(9):492-494, May 1, 1961.

22. Ogilvie, K. W., Bryant, D. A., and Davis, L. R., "Rocket Observations of Solar Protons during the November 1960 Event," in *Proc. Internat. Conf. on Cosmic Rays and the Earth Storm, Kyoto, September 1961. II. Joint Sessions*, Tokyo: Physical Society of Japan, 1962, pp. 317-319.

23. Leinbach, H. and Reid, G. C., "Polar Cap Absorption During the Solar Cosmic Ray Outbursts of July 1959," in: International Union of Geodesy and Geophysics, *Symposium on the July 1959 Events and Associated Phenomena, Helsinki, July 1960*, Paris: Institut Géographique National, 1960, pp. 145-150.

24. Ortner, J., Leinbach, H. and Sugiura, M., "The Geomagnetic Storm Effect on Polar Cap Absorption," *Arkiv för Geofysik* 3:429-434, 1961.

25. Leinbach, H., "Some Observations of Daytime Recoveries During Polar Cap Absorption Events," *Arkiv för Geofysik* 3:427, 1961 (Abstract).

26. Bryant, D. A., Cline, T. L., et al., "Results from the Goddard Cosmic Ray Experiments on Explorer XII," Presented at Explorer XII Symposium, Goddard Space Flight Center, January 1962.

27. Van Allen, J. A., Frank, L. A., et al., "Coordinated Injun I—Explorer XII Observations of Solar Cosmic Rays, 28 September to 4 October 1961," Presented at Explorer XII Symposium, Goddard Space Flight Center, January 1962.

28. Simpson, J. A. and Fenton, K. B., "The Neutron Monitor," Univ. Chicago, 1955 (unpublished).

29. Webber, W. R. and Quenby, J. J., "On the Derivation of Cosmic Ray Specific Yield Functions," *Phil. Mag.* 4(41):654-664, May 1959.

30. Schlüter, A., "Störmer Orbits of Low Energy," *Supplemento al Nuovo Cimento* 8(2):349-357, 1958.

31. Carmichael, H. and Steljes, J. F., "Review of Recent High Energy Solar Particle Events Including November 1960," Atomic Energy of Canada Ltd., AECL-1387 (CRGP-1056) October 30, 1961; Also *Proc. Internat. Conf. on Cosmic Rays and the Earth Storm, Kyoto, September 1961. II. Joint Sessions*, Tokyo: Physical Society of Japan, 1962, pp. 337-344.

32. McCracken, K. G., "The Cosmic-Ray Flare Effect. 1. Some New Methods of Analysis," *J. Geophys. Res.* 67(2):423-434, February 1962.

_____, "The Cosmic-Ray Flare Effect. 2. The Flare Effects of May 4, November 12, and November 15, 1960," *ibid.*, pp. 435-446.

_____, "The Cosmic-Ray Flare Effect. 3. Deductions Regarding the Interplanetary Magnetic Field," *ibid.*, pp. 447-458.

33. McDonald, F. B. and Webber, W. R., "The Variation of the Cosmic Ray Intensity During a Solar Cycle," in: *Space Research: Proc. 1st Internat. Space Sci. Sympos.*, Nice, January 1960, ed. by H. K. Bijl, Amsterdam: North-Holland Publ. Co., 1960, pp. 968-981.

34. Fenton, A. G., Fenton, K. B., and Rose, D. C., "The Variation of Sea Level Cosmic Ray Intensity Between 1954 and 1957," *Can. J. Phys.* 36(7):824-839, July 1958.

35. Winckler, J. R., "Cosmic-Ray Increase at High Altitude on February 23, 1956," *Phys. Rev.* 104(1):220, October 1, 1956.

36. Pfotzer, G., "On the Separation of Direct and Indirect Fractions of Solar Cosmic Radiation on February 23, 1956 and on the Difference in Steepness of Momentum Spectrum of These Two Components," *Supplemento al Nuovo Cimento* 8(2):180-187, 1958.

37. Meyer, P., Parker, E. N., and Simpson, J. A., "Solar Cosmic Rays of February 1956 and Their Propagation through Interplanetary Space," *Phys. Rev.* 104(3):768-783, November 1, 1956.

38. Dorman, L. I., "Cosmic Ray Variations," Moscow: State Publishing House for Technical and Theoretical Literature, 1957; Translation prepared by Technical Documents Liaison Office, Wright-Patterson Air Force Base, 1958.

39. Jelly, D. H., "Compiled Data for Polar Cap Absorption Events Observed at Churchill, June 1957 to June 1960," Canada, Defence Res. Telecommunications Establ. Rept. No. 1062, May 1961.

40. Anderson, K. A. and Enemark, D. C., "Observations of Solar Cosmic Rays Near the North Magnetic Pole," *J. Geophys. Res.* 65(9):2657-2671, September 1960.

41. Leinbach, H., Private Communication.

42. Freier, P. S., Ney, E. P., and Winckler, J. R., "Balloon Observation of Solar Cosmic Rays on March 26, 1958," *J. Geophys. Res.* 64(6):685-688, June 1959.

43. Hultqvist, B., Aarons, J., and Ortner, J., Effects of the Solar Flares of 7 July 1958," *Tellus* 11(3):319-331, August 1959.

44. Charakhch'yan, A. N., Tulinov, V. F., and Charakhch'yan, T. N., "Large Cosmic-Ray Intensity Fluctuations in the Stratosphere," *Zhurnal Eksperimental'noi i Teoreticheskoi Fiziki* 38(4):1031-1036, April 1960 (in Russian); Translation in *Soviet Physics—JETP* 11(4):742-746, October 1960.

45. Rymko, N. P., Tulinov, V. F., and Charakhch'yan, A. N., "A Case of a Sharp Increase in Cosmic-Ray Intensity in the Stratosphere," *Zhurnal Eksperimental'noi i Teoreticheskoi Fiziki* 36(6):1687-1689, June 1959 (in Russian); Translation in *Soviet Physics—JETP* 9(6):1202-1203, December 1959.

46. Anderson, K. A., Arnoldy, R., et al., "Observations of Low-Energy Solar Cosmic Rays from the Flare of 22 August 1958," *J. Geophys. Res.* 64(9):1133-1147, September 1959.

47. Van Allen, J. A., McIlwain, C. E., and Ludwig, G. H., "Radiation Observations with Satellite 1958 ϵ," *J. Geophys. Res.* 64(3):271-286, March 1959.

48. Rothwell, P. and McIlwain, C., "Satellite Observations of Solar Cosmic Rays," *Nature* 184(4681):138-140, July 18, 1959.

49. Freier, P. S., Private Communication.

50. Winckler, J. R. and Bhavsar, P. D., "Low-Energy Solar Cosmic Rays and the Geomagnetic Storm of May 12, 1959," *J. Geophys. Res.* 65(9):2637-2655, September 1960.

51. Ney, E. P., Winckler, J. R., and Freier, P. S., "Protons from the Sun on May 12, 1959, *Phys. Rev. Letters* 3(4):183-185, August 15, 1959.

52. Eriksen, K. W., Holt, O., and Landmark, B., "A Note on the Polar Absorption Event of 11-18 May 1959," *J. Atmos. Terrest. Phys.* 18(1):78-81, April 1960.

53. International Union of Geodesy and Geophysics, "Symposium on the July 1959 Events and Associated Phenomena, Helsinki, July 1960," Paris: Institut Géographique National, 1960.

54. Hartz, T. R. and Vogan, E. L., Private Communication.

55. Winckler, J. R., Bhavsar, P. D., and Peterson, L., "The Time Variations of Solar Cosmic Rays during July 1959 at Minneapolis," *J. Geophys. Res.* 66(4):995-1022, April 1961.

56. Webber, W. R., Private Communication.

57. Brown, R. R. and D'Arcy, R. G., "Observations of Solar Flare Radiation at High Latitude During the Period July 10-17, 1959," *Phys. Rev. Letters* 3(8):390-392, October 15, 1959.

58. Lin, W. C. and Van Allen, J. A., Private Communication; Also, Lin, W. C., "Observation of Galactic and Solar Cosmic Rays from October 13, 1959 to February 17, 1961 with Explorer VII (Satellite 1959 Iota)," State Univ. of Iowa SUI-61-16, August 1961 (Thesis submitted for M. S. degree).

59. Winckler, J. R., Masley, A. J., and May, T. C., "The High-Energy Cosmic-Ray Flare of May 4, 1960. 1. High-Altitude Ionization and Counter Measurements," *J. Geophys. Res.* 66(4):1023-1027, April 1961.

60. Winckler, J. R., Bhavsar, P. D., et al., "Delayed Propagation of Solar Cosmic Rays on September 3, 1960," *Phys. Rev. Letters* 6(9):488-491, May 1, 1961.

61. Winckler, J. R., Bhavsar, P. D., et al., Private Communication.

62. Steljes, J. F., Carmichael, H., and McCracken, K. G., "Characteristics and Fine Structure of the Large Cosmic-Ray Fluctuations in November 1960," *J. Geophys. Res.* 66(5):1363-1377, May 1961.

63. Ogilvie, K. W., Bryant, D. A., and Davis, L. R., "Rocket Observations of Solar Protons during the November 1960 Events, 1," *J. Geophys. Res.* 67(3):929-937, March 1962.

64. Biswas, S., Fichtel, C. E., and Guss, D. E., Private Communication.

65. Lockwood, J. A. and Shea, M. A., "Variations of the Cosmic Radiation in November 1960," *J. Geophys. Res.* 66(10):3083-3093, October 1961.

66. Manzano, J. R., Santochi, O. R., et al., "Cosmic Ray Phenomena during the November 1960 Solar Disturbances," *Notas de Fisica* 7(3):25-43, 1961.

67. Davis, L. R. and Ogilvie, K. W., "Rocket Observations of Solar Protons during the November 1960 Events; 2," *J. Geophys. Res.* 67(5):1711-1716, May 1962.

68. Guss, D. E., and Waddington, C. J., Private Communication.

69. Winckler, J. R., *Internat. Conf. on Cosmic Rays and the Earth Storm, Kyoto, 1961.*

70. Pieper, G. F., Bostrom, C. O., and O'Brien, B. J., "Detection of Low-Energy Solar Protons by Injun Satellite in July, 1961," Private Communication.

71. Fichtel, C. E., Guss, D. E., and Waddington, C. J., Private Communication.

72. O'Brien, B. J., and Van Allen, J. A., Private Communication.

73. Simpson, J. A., "Cosmic-Radiation Neutron Intensity Monitor," in: *Annals of the International Geophysical Year,* London: Pergamon Press, 1957, Vol. IV, pp. 351-373.

74. Jory, F. S., "Selected Cosmic-Ray Orbits in the Earth's Magnetic Field," *Phys. Rev.* 103(4):1068-1075, August 15, 1956.

75. Firor, J., "Cosmic Radiation Intensity-Time Variations and Their Origin. IV. Increases Associated with Solar Flares," *Phys. Rev.* 94(4):1017-1028, May 15, 1954.

76. Finch, H. F. and Leaton, B. R., "The Earth's Magnetic Field — Epoch 1955.0," *Monthly Not., Roy. Astronom. Soc. Geophys. Suppl.* 7(6):314-317, November 1957.

Paper A-5

INFORMATION ON SOLAR PROTON EVENTS (PCA's) DEDUCED FROM RADIO OBSERVATIONS

D. K. Bailey
National Bureau of Standards, Boulder

Solar proton events (SPE's) are generally described (parochially) by ionospheric workers as polar-cap absorption events (PCA's) and (ρddly) by cosmic-ray workers as solar cosmic-ray events. Ionospheric workers, using their traditional tool, the probing radio wave, in quite untraditional ways have been able to contribute in the last decade a considerable quantity of information about the nature and occurrence of these events. Moreover, the radio observations have been made continuously at fixed positions, whereas observations with particle detectors in balloons, rockets, and satellites are conspicuously lacking in continuity, either in space or time. Ground-based cosmic-ray monitors, while operating continuously, detect less than one-fifth of the events that are of interest in connection with the problem of radiation hazards in space.

The radio techniques do not observe directly the incoming protons, but rather observe the effects on the propagation of waves resulting from the abnormal ionization produced by the incoming protons in a height region from about balloon ceiling (30 km) to the E layer (110-120 km). This abnormal ionization is most important between about 45 and 85 km insofar as its influence on radio waves passing through it is concerned. Radio observations are capable of yielding quantitative information, not only about the onset and duration times of individual events but also, if carried on simultaneously at several suitably placed locations and with more than a single frequency, about departures from isotropy of the arriving protons and about the instantaneous spectrum and thus its time variation.

Until recently the radio techniques employed in the study of solar proton events have involved equipment that was designed for other purposes, and often only accidentally situated in favorable geographic positions. Thus one of the potentially most sensitive radio techniques, that of measuring phase and amplitude over short, high-latitude paths at low and very low frequencies, has scarcely been employed. On the other hand, because of great interest in the polar ionosphere and in auroral effects, there has been for many years, but especially during and since the IGY, an excellent network of high-latitude ionosondes and a fair network of fixed-frequency riometers. Some of the most valuable and certainly the most extensive and continuous observations have been obtained as a by-product of the desire of the USAF to have a communications system in the North Atlantic and Greenland region that would be immune to the aurorally associated polar blackouts. This system employing ionospheric-scatter propagation consists of five links, three of which have ionospheric midpoints inside the polar cap. The two remaining have ionospheric midpoints well outside the auroral zone but still in high latitudes. Continuous data, beginning in January, 1954, from several or all of the links of this system have been made available and have been analyzed for PCA events. Prior to January, 1954, similar

data exist from fewer links operating for the most part at higher and somewhat less sensitive frequencies. These earlier data extend the continuous period of study back to late 1951. Thus an entire solar cycle has been examined by the ionospheric-scatter technique.

The interpretation of this long series of ionospheric-scatter observations is continuing. It has been clarified by the simultaneous observations of certain of the more recent solar-proton events by riometers, and especially by particle detectors operated at high latitude at both balloon and rocket altitudes.

In order to assess and therefore to make sound decisions concerning the radiation hazard posed by solar-proton events, it is necessary to know their characteristics at the top of the polar atmosphere, or more generally in space at a distance from the earth such that the earth and its magnetic field no longer significantly affect the flux. Thus it is necessary to know:

1. The frequency of occurrence of solar proton events in relation to the solar cycle,

2. The statistics of occurrence of SPE's of different magnitudes described in terms of the evolution of their energy spectra from onset to the end of the period of detectability,

3. The statistics of the significant departures from nearly pure proton fluxes,

4. The statistics of departure from isotropy in space as indicated (a) at and near sunspot maximum, by differences in onset characteristics at different locations, and (b) at and near sunspot minimum, by evidence of impact zones and by evidence of much reduced "storage,"

5. The predictability of discrete events, and

6. The limitations on predictability.

The PCA observations by the ionospheric-scatter technique provide sound answers to (1) and partial answers to (2) and (4). They do not at present contribute much toward an answer to (3). Taken together with other solar observations they permit answers to (5) and (6). These latter answers, however, will perhaps not be well received. The nature of these various answers and partial answers will be described.

Paper A-6

STATISTICAL PREDICTION OF SOLAR PROTON EVENTS

James B. Weddell
North American Aviation, Inc., Downey, Calif.

Abstract

A method of correlating solar flares in time with several indices of activity of solar regions is described. The method determines the probability of occurrence of a flare if each of two indices exceeded given limits, and the average time between measurement of these indices and the outbreak of the flare. Significant correlations are listed; the most important is the tendency for major flares to occur in the second passage across the solar disk of regions exceeding 2000 millionths of the solar hemisphere in area, and which gave rise to small flares during their first passage. These criteria permit prediction of 69% of class 3 flares at least 14 days in advance. Flare positions have been correlated with the magnetic field in active regions. The field near the sites of flares tends to be frozen into the solar atmosphere to a greater extent than other portions of the field.

Introduction

The ability to predict the emission of energetic protons from the sun may eliminate or reduce the shielding requirements of manned space vehicles. If such prediction is to be useful, it must cover a time interval at least long enough for the crew to terminate their mission and return to earth after a warning of danger is made. The prediction method should seldom give false alarms which prevent space flights during periods free from solar proton events.

One present technique[1] uses sunspot penumbral areas to predict major solar flares, with which proton events are sometimes associated. This method permits flare prediction for only three days at a time. Another method[2], based on the areas and durations of calcium plage regions, gives five-day forecasts of "safe" periods during which no flares will occur. The areas and durations of many plage regions are such that safe periods cannot be forecast, although no flare actually occurs; the fraction of predicted safe time is thus greatly reduced near maxima of solar activity. Both of these methods are concerned only with observations made during a single rotation of the sun.

---

[1] K.A. Anderson, "Preliminary Study of Prediction Aspects of Solar Cosmic Ray Events," NASA Technical Note D-700, (April 1961).
[2] J.W. Evans, Private communication.

Correlation Method

We have developed a method of correlating the occurrence of flares with combinations of several indices of solar activity measured by arbitrary times before a flare. By simultaneously correlating several characteristics of a solar active region, we can more nearly identify the necessary and sufficient conditions for a major flare or proton event. By relating the times of occurrence of flares to the times of observation of the corresponding active regions during previous rotations of the sun, we open the possibility of predicting flares three weeks or more in advance.

Solar activity indices studied thus far include the area, central intensity, and duration of calcium plages, the duration of 200-Mcs and 3300 - Mcs radio noise emission from active regions[3], and the longitudinal component of the magnetic field in active regions. The area and duration of flares and their accompaniment by proton events have been considered. Published sources of data are listed as references[4-7].

To illustrate the correlation method by a hypothetical example, let A and B be two quantitative measures of active solar regions (e.g., the area of a plage region and its brightness temperature in 3300 - Mcs radio emission). Let a_1, a_2, ... , a_n be the magnitudes of A measured at times t_1, t_2, ..., t_n; let b_{n+1}, b_{n+2}, ..., b_{2n} be the magnitudes of B measured at times t_{n+1}, t_{n+2}, ..., t_{2n}. Some measurements of A and B may have been simultaneous. Let f_{2n+1}, f_{2n+2}, ..., f_{3n} be the magnitudes of some aspect of a flares (e.g., its area) measured at times t_{2n+1}, t_{2n+2}, ..., t_{3n}. We require:

$$t_{2n+K} > t_{n+K} \geqslant t_K,$$

$$1 \leqslant K \leqslant n.$$

The probabilities of the following events are calculated:

P(A,F): A is followed by a flare (i.e., in the region at which phenomenon A was observed).

P(B,F): B is followed by a flare.

P(A∩B,F): A is followed or accompanied by B, and B is then followed by a flare.

[3] G. Swarup, "Stanford Microwave Spectroheliograms for 1960 July," Stanford University, Stanford, Calif. (March 1962).

[4] "Compilations of Solar-Geophysical Data," Central Radio Propagation Laboratory, National Bureau of Standards, Boulder, Colo., (July 1957 to date, monthly).

[5] H.W. Dodson and E.R. Hedeman, "IGY Working List of Solar Flares," Mc Math-Hulbert Observatory, Pontiac, Mich., (1962).

[6] "Quarterly Bulletin on Solar Activity," Eidgenössiche Sternwarte, Zürich, Switzerland, (1917 - 1956).

[7] "Cartes Synoptiques de la Chromosphère Solaire et Catalogue de la Couche Superieure," Observatoire de Meudon, Paris, (1917 - 1956).

Lower limits a', b', and f' may be placed on a, b, and f. For example, the probability may be calculated that plages at least as large as 2000 millionths of the solar hemisphere have brightness temperatures at 3300 Mcs of at least 10^5 deg K, and that if so these regions are sites of flares at least as large as 10 sq deg.

Considering the j sets of observations for which $a_i \geq a'$, $b_{n+i} \geq b'$, $f_{zn+i} \geq f'$, the r.m.s. average time differences

$$\bar{t}_A = \left[\frac{1}{j} \sum_{i=1}^{j} (t_{2n+i} - t_i)^2 \right]^{\frac{1}{2}} , \qquad (2)$$

$$\bar{t}_B = \left[\frac{1}{j} \sum_{i=1}^{j} (t_{2n+i} - t_{n+i})^2 \right]^{\frac{1}{2}} , \qquad (3)$$

and the respective standard deviations

$$\sigma_A = \left[\frac{1}{j} \sum_{i=1}^{j} (t_{2n+i} - t_i - \bar{t}_A)^2 \right]^{\frac{1}{2}} , \qquad (4)$$

$$\sigma_B = \left[\frac{1}{j} \sum_{i=1}^{j} (t_{2n+i} - t_{n+i} - \bar{t}_B)^2 \right]^{\frac{1}{2}} \qquad (5)$$

are calculated. In our example, we find the r.m.s. average times between flares and the measurement of plage areas, and between flares and the measurements of radio brightness temperature, as well as the standard deviations of these times.

If $P(A \cap B, F) > 1/2$, $\bar{t}_A > 2\sigma_A$, and $\bar{t}_B > 2\sigma_B$, we consider that a statistically significant positive correlation exists, and that observations of A and B permit prediction of flares at least for time in advance.

Results

The following results have been obtained up to October 1962 on the basis of about 350 flares of class 2 and greater during 1958 through 1961:

1. The fraction of flares of class 2 and greater occurring at plages making at least the second passage across the disk was 0.67. The average time of the flare was 27 ± 4 days after the central meridian passage of the plage on the rotation previous to the flare.

2. The fraction of class 3 and 3+ flares occurring at plages making at least the second passage was 0.78.

3. The fraction of flares of class 2 and greater occuring at plages larger than 2000 millionths of the solar hemisphere was 0.91.

4. The fraction of flares of class 2 and greater occuring at plages which had been the sites of flares of any class during the previous rotation was 0.88.

Preliminary Prediction Method

If a plage region is the site of any flare during its first passage across the disk, and has an area of at least 2000 millionths of the solar hemisphere at its first central meridian passage, a warning of a major flare during the next rotation may be issued. This warning will include about 60% of flares of class 2 and greater, and 69% of class 3 and 3+ flares. Flares which occur by coincidence at other regions will increase the apparent accuracy of the warning.

The "false alarm" frequency of this prediction method has not been evaluated. The original warning covers the interval between the 21st and the 35th day after it is issued. When the active region reappears on the east limb of the sun on the 21st day following its first central meridian passage, the warning may be cancelled if either

(a) The plage area is smaller than 2000 millionths of the solar hemisphere, or

(b) the active region is free from sunspots.

Such cancellations reduce the effect of false alarms on the fraction of time during which space flight may be undertaken.

Relationship of Flares to Magnetic Field

The prediction method just tentatively proposed fails to predict a significant fraction — about 30% — of class 3 and 3+ flares. It may result in frequent false alarms, since some large active regions which are sites of flares during their first passage across the solar disk may not give rise to major flares during subsequent rotations. This method predicts flares rather than proton events, but it is known that some major flares are not associated with energetic protons near the earth. In order to overcome these limitations and to gain physical insight into the role of proton events in the total process of solar activity, we have begun a correlation of proton-event flares and other large flares with solar magnetic fields.

Solar magnetograms[8] obtained at Mount Wilson Observatory[9] were reproduced. The solar magnetograph measures the component of the magnetic field at the reversing layer in the observer's line of sight. Isogauss curves, or lines of constant magnetic field, were constructed from the magnetrograms. The position of a major flare associated with a given active region was translated in heliographic longitude to compensate for solar rotation between the time of occurrence of the flare and the time of measurement of the magnetic field.

---

[8]H.W. Babcock and H.D. Babcock, Publ. Astron. Soc. Pacific 71, 165 (1959).
[9]H.W. Babcock, Astrophys. J. 118, 387 (1953).

Figure 1 is a typical family of isogauss curves of a single active region. Two flares which occurred within a few days of the date of the magnetogram are shown; the crosses indicate the translated points at which the flares broke out, and the circles have areas equal to the maximum extent of the flares. It is not surprising that the points of outbreak of the flares lie very nearly on the line of zero longitudinal magnetic field. This is in accord with the observation of Severnyi[10] that flares break out beneath the highest points of dark filaments and loop prominences; these points correspond to zero radial magnetic field. Near the center of the solar disk, the radial and longitudinal components of the field are equivalent.

Figure 2 is the family of isogauss curves. Curves of the same region that was shown in Fig. 1, but measured during the previous solar rotation; this was the first passage of the region across the disk. The translated flare positions are also shown, and they again lie near the line of zero longitudinal magnetic field. This shows that the line of zero field in the vicinity of the flare sites is stationary relative to the material of the reversing layer. The other parts of the line of zero field, as well as the isogauss curves of non-zero field, exhibit marked displacement and distortion in the course of one solar rotation.

Let us list some alternative conditions which could cause parts of the line of zero field to be stationary in the ionized gaseous medium containing the field. An approximate condition for a magnetic field to be frozen into a plasma is that the magnetic Reynolds number[11]

$$R_m = \mu \sigma u L \gg 1 \qquad (6)$$

where μ is the magnetic permeability, σ is the electric charge density, u is the transport velocity of the plasma, and L is the length such that

$$\frac{F_m}{F_d} = \frac{JBL}{\rho u^2} \qquad (7)$$

In Eq. 7, F_m is the magnetic force exerted on the plasma, F_d is the dynamic force exerted on the plasma due to gravity, pressure gradients, and radiation pressure; J is the electric current density, induced in the plasma by its motion in the field, B is the magnetic field intensity, and ρ is the mass density of the plasma. Now

$$J = K \sigma u B \quad , \qquad (8)$$

where K is a constant, so

$$R_m = \frac{F_m \rho \mu u^2 K}{F_d B^2} \qquad (9)$$

Since the plasma is in approximate dynamic equilibrium near the flare sites, F_m and F_d are comparable in magnitude and their ratio varies slowly with position

[10] A.B. Severnyi, Soviet Astron. 1, 668 (1957).
[11] J.E. Drummond, "Plasma Physics," pp. 172-3 McGraw-Hill Book Co.,

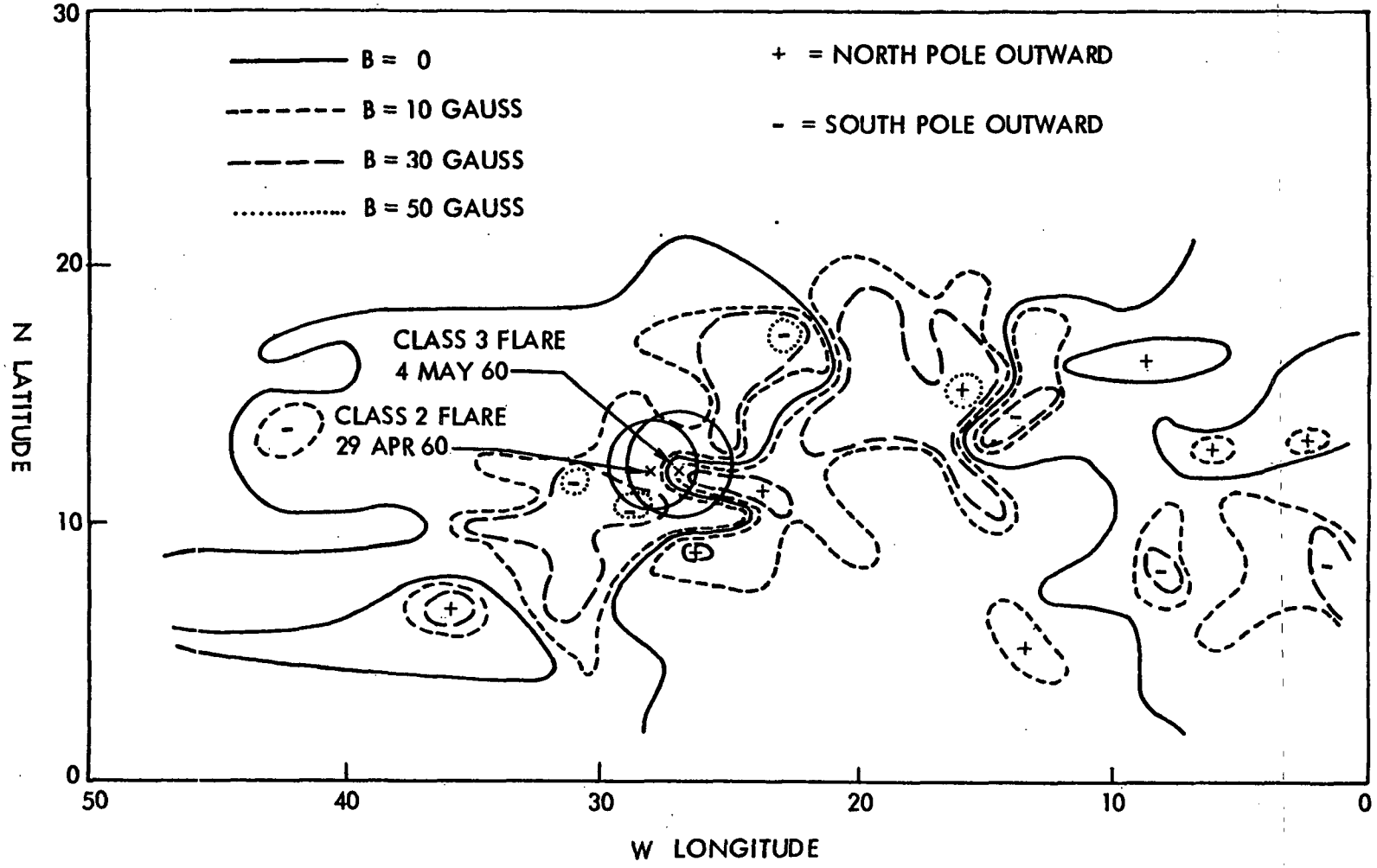

Figure 1. Isogauss Curves of McMath Region 5642. 29 April 1960

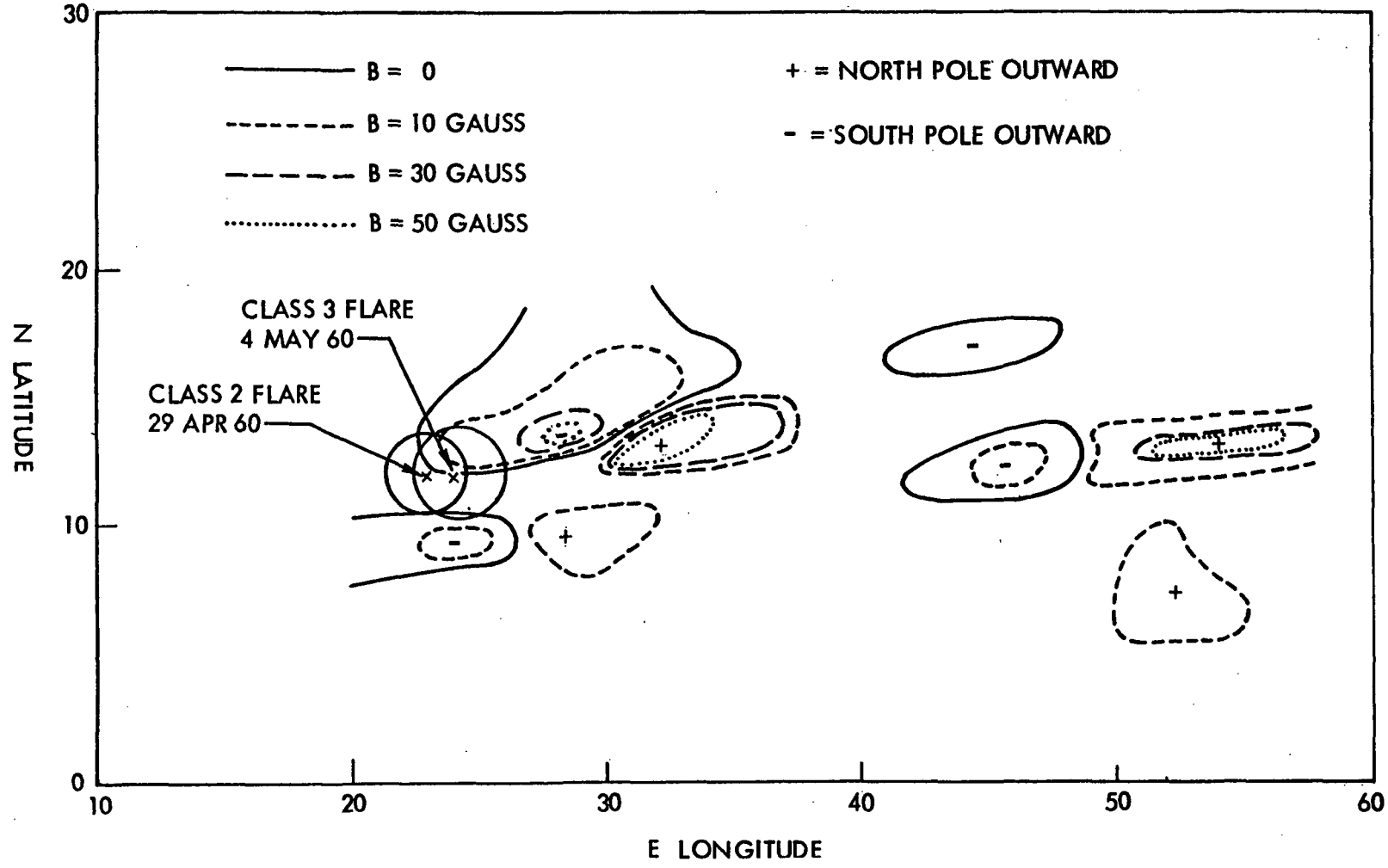

Figure 2. Isogauss Curves of McMath Region 5616, 29 March 1960

and time. If B is small, R_m is obviously large. But the total magnetic field is not necessarily small along lines where the longitudinal component of the field is zero. The transport velocity of the plasma is small, as evidenced by its rather steady participation in the rotation of the sun. The remaining way in which R_m can be large is for the plasma density ρ to be large.

Measurement of the transverse component of the magnetic field, or of the density in the reversing layer and lower chromosphere, would shed much light on this problem. Magnetograms of regions near the limb measure the component of the field tangential to the sun and in the line of sight. These magnetograms can be compared to those of the same region near the central meridian. If it is assumed that the field is essentially constant in magnitude and direction for 5 or 6 days, two of the three components of the field can be inferred.

It must be pointed out that the correlation of flare positions with magnetic field patterns does not yet include a statistically significant number of cases. The magnetic characteristics which are conducive to major flares or to proton events remain to be identified. The further study of magnetism in active solar regions is expected to improve the prediction of proton events and to increase our understanding of the behavior of the sun.

Acknowledgements

The author is indebted to Robert Howard of Mount Wilson Observatory, who made available the original magnetograms. He appreciates valuable discussions with Helen Dodson of Mc Math-Hulbert Observatory, and John W. Evans and Edward Dennison of Sacramento Peak Observatory.

Paper A-7

COMMENTS ON THE PRODUCTION OF SOLAR HIGH ENERGY PARTICLES

M. C. Chapman, R. E. Fortney, and M. R. Morrison
Northrop Space Laboratories

Abstract

A general qualitative model for the production of solar high-energy particles (SHEP) which can explain several observed flare phenomena is used in the analysis of a specific flare event. The model, incorporating the work of several Russians and Americans, explains the occurrence of solar radio emission, the initial anisotropic and later isotropic distribution of flare particles, Forbush decreases in cosmic ray intensity, decreases in cosmic radio noise, and fluctuations in the earth's magnetic field due to solar flare particles. Also qualitatively explained are such phenomena as the occurrence of shock waves during flare events, observed surges in the active region, and movement of magnetic "bumps" before the start of the flare. The model may be briefly described as follows: magnetic fields in active region contain "bumps" which move toward nodal points in the field. A conversion of energy can occur by the annihilation of magnetic fields and the contraction of the conducting medium. This contraction results in a shock wave which propagates opposite to the flow of gas. High temperatures behind the shock wave allow thermonuclear reactions to occur, producing particles which are further accelerated by the moving magnetic walls. The plasma between the magnetic walls is expelled perpendicular to the compression and carries "frozen-in" fields with it into the upper chromosphere or corona. This extended field-plasma-particle region constitutes the magnetic trap above the region from which it was generated, and determines the spectra of particles leaking from it. Energetic particles accelerated by the shock fronts fill the region and cause it to expand with an increase of energy; however, the high energy particles are not easily trapped and can escape, decreasing the energy and causing the trap to contract. This contraction will lead to further acceleration of the remaining particles. The non-equilibrium fluctuation will continue until particle diffusion does not change the energy sufficiently to cause large scale variations in

pressures. The initial ejection of the high energy particles could occur in fast bursts, after which the trapping region would assume a quasi-equilibrium configuration; a slower diffusion of less energetic particles will now occur. The trap, situated in the magnetic fields of the active region, is carried out into space by the solar corpuscular streams; as the region moves outward the volume increases (perhaps eventually encompassing the earth) and the field strength decreases, so that the trapping effectiveness is reduced and the particles escape easily into the stream.

Introduction

In commenting on the production of high energy particles from the sun, one is led to a reverse analogy using the case of particle accelerators here on earth. The accelerators were developed over a period of years and are well understood, while the particles emerging from the beam target are still being investigated. In the case of solar flares we have information on the particles from the beam after it strikes the target (the earth), however, the method of accelerating these particles is still not well understood.

This paper will present a model for the production of high energy particles from flares on the sun, and using published experimental data, will show the consistency of the model with observations.

Sections will be devoted to background information on solar physics, production of SHEP (solar high energy particles), and experimental verification.

Background

A brief discussion of the sun is now presented as background information on the environment in which flares occur.

It is convenient to divide the sun into four concentric regions with more or less well-defined properties (Figure 1);[1] these are the interior, the photosphere, the chromosphere, and the corona. The interior may be

---

1. Goldberg, L., "The Sun," Science in Space, Chap.VI, National Academy of Sciences - National Research Council, Washington, D.C., 1960.

subdivided further into (a) a core, in which radiant energy is produced by thermonuclear reactions, predominantly near the center, and through which it travels by radiative transfer toward the outside; and (b) a convective layer which extends to just below the visible exterior and is probably no more than 1/5 the radius thick. The temperature, pressure, and density decline through the interior from extremely high values at the center to relatively low values at the visible surface.

The photosphere is the apparent surface from which practically all optical radiation comes. The radiation contains contributions from many different layers, but its intensity is approximately equal to that radiated by the gas at an optical depth of one. At one A.U. a layer of unit optical depth seen edge-on subtends less than 1" of arc, and therefore appears sharp. The continuous spectrum of this radiation is a mean of near black-body radiation whose temperature ranges from perhaps 4500°K to 7500°K; the resulting blended spectrum resembles that of a black body near 6000°K at the center of the disk, while near the limb, along oblique lines of sight where the contribution of the deeper, hotter layers is proportionately less, the continuous spectrum corresponds to a lower temperature. The effective temperature which most nearly matches the continuous spectrum of sunlight integrated over the whole visible disk is about 5750°K.

The photosphere appears to be mottled with small areas slightly hotter and brighter than their surroundings and having a mean lifetime of several minutes. These granules appear to be regions where currents emerge with upward velocities of the order of 1 km/sec. The photosphere also is the region where sunspots and faculae are located.

The chromosphere is a thin transition region lying between the relatively cool outer layers of the photosphere and the million-degree corona. It is extremely inhomogeneous, and small volumes are far from being in a steady state. The normal structure of the chromosphere consists of fairly closely packed spicules - small jet-like prominences with lifetimes of the order of several minutes and upward velocities of the order of 20 km/sec - whose tops reach a height of roughly 10,000 km. The appearance of the chromosphere in the light of H-α has been compared to a prairie fire. There is little uniformity of opinion for a model of the chromosphere except perhaps on the following: the region below 6000 km is complex and inhomogeneous, probably comprising cells of high and low temperature, perhaps as different as 30,000° and 4000°; in the upper chromosphere the temperature rises steadily and rapidly to several hundred thousand degrees at the base of the corona. There is no sharp division between the top of the chromosphere and the base of the corona

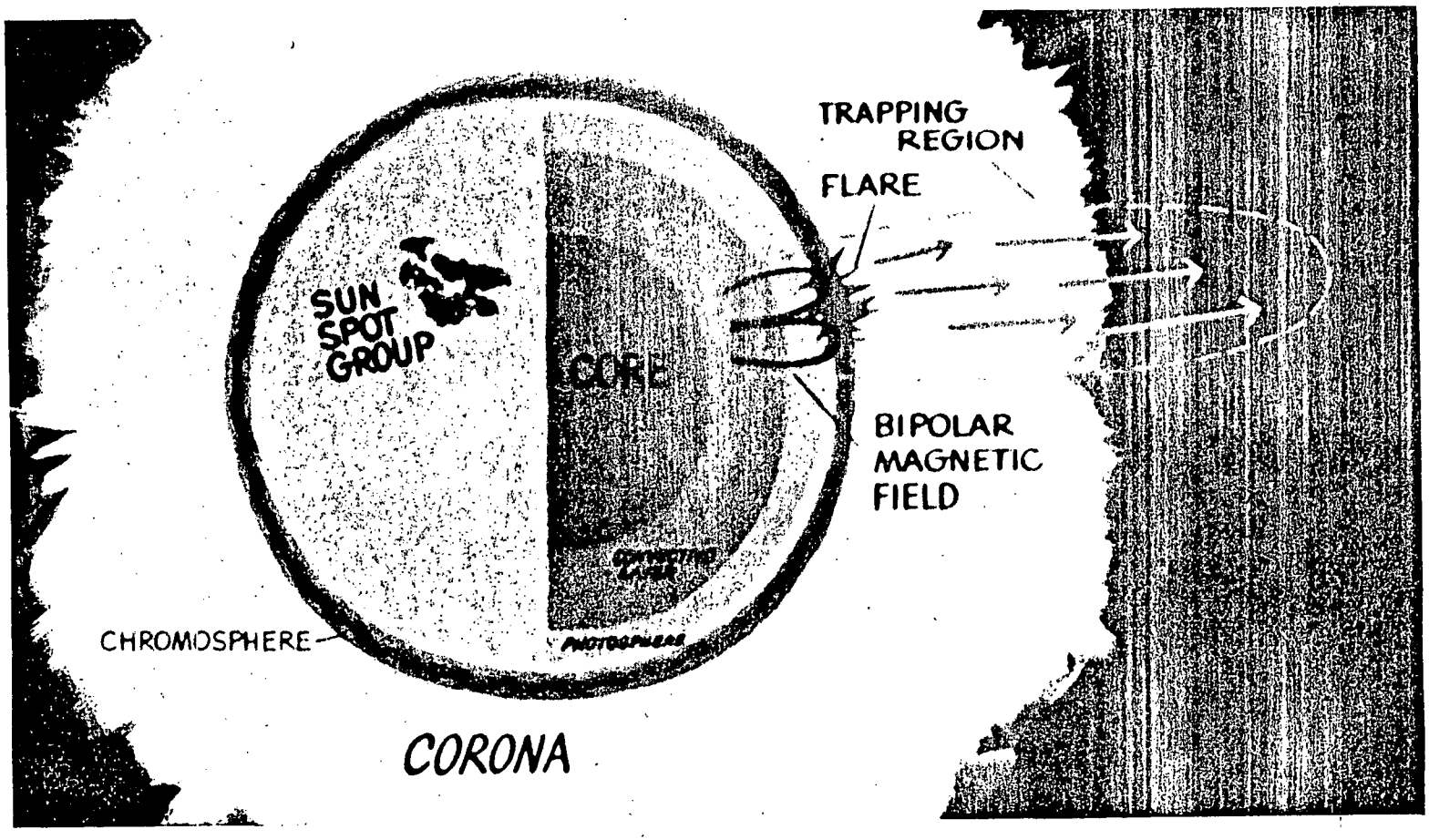

Figure 1. Structure of the Sun

since the tops of spicules sometimes project into the corona. Types of activity associated most closely with the chromosphere are flares, plages, and prominences.

The corona is the very tenuous outer atmosphere of the sun, which can be traced out into space for a distance of several solar radii. The intensity of coronal light is approximately 10^{-6} of the total sunlight, and most of this is continuous radiation from the photosphere scattered by electrons of the corona. Most of the sun's x-radiation originates in the corona and in certain active regions of the chromosphere. The kinetic temperature of the corona is of the order of 10^{6}°K.

The corona exhibits a considerable amount of both regular and irregular structure. The regular structure goes through a cycle in phase with the 11-year activity cycle, such that at sunspot minimum the corona shows broad extensions above the equatorial region and fine striated streamers fanning out from each pole, while at sunspot maximum the structure is more nearly the same over equator and pole, with polar streamers less pronounced. The corona also shows localized inhomogeneities, such as regions of greater radio opacity, and "hot spots" over regions of obvious activity in the chromosphere.

The sun's magnetic field can be approximated as an axisymmetric dipole field with a mean intensity in the photosphere of the order of 1-2 gauss. The field is assumed to be generally radial at the orbit of the earth, but at a distance somewhere between the orbits of Mars and Jupiter, it is assumed to become disordered from spiralling due to the sun's rotation.

All internal lines of force are assumed to lie in a relatively thin submerged layer at a depth of the order of 0.1 R that stretches between $\pm$ 55° latitude. H. W. Babcock[2] has shown how the magnetic lines of force are twisted due to the sun's rotation and then are floated to the surface of the photosphere and emerge as bipolar magnetic regions. These regions are associated with sunspots and may exist in varying forms of complexity. Therefore the sunspots themselves are classified according to these magnetic fields: α = unipolar, β = bipolar, γ = complex, and $\beta\gamma$ = semicomplex. The following is a qualitative description of the four basic spot types.

α : Unipolar groups are single spots or groups of spots having the same magnetic polarity.

β : Bipolar groups in their simplest form consist of two spots of opposite polarity. Often the bipolar group is a stream of spots.

---

2. Babcock, H. W., "The Topology of the Sun's Magnetic Field and the 22-Year Cycle," Mount Wilson and Palomar Observatories, Carnegie Institute of Washington, California Institute of Technology, 1960.

$\beta\gamma$: Semicomplex groups have bipolar characteristics, but no clearly marked dividing line between the spots of opposite polarity

γ : Complex groups have polarities so irregularly distributed that they cannot be classified as bipolar; sharply bounded regions of opposite polarity sometimes exist within the same penumbra.

The sunspots and their associated magnetic fields furnish the environment for the catastrophic disturbances known as solar flares. The flare occurs usually with a sudden onset near the neutral point (boundary) between two opposing spot-connected fields where the local field intensity is close to zero.[3] The region occupied by the flare expands during the lifetime of the flare ($\simeq 10^3$ sec), with velocities of several km/sec, and may attain linear dimensions of 10^{10} cm, and it is assumed that the depth of the region is of the order of 5×10^8 cm. Thus, a flare volume may be $V \approx 5 \times 10^{28}$ cm^3.

The energy radiated by the flare may best be described in the following breakdown:

- The visible radiation has been observed to be of the order of magnitude of $10^{27} - 10^{28}$ ergs.
- The energy of X-radiation has been observed to be also $\approx 10^{27} - 10^{28}$ ergs.
- The energy carried away by SHEP's is approximately $10^{31} - 10^{32}$ ergs.
- The energy release from decreases in magnetic field gradients in the flare region is roughly $10^{27} - 10^{28}$ ergs.
- The thermal energy is of the order of $10^{27} - 10^{28}$ ergs.

---

3. Chapman, M. C., and Morrison, M. R., A Summary of Natural Particulate Radiation in Space, ASD-TDR-62-606, p. 35 (1962).

A short development of solar flare phenomena as seen from the earth, would be as follows (Fig. 2).[4] The flare is observed usually at time 1 hour to emit light in the optical, ultraviolet, and X-ray regions of the electromagnetic spectrum (Profile 1). These emissions rise rapidly to a peak and then die off within a few hours. At the same time, bursts of high frequency radio emission are observed (Profile 2), exhibiting approximately the same rise and decay profile as the optical emissions. Low frequency emissions (Profile 3) also occur in burst form and with a total intensity rise time similar to the previous effects, but the maximum of the profile is longer and the decay in time is slower, persisting for as long as 12 hours.

Solar high energy particles (SHEP) are observed to arrive over the poles of the earth some time after the electromagnetic observations of the flare event, this delay being due to propagation times greater than that required for electromagnetic radiation. The SHEP intensity (Profile 4) is observed to have a sharp rise time with irregular fluctuations near the maximum, and then to decay slowly with time; the effects still being observed for periods as long as days.

Profile 7 shows that the earth's magnetic field is undisturbed by the previously discussed effects (Profiles 1 through 4). However, at some time which may be 24 hours after the observed flare, the geomagnetic field suffers violent fluctuations. This effect is due to a solar plasma of low energy charged particles (protons and electrons) colliding with the earth's field, and causing it to contract, deform and spring back. The effect of the perturbed geomagnetic field on SHEP arrival is indicated in Profile 4. The structure observed at times 30 through 38 hours depicts the arrival of SHEP over regions on the earth at low latitudes, where they were previously forbidden due to the geomagnetic cutoff of the particles.

The galactic cosmic ray intensity (Profile 5) follows the same general form as does the earth's magnetic field. The decrease in cosmic ray intensity is caused by the particles being deflected by magnetic fields "frozen" in the solar plasma. Thus, when the solar plasma has reached the earth's field and perturbed it, many of the galactic cosmic rays in the vicinity of the earth cannot penetrate both the plasma and the field, and the previously observed intensity decreases. As the solar plasma passes the earth, both the geomagnetic field and the cosmic ray intensity recover and approach normal levels.

The cosmic radio noise (Profile 6) is affected by arrival of three emissions from the sun, i.e., ultraviolet and X-rays, SHEP, and solar plasma. Since these radio emissions must penetrate the ionosphere, the conditions there greatly influence their propagation. Coincident with the

---

4. Ibid., p. 32-35.

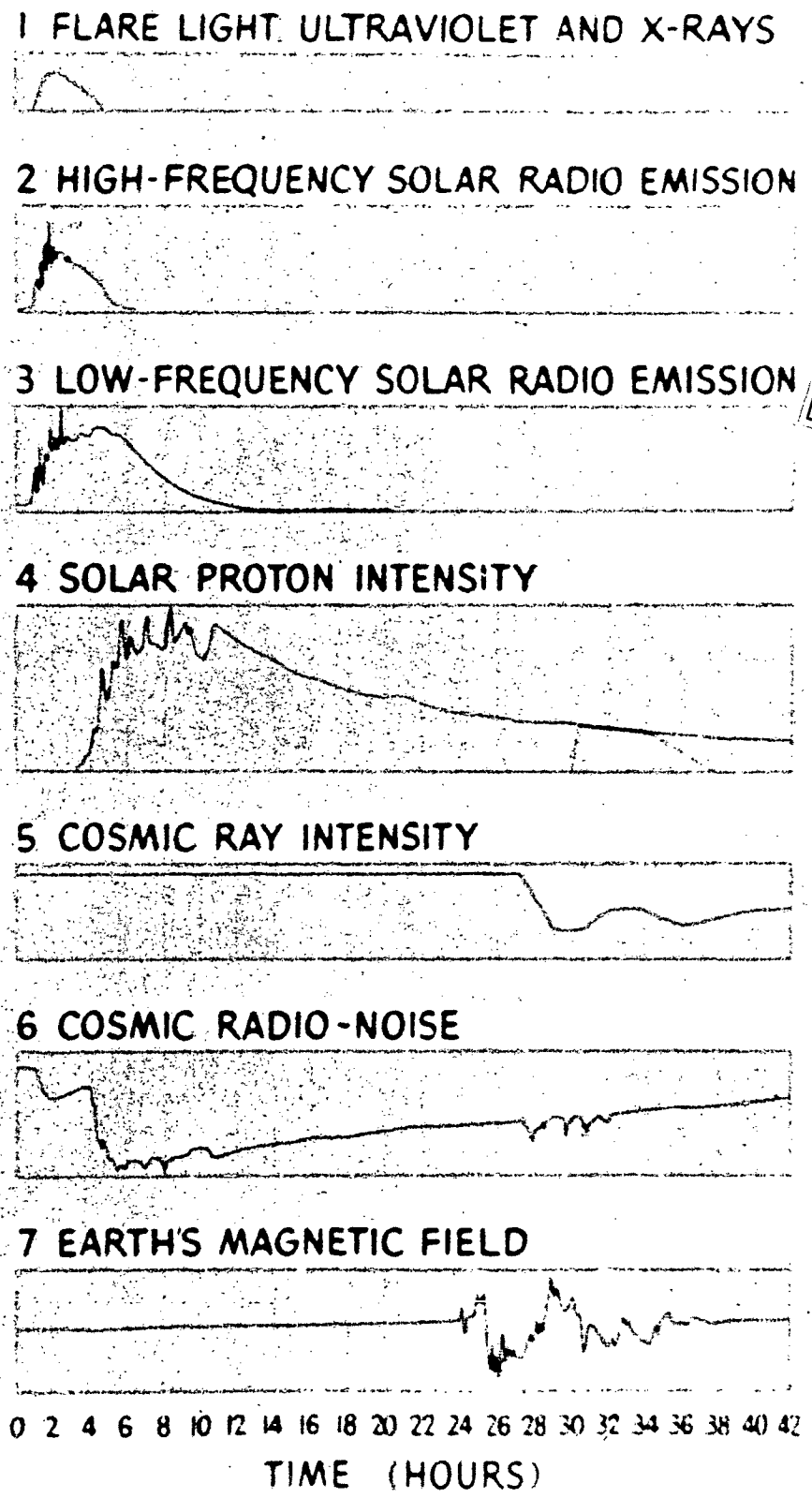

Figure 2. Development of a Solar Flare Event

emission of X-rays from the sun (allowing for a time of flight to the earth of 8 minutes), the reception of cosmic radio noise is decreased (times 1 through 4 hours). This is due to the increase in ionization in the ionosphere caused by the solar ultraviolet and X-rays, making it more opaque to transmission of the radio signals. This opacity is further increased by the arrival of the SHEP (times 4 through 24 hours) which produce additional ionization. The fine structure fluctuations in the recovery of the radio noise reception (times 27 through 32 hours) is due to the solar plasma disturbing the field and allowing additional particles to be dumped into the ionosphere, producing more ionization and thus increased opacity.

It can be seen that solar flare events produce varied geophysical phenomena and greatly influence the space environment, and with the advent of space exploration, flares are being studied with increased interest due to the radiation hazard they present to both manned and unmanned space flight.

SHEP Production Model

A. Energy Conversion

The flare event has its "roots" deep in the photosphere, actually occurs in the chromosphere, and extends into the corona. The flare processes that occur in the photosphere are not well known; however, it is thought that either ring currents are generated which rise into the chromosphere, or mutual destruction of magnetic fields leads to the observed chromospheric effects. The result of either of these two processes is a change in the configuration of chromospheric magnetic fields. Obviously, emergence of ring currents will produce this effect. However, the self-destruction of fields is a very attractive hypothesis, and could occur in the following manner.[5] Two tubes of a magnetic field could combine under favorable conditions, resulting in a destruction of a part of the field. These conditions require that two tubes collide such that the transverse components of the fields are parallel, and the longitudinal components antiparallel. If the gas conditions are favorable for field diffusion, i.e., low temperature and ionization, then the "inner" transverse field would diffuse and result in a decrease of the magnetic pressure in the gas, which would then contract due to the greater "external" magnetic field pressure. If this process were to occur in the chromosphere where the gas density is low and the internal field pressure is a large part of the total internal pressure, the destruction of this field would allow contraction and heating of the region. This heating would increase the conductivity and thus inhibit the magnetic field diffusion. This restriction does not occur in the photosphere, where the particle density is high and thus the internal thermal energy is greater than the internal field energy. These fields are relatively free to diffuse, and large contractions of the region will not result. However, since the chromospheric fields are rooted in this region, a relatively small

---

5. Shabanskii, V. P. "On the Origin and Evolution of Solar Flares and the Generation of Cosmic Rays in Them," Soviet Astronomy - AJ, Vol. 5, No. 5, March-April 1962.

SHEP PRODUCTION

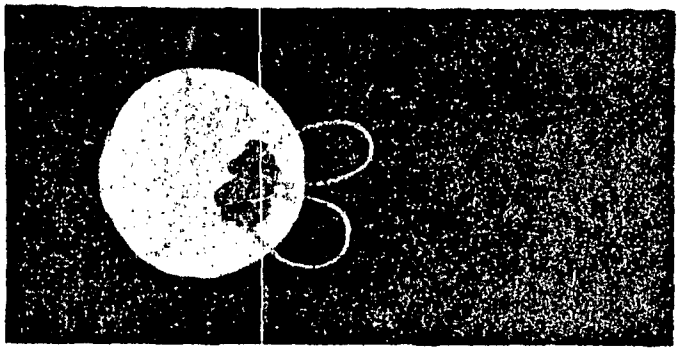

SUNSPOT GROUP WITH TWO BIPOLAR MAGNETIC FIELDS. MOVEMENT OF MAGNETIC BUMPS TOWARD NODAL POINT OF FIELD RESULTING IN SHOCK WAVES & BEGINNING OF FLARE.

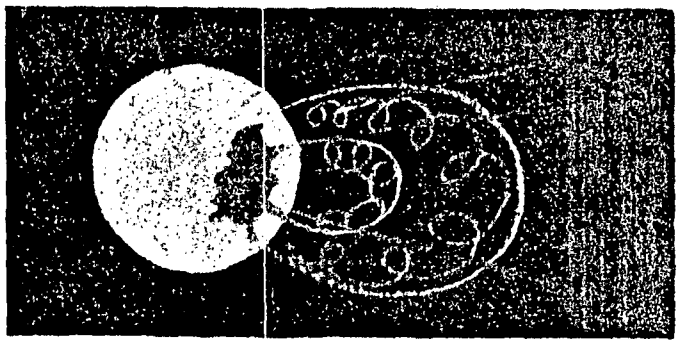

VISUAL PHENOMENA, ACCELERATION OF PARTICLES & EJECTION OF PLASMA FROM MOVING WALLS RESULTING IN FLUCTUATING TRAPPING REGION, LEAKAGE OF HIGH ENERGY PARTICLES PRODUCING INITIAL ANISOTROPIC DISTRIBUTION.

Figure 3. SHEP Production Model

change in magnetic field in the photosphere will induce a change in the chromospheric field, and due to lower gas densities, significant contraction of a region can be produced.

The protrusion of the flux tubes into the chromosphere results in sunspot magnetic fields of different polarities. The complexity of these fields results in several maxima and neutral points in the region. The plasma near a neutral point is in an unstable condition, the gradient of the magnetic pressure will tend to compress the region, and the region resists this compression by the gas pressure.

If the field gradient is high initially, then the compression forces increase more rapidly than the opposing gas pressure, and the pinch effect can occur.[6] However, before the compression proceeds very far, shock waves can be produced on either side of the neutral plane. Pressure discontinuities behind the shock waves, which propagate toward each other, tend to retard the compression. As the shock wave passes, the plasma expands behind it, leading to an increase in the flare area. The shock waves collide and are reflected; in collision, impulsive heating results in temperatures of 10^7 °K, which can sustain thermonuclear reactions. The chromospheric region normally exhibits temperatures of $\lesssim 10^4$ °K, and densities of $\sim 10^{13}$ cm^{-3}, as opposed to the photosphere where temperatures are lower and densities higher ($\sim 10^{17}$ cm^{-3}). The flare may last $> 10^3$ seconds, and have expansion velocities of 10^3 km sec^{-1}. The initial magnetic fields diffuse and are dispersed during this process, leading to different distributions after a flare.

The heated region where thermonuclear reactions can occur supplies the injection source for high energy particle accelerations. The reactions produce helium nuclei and protons with energies of $\sim$4 Mev and $\sim$3 - 14 Mev, respectively. It is necessary that the majority of the particles to be accelerated be injected with some sufficiently high initial energy, since the particle undergoing accelerations must gain energy in the face of retarding, or loss, mechanisms. The plasma (or gases) in the chromosphere and corona of the sun are sufficiently dense so that an accelerated particle loses energy through an "ionization" process in traversing them. Since ionization loss is a decreasing function of increasing particle energy, a low energy particle may suffer such great ionization losses that the acceleration process may never dominate. The rate of energy gain of a particle from acceleration processes rises approximately log linearly with particle energy, whereas the ionization loss decreases according to a power law. Thus, if a particle is injected with an energy greater than the intersection of these curves, it will always experience a net gain in energy. Also, it is true that, for equal charge, a particle of sufficiently greater mass can experience a net acceleration gain without injection, since the energy loss curve will be shifted toward higher energies.

---

6. Severnyi, A. B., "Nonstationary Processes in Solar Flares as a Manifestation of the Pinch Effect."

The accelerations occur when a particle is reflected between magnetohydrodynamic shock waves converging toward a neutral point. The particle will then be accelerated by successive reflections until it escapes the system. This mechanism could lead to a 100% increase in the energy of a relativistic particle in approximately 50 collisions if the front has a velocity of 10^3 km sec^{-1}.[7]

The plasma contained by the moving magnetic "walls" is not only compressed, but is also ejected from the region transverse to the motion of the walls. The plasma is "squeezed" both out of the region into the corona, and into the deeper parts of the sun. The outward streaming plasma carries with it energetic particles and frozen magnetic fields, and rises into the magnetic field region above the seat of the flare in the sunspot.

B. Trapping Region

The fields above sunspot groups during flares reach values of hundreds of gauss; thus, the expelled plasma and energetic particles push out into this field, forming a trapping region. Calculations of particle radii of curvature show that this region has sufficient field strength to trap Bev particles. The pressure of the expelled plasma causes the region to swell and extend outward from the sun. However, the very high energy particles do not remain trapped, but leak out of the trap. This then decreases the internal energy, and the region contracts. The contraction leads to additional acceleration of the remaining particles, of which the higher energies readily escape. Thus the region experiences a fluctuation until the energy of the remaining particles falls to a value such that they do not escape readily. If a rough dipole form is assumed for the trapping field, then the diffusion of particles out of this can be shown to be of the form

$$W_D = \frac{\nabla H}{H} \quad \frac{\beta^2 c^2}{W}$$

where W is the gyro frequency of the particles.

It has been shown that the energy spectrum of the particles can be calculated from a method similar to that used in galactic cosmic ray investigations.[5] The differential energy spectrum of the escaped particles is of the form $N(E) = CE^{-\alpha}$, where α has been calculated to be ≈ 3.5 for early stages of a flare. However, as the fluctuations cease, the lower energy particles will show a different spectrum due to perturbations from surrounding low strength fields. The trapping region now continues to push out against the sunspot field, with particles leaking out, and thus

7. Ginzburg, V. L., "Cosmic Rays on the Earth and In the Universe," Soviet Physics Uspekhi, Vol. 4, No. 4, January-February, 1962.

SHEP PRODUCTION

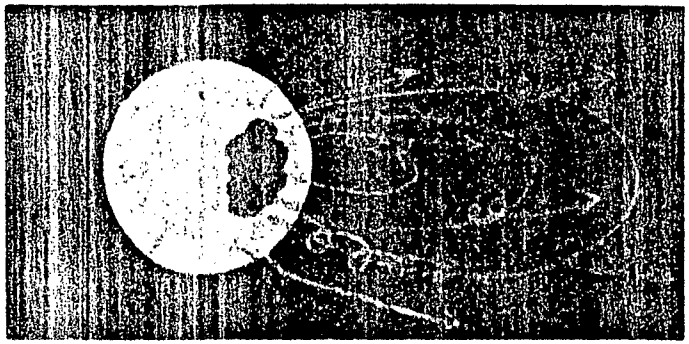

QUASI-EQUILIBRIUM TRAPPING REGION WITH START OF SLOW DIFFUSION OF PARTICLES OUT OF TRAP. EXTENSION OF TRAPPING REGION INTO RADIAL FIELD LEADING TO ISOTROPIC DISTRIBUTION OF LEAKAGE PARTICLES

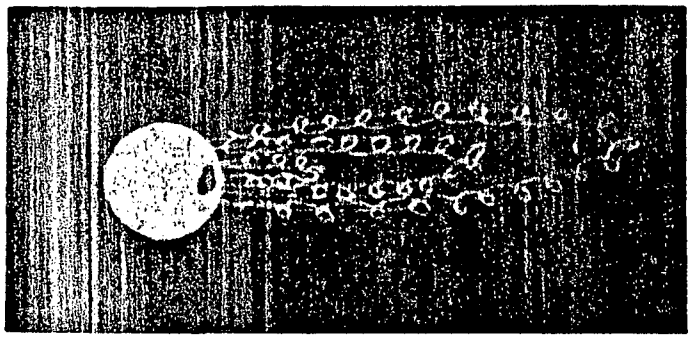

TRAPPING REGION EXTENDING TO THE ORBIT OF THE EARTH GIVING ISOTROPIC DISTRIBUTION OF PARTICLES. MAGNETIC FIELDS OF TRAP NOW AFFECT INTERPLANETARY CONDITIONS FOR FURTHER FLARE EVENTS.

Figure 4. SHEP Production Model

the internal energy decreases (assuming the source has ceased). However, the volume contained by the fields (which are still rooted in the photosphere) has increased, and thus the trapping effectiveness decreases as the field strength decreases.

Particles in the Mev energy range could be trapped for significant lengths of time, during which they lose energy through collision losses in the plasma. The rate of change of velocity for fast protons in hydrogen plasma can be expressed as a function of the plasma density and temperature. A lifetime for a high energy particle, defined as the time required for the particle to lose one-half of its energy, can be obtained from this expression, and is given as [8]

$$t_{\frac{1}{2}} = 0.64\, v^3\, mM \left\{ 12\,\pi e^4 N \ln \frac{2mv^2}{e^2} \left(\frac{kT}{4\pi N e^2}\right)^{\frac{1}{2}} \right\}$$

where N,T are the plasma density, temperature; m and M are the electron and proton masses, and v is the particle velocity. If the particle velocity is equal to, or less than, the average velocity of the plasma electrons, then v should be replaced by v_e. At a density of 10^7 cm^{-3}, and temperature of 10^5K, the lifetime of a 10 Mev proton is approximately 41 hours. Thus the concept of a trapping region which contains energetic particles and allows them to leak out in time is consistent with particle energy lifetimes in the coronal regions.

The trap is expanded into the corona and space by the pressure of the energetic particles within the region. This region continues to propagate through space, loosely guided by the radial field of the sun, or perhaps flowing along a path swept out by a previous event. Thus, west limb flare particles usually reach the earth sooner than do those from east limb flares; in fact, it is difficult for east limb flares to produce significant radiation at the earth. Since the velocity of propagation of the region is dependent upon the internal pressure (as well as the field), the delay time of magnetic storm onset at the earth is related to the number of high energy particles produced.

The early stages of the flare event, which produce the initial high energy particles and "squeeze" out the plasma from between the moving magnetic walls, could lead to an initial anisotropic distribution of high energy particles. These particles, if of very high energy, could penetrate the magnetic trap relatively easily, and escape into space to be loosely guided by the general radial field. As the event progresses, the higher energy particles are lost and the region expands, with the lower energy particles escaping after many deflections. Thus the initial high energy particle anisotropy should decay into low energy isotropy. The

---

8. Fireman, E. L., "Density of the Solar Flare Plasma," Smithsonian Astrophysical Observatory, (Private Communication).

balance of this anisotropic - isotropic stage should be a function of the energy of particles produced, the configuration and strength of the magnetic trap and the frozen-in fields, and the perturbations due to irregularities in the interplanetary field. The front of this extended trapping region could eventually reach the earth, resulting in a Forbush decrease of galactic cosmic rays, and the onset of a magnetic storm. At this time, due to the energy dependence of the diffusion of the particles out of the region, the trap should contain a preponderance of low energy particles.

Experimental Verification

Observations pertinent to verification of the model will be discussed in this section. The model predicts that the delay in arrival of the SHEP will differ from that of direct propagation due to trapping in the region above the flare. Thus, the flux-energy spectrum should charge in time as the particles escape from the trap. Evidence for this phenomenon is presented in Figure 5, which shows the data of Bryant.[9] The first particles to arrive are of high energy and low intensity; as the event progresses the spectrum changes, becoming more intense and steeped to low energies. Variations in the specific spectra can be expected for various flare events; however, the general feature of a buildup in flux and steepness of spectra should hold. It should be noted that portions of the spectra might not be observed for an event, such as perhaps an east limb flare, if propagation conditions are such that the particles are guided past the earth at one time, whereas the earth might move into their path at another time during the event. The shift of the intensity maxima to lower energies is shown in Figure 6 for the flare of 28 September 1961. The maxima are seen to shift to lower energies as time increases. The time integrated differential flux-energy spectra, normalized to 1 proton/cm^2 steradian with energy greater than 100 Mev is shown in Figure 7 for the flare of 28 September 1961. This curve can be approximated by a power law of the form

$$N(E) = CE^{-\alpha}$$

where α has been observed to change for various events. However, this is of the form that one would expect from considerations of the flare accelerations and trapping region.

---

9. Bryant, D. A., et al., "Solar Cosmic Rays Following the Flare of September 28, 1961," Paper at American Geophysical Union Meeting, Washington, D.C., (April 1962).

INSTANTANEOUS DIFFERENTIAL FLUX FOR VARIOUS TIMES

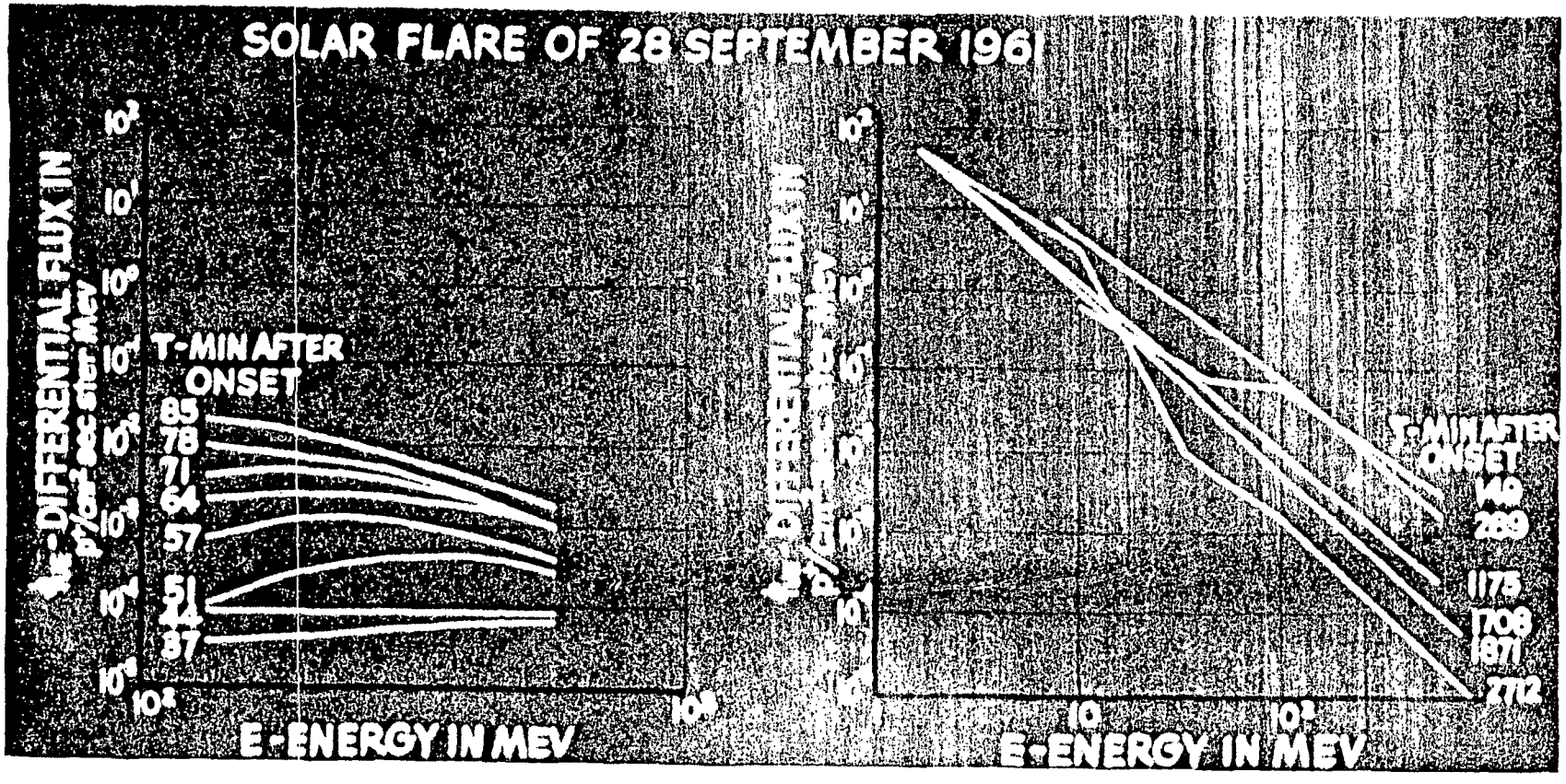

Figure 5. Solar Flare Flux - Energy Spectra

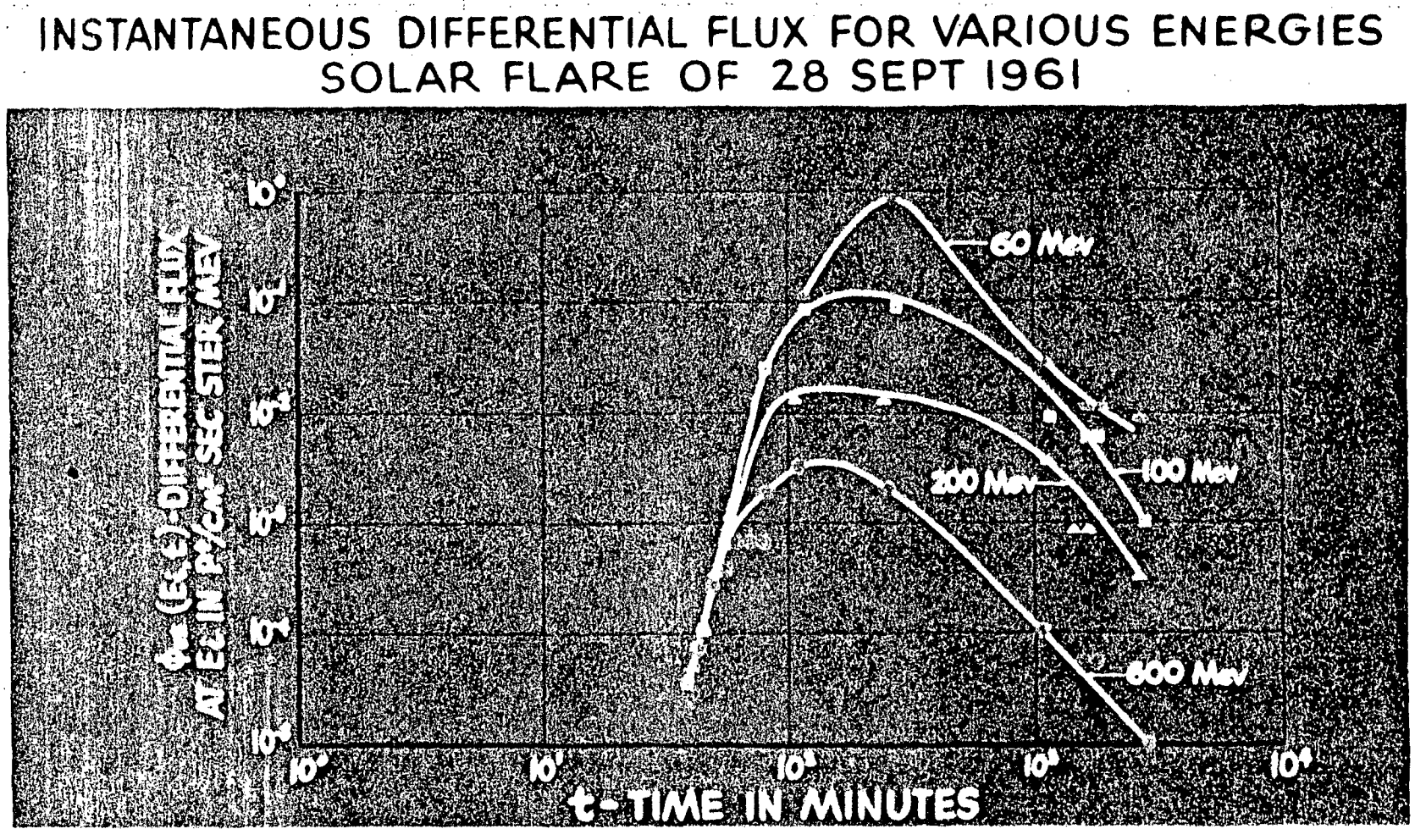

Figure 6. Solar Flare Intensity Maximum

TIME INTEGRATED NORMALIZED DIFFERENTIAL FLUX FOR SOLAR FLARE OF 28 SEPTEMBER 1961

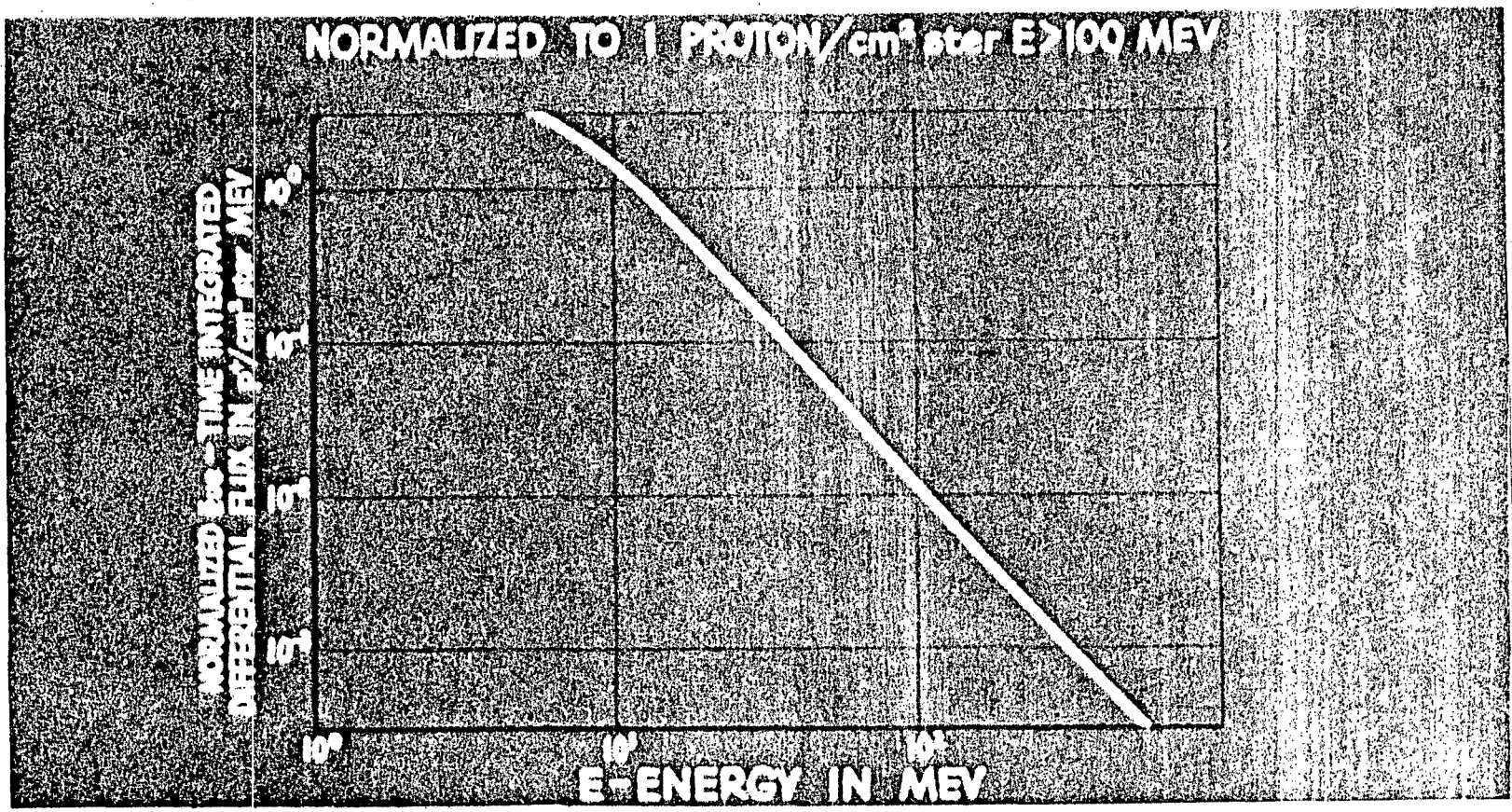

Figure 7. Time Integrated Solar Flare Spectrum

Much work has been done with radio astronomy and the radio noise from the sun has been classified into types. Some of these types have been found to correspond to radiations from particles in the chromosphere and corona can be correlated with flare events.

The following table lists the types of radio noise and the particle radiations that are believed to cause the noise.[10]

Solar Radio Noise

Type	Characteristic Duration	Probable Cause
Centimeter	Minutes	Synchrotron radiation from relativistic electrons.
Type II	Minutes	Excitation of coronal plasma oscillations by high energy particles that are probably trapped in a magneto-dynamic wave.
Type III	Seconds	Excitation of coronal plasma oscillations by high energy particles that pass through the corona freely.
Type IV	Hours	Synchrotron radiation from relativistic electrons.
Type V	Minutes	Excitation of coronal plasma oscillations by particles ejected during a flare. The particles rapidly diffuse from trapping region.
Radio Storms	Days	Excitation of coronal plasma oscillations by particles ejected during a flare. The particles slowly diffuse from trapping region.

As can be seen from the table, the kinds of particles causing the specific types of radio emission can be determined. Thus, Types II, II, V and Radio Storms agree well with a model which predicts a trapping region following a flare event. Types II and III correspond to the high energy particles that are not trapped in the region while type V and radio storms can be correlated to the diffusion of medium and low energy particles from the trap.

---

10. Denisse, J. F., "Solar Radio Phenomena and Their Physical Interpretation," NASA TT F-72, September 1961.

The change in magnetic field configuration of a sunspot group during a flare event has been observed by Gopasyuk,[11] in which he was able to distinguish "humps" of magnetic field intensity. Assignments of isogauss contours and magnitude of displacement have been made, which show, in general, that the displacement is in the direction of flare nodes (neutral points), and that these displacements do not occur in the absence of flare events. These field changes are consistent with the early stages of the flare event when compression and gas movements are in evidence. It has also been observed [12] that strong magnetic fields (hundreds of gauss) are carried thousands of kilometers above the edge of the solar disk. These fields correspond to the trapping region fields which are carried outward by the expelled plasma and energetic particles.

The observation of polar cap absorption verified another feature of the model, which discusses propagation from the sun to the earth. It has been observed [13] that SHEP stream into the polar cap regions some time after the flare occurs. At some later time, after the onset of the magnetic storm, the flare region produced another flare, and these new protons arrived much faster at the poles than did the initial protons from the first flare. This corresponds to the second flare particles following the path "carved out" by the preceding flare's trapping region, which remains rooted in the sun, but extended out and encompassing the earth. The presence of the plasma cloud near the earth results in a Forbush decrease in galactic cosmic rays, which became more severe when the plasma cloud was preceded by SHEP, than when no SHEP were observed. It is the presence of these SHEP in a flare event which makes possible the carrying-out of large magnetic fields from the sun, resulting in a strong Forbush decrease. To sum up, a SHEP flare will exhibit shorter storm delay time, lower SC amplitude, and stronger Forbush decrease than will a non-SHEP flare.

---

11. Gopasyuk, S. I., Variations of the Magnetic Field and Sunspot Configurations During Solar Flares - A Determination of the Total Energy of Flares, Soviet Astronomy - AJ, Vol. 5, No. 2, September-October 1961.

12. Severnyi, A. B., "Generation of Flares by Varying Magnetic Fields on the Sun," Soviet Astronomy - AJ, Vol. 5, No. 3, November-December 1961.

13. Dvoryashin, A.A., et al., "Active Solar Regions and Their Corpuscular Emission," Soviet Astronomy - AJ, Vol. 5, No. 3, November-December 1961.

The shock waves produced by the change in field gradient and subsequent compression of the flare region have been photographed.[14] The photographs clearly show the shock waves moving through the active region, and the region expanding. Also, through an ingeneous technique, a wavelength shift is used to show plasma ejected toward the earth in a color different than that for plasma falling back into the region. Thus the ejection of a plasma during the bright phase of a flare event has been directly photographed.

The anisotropy of the initial radiation arriving at the earth from a flare has been observed.[15] This early anisotropy seemed to come from a source located approximately 50^{o} to the west of the earth sun line, (Figure 8), which corresponds to the initial high energy particles escaping immediately from the flare trap,and being loosely guided to the earth by the spiralled field of the sun. It was observed for one event that the anisotropic SHEP arrived in bursts, which would correspond to the early fluctuations of the non-equilibrium trapping region above the flare site. The anisotropic phase of SHEP arrival is observed to vary in time, which is consistent with varying production and trapping conditions on the sun; the anisotropy decays into isotropy in a matter of minutes to a few hours.

Spectroscopic observations of flare phenomena[12] lends evidence for emission of a stream of radiating plasma having a velocity of the order of 10^{3} km sec^{-1}. These observations are of wings of hydrogen emission lines, upon which asymmetric "whiskers" are imposed. The investigations of these profiles yield good first approximations due to doppler broadening, but better agreement is obtained if velocity gradient broadening is used. Thus direct observations consistent with fast particle stream motion, both in and out of a flare region, have been made.

---

14. Ramsey, H. E., Lockheed California Company (Private Communication)

15. McCracken, K.G., "The Cosmic Ray Flare Effect," Jour.of Geophys.Res., Vol. 67, No. 2, February 1962.

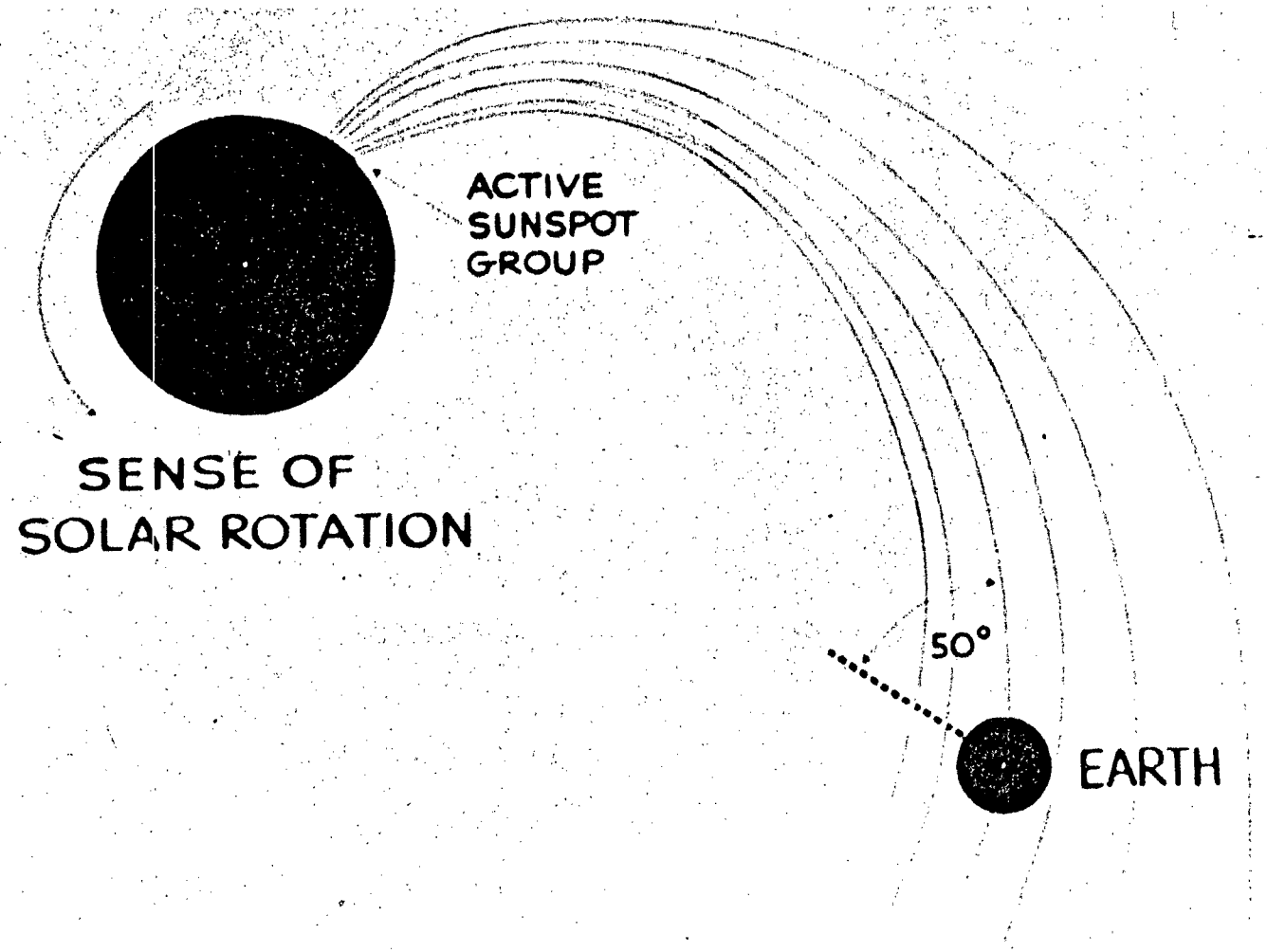

Figure 8. Solar Flare Anisotropy

Paper B-1

RADIATION DAMAGE TO SOLAR CELLS

J. A. Baicker and P. Rappaport
RCA Laboratories
Princeton, N. J.

Abstract

The construction, operation, and performance characteristics of solar cells are described. The radiation damage process is discussed, and details of proton and electron damage to silicon cells presented. The degradation of the photovoltaic current-voltage characteristics and the spectral response is shown, and a comparison made of various types of solar cells, including silicon, gallium arsenide and cadmium sulfide. Differences between p/n and n/p silicon cells are discussed and explained in terms of basic properties of the radiation defects.

I. Introduction

When solar cells were first suggested as space power supplies it was expected, based on cosmic ray intensities, that their operating lives would extend for thousands of years. However, with the discovery in 1958 of the Van Allen radiation belts it was recognized that solar cell lifetimes would be reduced to months or even less in the most intense regions. For many of the low energy electrons and protons in these belts simple quartz or sapphire shielding over the solar cells could be quite effective. Now, with the creation of the artificial radiation belt, the solar cell damage problem is quite serious and under some conditions the conventional solar cell may last for only days. This is a result of the large number of relatively high energy electrons that were produced by the high altitude bomb blast, and against which solar cells cannot be easily shielded. In this paper we will discuss solar cell radiation damage, and discuss how some of the deleterious effects may be counteracted.

First, we will describe the operation of solar cells and discuss the physical phenomena that occur when they are subjected to high energy particle radiation. The latest damage data for electrons and protons will be presented, with the general conclusion that solar cells will continue to be quite useful as space power supplies.

It is well-known that solar cells are among the most vulnerable components used in space vehicles. This is true for two reasons: (1) solar cells require long minority carrier lifetimes for efficient operation, and the lifetime is the most sensitive to radiation of all semiconductor properties, and (2) they are mounted on the exterior of the satellite in an exposed position with at most a minor amount of transparent shielding.

II. Description of Solar Cells

Several papers such as Chapin et. al.[1], Prince[2], and Rappaport[3] describe the solar cell. The basic operation is illustrated in Fig. 1. A wafer of n-type silicon is fired so as to produce a shallow-diffused surface layer of p-type silicon, and ohmic contacts are applied to both n and p regions.* When the cell is illuminated, photons with energy greater than the energy gap of the silicon generate electron-hole pairs both in the surface and base regions of the cell. These pairs are free to diffuse through the material, and those minority carriers that reach the vicinity of the space charge region near the junction are swept across the junction by the electric field. The collected carriers constitute an electric current, and can generate a voltage across an external load. Fig. 2 illustrates the typical junction i-V characteristics in the dark and under illumination. The shaded area is the region in which power is delivered to a load; notice that the cell operates with the junction biased in the forward direction, while the current flows in the reverse direction.

The spectral response of a solar cell having a 1 micron junction depth is shown in Fig. 3. The base response characteristically goes to zero at both long and short wavelength limits. This can be understood as follows: at long wavelengths the light photons have insufficient energy to produce pairs, and at the short wavelength extreme the optical absorption constant is so large that the light is totally absorbed in the 1 micron surface layer, and cannot penetrate into the base region. The surface response goes to zero at long wavelengths and approaches a constant value in the short wavelength limit, when the light is all absorbed at the surface of the cell in a layer that is thin compared with both the junction depth and the minority carrier diffusion length in the surface layer.

---

* The abbreviation p/n will be used to designate cells having n-type base material and p-type surface layers, and n/p for the reverse.

1. D. M. Chapin, C. S. Fuller and G. L. Pearson, J. Applied Phys. 25 676 (1954).

2. M. B. Prince, J. Applied Phys. 26 534 (1955).

3. P. Rappaport, RCA Review 20 373 (1959).

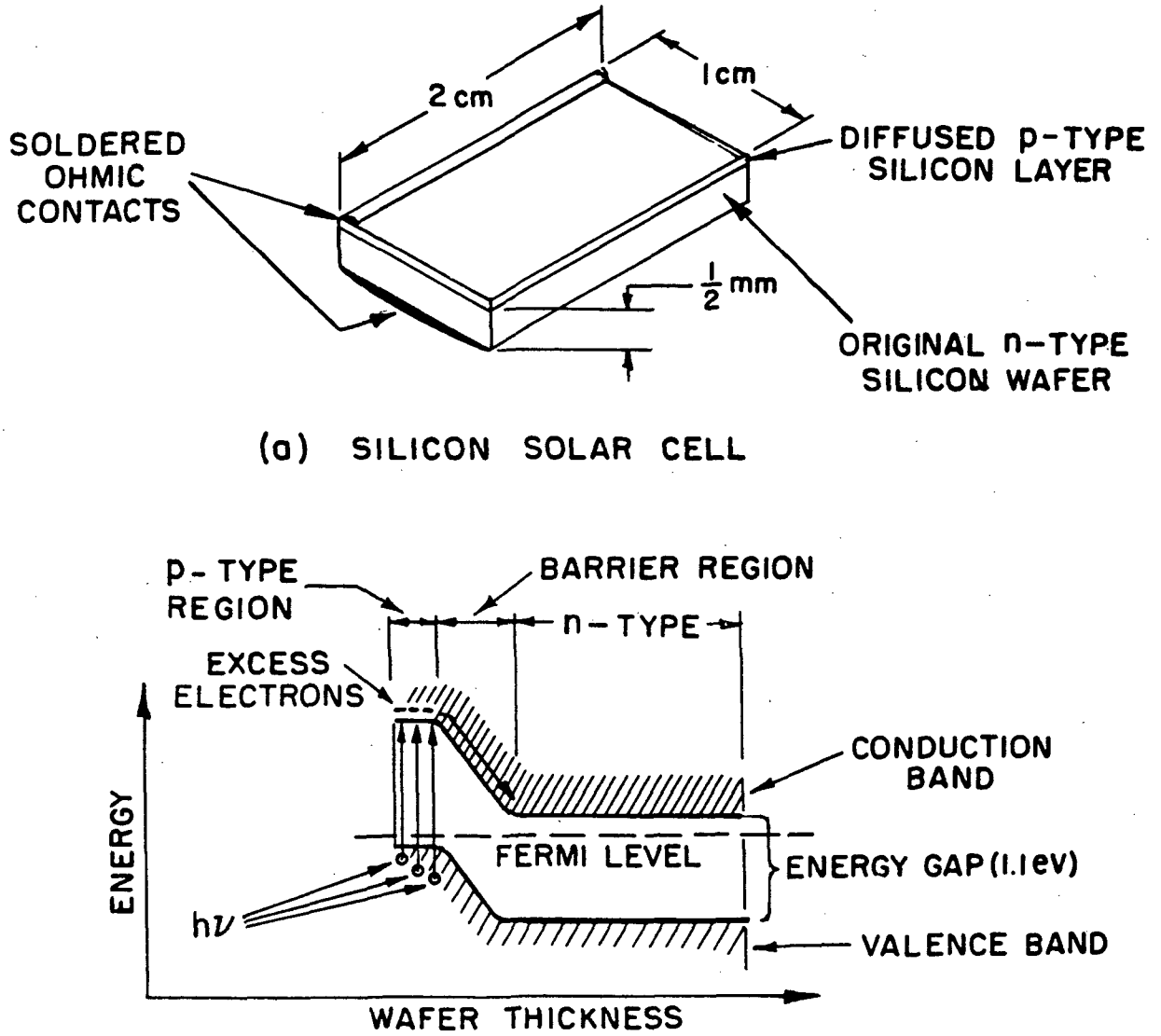

FIG. 1 Schematic diagram of a solar cell.

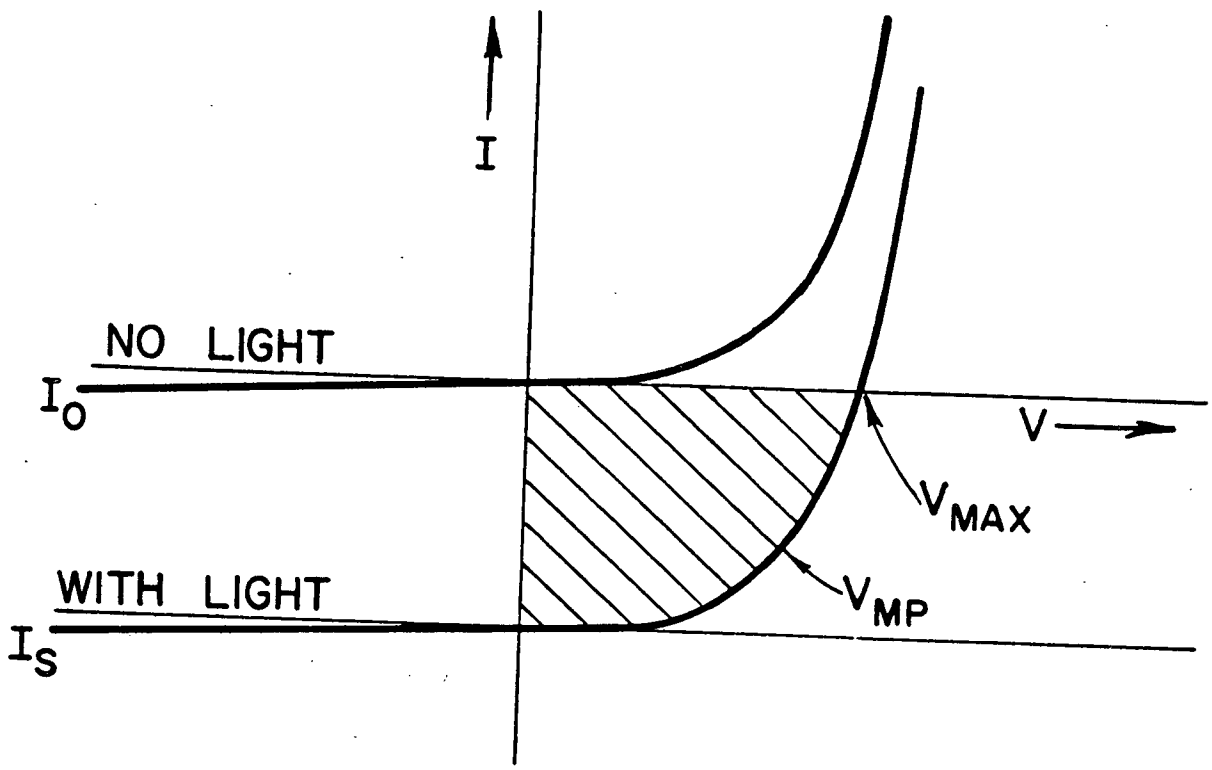

FIG. 2 Current-voltage characteristic of a solar cell.

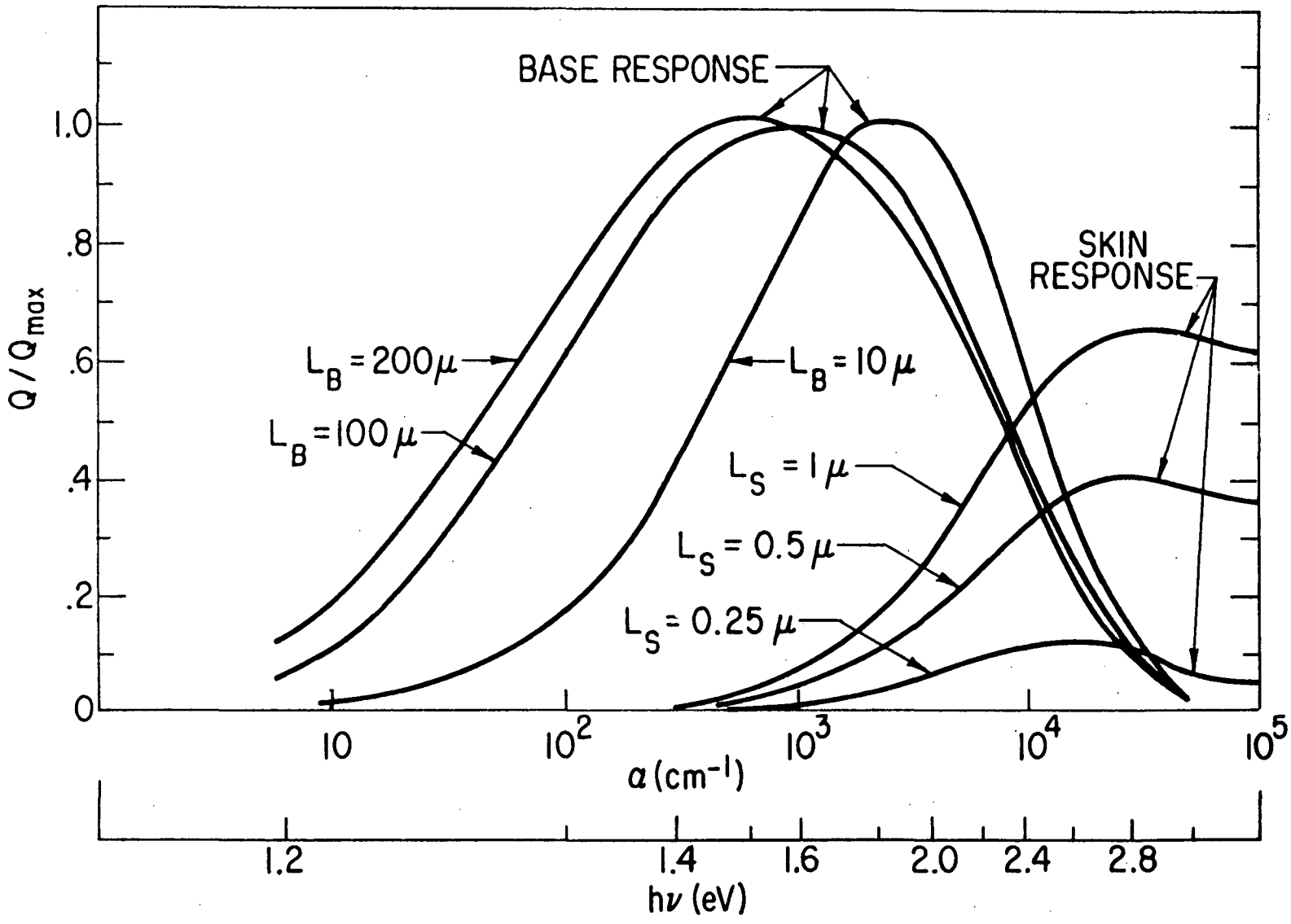

FIG. 3 Theoretical spectral response of a solar cell with a one-micron deep junction.

Figure 4 shows a typical spectral response curve, showing how it can be resolved into base and surface contributions. Note that the surface response is much smaller than the base response, a characteristic of practically all silicon cells. This is caused by two circumstances; (1) the optical absorption spectrum of silicon is such that for both sunlight and tungsten light over 75% of the radiant energy is absorbed in the base of the cell, and (2) the minority carrier diffusion length in the highly-doped surface layer is less than 1 micron, compared with 100 microns or more in the base.

This feature does not occur in solar cells made of other materials, such as gallium arsenide, for example.

The possibility of increasing the surface response by reducing the junction depth has been explored by several workers in the field. In addition to increasing the overall conversion efficiency the added surface response has the effect of shifting the peak of the spectral response towards the blue, and hence these cells are sometimes called "blue-shifted" cells.

Cells with 1/4 micron junction depths have been made; their surface response is considerably greater than the standard 1 micron junction depth cells, but the thin surface layer adds to the series resistance of the cells, and the overall efficiency is reduced. The series resistance loss can be minimized by providing a conducting grid on the surface.

Some of the performance characteristics of silicon solar cells are:

Efficiency in sunlight	10-11%	
Efficiency in tungsten light	13-14%	
Open-Circuit voltage	0.55 volt	Illuminated with 100 mw/cm^2
Short-circuit current	25-30 ma/cm^2	

III. Damage Process

It is evident that a solar cell requires a long minority carrier diffusion length for its efficient operation. With care in manufacture the diffusion length in the base is approximately 100μ. Upon bombardment with high energy particles silicon atoms are displaced from their normal lattice positions. The resulting lattice defects may act as recombination centers for electrons in the conduction band or holes in

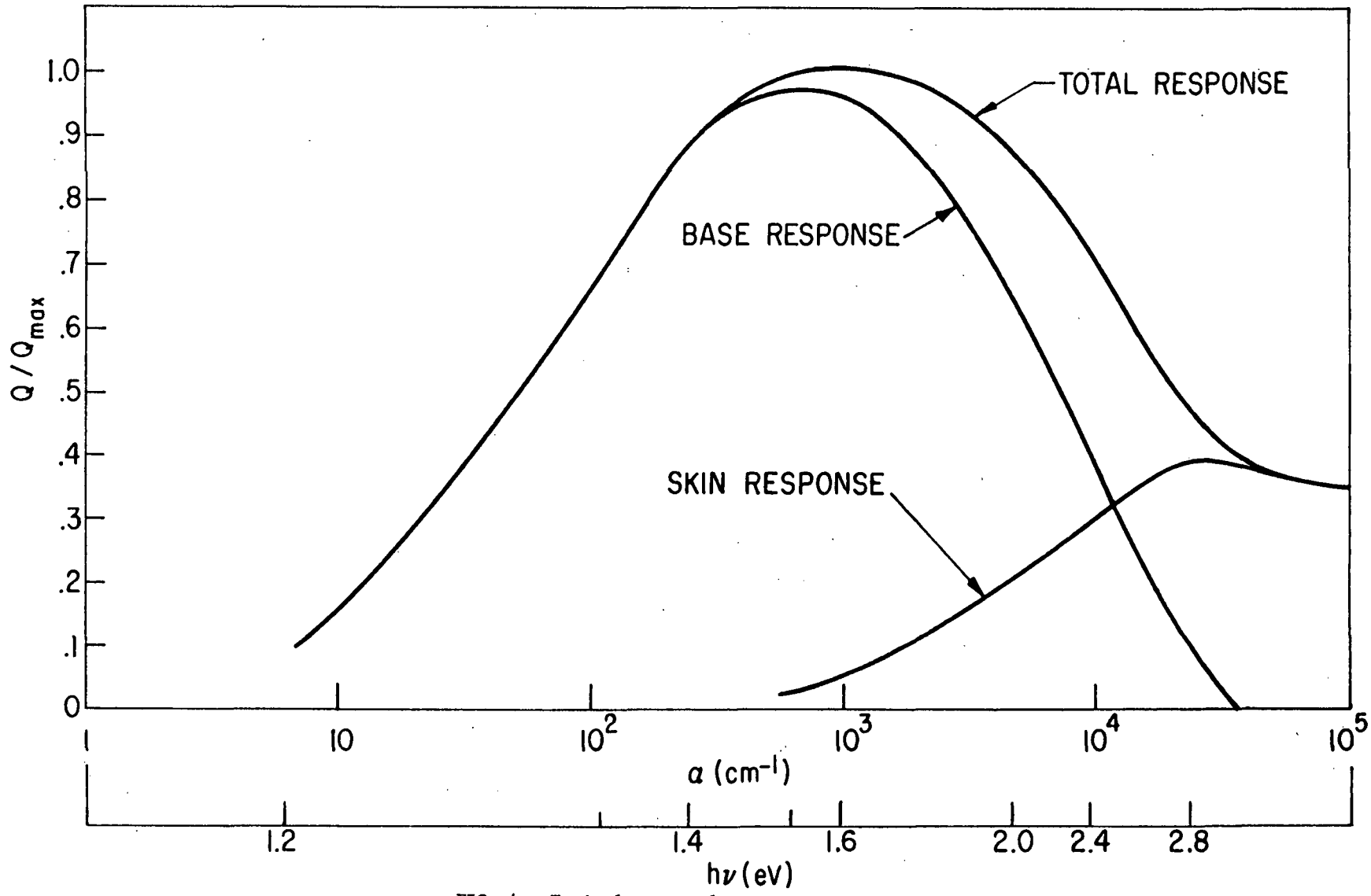

FIG. 4 Typical spectral response for a silicon solar cell.

the valence band, depending on whether the silicon is p-type or n-type. The recombination process occurs as the center first captures a minority carrier and subsequently captures a majority carrier. One electron-hole pair is annihilated in the process, and the center is left in its original charge state. The lifetime of excess carriers, τ, is reduced by the introduction of recombination centers according to the equation

$$\frac{1}{\tau} = \frac{1}{\tau_o} + N_r \sigma_r v f \qquad (1)$$

where τ_o is the lifetime before irradiation, σ_r is the recombination cross section, v is the thermal velocity of the minority carriers, N_r is the recombination center density and f is a statistical occupancy factor that is near unity in most practical cases. The diffusion length $L = (D\tau)^{1/2}$, where D is the diffusion constant, is reduced accordingly.

The first sign of damage to a cell is a reduction of the diffusion length in the base material. The diffusion length being very short in the surface region, it requires a much heavier irradiation before surface damage can be seen. As Fig. 3 shows, the red response will be the first to be affected; red light generates carriers deep in the cell, and a long diffusion length is required for collection.

IV. Results

Figure 5 shows a typical family of i-V curves before and after a number of successive irradiations. The principal loss is to the cell current; the voltage decrease is much smaller. Fig. 6 shows a typical spectral response before and after irradiation; as expected, the degradation is greatest at long wavelengths. The shallow-junction ("blue-shifted") cells are more radiation resistant than the standard cells because of their greater base response in the blue as well as their greater surface response.

The output is shown as a function of total irradiation in Fig. 7, for standard p/n and n/p silicon cells under electron and proton bombardment. The electron fluxes required for a 25% degradation in the conversion efficiency are shown as a function of electron energy in Fig. 8, for standard one-micron junction depth p/n and n/p cells. (4-8)

4. W. L. Brown and G. L. Pearson, BTL Technical Memornadum, April 1960 (unpublished).
5. P. Berman, Transitron Electronic Corp. Report. Oct 1960 (unpublished).
6. R. G. Downing Space Technology Labs Report, TR 60-0000-04057 Feb. 1960 (unpublished).
7. J. A. Baicker and B. W. Faughnan, J. Applied Phys 33 3271 (1962).
8. J. J. Wysocki and J. Scott-Monck, Personal Communication.

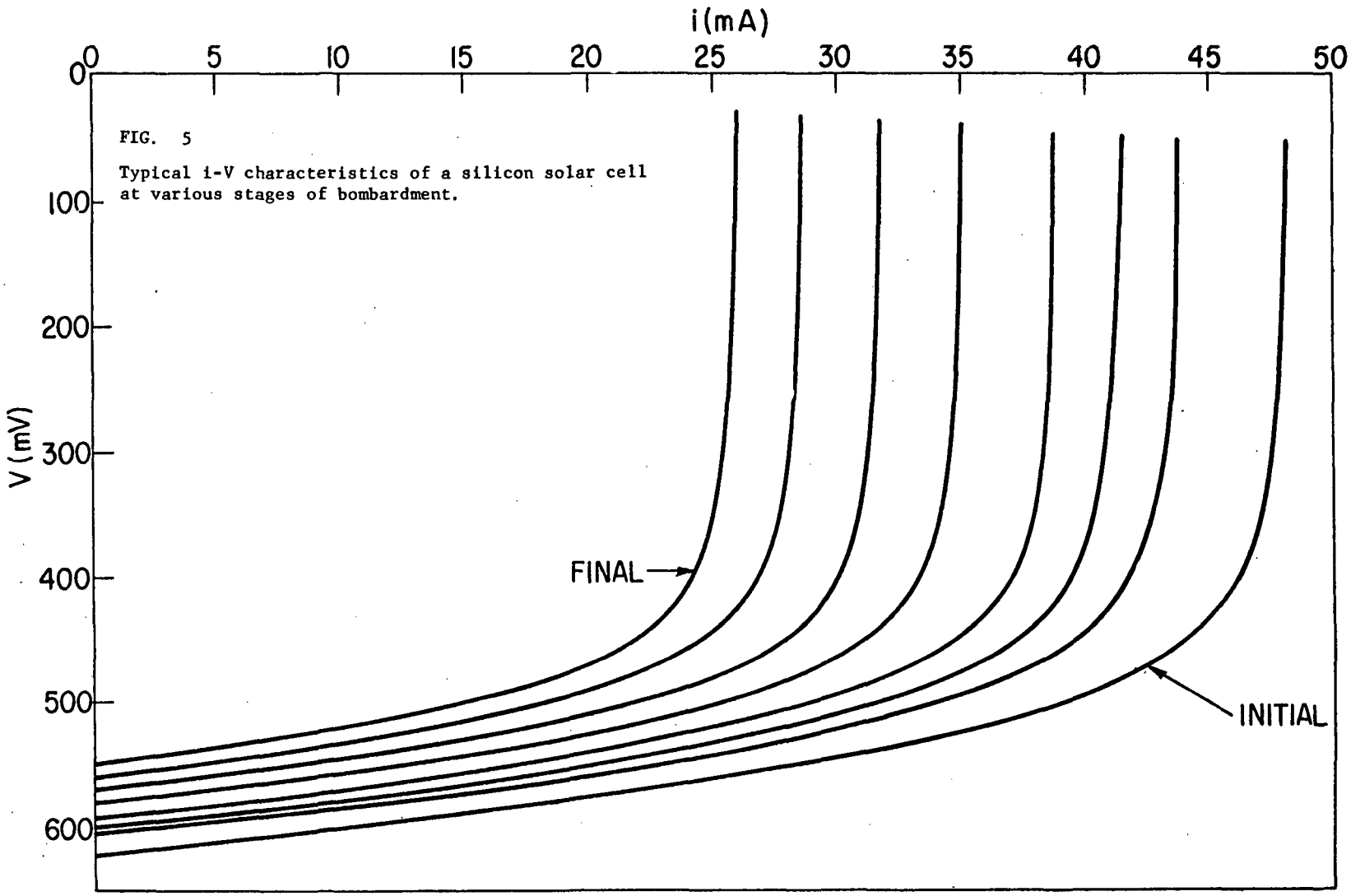

FIG. 5

Typical i-V characteristics of a silicon solar cell at various stages of bombardment.

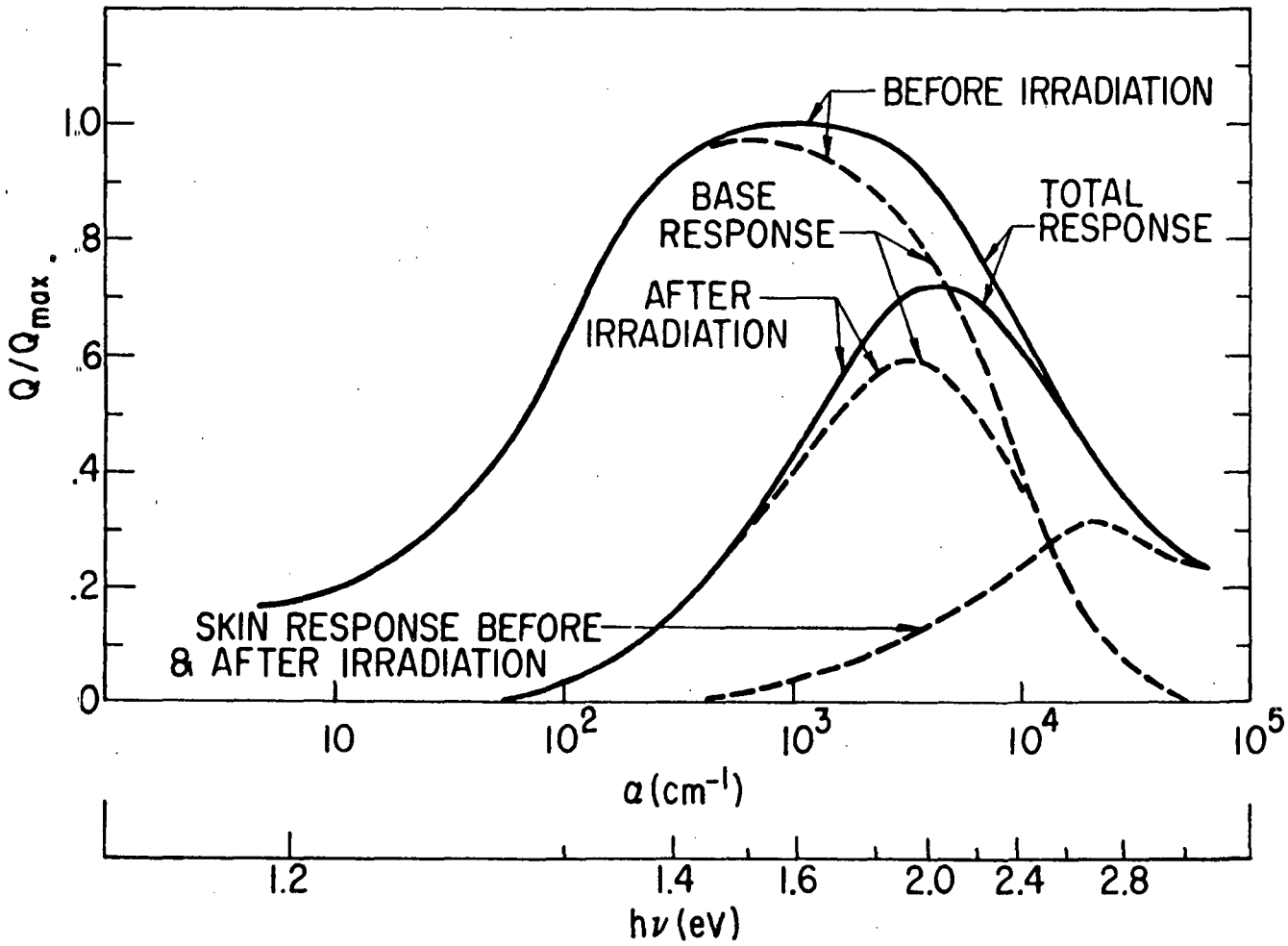

FIG. 6 Spectral response of a silicon solar cell before and after irradiation.

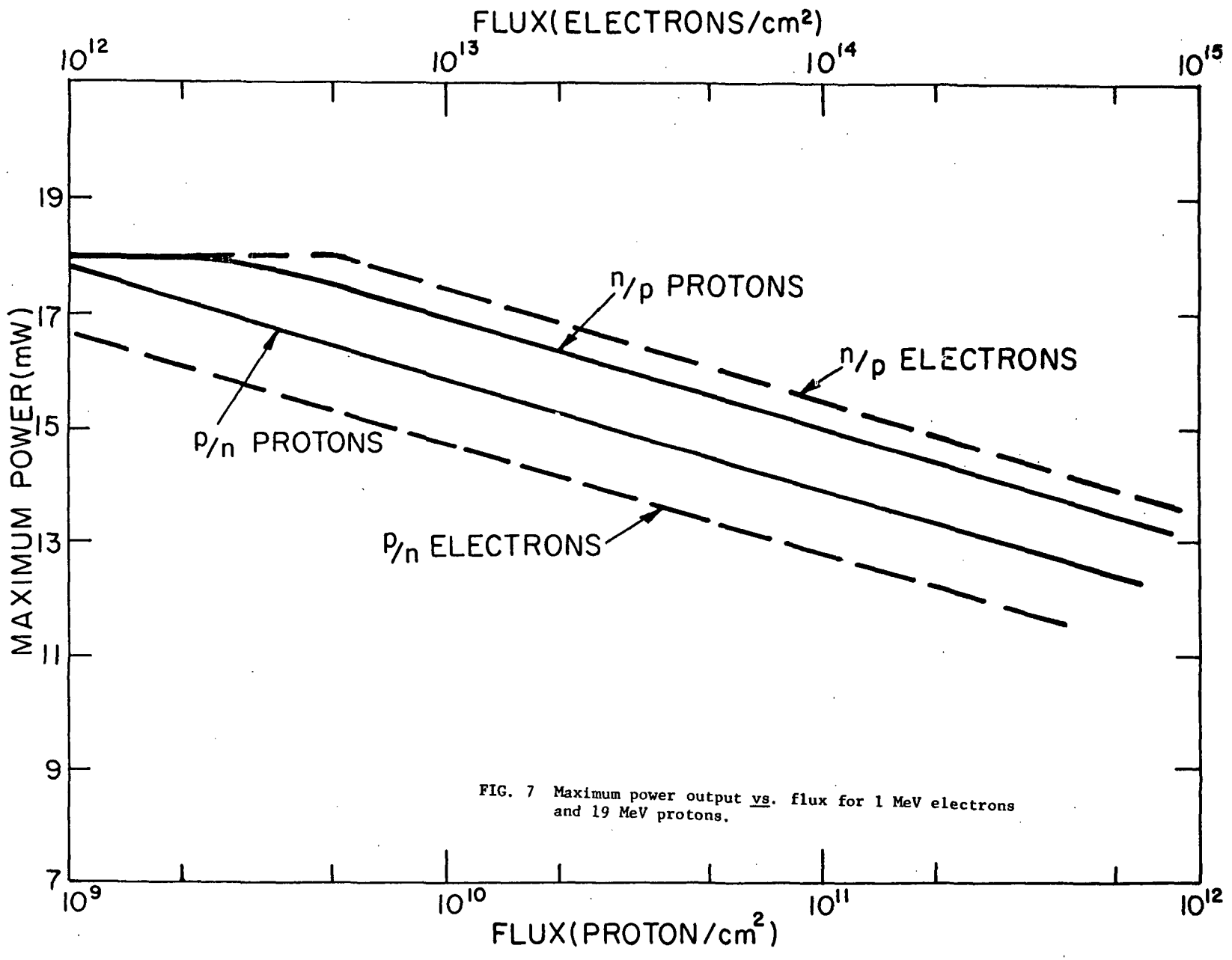

FIG. 7 Maximum power output vs. flux for 1 MeV electrons and 19 MeV protons.

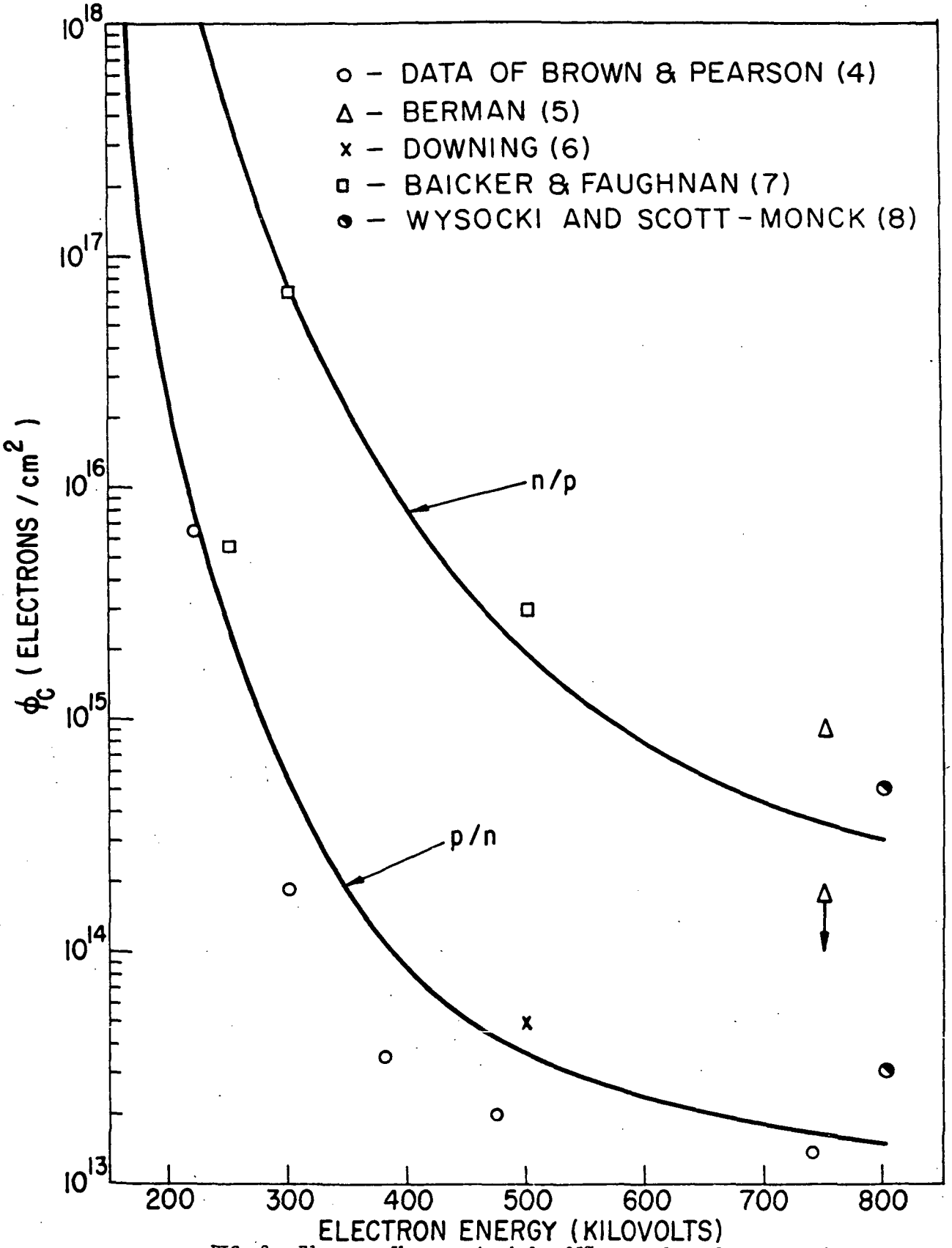

FIG. 8 Electron flux required for 25% power loss for standard p/n and n/p silicon solar cells vs. bombarding energy.

There has been considerable conjecture regarding the large difference between p/n and n/p silicon cells. This phenomenon is a result of the basic character of the recombination centers which are produced by bombardment. The simplest type of recombination center has two different charge states, one neutral and the other charge state either positive if the center is a net donor or negative if the charge state is a net acceptor. As a result of the coulomb forces a donor-like center will have a large electron-capture cross section when it is in its positive charge state, and it will have a relatively much smaller hole capture cross section when in its neutral charge state. If both donor-like and acceptor-like centers are present, the recombination process in n-type silicon will tend to be dominated by the net acceptors and in p-type by the net donors, barring enormous differences in the concentrations of the two different species. There is now substantial evidence that a multiplicity of different defects are produced in silicon by irradiation and the dominant recombination centers are indeed different in n-type and p-type silicon. They are produced in different concentrations, and have different minority capture cross sections, and it would in fact be purely coincidence if the radiation damage rates were the same in both types of silicon.

The energy dependence of the damage rate under proton bombardment is shown in Fig. 9. There should really be two curves, one for p/n and the other for n/p cells, with about a factor of 3 or 4 separating them, but the fluctuations within any given group of apparently identical cells in nearly a factor of 10, and so only an average curve is shown.

Shielding Effectiveness

Since the July 9th nuclear explosion which is generally conceded to have injected large numbers of energetic electrons into trapped orbits there has been a rapid deterioration of power on satellites traveling in the radiation region with one notable exception, the Bell Telstar. The Telstar system was different from the others on two accounts: it utilized n/p silicon cells for the first time and each cell was protected by a moderate amount of transparent shielding (30 mils of sapphire). The question of just how effective the 30-mil shield is, is rather difficult to answer, for either proton or electron fluxes, (for different reasons). In the proton case it isn't too difficult to calculate what will happen to a monoenergetic beam passing through a relatively thin layer of shielding. The difficulty occurs

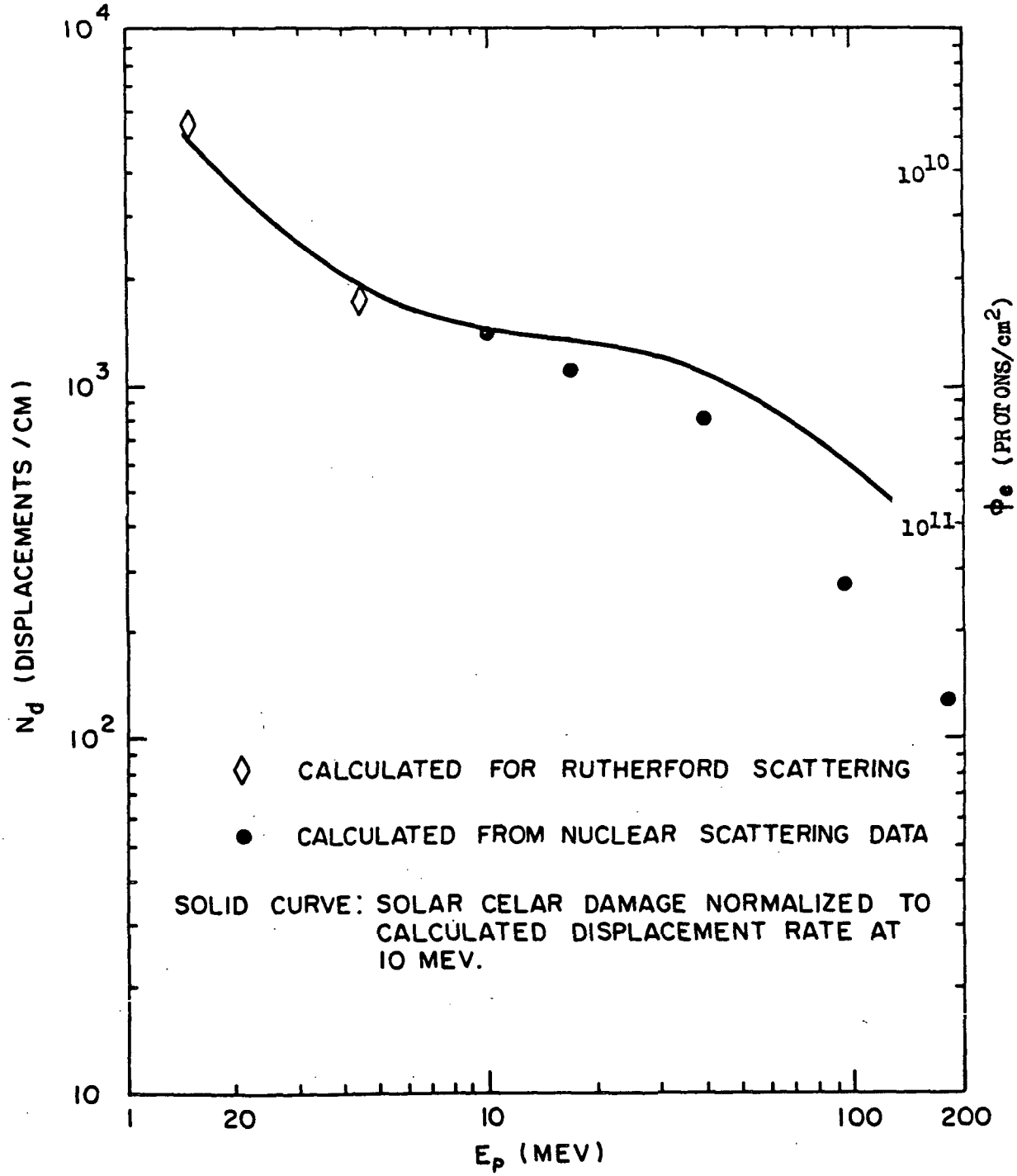

FIG. 9 Relative proton damage rate vs. bombarding energy.

because the proton spectrum has not been measured down to sufficiently low energies to account for the entire damage-producing flux. The energy spectrum increases very rapidly at low energies, and as Fig. 9 indicates the low-energy protons are at least as important to an unprotected cell as the high-energy protons. If we make the arbitrary assumption that the intensity is constant from zero to 10 Mev, and then drops off in a manner as reported by Freden and White and Naugle and Kniffen at higher energies, then we would conclude that 10 mils of sapphire would reduce the proton damage by roughly a factor of 10. A 30-mil sapphire shield would reduce the proton damage by a factor of 200, on the same assumption regarding the low energy spectrum. If, as one would suspect, the intensity continues to increase below 10 Mev the improvement due to shielding will be even greater than these figures.

In the electron case the shielding question is more difficult to answer. Electrons are not slowed down in as uniform a fashion as protons are, and there is even more diversity among the reported electron fluxes than among the proton fluxes. For a "fission-electron" spectrum such as was trapped after the Johnston Island explosion the shielding effectiveness will not be nearly as great as the approximate figures given above for the proton case. It has been estimated that the shielding reduces the damage by only a factor of two in the electron flux.[9] The principal advantage of the Telstar over the earlier satellites has come about through the use of n/p solar cells.

V. Gallium Arsenide

Photovoltaic effects are seen in practically all semiconductors, and many have been considered for energy conversion purposes. Of these, gallium arsenide and cadmium sulfide are the nearest to being practical (i.e., competitive with silicon).

Gallium arsenide photovoltaic cells are similar to silicon cells in construction. A wafer of n-type material has a p-type surface layer roughly 1μ deep. The principal difference between silicon and gallium arsenide is a consequence of the optical absorption spectra of the two materials. In GaAs the absorption constant rises very steeply above the fundamental edge, and as a result all of the carriers are generated in a very shallow layer ($\sim$ 1 micron) in the p-type surface. This is in constrast with silicon where the optical absorption rises more slowly and light can penetrate deeply into the base region. Solar cells with 10% solar conversion efficiency have been made using gallium arsenide,

9. W. L. Brown, Personal Communication

and since the active region of the cells is confined to the shallow surface layer a higher flux of damaging radiation is required to affect the output of these cells than is required for comparable silicon cells. The difference between the spectral response before and after irradiation for gallium arsenide and silicon is shown in Fig. 10.

Cadmium sulfide photovoltaic cells are the latest addition to the family, and since the exact mechanism for their operation isn't understood the present discussion will be qualitative. Cadmium sulfide cells are quite different from either gallium arsenide or silicon cells; a thin evaporated polycrystalline layer of n-type cadmium sulfide is deposited on a conducting backing, either metal or glass with a transparent conducting film, the materials being chosen to effect an ohmic contact. A surface layer of copper is deposited on top of the cadmium sulfide, and produces a surface barrier type junction.
In addition to the obvious difference in construction, the method of operation is different from silicon and GaAs. Light which is below the fundamental absorption edge can pass through the cadmium sulfide and strike the copper interface, where it is absorbed and produces carriers by a process which may be similar to photoemission. In contrast with silicon and GaAs little or no carrier diffusion is required, and hence the device is extremely difficult to damage. The maximum efficiency obtained up to now is in the neighborhood of 4-5%.

A comparison of the damage susceptibility of the various types of solar cell is given in Table I. The figures are all related to standard silicon p/n cells. The actual flux required for a given degradation can be obtained from Figures 8 and 9. Fig. 7 gives detailed numbers for 1 MeV electrons and 19 MeV protons.

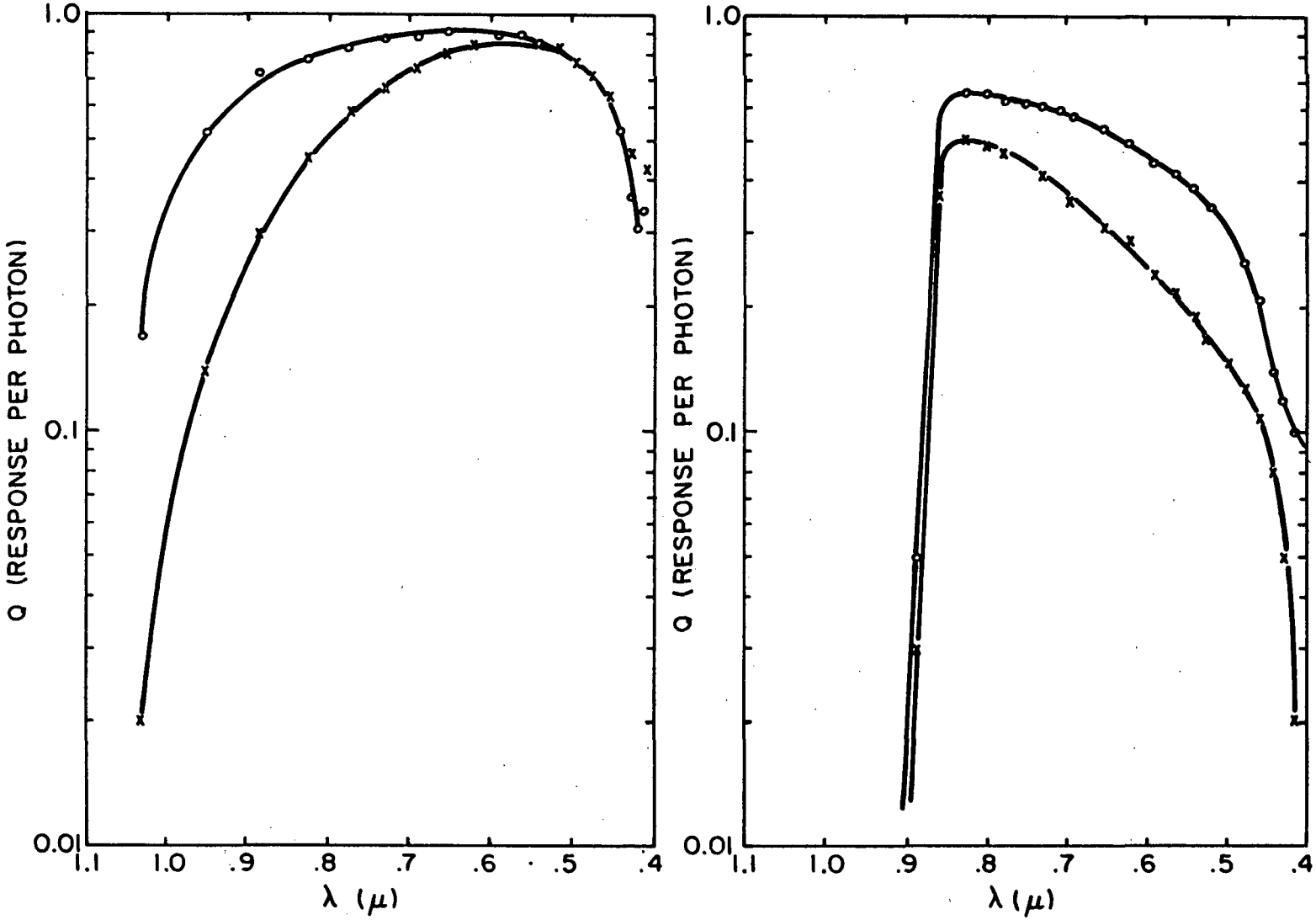

FIG 10 Comparison of the spectral response of a silicon and a GaAs solar cell before and after irradiation.

TABLE I

Comparison of Solar Cell Damage Rates
Relative Fluxes Required for Equivalent Degradation

Each Line Has Been Separately Normalized

	SILICON				GaAs
	Standard		Shallow Junction		
	(p/n)	(n/p)	(p/n)	(n/p)	
.5 MeV electrons	1	40			
1 MeV "	1	40	1.3	50	50
6 MeV "	x		1	10	100
1.8 MeV protons	1	4			60
8 MeV "	1	3			
19 MeV "	1	4		20	80
95 MeV "	1			10	60

VI. Summary

It is obvious from this discussion that there are still a number of gaps in our understanding of the radiation damage problem as it applies to semiconductor devices in general. We know very little about the physical identify of the radiation defects in silicon, and nothing about the defect centers in GaAs. There is a continuing effort at RCA and elsewhere to provide some of the answers, which we hope will be the first step in developing more damage-resistant devices.

Paper B-2

SURFACE EFFECTS OF RADIATION ON TRANSISTORS*

by

D. S. Peck, R. R. Blair, W. L. Brown, and F. M. Smits
Bell Telephone Laboratories, Incorporated
Murray Hill, New Jersey

I. Introduction

A wide variety of effects of high energy radiation on semiconductor materials and devices have been recognized and studied for a number of years. The major emphasis in this field has been on effects that involve the bulk properties of semiconductors. A great deal of progress has been made in understanding the processes that control bulk radiation phenomena[1] and in understanding the implications of these phenomena for semiconductor devices.[2] Radiation effects on semiconductor surfaces also have been observed[3], and this paper is concerned with some special aspects of surface phenomena that have recently come to light. In contrast to bulk effects, the surface radiation effects are very poorly understood and in general even poorly characterized. This paper will attempt to shed a little light on these complexities and indicate a type of measurement program that has been found appropriate for dealing with devices intended for use in a radiation environment such as that of the Van Allen Belts in space. It will fall short of providing a satisfactory understanding of the processes involved.

---

*This paper was published in the January 1963 issue of the Bell System Technical Journal; included here with the permission of the American Telephone and Telegraph Co.

[1]Partly supported by contract with Electron Technology Laboratories, Aeronautical Systems Division of the United States Air Force Systems Command.

The paper is arranged as follows: in Section II for perspective, a brief discussion of the two broad classes of bulk radiation effects. Section III, description of the early observations that provoked the present work. Section IV, a proposed model of the basic process. Section V, results of a number of experiments carried out to test the mechanisms of the process. Section VI, characterization of effects with significant numbers of devices. Section VII, the process of testing and selection undertaken for Telstar devices. Section VIII, Summary.

II. Bulk Radiation Effects

Bulk radiation effects can be placed in two broad classes that arise from (a) hole-electron pairs produced in the crystal by ionizing radiation and (b) defects in the semiconductor lattice produced by high energy particles. These phenomena often occur together but they result from quite different interactions of radiation with the solid and they have very different consequences in semiconductors.

II.1 Hole-electron pair formation

Figure 1a illustrates the first case. Any charged particle passing through a solid produces ionization through collisions with the bound electrons. These collisions excite electrons to the conduction band and leave holes in the valence band, producing electron-hole pairs in exact analogy with the production of pairs by light. Neutrons and gamma rays also cause ionization effects through intermediate reactions that

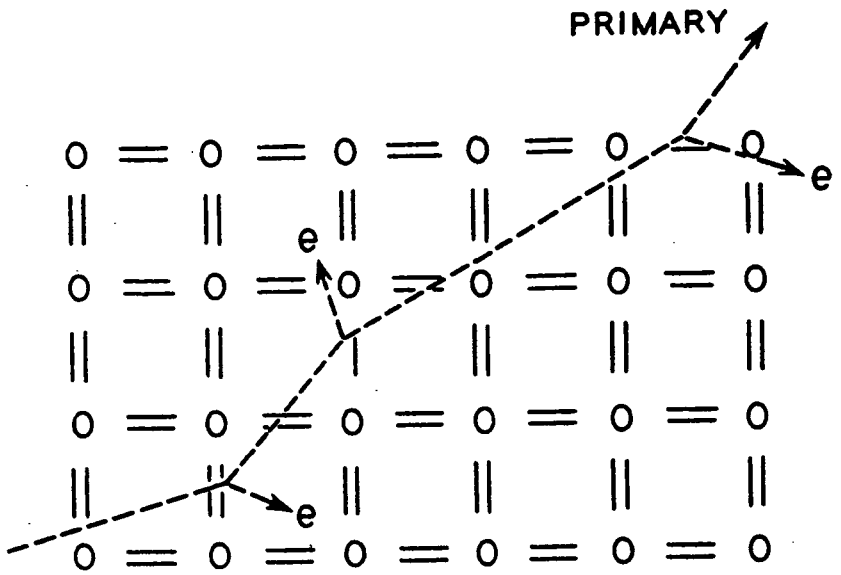

(a)

Production of hole-electron pairs by collision of a charged particle with electrons of a semiconductor.

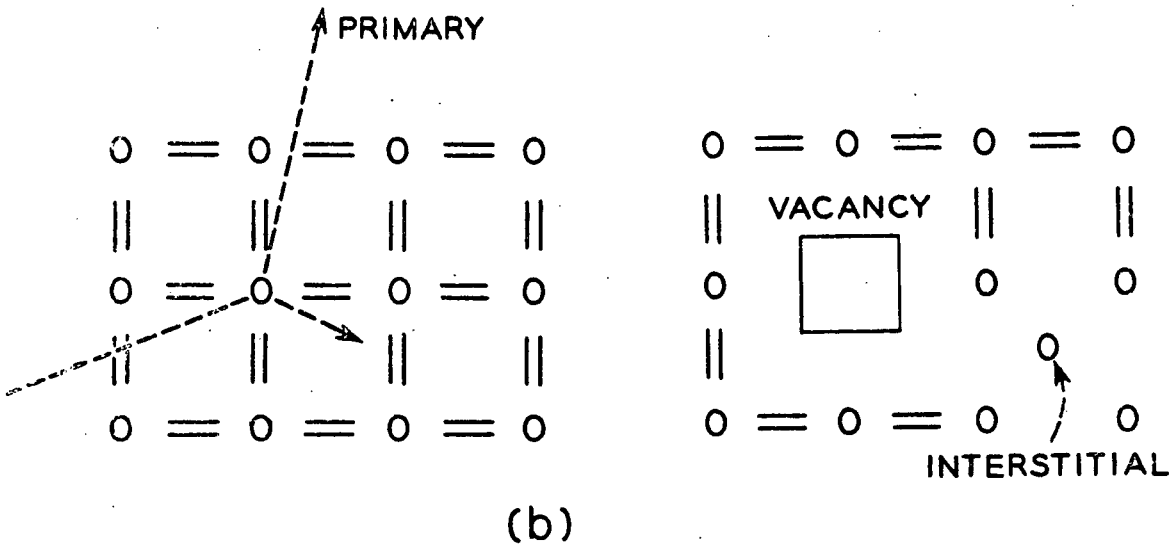

(b)

Production of lattice defects by collision of particles with the nuclei of a semiconductor.

Fig. 1

produce charged particles. As far as effects which depend on ionization are concerned, the particular particle involved is incidental; all that matters is how much energy is lost in

the solid. The number of hole-electron pairs produced is proportional to this energy loss.

The generated pairs tend to recombine with a time constant that is the conventional lifetime. Hence, all effects in this class are transient and persist only for the order of a lifetime after the excitation is removed. The pairs produced alter the conductivity of semiconducting materials. They also contribute currents in p-n junction diodes and transistors. Under pulsed ionizing radiation these effects can alter conductivities and currents by many orders of magnitude. On the other hand these effects can be very small in response to a single energetic particle and special p-n junction diodes may be required even to detect them.[4] A case of intermediate magnitude has been considered by Rosenzweig[5] who has used silicon solar cells to measure the intensity of moderate radiation fields.

II.2 Lattice damage

Figure 1b illustrates the other type of bulk radiation effect in semicondcutors that arises from collisions of energetic particles with the nuclei of the lattice. If such a collision transfers sufficient energy to the struck atom, it is capable of moving the atom from its normal lattice site to some interstitial position in the crystal. These events are rare by comparison with the ionization events of Fig. 1a, but they create permanent or at least semipermanent defects in the structure of the lattice. The most important consequence of these defects is reduction in

the carrier lifetime of the material. Increases in diode reverse current and decreases in transistor current gain are produced as functions of the time integral of the flux of particles. In contrast to the pair production of the paragraph above, this radiation damage is extremely dependent on the particular particle involved. Energetic protons, for example, are much more effective in producing damage than energetic electrons. This type of radiation effect is of major importance to the long term power conversion efficiency of solar cells in space. Detailed consideration of this problem can be found elsewhere[6].

III. The Surface Problem

Surface effects on semiconductor devices have an illustrious history of subtlety and perversity and it is no surprise to learn that radiation is an environmental factor that must be considered. Several years ago, before the present sophistication in surface processing, experiments were carried out in an attempt to characterize radiation surface effects[3] (changes in junction current, breakdown voltage, current gain, etc.). No systematic picture emerged, although surface cleanliness seemed certain to play some role.

Transistors that have evolved from refinements in junction formation and surface treatment techniques have, in the last few years, been examined in a variety of high energy neutron and gamma-ray environments. Particular attention has been given to bulk radiation damage effects on current gain

since these effects turned out to be serious (particularly for silicon) at the flux levels of current interest in the vicinity of nuclear reactors. Very substantial improvements in radiation tolerance have been found; however, no recent comprehensive work on the surface effects has been reported.

The relative stability of the characteristics of a particular type of diffused silicon transistor under radiation is illustrated in Fig. 2. The collector reverse current is displayed because it is a particularly sensitive indication of surface stability at the very low currents that are conventional in present silicon devices. The gamma ray radiation* used in this case is representative of ionizing radiation in general. The figure shows that after one hour tests with neither bias nor radiation or with either alone, the current is essentially unchanged. (Actually much longer tests under bias are conventionally made in checking device reliability with the same results as shown here.) However, when bias and gamma radiation are simultaneously applied two effects appear: there is a sudden rise in current and then an upward drift of current over many minutes. The sudden rise of about 0.02μa is largely due to ionization of the gas in the device can. The current drifts upward by another decade in the 45-minute exposure following

*Radiation dose is frequently expressed in "rads" which are a measure of the energy absorbed per unit mass of material. One rad is equivalent to absorption of 100 erg/gm. Such a dose would produce approximately 2×10^9 ion-electron pairs/cm^3 in atmospheric air or about 4×10^{13} electron-hole pairs/cm^3 in silicon.

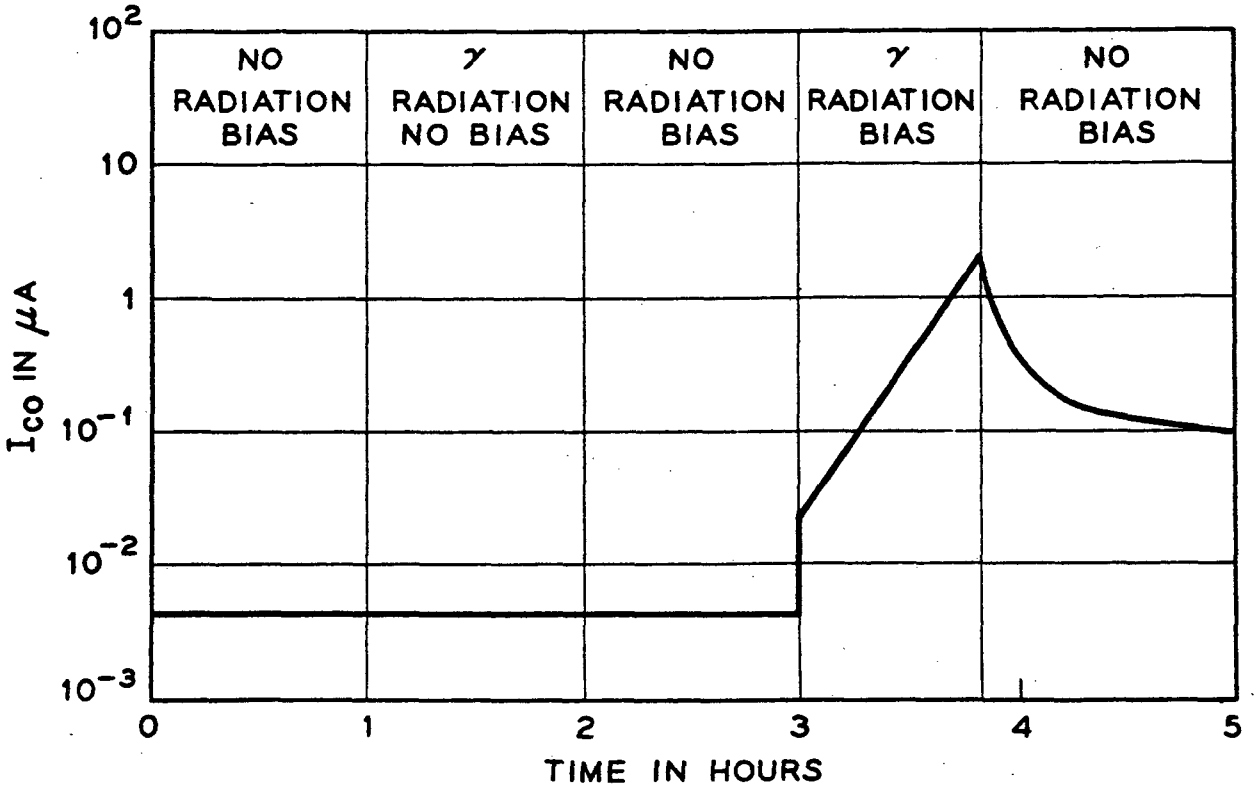

Fig. 2.

The response of I_{CBO} of a diffused silicon transistor to either radiation or bias alone or to both together. Radiation dose rate 8.5×10^5 rads/hr.

its rapid rise. When the gamma radiation is removed the current does not immediately drop back to its preirradiation value, but gradually declines and even after an hour is more than a decade too high. A drop of about 0.02μa must still occur at gamma ray turnoff, but this is so small compared with the level to which the current has drifted, that the drop is not visible.*

The drift up and the slow decay of the collector currents are surface effects produced by the radiation only when the collector junction is reverse-biased. This aspect of radiation sensitivity had not previously been reported. It represents a factor that must be considered for reliability of devices that must operate in any radiation environment including the high energy electron and proton belts found in outer space. The conclusion that these effects arise at the semiconductor surface can be reached in a number of ways. If they were bulk effects the marked influence of applied bias is quite unreasonable. Radiation defects created in a solid have been influenced by extremely high electric fields, but only to the extent of causing them to migrate very short distances in

*Ion currents to the electrical leads either in the device encapsulation or in the gamma radiation chamber pose a serious problem to measurements on devices at very low leakage currents in high radiation fields (10^5-10^6 rad/hr). It has often proved necessary to remove the device from the radiation environment momentarily for measurement. Because of recovery effects care must be taken to obtain measurements quickly and at uniform times after removal.

long times.[7] Furthermore, the decay of the effect occurs in a time that is very short for defect annealing in silicon. But more convincing is the sensitivity of the effect to the surface environment of the device inside its encapsulating can.

Figure 3 shows four typical n-p-n diffused silicon transistors of two types, each with two kinds of ambient atmosphere. Increases in collector current are observed in all four, but at quite different integrated gamma-ray doses. In both device types early current increases are associated with gas filling. In type B the evacuated device shows no measureable change until the integrated dose is in a range expected to cause substantial decreases in bulk lifetime. In this case, the influence of bias, although not shown in the figure, is practically nonexistent.

Not only is there a variation in the response depending on the gas filling of transistor cans, but there is also great variability among devices with a single type of filling. All evacuated units are slow to respond, but in the type B transistor only about half of the gas-filled units respond quickly. The other half are almost as stable as the evacuated units. This points again to a surface effect and to a broad spread in response arising from rather subtle differences in the surface chemistry. This lack of reproducibility complicates the study of the process involved and necessitates the use of statistical experiments, some of which will be reported in later sections.

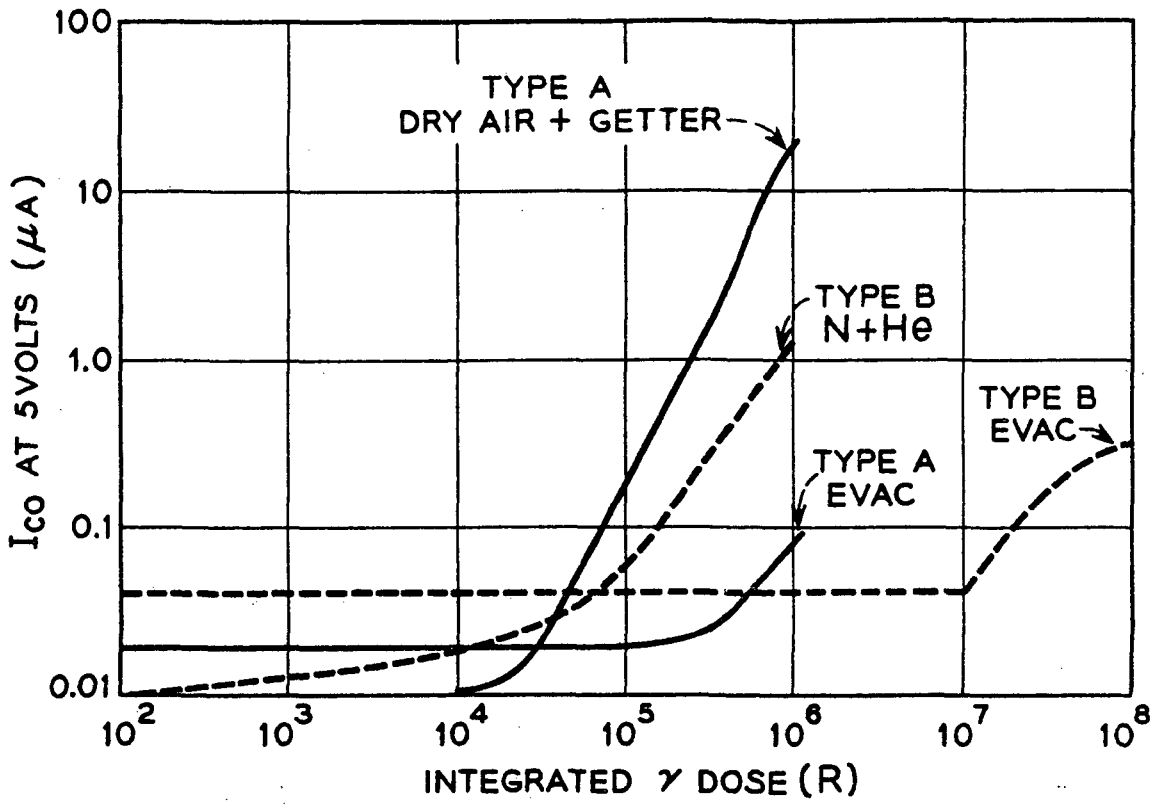

Fig. 3.

The radiation degradation of I_{CBO} of two types of diffused silicon transistors, evacuated or with gas filling. Radiation dose rate 8.5×10^5 rads/hr.

Before continuing to discuss the experimental observations we will introduce a simple model which describes some, but not all, of the effects, and provides a framework for the later discussion.

IV. A Model of the Process

Radiation, gas encapsulation, and device bias that seem to be essential to the effects shown in Section III can be combined in a simple model of the process. Fig. 4 illustrates the ingredients: the fringing field of a reverse biased collector junction on an n-p-n transistor and ions and electrons produced by gamma radiation in the gas of the encapsulation. The fringing field separates the electron-ion pairs, depositing electrons on the collector side of the junction and positive ions on the surface of the base. On both regions these charges tend to produce inversion layers at the surface, the effects being analogous for p-n-p and n-p-n devices. For simplicity only the inversion layer on the p-type base of an n-p-n transistor will be considered. A magnified view of the edge of the device might be as shown in Fig. 5. The positive ions induce an electron-rich inversion layer or "channel" on the base and in effect extend the collector region out over the base. The channel represents a grossly different surface than existed before. Since the junction between the electron-rich channel and the base material constitutes an extension of the collector-base junction, it contributes to the collector saturation current. In part this is simply because of the extra junction area. More importantly, because the channel junction is very close to the surface, the surface generation process can yield much more current per unit area than for the junction in the bulk. Furthermore, if the

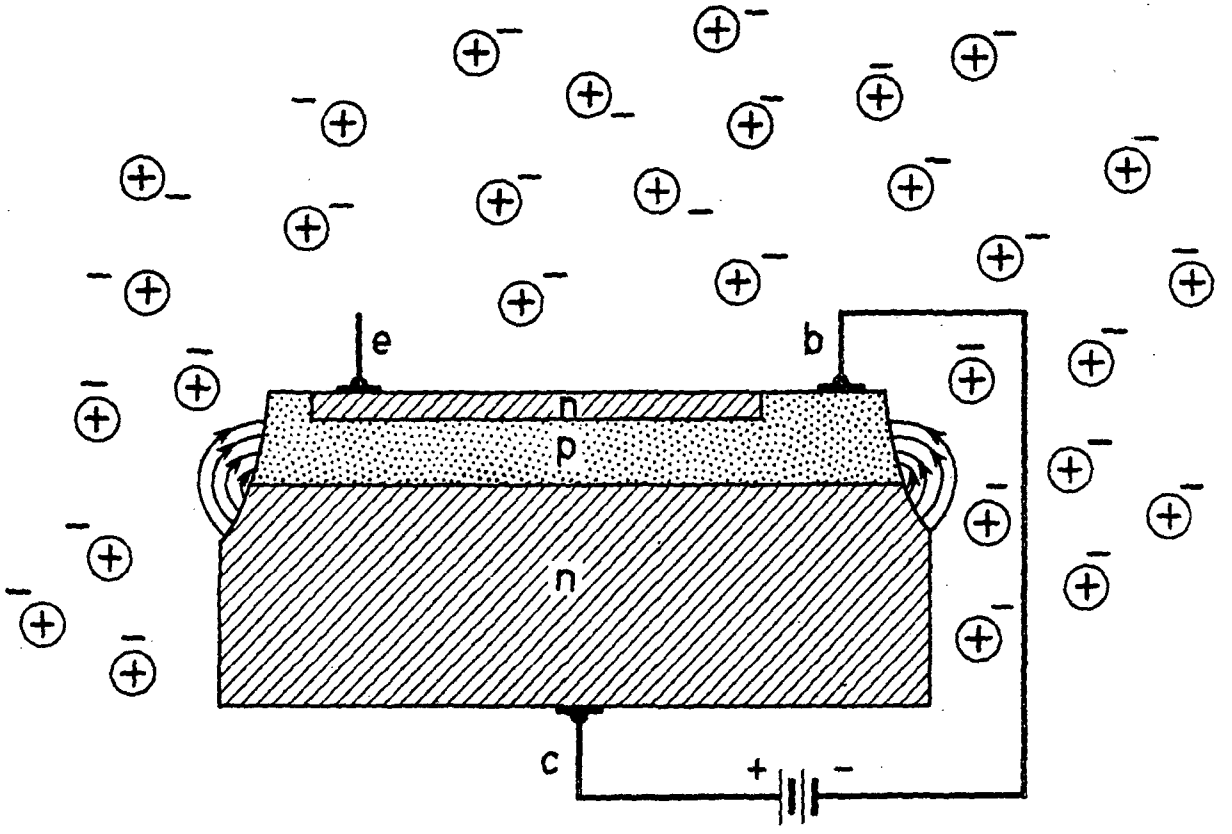

Fig. 4.

A model of a reverse biased transistor in a gas atmosphere ionized by radiation.

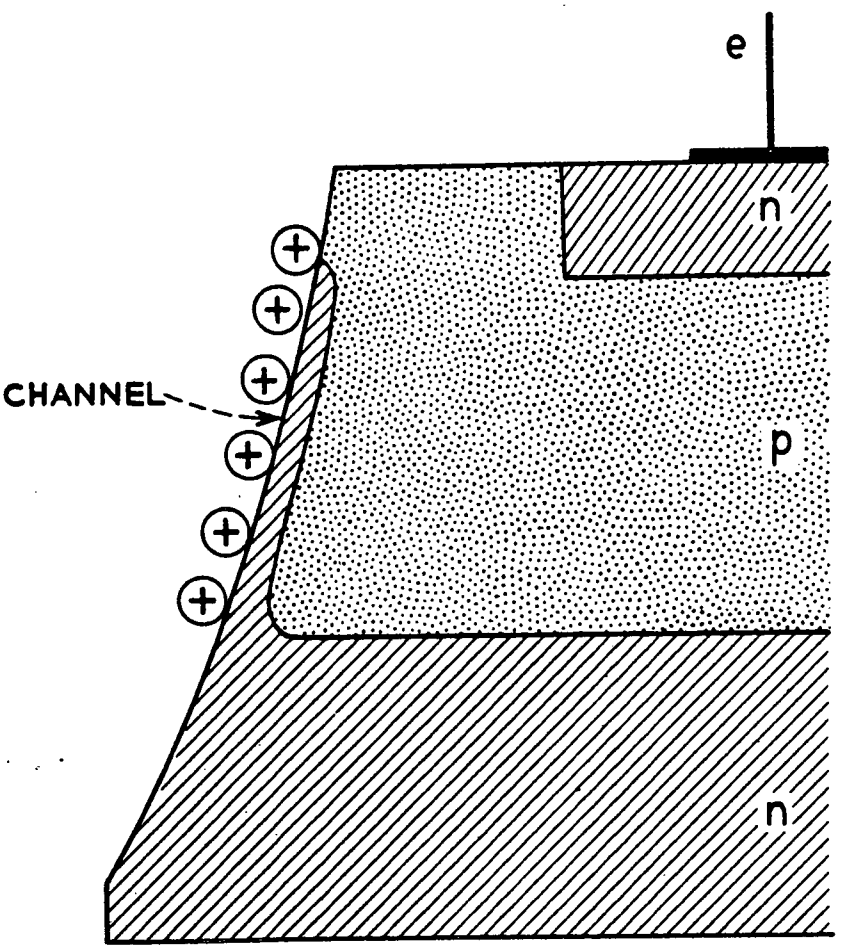

Fig. 5

Formation of a channel on the base of a transistor by + ion collection on the surface.

channel extends to the emitter it can add additional current to the collector by serving as a conducting path between the two. Channel effects on transistors and diodes have been studied previously in considerable detail[8] entirely unrelated to the presence of radiation. The basic channel characteristics of emitter-to-collector conductance, high emitter floating potential, and channel pinchoff have all been observed in connection with the present surface radiation effects on diffused silicon transistors.

We have so far considered only formation of a channel by charge collection in the collector fringing field, but a second possibility is shown in Fig. 6. In all the n-p-n diffused silicon transistors used in these experiments the collector is electrically tied to the encapsulating can of the device. Under collector reverse bias a field then exists throughout the whole can and of such a sign as to drift positive ions toward the surface of the device base. This feature can be expected to increase the ion-collection efficiency.

One may ask if there are enough ions produced in the gas of the can, by the radiation doses that have been used, to provide large channel effects. At an integrated dose of 10^4 rads (at which these effects may be substantial) and at atmospheric gas pressure (the normal device filling) a total of about 2×10^{13} ions per cc will have been produced. With a device enclosure of about 3×10^{-3} cc and a base layer area of about 10^{-3} cm^2, if all the ions were collected on the base, their concentration would be about $10^{14}/cm^2$. On typical base

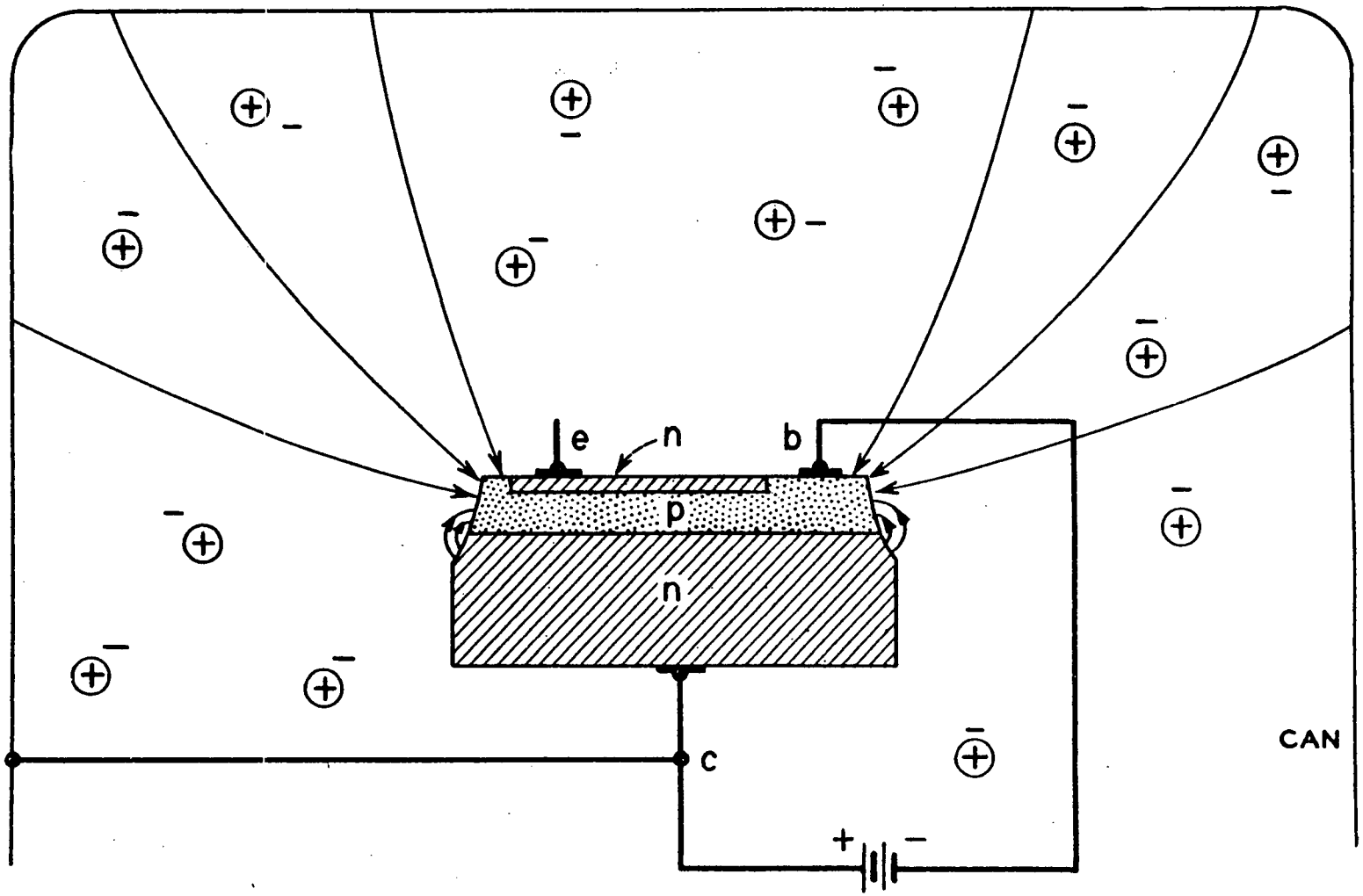

Fig. 6

The enhancement of ion collection at a transistor surface due to electron fields between the device and its encapsulating case.

material only about 10^{11} surface charges/cm^2 will be required to produce a channel. These several orders of magnitude margin are probably quite important because the efficiency of the surface charging process seems likely to be quite low. Furthermore, the process is far from a perfect charge integrator as we shall have occasion to observe in connection with reciprocity experiments in Section V.2.

The lack of reproducibility noted in Section III in connection with devices of the same type and same gas filling seems to necessitate an elaboration on the model. If ions of the gas are sufficient to produce a channel, why are there some devices with gas that are as stable as devices without? The gas ions themselves must not be the tenacious charge on the surface that forms the channel. The gas ions probably exchange their charge with residual contaminants on the device surface. Ionization of the surface contaminants directly is apparently too rare to be observed, since vacuum encapsulated devices show uniformly high surface stability. This is roughly reasonable since the probability of ionization of any single atom is estimated to be only about 10^{-5} at 10^4 rads. Even with a monolayer of residual surface contamination, the surface ion concentration would then be only about $10^9/cm^2$. Of course, if the gas ions are to do the job, they must be reasonably effective in finding and exchanging charge with the residual impurities. There seems to be margin for inefficiencies in these very rough numbers.

This model predicts a number of effects that can be tested:

1. The effect depends only on ionization, not on incident particle type.
2. The simplest form of the model suggests that the effect is cumulative and depends on total dose, not on dose rate.
3. The effect should be more pronounced at higher collector bias.
4. The electric field between the can and the semiconductor may influence ion collection.
5. The decay of the effect should be faster if the device is not under continuous bias and should be accelerated in the presence of radiation without bias.

The results of the experimental tests of these predictions are contained in the following section.

V. Tests of the Model

V.1 Ionization

If the ionization in the gas of the device encapsulation is essential, then just as in the case of the ionization effect in a semiconductor discussed in Section II.1, the type of energetic particle should not matter. The experiments in Section III were carried out with Co^{60} gamma rays which ionize through photo or Compton electrons that they produce. We have tested the model by comparing the results of 18 Mev proton irradiation with the Co^{60} gamma rays. The individual device response scatters so widely that the behavior of a number of similar devices is examined in each case. Figure 7 shows the collector reverse current versus radiation dose, for gamma rays in dashed lines and protons in solid lines. The dose is calculated simply from the amount of energy deposited in a gas (the gas of the encapsulation) by gamma rays and protons. The radiation intensity (dose per unit time) was approximately 10^6 rads/hr for the protons as well as for the gamma rays.

Within the spread of response observed, there is no significant difference between protons and gamma rays. If bulk damage in silicon were involved, one could expect a factor of 10 to 100 greater effect for the protons than for the gamma rays. (The bulk damage effect per particle comparing 18 Mev protons and 1.25 Mev gamma rays would be a factor of 10^4 to 10^5, but the scale in Fig. 7 is not particles but ionization, or energy loss, and the protons lose energy at a much higher rate

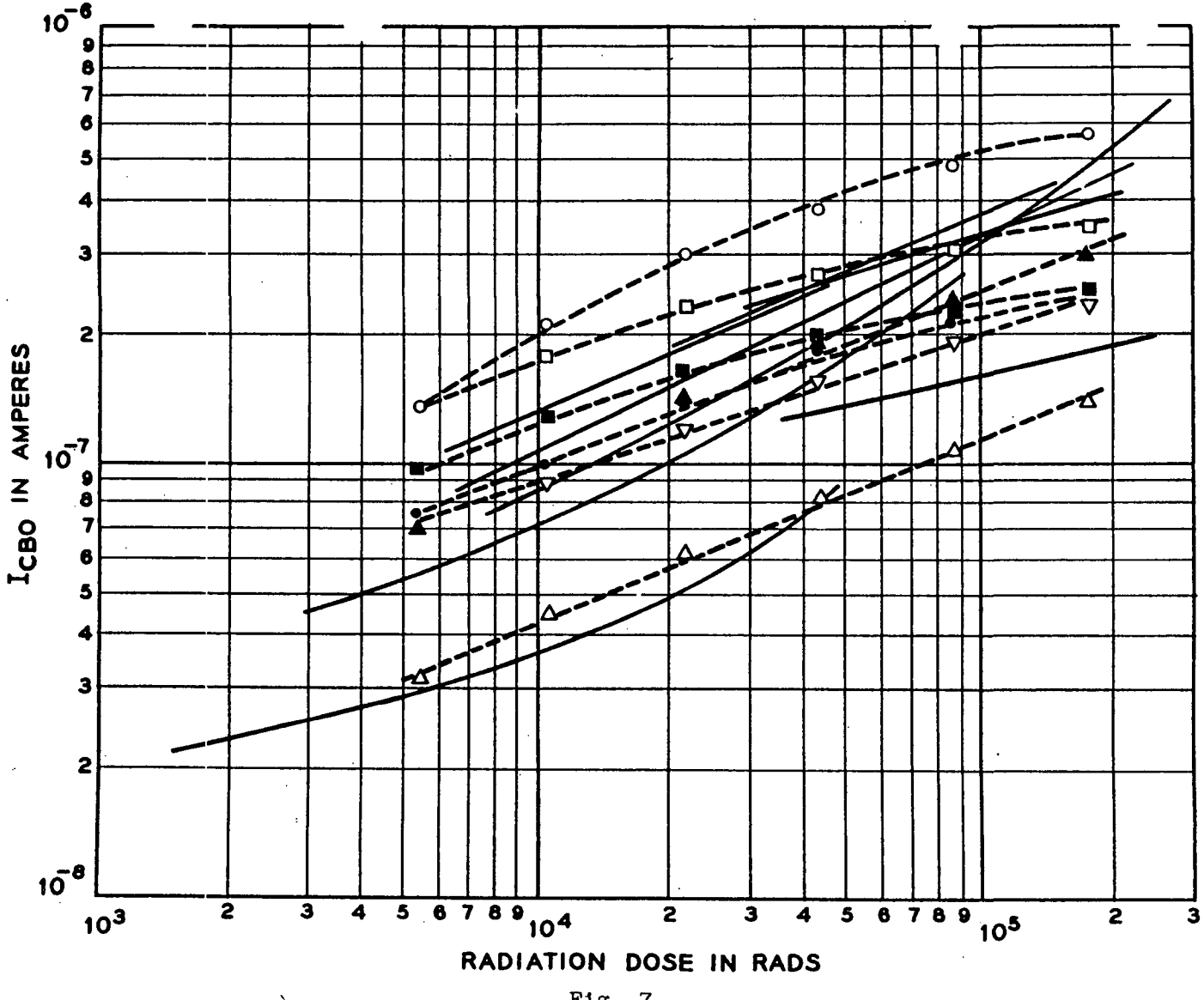

Fig. 7

Comparison of I_{CBO} changes under radiation by gamma rays (dashed lines) and protons (solid lines).

than gamma rays.) We conclude that ionization is essential to the mechanism of this surface radiation effect.

V.2 Reciprocity

The surface ionization effects may depend only on the total radiation dose or they may also depend on the dose rate. In the first case there is reciprocity between dose rate and time. Information on this point is relevant to understanding the process and is of immediate practical importance as well. The experiments are most easily performed at high dose rates, but the device reliability is also of concern in modest radiation fields.

In Fig. 2 recovery of the collector current following radiation was illustrated. The fact that recovery occurs at all when a device is removed from radiation but kept on bias proves that the observed result does not depend solely on the total dose. The ionized state of the surface at any time is not simply related to the total number of ions that have reached that surface.

Figure 8 shows the change of collector current vs. dose at two different high dose rate levels. The experiment was started at 8.5×10^5 rads/hr. After five minutes, when a dose of 7×10^4 rads had been delivered, the transistor was placed inside a lead shield that attenuated the gamma radiation by a factor of six. When a dose totaling 2.5×10^4 rads had been given the device, the attenuator was removed and the higher level radiation continued. After each attenuator change,

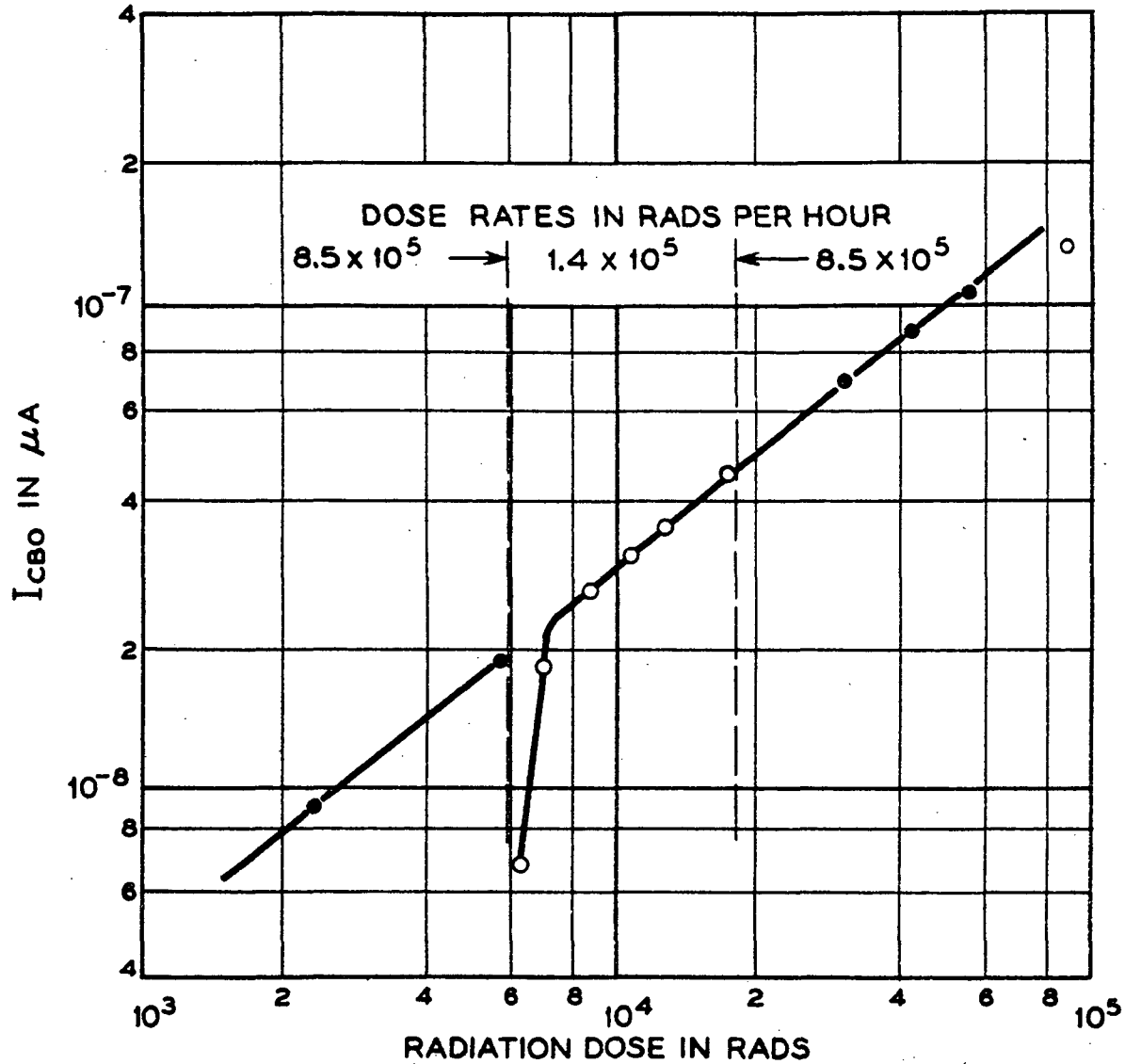

Fig. 8

Reciprocity of dose rate and time at two high radiation dose rate levels.

the collector current continues to rise in a smooth extension of the earlier portions of the curve. If the dose rate were important, the middle segment of the curve would be expected to have a different slope than the two ends. During the attenuator changes the device was out of the radiation for approximately a minute and the current had started to recover, as indicated by the first point taken at the lower dose rate. A comparable drop would have appeared at the second attenuator change, but the earliest measurement after reinsertion in the radiation field was not obtained soon enough for it to show.

The rapid re-establishment of a previous high response to radiation after some recovery from it, represents a memory in the process. This kind of memory has been seen repeatedly. Devices that were irradiated and have apparently completely recovered their original collector characteristics by standing out of radiation and even off bias, will still tend to re-establish their former response on a second radiation exposure. Even after several weeks, a device seems to retain a sensitivity to subsequent radiation as a result of an earlier exposure. There is some evidence that the memory can be removed by baking at approximately 100°C for a few hours.

The ionization produced by the radiation apparently has two functions: first, to produce some chemical species that are capable of ionization and second, to keep these species in an ionized state. The number of these centers would reflect the total radiation dose, but some minimum level of radiation would be required to keep them active.

We can draw the conclusion from Fig. 8 that, in the high-intensity region, dose is the important variable. Fig. 9 illustrates quite a different range. Here a device started its radiation history at only 10 rads/hr and established a pattern of current increase that is already determined at a dose less than 10^4 rads. Putting the device into the attenuated high-intensity source does not produce a simple continuation of the earlier curve, but rather produces a curve two and one-half orders of magnitude higher in current. This illustration is extreme and not many devices show this large a discontinuity, but essentially none give results that could be interpreted as simple reciprocity. Apparently over a dose-rate range this great, using the concept of the preceeding paragraph, the ionization-sensitive chemical entities are not fully ionized in the low radiation field.

5.3 Surface Effect vs. Collector Bias

Since the surface effects we have been considering are absent except under the simultaneous application of radiation and collector reverse bias, we expect to find that changing the bias will alter the effect. This can occur because of increases in efficiency of charge collection, but also because the increased junction field tends to bind the ions more tightly to the surface or distribute them to form a more extensive inversion region.

Figure 10 shows the effect of a sudden change in bias from 5 to 15 volts. One gains the impression that the

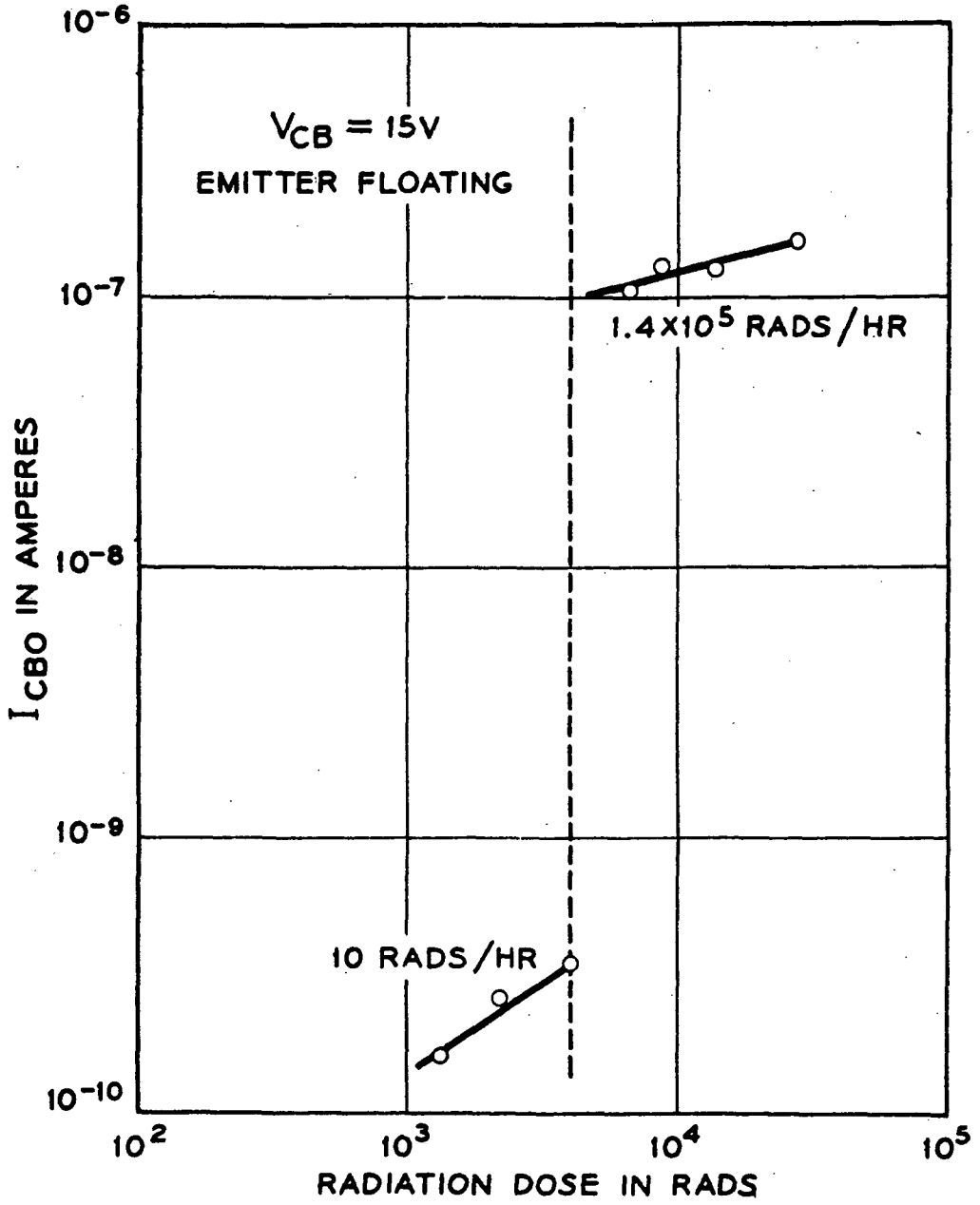

Fig. 9
Lack of reciprocity between high and low dose rates.

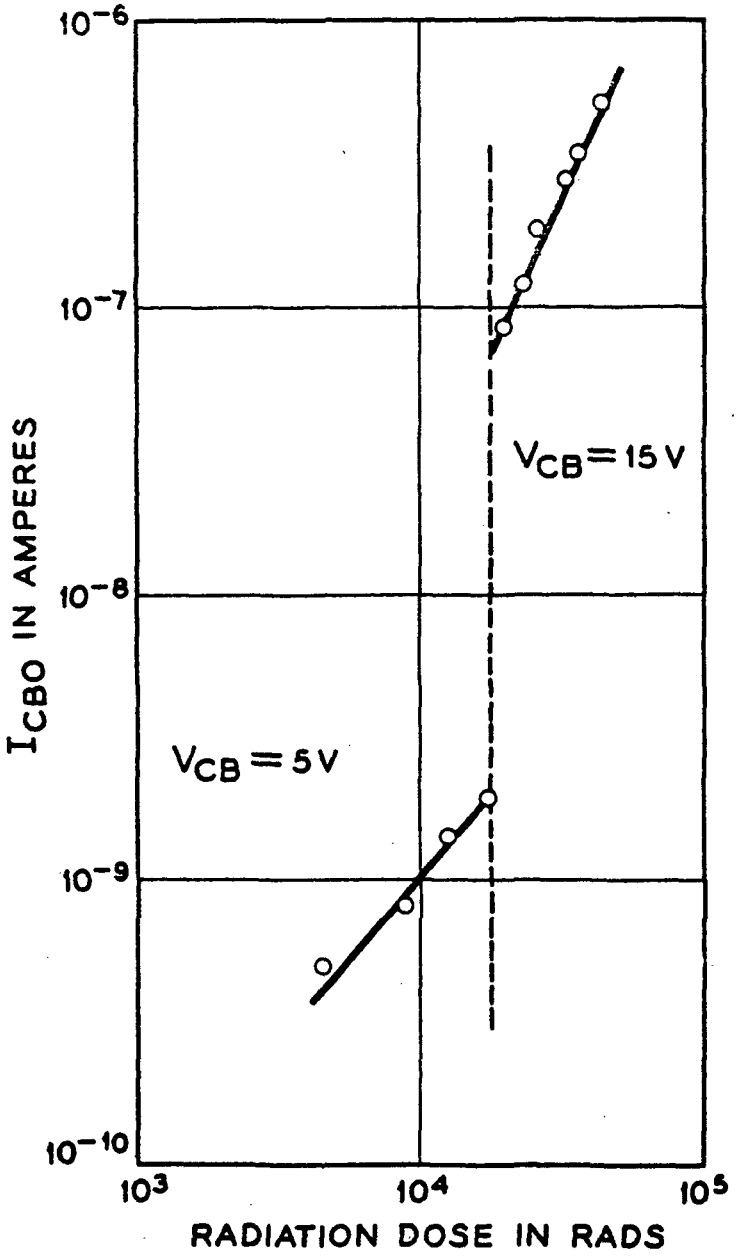

Fig. 10

Influence of change in collector bias on degradation of I_{CBO}. Dose rate 8.5×10^5 rads/hr.

current suddenly adjusts to a level and to a rate of change that are what they would have been if the entire dose had been given the device at the higher bias. If this impression is valid it would indicate that the effect at higher bias had not been retarded by the initial dose at low bias, and hence that ion collection was no different. In a plot like Fig. 10 it must be realized that the significance of the first dose rapidly diminishes in comparison with the total as one moves out along the second branch of the curve. It does seem possible to infer that a given number of ions on the surface give a larger current contribution at higher bias. Rearrangement in the new field and effective extension of the length of a surface channel can occur.

Figure 11 shows the response of transistors under radiation at different biases. Up to a dose of about 10^4 rads the current increase depends strongly on bias. Between 10^4 and 10^5 rads the slopes of the curves on this log-log plot are quite similar. Although only 4 units are illustrated in Fig. 11, the total group in the experiment was 80 and this pattern of behavior was quite consistent. Even beyond 10^5 rads where the slopes increase there is considerable uniformity between individuals and across the voltage range. This point is illustrated in a different way in Fig. 12 where the median behavior of a group of 10 to 12 devices at each bias is plotted at 6×10^3 rads and 6×10^4 rads. The pattern of bias

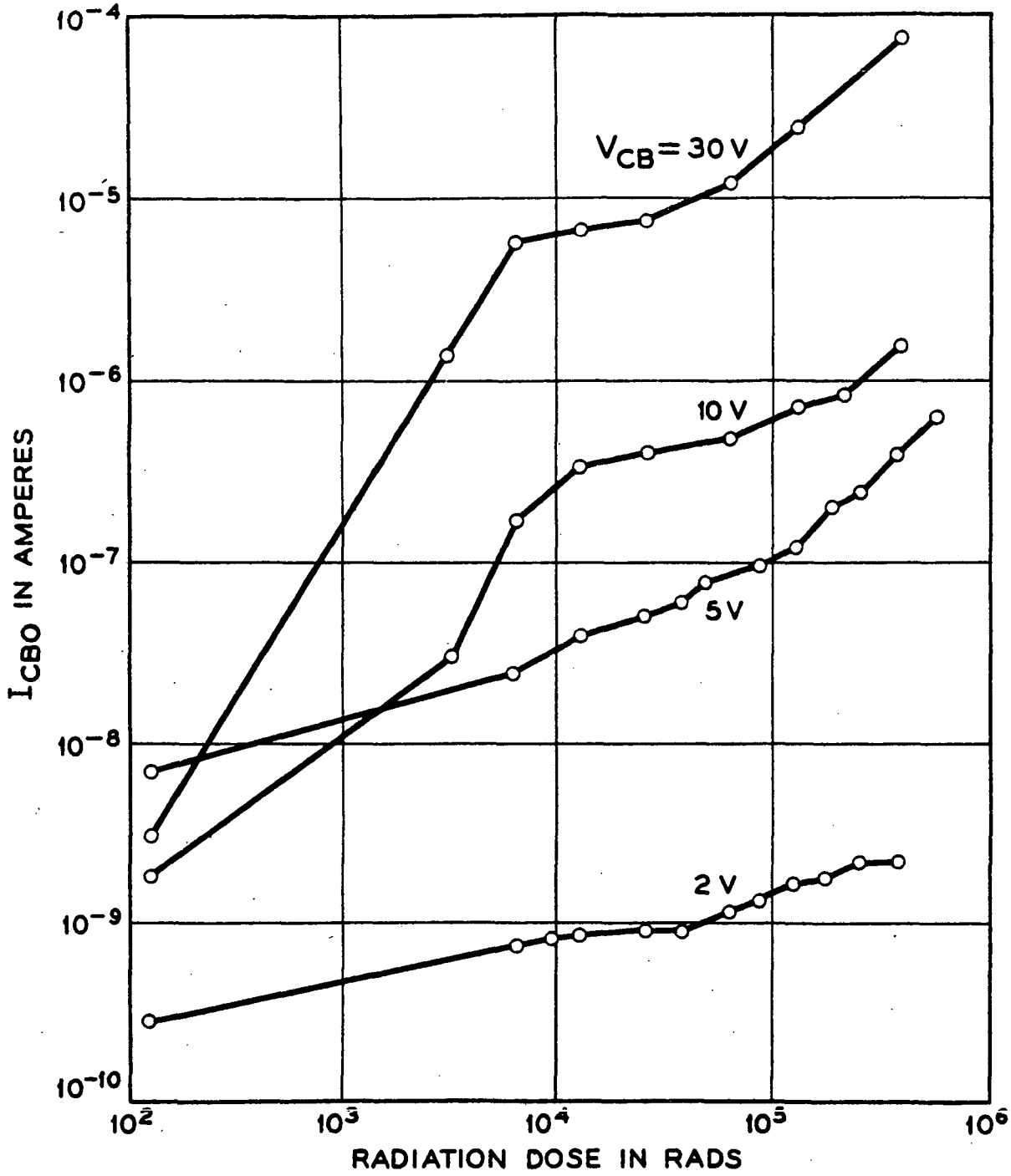

Fig. 11
Dependence of degradation in I_{CBO} on collector bias.

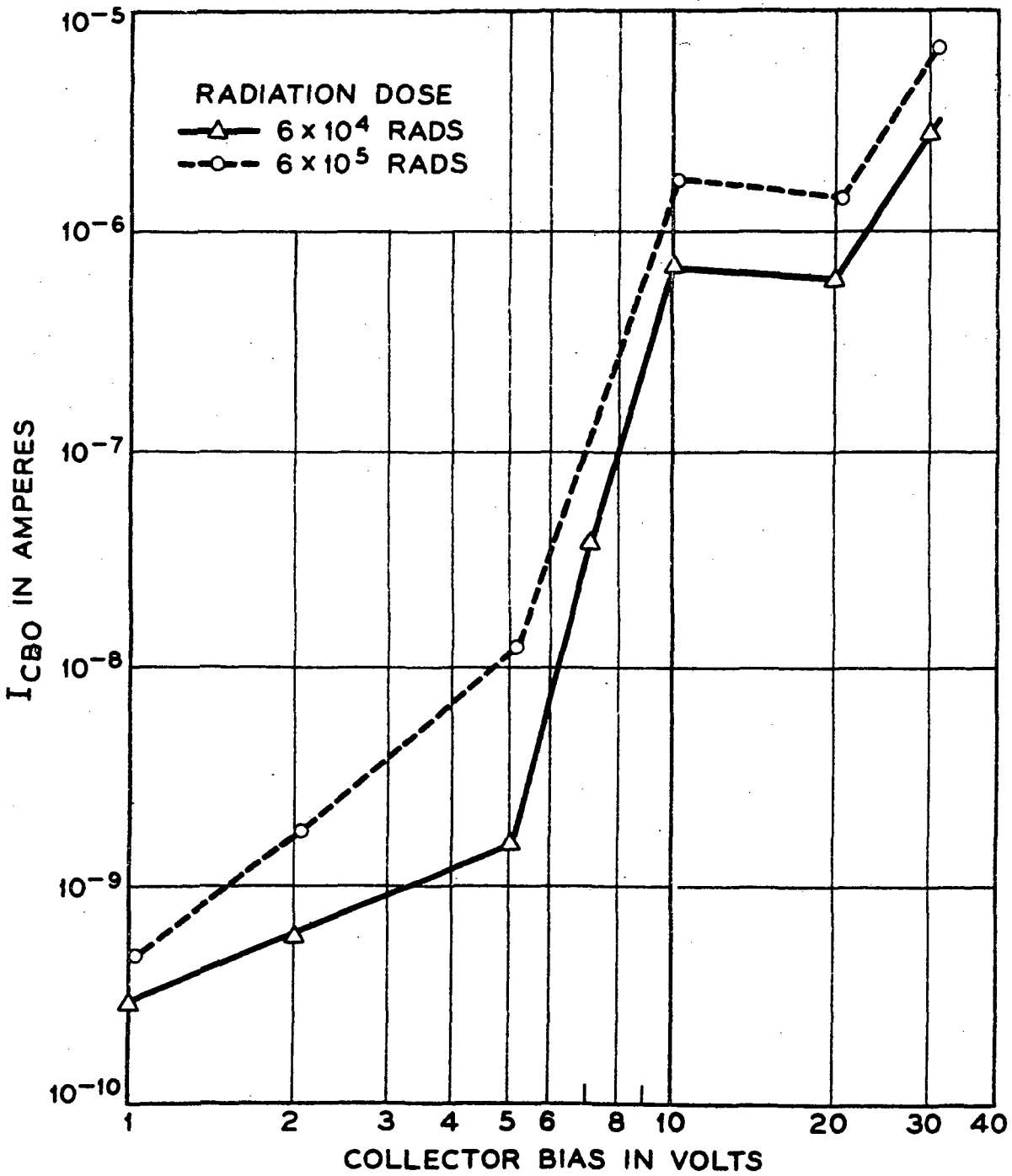

Fig. 12

Median behavior of I_{CBO} with collector bias at two integrated doses.

dependence is already established at the lower dose and is smoothly maintained after the further order-of-magnitude change in dose. The lump at 10 volts appears to be significant. If it is real, its explanation will require a clever refinement in the model.

We do indeed observe the anticipated increase in device degradation at higher bias. The consistency of the shape of the voltage dependence at doses greater than 10^4 rads strongly suggests that the dependence does not arise only from a difference in the numbers of available surface ions, but also from variation in the arrangement of ions and the influence of this arrangement on the current characteristics of the channel. The collection of charge does not seem to be the dominant variable over the voltage range examined.

Another indication that junction bias effects the arrangement of charge on a device surface is shown in Fig. 13. The characteristics observed after a total dose of about 10^7 rads and at a high dose rate may show considerable structure, depending on the rate at which the characteristic is swept out. Furthermore, the differences between the characteristics with slow and fast sweep show that rearrangements are not instantaneous. Note that here also a peak of I_{CBO} occurs in the vicinity of 10 volts.

5.4 Influence of Can Potential

It has been suggested that the electric field existing between the can and the transistor base by virtue of the bias on the collector junction may alter the collection of ions at

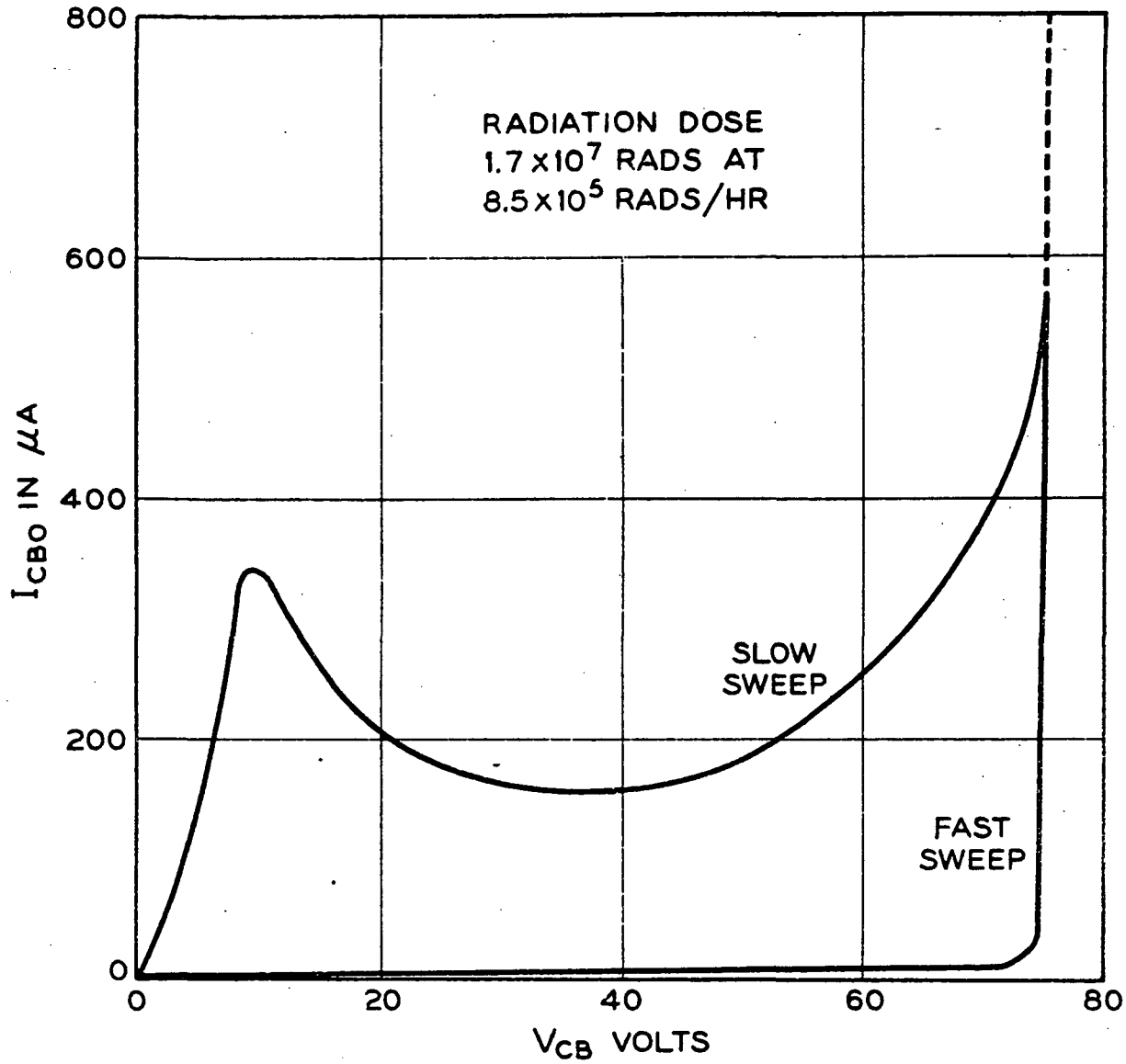

Fig. 13

Structure and drift in the reverse characteristics of a heavily irradiated transistor under radiation.

the semiconductor surface. This possibility has been examined using diffused silicon diodes, encapsulated in the same gaseous atmosphere as the diffused silicon transistors. Devices with the p-region common to the can and others with the n-region common were studied. There was no substantial difference in sensitivity to ionization in these cases. On the other hand it was found that by alteration of the device processing, devices of either polarity were insensitive. It is clear that in this case the chemical surface condition is of more vital importance than the can-to-diode bias.

No silicon transistor with reversible polarity to the can has been available, but a germanium transistor with all leads insulated from the can has been irradiated with reversal of the sign of can bias. The results are shown in Fig. 14. The device was irradiated at 8×10^5 rads/hr for one minute with the can negative with respect to the transistor base (the collector of which was continuously reverse biased) and then one minute with the can positive and so on for longer times as the irradiation proceeded. The leakage current is very clearly much more sensitive to positive potential on the can than to negative, a result consistent with the original picture of the role of positive ions in a channel on the transistor base. This experiment has been repeated several times with some lack of reproducibility. In some cases can bias makes much less difference than as shown in Fig. 14

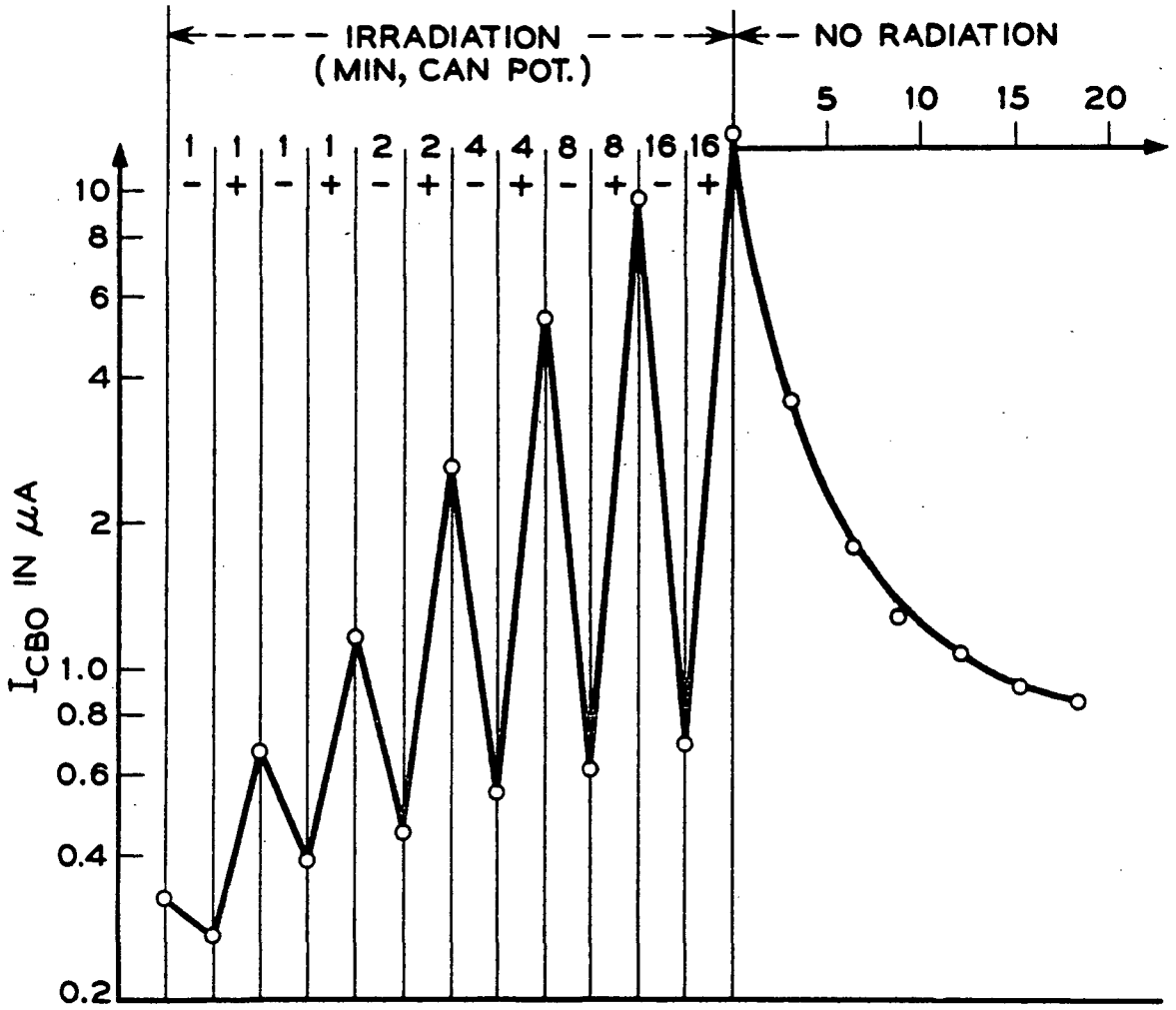

Fig. 14

The influence of the can to semiconductor potential on degradation in I_{CBO} of a germanium transistor.

and in two cases where the whole radiation effect was smaller, the dependence on can bias polarity was reversed.

There seems to be no question that the can-to-device potential can be important, but clear-cut evidence that positive ions rather than electrons (or negative ions) are always the important particle in transistor surface ionization effects has not been demonstrated.

5.5 Recovery

Recovery of the surface effects after an exposure to radiation has already been mentioned in connection with Figs. 2 and 8. The recovery is not exponential. In many cases, recovery under bias is well represented by a straight line on a log I_{CBO} vs log t plot, although the points at less than 0.5 min tend to fall below such a curve. The recovery represents a loss of charge at the surface, perhaps by neutralization from the interior in the absence of a radiation flux, but the memory effects suggest the active species do not actually leave the surface.

The comparison between recovery with and without bias is shown in Fig. 15. A transistor given a dose of 4.6×10^3 rads at 5 volts is shown, first recovering at this same bias and then recovering with the collector circuit open except momentarily for measurement. The decay is substantially accelerated in the zero bias condition. This is consistent with the idea that the ions are bound in place by the field but in its absence are free to diffuse on the

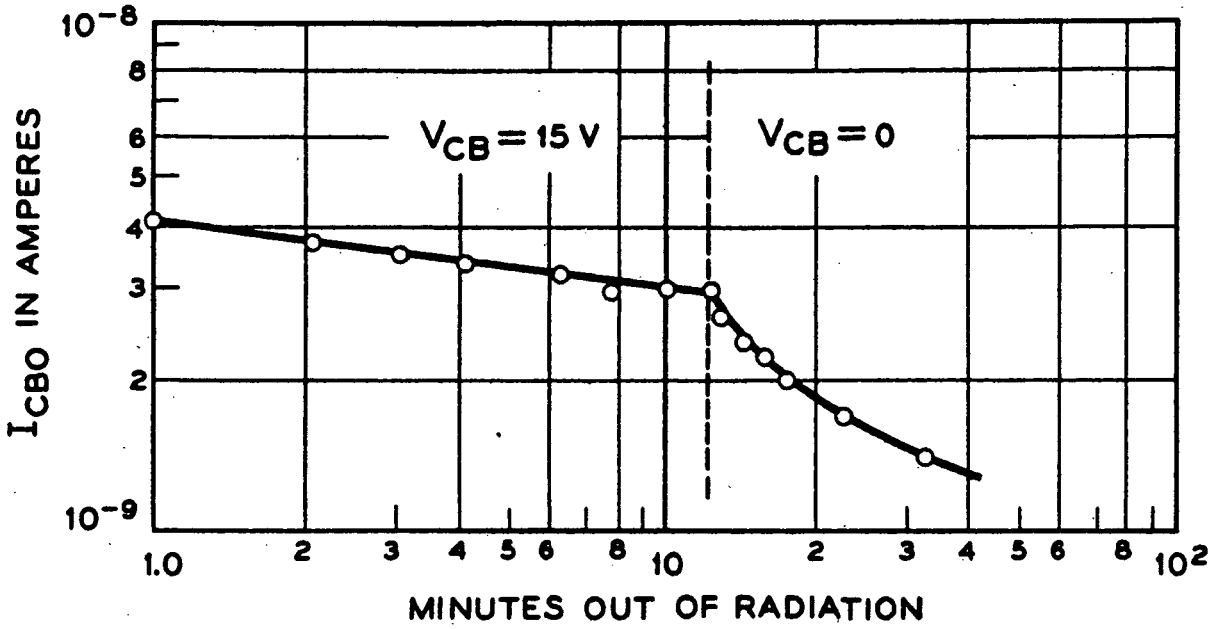

Fig. 15

Decay of the radiation effect with bias and without.

surface and will no longer be concentrated to produce an inversion layer. It has also been observed that with re-establishment of the bias the current rises before continuing its decay, suggesting that the ions are subject to recapture by the field. There is a loss in this process however, that may arise from the enhanced neutralization of the ions by electrons from the inversion layer when they are more numerous in the absence of reverse bias.

Figure 16 illustrates the effect of radiation on recovery. The upper curve was taken first and is a normal recovery with bias. The lower curve shows recovery from the same starting value in the 8×10^5 rads/hr gamma field without bias. The device is momentarily removed from radiation for measurement at 15 volts reverse bias. The recovery is substantially enhanced by the ionization in the absence of bias. This seems to be explained through neutralization of the charges on the semiconductor surface by the newly formed ions. Under bias the gas ions are directed by the junction field to strike the surface in places where they add to an inversion layer. In the absence of a field from applied bias, these ions tend to go wherever they can reduce fields produced by surface charges.

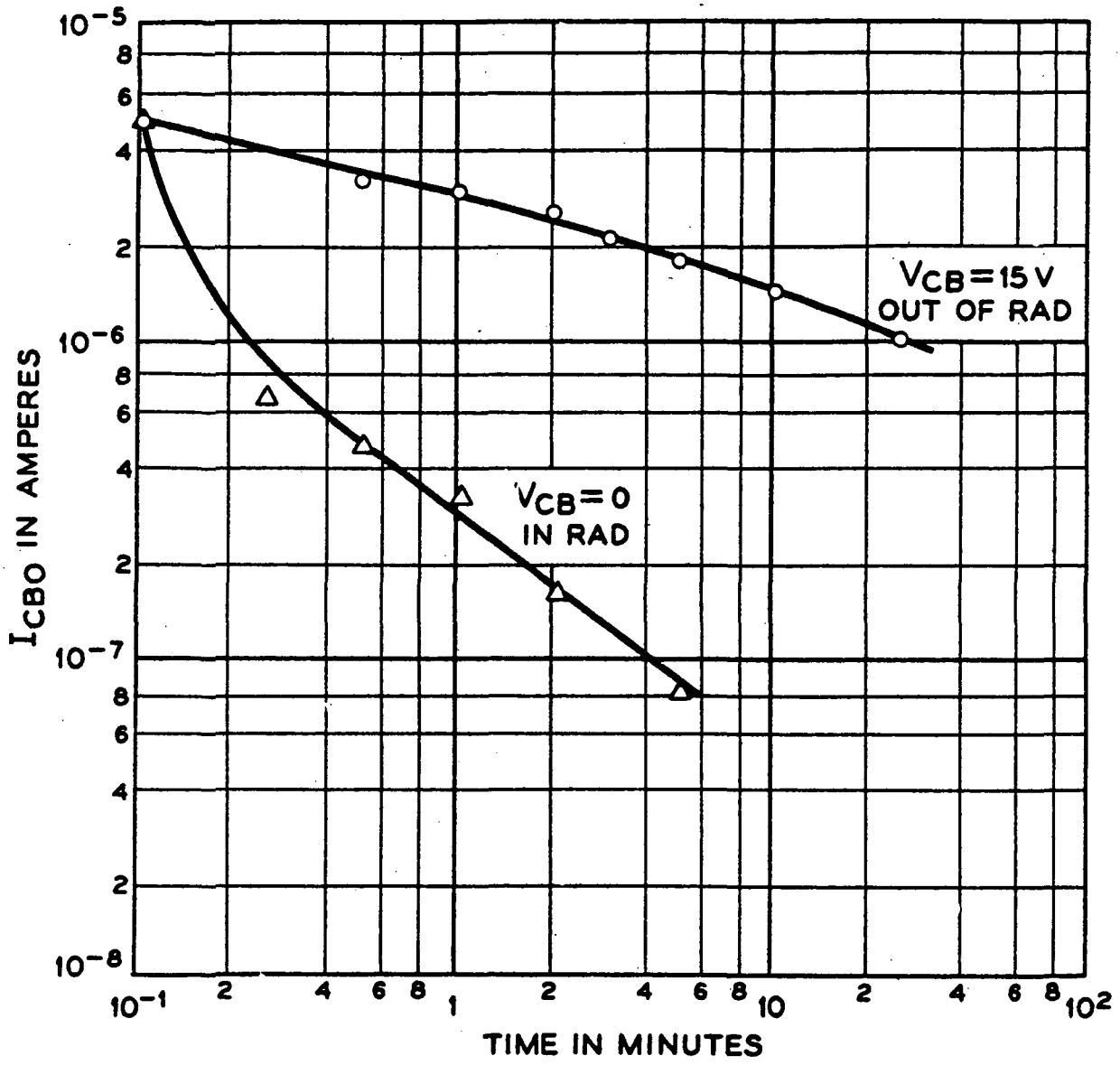

Fig. 16

Enhancement of the rate of recovery of I_{CBO} with radiation but without bias.

VI. Characterization of Effects with Significant Numbers of Devices

With the above background concerning the surface effects of ionizing radiation, and with recognition of the limited knowledge of the range of exact surface conditions existing in semiconductor devices, further tests were planned to establish the extent of the ionization effect in larger samples of devices. For the purpose of such a test program, a transistor type was selected which showed particular sensitivity to the combined effects of electrical bias and ionizing radiation. These transistors normally have quite low collector reverse currents, I_{CBO} (in the order of 10^{-10} amperes). They are therefore good subjects for study at relatively low gamma dose levels since small increases in I_{CBO} can readily be recognized. A large number of devices were available with sufficient power aging to indicate stability of characteristics, so that changes could clearly be attributed to the radiation exposure.

Although the measurements of gain of these transistors under gamma radiation indicate some change with dose, the changes are relatively smaller than those in the junction reverse current and are hence less subject to recognition of a specific pattern of change. The data presented here, therefore, relate specifically to the changes in I_{CBO}.

VI.1 Typical Pattern of Degradation with Dose

In order to determine the proper conditions for large scale evaluation, and to have some estimate of changes

to be expected, it is desirable to establish the pattern of change in characteristics. From the data presented in Section V on the various factors affecting degradation, there develops a typical pattern of degradation, at least for the type of diffused silicon transistor used, as shown in Fig. 17. In this log-log plot of I_{CBO} vs. integrated dose, four recognizable regions are indicated, an initial region of stability followed by three regions of change. The boundaries of the regions as indicated in Fig. 17 only depict representative variations and do not indicate actual limits of the device type.

As discussed in Section 5.3, the slopes of the degrading I_{CBO}'s become quite uniform among all units of this type beyond a total dose of about 10^4 rad, or beyond the variable Region 2. In Region 3 all units show slopes of approximately 1/2, and at about 10^5 rads there is a fairly distinct increase in slope, which distinguishes Region 4. Although these two regions are recognizable, they are of lesser importance in judging comparative usefulness of the devices in radiation than are the region of stability and the slope in Region 2.

The region of stability is indicated even in the early tests (see Fig. 3) and continues to show up, even at the lowest initial current levels, when the dose rate is low enough to allow measurements at sufficiently low total dose.

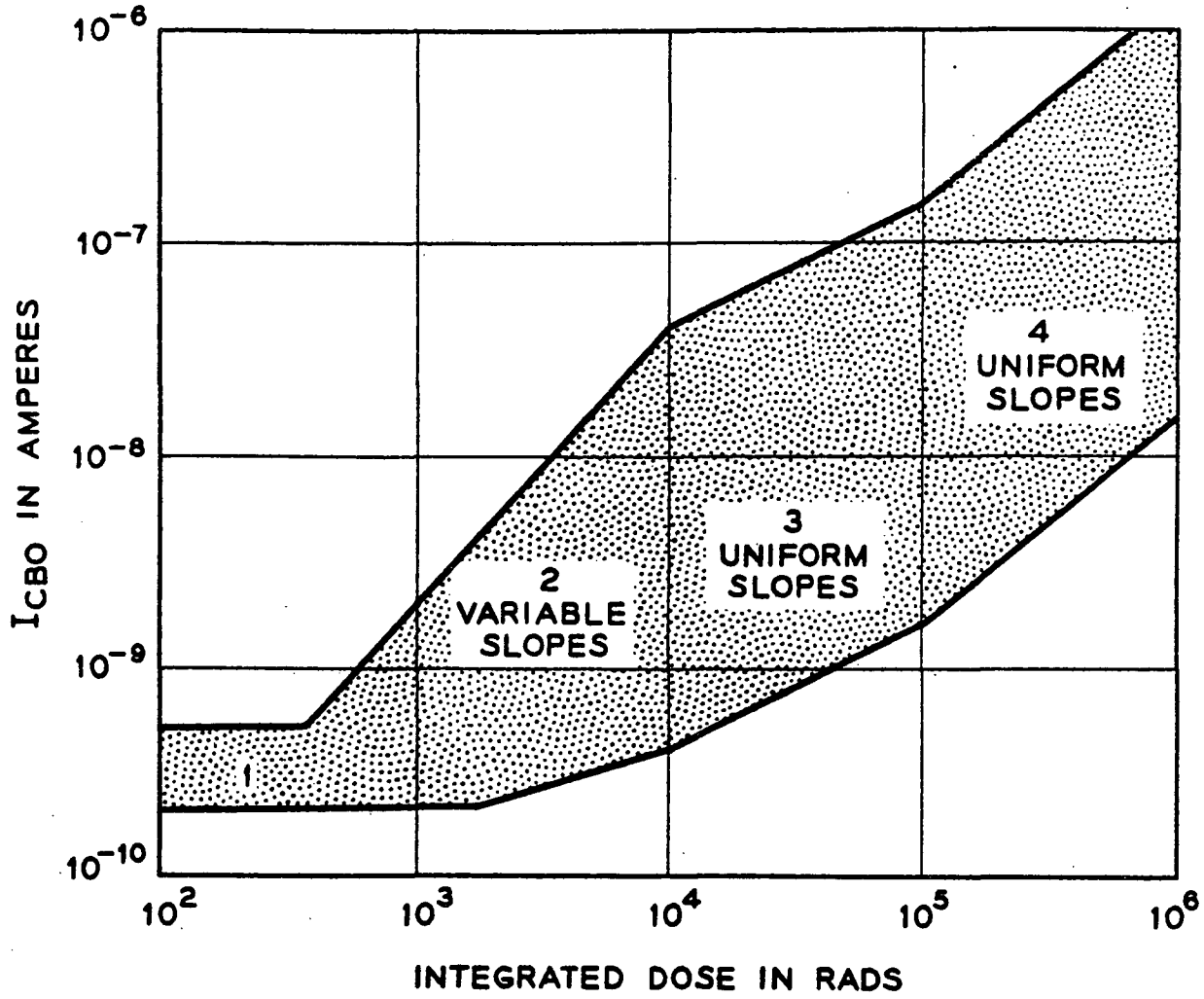

Fig. 17

The typical pattern of I_{CBO} degradation under radiation for a particular type of diffused silicon transistor.

The extent of Region 1, or the dose value at which an individual unit starts to degrade, is quite variable among units of a type, as well as between types, and is a significant point for further consideration of devices.

The transition into Region 2, where the units show a typical linear increase in log I_{CBO} with log of dose, is quite distinct in all observed cases. For this reason, data which show only the degrading slope in Region 2 (perhaps because a high dose rate causes the first measurement to be beyond Region 1) can be extrapolated with some confidence back to the preradiation value to achieve an estimate of the transition dose. Major features of Region 2 are extreme variations between individual devices of a type and considerable dependence on collector voltage. This dependence is shown in Fig. 11 by the variations in I_{CBO} values achieved at about 10^4 rad, apparently about the end of Region 2 for this type.

In general, there appears to be a consistency between Regions 1 and 2 in that those units which show the greatest change in Region 2 also tend to indicate the shortest period of stability in Region 1; and conversely, those showing smaller changes in Region 2 appear to have the longer period of initial stability. Within the range of actual initial values (from 8×10^{-11} to 2×10^{-9} amperes) however, there appears to be no correlation between the initial value and the subsequent severity of degradation.

VI.2 Distributions of Dose at Initiation of Degradation

With the recognition of the typical response of this transistor type to radiation, a question can first be asked regarding the variability in the extent of the region of stability, Region 1.

Figure 18 shows several plots of the distribution, on a normal probability scale, of the integrated dose at which degradation is initiated (the end of Region 1). The three lowest curves show the results obtained from exposure to gamma radiation at 8.5×10^5 rads/hr., 10 rads/hr., and 1 rad/hr., all with a collector bias of 15 volts and with no connection to the emitters. There appears to be only about a factor of 2 difference between the 8.5×10^5 rad/hr. and the 10 rad/hr. results. This evidence of reciprocity between the 8.5×10^5 rad/hr. dose and the 10 rad/hr. dose at the end of Region 1 is in contrast to the lack of reciprocity indicated in Fig. 9 which compares reverse currents in Region 2. On the other hand, the difference between the 1 rad/hr. and 10 rad/hr. distributions seems to indicate a breakdown of reciprocity, at this level, in the dose required to initiate degradation.

The two upper curves of Fig. 18 are obtained at 5 rad/hr. and with a forward bias on the emitters during radiation in addition to the reverse collector bias. One of these curves is on the same type (F-54273) as that of the lower distributions. The other distribution at 5 rad/hr. is

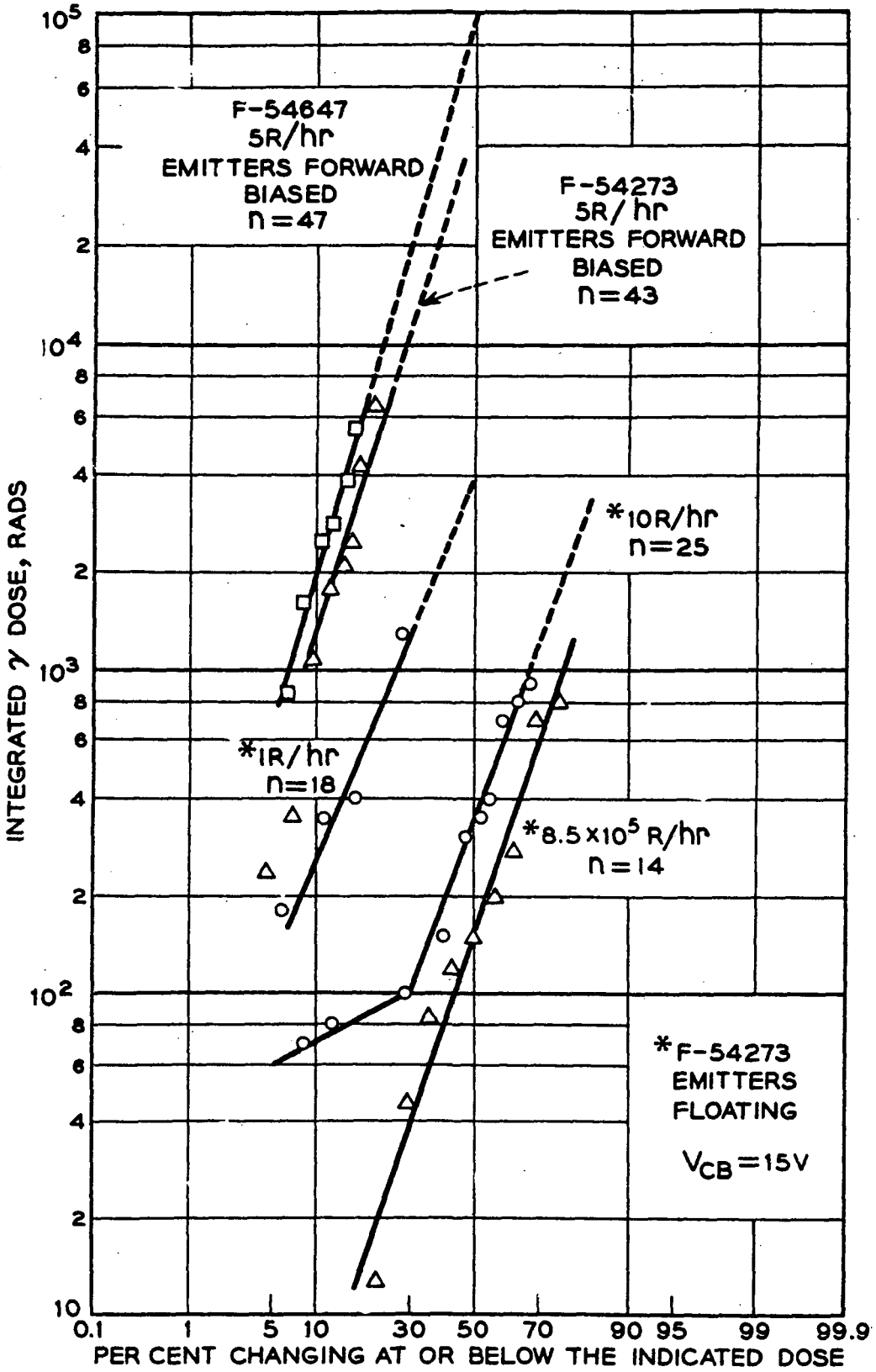

Fig. 18

Distribution of the radiation dose at initiation of degradation.

on another type (F-54647) which is basically the same but with a somewhat higher distribution of initial current gain. It would appear that the application of forward emitter bias causes an increase of roughly two orders of magnitude in the dose required for the onset of I_{CBO} degradation. This could result from the neutralization of positive charges on the surface of the base region by electrons injected into the base by the forward biased emitter.

VI.3 Distributions of I_{CBO} Increase

Figure 19 shows the distribution of the increase in collector reverse current resulting after 1.4×10^4 rads, which dose is past the completion of the variable Region 2. Here the I_{CBO}, on a log scale, is plotted on the normal probability scale. These data are on the same types of units represented in Fig. 18 and are obtained from radiation with the emitters forward biased. As in Fig. 18, the higher-gain type evidences a lesser degradation, having a longer region of stability as well as a smaller increase in I_{CBO} during Region 2. The excellent match to a log-normal distribution (except at very low currents where the data reflects the inaccuracy of measuring the difference between two nearly equal numbers) lends confidence to the interpretation that the break at the upper end of the distribution is caused by the transition into Region 3 of those units which have changed the most in the variable Region 2.

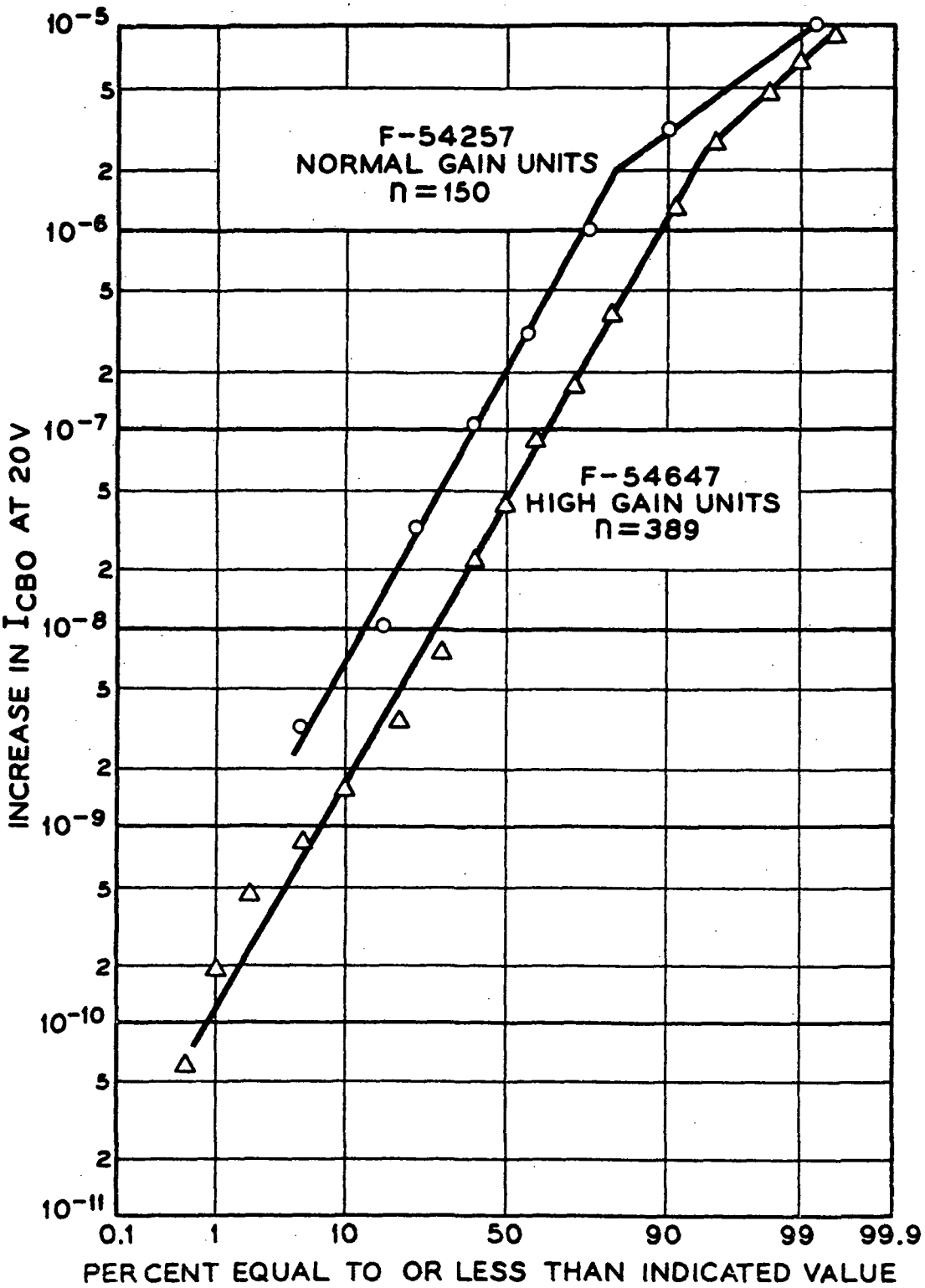

Fig. 19

Distribution of current degradation after a dose of 1.4×10^4 rad at 8.5×10^5 rads/hr.

The broad distributions of Figs. 5, 18, and 19 point up the necessity for relatively large-scale experiments in order to make valid comparisons between different test conditions or device types.

VI.4 Tests of Other Semiconductor Devices

Similar kinds of distributions and general responses to the various conditions affecting degradation under radiation have been found in other codes of diffused silicon transistors and silicon diodes which have been encapsulated with a gas filling.

Figure 20 shows, for example, the distribution of reverse current increase of a 1/4-watt diffused silicon diode after 3.7×10^4 rads at 7.4×10^5 rads/hr. The broken shape of the distribution may simply indicate that the devices did not come from a single product run. The lack of the distinct break in the distribution at high currents suggests that the transition to Region 3 may not exist, or exists at a different dose. It would appear that each type must be examined in detail for a good understanding, even empirical, of its performance under radiation.

One interesting variation to the kind of response indicated above is that of a type of silicon alloy transistor which contains a silicone grease. In this case a relatively minor degradation is observed during short periods at a high gamma dose rate, but more severe degradation occurs during

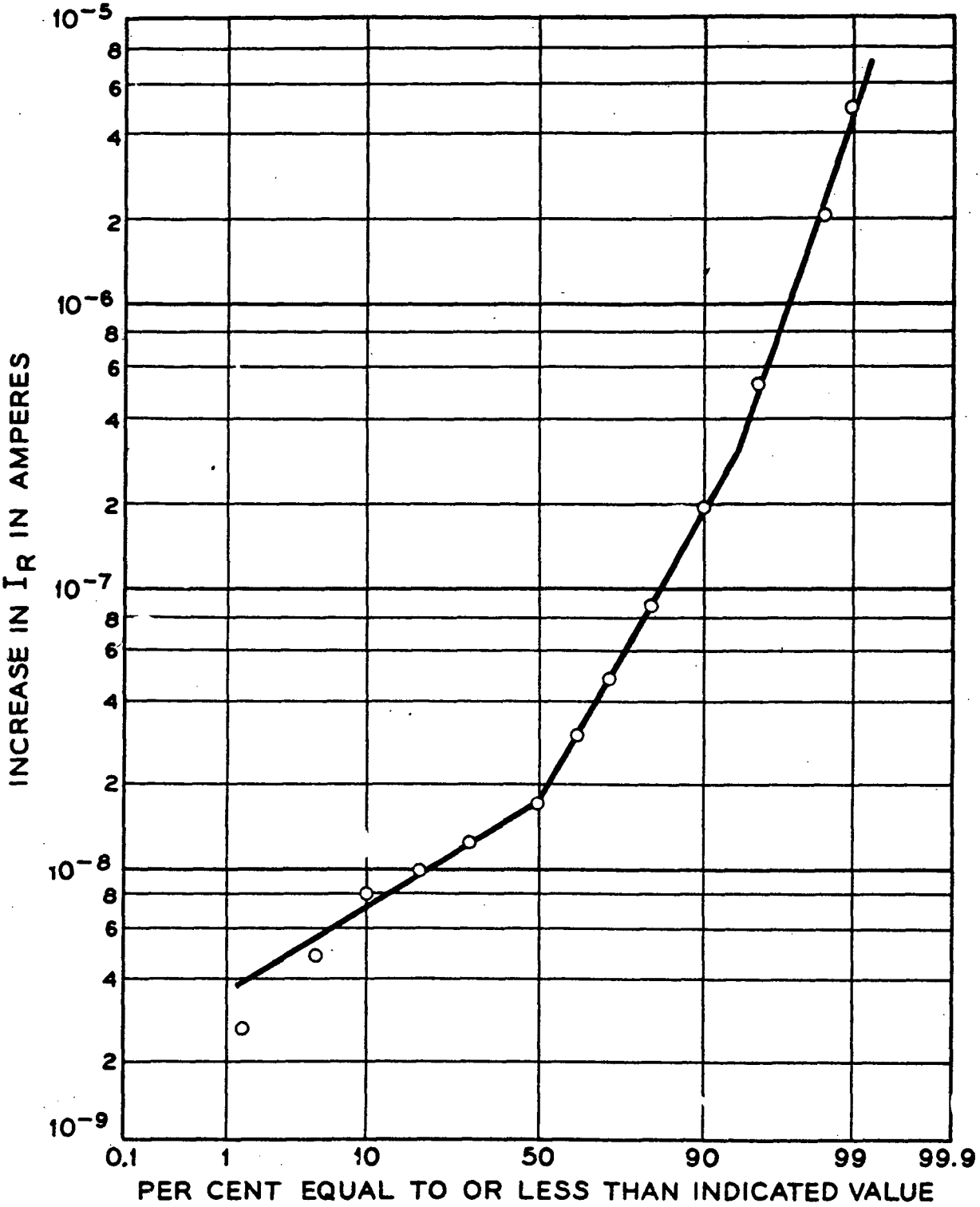

Fig. 20

Distribution of degradation of current in a type of diffused silicon diode at 3.7×10^4 rads.

the period subsequent to completion of the exposure. This is indicated in Fig. 21, a plot of collector reverse current vs. time after repeated exposures on an individual device. The device was exposed for several consecutive periods at 1.4×10^5 rad/hr, with current measurements subsequent to each exposure. The procedure was then continued at 8.5×10^5 rad/hr. Here each curve represents the I_{CBO} measurements subsequent to radiation for the total time indicated on the curve. I_{CBO} increases subsequent to the exposure, but may actually be decreased during the next exposure. After sufficient exposure, the devices evidence a saturation of the subsequent I_{CBO}, and also a saturation of the effect with continued exposure.

This saturation effect is confirmed at the 5 rad/hr. dose rate in Fig. 22, showing the I_{CBO} curves vs. integrated dose for two typical transistors of this type. Both show an eventual saturation of the curve and one shows an ultimate reduction which appears also to be typical of this type of transistor.

Several types of diffused germanium transistors have also been examined, with the general result that increases in I_{CBO} are relatively small (of the order of a factor of 3 or 4), and relatively consistent, until the dose reaches about 10^6 rads, where more drastic increases may be expected. The dependence on V_{CB} was relatively insignificant.

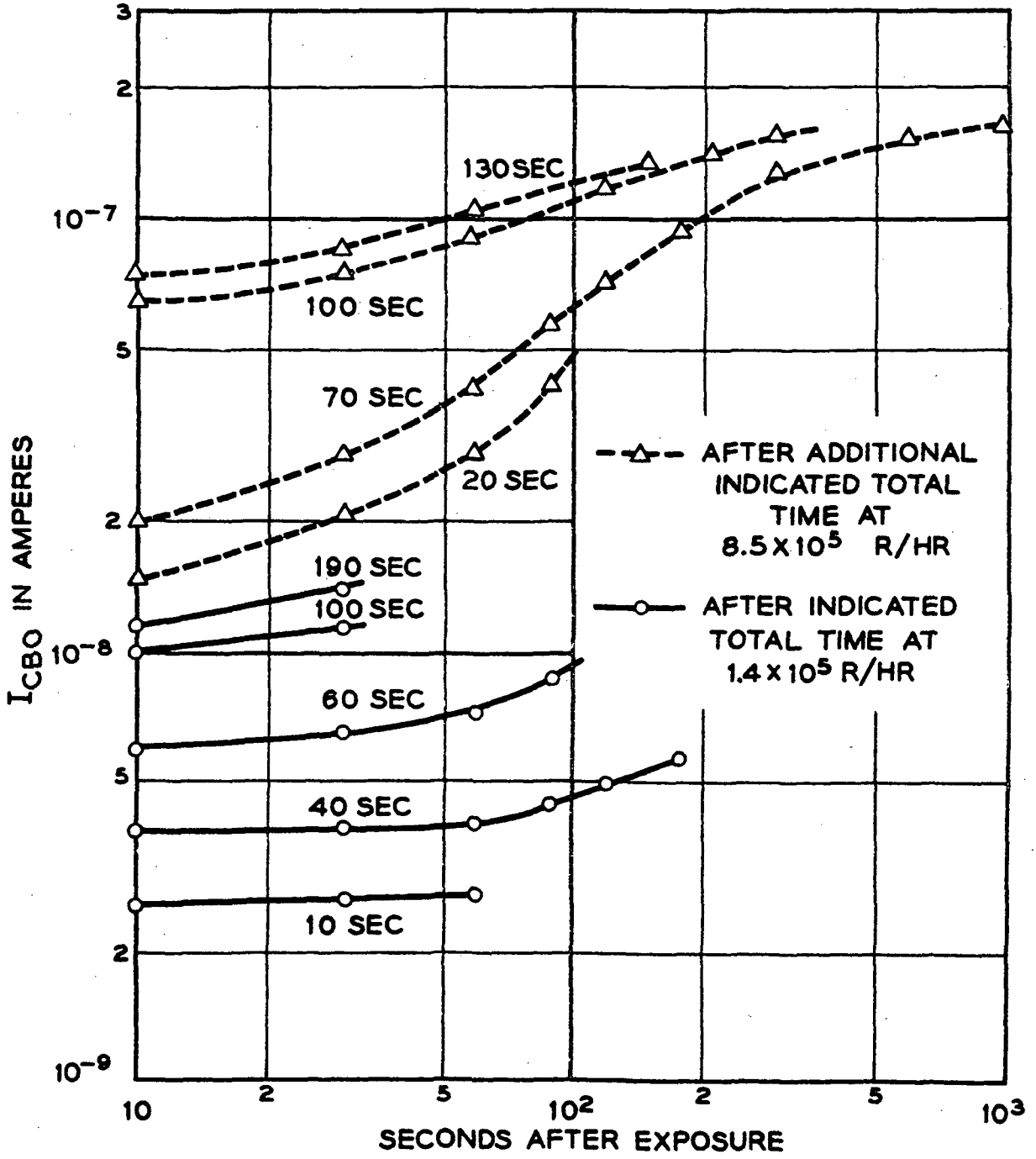

Fig. 21

The pattern of collector current response in a grease covered silicon transistor.

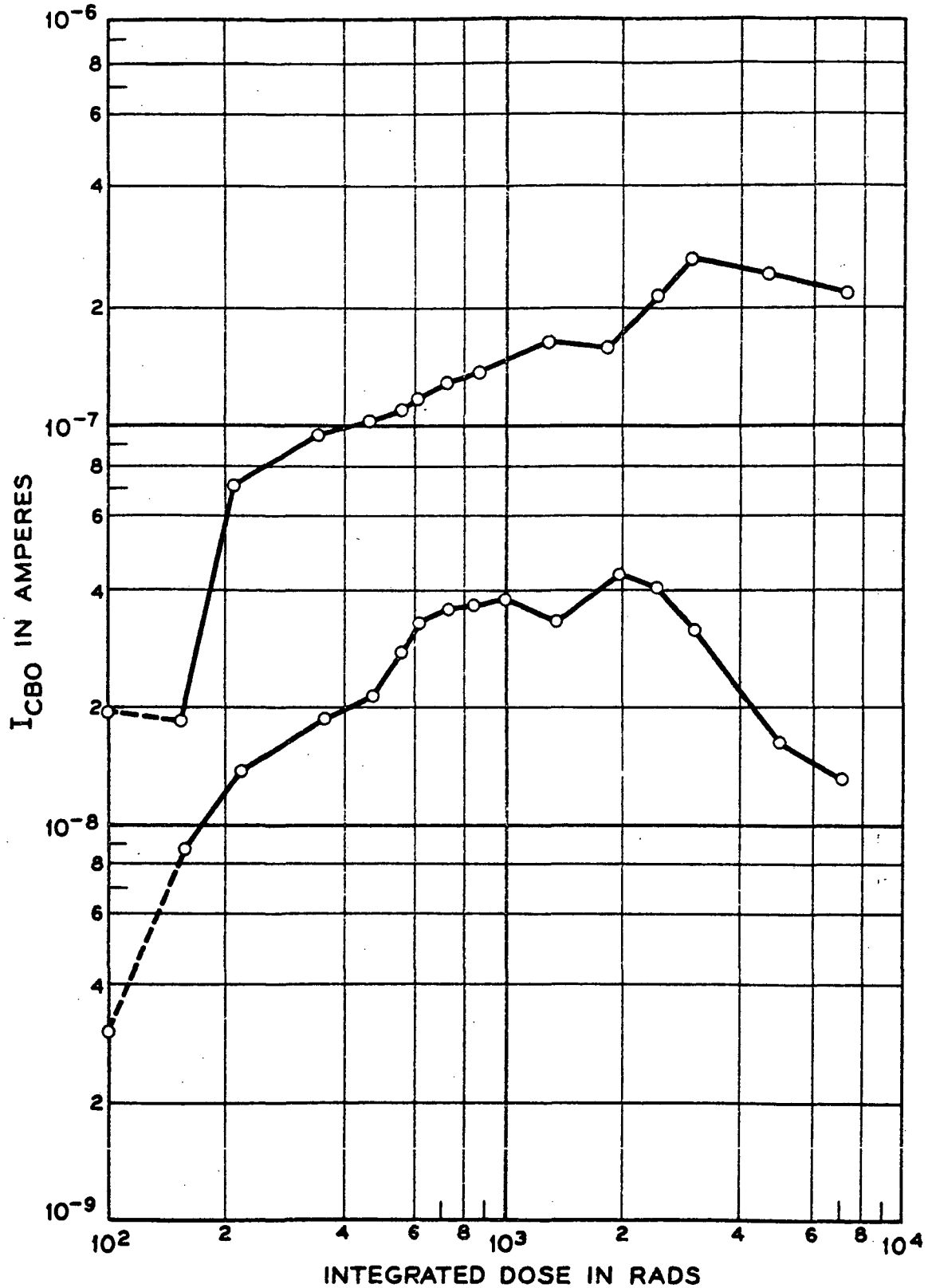

Fig. 22

The response of a grease covered silicon transistor under prolonged radiation at 5 rads/hr.

The effect of processing is evident in these types, however, with one group showing marked changes at about 10^4 rads, and another group having essentially no changes at 10^7 rads.

VII. Testing and Selection for Telstar Devices

The process of selecting the semiconductor components for use in the Telstar experimental communication satellite consisted of:

1. Qualification of design for reliability and performance as required in each application,
2. Fabrication,
3. Screening and preaging to assure satisfactory operation in the system environment,
4. Life testing,
5. Selection of the most stable devices.

At the time of recognition of surface effects from ionizing radiation (about October 1961), much of the life testing was already in process. Since the Telstar satellite was to orbit through the Van Allen radiation belt, the addition of radiation as an environmental factor was essential. Steps were therefore taken to determine the qualification of all types in the program and to study the screening and selection techniques that would be useful.

Figure 23 shows a plot of the estimated ionizing radiation intensity for components inside a satellite, as a function of the shielding of the components from the external environment. These curves refer to the ionization produced by protons only and were developed from existing estimates of the Van Allen belt particle fluxes. The upper and lower limit curves reflect the uncertainties in this estimate. For shielding thicknesses of

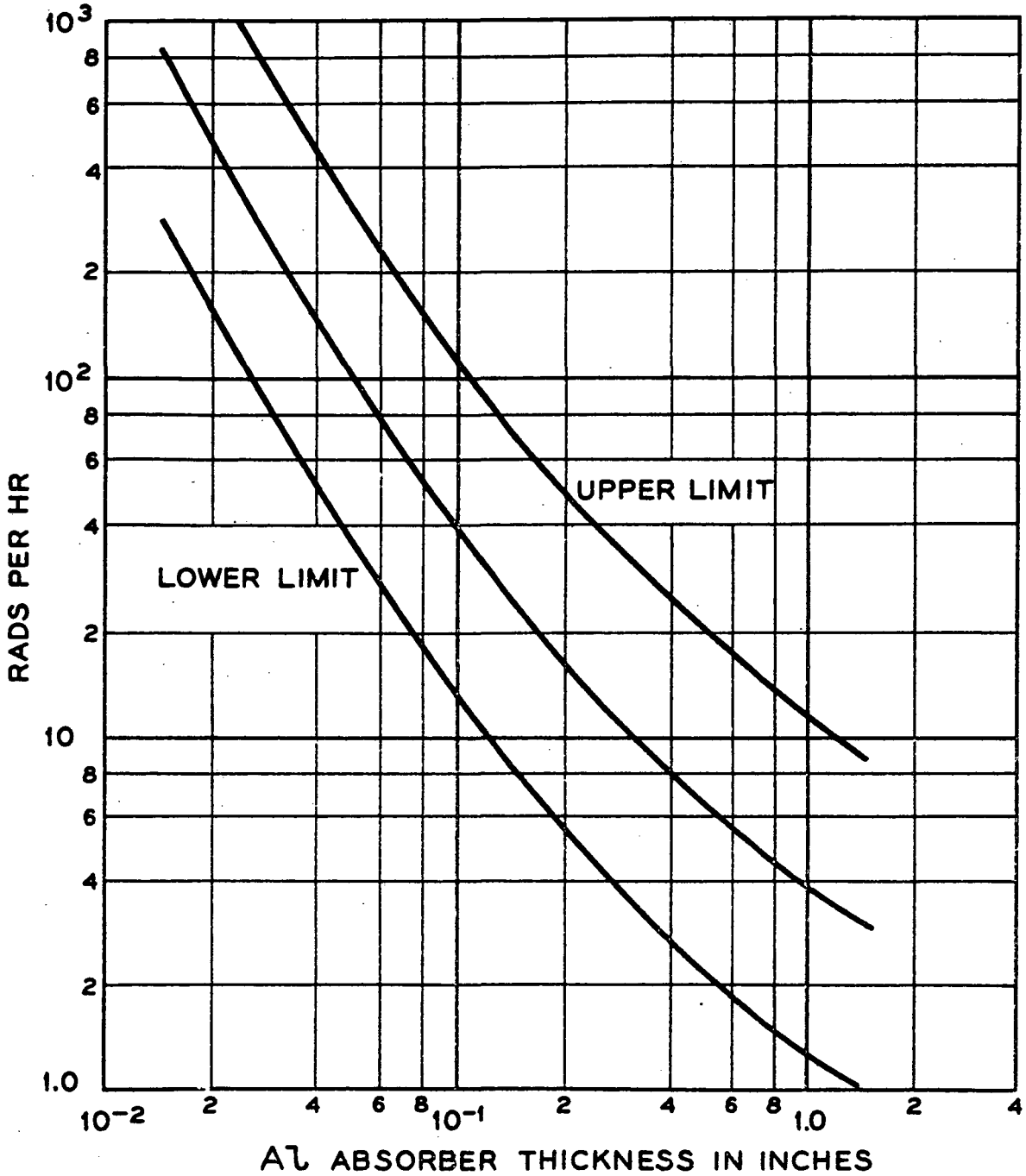

Fig. 23

The maximum radiation intensity anticipated in space due to high energy protons, as a function of the thickness of aluminum shielding.

less than 0.1 inch the electron contribution to ionization should be considered as well, but for Telstar, typical components are shielded by the equivalent of 0.5 to 1.0 inch of aluminum and only high energy protons are significant. The curves of Fig. 23 indicate that at this typical shielding, the radiation intensity would be a maximum of 10-20 rads/hr in the heart of the Van Allen belt. This results in a maximum average of 3-5 rads/hr over an entire orbit, considering Telstar's approximate 25% effective exposure to Van Allen radiation.

With this estimate of the maximum radiation environment, all device types were given a gamma exposure at 8.5×10^5 rads/hr for one minute (the equivalent of at least three months in orbit), followed by at least one week at 3 rads/hr. Any device type showing evidence of change in either condition was replaced or subjected to individual selection or screening. Device types showing no change were considered satisfactory. All of these devices were subject to a 15v reverse bias on the collector and an emitter current corresponding to the application.

The diffused silicon transistors F-54273 and F-54647 were used for experimental studies of screening and selection procedures. It is noted that the one minute dose of 1.4×10^4 rads (at 8.5×10^5 rads/hr) is not much beyond the variable Region 2 of Fig. 17 and should be very effective in providing a comparison between individuals. The study of the effectiveness of such a dose as a screening procedure was carried out through the following program:

1. Preradiation of a number of these transistors to screening exposures between 10 seconds and 6 minutes at 8.5×10^5 rad/hr and
2. Subsequent exposure at 5 rad/hr.

This permits an evaluation of the effect of the low dose rate after a screening dose.

Figure 24 shows the collector reverse current measurements of two units from this program, these being generally typical of the results of all of the devices. In this case, the measuring equipment was limited in sensitivity to about 10^{-9} amperes and the initial values prior to radiation are shown at this value although they may have been somewhat lower. Unit No. 762 is representative of those units which suffered a relatively minor increase in reverse current during the preradiation dose. During the subsequent radiation at 5 rad/hr, this unit returned quite rapidly to its original value remaining there until the dose became somewhat greater than 10^3 rads at which time it began to degrade in a fashion very similar to that expected from earlier tests. Unit No. 722 suffered a much greater change during the preradiation and took an appreciably longer time recovering toward its initial value. Before it fully recovered it reached the point of onset of final degradation and began to change quite rapidly. (A third type of response was seen in an occasional unit which degraded so severely during the preradiation that the subsequent low dose resulted in further increase in current and no recovery was evident at all.)

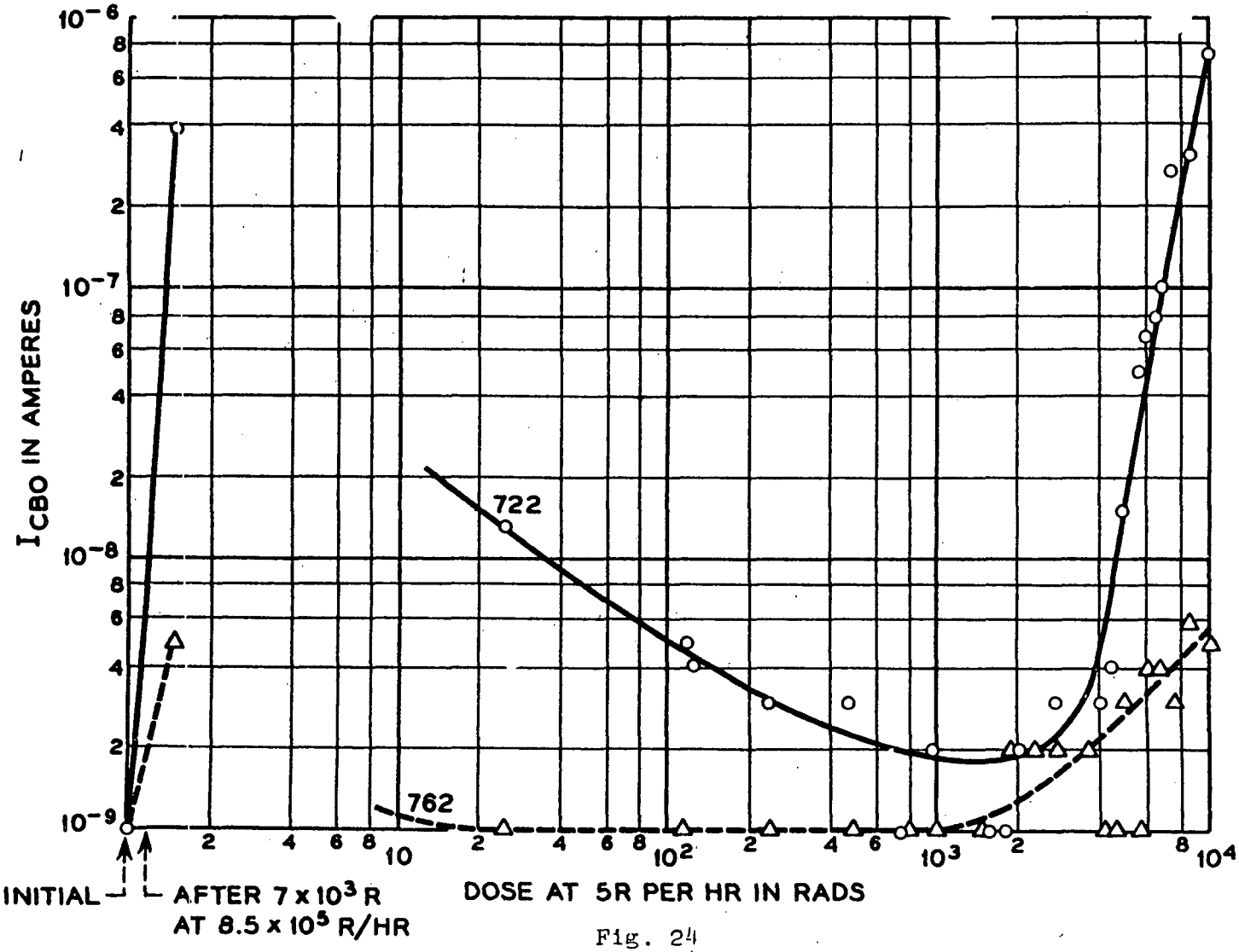

Fig. 24

The typical pattern of change in I_{CBO} in low-level radiation after a screening dose.

The influence of the screening dose on the distribution of onset of the final I_{CBO} degradation (at 5 rad/hr) is shown in Fig. 25 for four similar groups of 12 units each. One of these groups was irradiated at 5 rad/hr with no initial radiation at the high dose level. The other three groups were given an initial radiation at 8.5×10^5 rad/hr for different lengths of time to achieve the initial radiation dose indicated in the figure. It is seen that all of these distributions are essentially the same, indicating that the 5 rad/hr dose will cause a modification of the surface condition established by the high initial dose, causing the units to look eventually as if they had not received the initial dose. This is evidence of a contradiction to the principle of reciprocity of dose rate and time, in that the additional dose added at the 5 rad/hr rate does not normally cause a continuation in the degradation produced in the initial dose.

Another point of interest in Fig. 24 is the comparison of the I_{CBO} value resulting from the preradiation dose with that subsequently occurring after an equal dose at 5 rad/hr. Inspection of the two curves on Fig. 24 reveals that the currents at 7×10^3 rad are approaching those resulting from the preradiation dose. Fig. 26 shows a plot of the results of all the units so treated. The dashed line indicates the one-to-one correlation between the two current values, those points to the right of the line representing the units which during the 5 rad/hr exposure did not develop reverse currents as high as those obtained in the initial

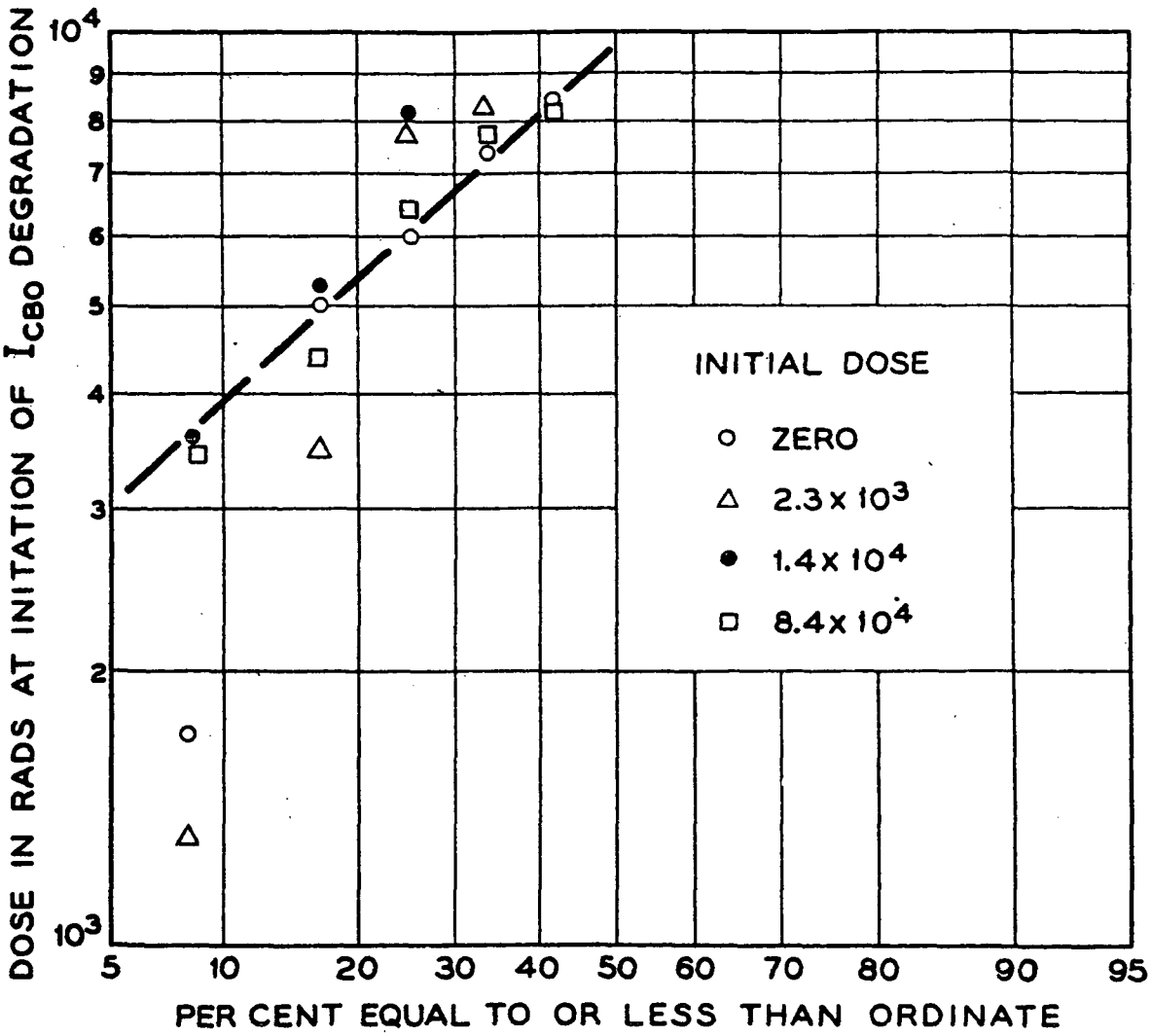

Fig. 25

Distribution in dose for initiation of degradation with and without preirradiation.

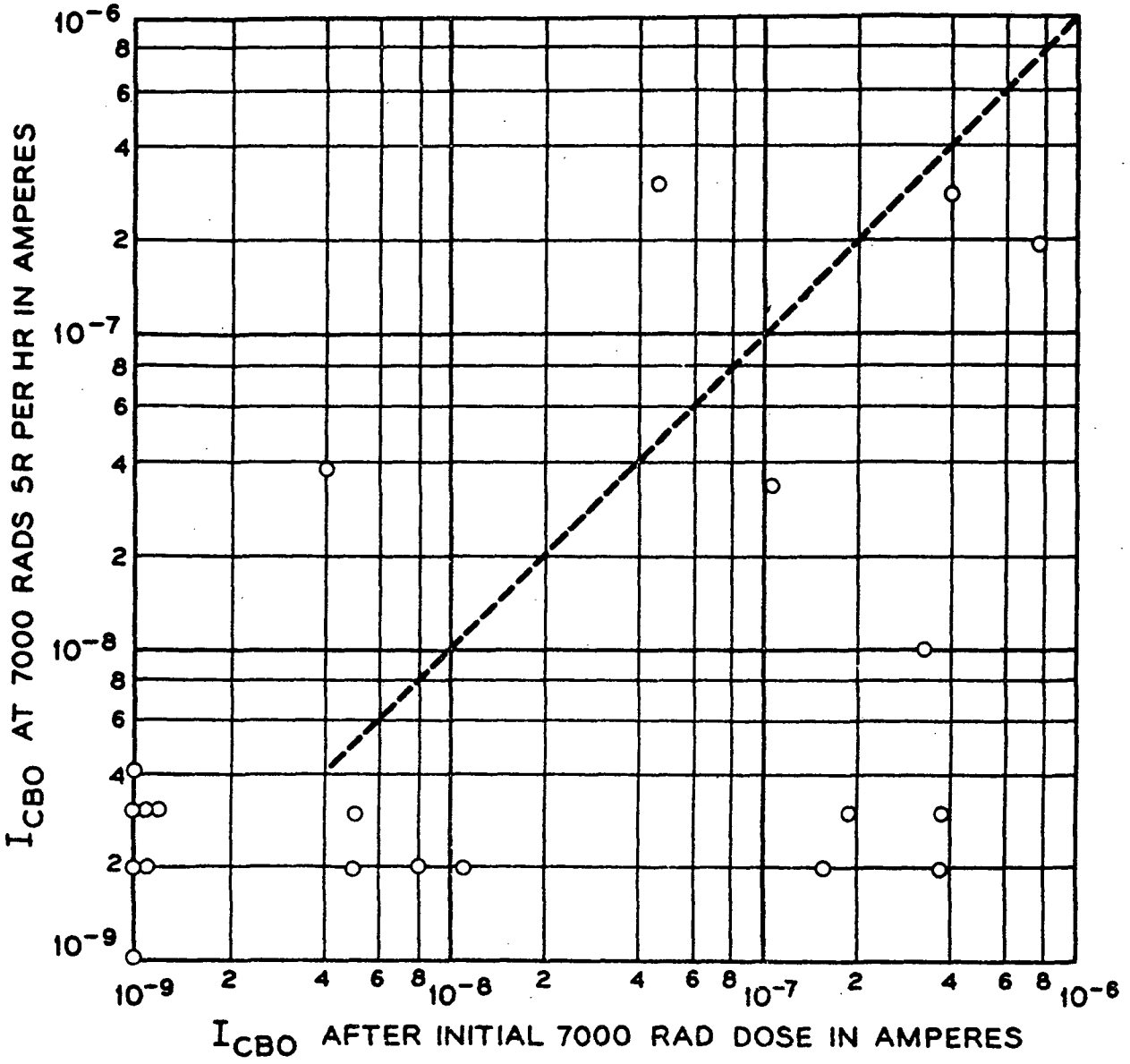

Fig. 26

Correlation of change in I_{CBO} after a screening dose at 8×10^5 rad/hr with subsequent changes at 5 rad/hr.

dose. This line was not extended below about 4×10^{-9} amperes because this was approaching the limit of sensitivity of equipment which was then in use. It is noted that all but two of the significant readings fall on the side of the one-to-one correlation line corresponding to larger changes after the preradiation dose than after the subsequent low dose rate exposure.

In some cases the lack of correlation is quite significant, the currents after the low dose rate exposure remaining below 10^{-8} amperes although quite large changes were observed after the screening dose. In these units, however, the changes in current gain after the low dose rate exposure were found to be appreciably greater than in those units which were more stable in the initial screening dose. Consequently, it is found that selecting of those units with I_{CBO} less than 10^{-8} amperes after the screening dose, would have eliminated 9 of the 10 units which subsequently degraded to either I_{CBO} values greater than 10^{-8} amperes or gains less than 50% of the initial gain. Of the 12 units good in these respects after the low dose rate exposure, only two would have been eliminated by selection following the screening dose. It is thus shown that selection on the basis of I_{CBO} after a screening dose is effective for this device type.

An indication of the effect of this screening on the distribution in degradation of I_{CBO} under low-level radiation exposure is given in Fig. 27. Both distributions are of I_{CBO}

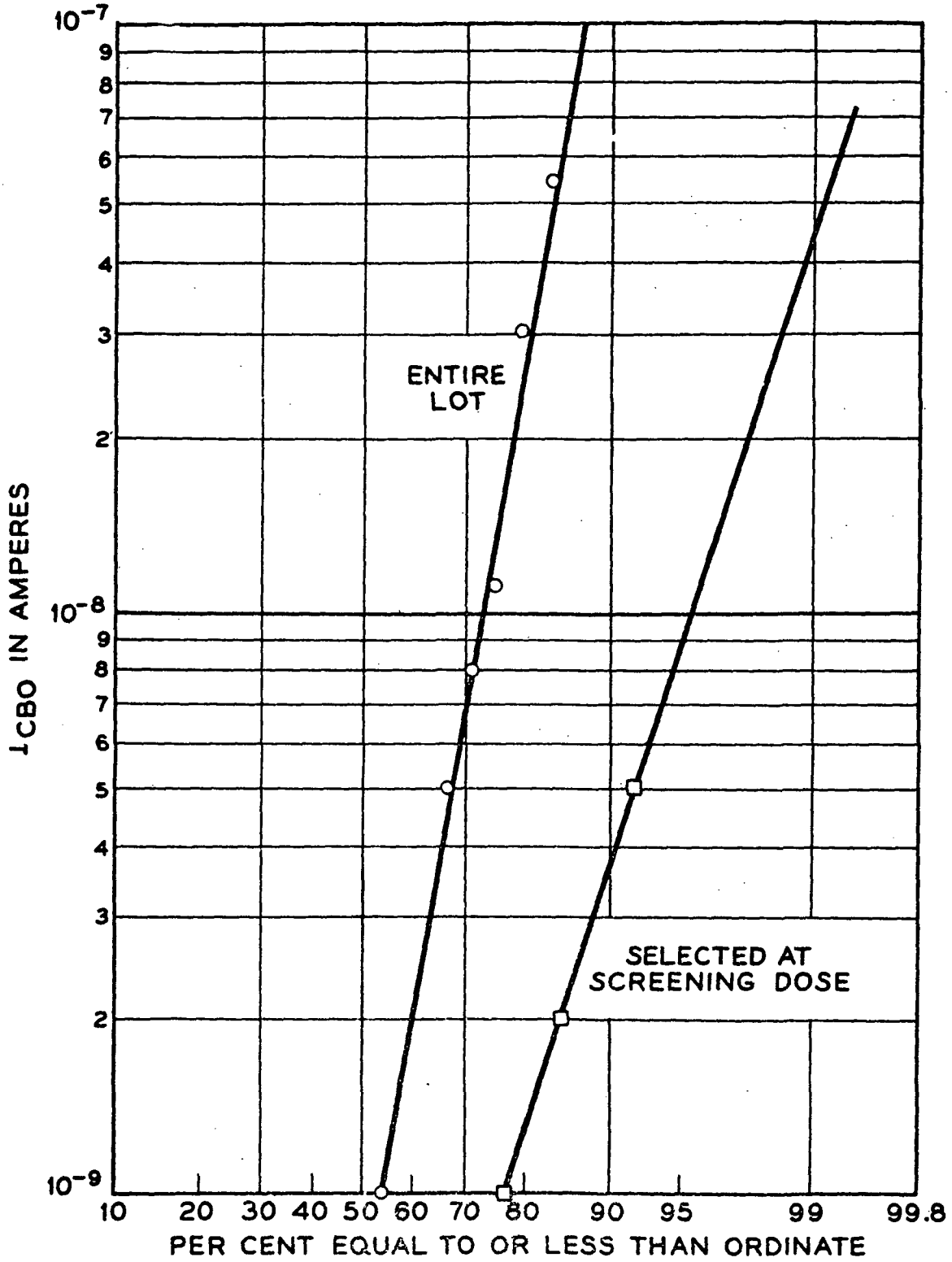

Fig. 27

Distribution of radiation response in screened and unscreened devices.

after exposure, first to 30 seconds at 8.5×10^5 rad/hr and then to 10^4 rad at 5 rad/hr. One distribution is of the entire sample of devices and the other is of only those which were selected for I_{CBO} less than 10^{-8} amperes after the initial dose. It is seen that an appreciable improvement is achieved by the screening procedure.

VIII. Summary

It has been found that changes can occur in semiconductor characteristics, because of surface effects of ionizing radiation in a device under electrical bias, at much lower doses than those required to produce surface effects in the absence of bias or to produce changes in the bulk of the semiconductor. These effects apparently arise from ionization in the gas of a device encapsulation and collection of ions on the device surface. The gas ions probably serve to produce and activate chemical species on the semiconductor which induce surface inversion layers that alter the junction characteristics. The chemical condition of the surface previous to irradiation is apparently involved in the process in a sensitive way. The effects observed depend on junction bias, envelope potential, and in many respects on total radiation dose rather than dose rate. The major features of these observations and of observations of the characteristics recovery of the surface effects after radiation under bias can be described by the ion-induced inversion layer model of the process.

In the time since the first direct observation of this effect, a comprehensive study of all types of semiconductor devices has not been attempted. Observations of several types, however, indicate that different types may respond quite differently to radiation, that the response may be quite dependent upon processing (and therefore upon production periods or batches), and that within a type the response may be quite variable between individual units.

One type of transistor was used for much of the experimental work of defining the radiation effect, and the I_{CBO} response was studied because the large changes facilitated comparative measurements. It is recognized that current gain and other surface-dependent characteristics can also be affected by radiation, and they should be observed in any evaluation of types, if critical in specific applications. It is hoped that the studies presented here will be a guide in formulating such evaluations.

It has also been found that at least some devices can be screened for sensitivity to radiation by means of a short-time, high-level dose, with correlation to subsequent low-level exposure results. Here, too, it is recognized that variations exist among types, and the usefulness of such screening operations should be evaluated for each type of interest.

It is hoped that further work will serve to provide more definitive results relating the radiation effects to a physical model and also to the surface conditions or processes contributing to the effect. These preliminary results can at least serve to expose the problem and to suggest the lines of further study and action.

Acknowledgments

The material presented here includes the contributions of many of the authors' colleagues. Of particular significance have been the efforts of E. P. Moyer, E. R. Schmid, J. Lange, of Bell Laboratories and G. L. Miller of Brooknaven National Laboratory.

REFERENCES

1. See Conference on Radiation Effects in Semiconductors. J. Appl. Phys. 30 (1959).
   G. D. Watkins, Corbitt, J. J. W., "Electron Paramagnetic Resonance of Defects in Irradiated Silicon."
2. Easley, J. W. and Dooley, J. A., "Fast Neutron Bombardment Reduction of Transistor Current Gain."
3. Proceedings of Second Conference on Nuclear Radiation Effects on Semiconductor Devices, Materials and Circuits. September 17 and 18, 1959.
4. See IRE Transaction on Nuclear Science. Vol NS-8, January 1, 1961. Solid State Radiation Detectors
5. Rosenzweig, W., "Diffusion Length Measurement by Means of Ionizing Radiation." BSTJ 41 1573 (1962).
6. Smits, F. M., Smith, K.D., Brown, W. L., "Solar Cells for Communication Satellites in the Van Allen Belt." Journal of the British Institution of Radio Engineers, 22 161 (1961).
7. Baruch, P., "Mobility of Radiation Induced Defects in Germanium." J. Appl. Phys. 32 653 (1961).
8. Kingston, R. H., "Review of Germanium Surface Phenomena." J. Appl. Phys. 27 101 (1956).

Paper B-3

NASA SPACE RADIATION EFFECTS LABORATORY

Dr. John Duberg* and Emanuel Rind**
NASA Langley Research Center

Abstract

Space particulate radiation from the Van Allen belts, and from cosmic and manmade sources have energies and fluxes which have produced and are capable of producing damage in matter and living organisms which comprise space mission payloads. Laboratories in space for the study of radiation effects are not available. NASA, Langley Research Center, Virginia has proposed a ground based Space Radiation Effects Laboratory which simulates most of the particulate energy spectrum found in space and can be used in an effective, accelerated, radiation research program by means of which deleterious radiation effects can be minimized or eliminated. To achieve these results in a minimum time, a 600-Mev, proton, synchrocyclotron of proven design with variable energy and variable external beam size, as well as a 1 to 30 Mev electron accelerator with the same capabilities have been incorporated into the proposed facility. Although these devices will be used as engineering tools, provision has been made to maintain the basic research capabilities of these accelerators. This will provide three Virginia institutions of higher learning, who will operate the laboratory jointly with the Langley Research Center, with the instruments necessary to conduct a basic research program. The plan of the proposed test areas reflect the latest advances in the state of the art as it pertains to both the engineering and basic experimental requirements in flexibility, radiation background levels, shielding, and isolation. NASA, Langley Research Center, Virginia, has been engaged in particulate radiation effects research in materials, components, dosimetry, devices, and instrumentation used in space missions. These efforts have been handicapped by the limited availability of time in existing accelerators which are being used for basic physics experiments. The proposed Space Radiation Effects Laboratory will provide the necessary facilities for conducting an expanding radiation effects research program using particulate radiation which simulates the space spectrum.

---

*Technical Assistant to the Associate Director.
**Aerospace Technologist.

Introduction

The Langley Research Center of NASA has had a special interest in the space environment insofar as it influences the design of space vehicle systems. Scientific exploration of space has revealed a number of hostile aspects of the environment. Perhaps the most significant of these is the particulate radiation associated with cosmic rays, solar flares, and that magnetically trapped in the radiation belts. The Langley Research Center has proposed a Space Radiation Effects Laboratory in which the particulate space radiation can be simulated, accelerated testing performed, and fundamental studies made in this problem area.

Particulate Radiation in Space

A brief review of our knowledge of the particulate radiations in space is appropriate and, as cosmic rays are familiar, they are used as a basis of comparison in figure 1.[1] The cosmic ray flux is comprised of approximately 85 percent protons, 13 percent helium nucleii and the remainder, heavy ions.[2] Only the proton spectrum is shown. Although the flux is low, protons from this source attain extreme energies in the Bevs. The upper energy limit has not been determined but there is reason to believe that it is much in excess of 10^6 Bev.

The proton spectra of three solar events are shown with an indication of their time variation. The dotted portions of the curves are extrapolations. Energies of 10 Bev may be attained but flux values for these high energies are very low. Integrated, instantaneous, omnidirectional fluxes down to a few Mev may exceed 10^6 protons/cm^2/sec. The solar event of February 23, 1956 would indicate that both flux and energy decrease with time. It is more commonly believed, however, that the event of November 12, 1960 is the more likely occurrence.[3] For this event, the flux values of the lower energies increase, as those of the higher energies decrease with time.

---

[1]Trutz Foelsche, Current Estimates of Radiation Doses in Space, NASA TN D-1267, 1962.

[2]F. B. McDonald, ed., contributed by G. E. Fichtel, D. E. Guss, H. H. Malitson, K. G. McCracken, K. W. Ogilvie, and W. R. Weber, Solar Proton Manual, NASA TR R.

[3]George J. Jacobs, ed. (With Appendix A by J. R. Winckler), Proceedings of Conference on Radiation Problems in Manned Space Flight, NASA TN D-588, 1960.

The protons trapped in the inner radiation belt have omnidirectional fluxes ranging from over 10^4 protons/cm^2/sec at energies greater than 40 Mev to fluxes of the order of 10^3 protons/cm^2/sec at energies greater than 550 Mev.

It is assumed that the electron fission energy spectrum shown in figure 2 would be obtained for manmade detonations of nuclear devices. The spectrum[4] is expressed in relative differential values. If the spectrum is integrated and normalized it yields the following results: 55 percent of the electrons have energies $\leq$1 Mev and 91 percent of the electrons have energies $\leq$3 Mev. The maximum electron energy is about 7 Mev.

The recent explosion of a nuclear device produced the electron spectrum of figure 2 and these electrons have been geographically located[5] in the position shown in figure 3. The naturally trapped protons and electrons of the radiation belts as previously reported are also shown and may be used as a basis of comparison. It can be seen that the new manmade belt contributes much of its intensity in the region previously referred to as the inner belt and thus increases the radiation damage problems of low-altitude space missions. The peak intensities of the electrons of this artificial belt equal if not exceed the maxima of the natural outer region when the latter's intensities are increased by magnetic storms.

The outer region is seen to be of a transient character and has variations in flux and energy due to solar activity. By far the greatest number of these electrons have energies below 1 Mev.[6] As indicated previously, however, the manmade belt has about 45 percent of its electrons with energies between 1 and 7 Mev. The addition of any manmade trapped electron radiation may pose an even greater hazard than that which is already present from the natural belt electrons.

---

[4]R. E. Carter, F. Reines, J. J. Wagner, and M. E. Wyman. Free Antineutrinos Absorption Cross Section. II. Expected Cross Section From Measurements of Fission Fragment Electron Spectrum. Phys. Rev., Vol. 113, No. 1, p. 280-6, January 1, 1959.

[5]Artificial Radiation Belt Discussed in Symposium at Goddard Space Center, W. N. Hess, P. Nakada, Science, Vol. 138, No. 3536, October 5, 1962, pp. 53-54.

[6]B. J. O'Brien, J. A. Van Allen, C. D. Laughlin, and L. A. Frank, Absolute Electron Intensities in the Heart of the Earth's Outer Radiation Zone. Jour. Geophys. Res. (Letter to the Editor), Vol. 67, No. 1, January 1962, pp. 397-403.

A brief summary of our knowledge of particulate radiation in space is given in table I.

TABLE I.- SUMMARY OF THE PROTON AND ELECTRON SPECTRA IN SPACE

PROTON SPECTRA

Low Energy	High Energy
Energy spectra $\leqq$22 Mev as obtained from Explorer XII data: 120 Kev < E < 4.5 Mev	Energy spectra from 22 Mev to 700 Mev
Flux (p/cm^2/sec) = 10^7 to 10^9	Total flux >2 × 10^4 p/cm^2/sec
	Intensity can vary by a factor of 2 to 3 with solar activity

ELECTRON SPECTRA

Low Energy	High Energy
Energy spectra <1.6 Mev	Energy spectra 1.6 < E < 6 Mev
E > 40 Kev, Flux < 10^8 e/cm^2/sec	Flux ≈ 2 × 10^5 e/cm^2/sec
E > 600 Kev,	Intensity can vary by a factor of
Flux $\geqq$ 5 × 10^6 e/cm^2/sec	50 to 100 with solar activity

Electron data obtained from Explorer XII.

SOLAR FLARES

Proton energy approaches 10 Bev. Fluxes vary with maximum values between 10^5 to 10^6 p/cm^2/sec. The greatest intensities occur at the low-energy values.

The proton data are divided into low energy, high energy, and solar flares. The low-energy data were reported at the symposium on the scientific results of Explorer XII, January 1962, by L. R. Davis and J. M. Williamson of the NASA, Goddard Space Flight Center. The low-energy range given was from 120 Kev to 4.5 Mev. This has been extended arbitrarily to 22 Mev, the upper limit for fixed frequency cyclotrons. The integral flux in this range is between 10^7 and 10^9 protons/cm^2/sec.

The high-energy-range data were obtained with Pioneer III and Explorer VII.[7] The low end has been taken from 22 Mev and extends to 700 Mev, the integral flux being greater than 2×10^4 protons/cm^2/sec.

The maximum integral energy flux of the solar flares vary between 10^5 to 10^6 protons/cm^2/sec with energies ranging from Kevs to about 10 Bev. The natural belt electrons have their highest intensities (between 10^8 to 10^9 e/cm^2/sec) at about $2\frac{1}{2}$ to 4 earth radii as measured from the earth's center. The manmade belt electrons have peak intensities greater than 10^9 e/cm^2/sec occurring at about 1.6 earth radii. The energies of both the manmade and naturally occurring electrons extend from a few Kev to 7 Mev.

Concept of the Space Radiation Effects Laboratory

Threshold doses for functional radiation damage[8] are shown for various materials and devices in figure 4. Unfortunately, most of this data is obtained from fission radiation which neither simulates space radiation as regards energy or type of radiation. This information is still useful in that it gives relative orders of magnitude of damaging doses and provides some means for determining the fluxes needed for accelerated space radiation damage studies.

The Langley Research Center in pursuing its research program for the experimental investigation of the effects of particulate radiation on items used in space missions, found, as have other investigators, that very limited beam time is available for engineering research using high-energy proton accelerators. The existing ones are being used almost full time for basic physics research experiments. To overcome this shortcoming without interference with the high-energy physics research effort, LRC, NASA, proposed construction of a Space Radiation Effects Laboratory which would encompass most of the space particulate radiation and which would utilize proton and electron accelerators as engineering tools as well as physics instruments.

---

[7]Guido Pizzela, C. E. McIlwain, and J. A. Van Allen, Time Variation of Intensity in the Earth's Inner Radiation Zone, October 1959 through December 1960, Jour. Geophys. Res., Vol. 67, No. 4, April 1962, pp. 1235-1253.

[8]S. N. Lehr, V. J. Tronolone, and P. V. Horton, Equipment Design Considerations for Space Environment, STL/TR-60-0000-09224, Space Tech. Lab, Inc., Sept. 1960.

Since over 90 percent of the space spectrum is below 1 Bev with fluxes less than 10^6 particles/cm^2/sec, and as the needs for the facility are immediate, a survey was made of existing accelerators having energies of this range and external beams which would permit accelerated space simulation for components with volumes of at least a cubic foot. The desire was to duplicate an existing, proven, design having the necessary features for accelerated space simulation, thus saving years of development time. The choice, based on availability, was narrowed to frequency modulated cyclotrons and alternating gradient synchrotrons. The synchrocyclotron design was chosen because its external flux was adequate for our purposes, whereas the external flux of the synchrotron machine was lower by about two orders of magnitude. Considerations of down time, beam extraction and overall proven reliability were additional factors in favor of the synchrocyclotron.

Particle Accelerators

There are four synchrocyclotrons in the world with energies of about 0.6 Bev or greater. The two behind the iron curtain were not considered. The other two are the machine at Berkeley, California (0.76 Bev) and the machine at CERN, Geneva, Switzerland (0.6 Bev). The CERN machine was designed for its stated energy and incorporated the most modern concepts of the day. The Berkeley machine has been redesigned and altered to bring it up from its initial lower energies to its present level and any design improvements of it and other existing accelerators were considered in the design of the CERN machine.[9] Since the CERN machine was the most modern, met our energy and flux requirements, and had a very good operational history, it was our final choice.

CERN Synchrocyclotron

Figure 5 is a photograph of the 600-Mev proton synchrocyclotron at CERN, Geneva, Switzerland. The overall size of the magnet is 36 feet wide by 21.3 feet deep by 20 feet high. It weighs 2500 tons, and is made up of 54 blocks weighing approximately 46 tons each. The height of the beam above the floor level is 4.1 feet and the magnet gap varies between 45 and 35 cm. The coils, which are water cooled, and made of aluminum, are about 25 feet in diameter, weigh about 60 tons, and produce 0.75 megawatt of heat at 1,750 amperes. The maximum radius R of proton path ($n = 0.2$) = 2.27 meters. The magnetic induction at $R = 2.27$ meters is 1.79 webers/meters^2; and at $R = 0$, the magnetic

---

[9]Bengt Hedin, Design of CERN Synchro-Cyclotron Magnet, CERN 55-3, Synchro-Cyclotron Division, January 14, 1955.

induction is 1.88 webers/meter^2. The vacuum chamber and connections are made of welded stainless steel and have a volume of 23 cubic meters. This is pumped down to about 10^{-6} torr using two oil diffusion and three roughing pumps.[10]

The radio frequency system uses a water-cooled tuning fork modulator which modulates the r-f frequency between 29 and 16.5 megacycles at 55 cps.[10]

The target systems shown in figure 6, although designed basically for high-energy physics research, lend themselves readily to engineering. There are eight internal flip targets to produce neutrons at radii corresponding to energies from 110 to 600 Mev. Negative mesons are obtained by use of a suitable target on a Fermi trolley. The external proton beam is obtained by means of a magnetic channel with suitable extraction devices and is brought to focus in a beam area of 15 cm^2. The external current is about 0.3 microamp ($\approx 10^{11}$-10^{12} protons/cm^2/sec).

For the SREL, the CERN accelerator and external beam will be modified to produce variable energy and beam area. As proposed, the proton energy variation will be from 600 Mev down to as low as 100 Mev and capabilities will exist for spreading the beam from 15 cm^2 to 900 cm^2 at the target area. With the existing external beam, a year in the belt could be simulated in minutes to weeks over these target areas.

Electron Linac

Capability will also exist for accelerating electrons from 1 Mev to 30 Mev with beam current in the range of 150 microamp. These parameters will simulate the electron space environment as well as being useful for basic physics research. The beam area and energy will be variable and the linear accelerator design will be used to attain the requisite energy. Figure 7 is the accelerator section of a 10-Mev electron linac. The 30-Mev linac requires one or two additional accelerator sections.

The layout shown in figure 8 has been proposed for the SREL electron linac. The beam could be used in the linac cave or with the beam handling equipment shown, piped into the adjacent test area.

---

[10]W. Genter, K. H Schmitter, S. Kortleven, B. Bollée, and F. Krienen, The CERN 600 Mev Synchrocyclotron at Geneva, Phillips Technical Review, Vol. 22, 1960/61, No. 5, March 1961.

Plan of the Space Radiation Effects Laboratory

The floor plan of the proposed Space Radiation Effects Laboratory is divided into three major areas as shown in figure 9. These are the test and beam handling area, the test setup area, and the support building. The test and beam handling area consists of two independent target areas, the electron accelerator cave, the proton accelerator cave, and the magnet hall which will contain the beam transport and handling for the proton accelerator. The two target areas are about 30 by 30 feet and these dimensions may be changed by moving the walls. One target area is arranged for receiving a combined electron and proton beam. Sufficient area has been allowed around both accelerators which permits ready access and normal maintenance without the inconvenience of moving shielding. Very large targets may be irradiated by piping the beam directly down the magnet hall. The shielding walls are about 18 feet thick. Overhead shielding is provided to reduce skyshine. In addition the proposed arrangement of the physics test areas will isolate them in a manner to give low radiation background, thus permitting the performance of very refined experiments. The setup area allows test setups and measurements to be made without disturbance prior to installation into the target areas. Large vertical lift doors separate the target area from the setup area. The combined test and setup areas occupy approximately 37,000 square feet.

The support building is conveniently located next to the setup areas. It consists of two floors and a basement which will contain the control room and monitoring system for the accelerators, laboratory space, shop facilities, office space, counting areas, etc. The two floors have an area of about 17,000 square feet.

The section view, figure 10, is taken through the synchrocylotron cave, and shows the relationship of the test setup area with the support building and test areas. Also shown are the head room for the overhead crane and the support and pilings needed around the accelerator.

Research Program

In accord with the objectives of minimizing or eliminating the effects of space radiation on all items which comprise space missions we have outlined a research program part of which is already underway in the following areas: materials, these will include seals, cements, plastics, lubricants, solder, damping materials, phosphors, insulators, etc.; external surfaces such as coatings, transparent materials, and optical components; devices such as magnetic, electronic, and solid state; shielding will cover magnetic as well as various bulk configurations; detection encompasses design, development, testing and calibration of new detecting devices; dosimetry will include experimental studies of radiation levels and doses delivered to different

areas and constituents of space vehicles; environmental contamination will deal with the ability of radiation to produce corrosive, noxious, atmospheres, for example, ozone and nitrous oxides in closed ecological systems; sputtering phenomena; activation resulting from radiation; chemistry of elastomers and polymers; spectroscopy for the study of radiation induced changes will include nuclear magnetic resonance, electron paramagnetic resonance, infra-red and visible light, electron microscopy, X-ray techniques, and mass spectroscopy; thin films; experimental validation of theoretical studies; biological research including synergistic effects; health physics; and basic physics research.

Operation of Laboratory

The tentative operational plan for the SREL provides for William and Mary, the University of Virginia, and Virginia Polytechnical Institute organized as the Virginia Associates Research Center (VARC), to supply the operational personnel for SREL. The participating universities of VARC will also establish a basic physics research program sponsored by government grant, industry grants, or self-initiated. Other institutions requiring a facility with high-energy capability for basic research can cooperate with VARC. Programs for accelerator improvement and development may also be undertaken by VARC. The Langley Research Center will conduct the engineering, applications, and basic research phases associated with the space environment. Other NASA Laboratories, government agencies, and industry under NASA contract will operate through the Langley Research Center.

Concluding Remarks

An architect's rendering of the Space Radiations Effects Laboratory is shown in figure 11. This will be located in the city of Newport News, Virginia within 15 miles of the Langley Research Center, and will lie in a site occupying approximately 100 acres. The principal intent of the Space Radiation Effects Laboratory was to provide a facility in which investigations simulating the space environment could be performed and the results used to increase the reliability and safety of spacecraft and space missions. As the project has now evolved, the Laboratory will serve a dual function. In one capacity, it will support an engineering program aimed at increasing the reliability and safety of spacecraft and missions. In the other, it will provide our universities and colleges with the instruments by which they can conduct basic research in high-energy physics as well as expanding their graduate program in this field. Thus, by providing a facility whereby both these endeavors can be conducted concurrently, two vital needs are simultaneously fulfilled.

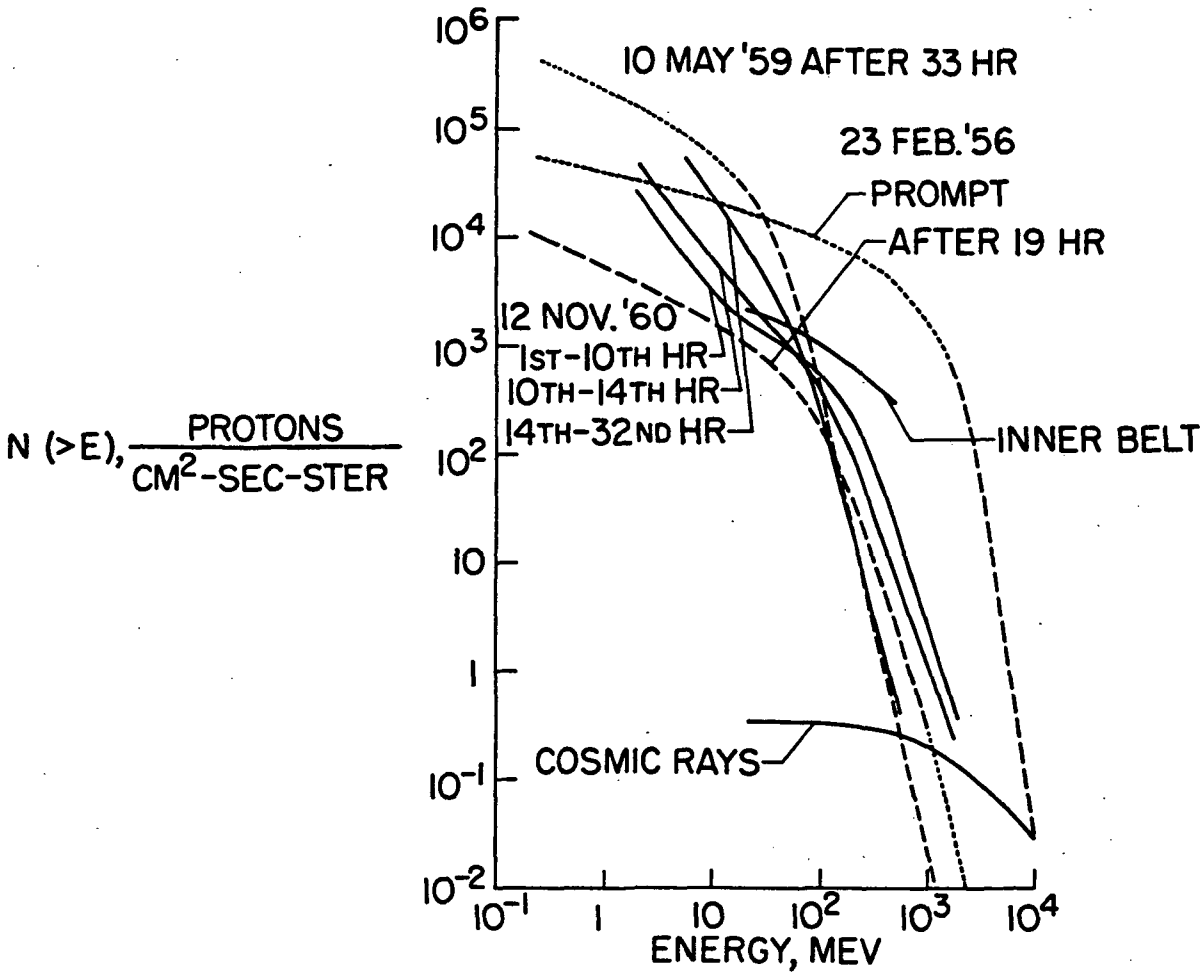

NASA

Figure 1.- The instantaneous integral energy spectra of cosmic rays, solar flare protons, and protons in the inner Van Allen belt. Dotted curves indicate extrapolations of measured data. (From ref. 1.)

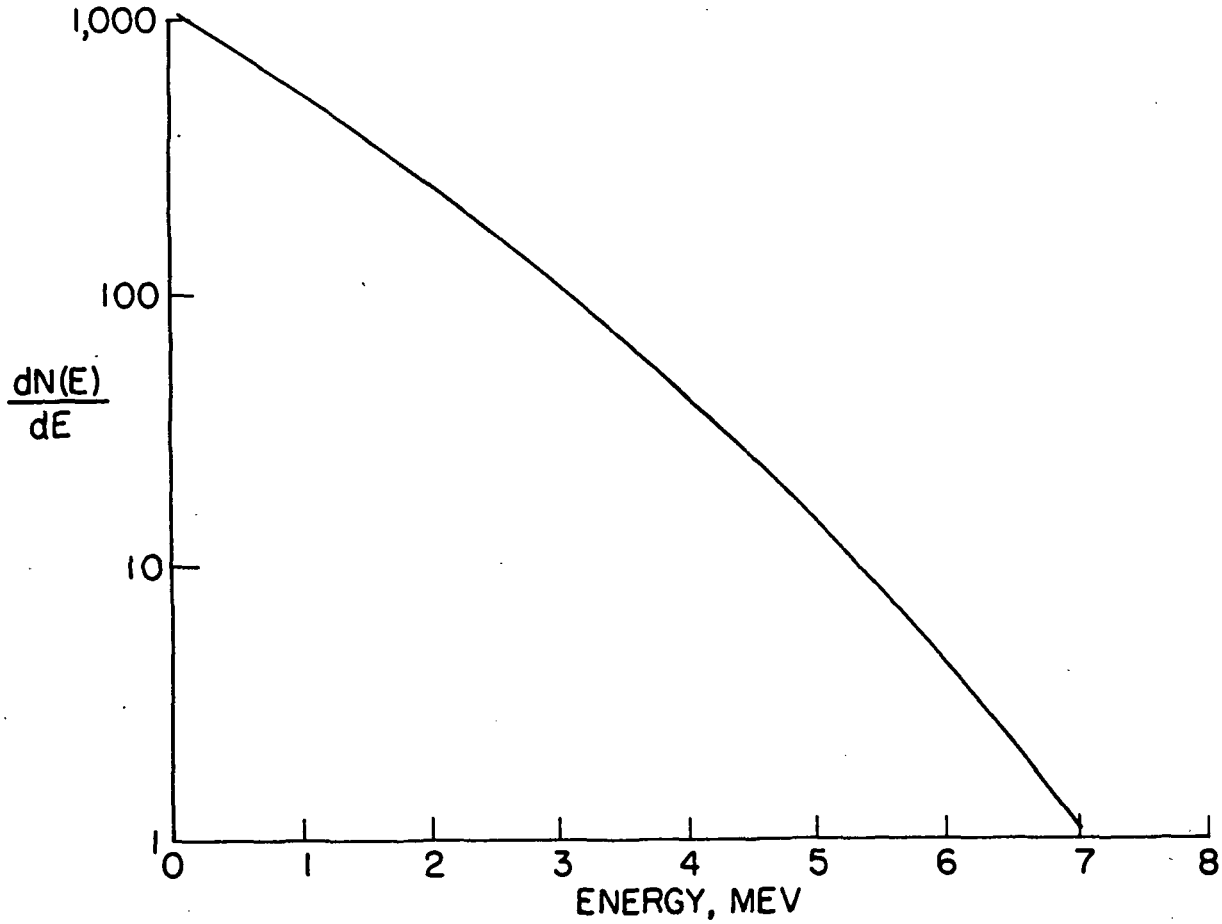

NASA

Figure 2.- Electron fission energy spectrum. (From ref. 4.)

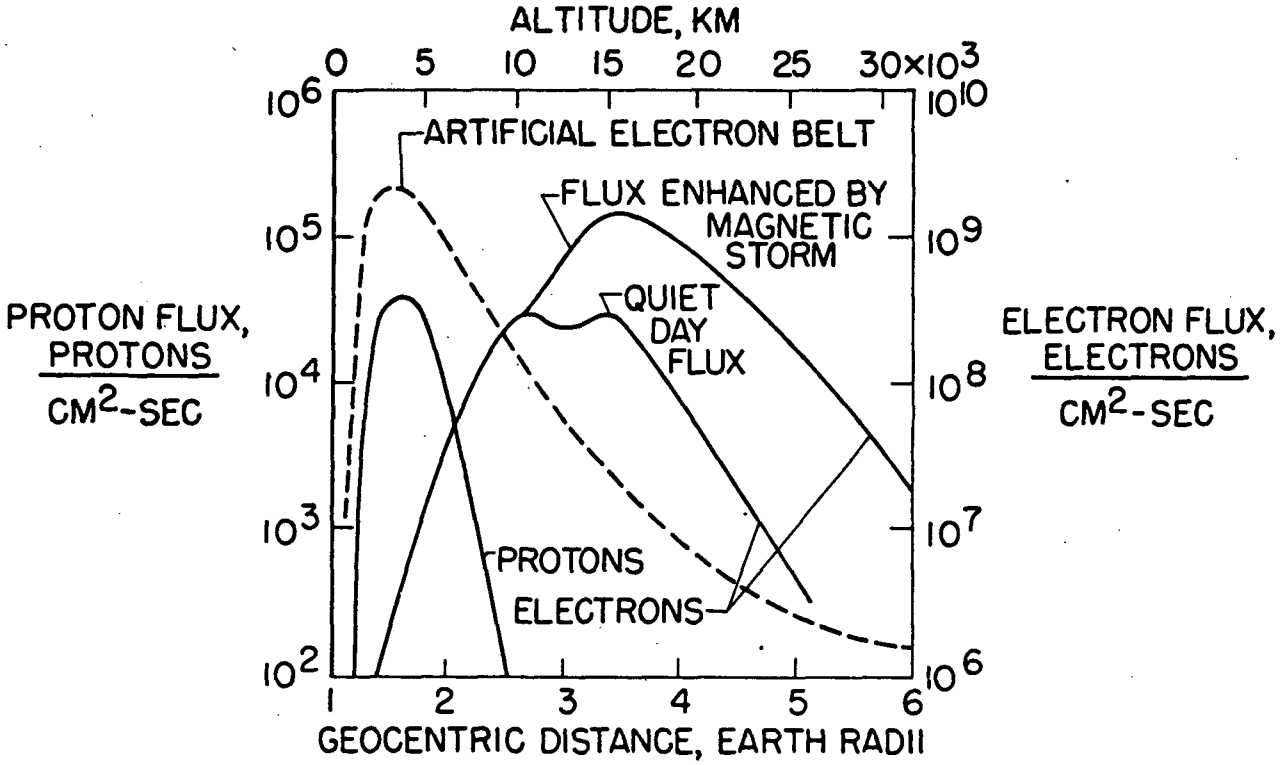

NASA

Figure 3.- Man-made electron belt shown relative to the existing electron and proton distributions. (From ref. 5.) The approximate variation of flux with geocentric distance and altitude in the plane of the geomagnetic equator is depicted.

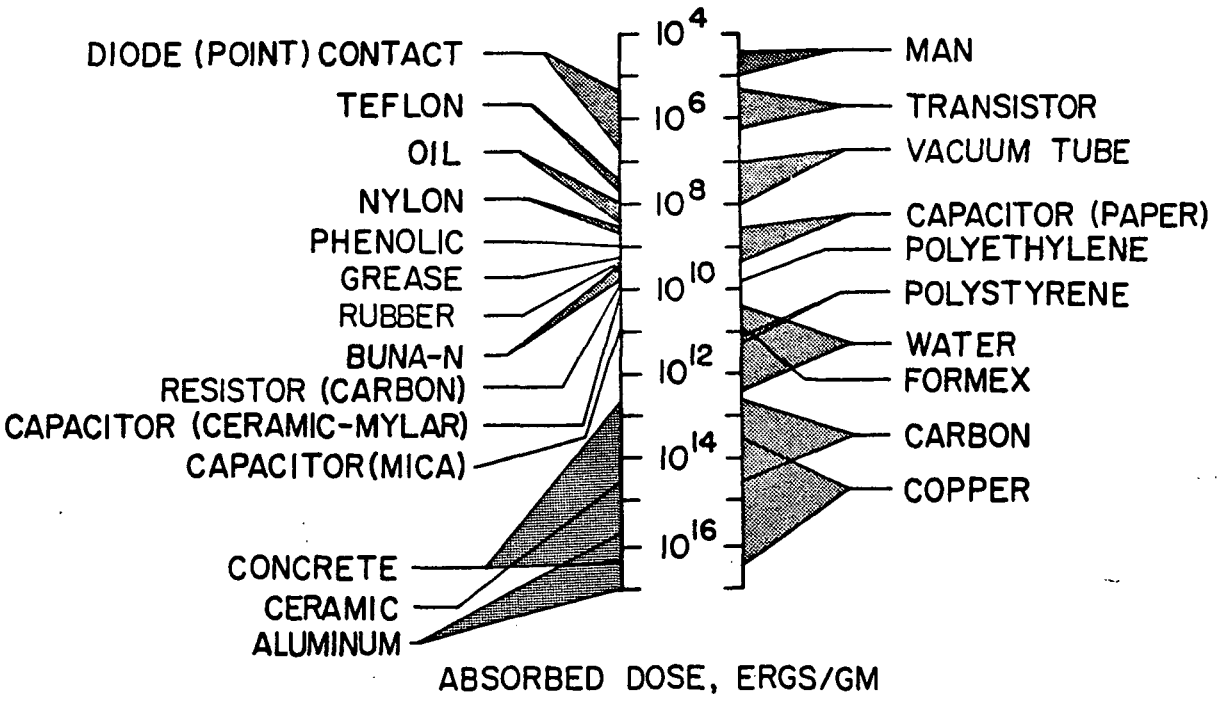

NASA

Figure 4.- Threshold dose for functional radiation damage as given in ref. 8. (Note that the absorbed dose in rads can be obtained by multiplying the dose in ergs/gm by 10^{-2}.)

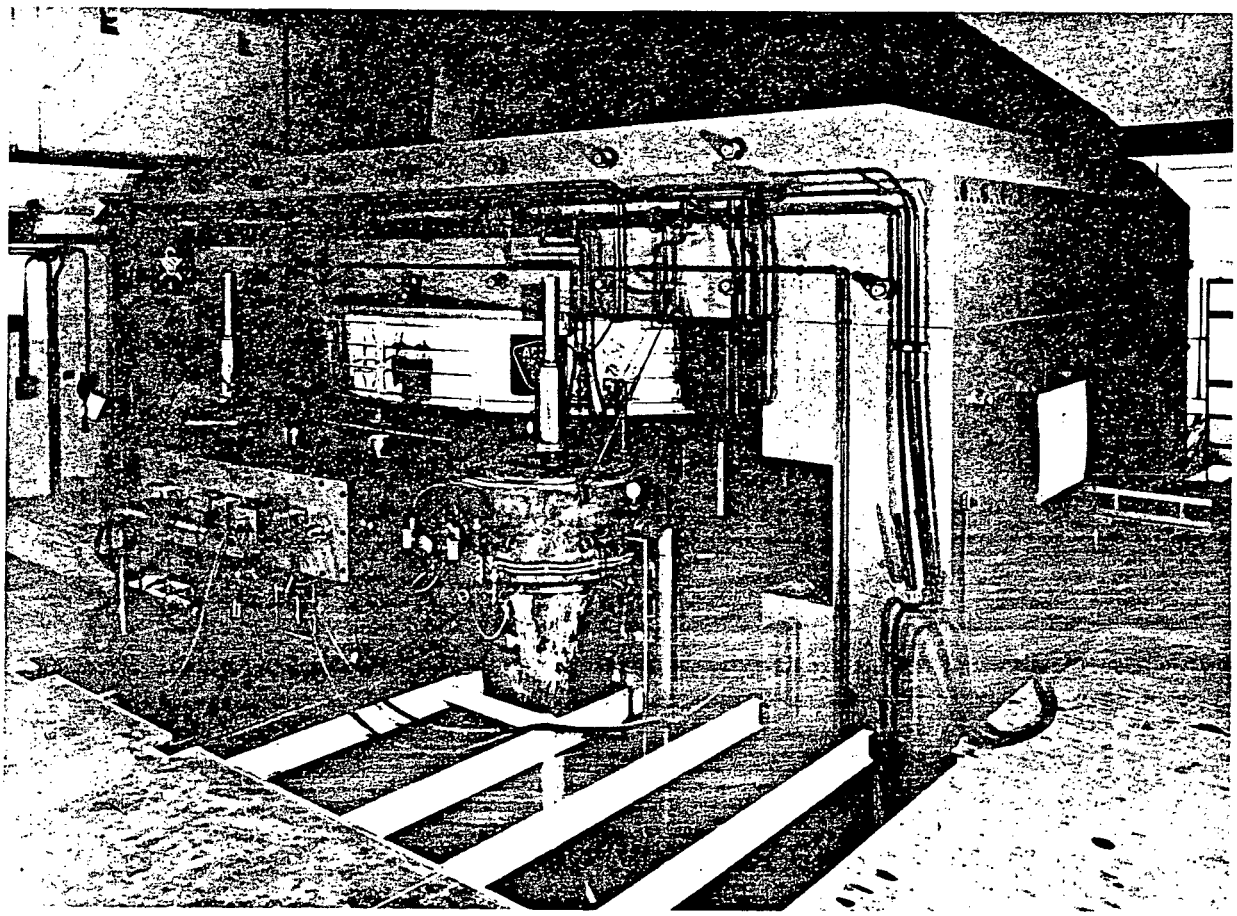

NASA
L-62-1046.1

Figure 5.- CERN 600-MEV Synchrocyclotron.

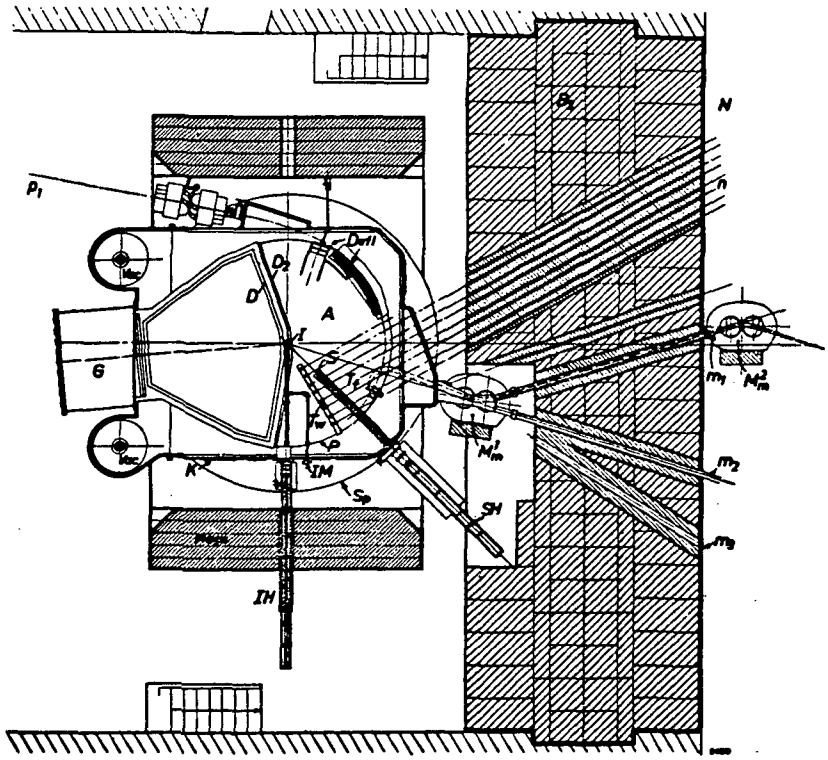

NASA

Figure 6.- Target systems for the CERN 600-MEV synchrocyclotron.

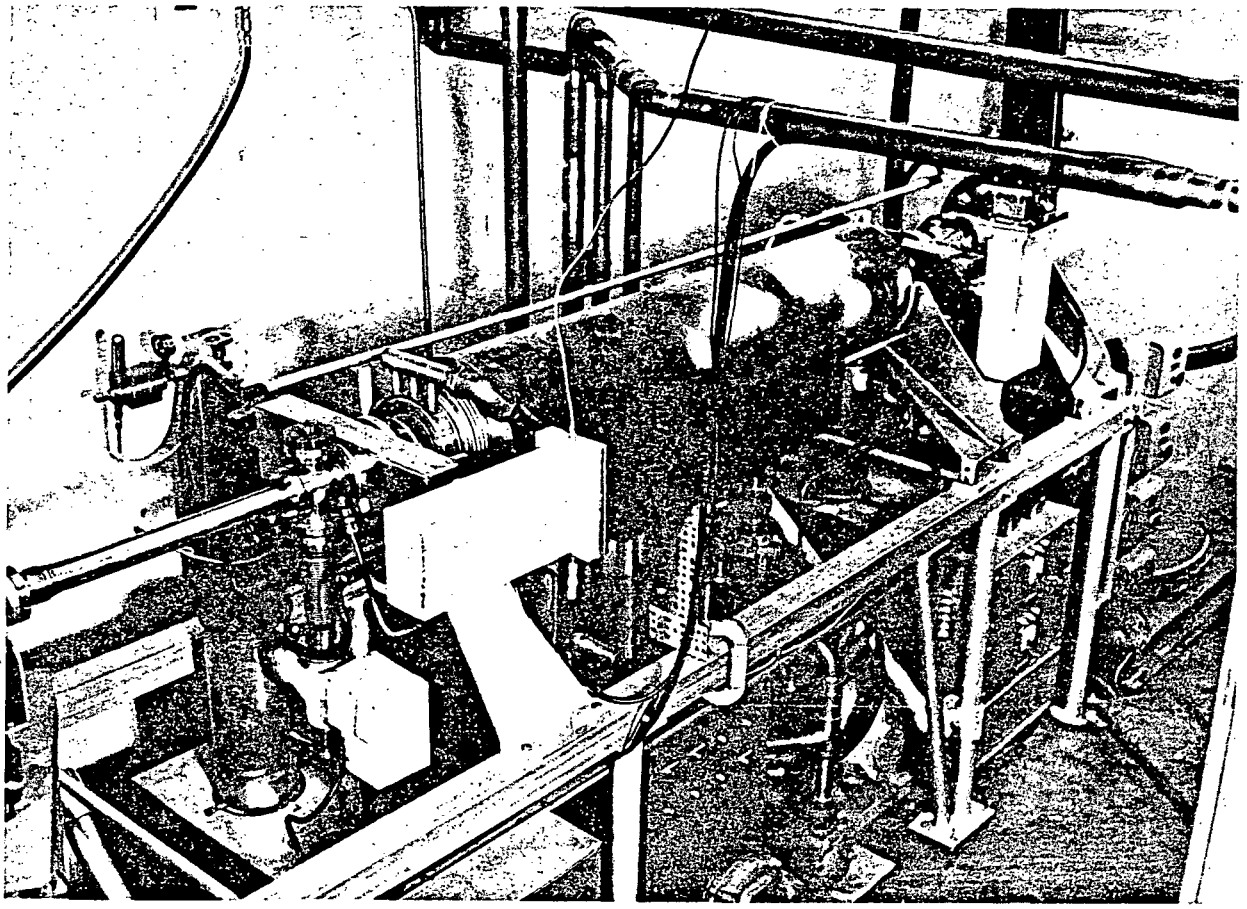

NASA
L-62-1045.1

Figure 7.- Accelerating section of a 10-MEV electron linac.

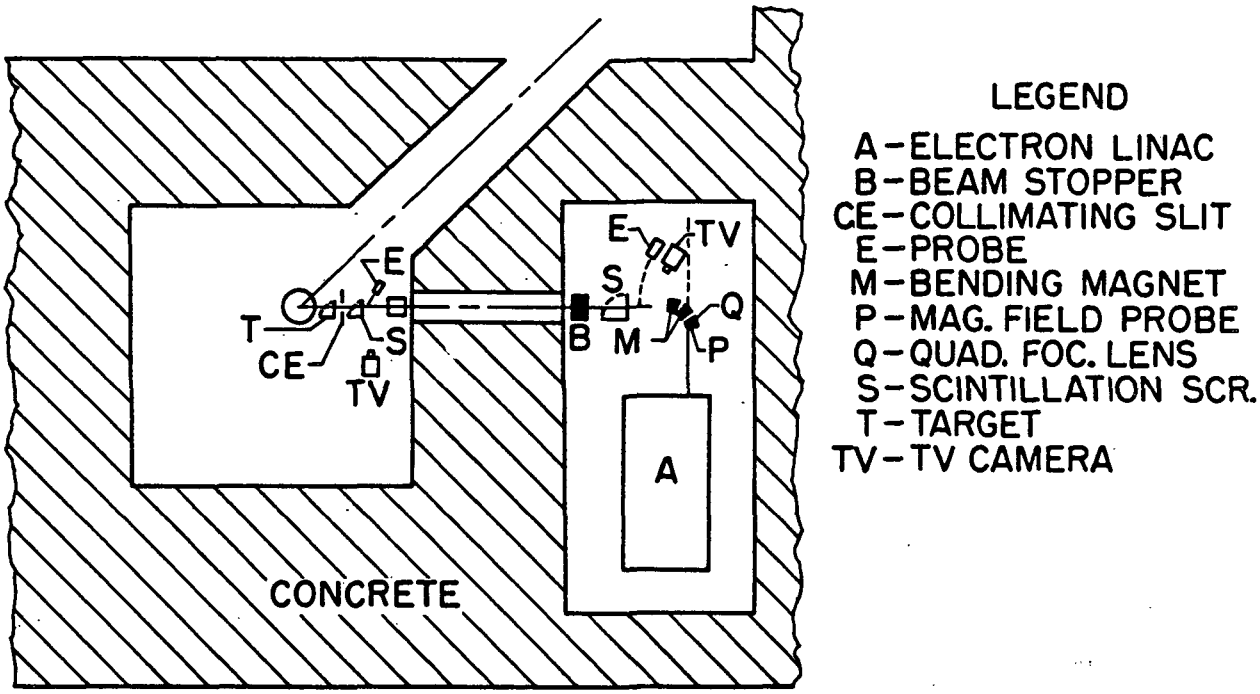

NASA

Figure 8.- Schematic of the electron linac proposed for SREL.

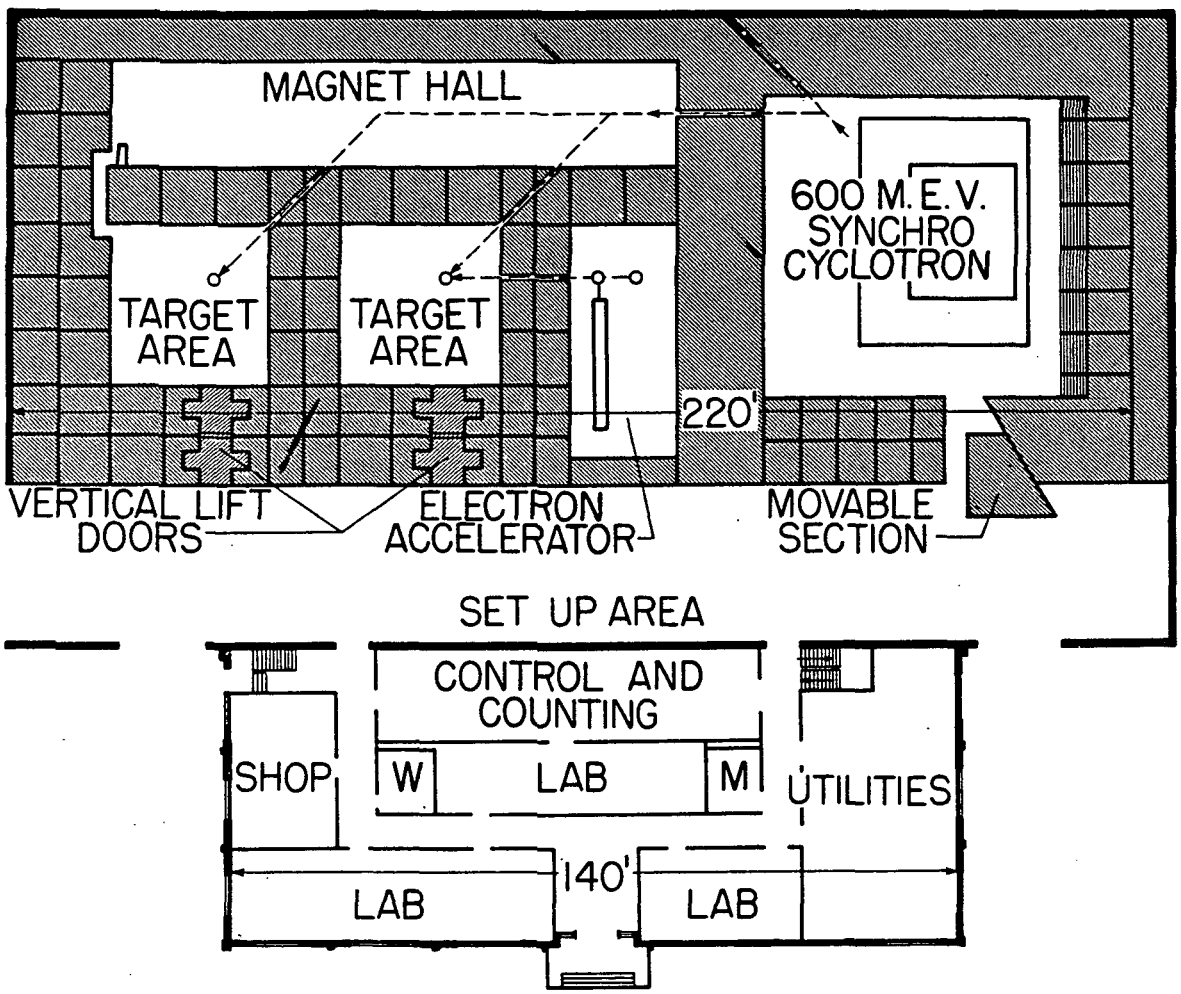

NASA

Figure 9.- Plan view of the Space Radiation Effects Laboratory.

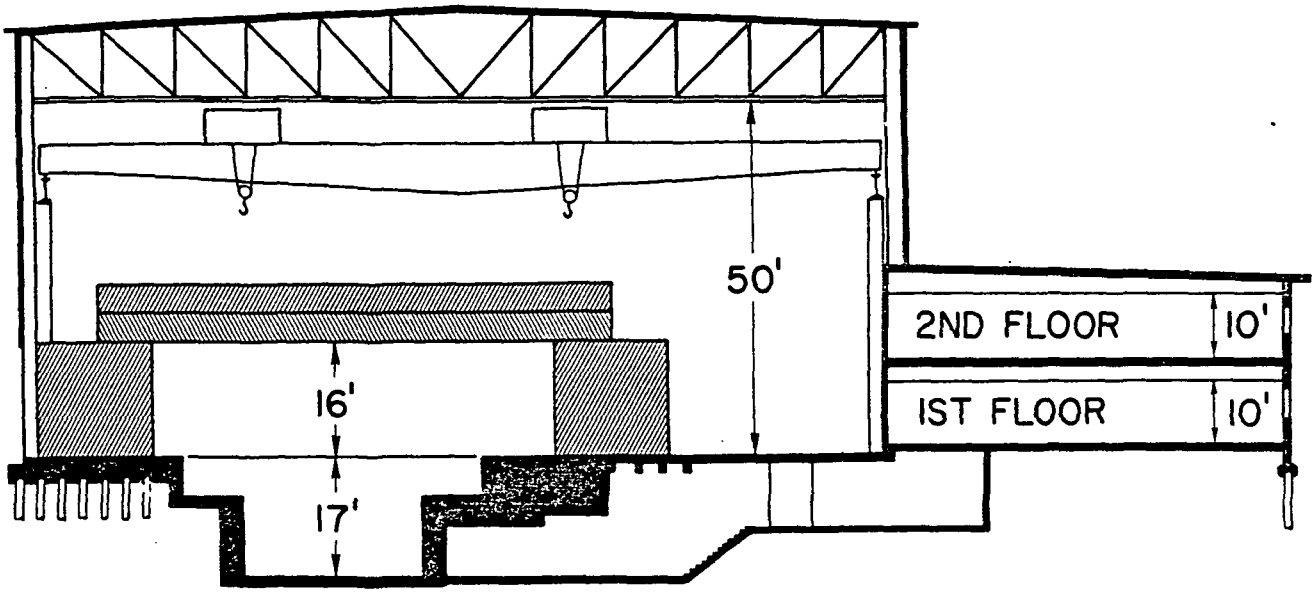

NASA

Figure 10.- Section of the Space Radiation Effects Laboratory taken through the synchrocyclotron cave.

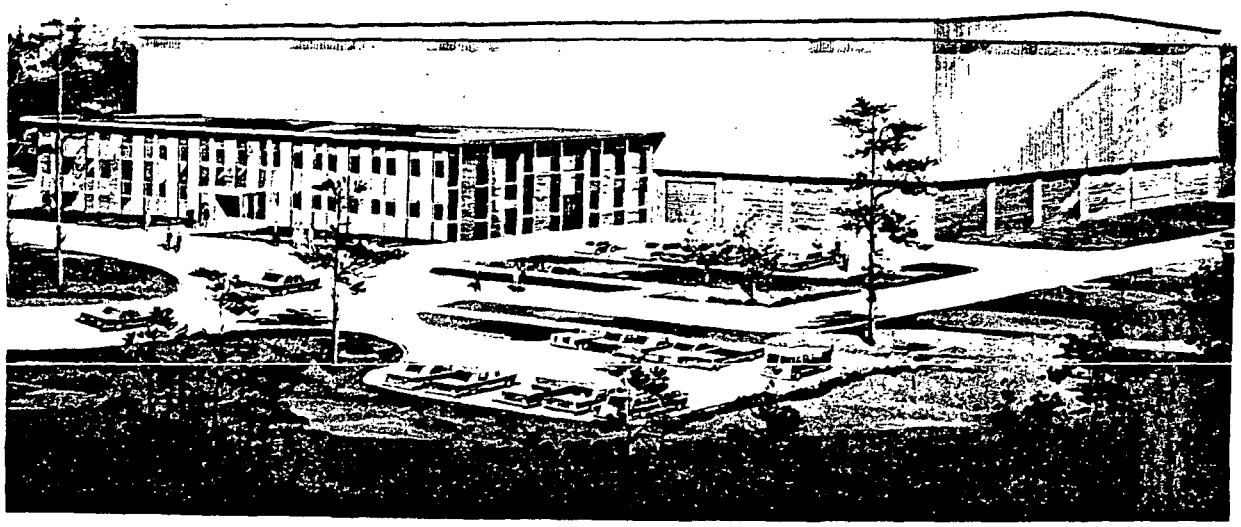

NASA
L-62-1043

Figure 11.- Architect's perspective rendering of the Space Radiation Effects Laboratory.

Paper B-4

THE EFFECTS OF PROTONS ON SEMICONDUCTOR DEVICES

William C. Honaker*
NASA Langley Research Center

Abstract

Experimental results are presented covering the data obtained from the bombardment of several transistors with 40 and 440 Mev protons. The data indicated a proton energy as well as a transistor frequency dependence on degradation. Figures are presented showing relative degradation of transistors with integrated flux.

Introduction

The presence of high-energy protons in the earth's radiation belts and in solar flares poses a problem in the design of circuits utilizing transistors for space application. The flux above an energy of 25 Mev in the inner belt is approximately 2.5×10^4 protons/cm^2/sec with the differential energy spectrum varying as $E^{-3.4}$. The proton energy ranges up to approximately 600 Mev (refs. 1 and 2). The proton flux in an extreme solar flare may be as high as 10^6 protons/cm^2/sec. In some high-energy events the proton energies extend into the billion electron volt (Bev) range (ref. 3).

Damage produced in solids by charged-particle bombardment has been considered theoretically in references 4 and 5. Most of the theory for such damage has been arrived at by using pure-element models with no definite correlation existing with a transistor junction; thus, a definite need for experimental data exists. This report presents data obtained during experimental testing of several types of transistors. If transient damage effects such as ionization are neglected, the primary damage produced in pure silicon and germanium is the creation of Frenkel defects (vacancy-interstitual pairs). This is the vacancy created by knocking an atom from its normal lattice site and having it come to rest at an interstitual position within a lattice structure. The defects that are formed affect the electrical characteristics of a semiconductor by providing recombination and trapping sites which can reduce the number of carriers and result in a decrease in carrier lifetime (refs. 6 and 7).

---

*Aerospace Technologist.

Only a limited amount of work has been accomplished with protons in the study of radiation damage on semiconductors (ref. 8). Results of bombardment with 40 and 440 protons presented in the present report show the extent to which transistors are damaged when they are subjected to a total proton flux in the order of 10^{12} protons/cm^2. With a knowledge of the proton spectrum in the radiation belts and in solar flares, an estimate can be made of the lifetime of the various transistors subjected to these environments.

Apparatus and Procedure

University of Minnesota Test

A total of 75 transistors were irradiated with 40 Mev protons by utilizing the linac accelerator at the University of Minnesota. The accelerator is capable of producing a time-average beam current of 10^{-8} amperes (approximately 6×10^{10} protons/sec). The cross-sectional area of the proton beam is approximately 1.25 square centimeters.

The experimental setup used during irradiation tests at the University of Minnesota is shown in figure 1. The transistors were mounted in individual ports on an aluminum disk and were remotely positioned in the proton beam. A cam-controlled electric motor automatically positioned each transistor in the proton beam for 10 minutes at a beam flux rate of 3×10^9 protons/cm^2/sec or a total flux of 1.8×10^{12}. A zinc sulfide phosphor (silver activated) was placed on the aluminum disk in a position corresponding to that of the transistors and was alined with the proton-beam pipe exit. The center of the proton beam was visually located by using a closed-circuit television system to determine the location of the beam-excited portion of the phosphor. By marking the excited portion on the television monitoring screen, each transistor could be properly positioned within the marked area corresponding to the proton beam. During the experiments, the beam flux was monitored by means of a Faraday cup mounted behind the transistors. Periodic checks were made on the beam flux level through a vacant space in the aluminum disk.

During irradiation the transistors were operated in an active circuit. The transistor parameters which were monitored and recorded on a direct-writing oscillograph recorder included collector current, I_C; small-signal current gain, h_{fe}; and leakage current, I_{CBO}. The base current I_B was held constant during the irradiation. Pretest and post-test measurements on each type of transistor were made both at the Langley Research Center (LRC) as well as by the manufacturer, with the

exception of the 2N146 and 2N337 transistors for which no manufacturers' data were obtained.

Carnegie Institute of Technology Test

A total of 20 transistors were irradiated by utilizing the 440 Mev proton synchrocyclotron at the Carnegie Institute of Technology. The synchrocyclotron is capable of producing a time-average beam current of 2×10^7 protons/cm^2/sec. The cross-sectional area of the proton beam at the external port is approximately 25 square centimeters.

The method used for exposing the transistors to the beam in this experiment differed from the method used at the University of Minnesota in that the larger cross-sectional area of the beam permitted the irradiation of several transistors at the same time with each bombardment lasting approximately 6 hours. Due to the nonuniformity of the cross-sectional area of the proton beam, a profile survey was made with a scintillation counter. The positions of the various transistors in the beam were carefully determined, and total dosages were arrived at by using the beam-profile plots. The beam current was measured before and during irradiation by using a helium-filled ionization chamber mounted between the beam exit port and the specimen and operated at 2 lb/sq in. above atmospheric pressure. The transistors exposed to the beam were mounted on a bracket supported by a junction box attached to a tripod. The transistor parameters measured before, during, and after irradiation were the same as those of the University of Minnesota experiments except that no manufacturer's data were obtained. Also, the number of transistors irradiated was fewer because of the lower beam flux and the longer irradiation time.

Discussion and Results

Figure 2 shows seven 2N146 (NPN) germanium, low-frequency transistors which were irradiated with 40 Mev protons. The average change in gain was a decrease of 70 percent at a total flux of 1.8×10^{12} p/cm^2, which was found to be typical for low-frequency germanium devices. Figure 3 is a plot of six, 2N743, NPN, high-frequency silicon transistors with small signal current gain plotted against integrated proton flux. The change was about a 12-percent decrease at a total flux of 1.8×10^{12} p/cm^2 or approximately one-sixth the damage sustained by the low-frequency transistor in figure 2. In figure 4 a plot is shown of a 2N337, NPN, silicon low-frequency transistor. This device was damaged by about 85 percent of its original value after a dose of 1.8×10^{12} p/cm^2. The extent of damage was about the same as for the low-frequency germanium device.

To give an idea of the frequency dependence on transistor damage figure 5 shows a 2N1302 transistor having an alpha cutoff frequency of 0.5 megacycle and a 2N224 transistor with an alpha cutoff frequency of 4.5 megacycles. The difference in frequencies here is approximately an order of magnitude and the difference in change in gain is 20 percent. The change would be approximately the same for other orders of magnitude change in frequency but this can also vary with materials and type of junction.

The 2N1302 shown in figure 5 was one of the devices irradiated at both 40 and 440 Mev. Figure 6 shows the relative damage at these two energies for a medium frequency transistor. The relative change at the two energies at 3×10^{11} p/cm^2 was approximately a factor of 3 for this transistor. A comparison can be made between this NPN germanium device and a PNP germanium device shown in figure 7. Figure 7 is basically the same type of plot as figure 6 except that a 2N224, PNP, germanium transistor is irradiated in figure 7. The relative change in the 40 and 440 Mev bombardment again is approximately a factor of 3 at identical fluxes. Note the initial increase in gain and then a decrease. This phenomenon is noticed in PNP germanium junctions but not in NPN germanium junctions.

Table I gives a complete list of transistors bombarded with 40 Mev protons and shows the type junction, material, alpha cutoff frequency and the average change in each transistor gain at a total flux of 1.82×10^{12} protons/cm^2. The averages were arrived at using six or seven transistors at the same proton dose and the changes noted ranged from an increase of 10 percent for the 2N128 PNP germanium transistor to a decrease of 85 percent for the 2N337 NPN silicon device.

For a good comparison between NPN and PNP junction, the second transistor the 2N1302 which changes by 65 percent and the sixth a 2N1303 which changed by 23 percent are nearly the same device except for the type junction; here it is evident that the PNP junction is more resistant to proton irradiation.

In table II, if one can assume a tolerable operating level of 0.7, the original gain of a transistor and a flux of 5×10^4 p/cm^2/sec in the space environment, then the lifetime of the various transistors irradiated is given in the right-hand column which extends from 30 to 418 days.

References

1. Smith, R. V., Fisher, P. C., Imhof, W. L., and Reagan, J. B.: Midas IV Proton Measurement in the Inner Van Allen Belt. [Rep.] 3-77-62-6 (Contract AF 19(604)-8028) Nuclear Phys. Dept., Lockheed Missiles and Space Corp., Feb. 1962.

2. Freden, Stanley C., and White, R. Stephen: Protons in the Earth Magnetic Field. Phys. Rev. Letters, vol. 3, no. 1, July 1, 1959, pp. 9-11.

3. Foelsche, Trutz: Current Estimates of Radiation Doses in Space. NASA TN D-1267, 1962.

4. Seitz, Frederick, and Koehler, J. S.: Displacement of Atoms During Irradiation. Solid State Physics, Vol. 2, Frederick Seitz and David Turnbull, eds., Academic Press, Inc. (New York), 1956, pp. 305-448.

5. Mitchell, E. W. J.: The Effect of Radiation Damage on the Electronic Properties of Solids. British Jour. Appl. Phys., vol. 8, no. 5, May 1957, pp. 179-189.

6. Denny, J. M., and Pomeroy, D.: Radiation Damage and Transistor Life in Satellites. Proc. IRE, vol. 48, no. 5, May 1960, pp. 950-952.

7. Billington, Douglas S., and Crawford, James H., Jr.: Radiation Damage in Solids. Princeton University Press, 1961.

8. Hulten, W. C., Honaker, W. C., and Patterson, John L.: Irradiation Effects of 22 and 240 Mev Protons on Several Transistors and Solar Cells. NASA TN D-718, 1961.

TABLE I

RELATIVE DAMAGE TO Si AND Ge TYPE TRANSISTORS
40 MEV PROTONS - TOTAL FLUX 1.82×10^{12} CM^{-2}

TRANSISTOR	TYPE	DESCRIPTION	$f_{\alpha b}$ MC	Δh_{fe} PERCENT
2 N 859	PNP Si	ALLOY JUNCTION	17	78
2 N 1302	NPN Ge	ALLOY JUNCTION	4.5	65
2 N 224	PNP Ge	ALLOY JUNCTION	0.5	85
2 N 1305	PNP Ge	ALLOY JUNCTION	8	65
2 N 1303	PNP Ge	ALLOY JUNCTION	4.5	23
2 N 526	PNP Ge	ALLOY JUNCTION	3	65
2 N 337	NPN Si	GROWN JUNCTION	30	85
2 N 146	NPN Ge	GROWN JUNCTION	13	70
2 N 169A	NPN Ge	RATE GROWN	9	50
2 N 743	NPN Si	DIFFUSED MESA	500	12
2 N 128	PNP Ge	SURFACE BARRIER	60	+10

TABLE II

FLUX TOLERANCE $\frac{h_{fe}(\phi)}{h_{fe}(0)} = 0.7$

TRANSISTOR TYPE	MAXIMUM PROTON FLUX (10^{11}/CM^2)	PROTON ENERGY	SIMULATED TIME IN DAYS IN A PROTON FLUX OF 5×10^4 P/cm^2/SEC
2N 337	1.3	40 MEV	30
2N 224	1.5	↓	35
2N 146	2		46.5
2N 859	2.5		58.1
2N 1305	5		116.3
2N 1302	5		116.3
2N 526	6.5		151.2
2N 169A	7		162.8
2N 1303	18		418.6
2N 743	>18		>418.6
2N 128	>18		>418.6

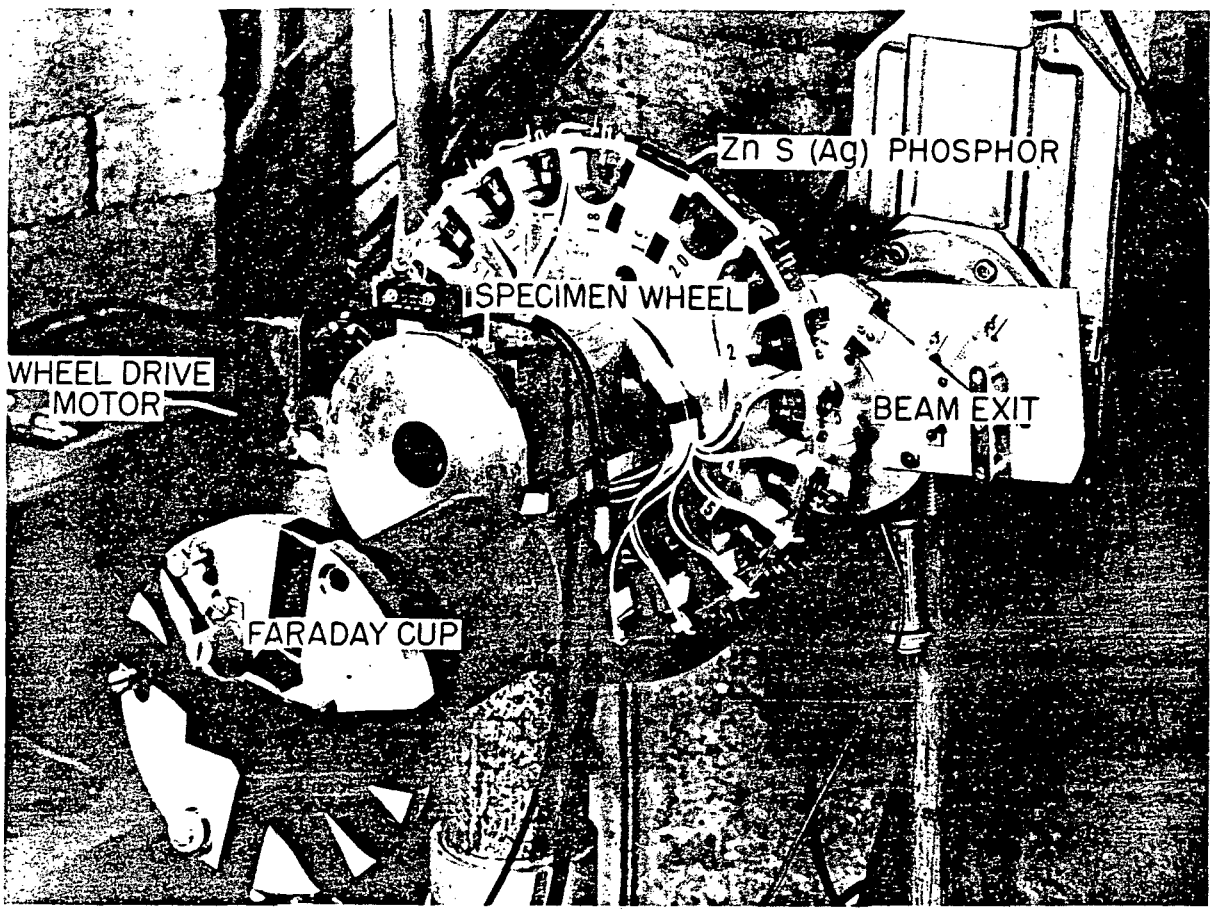

NASA
L-62-1017

Figure 1.- Transistor positioning device in the 40 Mev beam.

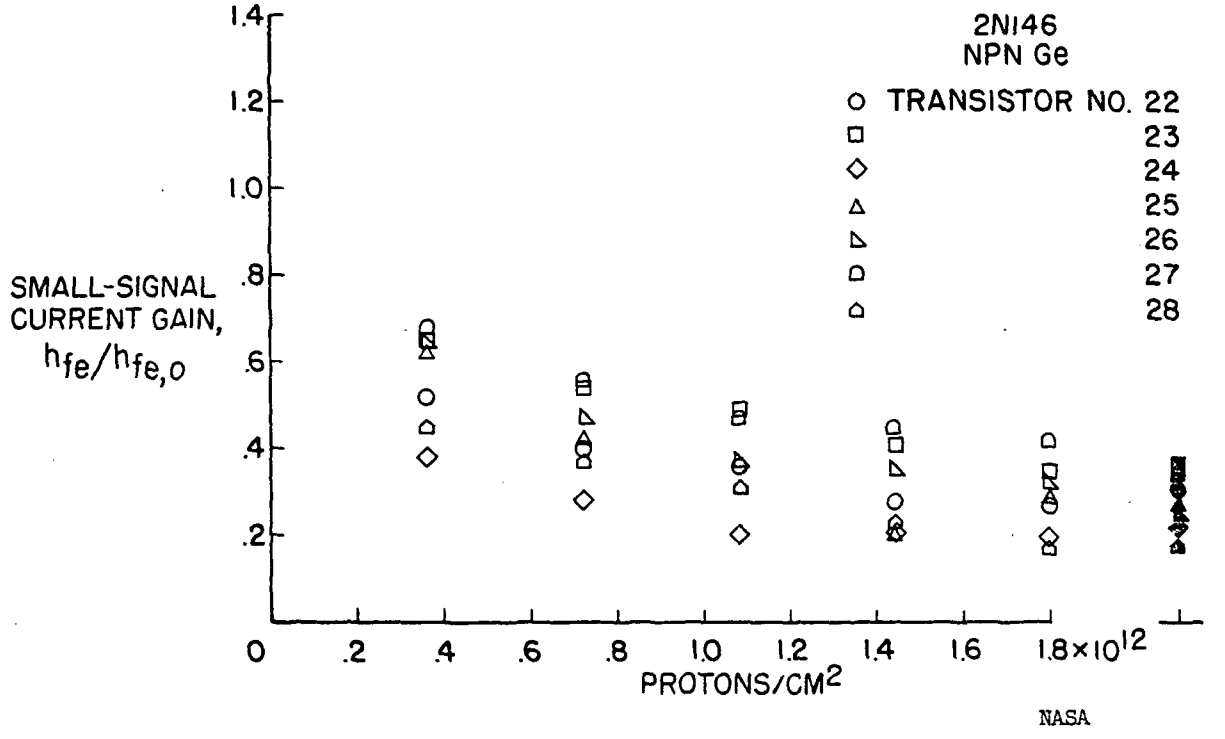

Figure 2.- 40 Mev proton damage.

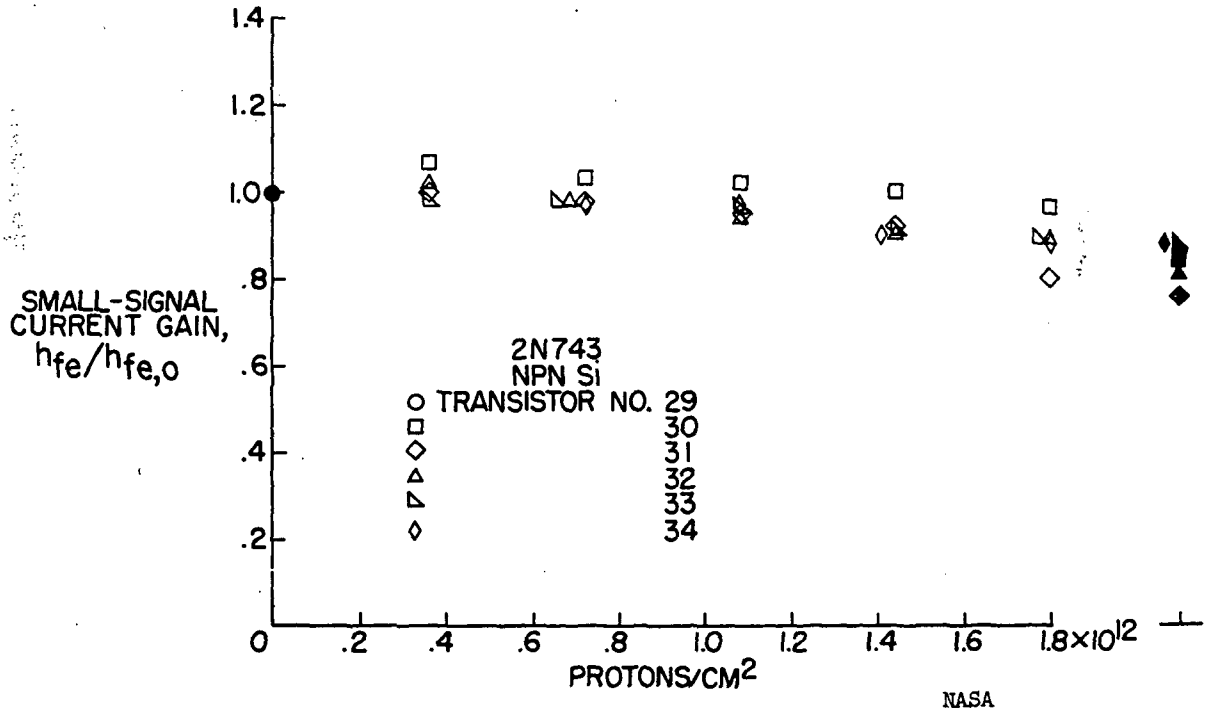

Figure 3.- 40 Mev proton damage.

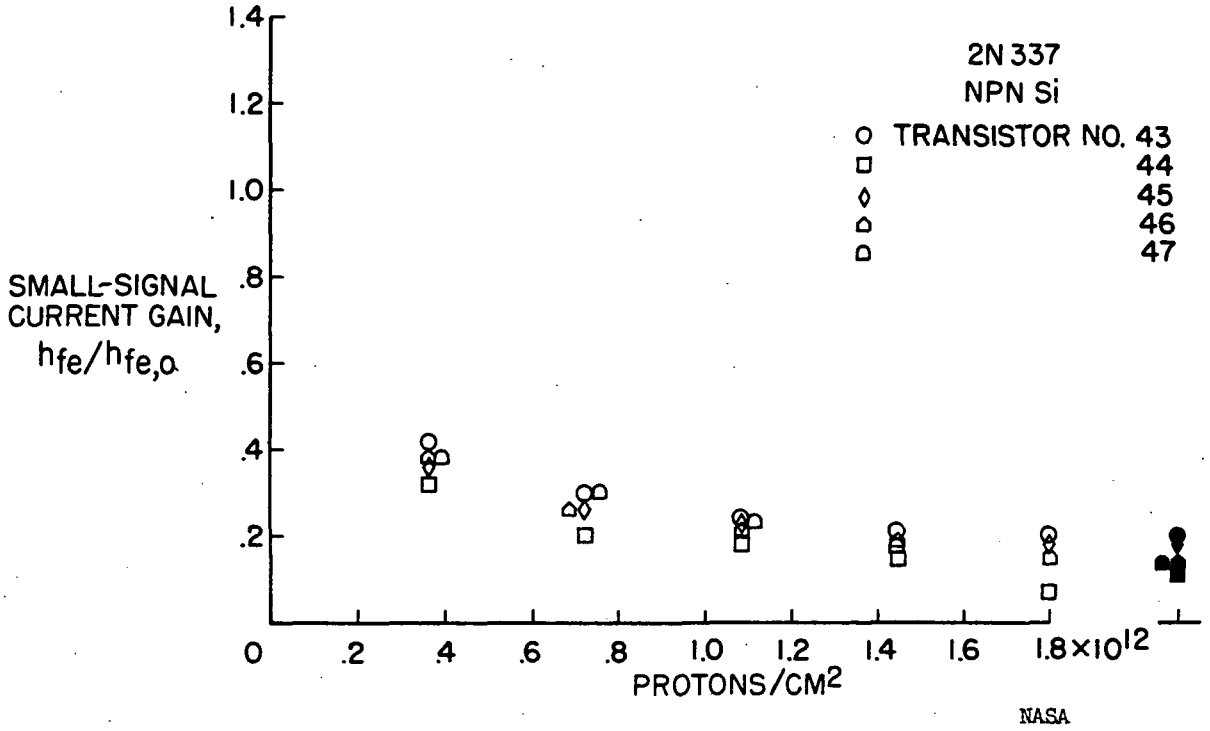

Figure 4.- 40 Mev proton damage.

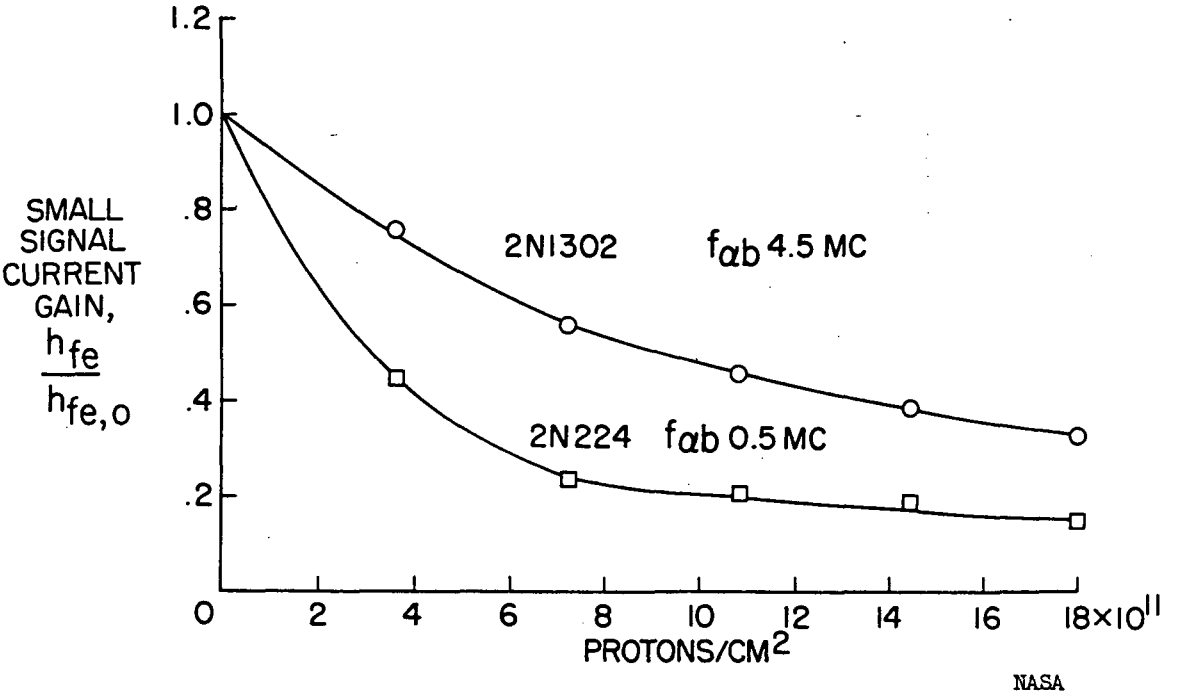

Figure 5.- Proton damage versus alpha cutoff.

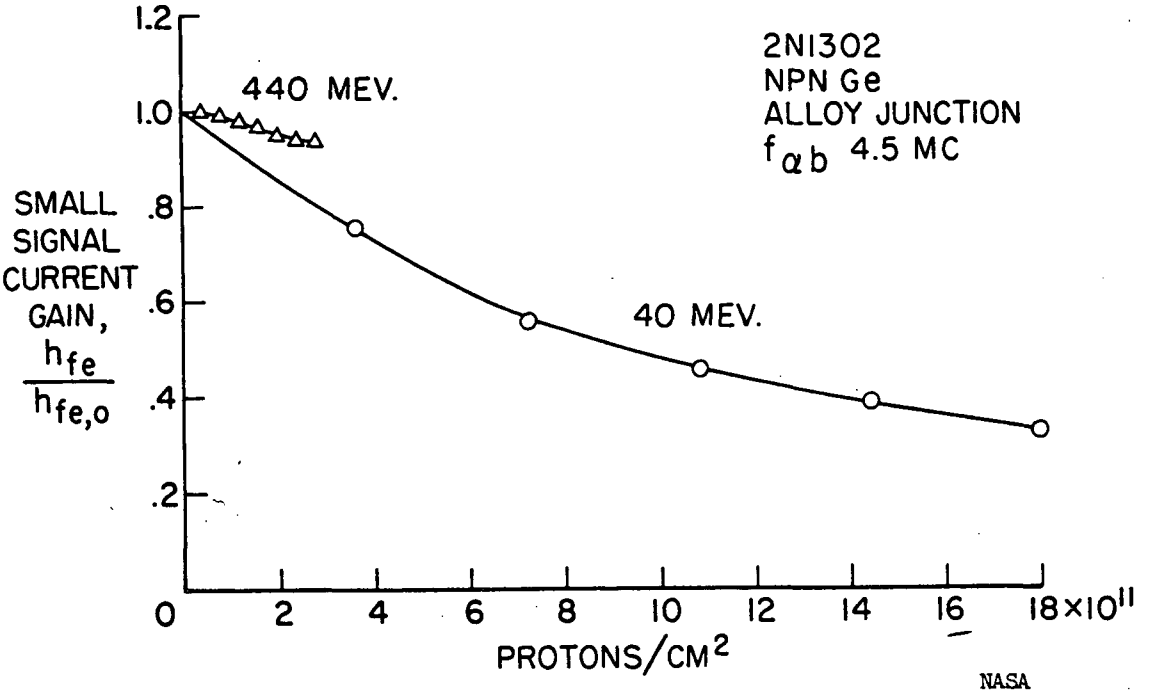

Figure 6.- Proton damage versus energy.

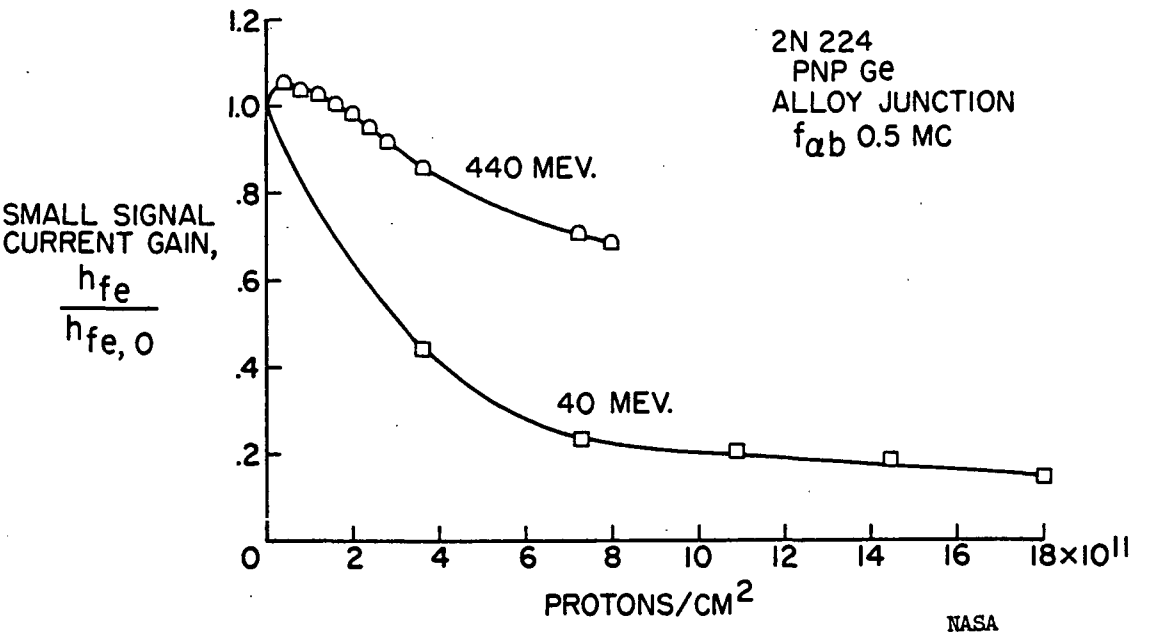

Figure 7.- Proton damage versus energy.

Paper B-5

PROTON RADIATION DAMAGE IN SEMICONDUCTOR DEVICES

D. A. Gandolfo*, D. M. Arnold*, J. A. Baicker**,
H. Flicker**, J. R. Parker*, J. Vilms**, J. Vollmer*,
Radio Corporation of America

Abstract

The objective of the present study is to interpret observed changes in transistor electrical characteristics in terms of fundamental damage in the semiconductor crystal structure and, in so doing, to predict the effects of proton bombardment. Proton and neutron displacement production rates are calculated. These are used in conjunction with neutron irradiation data and an assumed similarity of defect clusters to determine the effects of protons on transistors. Reasonable agreement with experiment is obtained. The expected lives of transistors in satellites orbiting in the inner Van Allen belt are given.

Introduction

It has become important to understand and be able to predict the extent of proton damage to semiconductor devices. Accordingly, the objective of the study reported here is to interpret the observed changes in electrical characteristics of transistors in terms of fundamental damage to the semiconductor crystal structure and in so doing, to predict the effects of proton bombardment.

The method is as follows. First, the rate of production of lattice displacements is calculated at various proton energies. Next the rate of production of lattice displacements for neutron bombardment is calculated. Finally damage constants for neutron irradiation, determined from existing data, are converted into damage constants for proton irradiation by means of the calculated displacement rates. With these, the effect of proton bombardment on transistors is computed.

*Applied Research, Camden, New Jersey
**David Sarnoff Research Center, Princeton, New Jersey

Displacement Calculations

According to the theory discussed, for example, by Seitz and Koehler[1], Dienes and Vineyard[2] and Billington and Crawford[3] the displacement production rate is given by

$$R_D = \int_{E_d}^{T_m} n_{si}\, g(T)\, \frac{d\sigma}{d\Omega}(T)\, dT \qquad (1)$$

where: R_d is the displacement density per unit flux of incident particles.

n_{si} is the number of target silicon atoms per unit volume.

$g(T)$ is the defect cascade function, i.e. the expected total number of displacements produced by a primary recoil of energy T.

$\frac{d\sigma}{d\Omega}(T)$ is the differential elastic scattering cross section.

E_d is the displacement threshold, i.e. the energy which must be imparted to a target atom to displace it from its equilibrium site.

T_m is the maximum recoil energy which may be imparted to a target atom by an incident particle with a given energy.

The variable of integration in this expression is T, the energy of the primary recoil. T is related to the energy of the incident particle, E_{inc}, and the C.M. angle, θ, through which it is deflected by

$$T = \frac{4\left(\frac{m}{M}\right)E_{inc}}{\left[1+\left(\frac{m}{M}\right)\right]^2}\sin^2\frac{\theta}{2} \qquad (2)$$

where m is the proton mass and M is the silicon mass.

First, the proton displacement rate will be considered. At low bombarding energies one would expect coulomb forces to dominate the proton-silicon interaction, and as will be pointed out later, the

1. F. Seitz and J. S. Koehler, Solid State Physics, (Ed. by F. Seitz and D. Turnbull) Academic Press, N. Y. 1956, Vol. 2, P. 305.

2. G. J. Dienes and G. H. Vineyard, Radiation Effects in Solids, Interscience, N. Y. 1957.

3. D. S. Billington and J. H. Crawford, Radiation Damage in Solids, Princeton University press, Princeton, 1961.

radiation damage data for protons below 10 MeV is consistent with Rutherford scattering calculations. Above 10 MeV, however, the proton-silicon interaction must be modified to include nuclear forces. The principal result is a slight, though important, enhancement of the elastic cross section mainly at large scattering angles. This enhancement does not produce an observable increase in the number of primary proton-silicon collisions, but the few extra collisions that result generally involve a large momentum transfer, on the average, and consequently a large number of secondary lattice displacements. At very high energies (above 100 MeV) a complete account of the displacement production rate requires the inclusion of a number of inelastic processess as well as elastic scattering.

In the absence of data on the scattering of protons by silicon, the proton-aluminum cross sections have been used for these calculations. The justification for this is a logical consequence of the nuclear optical model, which fits the elastic proton scattering data with considerable accuracy over the energy range from 10 to 100 MeV, and for nuclei throughout practically the entire periodic table. Since the optical model parameters are slowly varying functions of atomic weight, going from A=27 to A=28 requires practically no correction.

The proton displacement rate is shown as a function of proton energy in Fig. 1.

The solid curve shown in this figure is a compilation of silicon solar cell damage data from several sources. The two lowest-energy points shown, at 1.5 and 4.5 MeV were calculated from Rutherford scattering, and the upper five points from p+Al elastic scattering data. The solid curve has been normalized to the computed displacement rate at E_p = 10 MeV.

There are two interesting features about this figure. The first is that at proton energies as low as 10 MeV there is a perceptible contribution to the total lattice displacement rate caused by nuclear-elastic scattering. The second interesting point is that elastic scattering is sufficient to give a fairly good account of the total displacement rate for proton energies as high as 100 MeV. At 180 MeV the solar cell damage rate is 2.5 times what one would expect from elastic scattering alone.

Next, the displacement production rate for neutrons is calculated using Eq. 1, and making the same assumptions that were made in the proton displacement calculation regarding the applicability of n + Al data to silicon. The results of the calculation are given in Fig. 2 which shows the displacement rate over the energy interval, 0 to 10 MeV. The weighted average of the displacement rate for a fission spectrum is shown as $\overline{R}_{DN}$. The fission spectrum is the energy spectrum of prompt fission neutrons and is a good approximation to the energy spectrum of neutrons produced by pulsed reactors such as the Godiva and Kukla facilities.

Lifetime Damage Constant

Next attention will be turned to the electrical property of semiconductors which is most affected by radiation, namely the minority carrier lifetime. In semiconductors like germanium and silicon where direct band to band recombination is forbidden, the recombination rate is directly proportional to the number of traps or centers at which recombination can take place. The minority carrier lifetime is of course inversely related to the recombination rate; therefore, to the number of traps. According to these considerations the lifetime may be written as

$$\frac{1}{\tau} = C\, N_t\, (\varphi) \tag{3}$$

where C is related to the capture cross section of the centers for minority carriers, the energy levels of the centers, the Fermi level of the material and the thermal velocities of the carriers. C is assumed to be independent of the flux, φ. N_t is the number of traps and is, of course, a function of φ. Loferski and Rappaport[4-6] determined experimentally that the lifetime is related to the flux by

$$\frac{1}{\tau} = \frac{1}{\tau_o} + k\varphi \tag{4}$$

where τ_o is the pre-irradiation lifetime and k is the lifetime damage constant. Taking the derivative of $\frac{1}{\tau}$ with respect to φ one finds that

$$\frac{\partial\left(\frac{1}{\tau}\right)}{\partial\varphi} = C\,\frac{\partial N_t}{\partial\varphi} = k \tag{5}$$

Thus, k is simply the product of C and the rate of introduction of traps. At this point, it is assumed that the rate of introduction of traps is directly proportional to the displacement production rate. Further, it is assumed that the damage constants for protons and neutrons are related to the particle type only through the respective displacement rates. Therefore the damage constants for protons and neutrons may now be written

$$k_P = C' R_{DP};\ k_N = C' R_{DN} \tag{6}$$

4. P. Rappaport, Phys. Rev. 94, 1409(A) (1954).

5. J. J. Loferski and P. Rappaport, Phys. Rev. 98, 1861 (1955).

6. P. Rappaport and J. J. Loferski, Phys. Rev. 100, 126(A) (1955)

When C' is eliminated from Eq. 6, k_P is obtained in terms of k_N and the displacement rates

$$k_P = k_N \frac{R_{DP}}{R_{DN}} \tag{7}$$

k_N is determined from neutron irradiation experiments and R_{DP} and R_{DN} are calculated quantities.

The assumption that the damage constants are functions only of the total displacement production rates, independent of the type of particle producing the damage is an essential part of this study. However, it has been seen that for proton energies above 10 MeV nuclear-elastic scattering contributes significantly to the total displacement rate. The good agreement between the proton energy dependences of the damage rate and the displacement rate may be accounted for by assuming that all displacements are equally effective in producing electrical damage, regardless of whether they are produced in high concentration, as in the displacement spikes characteristic of nuclear-elastic scattering, or in very low concentration, as in the point defects generally characteristic of coulomb scattering.

Effects of Proton Bombardment on Transistors

Transistors and the effect of radiation induced lifetime changes on their performance will now be considered. Webster's[7] equation shows the dependence of the common emitter current gain, β, on the minority carrier lifetime

$$\frac{1}{\beta} = \frac{SA_S W}{A D} + \frac{\sigma_b W}{\sigma_e L_e} + \frac{1}{2} \frac{W^2}{D\tau} \tag{8}$$

where S is the surface recombination velocity, A_S is the effective area for surface recombination, W is the base width, A is the area of the conduction path, σ_b and σ_e are the conductivities of the base and emitter regions, L_e is the diffusion length in the emitter, D is the diffusion constant and τ is the minority carrier lifetime.

The first term on the right is the surface recombination term, the second is the injection efficiency term and the third is the volume recombination term. Terms one and two are assumed to be independent of the flux. Equation 8 may be rewritten, using Equation 4, to show explicitly the dependence on radiation induced lifetime changes

$$\frac{1}{\beta} = \frac{1}{\beta_0} + \alpha\varphi = \frac{1}{\beta_0} + \frac{1}{2} \frac{W^2}{D} k\varphi = \frac{1}{\beta_0} + \frac{.2}{f_{c\alpha}} k\varphi \tag{9}$$

---

[7] W. M. Webster, Proc. IRE 42, 914 (1954)

where $f_{c\alpha}$ is the alpha cutoff frequency of the device. This relationship has been checked experimentally by Messenger and Spratt[8] and Loferski[9]. In a neutron irradiation experiment where the flux is φ_N, the lifetime damage constant for neutrons, k_N, is measured. If the effect of a proton bombardment is to be calculated, $k_p\varphi_p$ must be substituted for $k_N\varphi_N$. Equation 7 shows how kp is determined from k_N and the calculated displacement rates R_{DN} and R_{DP}. Several sample calculations have been made to check the validity of the method outlined here. From the data of Puttcamp[10] of the Diamond Ordance Fuze Labs and Hicks[11], et. al. at Boeing, lifetime damage constants describing the degradation of β with neutron flux have been obtained. These have been used in conjunction with the method discussed above to compute lifetime damage constants for monoenergetic proton bombardment.

Using the damage constants thus obtained one may calculate the proton flux necessary to reduce the current gain of selected silicon transistors to a specified fraction of its initial value. The results of the calculation may be compared with the experimental results which Hulten and Honaker[12] obtained with 40 MeV protons.

Example 1: 2N743, npn mesa, $f_{c\alpha} \doteq 400$ Mc.

The data of Hulten and Honaker[12, 13](average of 6 units) showed that a flux of 1.8×10^{12} protons/cm^2 at 40 MeV reduced β to $.85\beta_o$. From Puttcamp's neutron irradiation of the 2N697, npn mesa, $f_{c\alpha} \doteq 150$ Mc, one finds

$$\alpha_N \text{ (average of 4 units)} = 1.8 \times 10^{-15} \text{ nvt}^{-1}$$

and

$$\alpha_P = \frac{150}{400} \times \frac{1000}{380} \alpha_N = 1.8 \times 10^{-15} \text{ per unit proton flux.}$$

8. G. C. Messenger and J. P. Spratt, Proc. IRE, 46, 1038 (1958)

9. J. J. Loferski, J. Appl. Phys. 29, 35 (1958)

10. Robert Puttcamp, Diamond Ordance Fuze Laboratories TR-975 (AD 270264) 27 November 1961.

11. D. A. Hicks, D. V. Keller, J. B. Robison, R. K. Durkee, J. R. Orr, B. M. Clarke, Boeing Airplane Company, Report D5-2880, 1 December 1958.

12. W. C. Hulten, "Radiation Effects of 40 and 440 MeV Protons on Transistors," Society of Aerospace Material and Process Engineers Symposium, St. Louis, May 7-9, 1962.

13. W. C. Honaker, "The Effects of Protons on Semiconductor Devices," Protection against Radiation Hazards in Space, Gatlinburg, November 5 - 7, 1962.

Using this α_p to calculate the proton flux necessary to reduce β to $.85\beta_o$ one finds

$$\varphi_{calc} = 2.2 \times 10^{12} \text{ protons/cm}^2$$

and

$$\frac{\varphi_{calc}}{\varphi_{exp}} = 1.2$$

Example 2: 2 N859, pnp alloy, $f_{c\alpha} \doteq 14$ Mc.

The data of Hulten and Honaker (average of 6 units) showed that a flux of $.7 \times 10^{12}$ protons/cm^2 at 40 MeV reduced β to $.5\beta_o$. From the neutron irradiation by Hicks et. al. of the 2N495, also a pnp alloy, with $f_{c\alpha} \doteq 35$ Mc one finds

$$k_N = 3.2 \times 10^{-7} \text{ nvt}^{-1} \text{ sec}^{-1}$$

and

$$\alpha_p = \frac{.2}{14 \times 10^6} \times \frac{1000}{380} \times k_N = 1.23 \times 10^{-14} \text{ per unit proton flux}$$

Using this α_p to calculate the proton flux required to reduce β to $.5\beta_o$ one finds

$$\varphi_{calc} = 1.5 \times 10^{12} \text{ protons/cm}^2$$

and

$$\frac{\varphi_{calc}}{\varphi_{exp}} = 2.2$$

The agreement in the case of the 2N743 is quite good. For the 2N859 it is less good but still satisfactory in light of the scatter in the proton irradiation data.

Transistors in Satellites

Having checked the method in two cases where comparable neutron and proton data exist, one may proceed to the calculation of the expected life of selected groups of transistors in a hypothetical proton flux. The flux is an idealized representation of that which might be experienced by a device aboard a satellite whose orbit is in the most intense region of the Inner Van Allen Belt. This idealized proton spectrum has been constructed from the data of Heckman and Armstrong[14] and is shown in Figure 3. The expected life of the devices has been calculated from

14. Harry H. Heckman and Alice H. Armstrong, J. Geophys. Research 67, 1255 (1962).

$$T_{(.5\beta_o)} = \frac{2D}{W^2\beta_o} \times \frac{R_{DN}}{k_N} \times \frac{1}{R_{DP}\Phi_P} \qquad (10)$$

where k_N is the average lifetime damage constant for p or n type silicon as given by Messenger and Spratt and Φ_P is the proton flux rate in particles/cm^2-sec. Results of this calculation are shown in Figure 4. Table 1 lists the type numbers and some properties of the transistors in the groups indicated by the numbers in Figure 4.

Table 1. Satellite Transistors

Group Number	W(cm.)	f_c (Mc)	Transistor Types
1	5.1×10^{-5}	> 500	2N709 2N917
2	1.02×10^{-4}	$200 < f_{c\alpha} < 500$	2N916 2N914 2N708
3	1.9×10^{-4}	$50 < f_{c\alpha} < 200$	2N718A 2N1613 2N1893 2N910
4	3×10^{-4}	$20 < f_{c\alpha} < 50$	2N1675 2N930
5	1.27×10^{-3}	$2 < f_{c\alpha} < 10$	2N560 2N657
6	2.3×10^{-3}	$.5 < f_{c\alpha} < 1.5$	2N1485 2N2016
PNP	1.2×10^{-4} 1.2×10^{-4} 1.5×10^{-4}	~ 100	2N995 2N869 2N1132

To be noted in Figure 4 is the superiority of transistors with thin bases (corresponding to high alpha cutoff frequency) and low initial current gain.

Summary and Conclusions

The displacement production rates for protons and neutrons have been calculated and used with neutron irradiation data to predict proton damage.

The lattice displacement rate produced by elastic scattering of protons has been calculated as a function of energy and compared with the observed proton damage rate for silicon solar cells. For energies up to nearly 100 MeV the agreement is quite good. As might be expected, at higher energies where nuclear reactions assume increasing importance the damage rate exceeds the displacement rate calculated from elastic scattering alone.

The effect of protons on transistors has been calculated with the use of a lifetime damage constant measured under neutron irradiation and the ratio of the calculated displacement rates. The good agreement with available data indicates that the assumptions made earlier are reasonable, and a very useful consequence follows, namely that the large amount of existing neutron damage data may be converted to proton damage information in a rather simple manner.

Acknowledgments

The authors are grateful for the assistance of Mr. Henry Harmon of the Radio Corporation of America who provided much information about the physical and electrical characteristics of the transistors considered in this study, and for that of Mr. E. Rind of the National Aeronautics and Space Administration.

This study was performed under NASA contract NASI-1654.

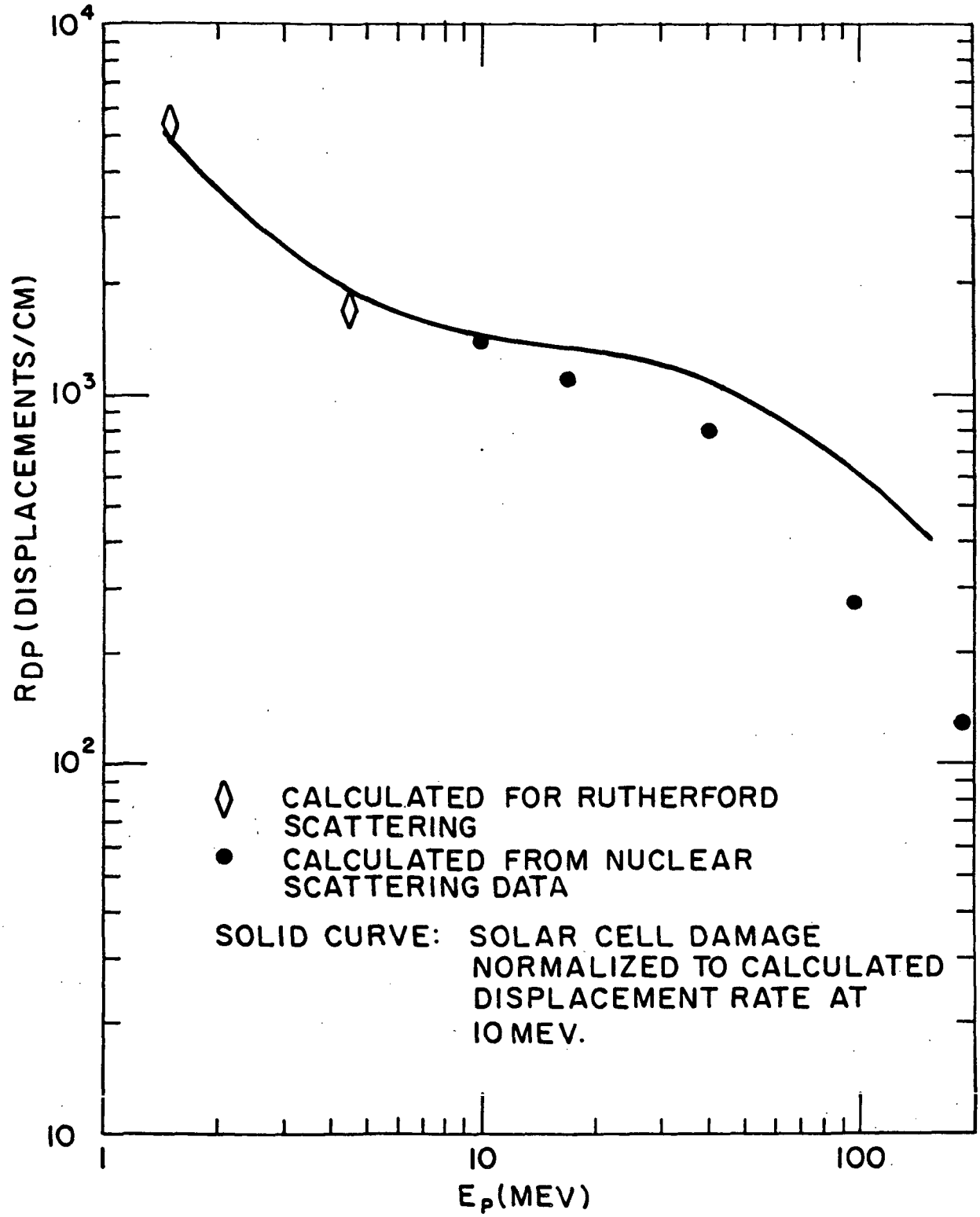

Figure 1. The number of lattice displacements, R_{DP}, per centimeter along the track of an incident proton of energy, E_P. Ionization effects by the primary recoiling silicon atom have been neglected.

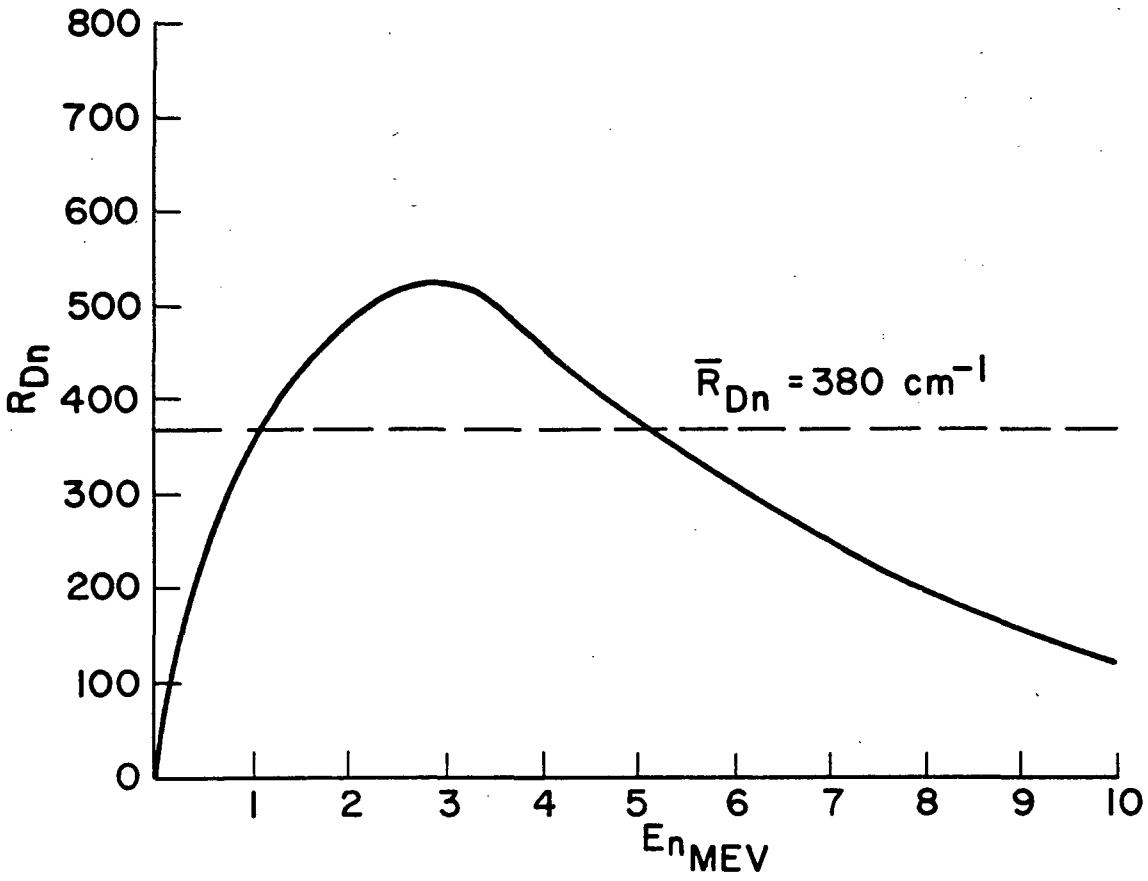

Figure 2. The number of lattice displacements, R_{DN}, per centimeter along the track of an incident neutron of energy, E_N.

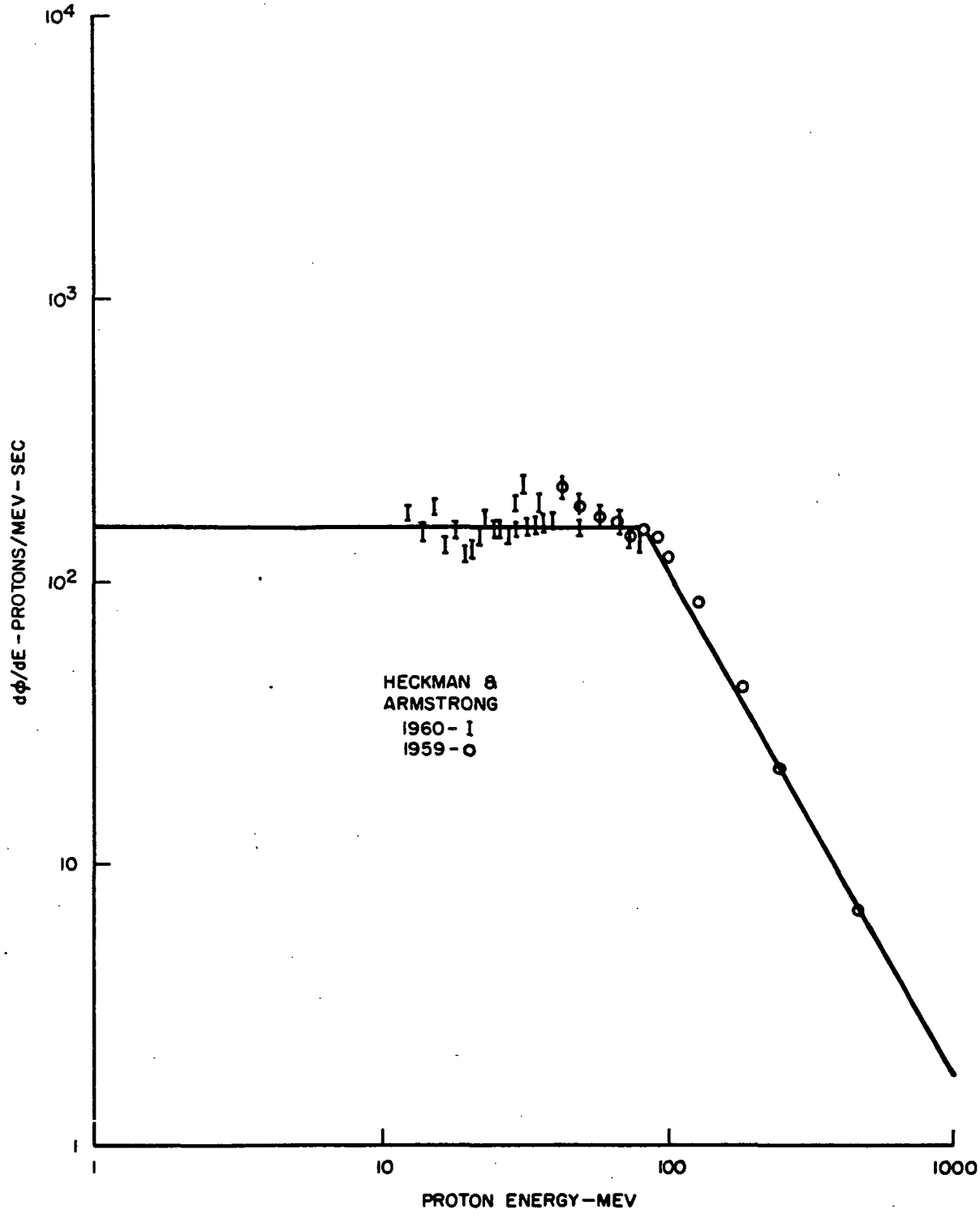

Figure 3. Idealized proton spectrum for the Inner Van Allen Belt. The shape of the spectrum is based on the data of Heckman and Armstrong,(9) but the curve has been normalized to Van Allen's total of 2×10^4 protons/cm^2-sec above 40 Mev.

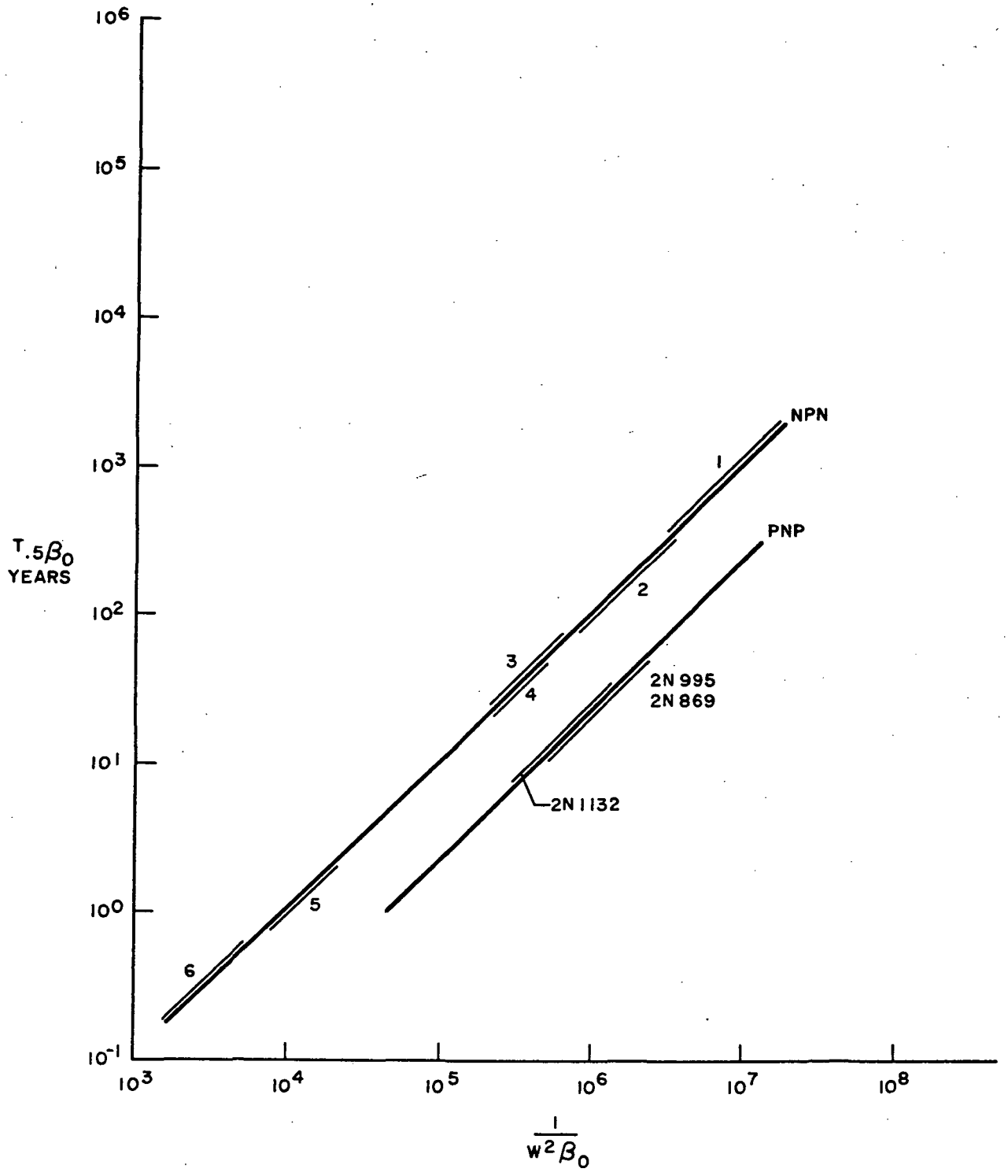

Figure 4. Time in Inner Van Allen Belt flux shown in Figure 3 for 50% reduction in current gain as a function of base width, W, and inital gain, β_o.

Paper B-6

SOLAR CELL DEGRADATION BY PROTONS IN SPACE

Richard Madey
Republic Aviation Corporation

Abstract

An analytic expression for the decrease in efficiency of a solar cell behind a protective cover glass exposed to a spectral distribution of protons is formulated on the basis that the time rate of decrease in output power is proportional to the proton dose rate absorbed at the surface of the solar cell. The decrease in the maximum power output ΔP of a solar cell exposed to protons in space is found to be

$$\Delta P = 1/2\ P_o \ln(1 + \bar{\epsilon} L_i^2 D)\ , \qquad (1)$$

where D is the absorbed dose of protons at the surface of the solar cell behind a protective cover glass, and L_i is the initial value of the diffusion length of the minority carriers of the solar cell corresponding to the initial maximum power output P_i. The dependence of L_i on P_i is found from the data of Smits, Smith, and Brown[1] to be represented by

$$L_i = L_o e^{P_i/P_o} \qquad (10 \text{ mw} < P_i < 20 \text{ mw}) \qquad (2)$$

For an n-on-p cell, $L_o = 0.234$ micron and $P_o = 3.13$ milliwatts. The quantity $\bar{\epsilon}$ is a radiation damage factor averaged over the absorbed dose rate from a spectral

---

1. F.M. Smits, K.D. Smith, and W.L. Brown, "Solar Cells for Communications Satellites in the Van Allen Belt," J. Brit. IRE 22 (2), 161 (August, 1961).

distribution of protons. The energy dependence of ϵ is obtained from experimental data[2,3] on the change in the reciprocal squared diffusion length per unit integrated proton flux, I, versus proton energy E. Actually, ϵ is defined by

$$\frac{d\,(1/L^2)}{d\,I} = \epsilon \quad \frac{dE}{dR_o} \tag{3}$$

where dE/dR_o is the specific ionization energy loss in the material of the solar cell.

The decrease in the maximum power output of an n-on-p silicon solar cell exposed to the solar flare of 12 November 1960 is calculated as a function of the thickness of protective cover glass for a power-law representation of the differential flux spectrum of the incident protons.

Introduction

Energetic protons in space bombard the active material of solar cells which supply power for satellites and space probes. Radiation damage to a solar cell results in a decrease in its power output. This degradation in the efficiency of a solar cell must be taken into account in the design of a solar cell power supply. The number of solar cells required to furnish a specified power output throughout a given mission will depend upon the decrease in power output expected during the mission. Some degradation can be prevented at the expense of additional weight by increasing the thickness of the protective cover glass. In order to be able to optimize the design of solar cell power supplies exposed to protons in space, it is useful to obtain an analytic representation for the decrease in power output of a solar cell behind a cover glass of arbitrary thickness.

---

2. W.L. Brown, "Damage to Semiconductors from Space Radiation," Presented at the American Rocket Society Space Nuclear Conference on May 3, 1961, at Gatlinburg, Tennessee.

3. W. Rosenzweig, F.M. Smits, and W.L. Brown, "Energy Dependence of Proton Irradiation Damage in Silicon," Bull. Am. Phys. Soc. II 7 (7), 437 (August 27, 1962).

Theory

Basic Assumption

In order to derive a formula for the decrease in the power output of a solar cell exposed to protons in space, we have made the assumption that dP/dt, the time rate of decrease in the output power of the solar cell, is proportional to the proton dose rate W absorbed at the front surface of the solar cell. Formally, we write

$$-\frac{dP}{dt} = F(P)\,W \tag{4}$$

where F(P) is a factor of proportionality which depends upon the instantaneous power level P of the solar cell. F(P) represents the differential decrease in power of the solar cell per unit of absorbed dose. If dP/dt is expressed in units of milliwatts/hour and W is in rads/hour, then F(P) is in units of milliwatts/rad.

Evaluation of Proportionality Factor F(P)

The proton dose rate absorbed at the surface of the solar cell behind a protective cover glass is given by the following integral:

$$W(\text{Mev/sec gm Si}) = \int \left(\frac{dE}{dR_o}\right) dR \int n'(R,\Omega)\, d\Omega\ , \tag{5}$$

where dE/dR_o is the specific ionization energy loss in Mev per gram per cm^2 of the material of the solar cell for protons of energy E, corresponding to the residual range R in the material of the cover glass. The zero subscript of dE/dR_o refers to the material of the solar cell (e.g., silicon). The differential quantity $n'(R,\Omega)\, dR\, d\Omega$ represents the number of protons emerging from the cover glass in a direction Ω in $d\Omega$ with a residual range (in the material of the cover glass) between R and R + dR.

For a spectrum of protons incident on the solar cell, the time rate of decrease in the output power is given by

$$-\frac{dP}{dt} = \int \frac{dP}{dI}\, dR \int n'(R,\Omega)\, d\Omega, \tag{6}$$

where dP/dI is the change in output power per unit time-integrated proton flux, and $dR \int n'(R,\Omega) d\Omega$ represents the number of protons

incident on the solar cell with residual ranges between R and R + dR crossing a unit area per unit time from all directions. The primed notation is used to denote that the unidirectional differential range spectrum, $n'(R, \Omega)$, at the solar cell is a degraded spectrum, the incident spectrum in space being degraded by a cover glass protecting the solar cell.

In the integrand of Eq. 6, the quantity dP/dI may be rewritten as a product of two factors:

$$\frac{dP}{dI} = \frac{dP}{d(1/L^2)} \frac{d(1/L^2)}{dI} = f(P)\, g(E), \tag{7}$$

where L is the diffusion length of the minority carriers in the material of the solar cell. The right-hand member of Eq. 7 is written in recognition of the fact that the first factor, f(P), will depend only on the power output of the solar cell and the second factor, g(E), will depend only on the proton energy.

The sensitive thickness of the solar cell is equal to the diffusion length of the minority carriers in the bulk material. The diffusion length is the average distance traveled by an excess minority carrier before recombining with a majority carrier. Values of the diffusion length range from 200 μ down to a few microns, depending upon the conductivity type, resistivity, and irradiation history of a cell.

From the data of Smits, Smith and Brown[1], the dependence of the maximum power output on diffusion length of an n-on-p solar cell may be represented by an exponential function as follows:

$$L \text{ (microns)} = L_o e^{P/P_o} \qquad (10 \text{ mw} < P < 20 \text{ mw}) \tag{8}$$

where $L_o = 0.234$ micron and $P_o = 3.13$ milliwatts. In Fig. 1, this analytical representation is compared with the data of Smits et al. They measured output characteristics of 92 solar cells under electron bombardment. From their measurements, they constructed curves of median power output versus voltage under outer space illumination with the integrated electron flux and the diffusion length as parameters. The dependence of the maximum power output on diffusion length is obtained from this data.

Thus, from Eq. 8, we find that

$$f(P) \equiv \frac{dP}{d(1/L^2)} = \frac{1}{2} P_o L_o^2 e^{2P/P_o} = \frac{1}{2} P_o L^2 \tag{9}$$

Now, let us write the energy-dependent factor as a product of two factors:

$$g(E) \equiv \frac{d(1/L^2)}{dI} = \epsilon \frac{dE}{dR_o} \tag{10}$$

where dE/dR_o is the specific ionization energy loss in the material of the solar cell, and ϵ is a radiation damage coefficient. The value of ϵ will be determined from experiment. After substituting Eqs. 7, 9, and 10 in Eq. 6, we obtain

$$-\frac{dP}{dt} = f(P) \int \epsilon \left(\frac{dE}{dR_o}\right) dR \int n'(R,\Omega)\, d\Omega. \tag{11}$$

We may rewrite Eq. 11 as follows:

$$-\frac{dP}{dt} = f(P)\, \bar{\epsilon}\, W \equiv F(P)\, W \tag{12}$$

where

$$F(P) \equiv \bar{\epsilon}\, f(P) = \frac{1}{2}\, \bar{\epsilon}\, P_o L^2 \tag{13}$$

and

$$\bar{\epsilon} \equiv \frac{\int \epsilon \left(\frac{dE}{dR_o}\right) dR \int n'(R, \Omega)\, d\Omega}{\int \frac{dE}{dR_o}\, dR \int n'(R, \Omega)\, d\Omega} \tag{14}$$

The dependence of the diffusion length on proton energy has been measured by Bell Telephone Laboratory workers[2,3] at various proton accelerators. These workers have reported their data in a plot of $d(1/L^2)/dI$ vs. proton energy. The first data of this type, reported by W.L. Brown[2], are shown in Fig. 2. Later, Rosenzweig, Smits, and Brown[3] reported similar data, shown in Fig. 3. We have shown both sets of data in a slightly different form in Fig. 4, where we have plotted ϵ vs. proton energy.

Decrease in Maximum Power Output

In order to obtain an expression for the decrease in the maximum power output of a solar cell, we integrate Eq. 12:

$$\text{Absorbed dose } D \equiv \int_{t_i}^{t_f} W dt = -\int_{P_i}^{P_f} \frac{dP}{F(P)} \equiv I(P)$$

where the subscripts i and f on the limits of the integrals denote initial and final values of the power and time. The result of integration is

$$\Delta P \equiv P_i - P_f = \frac{1}{2} P_o \ln(1 + \bar{\epsilon} L_i^2 D) \qquad (16)$$

where, from Eq. 8, L_i designates the value of the diffusion length of the minority carriers of the solar cell corresponding to the initial power P_i.

Upon substituting the values $P_o = 3.13$ milliwatts, $L_o = 2.34 \times 10^{-5}$ cm, $\bar{\epsilon} = 7.48 \times 10^{-8}$ gm/cm^2-Mev $= 4.67$ Rad^{-1}-cm^{-2}, Eq. 16 becomes

$$\Delta P \text{ (mw)} = 1.565 \ln \left[1 + 0.25 \times 10^{-8} e^{0.639 P_i} D \text{ (rads)}\right].$$

In Fig. 5, we plot the decrease in the maximum power output as a function of the absorbed dose of protons at the surface of the solar cell.

Absorbed Surface Dose Rate as a Function of Cover Glass Thickness

In order to determine the dependence of W, the proton dose rate absorbed at the surface of the solar cell, upon the thickness x in gm/cm^2 of a protective cover glass, it is necessary to integrate Eq. 5 for the dose rate. We have obtained an analytic expression relating the dose rate to the cover glass thickness on the following basis:

(a) An isotropic differential spectrum of protons is incident on a protective cover glass in plane geometry from the upper hemisphere. We represent the incident flux spectrum by a power law of the form

$$j \text{ (p/cm}^2\text{-sec-Mev)} = 2 \pi C E^{-\gamma}. \qquad (17)$$

(b) The range-energy relation for protons in matter is representable by a power law of the form

$$R \text{ (gm/cm}^2\text{)} = K E^{\alpha} \qquad (18)$$

where the constants K (gm/cm^2-Mev$^{\alpha}$) and α depend on the material.

The result of integration, written in terms of the incident flux, is

$$W \text{ (rads/hr)} = 5.76 \times 10^{-5} \frac{B(p,q)}{(1+p)\alpha \alpha_o K_o} E_x^{2-\alpha_o} j(E_x) \qquad (19)$$

where E_x is the proton energy required to just penetrate a cover glass thickness (gm/cm^2); α_o and K_o denote values for the material of the solar cell (e.g., silicon); α and K represent values for the material of the cover glass (e.g., sapphire); $B(p,q)$ is the beta function; and

$$p = (\gamma + \alpha_o - 2)/\alpha \tag{20}$$

$$q = (1 + \alpha - \alpha_o)/\alpha \tag{21}$$

Alternatively, by making use of the range-energy relationship, we may rewrite Eq. 19 directly in terms of the cover glass thickness:

$$W(t,x) = 5.76 \times 10^{-5} \frac{2\pi\, C(t)\, B(p,q)}{(1+p)\,\alpha\,\alpha_o\, K_o} \left(\frac{K}{x}\right)^p \tag{22}$$

Application to the Solar Flare of 12 November 1960

Characteristics of the Proton Spectrum

The integral proton spectrum has been measured[4] at energies as low as 2 Mev at 5 hours and 27 minutes after the peak of the optical flare on 12 November 1960. From the reported values of the spectral parameters (viz., $\gamma - 1 = 1.7 \pm 0.2$ in the energy interval from 2 Mev to 100 Mev and $N(> 2\ \text{Mev}) = 3 \times 10^4$ protons/cm^2-sec-steradian), the spectral exponent $\gamma = 2.7$ in the energy interval from 2 Mev to 100 Mev and the spectral coefficient $C(t_o) = 1.66 \times 10^5$ protons/cm^2-sec-steradian-Mev$^{\gamma-1}$ at $t_o = 5.5$ hours after the flare peak.

Absorbed Dose Rate at Time t_o

If we substitute numerical values in Eq. 22, the proton dose rate absorbed at time t_o at the surface of a silicon solar cell becomes

$$W(t_o, x) = 1.1\, x^{-1.4} . \tag{23}$$

---

4. K.W. Ogilvie, D.A. Bryant, and L.R. Davis, "Rocket Observations of Solar Protons During the November 12, 1960 Event," NASA Goddard Space Flight Center Contributions to the 1961 Kyoto Conference on Cosmic Rays and the Earth Storm. Also, K.W. Ogilvie, and L.R. Davis, "Rocket Observations of Solar Protons," presented at Forty-Second Annual Meeting, American Geophysical Union, Washington, D.C. (April 18-21, 1961).

Equation 53 is plotted in Fig. 6.

Absorbed Dose

We may estimate the integral for the absorbed dose in the approximation that the spectral exponent γ and hence the parameter p in Eq. 22 for the absorbed dose rate is independent of time t. In this approximation, the absorbed dose may be written

$$D = W(t_o, x)\ \overline{\Delta t} \tag{24}$$

where $\overline{\Delta t}$ is the effective duration of the flare. We have found $\Delta t = 2.36 \times 10^5$ seconds = 65.6 hours from the data of Fichtel, Guss, and Ogilvie[5] on the time dependence of the integral proton flux above 20 Mev.

Thus, the absorbed dose as a function of cover glass thickness $x(gm/cm^2)$ for the solar flare of 12 November 1960 is

$$D\ (rads) = 71\ x^{-1.4}. \tag{25}$$

Equation 25 is plotted in Fig. 7.

Decrease in Maximum Power Output vs. Thickness of Protective Cover Glass

Finally, the percentage decrease in maximum power output of an n-on-p silicon solar cell exposed to protons from the solar flare of 12 November 1960 is given by

$$\frac{\Delta P}{P_i} = \frac{1.565}{P_i} \ln\left(1 + 1.82 \times 10^{-7}\, e^{0.639 P_i}\, x^{-1.4}\right) \tag{26}$$

where the powers P_i and P_f are expressed in milliwatts, and x is in gms/cm^2 of cover glass. Equation (26) is plotted in Fig. 8.

---

5. C.E. Fichtel, D.E. Guss, and K.W. Ogilvie, Private Communication.

Acknowledgements

The author gratefully acknowledges the assistance of Messrs. Howard Oringer and F. M. Sisavic in performing calculations and plotting figures.

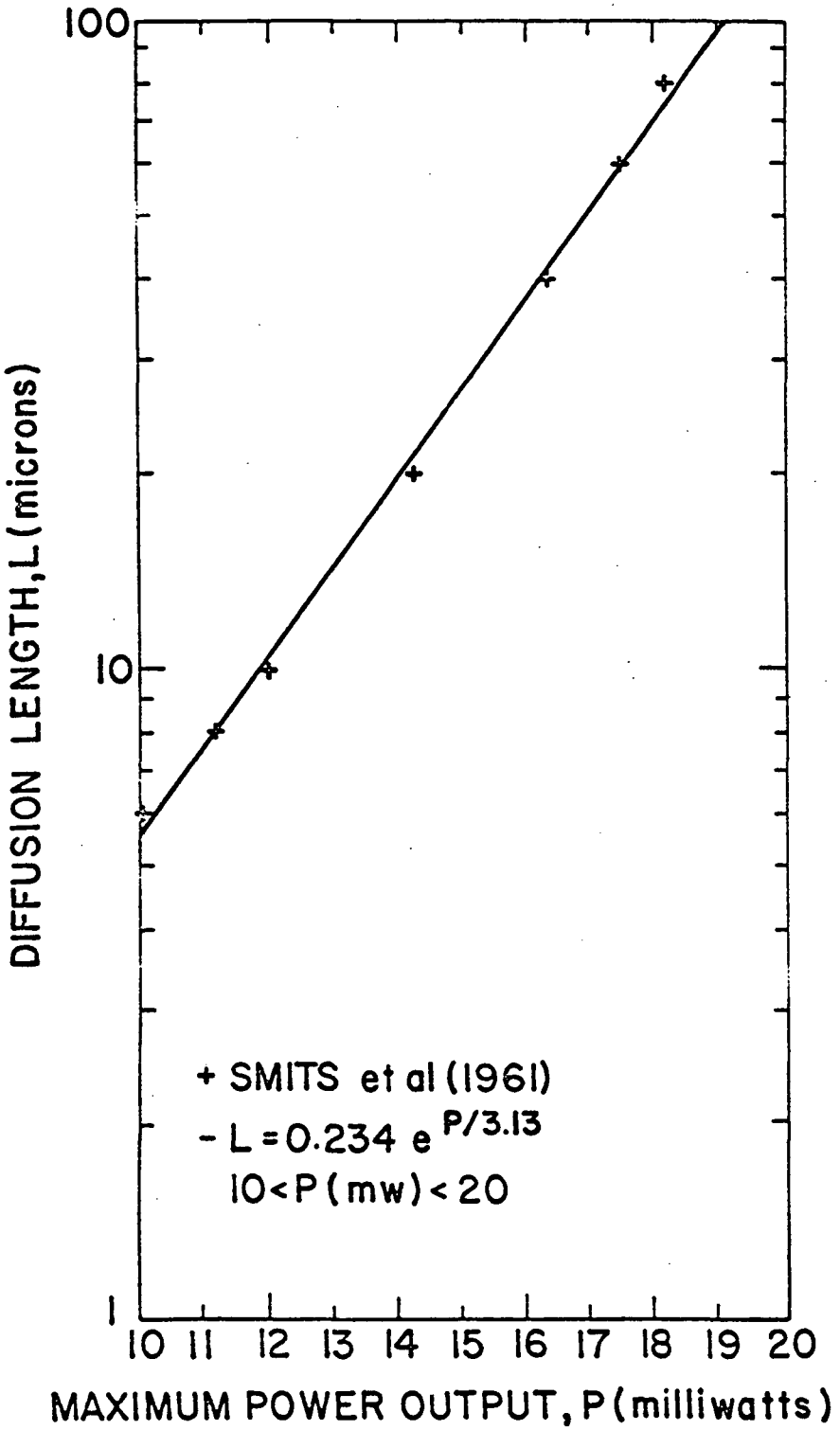

Figure 1. Diffusion Length of Minority Carriers of an n-on-p Solar Cell vs. Maximum Power Output.

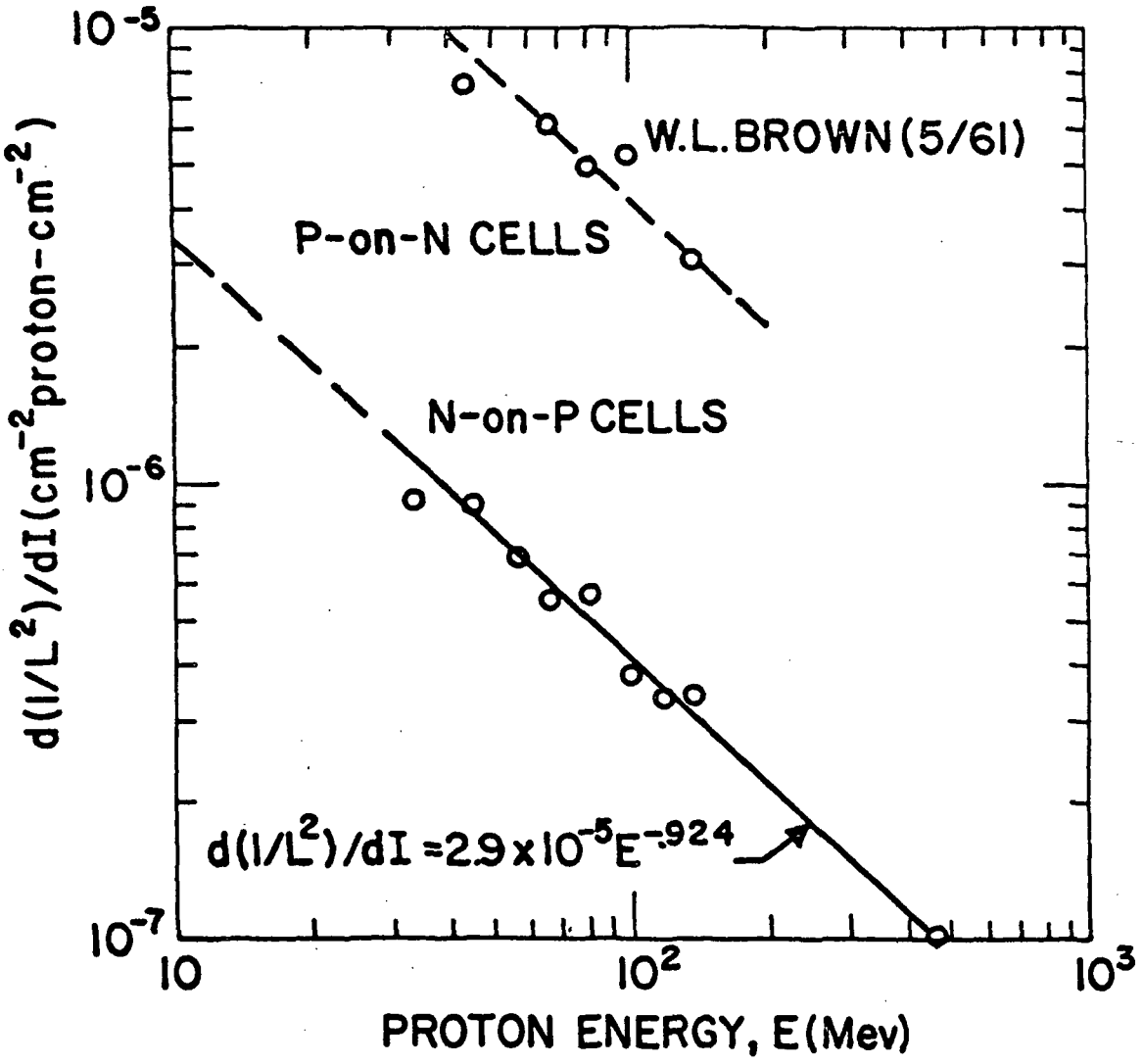

Figure 2. Change in Reciprocal Squared Diffusion Length per Unit Integrated Proton Flux for Solar Cells vs. Proton Energy. Data from W.L. Brown (May 1961).

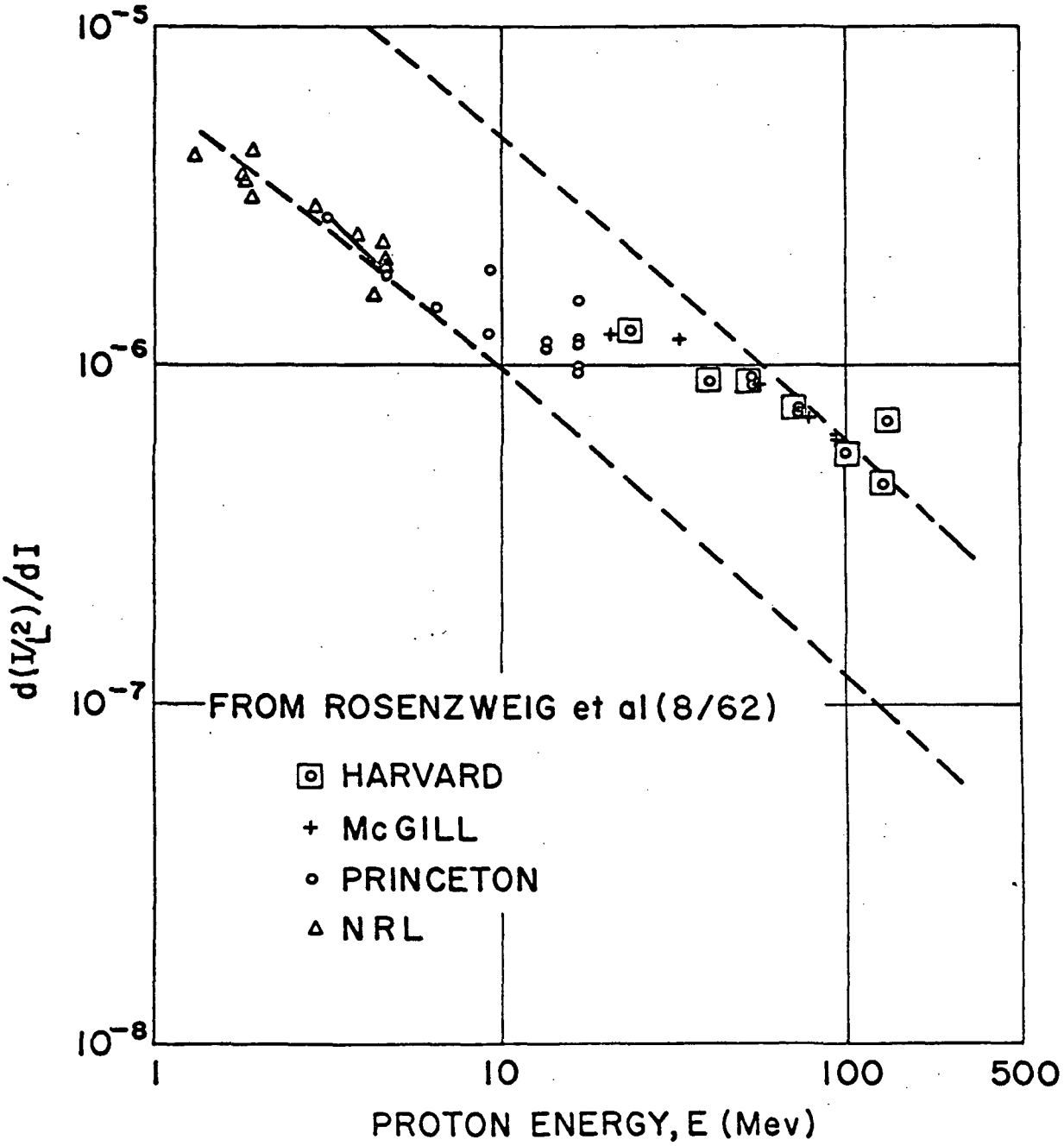

Figure 3. Change in Reciprocal Squared Diffusion Length per Unit Integrated Proton Flux for Solar Cells vs. Proton Energy. Data from Rosenzweig et al. (August 1962).

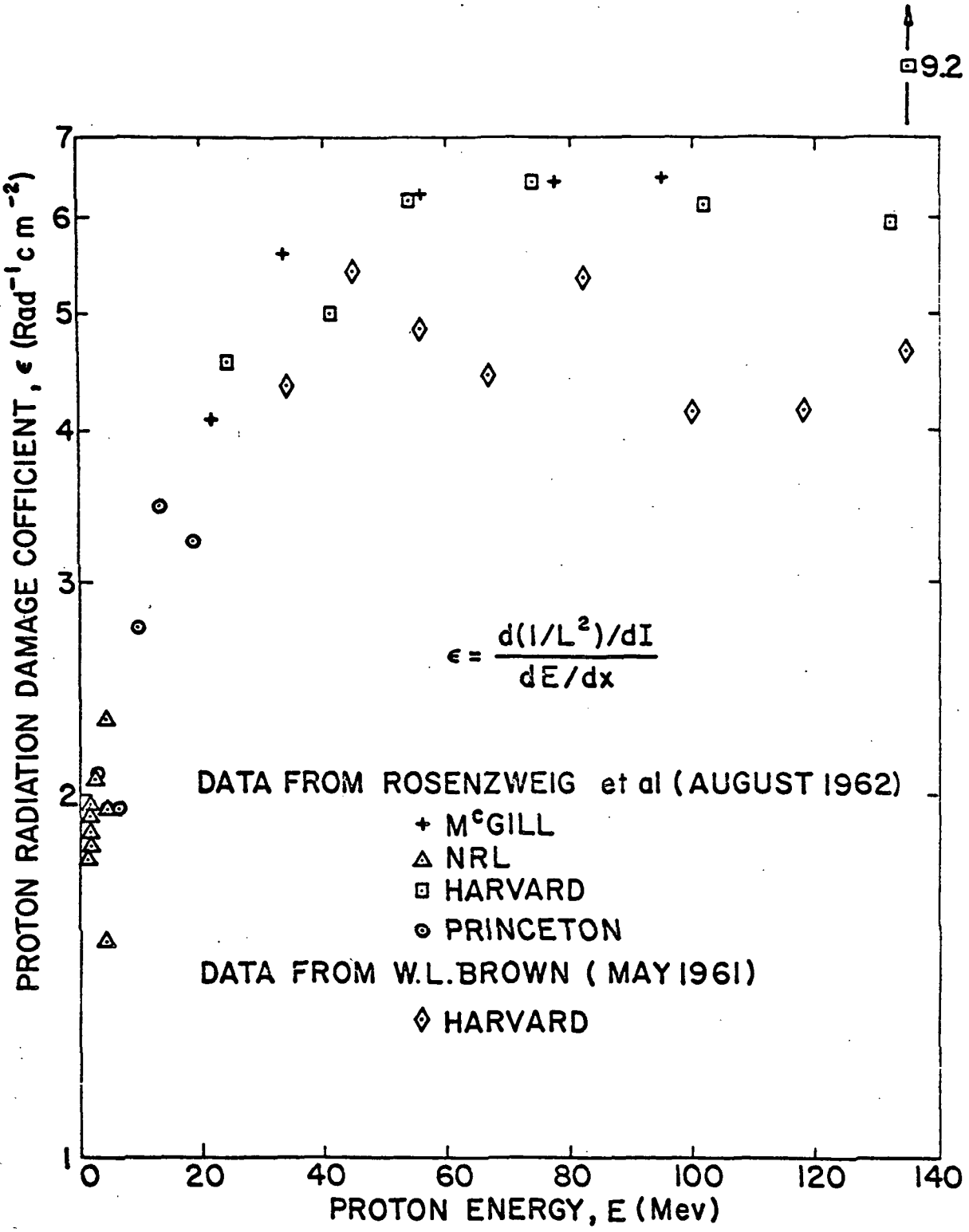

Figure 4. Proton Radiation Damage Coefficient for Solar Cells vs. Proton Energy.

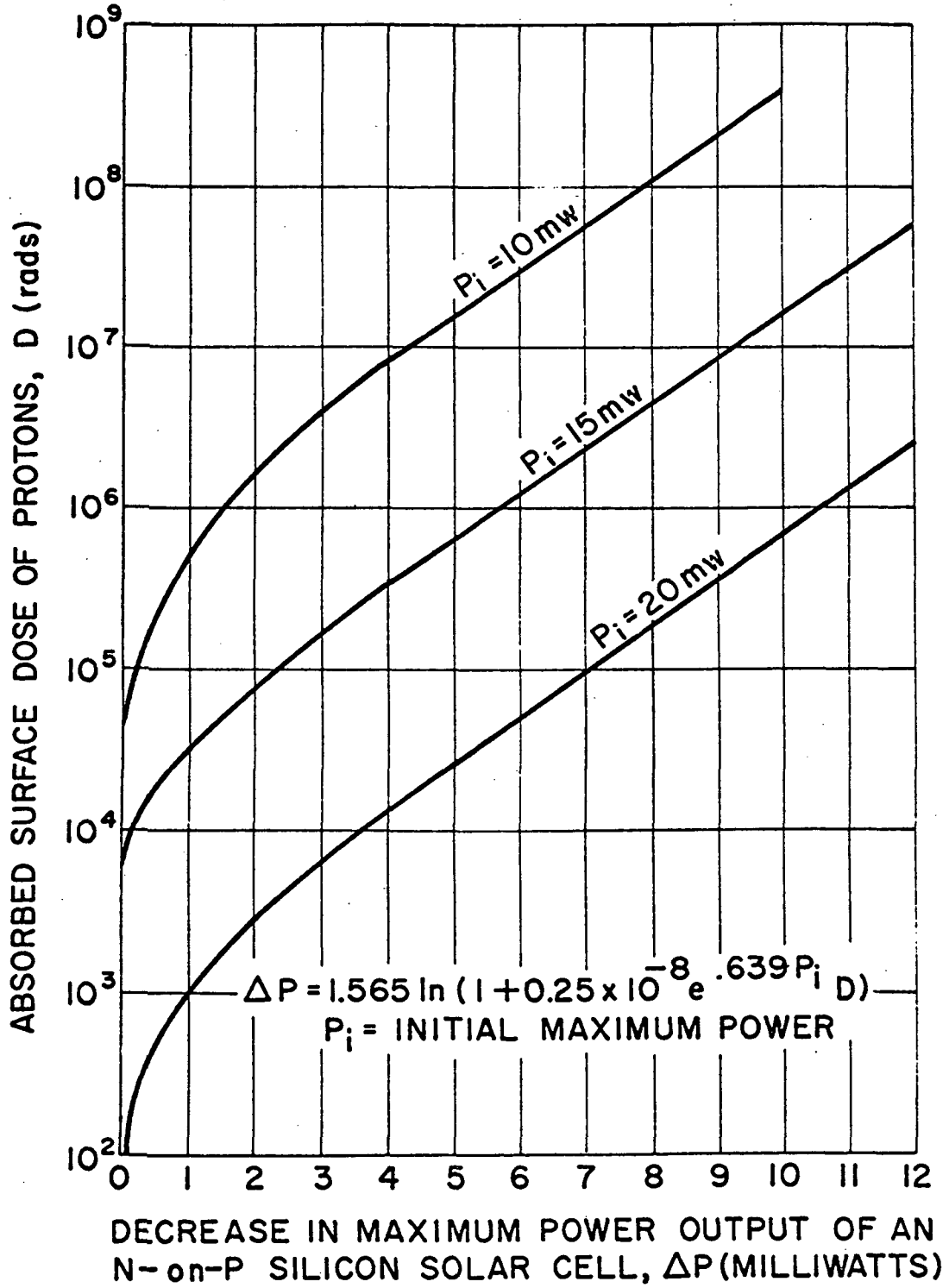

Figure 5. Decrease in Maximum Power Output of an n-on-p Silicon Solar Cell vs. Absorbed Dose of Protons at the Silicon Surface Layer Behind a Protective Cover Glass with the Initial Value of the Maximum Power Output as a Parameter.

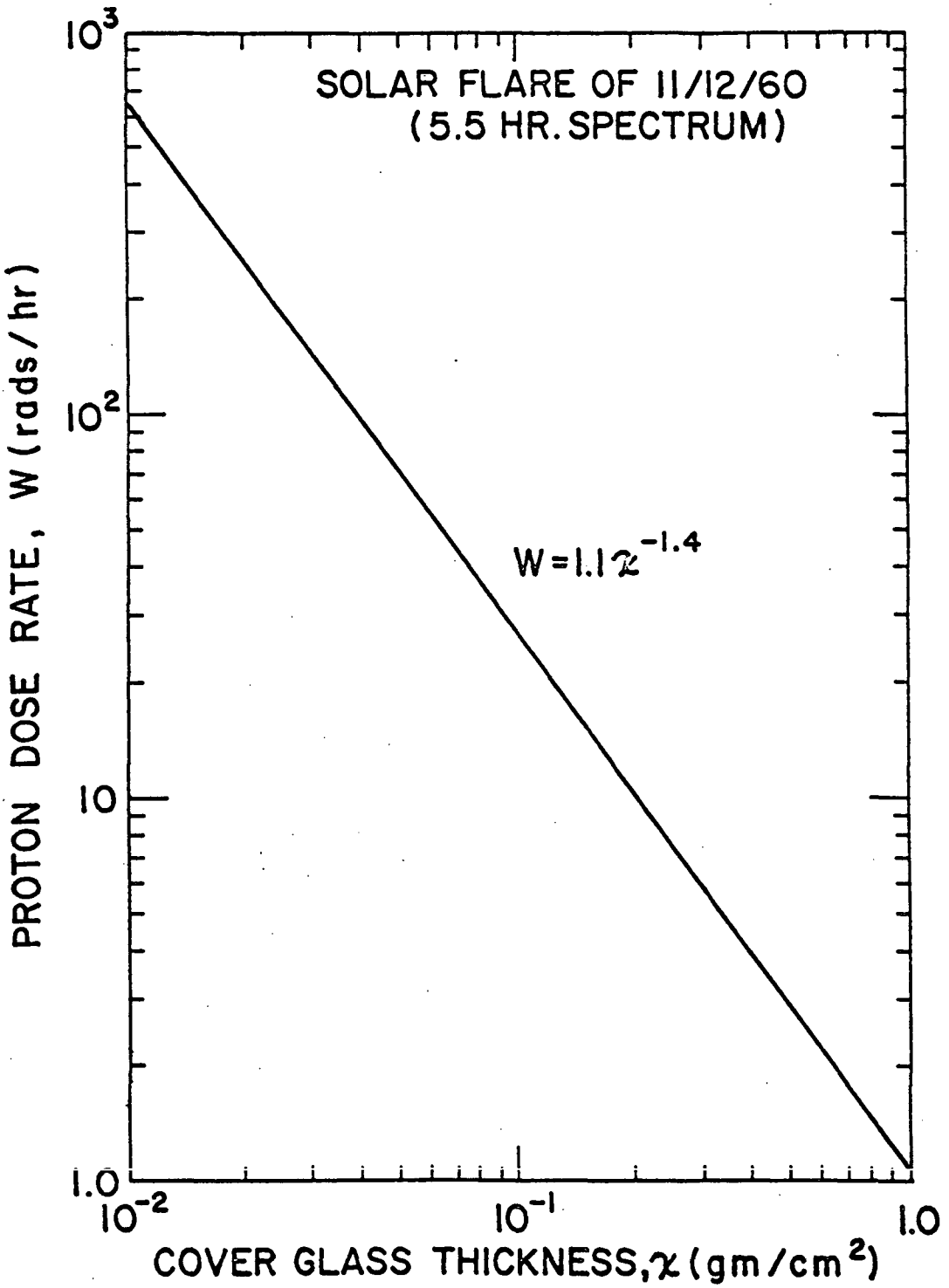

Figure 6. Proton Dose Rate (in rads/hour) from the 5.5 Hour Spectrum of the Solar Flare of 12 November 1960 vs. Thickness (in gm/cm^2) of Protective Cover Glass.

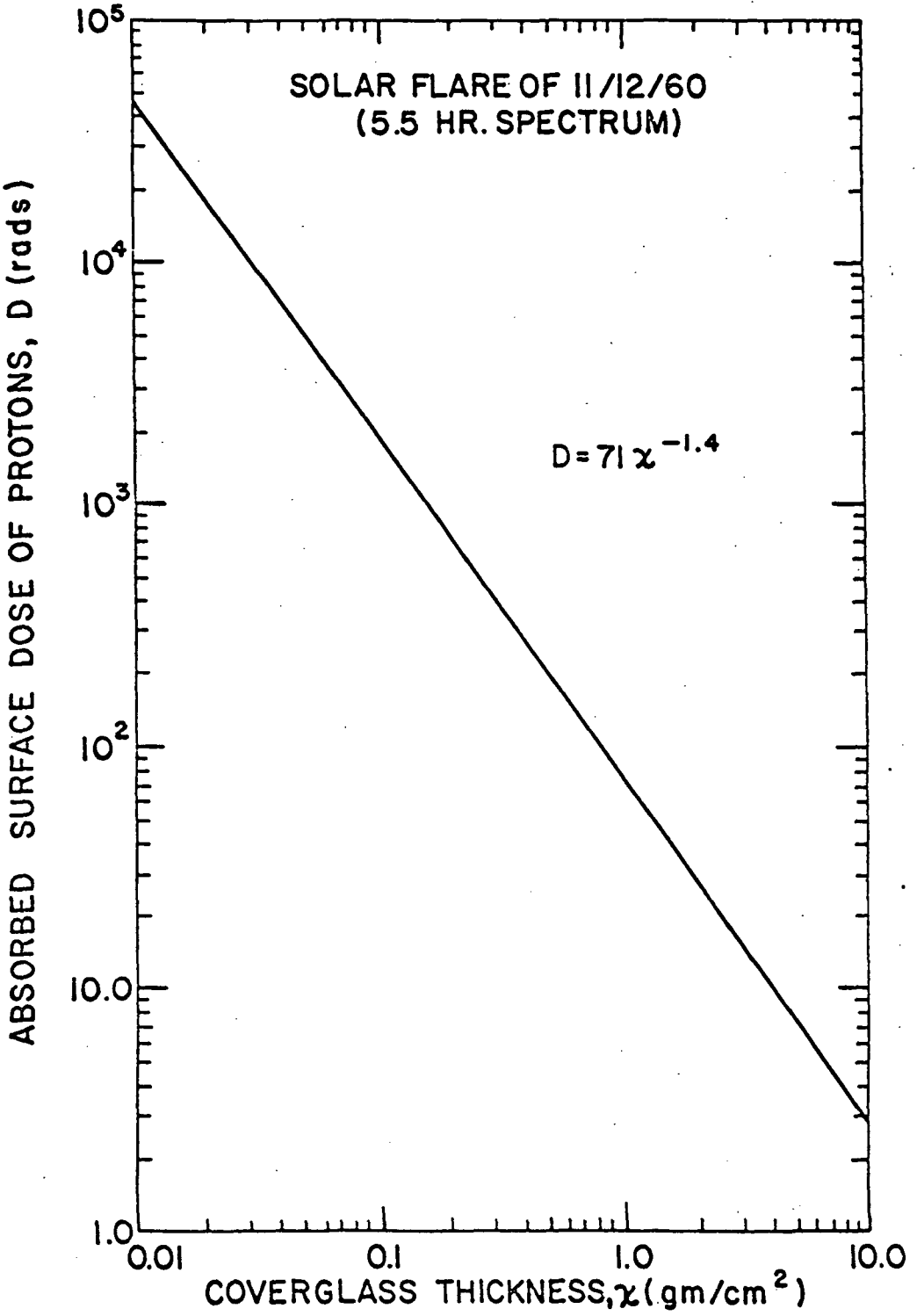

Figure 7. Surface Dose of Protons Absorbed From the Solar Flare of 12 November 1960 vs. Thickness of Protective Cover Glass.

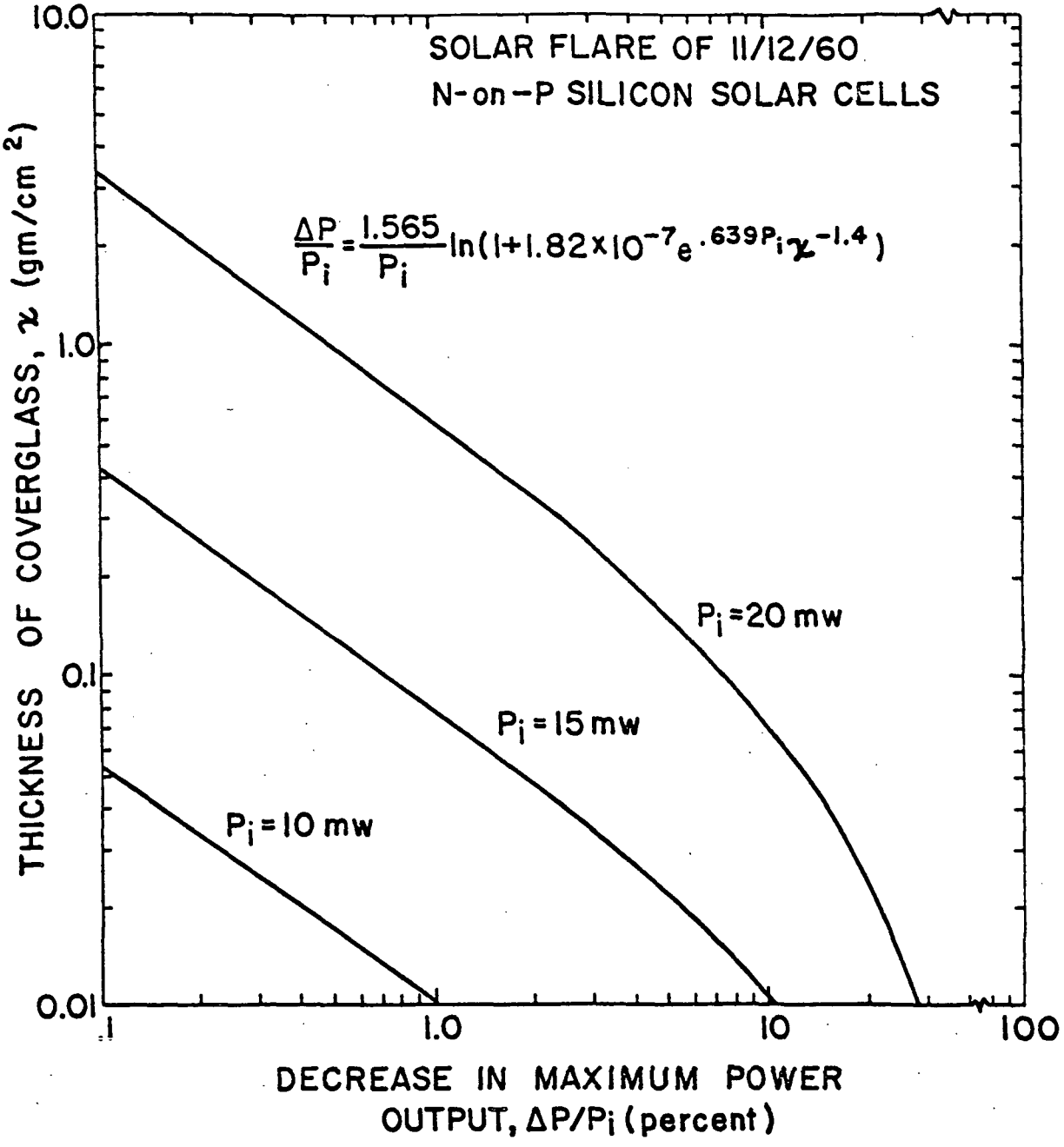

Figure 8. Decrease in Maximum Power Output vs. Thickness in gm/cm^2 of Protective Cover Glass for the Solar Flare of 12 November 1960, With the Initial Value of the Maximum Power Output as a Parameter.

Paper B-7

EFFECT OF ELECTRON IRRADIATION ON THE MECHANICAL PROPERTIES OF A COMPOSITE FOIL FOR INFLATABLE SATELLITES

Thomas G. James*
NASA Langley Research Center

Abstract

The primary effect of electron irradiation on the Echo II skin material is an increased brittleness which leads to an early and brittle failure in both the burst strength and ultimate strength tests. Severe surface damage, which occurs at doses on the order of 10^{17} e/cm^2, causes mechanical damage to the aluminum foil portion of the skin and may lead to changes in the temperature control characteristics of the surface.

Introduction

Some months after the 100-foot-diameter Echo I balloon was put into orbit, it became apparent from both optical and radar observations that the balloon was no longer a smooth sphere. Presumably the inflation gases had leaked out by this time leaving the balloon somewhat wrinkled because the 1/2-mil aluminized mylar of which it was made had no inherent stiffness. The next passive communication satellite, the 135-foot-diameter Echo II balloon, will have a much stiffer skin so that it is hoped the balloon will remain smooth and spherical after the initial inflation pressure is lost. The Echo II skin is made of 0.35-mil-thick mylar with 0.2-mil-thick aluminum glued on either side. Both outer aluminum surfaces are given an alodine coating for temperature-control purposes. (See fig. 1.)

This satellite and subsequent similar satellites will have to remain for many years in the space environment, which in this case includes the magnetically trapped radiation, both the natural Van Allen belt and the new artificial electron belt. As a result of the high-altitude nuclear explosion of July 9, 1962, Echo II, which will orbit at an altitude of about 1,000 km, will be exposed to a flux of between 10^8 and 10^9 e/cm^2/sec. The study presented herein was made in order to determine the extent to which the electron radiation part of this environment will damage the Echo II type composite foil in the course of many years in orbit. Samples of the Echo II foil were irradiated with electrons of energies up to 1.2 Mev, with total doses representing those incurred during many years in orbit.

---

*Aerospace Technologist.

Symbols

e	electron
E	modulus of elasticity, used herein as the secant modulus at 1-percent elongation, $lb/in.^2$
Kev	thousand electron volts
Mev	million electron volts
S_{ULT}	ultimate tensile stress
μa	microamperes

Tests And Equipment

Test Setup

The accelerator used in these tests was a constant-voltage cascaded-rectifier type - a Radiation Dynamics Model No. PEA-1.0 Dynamitron. This accelerator is capable of producing fluxes of electrons with intensities as great as 10 milliamperes and with kinetic energies varying from 50 Kev to 1.20 Mev. The experimental test setup is shown in figure 2. The beam enters from the accelerator at the left-hand side and passes down the beam tube through a scanning magnet which scans it vertically in the scan horn at approximately 10 cycles per second. The beam then passes into the air through a blower-cooled, 2-mil-thick titanium window. The foil sample is suspended in the beam at a distance of approximately 6 inches from the titanium window. The clamps that hold the foil are mounted approximately $1\frac{1}{2}$ inches in front of a solid aluminum support plate. The current density was measured by means of a 1- by 2-cm aluminum plate mounted on, and insulated from, the foil itself. The current captured by this small plate was measured by passing it to ground through an electrometer. The current captured by the support plate was also passed to ground through an electrometer in order to monitor the total output of the accelerator. The foil itself was grounded in order to avoid any charge-buildup effects. The kinetic energy of the electrons at the location of the foil was determined by measuring the extreme range of electrons in aluminum at this location. The uniformity of the beam intensity was determined through the use of cobalt glass dosimetry. An area of approximately 2 by 15 inches was found to be uniform to within ±5 percent.

Mechanical Tests.- All data were obtained by means of post-irradiation tests. Six mechanical properties were studied. From the stress-strain curves measured on a Thwing-Albert Model 30LT tensile tester, the modulus of elasticity, ultimate strength, and percent elongation were determined. A standard Mullen tester was used to determine the burst strength of the skin. A Sheffield Micro-Hardness tester was used to measure the Vickers hardness of the surface of the foil. Several 1/3 cm^2 pieces of foil were weighed on a Cahn Electrobalance to determine the weight per square centimeter.

Results And Discussion

Effect of Dose Rate

Since the dose rate in these tests is necessarily higher than that in space, the initial portion of this investigation was a study of possible dose rate effects on the foils. A portion of the results of this study can be seen in figure 3. Each of the samples was given the same total dose of 3.156×10^{16} e/cm^2. This total dose, at 10^8 $e/cm^2/sec$, represents about 10 years in orbit; at 10^9 $e/cm^2/sec$, the corresponding time would be 1 year. In all cases the energy used was 1.20 Mev.

Figure 3 shows the percent change in these mechanical properties as a function of the dose rate in microamperes per square centimeter. It is apparent that dose rate has no significant effect for dose rates less than 1.12 $\mu a/cm^2$. There are, however, significant effects of dose rates much above 1.12 $\mu a/cm^2$. A dose rate of 1.12 $\mu a/cm^2$ is two or three orders of magnitude greater than the maximum dose rates in space. In general, it is seen that the damage is less for the higher dose rates. The lessened damage at high dose rates may be a result of severe heating at these dose rates; however, previously published work[1] indicates a similar trend with respect to the electrical properties of mylar. Since no significant dose rate effects are observed at a dose rate of 1.12 $\mu a/cm^2$, this value was selected for use in all subsequent tests.

Effect of Total Dose

The most significant data from the viewpoint of lifetime in the space environment is that showing the effect of total dose. Figure 4 shows the effects of total dose on the mechanical properties for an

1. The Effect of Nuclear Radiation on Elastomeric and Plastic Materials. Radiation Effects Information Center (Battelle Memorial Institute), Report No. 3, First Addendum, May 31, 1959, p. 27.

energy of 1.2 Mev. The doses shown here, at a flux level of 10^8 e/cm^2/sec, correspond to times in orbit ranging from 6 months to 50 years; at 10^9 e/cm^2/sec, the corresponding times are 18 days to 5 years. The most notable effect is a rapid degradation of the percent elongation, which is reduced by about 25 percent even at the lowest dose. This is reflected at somewhat higher doses in the early and brittle failure of both the burst strength and ultimate strength tests. The modulus of elasticity, hardness, and cot/cm^2 are essentially unchanged at least to such doses as it was possible to measure these quantities.

It will be observed that the last two points are missing for both the modulus of elasticity and hardness. The modulus of elasticity as used throughout this paper is the secant modulus at 1-percent elongation. For the two highest doses the percent elongation was less than 1 percent and, consequently, the modulus could not be measured. The degree of surface damage at these doses was such that a clean indentation could not be obtained with the microhardness tester. These surface effects will be discussed more fully in a later part of this paper.

The fact that these properties fall into two groups, one of which shows major changes and the other essentially none, is of interest since it indicates which portion of the foil has sustained the major portion of damage. It is to be noted that, in the tests of the unirradiated and lightly irradiated foils the aluminum fails long before the mylar in both the burst and tensile tests. Thus, except perhaps for the highest doses, these properties indicate almost solely the condition of the mylar. At the highest doses, there must be some damage to the aluminum, since the aluminum by itself should be able to carry about 15 percent of the initial ultimate tensile strength, whereas at the highest doses, the irradiated specimen retained only 5 percent of its tensile strength. The additional loss, however, is probably not a direct radiation effect. This point will be discussed later in this paper. On the other hand, the modulus of elasticity, which is measured in the initial portion of the stress-strain curve, and hardness, which is measured by indenting the aluminum surface, are primarily indicative of the condition of the aluminum. It will further be noticed that the aluminum surface protects the mylar from either weight loss due to outgassing or weight gain from oxidation reactions. Thus this property is primarily an indication of the integrity of the aluminum foil rather than of the mylar substrate. The conclusion, therefore, is that the mylar has sustained essentially all of the radiation damage and that the aluminum was essentially unaffected by radiation.

Surface Effects

A notable feature of the tests involving very high doses is the severe damage to the surface. A photograph of the surface after a dose

of 1.578×10^{17} e/cm^2 is shown in figure 5. This photograph is typical of the test results at all energies. The surface is seen to be markedly distorted and bubbled as a result of the internal pressure resulting from outgassing of the material in the foil. This is a radiation effect rather than a heating effect, since heating in an oven for several days at similar temperatures does not produce the same effect.

No proof has been obtained as yet as to whether the gas originated in the glue, the mylar, or both. The initial suspicion, however, points to the glue as a major factor since many of the bubbles are sharply defined on one side of the foil but only more softly defined on the other side. This asymmetry would indicate that the bubbles are not within the mylar but are rather at the interface between the mylar and the aluminum. Further tests are planned of samples prepared by vapor depositing the aluminum on the mylar without any glue as well as of samples with two sheets of aluminum foil glued together without the intermediate mylar. A comparison of the results of these tests with the present results should indicate the extent to which each portion of the foil is responsible for the outgassing.

The temperature of the balloon is determined by the optical characteristics of its surface. Thus, any change in the ratio of absorptance to emittance of the surface will affect the equilibrium temperature and could be more dangerous than the mechanical damage previously shown. The surface change shown here will doubtless produce some changes in the absorptance and the emittance. Tests are now in progress to determine the extent of these changes.

As was mentioned previously, there is some damage to the ultimate strength of the aluminum foil itself. The effect is somewhat unexpected since radiation doses of this type and magnitude do not generally affect metals. It would appear that the mechanical damage due to outgassing, rather than irradiation itself, is probably responsible for the damage to the aluminum.

Effect of Kinetic Energy

So far all of the results given herein have been for electron energies of 1.2 Mev. The electrons in space, however, encompass a broad spectrum of energies ranging from almost zero to several Mev. It is necessary to investigate all energies in this spectrum in order to obtain a reasonable picture of the effect of the space environment. Figure 6 shows the effect of kinetic energy on the results for a fixed total dose. In this case all of the samples were given the same total dose of approximately 6.31×10^{15} e/cm^2. At a dose rate of 10^8 e/cm^2/sec this total dose represents 2 years in orbit; and at 10^9 e/cm^2/sec, a little over 2 months. It will be observed that, for those properties which are affected, the degree of damage increases as the energy

decreases, except for the very lowest energy, where the electrons do not completely penetrate the foil. In studying the energy spectrum in space it is apparent that there are many more electrons with energies below 1.2 Mev than above 1.2 Mev. Thus, in assessing the damage to the material in space, it may be concluded that the increased damage potential of the lower energy electrons will probably lead to somewhat more severe damage than that demonstrated at 1.2 Mev in figure 4.

The increase in damage with lower energies is a reasonable result. It is observed that the foil is very thin so that at all energies except the lowest the electrons pass completely through the foil and thus have essentially a constant path length. In traversing this constant path the lower energy electrons, with their higher rate of linear energy transfer, deposit more energy in the foil and consequently do more damage.

Concluding Remarks

The results of this study on the effects of electron radiation on the mechanical properties of the Echo II material indicated that:

1. The primary effect of electron irradiation is an increased brittleness of the foil, resulting at higher doses in the early and brittle failure of the foil in tensile-strength and burst-strength tests.

2. Severe surface damage occurs at the highest doses used in this study. This damage results in mechanical damage to the aluminum foil.

3. The damage due to electron irradiation increases as the energy of the electrons decreases, at least until the point when electrons no longer completely penetrate the foil.

4. Dose rate effects in the material are negligible until rates at least two or three orders of magnitude higher than those in space are used.

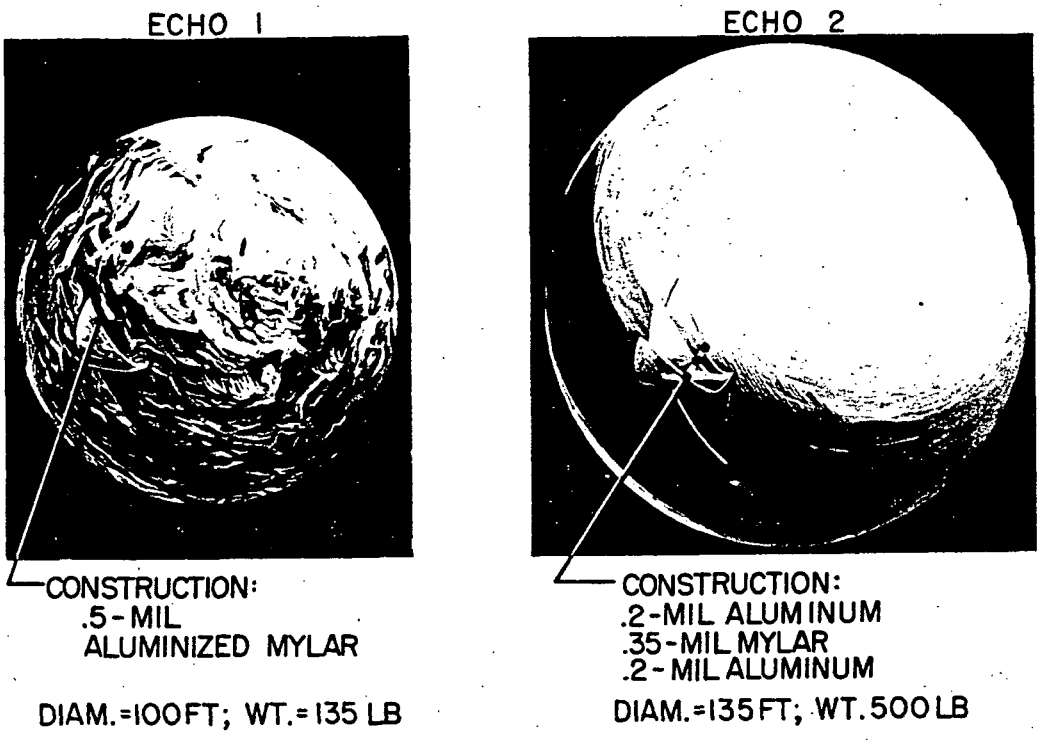

NASA
L-62-8554

Figure 1.- Construction of echo satellites.

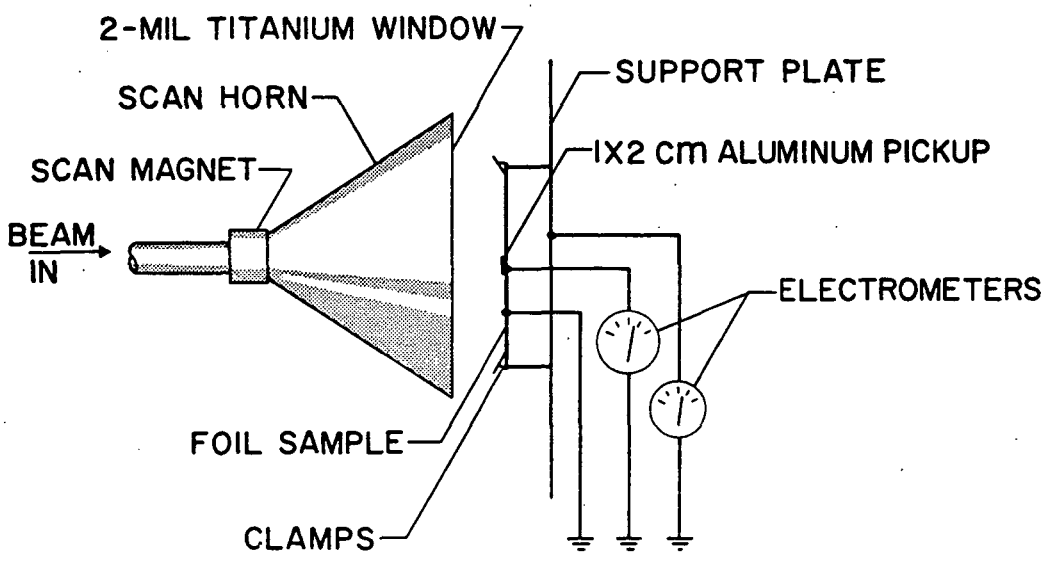

NASA

Figure 2.- Experimental arrangement.

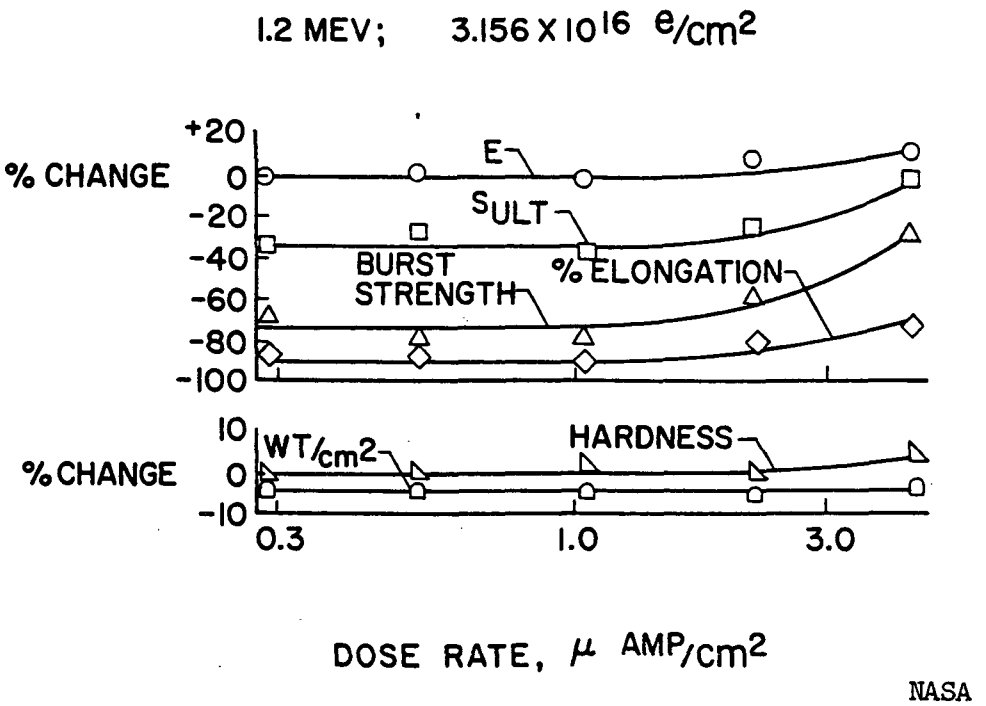

NASA

Figure 3.- Effect of dose rate.

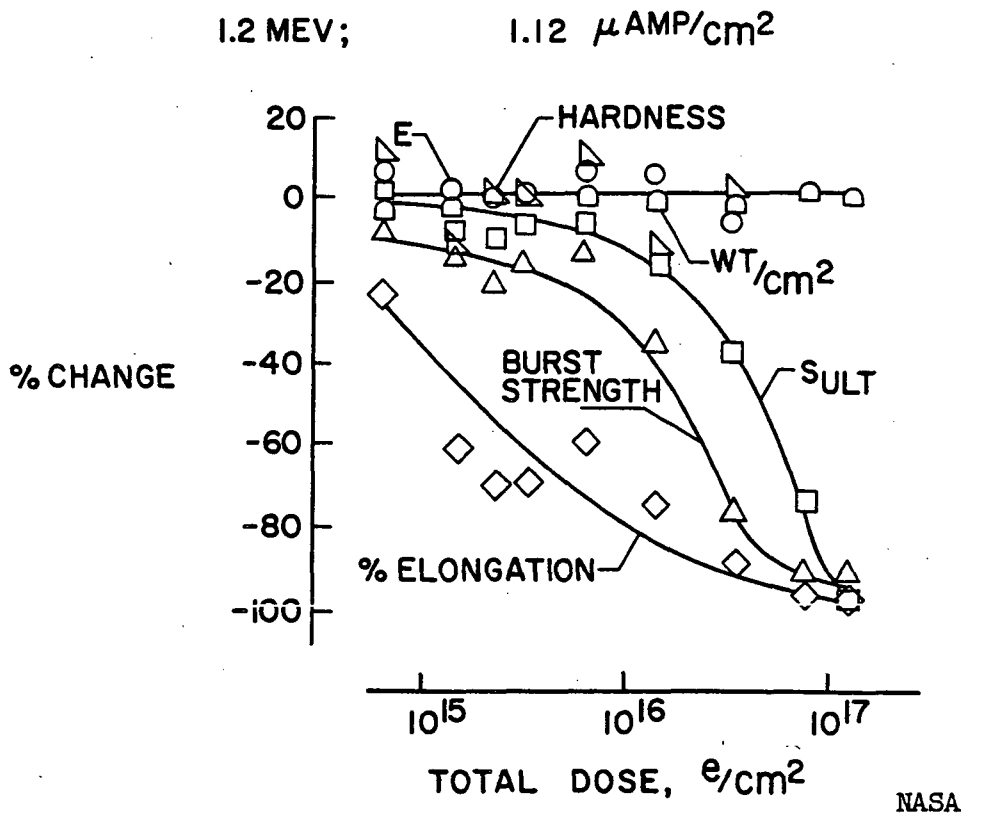

NASA

Figure 4.- Effect of total dose.

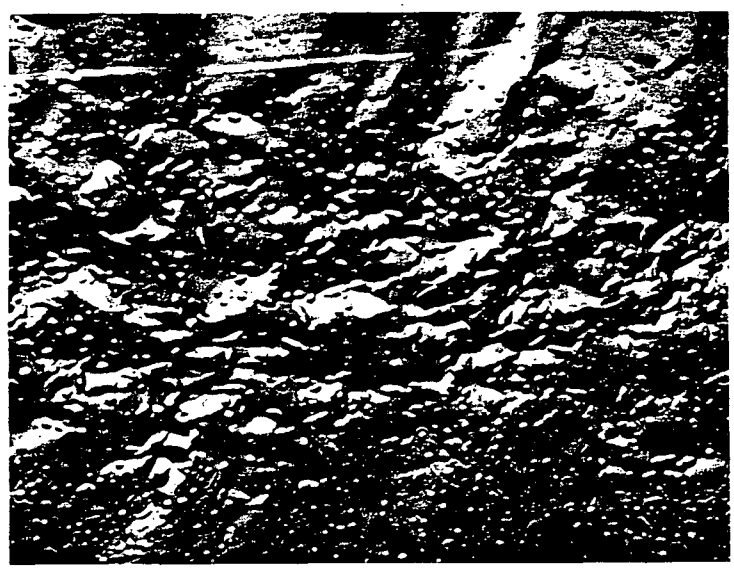

NASA

Figure 5.- Surface after 1.578×10^{17} e/cm^2.

6.31×10^{15} e/cm^2 1.12 μa/cm^2

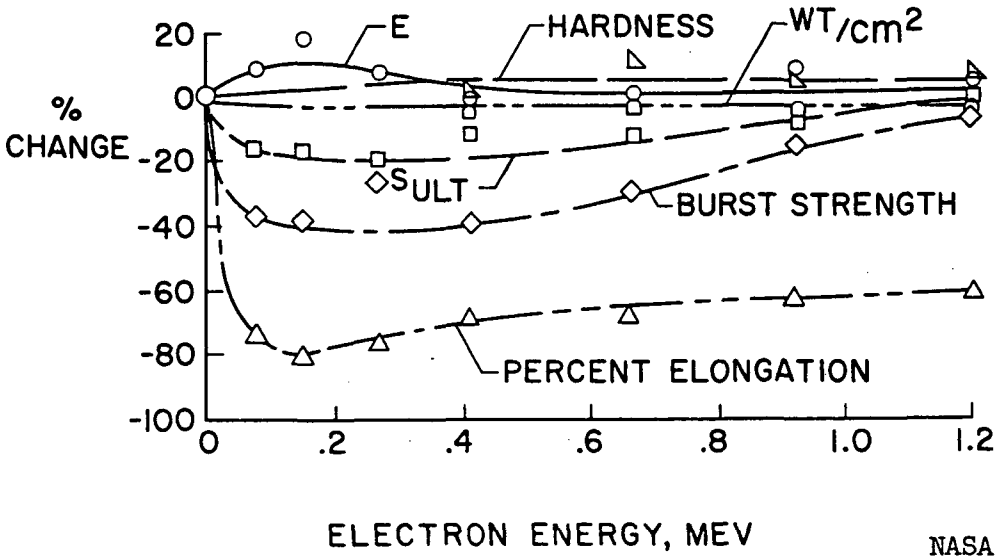

NASA

Figure 6.- Effect of electron energy.

Paper C-1

ACUTE EFFECTS OF RADIATION EXPOSURE IN MAN

J.J.Nickson,M.D.
Memorial Hospital & Sloan Kettering Institute
New York City,N.Y.

Abstract

The data to be discussed today will be derived primarily from observations in man. For the most part, the events to be described will take place less than three months after the onset of the exposure. The data arises from three sorts of observation; first, those on patients who receive total body radiation in an attempt to ameliorate some ailment; second, accounts of nuclear accidents involving reactors; and third, the consequences of exposure to the events after the use or testing of nuclear weapons.

Historically, total body radiation as a medical tool was first suggested in 1907. Its use, however, may be said to have begun in 1923, and it has been used intermittently since. Medically, however, use of total body radiation may be divided into two broad components; first, when its use derives from the intent to modify a disease process itself; second, when it is used in an attempt to suppress immune mechanisms sometimes also associated with an attempt to suppress a disease process.

An acute syndrome may be divided into events associated with effects upon the function of the marrow, upon the epithelium or the gastrointestinal tract, upon the skin, and upon the central nervous system. The number of observations relating to biochemcial alterations is increasing.

These changes will be described and discussed. Major emphasis will be given to those abnormalities from which recovery may occur.

Finally, an attempt will be made to relate dose time considerations to the kinds of effects seen.

Introduction

This is clearly a large and diffuse subject. Since it is my impression that our major interest today relates to the effects noted after either total body exposure or after exposure of substantial segments of the body, information about the after-effects of radiation will be limited to those after exposure. The term "acute" is defined as those effects occurring within 30 days. It is recognized that the definition is somewhat arbitrary, but again, in the time allotted some narrowing of the area under discussion must be accepted.

Areas of Information

The information with regard to humans comes from three broad categories: patients; occupational exposure; and military usage. Data has been derived from deliberate exposure of patients, usually those suffering with malignant disease, to whom total body irradiation was given as a means of attempting to modify favorably the course of the disease. Information of this sort begins to appear in the literature in the 1920's and perhaps 50 papers have been written on the consequences of exposure of such patients. Except for the few papers since the last war, exposure was to low doses, or to low dose-time levels, and to x-rays of quite low energies, from 180 to 250 Kvp. As a consequence, the distribution of energy within the patient is inhomogenous. In the absence of detailed dosimetry, the total energy deposited varies considerably and is subject to uncertainty when one attempts to think about it today.

A second category is that following irradiation of patients to high dose levels, several hundred of roentgens in a single exposure. The radiation is given with two objectives in mind: first, to suppress the activity of the neoplastic cells, and second, to modify the immune response of the patient by suppression of the hematopoetic system, with subsequent bone marrow grafting to support life. A third category, with relatively few representatives as yet, consists of patients with non-neoplastic disease who are given radiation with the sole objective of suppressing the immune mechanism, to be followed by an organ transplant.

In general, patient exposure has been to photons only. Dosimetry, as noted above, is subject to some uncertainty. The data has the merit that the time of exposure is known with certainty. Further, in most cases and certainly in almost all recent cases, base-line laboratory values have been determined.

Occupational exposure of sufficient magnitude to be relevant here commonly has followed accidents with nuclear reactors. Wald and Thoma [1] have summarized these data. Here, the exposure to ionizing radiation is commonly a mixed one. The exact values are subject to several kinds of uncertainty. First, the absolute amount of energy absorbed is open to question. Second, the knowledge of the mixture of particulate and electromagnetic radiation is uncertain. Third, the estimation of dosage depends, at least in some of the incidents, upon assumption as to the relative biological effectiveness of the various components. Naturally, these studies commonly are not preceded by detailed baseline observations of hematologic or bio-chemical values. The individuals involved are normally healthy, or at least capable of performing a day's work

Finally, there is some information from military usage of nuclear weapons either in combat or in testing situations. Information exists from Hiroshima and Nagasaki incidents, from the exposure of the polynesians, and from the Japanese on the Fortunate Dragon. Such information is derived from more or less random selection of the available population. No baseline studies exist. The interpretation of data may be further clouded by the presence of other kinds of trauma, frequently of sufficient magnitude by itself to cause severe illness or death of the individual.

Description of Syndrome

Three modes of death following exposure to ionizing radiation have been identified in the laboratory mammal and in man.

The first mode involves or appears to result from damage of the central nervous system and is called the "CNS" pattern, on which Dr. Langham [2] and his group have worked extensively. This occurs in mammals at dose levels of the order of tens of thousands of roentgens. In laboratory mammals, death occurs in a few hours. Convulsions are a permanent feature and are associated with profound electrolyte and fluid balance abnormalities. It seems reasonable to assume that some of the exposures at Nagasaki and Hiroshima were sufficient to induce this pattern of death. Death would have occurred before hospitalization

---

[1] N.Wald and G.E. Thoma,Jr.,Radiation Accidents: Medical Aspects of Neutron and Gamma-Ray Exposures, ORNL-2748,AEC,Oak Ridge National Laboratory, Oak Ridge Tenn.,2/21/61,pp.1-177.

[2] W.Langham,K.T.Woodward,S.M.Rothermel, P.S.Harris, C.C.Lushbaugh, and J.B.Storer, Studies of the Effect of Rapidly Delivered, Massive Doses of Gamma-Rays on Mammals, Rad.Res. 5,404,(1956).

IN MOST CASES IF NOT ALL INSTANCES. ONE LABORATORY ACCIDENT WAS FOLLOWED BY A PATTERN OF DEATH OF THIS SORT. DOSAGE ESTIMATIONS FOR THE UPPER HALF OF THE BODY WERE OF THE RIGHT ORDER.

THE SECOND OR GASTROINTESTINAL PATTERN OF DEATH OCCURS IN LARGE MAMMALS WITH DOSES OF THE ORDER OF A FEW THOUSAND ROENTGENS (1500+ R). HERE, DEATH INTERVENES AS A RESULT OF ELECTROLYTE AND FLUID LOSSES DUE TO DENUDATION OF THE GASTROINTESTINAL TRACT EPITHELIUM. DEATH USUALLY OCCURS BETWEEN FIVE TO EIGHT DAYS.

THE THIRD AND THE COMMONLY OBSERVED PATTERN OF DEATH IS A CONSEQUENCE OF INJURY TO THE HEMATOPOETIC SYSTEM. THE USUALLY GIVEN LD-50 ESTIMATES FOR MAN RELATE TO THIS PATTERN OF DEATH. AN ACCURATE LD-50/30 DAY FOR MAN IS NOT KNOWN. VALUES FOR LABORATORY PRIMATES ARE IN THE RANGE OF 450 TO 550 R. THE LD-50/30 DAY DOSE GUESSES FOR MAN USUALLY CENTER AROUND 500 R. IN EXAMINING THE EVIDENCE PREPARING FOR THE DISCUSSION TODAY, AND GIVING CONSIDERABLE WEIGHT TO RECENT STUDIES IN PATIENTS RECEIVING ABOUT 400 RADS WITH AND WITHOUT BONE MARROW GRAFT, AND ALSO TO SOME INDIRECT EVIDENCE, I HAVE COME TO FEEL THAT THE LD-50/30 DAY FOR MAN MAY WELL BY HIGHER THAN ≈500 R, AND MAY BE IN THE RANGE OF 650 TO 700 R.

THE CONSEQUENCE OF EXPOSURE TO DOSES OF APPROXIMATELY 500 R MAY BE SUMMARIZED AS FOLLOWS:

NAUSEA AND VOMITING, USUALLY OF SHORT DURATION, BEGINNING MINUTES OR HOURS AFTER EXPOSURE AND LASTING ABOUT 24 HOURS. FOLLOWING THIS, THE PATIENT MAY FEEL WEAK AND LETHARGIC, BUT HAS NOT SPECIFIC SYMPTOMS OR SIGNS UNTIL ABOUT THE FOURTH DAY WHEN DIARRHEA COMMONLY APPEARS. DIARRHEA MAY PERSIST FOR THREE OR FOUR DAYS AND MAY BE ASSOCIATED WITH ANOREXIA, WEIGHT LOSS, AND SIGNS OF DEHYDRATION, IF SEVERE.

FEVER RESULTING FROM INFECTION MAY DEVELOP BY THE NINTH DAY. COMMONLY, THIS IS THE RESULT OF INVASION OF THE LYMPHATIC SYSTEM AND BLOOD STREAM BY ORGANISMS NORMALLY RESIDING WITHIN THE LUMEN OF THE GASTROINTESTINAL TRACT. INFECTION DEVELOPS BECAUSE OF THE POST RADIATION SUPPRESSION OF THE IMMUNE SYSTEM, THE DECREASE OF THE WBC, AND BECAUSE OF THE LOSS OF THE EPITHELIAL BARRIER NORMALLY PRESENT.

AROUND THE TWELFTH TO FOURTEENTH DAY, IF INFECTION HAS NOT BEEN A FATAL COMPLICATION, EVIDENCES OF DISTURBANCES IN THE BLOOD'S ABILITY TO CLOT MAY APPEAR AS EVIDENCED BY PETECHIAE IN THE SKIN, NOSEBLEEDS, BLEEDING OF GUNS, AND BLOOD IN STOOL. IF BLOOD LOSS ALONE OR IN COMBINATION WITH INFECTIOUS COMPLICATIONS IS SUFFICIENT

DEATH MAY OCCUR DURING THE THIRD WEEK AFTER RADIATION. PATIENTS WHO SURVIVE THIS PERIOD USUALLY RECOVER SLOWLY, THE PERIOD OF RECOVERY LASTING SEVERAL MONTHS.

SUBLETHAL DOSAGES

PERHAPS THE BEST AND MOST ORDERLY STUDY RELATING TO THE CONSEQUENCES OF LOWER DOSES IS THAT REPORTED BY MILLER AND FLETCHER [3] IN 1961. IN THIS REPORT THE PERIODS OF OBSERVATION WERE LIMITED USUALLY TO 14 DAYS AND INVOLVED IN ALL 263 PATIENTS. THIRTY PATIENTS RECEIVED 200 R. NAUSEA AND VOMITING OCCURRED IN 17 OF THE 30 PATIENTS AND WAS SEVERE AND PERSISTENT IN ONE PATIENT ONLY. THE TYPICAL EPISODE OCCURRED ABOUT TWO HOURS AFTER IRRADIATION WAS COMPLETED. NAUSEA WAS NOTED FOR 10 TO 15 MINUTES, FOLLOWED BY VOMITING OF BRIEF DURATION. THEREAFTER THE PATIENT FELT NO FURTHER NAUSEA, AND NO MORE VOMITING OCCURRED. THE MAJORITY OF THESE PATIENTS CONTINUED THEIR NORMAL ACTIVITIES; IN A FEW INSTANCES THIS INCLUDED MANUAL LABOR.

SEVENTEEN PATIENTS RECEIVED DOSES RANGING FROM 125 TO 200 R; SEVEN OF THESE SHOWED NAUSEA AND VOMITING. EIGHTEEN PATIENTS RECEIVED 100 R; NONE SHOWED NAUSEA AND VOMITING. NONE OF THE PATIENTS RECEIVING DOSES LESS THAN 100 R SHOWED NAUSEA AND VOMITING. NONE SHOWED ANY OF THE EVIDENCES OF INFECTION OR OF HEMORRHAGIC DIFFICULTIES NOTED ABOVE.

WEAKNESS AND LETHARGY WAS NOTED IN ONLY THREE PATIENTS, ALL WERE FROM THE GROUP EXPOSED TO 200 R.

OUR EXPERIENCE WITH ABOUT 50 PATIENTS IS CONSISTENT WITH THE MILLER AND FLETCHER DATA. NAUSEA AND VOMITING HAS BEEN SEVERE IN ONLY ONE OF OUR PATIENTS; THIS WAS A PATIENT OF A VERY NERVOUS TEMPERAMENT, AND IT IS OUR BELIEF THAT THE NAUSEA AND VOMITING, WHILE IT MAY HAVE BEEN INDUCED BY THE 175 R GIVEN HER, WAS ALMOST CERTAINLY INTENSIFIED BY HER APPREHENSIONS.

HEMATOLOGIC DATA HAS BEEN OVERWHELMINGLY THE LABORATORY INDEX OF RADIATION DAMAGE TO DATE. AGAIN REFERRING TO MILLER'S AND FLETCHER'S DATA IN THE 200 R GROUP, THE WBC HAD DROPPED TO A LEVEL WITH A SIGNIFICANCE OF 0.01 BY THE SEVENTH POST-TREATMENT DAY. RED BLOOD CELL AND HEMAOGLOBIN VALUES SHOWED NO SIGNFICIANT CHANGES DURING THE PERIOD OF OBSERVATION. IN VIEW OF OUR OWN STUDIES, WHICH WILL BE COMMENTED UPON LATER, THIS IS NOT SURPRISING. LITTLE CHANGE IN THE PLATELET COUNTS WAS SEEN IN THE FIRST TEN DAYS AFTER TOTAL BODY TREATMENT.

FOR THE FOUR PATIENTS FOLLOWED LONGER THAN TEN DAYS THE PLATELET COUNTS REACHED A MINIMUM AT SEVEN WEEKS, FIVE WEEKS, FOUR WEEKS AND THREE WEEKS.

---

[3] L.S.MILLER AND G.H.FLETCHER AND H.B.GERSTNER, RADIOLOGICAL OBSERVATIONS ON CANCER PATIENTS TREATED WITH WHOLE-BODY X-IRRADIATION, RAD.RES. 8,150,(1961).

Doses of 125 to 175 r were followed by a depression in the white count with a significance of 0.01 on the seventh day. For the lymphocyte count there was a depression significance at the same level on the fourth day. The 100 r doses were followed by a fall in the lymphocyte count significant by the second day, but no significant effects was noted on the total white blood cell count. The authors concluded that doses of 100 r could be detected by the drop in the lymphocyte count; but doses below that level could not be so detected.

In our series of 11 patients, without disease of the blood forming organs, who received doses in excess of 120 r, the mean time of 50 per cent of the pre-irradiation white count was 24 days. The mean time to ten to 15 per cent of the pre-irradiation value was 31 days. Abnormal bleeding as a clinical problem is not commented upon in Dr. Fletcher's and Dr. Miller's paper. In our series abnormal bleeding occurred in several patients during the fourth week after exposure, but was a serious clinical problem in one patient only. Maximal depression of the platelet count after 100 to 175 r occurs at 20 to 30 days.

Summary and Conclusion

Radiation in sufficiently large amounts can without question produce signs and symptoms in man, primarily relating to injury to the gastrointestinal tract, and immune mechanisms, and to other evidences of suppression of hematologic function. With doses of 200 r or less in a single exposure, nausea and vomiting of relatively short duration is the only symptom which has been described. With doses of 100 r or less the probability of even nausea occurring is small and perhaps absent.

Paper C-2

LATE EFFECTS IN MAN FOLLOWING EXPOSURE TO IONIZING RADIATIONS

Douglas Grahn

Division of Biological and Medical Research, Argonne National Laboratory

The problems before the National Aeronautics and Space Administration concerning the potential biological hazards of radiation exposure are familiar ones to other agencies, such as the Atomic Energy Commission. The "late effects" or manifestations of chronic radiation injury have been of particular concern to the AEC and for the same reasons they concern the NASA; chronic injury is cumulative, though subtle and often undetected, and can be the limiting factor for individual exposure histories.

Although a considerable amount of experimental effort has been expended on late-effects problems, completely satisfactory answers are not yet available for man. This is largely due to the necessity of projecting expectations for man on the basis of experience in laboratory animals. Available direct human experience can be drawn upon, but even this can only serve to "spot check" certain predictions. At present the most thorough examination of man's response to radiation involves the Hiroshima-Nagasaki survivorship study under the jurisdiction of the Atomic Bomb Casualty Commission.[1] Other studies include the follow-up of criticality accident cases. All things considered, our information is best for doses that induce acute injury and it becomes progressively more uncertain as dose declines. Statements regarding the chronic effects of fallout radiation, for example, are almost entirely conjectural - lacking experimental validation. By and large, the same can be said for any projected effects of exposure to space radiation, with the exception that here we can be dealing with bursts of exposure to higher doses in the range of present experience.

The late effects of radiation exposure have to be examined in two broad categories; somatic and genetic. The somatic effects are those found in the irradiated individual; the genetic effects are those transmitted or transmissable to the offspring as a result of radiation-induced change in the reproductive tissues. Before discussing the biological expectations however, some comments are required concerning the physical exposure parameters.

---

[1] A research agency of the U. S. National Academy of Sciences - National Research Council supported by a contract with the U. S. Atomic Energy Commission.

Temporal and geometric aspects of exposure to space radiation

The ambient radiations in space are characterized by their heterogeneity, not only in the variety of both particulate and electromagnetic radiations but also in the energy levels of these radiations (Newell and Naugle, 1960). Since these factors are discussed elsewhere in the proceedings, my comments will be restricted to the general consequences of this heterogeneity for the hazards evaluation problem.

A heterogeneous energy spectrum of the incident radiation will produce a very non-uniform distribution of dosage in depth, if the spectrum includes a large low energy component. For photons, this would involve energies below 120-135 kvp (Grahn et al., 1956). For protons, energies generally below 100 Mev would have an inadequate range in water (Rich and Madey, 1954), and consequently wet tissue, to assure uniform depth dosage. It becomes extremely difficult to define the level of injury when the exposure dose in air may vary from two to twenty times greater than the midline tissue dose. The use of the midline dose, or other measures, such as exit dose or gram-roentgen dose, is not recommended for the definition of exposure level. There is evidence, however, to support the hypothesis that the biologically effective dose is best defined as the average dose to the bone marrow for both acute and chronic measures of injury (Grahn et al., 1956; Grahn and Sacher, 1958; Alpen et al., 1958). This problem is especially difficult when dealing with heterochromatic x or γ radiation, since absorption in bone exaggerates the non-uniformity by preferentially shielding the bone marrow. Any bremsstrahlung or secondary x or γ radiation produced by shielding or capsule materials may be in this low energy range. Protons, on the other hand, are not more effectively stopped by bone than by soft tissue, but the wide energy range for galactic and solar flare protons causes the depth dose curve to be very steep (Figure 1). As seen in Figure 1, this would lead to an extremely heterogeneous marrow dosage. In comparison to the flare proton, the geomagnetically trapped proton belt has a more uniform energy spectrum and consequently a flatter depth-dose distribution.

The actual dose in depth for any circumstance would have to be calculated from the observed differential energy spectrum; and each event is going to differ from every other event. Thus, complete monitoring of all radiation

events to which an astronaut may be exposed will be required if any sensible statements on radiation exposure stacus are to be made.

In addition to the problem of non-uniform depth dosage, there is the question of "non-random" exposure due to the extremely high local doses that will occur in cells and tissues from the passage of high energy heavy particles. In this situation, small groups of cells may be severely injured while surrounding tissue will remain unscathed. The acute and chronic effects of this type of exposure are not really understood but some comments will be made on the basis of experience with fission neutrons.

Lastly, the time pattern of exposure will be unpredictable and irregular. For example, there would be a pulse or brief period of exposure during transit of the Van Allen belts. The random occurrence of solar events would give rise to additional pulses. All of these could vary in total dose, dose rate and depth dose. Throughout a mission, there would also be a continuous low level exposure to the galactic cosmic radiation. The ultimate biological effect is known to vary with the pattern of exposure (see Figure 2 below) but because of the pulse-like nature of the exposure under discussion, it would be difficult to "assign" an individual to either a predominantly single dose exposure or continuous exposure. If the total dose remains below 50 r, it will make little difference, but it is obvious from Figure 2 that brief, single-dose, high-intensity exposures to total doses of 100 r or more can be followed by a more exaggerated chronic syndrome.

The above remarks and these below concerning somatic hazards are all based on the assumption that whole-body exposure pertains. If partial-body exposure occurs, or is deliberately planned as a protective measure, prediction of late effects becomes essentially impossible for man. The value of bone-marrow shielding as protection against both acute and chronic radiation injury is well recognized and documented for experimental animals (Thomson, 1962), but is quantitatively unevaluated for humans.

Somatic hazards

There is a variety of ways of evaluating the long term biological hazards, but the most readily quantitated measure of chronic injury is simply survival

time or life shortening. The general relationship between dose and the reduction of life expectancy is shown in Figure 2 for the mouse; the species from which we gain most of our knowledge of mammalian radiobiology. The figure indicates what might be called the limiting conditions - the exposure situations that give the maximum and minimum late effect. As indicated above, any exposure to the radiations in space during an extended mission will lie somewhere between the two extremes. If shielding is adequate so that total doses per mission are less than 50 r, late somatic effects can probably be predicted on the assumption of a continuous exposure. The expectations for man are suggested in Figure 3, according to the date and calculations of Sacher (1960) and Sacher and Grahn (1963).

The curve is described by the equation: $Y = 45e^{-1.05D}$ where Y is the predicted after-expectation of life under exposure of D roentgens per day. This relationship is exceptionally accurate for mouse populations and it is applied to man on the assumption that responses to radiation will be in proportion to the ratio of life expectancies (Sacher, 1960). In simplest terms, it states that the life shortening effect in man is about one day per roentgen, when this is accumulated in a reasonably protracted manner.

One should hasten to add that at doses probably below 0.3 r/day (for man) the actual effects are still quite unpredictable. In the mouse, for example, at comparable doses (below 10 r/day), where life shortening amounts to 15% and less, there is a great deal of variability in the response. There is extensive dependence upon environmental factors such as disease pressure, and the innate viability of the individual, (Grahn and Sacher, unpublished data).

In general, the mouse strains with shorter life expectancies tend to demonstrate little or no life shortening at doses below 10 r/day and occasionally a small increase in life expectancy over the control. Longer lived strains generally tend to show some degree of life shortening at even the lowest doses. Shorter-lived animals have the higher mortality from infectious disease and independent control samples show a wide variance of mean life expectation. The irradiated mice that are from the short-lived group may have their mortality rate from infectious disease depressed below this age-specific control, thus they

may show some over-survival. Longer-lived mice are more invariant in their normal survival times and appear to be subjected to a minimum of infectious disease pressure, whether or not they are irradiated.

It is very likely that the astronaut populations will be analogous to those mouse populations that have a better than average life expectancy and a low infectious disease incidence. In other words, they undoubtedly have a low background noise level and even at very low radiation doses, a significant signal-to-noise ratio will exist and thus some degree of chronic injury could be manifested.

The next question asked is - why does an irradiated population die sooner? Generally, chronic radiation injury is expressed by an increase in the age - specific death rates over those seen in unirradiated populations. The causes of death normally found in a population are also found in the irradiated group. There is no unique pathology associated with chronic radiation injury.

Certain causes of death are increased in incidence more than others - leukemia, for example, is readily induced by radiation. Although radiation-induced leukemia has been the subject of extensive research, the most pertinent data are still those being obtained in the Japanese survivors. A recent summary by Brill et al. (1962) substantiates earlier interpretations that above 50-100 r, the increase is linear with dose at a rate of 1 to 2 x 10^{-6}/r/year during the first 15 years post-exposure. This is an average figure for all age groups and would be slightly less for a group of adults between 30 and 40 years of age, at least for acute leukemias. The data are uncertain at doses below 50 r but tend to demonstrate a positive effect.

Radiation-induced leukemia has a phasic response pattern in time. The peak year of incidence in Japan was 1952 - seven years post-exposure - and it has been dropping steadily since then. Undoubtedly some life shortening effect will be specifically attributed to leukemia when the study is complete. Such an effect has been statistically isolated in mouse populations (Grahn, 1960).

Other neoplastic diseases are also increased following irradiation and again, early reports from the Japanese studies indicate a positive dose-response

relation for all age groups. Specifically, carcinoma of the stomach, lungs and ovaries was shown to be increased during a 20-month survey period in 1958-1959 (Hollingsworth et al., 1962).

The incidence of cataracts in the Japanese is very low (<1%) but this could be a more common sequel of exposure to space radiation due to their high LET component and high surface dose.

Earlier, it was noted that the high LET radiations may have a somewhat modified pattern of chronic injury as a result of the greater localization of energy deposition. Experience with fission neutrons indicates what can occur when geometric factors are appropriate. Nowell et al. (1958) reported that neutron exposure induces a four-fold greater incidence of stomach cancer in the mouse than does x-ray exposure (36% vs 9%). This is attributed to the fact that the mouse is small enough for the deep tissues to be largely irradiated by the high LET recoil protons from the neutron interaction. Thus, the glandular epithelium is subjected to extensive local damage along the proton track while comparable doses of x-irradiation produce a more diffuse level of injury. The cellular and local physiologic sequelae are such as to produce a higher incidence of gastric carcinoma from the neutron exposure.

This interpretation is supported by the observation that neutron induction of cell damage in the mouse's intestinal wall has an RBE of 6-8 while the concurrent acute lethal response has an RBE of 2-3 (Lesher and Vogel, 1958). In contrast, larger mammals, from the rat to the dog, do not evince the acute gastro-intestinal syndrome after fission neutron irradiation that characterizes the response of mice (Bond et al., 1956). Man would undoubtedly respond like other large mammals, since the deeper tissues would be irradiated almost entirely by thermal neutron capture gamma rays rather than by recoil protons. A more penetrating particulate radiation, such as high energy protons and heavy primaries, could produce a situation in man similar to that in the mouse exposed to fission neutrons.

The above noted case for gastric cancer induction is a clear example of a late effect that appears to be modified by the local geometric details of the energy transfer. Other cases more pertinent to space radiation exposure may be brought out if deep tissues were experimentally subjected to high LET radiations;

for example, if portions of the liver or intestine were exteriorized and exposed to charged particle beams from a HILAC.

Genetic hazards

One of the first questions that arises concerns the possibility of radiation-induced sterility. Unfortunately, good data on this point do not exist for man. What is known, along with animal experience, suggests that permanent sterility will not be induced at doses below acute lethal levels; unless a high local exposure of the gonads should occur. There may be a period of temporary sterility or reduced fertility following exposure to doses as low as 20 r, but present data from accident cases are incomplete or contradictory. One individual exposed to 12 r demonstrated a sharp reduction in sperm count (from 5×10^8/ml to 1×10^6/ml) over a period of seven months followed by an equal period of slow recovery (Hasterlik and Marinelli; 1956).

The Y-12 accident cases involved doses between 200 rad and 400 rad and some sperm counts were done (Andrews et al., 1961). Within 3 weeks, counts were low and sperm were generally non-motile. Absence of sperm, azoospermia, was noted in most of the cases for at least 9 months and reduced counts were noted at 22 months. The Vinca, Yugoslavia, accident cases, reported by Pendic (1961) and Jammet (1961) involved slightly higher doses; between 300 rad and 600 rad. Sperm counts began to decline by day 10 and within 3 months, 2 of the 4 surviving males showed azoospermia. Curiously, one individual who received a dose of 350 rad had nearly a normal sperm count 7-8 months after exposure while the other three males were azoospermic. Doses to the latter were between 400 and 600 rad. At 18 months post-exposure, one was normal, two were hypospermic and one still remained azoospermic.

While the above data are somewhat crude, the general course of events is typical of that seen in laboratory mammals; there is a pre-sterile period following irradiation, a sterile period, and a post-sterile period. The pre-sterile period in man probably lasts about 30 days. The sterile period may last months to years followed by a slow return to normal, but in some, this temporary sterility may not occur at all.

The importance of distinguishing between a pre-sterile and a post-sterile period lies in the type and frequency of mutations observed from matings in

these periods. Offspring produced in pre-sterile matings largely come from irradiated mature germ cells or spermatozoa. The mutation rate for recessive genes in these cells may be twice that observed in the spermatogonia or stem cells (Russell et al., 1958). In addition, the irradiated mature germ cells carry a high incidence of a mutational type rarely found in the immature cells - the dominant lethal. A recent survey of experimental data on dominant lethals in mice (Grahn, 1962) indicates that most act early in gestation, that the lethal effect is due to aberrant cell division and chromosome fragmentation, that the neutron: x-ray RBE is about 7, and that neutron dose-response data are linear with arithmetic dose compared to x-ray data which are more nearly linear to dose-squared. Thus, the particulate radiations of space may present an extra threat because of their dense ionization tracks and greater probability of inducing genetically lethal effects. This period of increased genetic hazard may only be of two months duration, however, according to recently reported data on the cycle of spermatogenesis in man (Heller, 1962).

Mutations observed in the post-sterile period are predominantly recessive, and about three-fourths of these may be lethal in mice (Russell and Russell, 1959) The mutation rate is lower for those mutations induced in gonia and lower still if the dose rate is less than 1 r/minute (Russell et al., 1958). Table 1 summarizes the mutation rate data in mice for the two sexes. These figures can be generally accepted as indicative of the radiation-induced mutation rate in man, at least within a factor of two. Again it can be seen that close monitoring of the exposure pattern will be required in order to assign a given exposure to the 'acute' or 'chronic' mutation rate categories.

What is the probability that a given germ cell will carry a recessive mutation? From the mouse data, this can be calculated as lying between 1 chance in 20 and 1 chance in 5, for immature germ cells following an exposure of 100 r and assuming there are 10^4 genes. Obviously, exact figures cannot be given, but the probability is certainly small for doses appreciably below 100 r. In addition, the chance of expression in the immediate offspring is probably only 1 in 25 or less (Morton et al., 1956).

Thus, there may be less than one chance in a hundred of a radiation-induced recessive mutation appearing in the first generation when the parent has

received a dose of 100 r. This seemingly low probability should not allow us to relinquish our obligation to minimize the genetic hazard.

Detrimental genes may express themselves in the population in a number of ways. These include:

a. Increase in frequency of stillbirths.
b. Shifts in sex ratio attributable to sex-linked lethal mutations.
c. Increase in mortality rate from birth to 10 years of age.
d. Increase in incidence of congenital abnormalities.
e. Decrease in life expectancy.
f. Decrease in birth weight.
g. Increase in variance of metrical traits.

The reader is referred for further detail to other reviews and reports by Grahn (1962), Neel and Schull (1956), and Stern (1960).

The major point to be made is that genetic damage can linger in the population for many generations. The probability of expression in the first generation offspring is usually low enough to produce a misleading confidence that no damage has been done. The issue will not be pressed here since the genetic hazard is probably not a major one. Most of the astronauts may be beyond median reproductive age - about 30 years - and therefore will not transmit any induced mutations. Also, this is a very small group whose genetic impact on the population will be equally small.

Assessment of hazards

The above remarks introduce the most difficult judgments of all - the value judgments on the rationalization of all of the risks involved in extended space flight missions. It is the writer's opinion that presently accepted standards of operational radiation safety for occupational and emergency situations have little meaning for these flight missions. Final judgments will depend not only on biological and medical considerations of radiation safety but also on the total complex of engineering and bioastronautics capabilities. However, it would be a pity to lose an otherwise successful mission, with all of its complications of launch, guidance and instrumentation, because of inadequate consideration of an old-fashioned hazard like radiation.

Undoubtedly, the shielding considerations should concern themselves primarily with the avoidance of acute radiation symptomatology. Any plan for the continued utilization of experienced personnel, however, will have to take chronic injury parameters into account.

In this regard, somatic endpoints are in part medically manageable so that valuable personnel need not be subjected to any maximum calculable risk; the risk based upon total absorbed dose. Genetic endpoints, in a sense, are not biologically controllable, but the hazard here is statistically manageable in that only a tiny fraction of the total reproductive population is involved.

Thus, as indicated, the judgments become almost wholly value judgments, but, fortunately, the data for establishing realistic probability statements of radiation hazards are becoming available. With these, the radiation hazards can be quantitatively evaluated along with all other risks in terms of the precautions required to insure mission success.

REFERENCES

Alpen, E. L., D. M. Jones, H. H. Hechter and V. P. Bond. 1958. The comparative biological response of dogs to 250 kvp and 100 kvp x-rays. Radiology 70: 541-550.

Andrews, G. A., B. W. Sitterson, A. L. Kretchmar and M. Bracer. 1961. Criticality accident at the Y-12 plant. In: Diagnosis and Treatment of Acute Radiation Injury. New York: Internat. Documents Service, Columbia Univ. Press, p. 27-48.

Bond, V. P., R. E. Carter, J. S. Robertson, P. H. Seymour and H. H. Hechter. 1956. The effects of total-body fast neutron irradiation in dogs. Radiation Research 4: 139-53.

Brill, A. B., M. Tomonaga and R. M. Heyssel. 1962. Leukemia in man following exposure to ionizing radiation. Ann. Internal Med. 56: 590-609.

Grahn, D. 1960. The genetic control of physiological processes: The genetics of radiation toxicity in animals. In: Radioisotopes in the Biosphere, R. S. Caldecott, Ed., Minneapolis: Univ. of Minnesota, p. 181-200.

Grahn, D. 1962. Methods in mammalian radiation genetics. In: Methodology in Mammalian Genetics, W. Burdette, Ed., San Francisco: Holden-Day.

Grahn, D. and G. A. Sacher. 1958. Chronic radiation mortality in mice after single whole-body exposure to 250, 135, and 80 kvp x-rays. Radiation Research 8: 187-194.

Grahn, D., G. A. Sacher, and H. A. Walton. 1956. Comparative effectiveness of several x-ray qualities for acute lethality in mice and rabbits. Radiation Research 4: 228-242.

Hasterlik, R. J. and L. D. Marinelli. 1956. Physical dosimetry and clinical observations on four human beings involved in an accidental critical assembly excursion. Proc. I Internat. Conf. Peaceful Uses of Atomic Energy 11: 25-34.

Heller, C. G., L. J. Matson, D. J. Moore and Y. Clermont. 1962. Rate of spermatogenesis in man determined by incorporating initiated thymidine into testes. In: Symposium on the Effects of Ionizing Radiation on the Reproduction System. In Press.

Hollingsworth, S. W., G. W. Beebe, M. Ishido and A. B. Brill. 1962. Medical findings and methodology of studies by the atomic bomb casualty commission on atomic bomb survivors in Hiroshima and Nagasaki. In: The Use of Vital and Health Statistics for Genetic and Radiation Studies. A/AC.82/Seminar, United Nations, N. Y. p. 77-100.

Jammet, H. P. 1961. Treatment of victims of the zero-energy reactor accident at Vinca. In: Diagnosis and Treatment of Acute Radiation Injury. New York: Internat. Doc. Serv., Columbia Univ. Press, p. 83-104.

Lesher, S. and H. H. Vogel. 1958. A comparative histological study of duodenal damage produced by fission neutrons and Co^{60} γ-rays. Radiation Research 9: 560-571.

Morton, N. E., J. F. Crow and H. J. Muller. 1956. An estimate of the mutational damage in man from data on consaguineous marriages. Proc. Natl. Acad. Sci. 42: 855-63.

Neel, J. V. and W. J. Schull. 1956. The effect of exposure to the atomic bombs on pregnancy terminations in Hiroshima and Nagasaki. National Acad. Science. National Research Council Report No. 461. Washington D. D.

Newell, H. E. and J. E. Naugle. 1960. Radiation environment in space. Science 132: 1465-1472.

Nowell, P. C., L. J. Cole and M. E. Ellis. 1958. Neoplasms of the glandular stomach in mice irradiated with x-rays or fast neutrons. Cancer Research 18: 257-260.

Pendic, B. 1961. The zero energy reactor accident at Vinca. In: Diagnosis and Treatment of Acute Radiation Injury. New York: Internat. Doc. Serv., Columbia Univ. Press, p. 67-82.

Rich, M. and R. Madey. 1954. Range-energy tables. University of California Radiation Lab. Report, UCRL-2301. U. S. Atomic Energy Commission.

Russell, W. L. and L. B. Russell. 1959. The genetic and phenotypic characteristics of radiation-induced mutations in mice. Radiation Research (Suppl.) 1: 296-305.

Russell, W. L., L. B. Russell and E. M. Kelly. 1958. Radiation dose rate and mutation frequency. Science 128: 1546-1550.

Sacher, G. A. 1960. Problems in the extrapolation of long-term effects from animals to man. In: The Delayed Effects of Whole-Body Radiation. B. B. Watson, Ed., Baltimore: Johns Hopkins Press, p. 3-10.

Sacher, G. A. and D. Grahn. 1963. Survival of mice under duration-of-life exposure to gamma rays. I. Dosage-survival relations and the lethality function. In preparation.

Stern, C. 1960. Principles of Human Genetics. 2nd Ed. San Francisco: W. H. Freeman and Company.

Thomson, J. F. 1962. Radiation Protection in Mammals. New York: Reinhold Publishing Co.

TABLE 1

RADIATION-INDUCED MUTATION RATE IN MICE

(Adapted from data of W. L. Russell, ORNL)

Observed mutation rate	Sex	Cell stage	Radiation exposure
45×10^{-8}/r/gene	Male	Postgonial	Acute or chronic
21×10^{-8}/r/gene	Male	Gonial	Acute
5×10^{-8}/r/gene	Male	Gonial	Chronic
31×10^{-8}/r/gene	Female	Oocyte	Acute
4×10^{-8}/r/gene	Female	Oocyte	Chronic
0.7×10^{-5}/gene	Male and female	All stages	Unirradiated

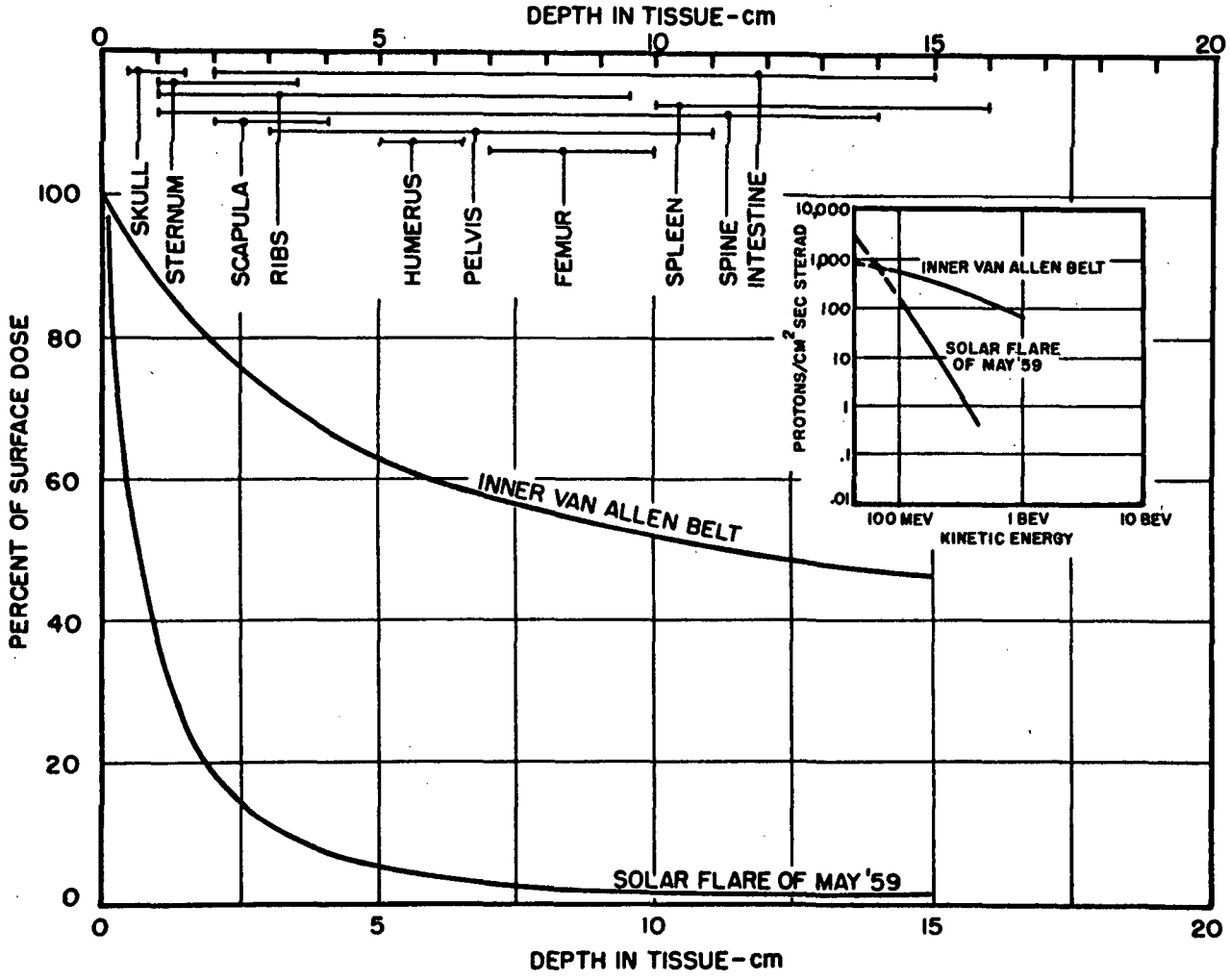

Figure 1. Depth dose as percentage of surface dose for a solar flare protons compared with inner Van Allen belt protons. Note general location of regions of active bone marrow in relation to depth dose.

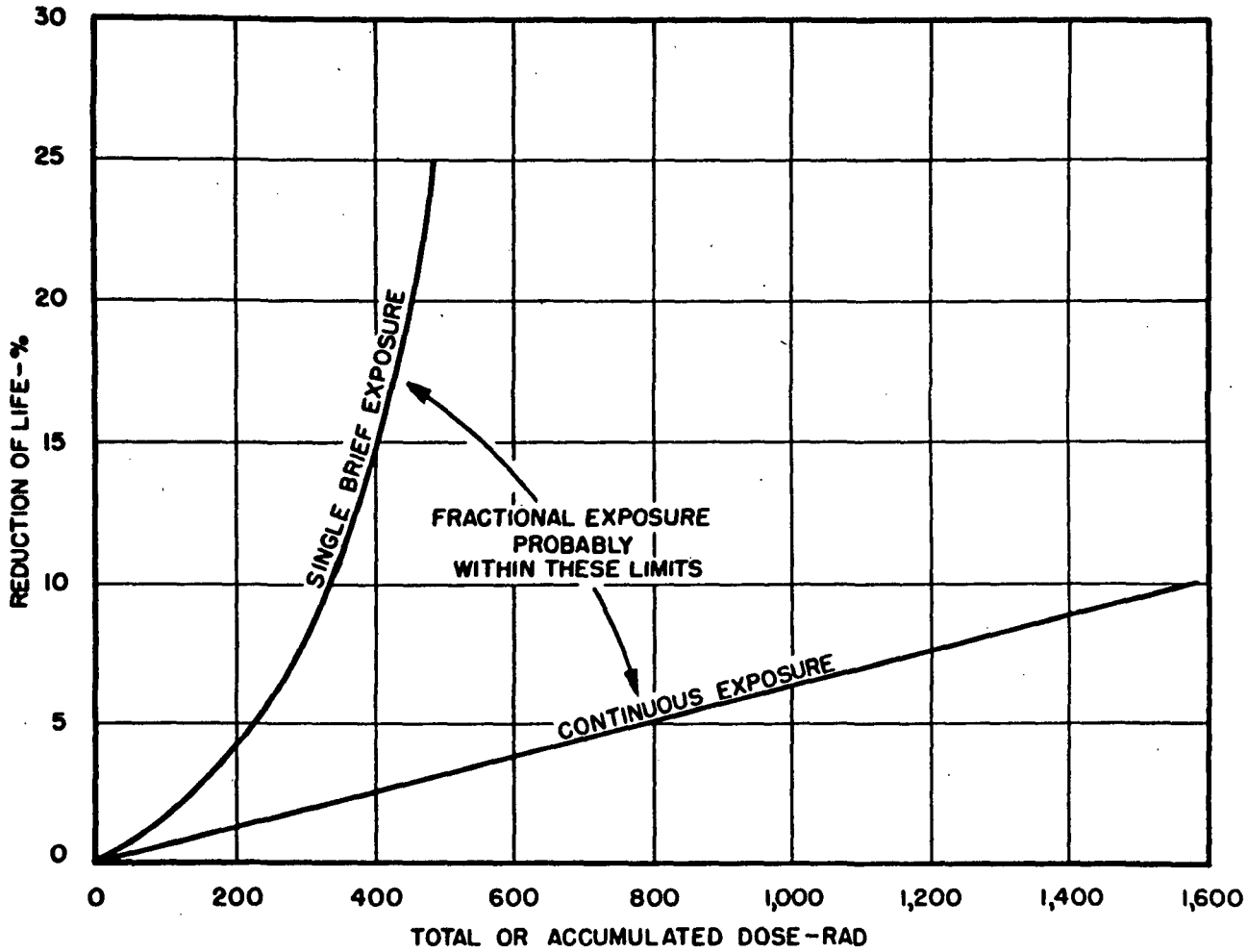

Figure 2. Idealized relation between life shortening and radiation dose for the laboratory mouse. Generally descriptive of expectations for man on the indicated basis of "percent reduction of life".

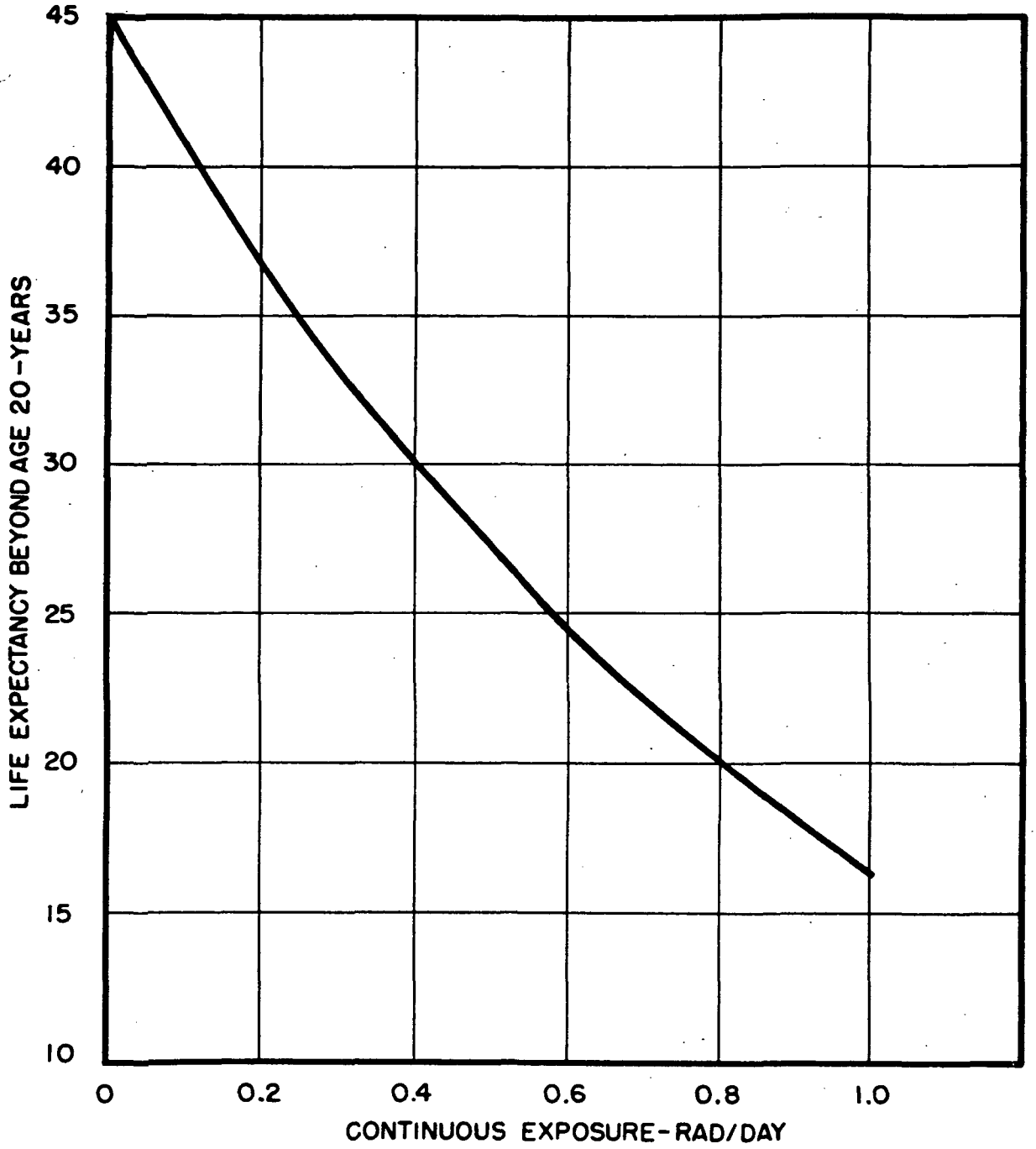

Figure 3. Prediction of life expectancy for man exposed to daily doses of radiation.

Paper C-3

SOME SPECIFIC CONSIDERATIONS OF THE POTENTIAL HAZARDS OF HEAVY PRIMARY COSMIC RAYS*

Howard J. Curtis

Biology Department, Brookhaven National Laboratory, Upton, N. Y.

INTRODUCTION

The radiations of the Van Allen belts and the solar flares consist primarily of electrons and protons, the biological effects of which are reasonably well known. However, there is a very small component of the galactic cosmic rays which consists of stripped atomic nuclei of atoms as heavy as iron. The biological effects of such particles have not been extensively investigated because it is impossible to produce them in the laboratory with an energy high enough to use for mammalian experiments. Consequently it has been necessary to approach the problem by indirect methods.

The distribution of these particles is shown in Fig. 1, as estimated by Dainton et al. (1). It will be seen that most of the particles are of the very light elements and only a few heavy ones. For the elements lighter than carbon it seems safe to assume that the radiobiological effects are quite similar to those of protons or alpha particles and consequently the dose can be calculated in the usual way. Schaefer (2) has calculated this dose to be of the order of 40 m rep/day. This by itself, while it should not be ignored, would not seem to pose a very serious hazard for space travel.

* Research carried out at Brookhaven National Laboratory under the auspices of the U. S. Atomic Energy Commission.

But the particles heavier than carbon constitute a special hazard. Schaefer (2) has pointed this out a number of years ago and at that time performed much of the necessary calculation. He showed that when these heavy particles enter tissue one of two things may happen. Especially at very high energies a nuclear reaction may take place which results in a nuclear disintegration and star formation. In this the energy of the particle is widely spread throughout the tissue, and does not concentrate enough at any one spot to constitute a new type of effect. However, some of the particles, especially at low energies, slow down by interaction with the electrons of the tissue and this produces very energetic delta rays, especially near the end of the track. This leads to a very dense ionization track, and Schaefer (2) has computed that within this track, known as a "thindown," the radiation dose may be as high as 10,000 rads at the center, and decreases to low values at the edges. The track may be as much as 0.025 mm in diameter and about 1.5 mm long. Schaefer (2) has computed that there might be as many as 100 such hits per hour in an average man in interstellar space and there would be several thousand cells irradiated in each "hit." It thus appears there would be "hot spots" in the tissue in which the dose might be quite high, even though the over-all dose is quite low.

The proportion of particles which would be stopped in tissue by nuclear reactions as compared to those stopped as thindowns has been estimated by Schaefer (2) and is shown in Fig. 2 as a function of energy. It is seen that practically all particles having energies greater than 10^9 e.v./nucleon will be stopped by nuclear reactions and so need not be considered here.

The magnetic field of the earth forms an effective shield for the equatorial region of the earth for everything except a few of the most energetic of these particles. At higher latitudes more of the low energy particles will be present. Schaefer (2) has also estimated the energy spectrum of these particles at various latitudes and this spectrum is shown in Fig. 3 for 55° latitude. The extrapolation of the spectrum shown in Fig. 3 to lower energies is the spectrum for the polar region and this is also presumably the spectrum which would exist in outer space. The shaded portion of the figure shows the particles at 55° which would probably form thindowns in tissue, and at the polar regions practically all particles below 1 BEV per nucleon would form thindowns. Thus in outer space more than half of all the heavy particles would be in the energy range to produce thindown hits.

A complete discussion of shielding problems in connection with these particles is out of place here. Suffice it to say there are two facets to the shielding problem; that for the relatively low energy particles (< 1 BEV/nucleon) and that for the high energy ones. For the former, a reasonable amount of shielding, for example 6 g/cm^2 of a low molecular weight material, would only serve to make the situation worse because it would slow down the particles enough to cause more thindown tracks in a man. It would be necessary to increase the shielding to more than 20 g/cm^2 before the numbers of these thindowns would be substantially reduced. It would be equally difficult to shield against the high energy particles. Here one would rely on star formation within the material, and the cross section is independent of the energy of the particle and depends only on the nuclear cross section. Since the nuclear cross sections are relatively greater for the light elements, on a g/cm^2 basis,

light elements would be preferable for shielding here. Again it would take more than 20 g/cm^2 for effective shielding.

In order to approach the problem of the radiobiological effect of these particles from an experimental point of view it is necessary either to send biological materials to very high altitudes in the polar region, or to generate such particles in an accelerator. The latter has been accomplished only for energies up to 10 mev/nucleon and this is energetic enough only for work with single cells and tells us almost nothing about the effect in mammals. Chase (3) has sent black mice in balloons to the top of the atmosphere to observe greying of the hair in these mice. If the heavy particles are as destructive as expected, these mice should have grown a grey hair from each of the hair follicles hit by a thindown. In the 1954 series there was a very impressive increase in greying in mice flown in the polar region as compared to mice flown at lower latitudes. Fig. 4 shows a photograph of one such mouse. It is easy to see that if all the organs of the body were affected like the hair on the mouse in Fig. 4 after an exposure of only one day, space flight might be quite hazardous. However, the experiment was repeated in 1955, presumably under more rigidly controlled conditions, and no increase in greying was observed. The experiments were stopped at this point in a very inconclusive state, but with the impression that the thindowns might be quite destructive.

Other attempts have been made to measure the radiobiological effect of these particles by sending animals, including monkeys, to the top of the atmosphere with nuclear emulsions attached to them in an attempt to relate cellular damage, usually in the brain, to the thindown hits re-

corded in the emulsions. However, there are so few hits, and the geometrical considerations are so difficult, that nothing has been observed.

In order to try to get at the problem an indirect experimental approach has been developed (4). The biological effect from these particles must be due almost entirely to the delta rays which are generated by the passage of the particle, and it is these rays which cause almost all of the dense ionization of the track. From a radiobiological point of view the effect should be the same if the same ionization pattern were produced in another way. The approach used was to confine the deuteron beam from the 60" Brookhaven cyclotron in a beam which could be as small as 0.025 mm in diameter which is about the same maximum diameter for a heavy particle track. The difference would be that the particle track has maximum ionization at the center and decreases nearly to zero at the edge, while the microbeam presents a uniform ionization over the whole beam profile. By adjusting the exposure in this beam any desired ionization density could be achieved and thus any desired dosage. The experimental arrangement was such that the beam could be directed to any desired point within an accuracy of about 0.050 mm, so the part of the animal irradiated could be marked for later examination. The experimental arrangement is shown in Fig. 5 and a photograph of a mouse in position for irradiation shown in Fig. 6.

RESULTS

Irradiation of hair follicles

Since the only direct biological effect ever recorded for the heavy particles was that of greying of hair, it was felt to be important to use the greying response as one of the test objects for the microbeam

studies since this should give a direct comparison (5).

It was found to be not possible to locate an irradiated hair follicle some three months later, so the microbeam had to be modified for the study on hair. Two apertures were used. Both were formed as crossed slits, one with the slits 0.025 mm and the other 0.25 mm wide. In one of the quadrants of each aperture there was a hole 1 mm in diameter. The resulting 1 mm beam was large enough to hit many hair follicles and if the dose was more than about 500 rads, a small spot of grey hairs, the marker spot, would be visible 5 to 10 weeks later. Knowing the relationship between the spot and the slits, one can look for grey hairs along the slits.

It was found that whenever grey hairs appeared in the spot, they also appeared in the 0.25 mm slits. Further, the grey hairs were strictly confined to the region of the slits, and there was no spread of the influence of the irradiation beyond the irradiated volume. Two exposures are shown on one mouse in Fig. 7.

For the 0.025 mm slits, the results were not quite so definite because the hair follicles themselves are more than 0.025 mm in diameter so it would take a direct hit on the center to cause greying. Further, the follicles are as much as 0.2 mm apart so one would expect only a very few of them to be exactly in line. Nevertheless, whenever the spot was grey there were at least a few grey hairs along the line of the slit.

These experiments established that the threshold dose for greying is about 500 rads, and this is independent of the volume of tissue irradiated as long as the follicle is hit. This result supports Chase's results and gives a strong indication that the microbeam does simulate the

biological effect of a heavy particle.

Brain irradiation

One would expect that damage to the brain would be the greatest hazard from these particles since there are very small volumes of the brain which control very vital processes such as temperature regulation.

The microbeam was directed at the cerebral cortex of mice, and after varying periods of time up to 240 days, the mice were sacrificed and the brains examined histologically for damage (6, 7). First a wide beam 1 mm in diameter was used in order to make sure the dosage measurement was correct, since results should be predictable from x-ray experience on this broad a beam. Here it was found that at about 14,000 rads there was complete destruction of the cortex in the beam path, as predicted from x-ray work. The same dose was then administered through the 0.025 mm beam and absolutely no effect was observed at any interval. Since the maximum dose expected at the center of a heavy particle track is about 10,000 rads, it would seem that these particles would have very little effect on the brain.

It was felt to be important to find the "factor of safety" for this effect, and consequently the dose in the microbeam was increased to the point where an effect was observed. It was found necessary to go to 400,000 rads before the neurous of the brain were destroyed. These effects are illustrated in Fig. 8.

The explanation for this extreme insensitivity of the brain to a very narrow beam probably lies in the facts (a) that blood capillaries are moderately sensitive to radiation and so most radiation damage to the brain is through capillary damage. Since the capillaries are about 0.065 mm

apart in the mouse brain, the microbeam would largely miss them, and even if it did hit an occasional one, the factor of safety should be great enough to sustain this loss without damage to the neurons. (b) The neurons never undergo cell division, and it is well known that cells can withstand enormous doses of radiation if they are not required to divide. It has not yet been determined that these cells are functional, but it seems quite likely that after a dose of 10,000 rads they would be, since it takes such an enormous dose to cause destruction.

It thus appears that in this most critical organ these particles will not present a serious problem.

Irradiation of the eye

The organ next most vulnerable for the particles would be the eye. Radiation cataracts are well known, and the high LET radiations are especially effective in causing these cataracts. It could be reasoned that a thindown hit in the lens epithelium would cause a minute disruption of the lens fibers which would grow to a full cataract. Further, there is no capillary circulation in this tissue and the epithelial cells undergo cell division at a rather rapid rate. Thus the situation is quite different from that of the brain and one might expect damage at a low dose.

The microbeam was directed to the generative zone of the lens in the mouse eye and the animals were examined periodically with a slit lamp and some were sacrificed for histological examination (8). When the 1 mm beam was used cataracts were formed with doses as low as 1000 rads as expected. With the 0.025 mm beam cells which were in the beam path had a high probability of turning into a bazar cell which might lead to

a cataract. However, the beam was so small that only one or two cells were hit at a time. As these cells migrated toward the posterior pole they were sloughed off and absorbed, presumably by pressure of the surrounding normal cells. They never formed even a small cataract, so it apparently takes a cluster of abnormal cells to be stable enough to cause a persisting cataract. The dose necessary to cause abnormal cell formation by the microbeam is about the same as for the 1 mm beam.

The fact that the damage produced is independent of beam size is in accord with expectations and is in agreement with the explanation given for the action of these beams in the brain.

Here again it seems that the heavy particles will not be a serious hazard for space flight.

DISCUSSION

From these results one can estimate the effect of these heavy particles on the other organs of the body and on the body as a whole. The occasional loss of individual cells or small groups of cells in organs such as the skin which are continually undergoing cell division should be of no concern since the damaged or dead cells will be quickly replaced. The loss of individual cells in the brain or musculature is in progress continually as a normal part of the aging process. It would take a very long exposure to these heavy particles in outer space to cause a loss significantly greater than occurs spontaneously. Other organs such as the liver or kidney would likewise cause no concern. Greying of the hair seems to be the one real possibility but fortunately this is not serious. There would be some genetic

effect but this would be very minor.

It would thus seem safe to conclude that this hazard will not be very great, but the subject is important enough so it would be well to check one or two of these points by biological experiments in satellites.

SUMMARY

The ionization produced by the heavy cosmic ray particles is almost entirely highly concentrated along single tracks, and the microscopic dose in tissue within these tracks may be quite high but the overall dose rate from these particles in outer space would be very low. These particles cannot be produced in the laboratory so a microbeam of deuterons has been developed which simulates the ionization pattern of these particles. Using this microbeam on mice it is found that this type of radiation causes very little effect in either the brain or the eye, and presumably also in other vital organs. However, it will cause greying of the hair. It is concluded that this type of radiation will not cause a serious hazard for space flight.

REFERENCES

1. Dainton, A. D., P. H. Fowler and D. W. Kent. The abundance of lithium, beryllium and boron in the primary cosmic radiation. Phil. Mag. 43: 729-752 (1952).
2. Schaefer, H. J. Theory of protection of man in the region of the primary cosmic radiation. J. Aviation Med. 24: 338-350 (1954).
3. Chase, H. G. and J. S. Post. Damage and repair in mammalian tissues exposed to cosmic ray heavy nuclei. J. Aviation Med. 29: 533-540 (1956).
4. Baker, C. D., H. J. Curtis, W. Zeman and R. G. Woodley. The design and calibration of a deuteron microbeam for biological studies. Radiation Res. 15: 489-495 (1961).
5. Curtis, H. J. The effect of a deuteron microbeam on greying of hair. Radiation Res. (in press).
6. Zeman, W., H. J. Curtis, K. L. Gebhard and W. Haymaker. Tolerance of mouse brain tissue to high energy deuterons. Science 130: 1760-1761 (1959).
7. Zeman, W., H. J. Curtis and C. P. Baker. Histopathologic effect of high energy particle microbeams on the visual cortex of the mouse brain. Radiation Res. 15: 496-514 (1961).
8. Von Sallmann, L., H. J. Curtis and P. Grimes. The effect of a deuteron microbeam on the mouse crystalline lens. Arch. Ophthalmol. 67: 163-170 (1962).

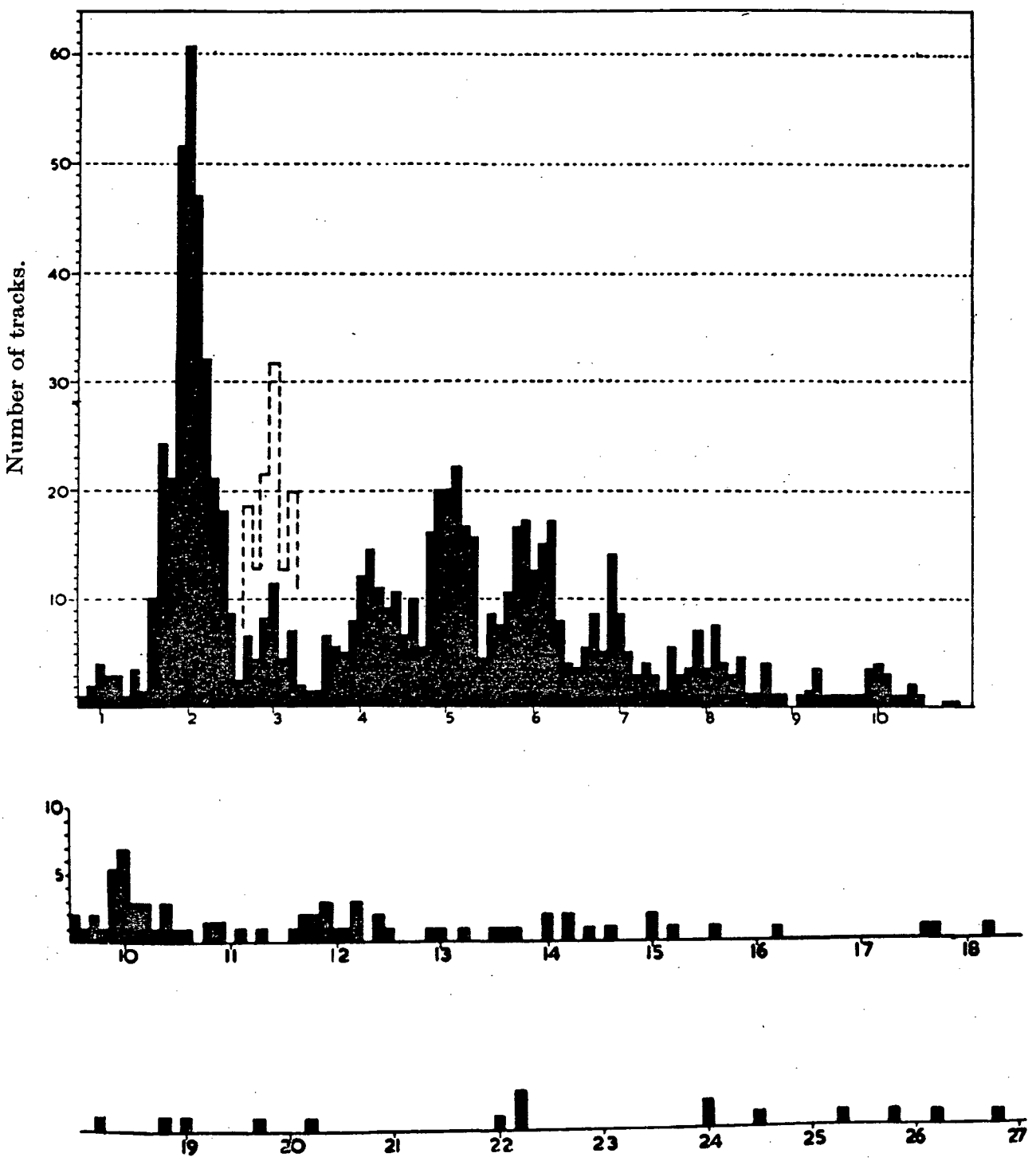

Fig. 1. Distribution of numbers of heavy particles in outer space (from Dainton, Fowler and Kent (1)).

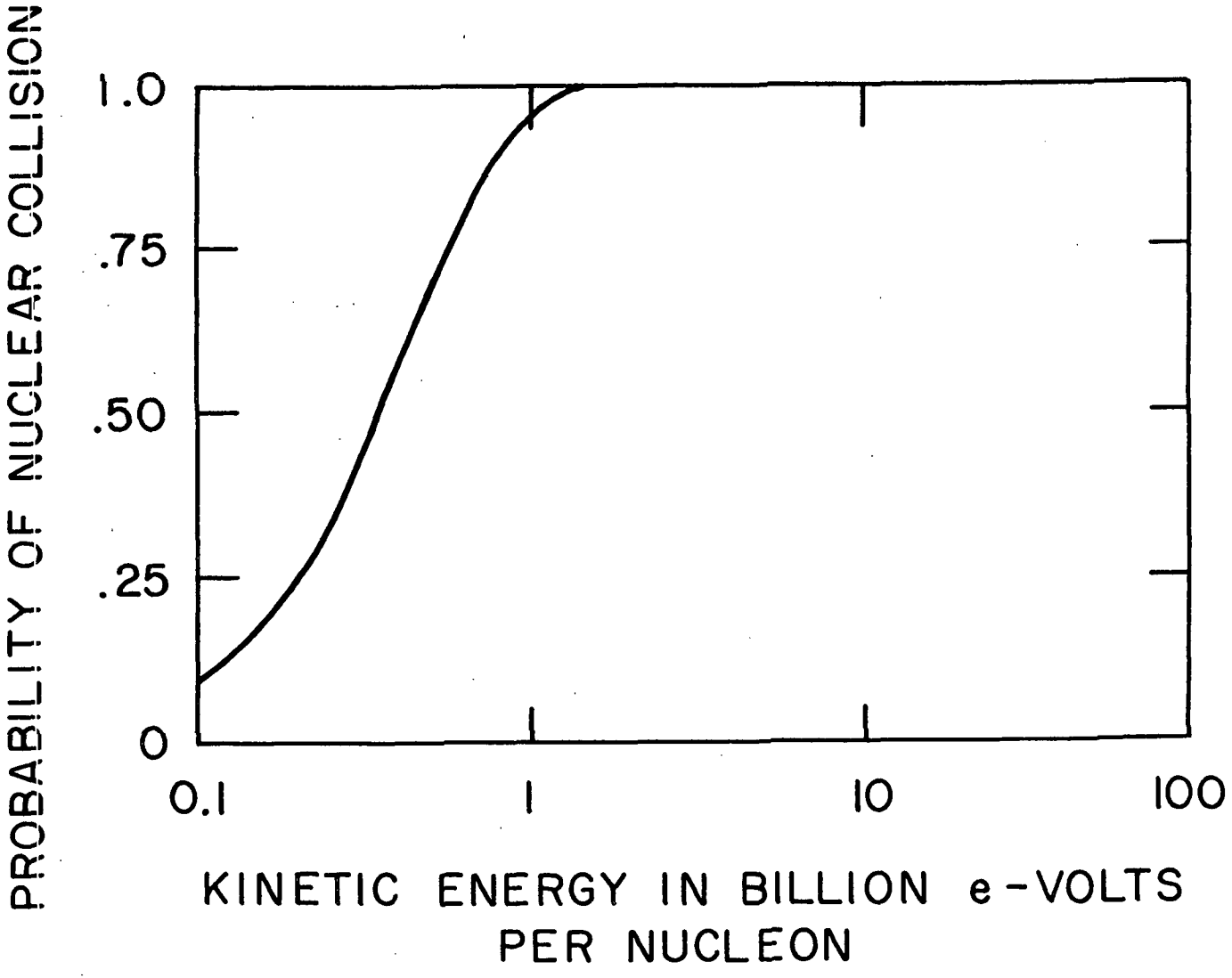

Fig. 2. Probability of a nuclear reaction as a function of energy for heavy particles (from Schaefer (2)).

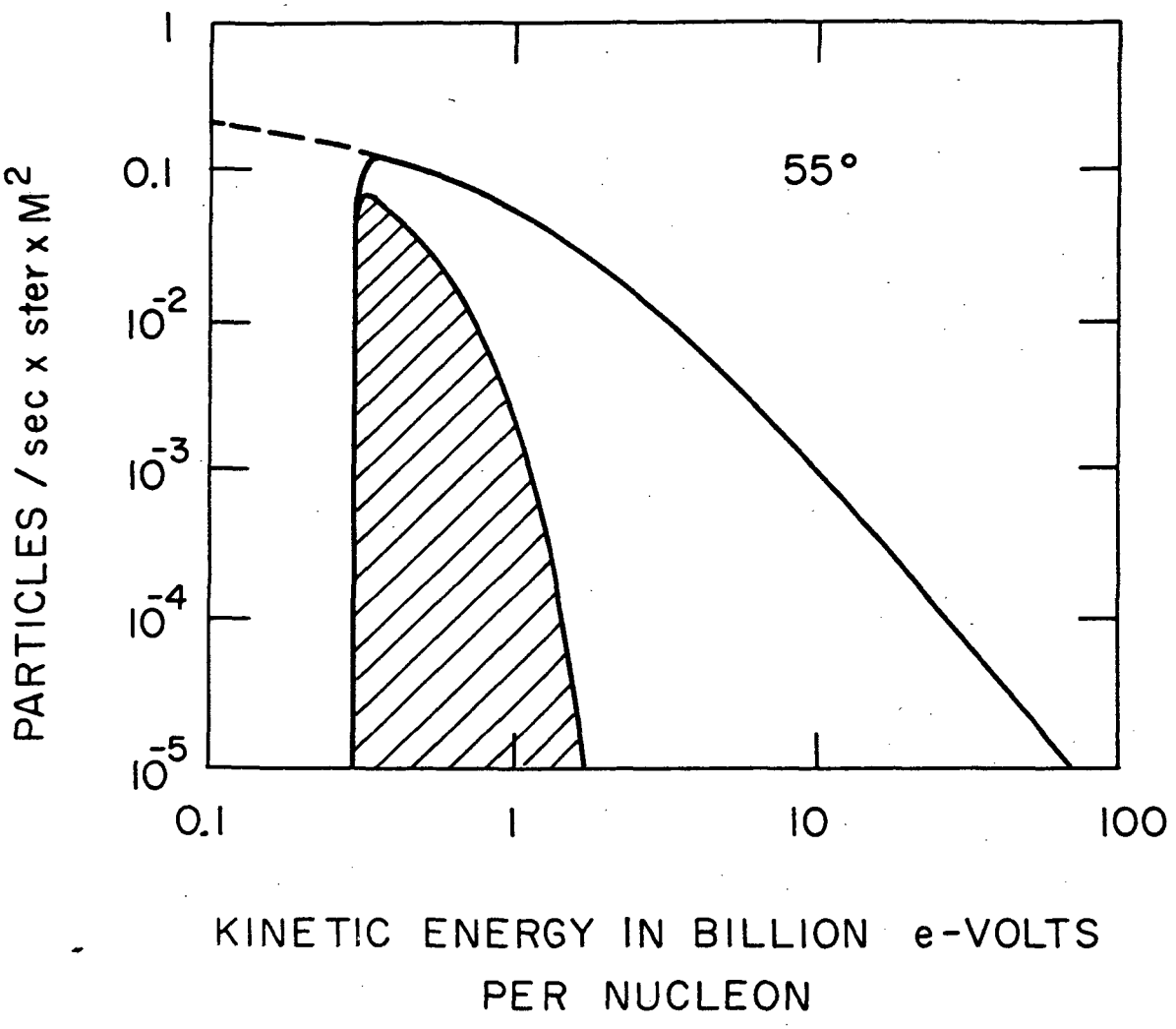

Fig. 3. Energy distribution of particles in the CNO group of primary cosmic radiation above the atmosphere at 55° latitude. The shaded portion indicates the numbers which will probably cause thindowns in tissue. At the polar region there would be no magnetic cut-off so the very low energy particles would be present, and the dotted line represents these additional particles present at the poles, and this same spectrum should hold true for outer space.

Fig. 4. Photograph of mouse exposed in balloon flight from Sault Ste. Marie in 1954 at an altitude of about 90,000 ft. for 35 hours (from Chase and Post (3)).

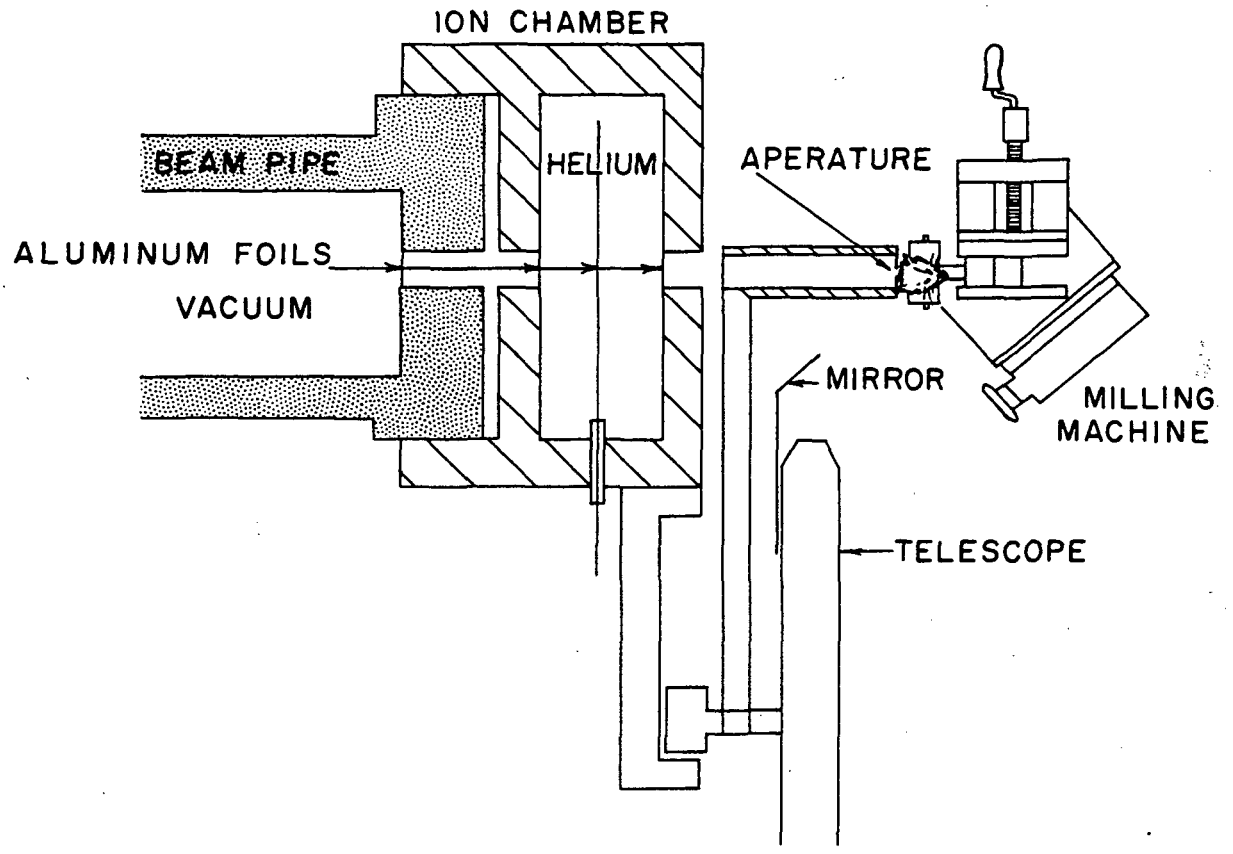

Fig. 5. Experimental arrangement for irradiation with the microbeam (from Baker, Curtis, Zeman and Woodley (4)).

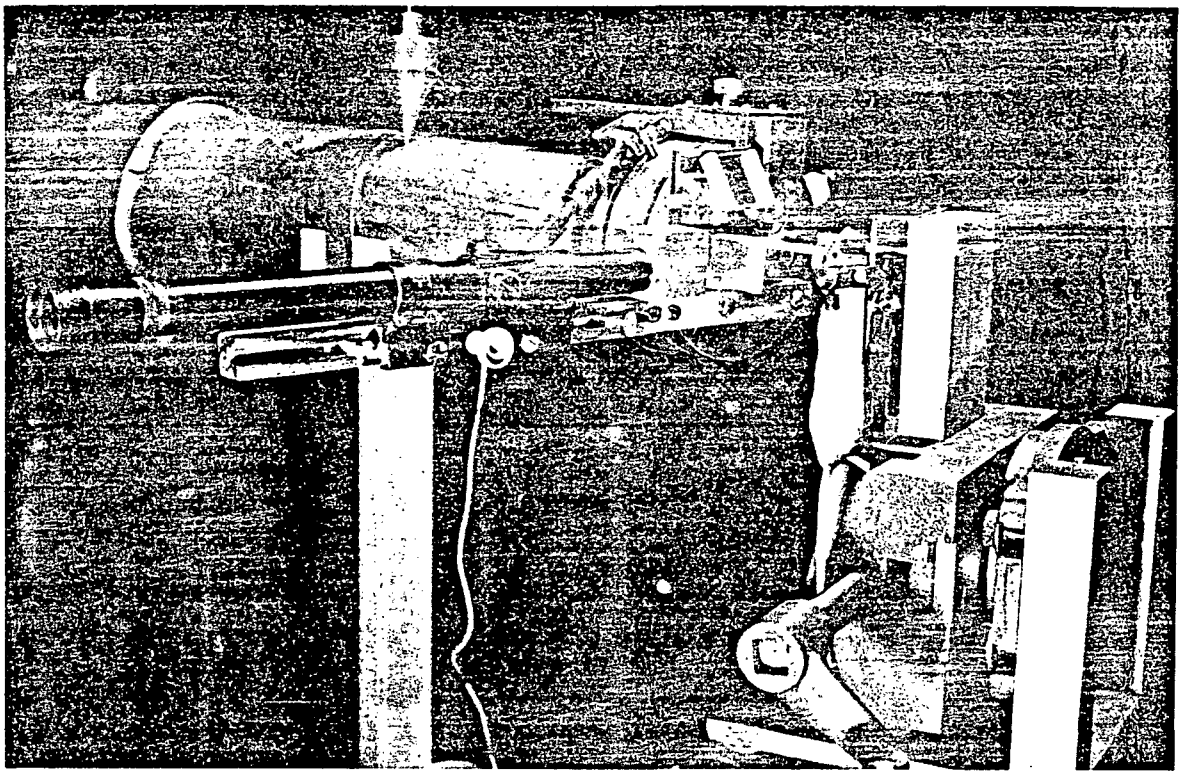

Fig. 6. Photograph of anaesthetized mouse in position for irradiation with the microbeam.

Fig. 7. Two exposures of the skin of a mouse through the 0.25 mm crossed slits with a dose of 800 rads. The marker spot is also visible (from Curtis (5)).

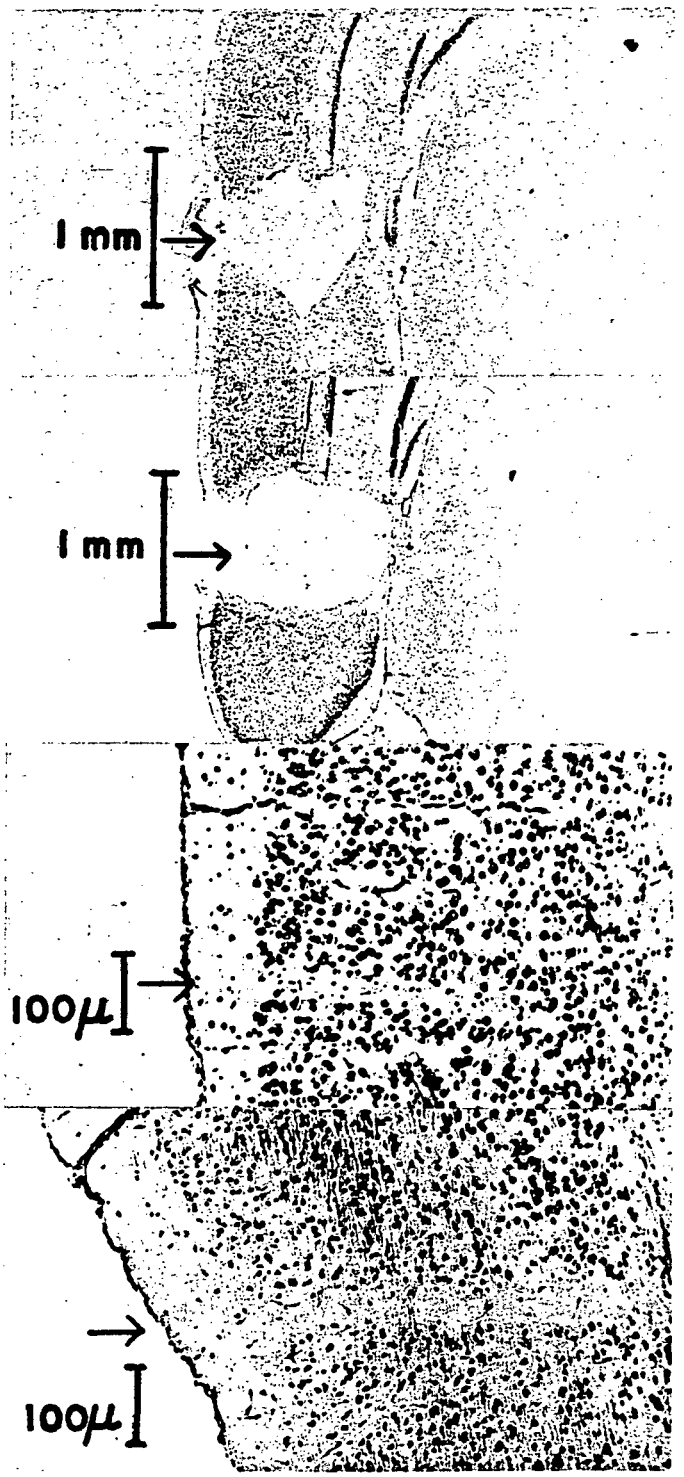

Fig. 8. Sections of mouse brain irradiated with deuteron beams. The arrows indicate the direction of the beam and the magnification can be judged from the scales (from Zeman, Curtis, Gebhard and Haymaker (6)).

Paper C-4

BIOLOGICAL EFFECTS OF HIGH ENERGY PROTONS

C. A. Sondhaus

Donner Laboratory
University of California
Berkeley, California

November 1962

ABSTRACT*

Proton fluxes of solar origin appear to constitute the main radiation hazard in space. Several semi-empirical experssions have been proposed to describe solar proton spectral energy distribution, and extensive dose calculations have been made on the basis of these estimates. Some uncertainties exist with regard to physical exposure factors, especially the variation of proton energy with time and the dependence of depth dose pattern on energy and exposure geometry. Similar uncertainties exist as to the degree of additivity of proton radiation doses both in time and with other stresses and as to differential effects between irradiated organ systems.

Since few terrestrial sources of proton radiation exist, radiobiological studies, especially on effects of high energy protons, have been rare. Existing data, which will be summarized, appear to indicate that protons of energies above about 50 Mev have an RBE close to 1, as would be expected on the basis of average LET distributions. Depth dose distribution may thus be a crucial factor determining degree of biological effect. Passage of the primary proton flux through shielding material or tissue also results in the production of secondary particles, including electrons, mesons, neutrons and recoil nuclei, as well as altering the proton energy distribution. Although it

---

*Presented by invitation at the Symposium on Protection Against Radiation Hazards in Space, Gatlinburg, Tennessee, November, 1962.

is to some extent possible to duplicate proton LET and depth dose geometry with gamma radiation, the secondary reactions comprise one of several reasons why biological studies with high energy proton beams are needed.

Total body irradiation of mice with 730MEV protons has yielded an RBE of 0.75 relative to 200 KVP X-rays and an $LD_{50(30)}$ dose of 775 rad for acute lethality, under conditions in which creation of secondaries was minimal and depth dose was uniform to about 5 per cent. The corresponding RBE found for splenic atrophy was about 1. In other experiments with primates, total body proton irradiation appeared to have an RBE of about 1 compared to Co^{60} gamma radiation.

Recent experimental data indicate that a peak of ionization, presumably due to secondary particles, occurs at a depth of about 30-40 gm/cm^2 when 730 Mev protons penetrate matter. Mouse studies are in progress at Berkeley to assess the radiological significance of this component. In addition, experiments with mice are under way to detect possible differences in organ mode of injury between protons and X-rays. Later series will include studies on the additivity of radiation dose and other stresses. All this work will be described.

At present, laboratory whole body exposure to a proton flux is impractical for large animals. Since exposures in space flight are almost certain to occur under omnidirectional conditions, and since a high but variable ratio of superficial to midline dose is expected to result from solar flare proton energy distributions, a means of irradiating large animals with the proton beam of the 184-inch cyclotron at Berkeley is being developed in such a way as to permit simulation of solar flare energy and geometry. Degradation of energy is brough about by a multiple Coulomb scattering target, with second-

otation of the animal around one axis normal to the beam and uniform rotation around the other, the angular dispersion produced in the emergent flux y the energy degradation process appears sufficient to generate isotropy ithout recourse to magnetic scanning or deflection techniques. Apparatus ow under construction, which will be described, should thus permit direct xperimental studies of biological effects, depth dose patterns and shielding onfigurations under approximately isotropic flux conditions.

BIOLOGICAL EFFECTS OF HIGH ENERGY PROTONS

C. A. Sondhaus

Donner Laboratory
University of California
Berkeley, California

November 1962

1. INTRODUCTION

It now seems quite probable that by the end of the present decade, manned lunar and deep-space flights will be a reality. These will certainly involve enorous difficulties and manifold hazards. The task which the biologist and the radiation physicist have to perform is that of developing an adequate understanding of the biologic effects of highly penetrating radiation, for it is evident that it is present everywhere in the vast reaches of space and must be reckoned with as soon as man leaves the protection of the terrestrial biosphere. Although it is not yet possible to define categorically the extent of the radiation problem in interplanetary travel, it is clear that the main component of the various space radiations is high-energy protons, particularly the intense proton fluxes which accompany visible outbursts from the sun. Because of the severe limitations in our ability to predict these phenomena or to carry enough shielding to eliminate their hazard, a basic inquiry into the biologic effects of high-energy protons is now of great practical importance.

In the relatively short time since this hazard has been known to exist, considerable effort has been expended in attempts to estimate the total dose that might be expected from proton irradiation in space. These efforts are hampered not only by the uncertainties in our physical knowledge of the energy-intensity-time relationships, but perhaps also equally by our uncertainty with regard to basic radiobiological parameters of proton exposure. It is not known, for example, whether dose rate, dose fractionation in time, combination of

irradiation with other physiological stresses, or mode of radiation injury to different organ systems in the mammal will modify biological response in the same way or to the same degree as has been found for other radiations. Such estimates as have been made are largely by calculation and extrapolation from other data, since there has been little opportunity to carry on controlled animal experiments in space and few sources of proton radiation are available for laboratory studies. It is the purpose of this paper to review some of the rather sparse experimental data which are already at hand, to summarize some experiments now in progress, and to report on some of our own work planned for the near future.

2. PHYSICAL DATA

On the basis of balloon and satellite data, Freden & White (1), Winckler (2), Bailey (3), Chupp et al (4) and others have proposed semi-empirical mathematical expressions to describe the energy and time distributions of solar flare protons. Evans (5) has presented the physical basis for a method of calculating the depth dose produced in a large volume of tissue irradiated omnidirectionally by an isotropic flux of protons of any energy or combination of energies. Schaefer, (6) using the assumed solar flare proton spectral energy distribution laws, has calculated the dose distribution in a spherical volume of tissue with and without a shield surrounding it.

Figure 1, from Schaefer, shows two of these energy distribution curves, illustrating the range of proton energy to be expected. Figure 2 shows the depth dose curves which he has calculated from these assumptions. It can be seen that great differences may exist in the distribution of dose with depth, and further that the vehicle shield or wall produces a marked hardening of the beam which penetrates it. The ratio of surface to midline dose can vary by a factor of 10 or more, depending on shield thickness and proton energy distribution. In Figure 3, an idealized set of curves of integral intensity vs time is shown, taken from the paper of Chupp, et al. It is seen that the high-energy

particles arrive earlier and persist for the shortest time; there is thus a shift of intensity with time for particles of a given energy and for the overall spectrum shape, making the net result rather complicated.

The importance of ionization density in relation to the biological effect of different radiations on mammalian tissue was realized in studies on whole mice and transplantable mouse tumors by Lawrence and others as early as 1935 (7). It was found at that time that the RBE of fast neutrons, will average linear energy transfer of about 20 Kev/μ, compared to 200 kv x-rays (average LET about 3 Kev/μ) was about 2. Since that time a number of studies have been made on the RBE of radiation with widely differing LET (8-10), and a rough pattern of the variation of RBE with LET has become evident. This is schematically indicated in the Figure 4. A few representative radiation types are marked along the abscissa at positons corresponding to their calculated average LET values. The work of a numberof investigators is summarized here, mainly from heavy particle studies on the Berkeley and Yale Hilacs together with some data on alpha particles.

The curve of RBE vs LET can apparently follow one of four different types with regard to the existence and height of a maximum, and the shape of the curve. The four rough categories are as follows: In curve I the RBE never exceeds one and decreases with increasing LET. This has been found to be the case with dry molecules, such as enzymes, and some phages and viruses for example. In the curve of type II, the RBE is found to peak at a value of about 2 for a LET between 100 and 200 keV per micron, and it falls below one thereafter. This behavior has been observed with small microbial and plant cells as well as with chromosome effects and mutations. The curve of type III shows a higher RBE than 1 for LET's of about 20 keV or higher, and again exhibits a peak in RBE in the LET range of 100 to 200 keV per micron, but this peak is now at a value of about 5. It then falls to 2 or 3 for higher LET radiation. Mammalian cells

appear to fall into this category, as do plant cells with large chromosomes, and the process of catacract formation for example. Dose rate dependence is observed here. In the type IV curve, the RBE reaches values beyond 10 at LET values of 100 or 200 keV per micron, but there are insufficient data at higher LET values to conclude even around LET values of about 10 keV per micron. This type of curve is seen with dried seeds and spores, also grasshopper heuroblasts, and the behavior seems to be related to special effects usually connected with a phase change or other physical variable.

In general, the curve of type III seems to be most pertinent to the case of human exposure to high LET radiation. Unfortunately, these data are not yet sufficient or accurate enough to draw clear-cut conclusions. It is to be expected, however, that not only dose distribution, but the distribution of LET will vary with depth in proton irradiation. Figure 5 illustrates Schaefer's calculation of the variation in specific ionization with depth in tissue for a proton beam of the energy spectrum prevailing in the inner Van Allen Belt. It is seen that the number of ion pairs produced per micron of tissue, which is related to LET, may be 5 or 10 times as high at the surface of the tissue as at the midline, depending on the thickness of the shield between the proton beam and the tissue surface.

It has been shown experimentally by J. Lyman and J. Howard in this Laboratory that ionization density builds up to a maximum value at some depth during the passage of a narrow beam of monoenergetic high-energy protons through an absorbing medium. This increase is probably due to the production of secondary protons as well as other charged particles including electrons, mesons, and recoil nuclei. At shallow depths, the ionization due to these secondary events more than compensates for the loss of ionization from reduction in primary beam intensity, the

latter caused by the inelastic collisions which produce the secondary events.

Figure 6 illustrates the effect of absorber thickness on beam ionization for lucite, lead and copper. It can be seen that the initial buildup of ionization in copper is higher than it is for lead, even though the ionization eventually falls off more rapidly. The converse is true for lucite vs lead and lucite vs copper.

These curves were obtained by placing successive layers of absorber between two ionization chambers aligned in the 730 meV proton beam of the 184-inch Cyclotron at Berkeley. They are plots of the ratio of the downstream chamber reading to the upstream chamber reading vs absorber thickness. In Figure 7, the full range of the 730 meV protons in lead is covered. A Bragg peak can be seen at the end of the range.

The prediction of secondary neutron spectra as well as other secondary particle fluxes produced by primary protons is described in the paper presented by Wallace in another session of this symposium. Of importance to the present discussion is the apparent contribution made by such secondary particle events to a dose component which is probably of high LET. This is present in addition to the calculated LET distribution of the primary proton beam whenever a thick shield or target is bombarded, and the influence of the higher LET component on biological effect needs to be evaluated under these conditions.

3. BIOLOGICAL STUDIES WITH HIGH-ENERGY PROTONS

a. Past Studies

A few studies on the biological effects of high-energy protons have been carried out in the past several years. In 1952 Tobias, et al, (11) exposed albino mice to 340 meV protons at the 184-inch Cyclotron in Berkeley, and made a

preliminary estimate of RBE, as having a value of "about 1" for $LD_{50(30)}$.

In 1960 at the Joliot-Curie Laboratory of the Institut du Radium in Paris, Bonet-Maury and collaborators (12) irradiated mice with 157 meV protons from their synchrocyclotron and determined an LD_{50} dose in eleven experiments on more than 500 animals. The proton beam was of circular cross section with a 90% isodose curve of radius 6 cm, determined photometrically by density measurement of photographic film exposed to the beam. Four mice could thus be irradiated simultaneously in thin perforated plastic tubes. It was estimated that the LET of the proton beam varied by about 10% during its passage through the animal in an anteroposterior direction. Dose rate was about 250 rad/min.

Litter-mate animals were used in the experiments. Following irradiation, the animals were weighed daily and the number of dead animals recorded. An eight-day LD_{50} dose was determined by log probit analysis.

Dosimetry of the beam was by both physical and chemical methods. An ion chamber with thin aluminum walls was used, containing air at atmospheric pressure. The total proton flux traversing the chamber during an experiment was calculated from saturation current measurement, and the isodose curves obtained photographically were then used to calculate the average flux through an individual animal and the corresponding absorbed dose. Aluminum and polyethylene mosaics were activated in the beam and the activity induced in each element was counted to check the photographic measurements. Discs of graphite were also placed with each animal and the C^{11} activity induced also served as a supplementary indication of dose. Ferrous sulphate dosimetry was also used; plastic tubes of the same size as the animals were filled with solution and irradiated in the same

way as the animals; dose measurement of optical density at 580 mμ was then made. Uniformity of dose among a group of animals was found to be within 5%.

The biological effects observed after proton exposure did not differ from those observed after exposure to x or gamma radiation: weight loss, anorexia, bloody diarrhea, etc., and reduction in general activity preceding death which occurred after the fourth day post-irradiation.

The $LD_{50(8\ day)}$ dose was found to be ± 80 rad. In order to determine an RBE, mice of the same lineage were exposed to 250 kv x-rays filtered by 0.3 mm Cu plus 2 mm Al, at a dose rate of 80 rad/min and a TSD of 46 cm. The $LD_{50(8\ day)}$ dose determined with 144 animals was 605 ± 30 rad. RBE of 157 meV protons compared to 250 kv x-rays was thus 0.77 ± 0.1. This value is close to the value of 0.7 observed for chromosome observations on vegetal cells of Allium and Vicia by Larsson and Kihlman, who used the 170 meV proton beam of the Uppsala synchrocyclotron in Sweden.

Zellmer and collaborators of the USAF School of Aerospace Medicine in San Antonio irradiated the eyes of forty-eight rhesus monkeys, macaca mulatta, with the 730 meV proton beam of the 184-inch Cyclotron at Berkeley, and found that the threshold dose necessary to produce clinical signs of injury was between 500 and 1000 rad. in comparison with Co^{60} gamma radiation an RBE of between 1 and 2 was estimated. (13).

In further experiments with primates this year, the same Air Force group, in collaboration with the Berkeley group, has studied total body radiation effects with 730 meV protons. Analysis of the data is not yet complete, but preliminary estimates indicate a $LD_{50(30)}$ of 395 rad for the 730 meV proton beam under essentially uniform exposure conditions. The dose rate was about 10 rad/min due to the scanning process

required for total body exposure of animals of this size. Figure 8 illustrates the pneumatic device which was developed by P. Bean and N. Yanni of UCLRL to enable the animal to be scanned by the small diameter beam.

Irradiation of this species with Co^{60} gamma radiation at a dose rate of the order of 100 rad/min indicated a $LD_{50(30)}$ value of 500 rad. The RBE thus appears to be around 1.4 for this end point, with most deaths occurring between seven and fifteen days post irradiation, suggesting an early bone marrow or late gut death. There is some evidence for a 20% dose buildup due to secondary particles.

These USAF primate studies are continuing with protons of other energies. 40 meV protons have been used at the University of Minnesota, 185 meV at the University of Uppsala, and 100 meV at Harvard thus far.

In a recent experiment with the 730 meV proton beam of the 184-inch Cyclotron at Berkeley, Wang, Lyman and Tobias (14) studied the RBE of 730 meV protons as compared with 200 kvp x-rays on mice following whole-body irradiation. The end points observed as indices of radiation lethality effects were a) the whole-body $LD_{50(30)}$; b) changes in spleen weight with dose following irradiation; and c) change in body weight with time after irradiation. Reproducibility of lethality experiments has been shown to be much enhanced with proper adherence to strictly controlled physical and biological experimental procedures and proper care of animals; the mice were therefore caged individually in labelled one-pint mason jars which were cleaned weekly and supplied with sterile wood shavings. Figure 9 illustrates the animal caging system. Namru strain Swiss mice white mice, random bred at the Laboratory were used--all five to seven weeks old, male

weighing 24 ± 5 gram. The mice were fed on Simonsen Laboratory white diet and water ad libitum.

Physical factors for the Phillips 200 kvp x-ray unit which was used were 200 kv, 15 ma, 0.25 cμ + 1.0 mm Al filter, for which the resulting HVL of the beam was 1.0 mm Cμ. A rotating positioning wheel was used; this is shown in Figure 10. The wheel rotated at 2.5 rpm and the dose rate delivered was 30 rad/min, as measured with a Victoreen condenser r-meter.

The proton beam was deflected from the Cyclotron, magnetically sorted and collimated by the quadrupole focussing method. After emergence from the vacuum system into the air, the protons form a nearly parallel homogeneous beam almost two inches in diameter. Slide 10 illustrates the exposure setup; a parallel plate ionization chamber of thin aluminum foils provided the dosimetry. As much as possible, the creation of secondary particles by passage of the beam through thick absorbers, as discussed earlier, was avoided in this experiment, and the ionization in the whole-mouse body was found by phantom measurements to be uniform within 5%. Dose rate was from 500 to 1000 rad/min, and each mouse was irradiated in an individual cylinder positioned in the beam by setting a wheel. In both x-ray and proton experiments twenty mice were exposed at each dose level; pre-and post-irradiation care was identical in both groups. The mice were followed for thirty days, dead animals were autopsied, and five of each group of survivors were sacrificed and the organs studied at the end of the experiment.

The resulting LD 50(30) for 730 meV protons was 775 rad, while that after 200 kvp x radiation was 580 rad (580 roentgens measured in phantom). Figure 11 shows the survival curves which were obtained. RBE of the protons relative to 200 kvp x-rays was found to be about 0.75. Since Upton et al (15) found about

the same RBE for Co^{60} gamma radiation in producing acute lethality in mice, this experiment suggests that the RBE of 730 meV protons is about the same as Co^{60} gamma rays, which is consistent with the findings that the respective LET distributions of the two radiations are quite similar.

Figure 12 shows the reduction in spleen weight observed at autopsy of those mice dead of radiation. More than 50% decrease in spleen weight occurred following similar doses of either x or proton radiation. RBE of 730 meV protons is about 1 compared to 200 kvp x-rays for splenic atrophy. More than 30-day survivors showed nearly normal spleens in both groups.

Figure 13 shows weight loss in the different dose groups with both radiations. Those mice which died always showed weight loss, in contrast to survivors. Rapidity of weight loss was directly proportional to the dose delivered. Both x and proton irradiated mice dying after irradiation showed a 25% weight loss during 13-16 days after 650-700 rads. The rapidity and degree of weight loss are an approximate index of RBE, which thus appears to be around 1 for this end point.

These results agree with the previous work cited earlier, using heavy particles with LET similar to 730 meV protons, as well as with earlier observations on high-energy deuterons. An RBE of less than 1 for 730 meV protons suggests that in spite of similar LET, the greater absorption in bone of 200 kvp x-rays may account for the lower proton RBE.

In order to study this question further, we are now beginning a series of experiments. In this study the time course of deaths is being followed in order to characterize the dominant mode of damage, with a view to distinguishing between "gut deaths" and "bone marrow deaths".

In the present study, in collaboration with J. Ashikawa, Simonsen Laboratory white Swiss mice have been used, all males 6-7 weeks old at irradiation and weighing 25 ± 4 gram. The animals were dipped on arrival and had been inoculated for ectomelia, a common problem in mouse colonies. Since dipping has been observed to produce a significant degree of spleen involution, the mice were placed in individual cages as described before and allowed to "come to equilibrium" physiologically for at least fifteen days. Diet and care were as previously described. At the time of irradiation, only those mice were selected which had gained weight or remained constant in weight.

Three dose rates were employed in the 730 meV proton irradiations: a) 1000 rad/min; b) 300 rad/min; and c) 100 rad/min. Exposure technique was as previously described. In the first two dose rate groups, total doses of 700, 800 and 900 rad were administered; in the 100 rad/min group, total doses were given of 600, 700, and 800 rad. The x-ray irradiation will be performed in two weeks. Both 100 kvp and 200 kvp irradiations are planned, at dose rates of 100 and 300 rad/min. We thus expect to allow for any dose rate effects which might appear.

Only preliminary impressions can be given here, as data is incomplete as yet. All mice irradiated in the first two dose rate groups have died within six days post irradiation. This strongly implies a predominantly gut death in these animals, with LD50 below 700 rad. This is to be compared with other experiments in which 250 kvp x-rays produced early gut death in mice only at total doses of 1200 rad whole-body; in the latter experiments, however, dose rate was presumably about 30 rad/min. An RBE for gut death somewhat higher than 1 for 730 meV protons is therefore suggested, but this may not necessarily be the case if dose rate differences are a factor. No definite conclusion can yet be drawn.

A series of additional mouse experiments is planned for the immediate future. In addition, several experiments with primates are planned in collaboration with Taketa et al of the Ames Laboratory biology group at Moffett Field. These studies will be aimed at answering several questions:

a. The transition curves for 730 meV protons indicate that a buildup of secondaries will occurr behind a shield. These are expected to have higher LET distributions than the primary beam, and hence to have higher RBE values, as previously mentioned. This effect can be studied with mouse exposures, and the first experiments will follow the present study. It should thus be possible to verify experimentally some of the effects predicted by calculation.

b. The additivity of two doses as a function of their separation in time will be studied in a further experiment, with the aim of estimating a recovery factor for high-energy protons in mice.

c. More detailed evaluation of hematopoetic criteria will also be made in future experiments. In addition, skin effects of both alpha and proton radiation will be studied as well as the degree of protection afforded by known agents. Finally, addition of other stresses such as temperature extremes or g-forces to that of radiation exposure will be studied.

4. MEDICAL CAVE MODIFICATIONS AT THE 184-INCH CYCLOTRON

The design portion of the modifications to be made on the Medical Cave at the 184-inch Cyclotron at Berkeley, California was started in February 1962. The aim of these changes was to permit high intensity proton irradiation of large animals. In order to perform whole-body radiation experiments with animals simulating solar flare radiation, two basic problems must be resolved.

The first is how to increase the beam intensity enough to give a reasonable exposure time. This can be accomplished only by the reduction of the amount of beam lost after it leaves the steering magnet. We propose to reduce the beam divergence by the use of a quadrupole magnet of large aperture (8-inch diameter) along with a larger aperture (8-inch diameter) beam tube. This will make it possible to focus the maximum number of protons on the target. This quadrupole magnet is on order. The design of the beam tube complex--including vacuum pipe, safety plug and a scattering target--is about 90% complete and about 50% of it is on order.

The second problem is one of protection of operating personnel from overdoses of radiation when such intense beams of protons are being directed into the Medical Cave. From our experience with such beams in the Physics Cave, we know that the present Medical Cave side walls must be increased to 12 feet equivalent of ordinary concrete, the back wall increased to 20 feet equivalent of ordinary concrete, the roof increased to 8 feet equivalent of ordinary concrete, and a solid shielding door provided. These increases amount to 140% for the side walls, 300% for the back wall, and 300% for the roof. Since the building is not large enough to accommodate a cave of adequate size with walls this thick of ordinary concrete, more massive material must be used so that a given amount of shielding may be obtained with thinner walls. This is being accomplished by using a U. S. Navy surplus steel and high-density aggregate concrete. The design, as shown in Figure 14, is complete, the required steel has been procured, the heavy aggregate is on order, and fabrication jobs for the required shielding blocks are out for bid.

The massiveness of the required shielding walls and the resulting increased floor loads necessitate reinforcing the floor in the Cyclotron building at the vicinity of the Medical Cave. A hydraulic-actuated door is available from the Physics Group; it requires a pit which can be provided when the floor is strengthened, and a slight modification to adjust it to the Medical Cave platform height. Designs on these modifications are complete, as are the designs of the platforms themselves, and both have been ordered.

The current schedule is to have all of the equipment available for installation by January 1963. This is based on the earliest possible shutdown, and depending on the Cyclotron schedule and overall modifications. It is estimated that a period of approximately three weeks will be required for installation.

Upon completion of the above modifications, it will be possible to irradiate up to a 300-pound animal with an alpha or proton beam under conditions simulating solar flare radiation. A whole body exposure of a large animal to an ommidirectional proton flux by use of the Cyclotron beam requires that certain criteria be met by suitable modifications in the beam characteristics. Among these are the following:

1. Beam Energy Variation

   Of several possible methods of producing variable energy proton beams, energy degradation by multiple coulomb scattering in passage through material appears to be most practical. Although intensity is lost and angular and energy dispersions are increased in a degraded beam, no modification of the accelerator magnetic field, or magnetic shielding-beam extraction techniques is required. Beam degradation thus does not

disturb the operation or construction of the cyclotron itself and experimental use can be achieved within a short time.

As scattering materials, lead, copper, aluminum, and carbon have been considered. Design calculations (16) show that degradation in graphite of the 730 meV beam to an energy of 100 meV, introduces an additional rms energy spread of less than ± 15 meV in the emergent beam, and less spread at higher degraded energies. Figure 15 shows that the rms angular dispersion of the emergent beam at this energy varies from 0.10 radian half angle for graphite to 0.36 radian for lead. Remanent intensity of the emergent beam after degradation to 100 meV is 7.5% for graphite and 16% for lead, as illustrated in Figure 16.

2. Broad Beam Geometry

In order to simulate a 4π or omnidirectional exposure, the usual narrow well-collimated beam emerging from the accelerator must be defocused or otherwise caused to diverge, or alternatively, must be made to scan the target by magnetic deflection. Here the angular dispersion introduced in the beam by scattering and energy degradation can be utilized. When combined with sinusoidal rotation of the target around one axis normal to the beam and uniform rotation around the other, the angular dispersion produced in the process of energy degradation appears sufficient to generate an isotropic exposure geometry, without recourse to magnetic scanning or deflection techniques. Figure 17 illustrates the animal rotator now under construction to serve this purpose.

It is concluded that sufficient angular dispersion is introduced by scattering in graphite to permit whole-body irradiation with target diameters up to three feet.

A hollow lucite sphere of this diameter containing an animal mounted in a frame can thus be rotated on the apparatus; Figure 18 illustrates the animal holder. The angular dispersion in graphite is low enough to compensate for its increased absorption loss at a given degraded energy, making graphite the scattering material of choice. The same conclusion is reached on the basis of the relative number of secondary neutrons produced in the scatterer, which is lowest for carbon.

The resulting proton energies and geometry of the exposure should simulate fairly adequately the solar flare condition by stepwise irradiation at several energies, thus permitting direct experimental study of biological effects, depth dose patterns, secondary production and shielding configurations.

This information will be of value not only in itself, but also in simulating space radiation exposure with Co^{60} or other radiation sources. The time available for biological research for the 184-inch Cyclotron is limited, but it is believed, nevertheless, that some important questions can be answered experimentally in regard to solar radiation problems with a relatively modest expenditure of time.

This study was supported by the National Aeronautics and Space Administration through the Atomic Energy Commission and Lawrence Radiation Laboratory, University of California.

REFERENCES

1. Freden, S.C. and R.S. White: Protons in the Earth's Magnetic Field; Phys. Rev. Letters 3, 9-10 (1959) and 3, 145 (1959).

2. Winckler, J.R.: This Symposium; see also Solar Influences on the Radiation Field in Space; Aerospace Med.32, 893-900 (1961).

3. Bailey, D. K.: Time Variations in the Energy Spectrum of Solar Cosmic Rays in Relation to the Radiation Hazard in Space; Nat'l Bureau of Standards, Boulder, Colo., 1960; see also Abnormal Ionization in the Lower Ionisphere Associated with Cosmic Ray Flux Enhancements; Proc. I.R.E. 47, 255 (1959).

4. Chupp, E.L., D.L. Dye, B.W. Mar, L.A. Oncley and R.W. Williams: Analysis of Solar Flare Hazard to Manned Space Systems; Boeing Report #D2-11608(1962).

5. Evans, R. D.: Principles for the Calculation of Radiation Dose Rates in Space Vehicles; Technical Report to the N.A.S.A.; A.D. Little Co. Report 63270-05-01, July 1961.

6. Schaefer, H. J.: Time Profile of Tissue Ionization Dosages for Bailey's Synthetic Spectrum of a Typical Solar Flare Event; U.S. Naval School of Av. Med.,Apr 4, 1962; see also Tissue Ionization Dosages in Proton Radiation Fields in Space; Aerospace Med. 31, 807-816 (1960).

7. Lawrence, J.H. and E.O. Lawrence: The Biological Action of Neutron Rays; Proc. Nat. Acad. Sci. 22, 124-133 (1936).

8. Storer, J.B., P.S. Harris, J.E. Furchner and W.H. Langham; The Relative Biological Effectiveness of Various Ionizing Radiations in Mammalian Systems; Rad. Res. 6, 188-288 (1957).

9. Fluke, D.J., A.C. Birge, J. Sayeg, T. Brustad and C.A. Tobias: Radiobiological Studies with Stripped Carbon Nuclei and Other Heavy Ions; Lawrence Radiation Laboratory Report UCRL-8078 (1958).

10. Brustad, T.: Study of the Radiosensitivity of Dry Preparations of Lysozyme, Trypsin and Deoxyribonuclease Exposed to Accelerated Nuclei of Hydrogen, Helium, Carbon, Oxygen and Neon; Rad. Res. Suppl.2, 65-74 (1960).

11. Tobias, C.A., H.O. Anger and J.H. Lawrence: Radiological Use of High Energy Deuterons and Alpha Particles; Am. J. Roent. Rad. Ther.Nucl.Med. 67, 1-27 (1952).

12. Bonet-Maury, P., A. Deysine, M. Frilley and C. Stefan: Relative Effectiveness of 151 Mev Protons; Comptes Rendus Acad. Sci.(Paris) 251, 3087-9(1960).

13. Zellmer, R.W. and R.G. Allen: Cosmic Radiation - Laboratory Observations; Aerospace Med. 32, 942-946 (1961).

14. Wang, C.C., J. Lyman and C.A. Tobias: Relative Biologic Effectiveness of 730 Mev Proton Particles for Acute Lethality in Mice; in Univ. Calif. Lawrence Radiation Laboratory Biol. & Med. Semiannual Report, Spring 1962; UCRL-10211, June, 1962.

15. Upton, A.C., F.P. Conte, G.S. Hurst and W.A. Mills: The Relative Biological Effectiveness of Fast Neutrons, X Rays and Gamma Rays for Acute Lethality in Mice (Abstract); Rad. Res. 3, 355 (1955).

16. Sondhaus, C.A. and R.W. Wallace: Solar Proton Exposure Simulation with the 184 Inch Cyclotron; Lawrence Radiation Laboratory Report UCRL-10447 (1962), (to be published); see also Wallace, R.W. and C.A. Sondhaus, This Symposium.

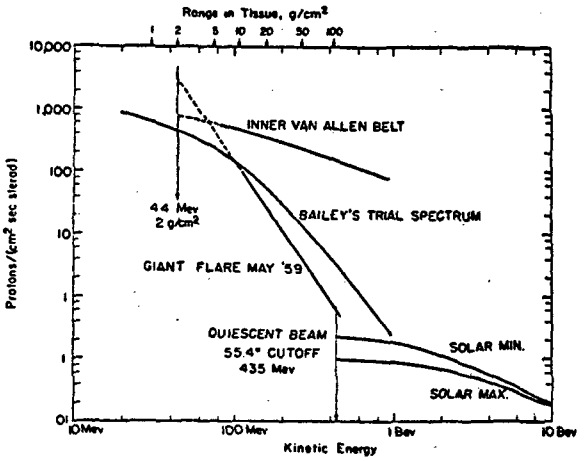

Fig. 1. Integral energy spectra of various proton radiation fields in space. Note enormous intensity of flare 59 spectrum observed at 55.4° magnetic latitude, i.e., in a magnetically forbidden region.

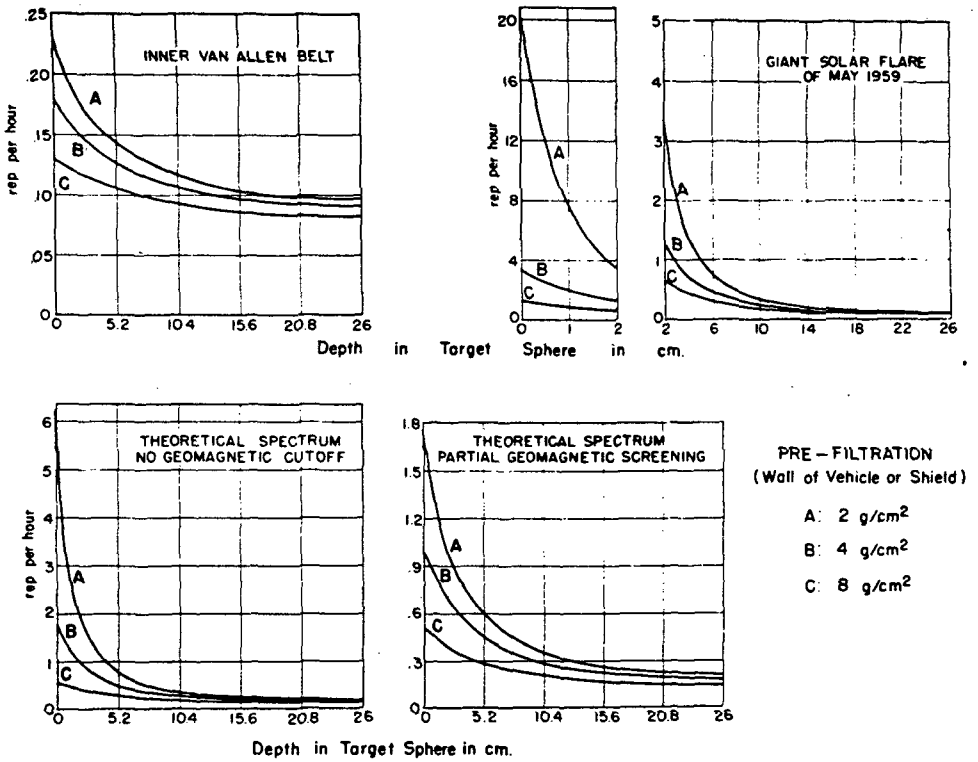

Fig. 2. Depth dose curves resulting from assumed solar flare energy distributions, as calculated for a spherical tissue volume (Schaefer).

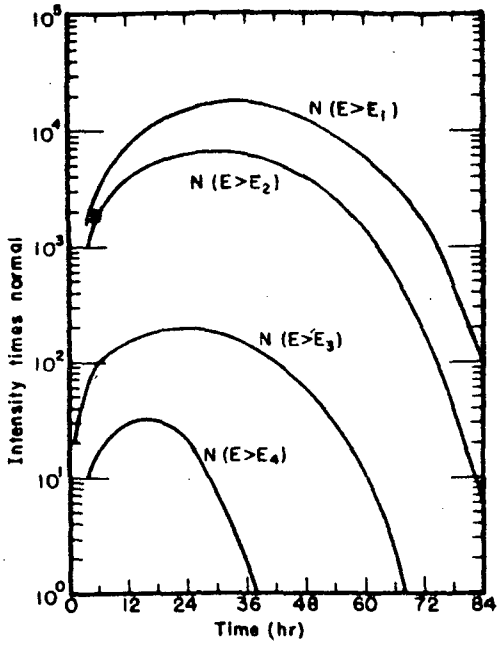

MU 26661

Fig. 3. Idealized set of curves of integral intensity vs. time (Chupp, et al.)

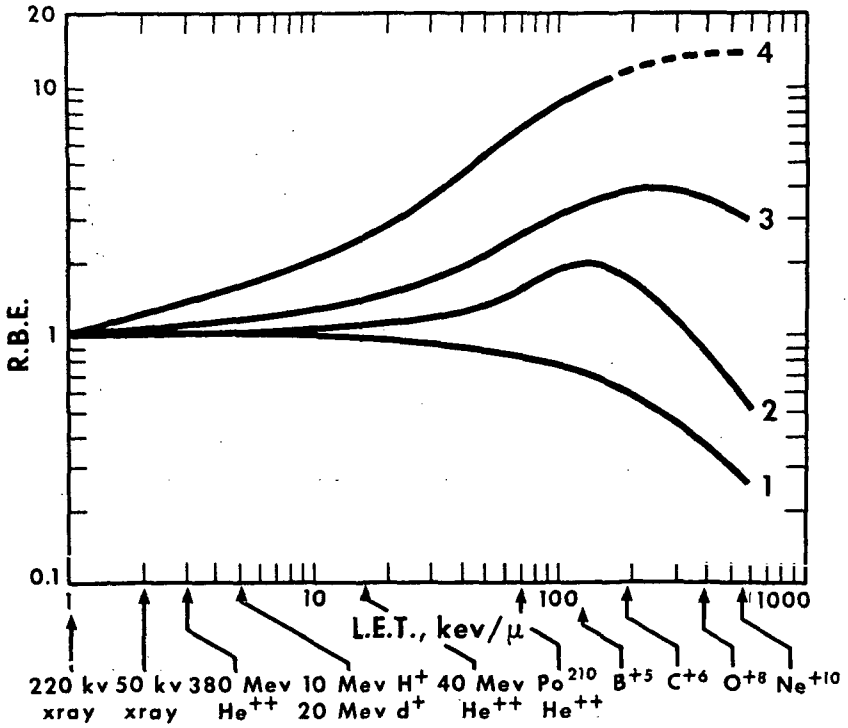

Fig. 4. Variation of Relative Biological Effectiveness with Linear Energy Transfer of radiation (idealized).

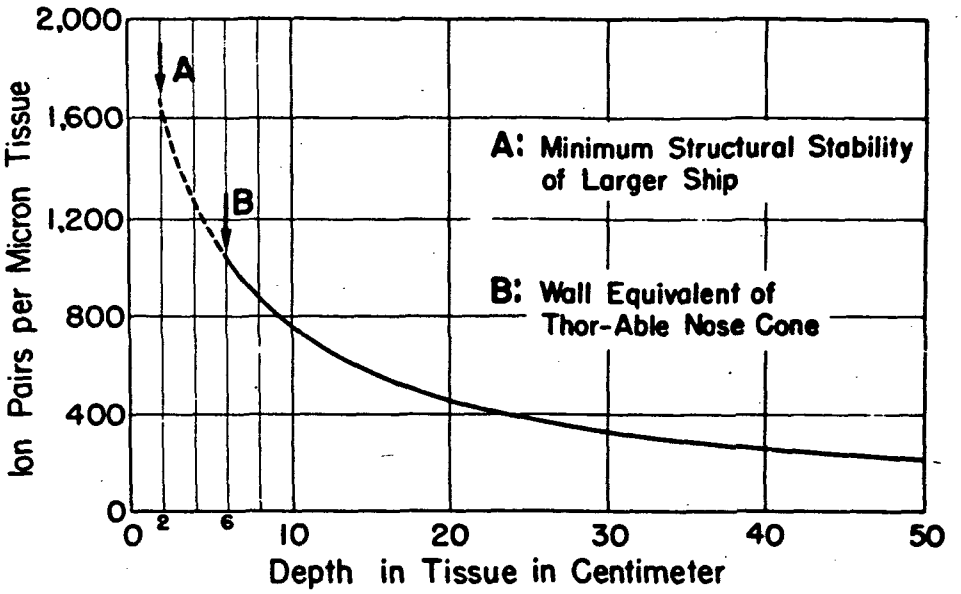

Fig. 5. Specific ionization vs. tissue depth for an assumed proton energy spectrum in Van Allen Belt (after Schaefer).

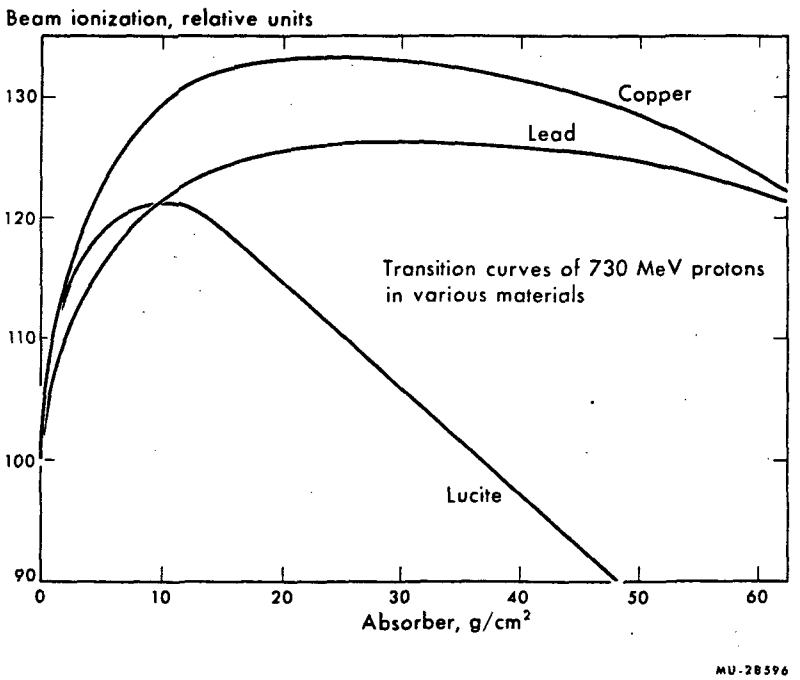

Fig. 6. Transition curves of 730 MeV protons in various materials.

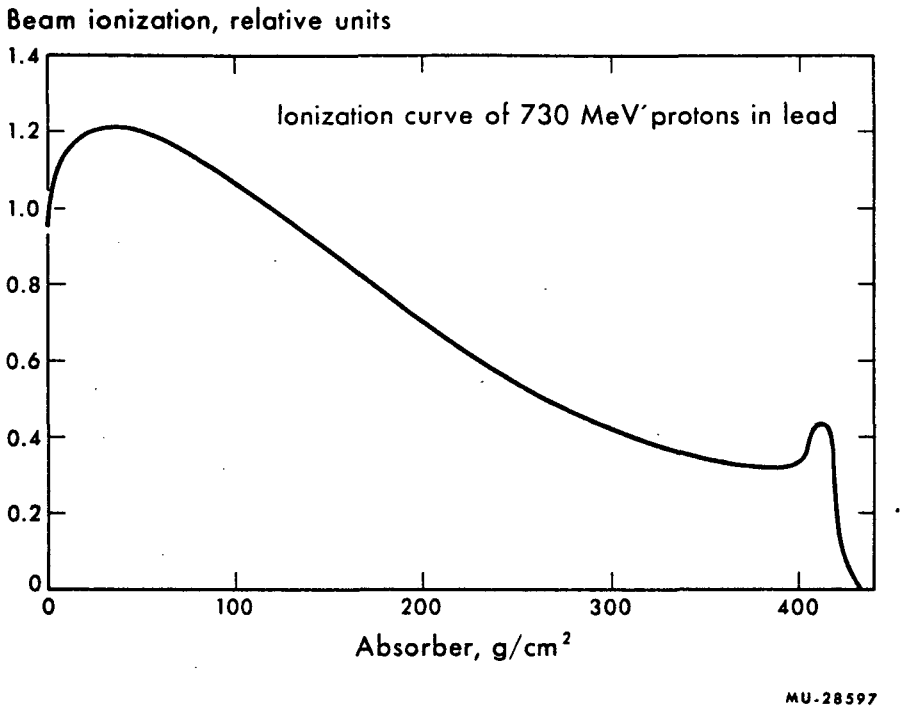

Fig.7. Transition curve of 730 MeV protons in lead - beam ionization vs. absorber thickness over full range.

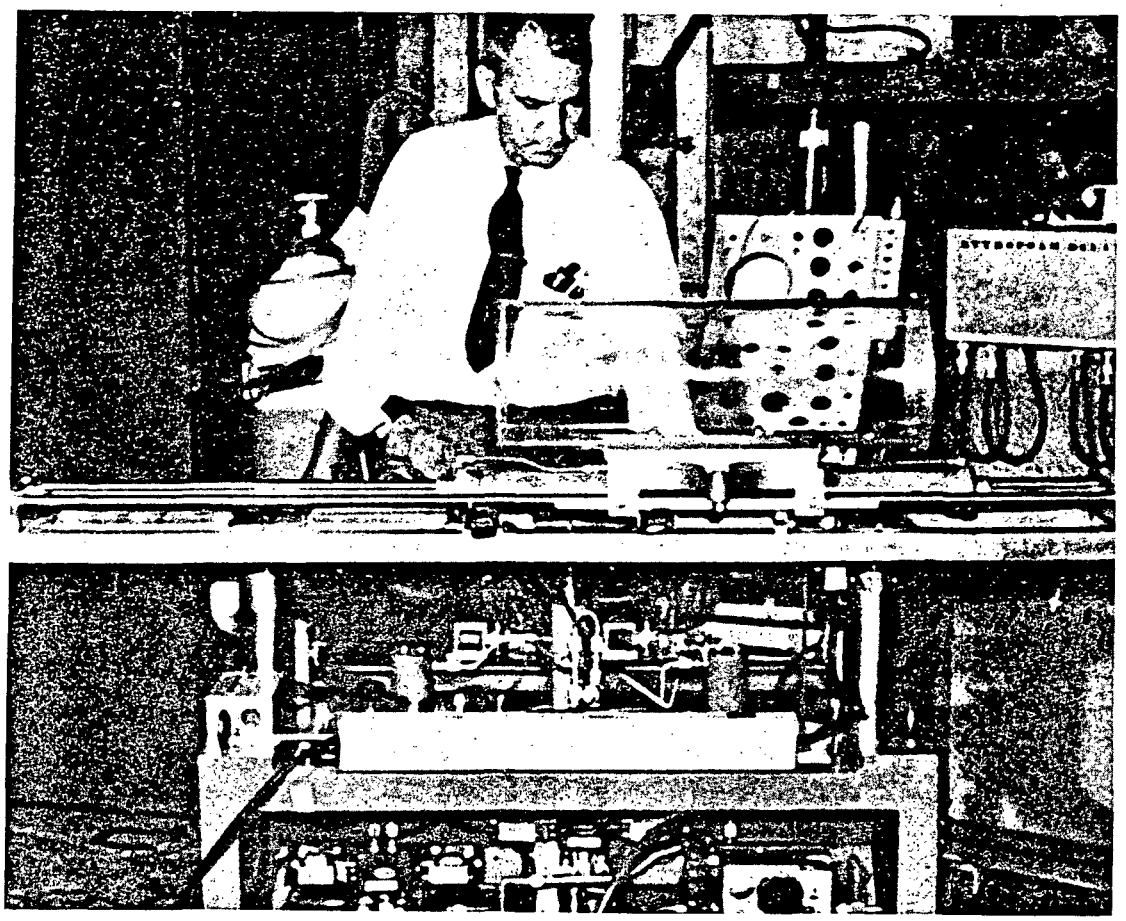

JHL-3048

Fig. 8. Pneumatically driven animal scanner for primate studies with 184" cyclotron proton beam.

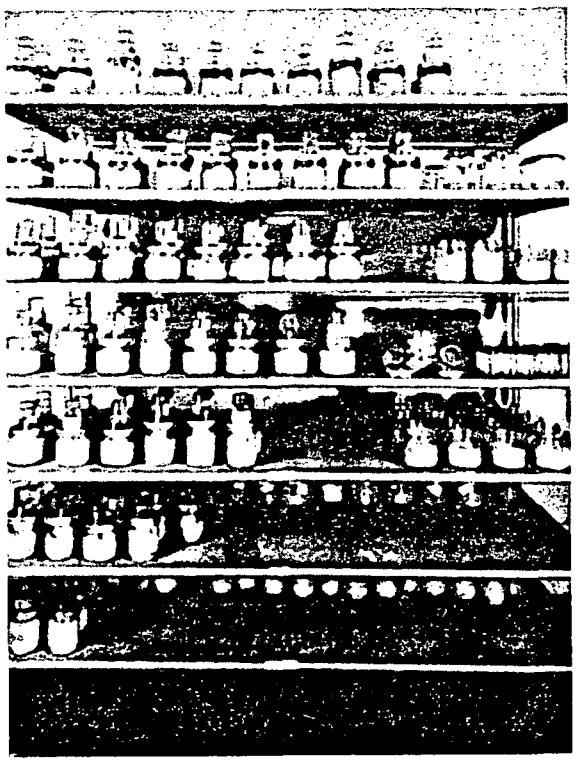

JHL-3167

Fig. 9. Individual caging system for proton-irradiated mice.

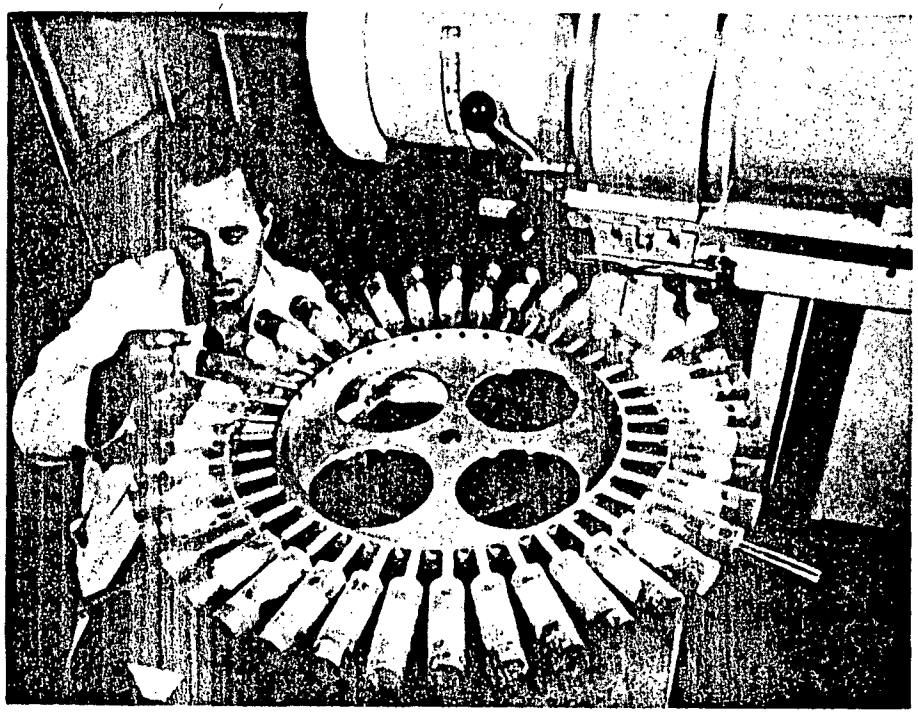

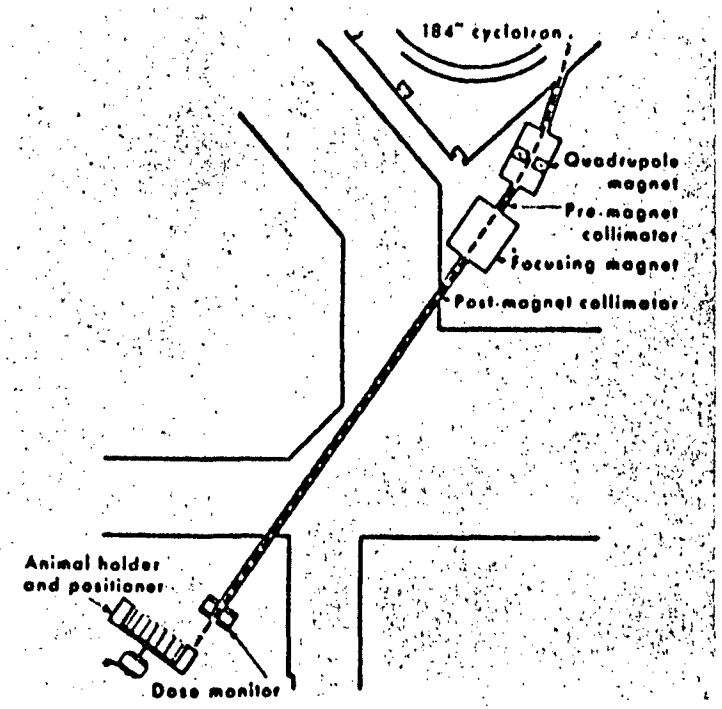

JHL-3173-C MU 27193

Fig. 10. (Left) Mouse irradiation wheel for X ray control experiments; (Right) Exposure setup for mouse irradiation with proton beam. The X ray wheel has now been converted to a positioner to increase maximum possible dose rate during irradiation. The proton beam mouse positioner exposes the animals postero-anteriorly, the X ray positioner dorsoventrally.

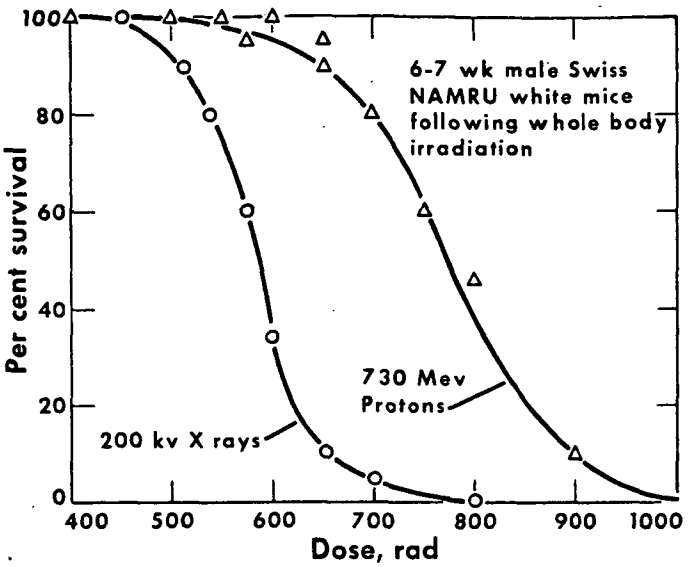

MU-27077

Fig. 11. Survival curves for proton irradiated and X irradiated mice.

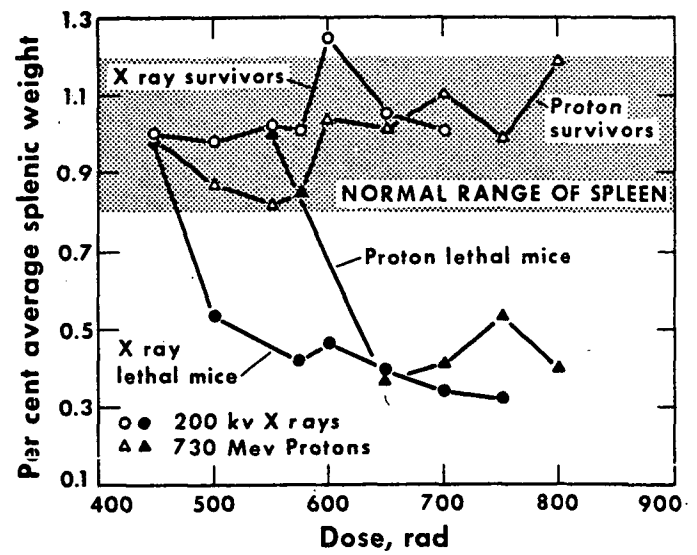

MU-27078

Fig. 12. Reduction in spleen weight for proton and X ray irradiated mice.

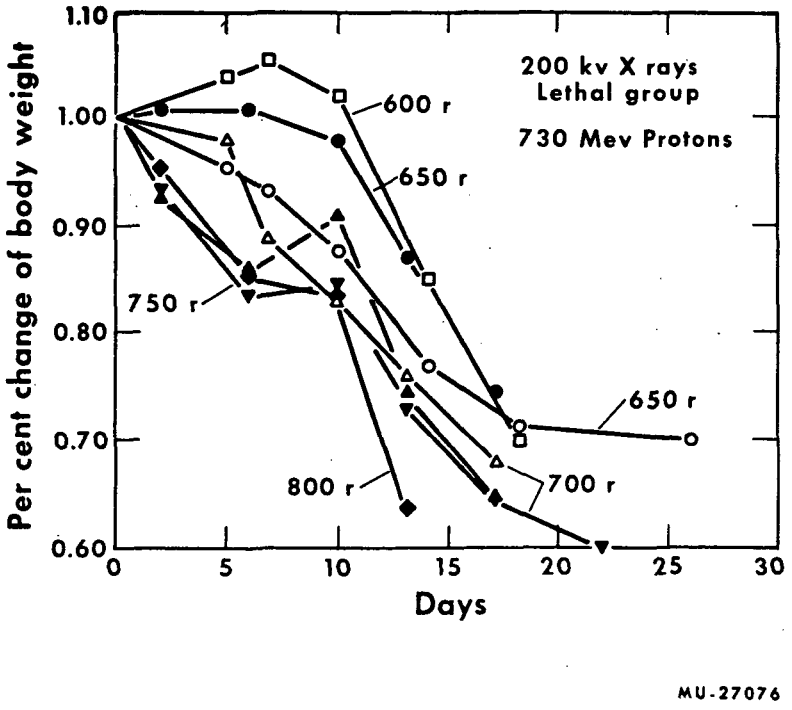

Fig. 13. Post-irradiation weight loss in proton and X - irradiated mice.

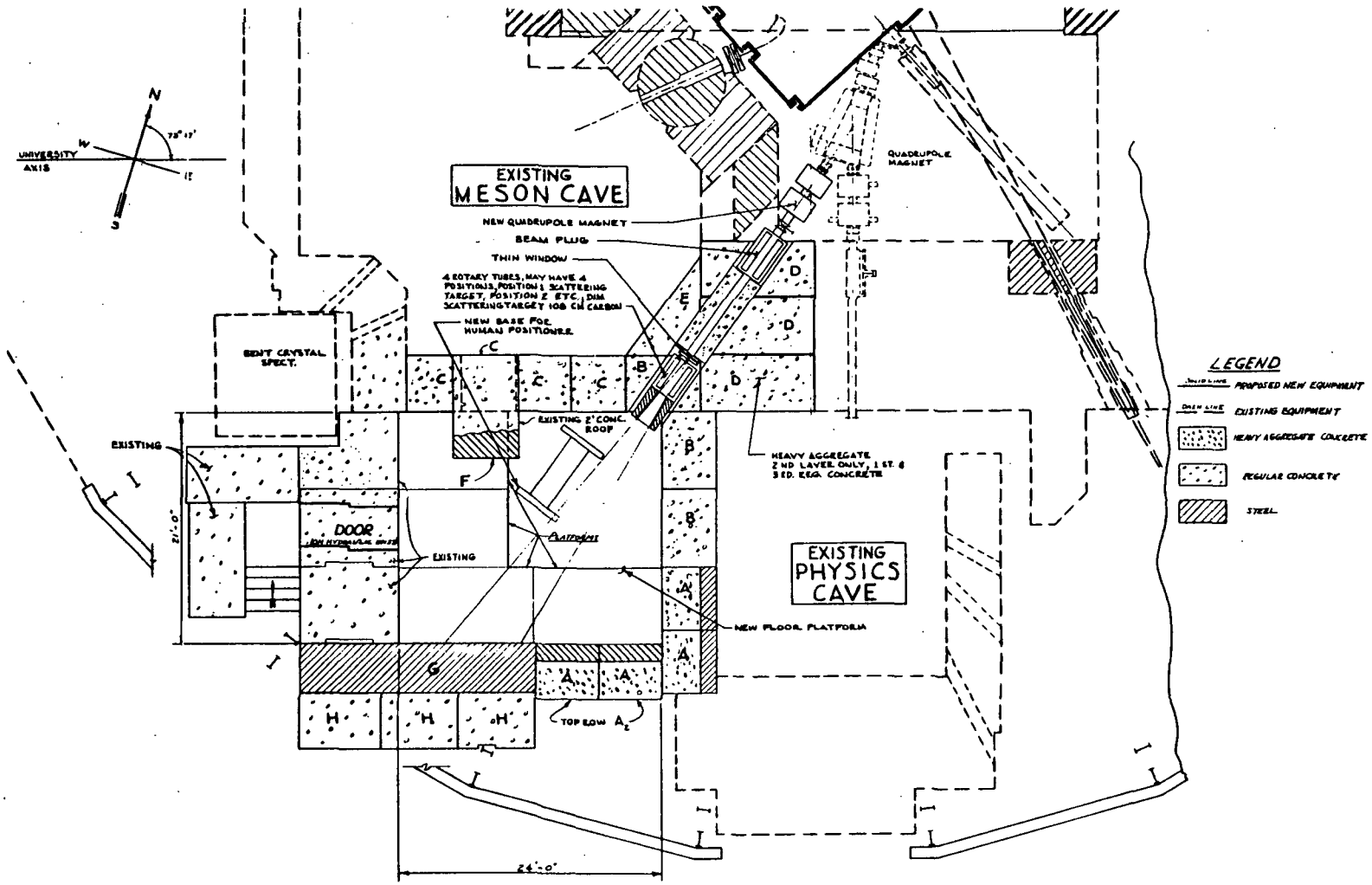

Fig. 14. Redesign of medical cave, 184 inch cyclotron, Berkeley.

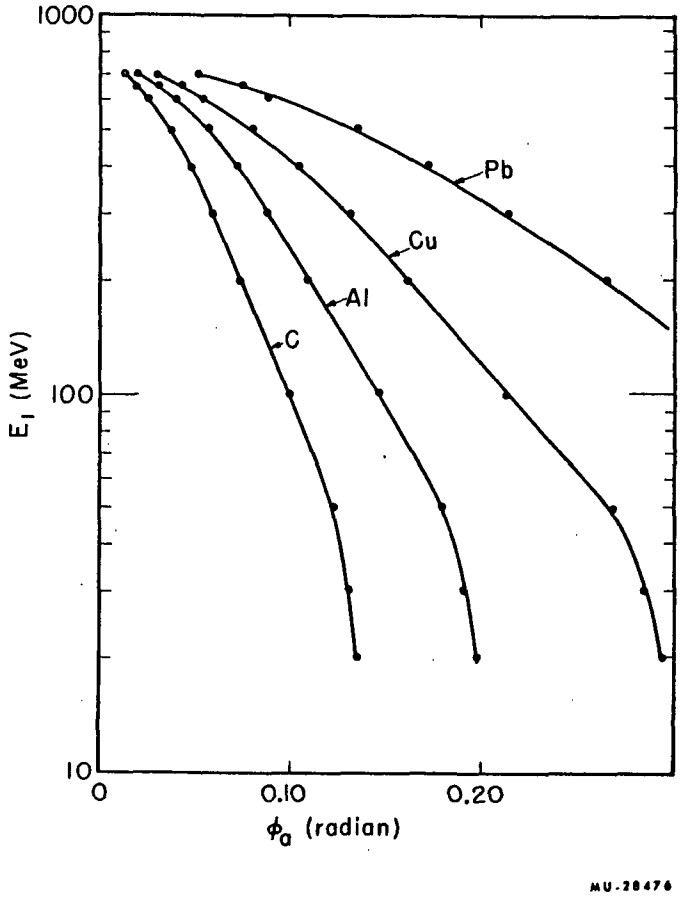

Fig. 15. Root-mean-square angular dispersion of emergent proton beam after degradation from 730 meV to 100 meV in various materials.

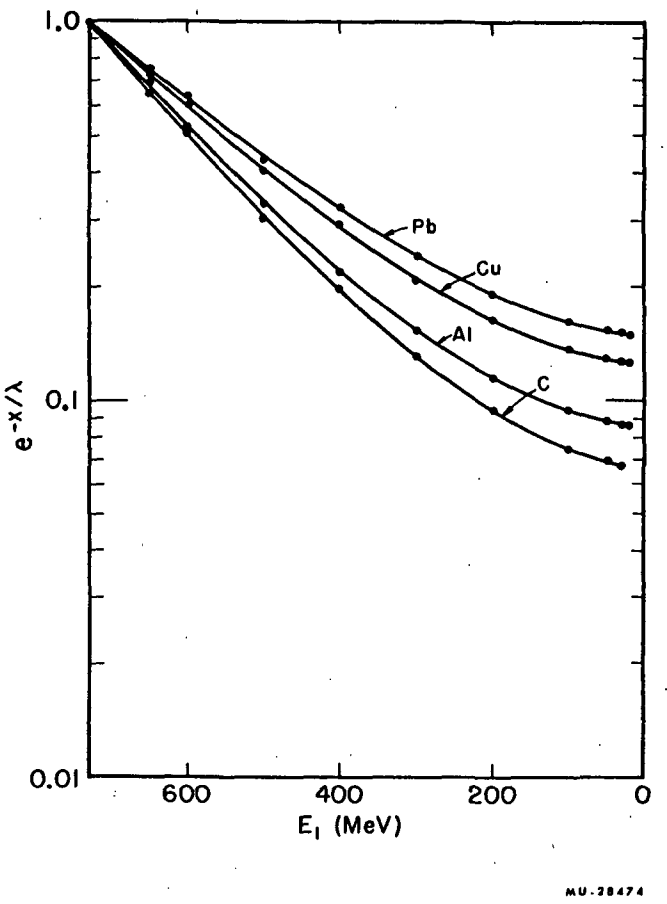

Fig. 16. Emergent proton beam intensity (fractional) after energy degradation from 730 to 100 meV in various absorbing materials.

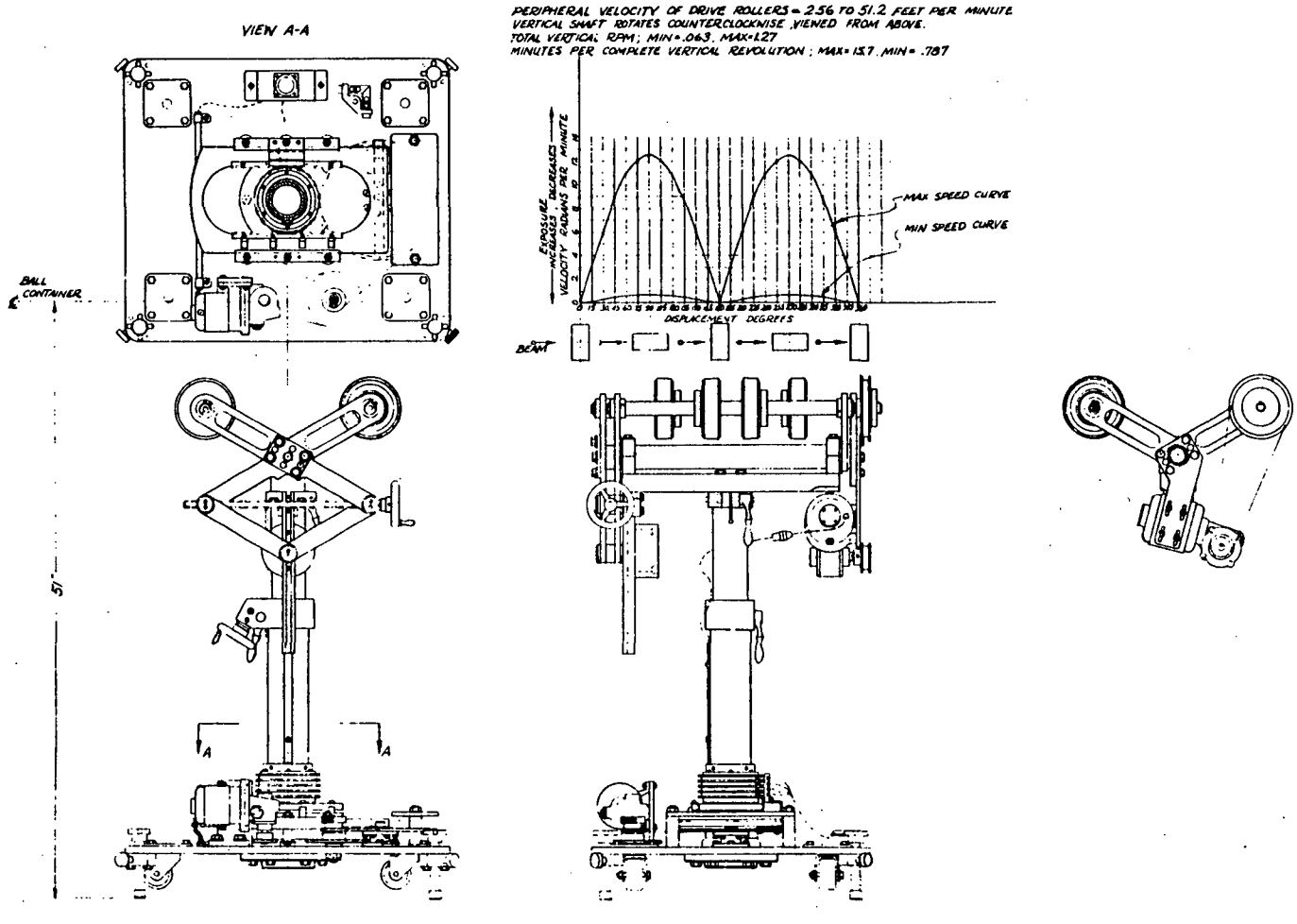

Fig. 17. Animal rotator for omnidirectional exposure of large animals to divergent, energy-degraded proton beam of 184" cyclotron, Berkeley.

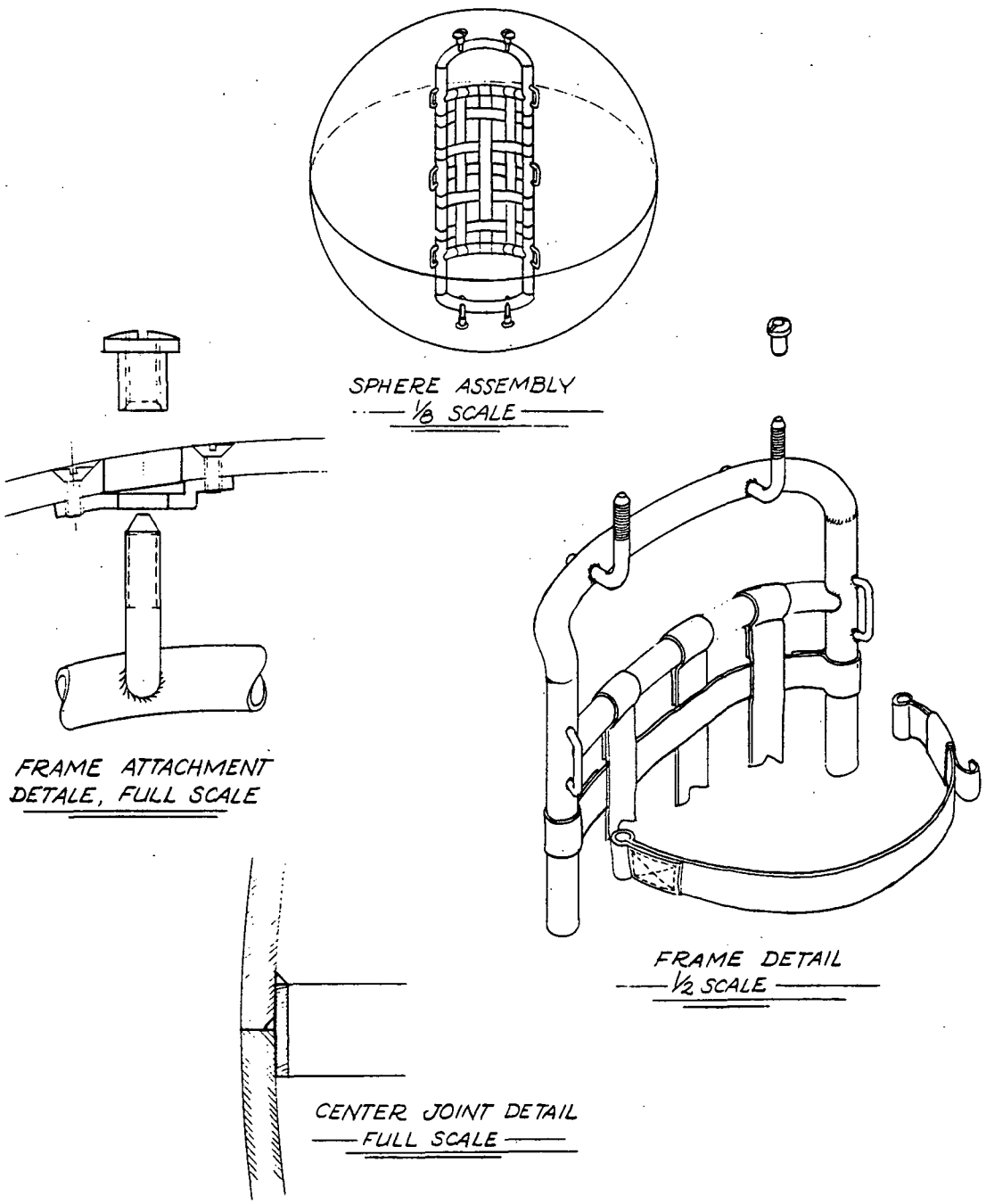

Fig. 18. Detail of animal holder, omnidirectional exposure apparatus for large animal proton irradiation.

Paper C-5

EFFECTS OF ACUTE RADIATION EXPOSURE ON HUMAN PERFORMANCE

R. B. Payne
USAF School of Aerospace Medicine

A literal and parsimonious interpretation of the assigned topic would allow the speaker to fulfill his obligation quite honestly in approximately four seconds, or about as long as one might require to say, "There are no effects as far as we know." But this response would leave us far from satisfied, and it would create the false impression that the problem had been studied exhaustively throughout all the critical categories of behavior under various kinds, rates, and amounts of ionizing radiation. The distressing fact is, of course, that only two systematic human studies on this subject have been reported in the Western literature, and these can scarcely be said to provide a useful grasp of the total problem.

Under the circumstances, therefore, it has seemed appropriate to broaden the empirical base of this discussion by reference to studies of lower animals. As many of you know, the Radiobiology Laboratory at Austin, Texas, operated jointly by the USAF School of Aerospace Medicine and the University of Texas, has devoted a prominent share of its energies over the past ten years to systematic studies of radiation effects on the behavior of M. mulata; and laboratories elsewhere have fed the burgeoning literature with behavioral studies of mice, rats, and dogs. Perhaps there are conditions and assumptions under which we should be willing to consider at least the infrahuman primate studies for whatever

implications they may have for the behavior of man.

First, however, there is a sense of obligation to explain the rationale for the study of behavior in a radioactive environment. What can such studies tell us that we cannot learn merely by observing the impact of ionizing radiation on the cells, tissues, and organs of the body?

Why Study Behavior?

The principal reason for sending man into the aerospace environment is to take advantage of his abilities and skills as an equipment operator, a trouble-shooter and maintenance specialist, an observer and interpreter of dynamic situations, and a maker of decisions. Mercury flights have already shown the operational flexibility which can be realized by including man as a system component, and the operational plans for such systems as Gemini and Apollo have already been modified to take advantage of this versatility. In other words, man's capabilities are operationally important and without substitute, and we must therefore be concerned about their preservation.

Man's capabilities are joint functions of many determinants, including, but not limited to, the functional properties of biological components and systems. Since biological components and systems constitute the targets of ionizing radiation, one might be tempted to argue, as indeed many have argued, that their study would provide a sufficient basis for inferences about the fate of behavior. Unfortunately, even after nearly a century of serious effort on the part of many scien-

should start with the human studies.

Human Studies

The Houston Studies

Background. The two experimental human studies were initiated in 1951 at the M.D. Anderson Hospital and Tumor Clinic of Houston, Texas, for the purpose of charting the effects of low-level ionizing radiation on some of the psychomotor capabilities relevant to the operation of aircraft. The director and staff of the hospital had long been interested in the comparative value of radiotherapy and chemotherapy for the treatment of generalized neoplastic disease, and they foresaw no valid criticism of collateral studies of biological and behavioral changes subsequent to the routine application of radiotherapy. All realized, of course, that ethical and moral considerations would necessitate compromises with some of the principles of experimental design. For example, medical considerations required that patients be assigned to treatment levels in accordance with professional judgment as to the severity of disease. Thus, the inability to employ random or stratified assignment methods virtually guaranteed some likelihood of confounding disease effects and treatment effects on the dependent variables. Further, language barriers, both of degree and kind, precluded the study of cognitive functions with available materials in which verbal comprehension occupied a central role. Despite such limitations, all agreed that the studies were feasible and desirable, and that negative results could be meaningfully interpreted and practically significant, even if

tific disciplines, we have not yet acquired more than a few of the concrete details about the way in which somatic events participate in behavior, although perhaps we have learned a great deal about the explanatory sterility of certain viewpoints. One consequence of our continued ignorance of these matters is that we are unable to forecast changes in behavior from observed changes in somatic functions with sufficient accuracy to predict the operational impact of biological damage, except, of course, under conditions of extreme insult. It is necessary, therefore, to observe and measure behavior directly in order to be able to say what is going to happen to it under specified exposure conditions. An ancillary product of such efforts may well turn out to be a better understanding of relationships between behavior and those events which occur inside the skin.

The foregoing premises have served as the foundation for modest but aggressive research efforts concentrated primarily at the USAF School of Aerospace Medicine. Such efforts have not been widespread among universities and other scientific institutions, for the resource requirements are formidable, and the monotonous occurrence of negative results soon blunts the enthusiasm of all but the most operationally minded investigators. Consequently, progress toward the achievement of a thoroughgoing research program has been slow. Many gaps are painfully evident, particularly with reference to dose dependency functions, relative behavioral effectiveness of different kinds of radiation, adequate coverage of the behavior spectrum, and the interactions of radiation effects with those of other stressors. Nevertheless a substantial amount of work has in fact been accomplished, and our review of it perhaps

the converse were not necessarily true.

Within the foregoing circumstances, two studies became possible throughout the next five years by virtue of close collaboration between the hospital and the USAF School of Aviation Medicine (Payne, 1959). The first study was concerned with the question whether a given air dose would have a greater effect when delivered in a single exposure than when delivered in a series of fractional exposures. The second study was organized as a straightforward dose-response study extending to relatively high exposure levels.

First Study. The first study was organized about the therapeutic circumstance that certain patients were treated with whole-body doses delivered in single exposures, while others were given equivalent total exposures in five equal increments separated by intervals on one hour. Psychomotor performance data obtained from both types of patients made it possible to test the prediction that performance level would be an inverse function of total dose, moreso with concentrated dosage than with temporally distributed dosage.

Subjects were male adults, usually in advanced stages of neoplastic disease not correctible by surgical intervention or localized radiation therapy. Ages ranged from 19 to 76 years.

Three well-known perceptual-motor tasks served as criteria of treatment effects. The USAF SAM Complex Coordination Test, shown in Figure 1, required the subject to coordinate the movements of a stick and rudder bar in order to match successive positions of three red lights with three green lights. Score consisted of the number of matches accomplished within standardized trial periods. The USAF SAM Two-Hand Coor-

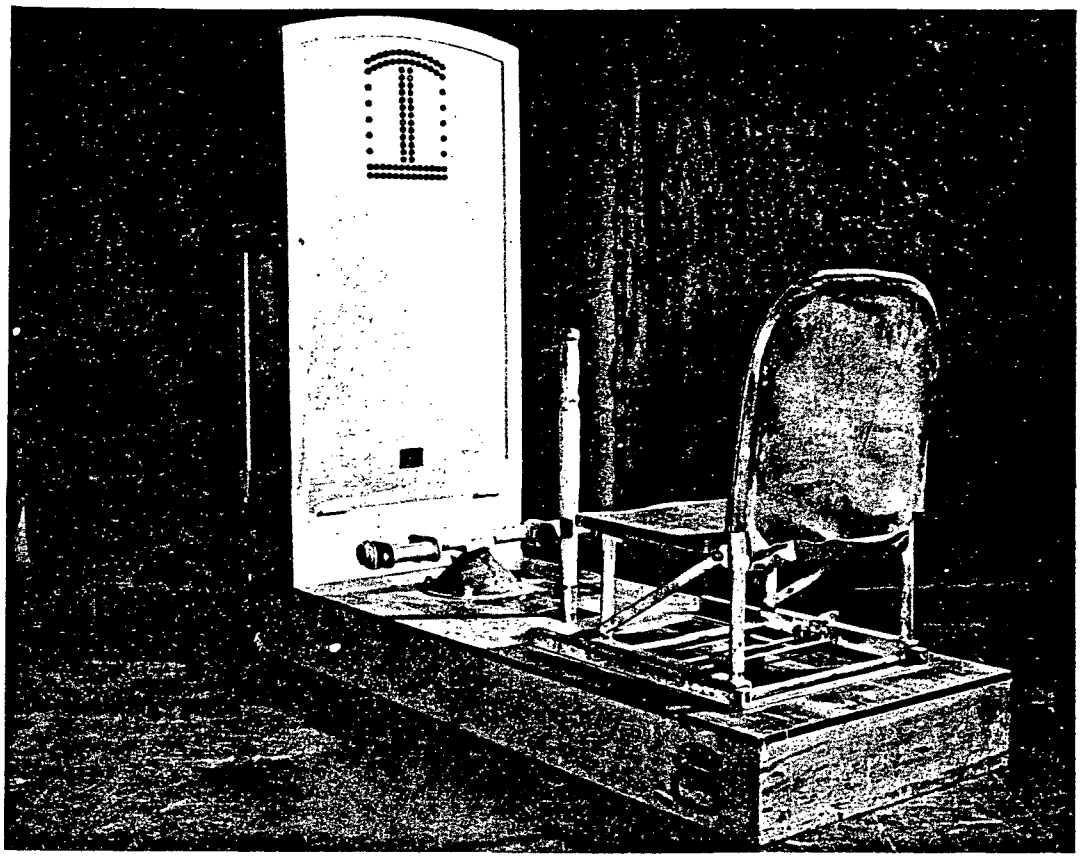

Figure 1. USAF SAM Complex Coordination Test

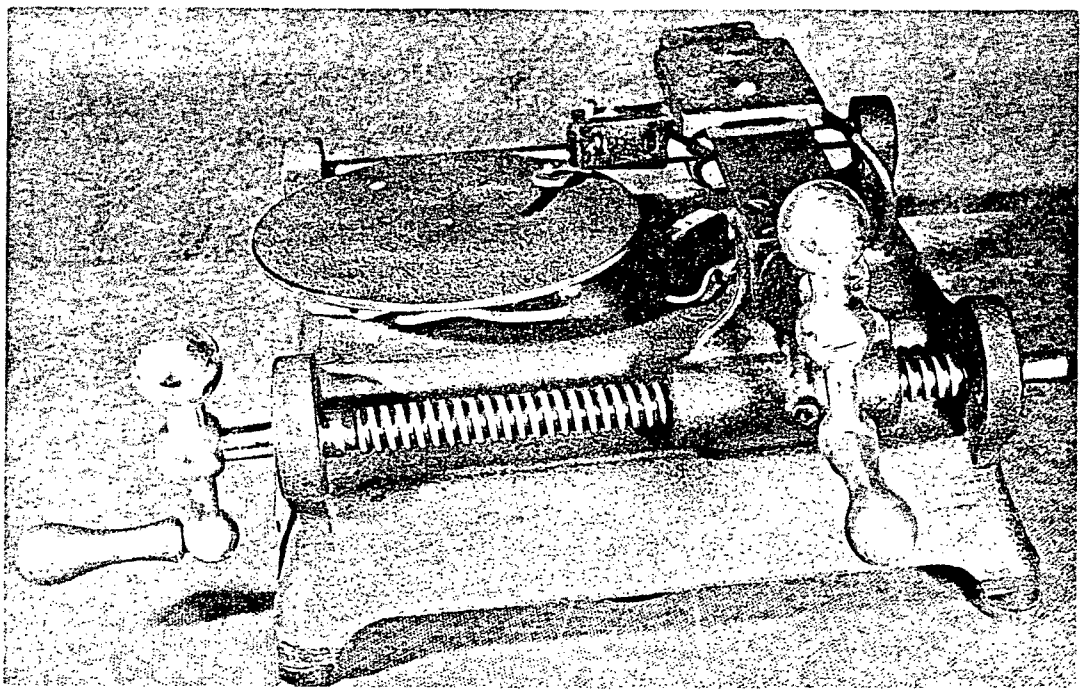

Figure 2. USAF SAM Two-Hand Coordination Test

dination Test, shown in Figure 2, required the subject to operate two lathe-like crank handles in order to keep a cursor positioned on an eccentrically moving target. Score consisted of the amount of time the pointer was on the target during standardized trial periods. Finally, the USAF SAM Rotary Pursuit Test, shown in Figure 3, required the subject to follow a rotating target with the tip of a stylus. Score consisted of time on target during standardized trial periods. All tests had been used successfully for the selection of aviation cadets during World War II, having been shown capable of accounting for a substantial portion of the variance of pilot training outcome. Thus, the behaviors under observation were relevant to flying proficiency, although they were by no means predictive of its entire factorial structure.

Three exposure levels were available for study: 15, 25, and 50 r, as measured in air at the position of a plane which bisected the patient. Each level was reached either by a single exposure or by five equal fractional exposures separated by an interval of 1 hour. Delivery was accomplished by a 400 kvp General Electric x-ray machine with Thoraeus III filtration having a half-value layer equivalent to 4.1 mm of copper. At the target distance of 300 cm, the output was approximately 0.95 r/min. One large field was used, the patient being treated in a lateral position with left and right sides alternated in proximity to the target. Air-wall ionization chambers (Farmer) were placed on the patient's skin during exposure in order to measure entrance and exit doses.

At about 0800 hours on the day of exposure, each subject was given formal test instructions and a standardized amount of preliminary practice on the three testing devices. Practice sessions were 2

minutes for the complex coordination and two-hand coordination tests, and 100 seconds (five 20-second trials separated by 10-second rests) for the rotary pursuit test. Following practice, the prescribed treatments were begun. One hour later the psychomotor testing sessions were resumed, and they were repeated thereafter at 2-hour intervals until six post-treatment sessions had been completed. Two testing sessions 8 hours apart were completed on the day following treatment. Additional testing was done on some of the subjects, but these data are not considered in the present study. Single-exposure subjects and multiple-exposure subjects within a given total exposure group were treated alike except that the latter were alternated between testing sessions and fractional treatment sessions until the five exposures had been accomplished.

Inasmuch as the performance under observation was measured early in the course of habit acquisition, two somewhat independent assessments of it were possible. The first was based simply on the total score achieved during the entire posttreatment testing sequence, while the second was an estimate of learning rate based upon the mean tangent of the angles defined by the abscissa of the performance curve and tangents drawn to successive equal segments of it. Both indexes were adjusted for multiple regression upon chronological age and pretreatment performance levels before the final analysis of posttreatment variation was performed. This adjustment had the general effect of (1) reducing the contribution of these factors and factors correlated with them (such as type and severity of disease) to posttreatment variation, and (2) increasing the precision with which final tests of significance could be made. What remained for the final analysis was the variation

attributable to the main experimental effects, their interaction, and residual differences between subjects.

Suffice it to say that only one of the six analyses (two criteria for each of three tests) provided even the slightest hint that performance was affected by the independent variables under consideration. An analysis of acquisition rate for the Rotary Pursuit Test, shown in Table 1, suggests that the effects of exposure level and method of delivery may have been correlated, i.e., the effects of treatment levels may not have been the same at all exposure levels. A plot of subclass means, shown in Figure 4, suggests that single exposures may have attenuated habit acquisition more than fractional exposures to the same levels, particularly at the highest level, in accordance with hypothesis.

Table 1. Analysis of variance of acquisition rate scores for Rotary Pursuit Test

Source	df	Mean Square	F	p
Doses	2	6.1888	< 1.00	
Methods	1	20.9941	2.05	.165
D x M	2	28.6785	2.79	.075
Error	70*	10.2589		
Total	75*			

*Reduced by 2df for regression of posttreatment scores (y) upon pretreatment scores (x) and chronological age (z).

$R_{y.xz} = .43$; $r_{zx} = -.16$; $r_{zy} = -.42$; $r_{xy} = .11$; $b_1 = .0043$; $b_2 = -.0900$

However, the probability levels associated with both methods and interaction effects are far from convincing, and the observed regressions of the two methods functions on the dosage variable are difficult to reconcile with the theoretical model.

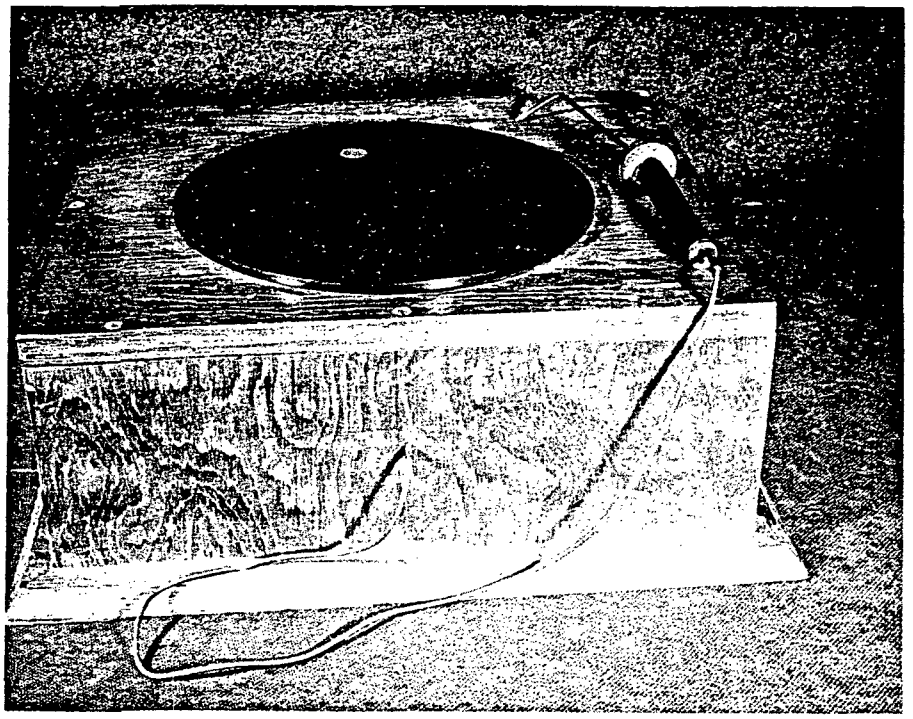

Figure 3. USAF SAM Rotary Pursuit Test

Second Study. Accumulated experience with therapeutic applications of whole-body radiation convinced the hospital staff of the wisdom of higher single doses than those which had been prescribed during the period covered by the first study. Consequently, it became possible to conduct psychomotor studies following single doses ranging from 0 to 200 roentgens (in air) in steps of 25 r, and special arrangements for hospitalization permitted the observations to extend over a period of 10 days beyond treatment.

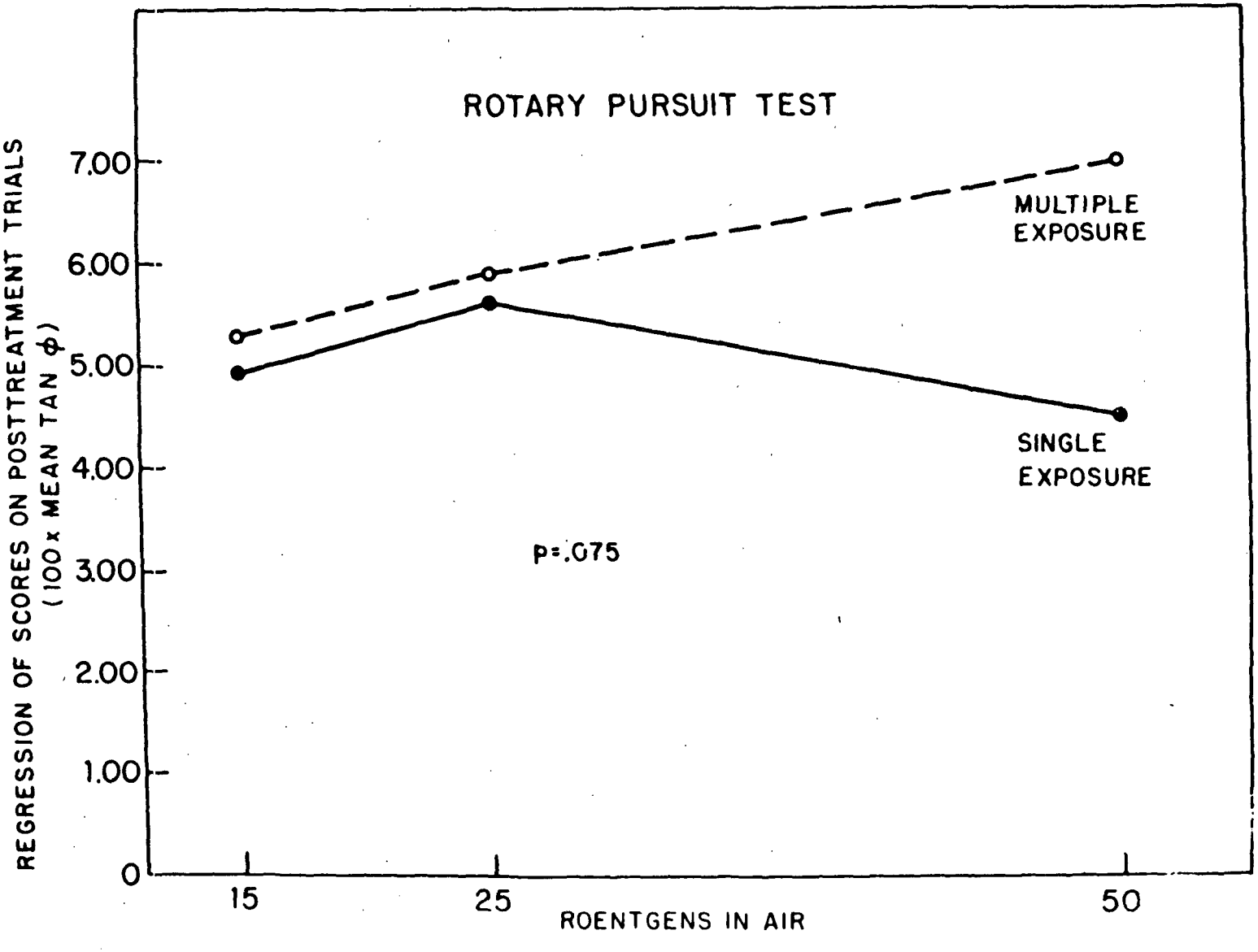

Figure 4. Rotary pursuit performance as a joint function of level and method of radiation exposure.

As before, subjects were adult males whose participation in the study was governed by their own consent and the judgment of the hospital staff. Ages ranged from 23 to 76 years. Testing devices were as previously described.

As before, patients were exposed in a lateral position with left and right sides alternated in proximity to the target. For approximately half the subjects, mostly those receiving below 75 r, the treatment was delivered as previously described. For the remainder, treatment was accomplished by a General Electric Maxitron operated at 250 kvp with a Thoraeus III filter providing half-value layer equivalent to about 3 mm of copper. Output was about 3.8 r/min. Nine exposure levels, ranging from 0 through 200 r in 25-r steps, were sampled. Each subject received his prescribed exposure in a single session.

Beginning at approximately 0800 hours each day for 4 days prior to exposure, each subject was allowed a practice session on each testing device. Practice sessions both before and after exposure were 4 minutes for complex coordination and two-hand coordination, and 300 seconds (fifteen 20-second trials separated by 10-second rests) for rotary pursuit. Exposure occurred on the morning of the fifth day. One hour later the first posttreatment testing session was held, and this was repeated each day at approximately the same time for 9 days thereafter. All subjects, including controls, were treated essentially alike except for the amount of radiation to which they were exposed.

Analyses of variation in posttreatment achievement levels for complex coordination and two-hand coordination were based on the forty one-minute performance samples obtained from each subject (10 days x 4

Table 2. Analysis of variance of adjusted posttreatment achievement levels for rotary pursuit

Source	df	Mean Square	F	p
Groups (doses)	7	23,086	< 1.00	ns
Ss treated alike	57	40,466		
Days	9	75,218	68.07	<.001
D x G	63	1,229	1.11	ns
Ss x D	513	1,105		
Trials/day	2	16,353	19.17	<.001
T x G	14	1,039	1.22	ns
Ss x T	114	853		
T x D	18	121	< 1.00	
T x D x G	126	272	1.14	ns
Ss x T x D	1,026	238		
Total	1,949*			

*Reduced by 60 df for regression coefficients, as follows: Ss treated alike (-2), Ss x D (-18), Sc x T (-4), and Ss x T x D (-36).

trials/day), while the analysis of rotary pursuit was based on the thirty 100-second performance samples from each subject (10 days x 3 trials/day). The scores of all subjects in each performance sample were adjusted for their multiple regression on chronological age and pretreatment achievement levels, and the residual variation of the

scores was then decomposed into main effects and interactions for determinations of statistical significance.

The outcomes for all testing devices are well represented by the analysis of rotary pursuit data, shown in Table 2. The highly significant variation associated with days and trials/day, when considered in conjunction with appropriate mean values, shows that significant amounts of learning occurred both within each day and from day to day. All radiation groups were essentially alike in this respect, as shown by the negligible interaction values, and there was no evidence of radiation impairment.

The data from each testing device were further analyzed in terms of the linear component of the habit acquisition curve, both within days and from day to day, but none of the analyses implicated radiation exposure as a significant source of variation. Comparable analyses were made in terms of the quadratic component of the acquisition curve. The results were negative for two-hand coordination and rotary pursuit, but those for complex coordination were significant, as shown in Table 3.

Table 3. Analysis of variance of quadratic component of scores by days for complex coordination

Source	df	Mean Square	F	p
Between radiation groups	8	.00282061	3.33	< .01
Within groups	58	.00084699		
Total	66			

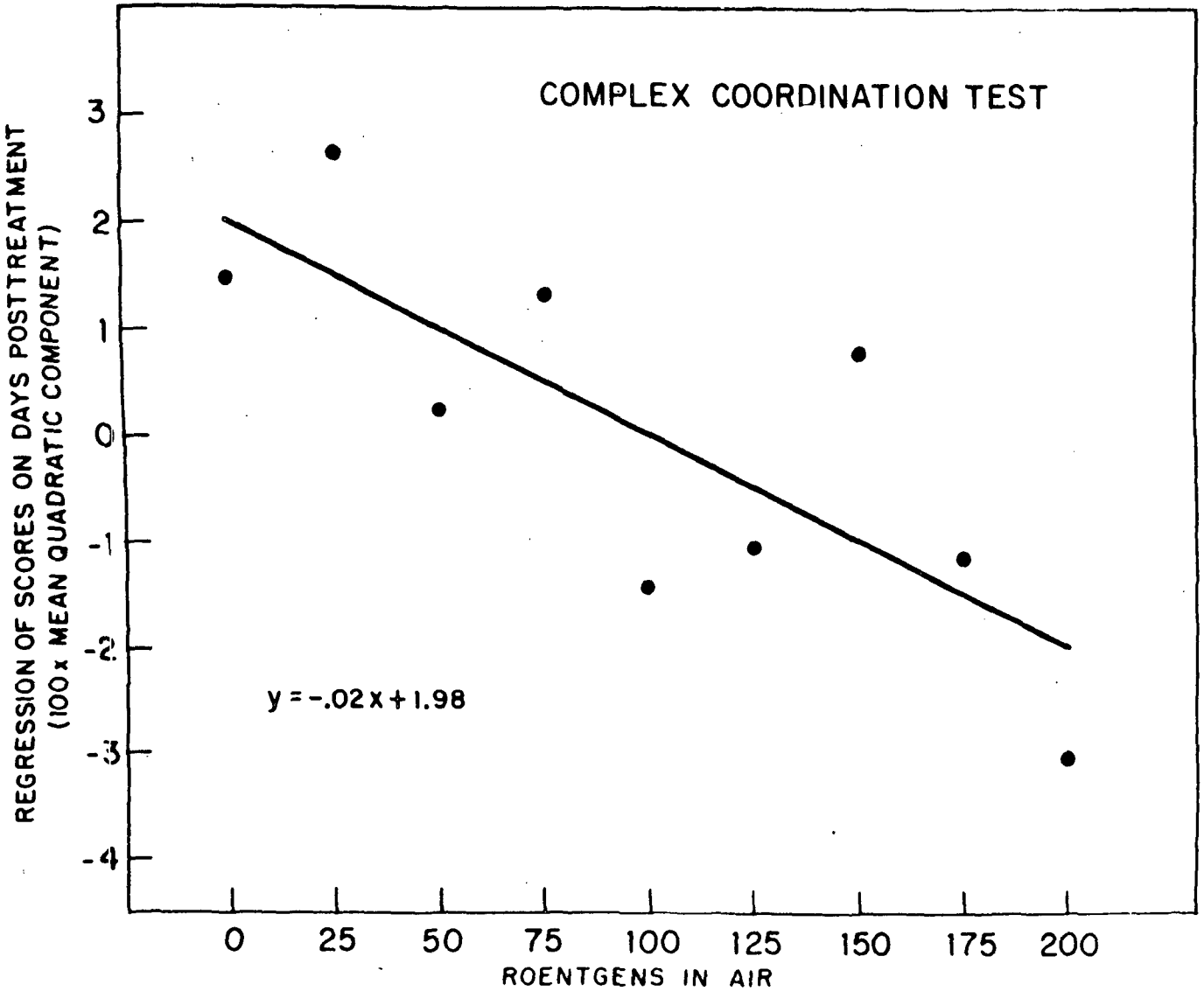

Figure 5. Quadratic component of complex coordination learning curve as a function of radiation exposure level.

A plot of the mean coefficients against exposure values, shown in Figure 5, suggests that the quadratic component of the 10-day performance curve became more negative the more intense the radiation exposure. In other words, the more intense the exposure, the more likely it was that performance was falling, rather than rising, toward the end of the 10-day period of measurement.

Except for the curvature aspect of the 10-day performance sequence for complex coordination, one can summarize these two studies by saying that there is no dependable evidence that exposure to ionizing radiation affected the variables measured. Whether this exception is a true radiation effect is debatable. It could just as well have been a disease effect, for we must presume that the prescribed exposure intensity bore some relationship to the true severity of the disease. Whatever its source, the effect probably represents progressive motoric weakness or fatigue in the operation of the spring-loaded controls rather than decrements in the cognitive aspects of the task. Finally, it seems important to re-emphasize that the application of these results to operational problems should be made with cautious regard for the medical status of the subjects and the limited relevance of experimental criteria.

Clinical Observations

Although lacking the precision of systematic experimental studies, certain observations acquired through clinical studies of bomb casualties, accidental exposures, and therapeutic experiences deserve careful

consideration because of their attention to what Furchtgott (1956) has called "behaviorally significant effects." For example, Keller (1946) noted fatigability as an almost universal complaint in his study of bomb casualties; and Gerstner (1957, 1958) commented on the appearance of listlessness, apathy, headache, and drowsiness "within a few hours" of exposure to radiotherapy. Miller, Fletcher, and Gerstner (1957) found about 50 percent of their patients showing fatigue, anorexia, and nausea shortly after radiotherapeutic exposures ranging from 125 to 175 r. Further studies of therapeutic experience by Levin, Schneider, and Gerstner (1959) observed that whole-body exposures of 150-200 r left patients asymptomatic for about an hour, but thereafter precipitated feelings of fatigue, apathy, dizziness, and headache, and produced appearances of depression and energy depletion. Thoma and Wald (1959) reported similar findings in their review of accidental exposures. Finally, Furchtgott (1952) reported studies, unavailable to him in original form, which suggested that radiation of the skin in "sub-erythemal doses" increased scotopic thresholds for several days and produced decrements in dark adaptation levels.

One, of course, cannot foresee with confidence what impact these effects might have on task performance, since high levels of training and motivation often sustain an operator to outstanding levels of achievement despite his infirmities. On the other hand, we can all agree that such effects represent potential liabilities that operators would be better off without.

The British Study

The sparse account of human studies would not be complete without reference to a recent paper by Frisby (1961). A British physician discovered one day that he had acquired a carcinoma of the tongue. As radiation therapy progressed, he came vaguely to feel that certain behavioral changes were taking place, and finally, after four weeks of this, he offered a psychologist an opportunity to study certain intellectual and perceptual functions by psychometric methods. Tests involving choice reaction time, cancellation, and fractions were administered twice daily (except Saturday and Sunday), sometimes by the psychologist and sometimes by the secretary, until a total of 6870 r had been delivered to the lesion, 5000 r to a nearby gland, and 7530 r to the skin. There was no evidence of radiation effect.

Infra-Human Primate Studies

The scarcity of human data may be regarded as compensated in part by a wide assortment of studies conducted on the infra-human primate, particularly on M. mulata. Whether such studies are truly useful depends, of course, on the validity of assumptions one makes about the phylogenetic continuity of behavioral processes. There are some who insist that there is a fundamental discontinuity between the behaviors of man and lower animals, and that little or nothing can be safely inferred about one from studies of the other. On the other hand, one should remember that such assertions are usually treated as hypotheses by those who study subhuman behavior, and the acceptance of the doctrine

before the fact would therefore seem to beg the question. Scholars in this field generally take the position that the study of lower animals promotes the understanding of human behavior to the degree that fundamental principles anticipate and embrace both sets of facts, an event which occurs more conclusively than most people today realize. From a clinical point of view it is interesting to note the conclusion drawn by Zellmer and Pickering (1960) that M. mulata demonstrates all the important aspects of the acute radiation syndrome. Diagnostic and prognostic signs (diarrhea, vomiting, purpura, anorexia, epilation, etc) occur about as frequently and with about the same latency as in humans, and the three modes of radiation death (CNS, gastrointestinal, and hematopoietic) are about as well illustrated. Thus there is a very substantial amount of conviction that M. mulata is an exceptionally suitable substitute for the human as an experimental animal. Fortunately so, for the study of lower primates permits the observation of complicated processes in their more elementary forms, and it permits the deliberate arrangement and control of a great variety of conditions for the satisfaction of experimental objectives.

Behavioral Methodology

The broad assortment of devices and techniques commonly used to study the animal's intellectual, perceptual, and motoric capabilities are described in any textbook of comparative psychology (e.g., Stone, 1951), as well as in the cited references, and any attempt to review them here would impose needlessly upon time and patience. In general, however, it may facilitate understanding to note that the investigator's

ability to observe and measure these processes entails two fundamental requirements. First, he must devise a problem the solution of which embodies the specified characteristics of such processes and falls within the anatomical and physiological capabilities of the organism. Second, he must provide an incentive which renders the solution worth the animal's effort. The rigor and precision with which he can study the processes depends in part upon the extent to which he can (a) control the environmental conditions and (b) quantify the responses in terms of their appropriateness, vigor, frequency, and latency.

The major categories of behavior which have served as focal points of research on the radiated monkey are (a) the learning and retention of discrimination habits, (b) the generalization of habits to novel situations, (c) the manipulation of environmental objects, (d) the delay of response to cues no longer present, (e) the breadth of attention to peripheral cues, (f) the solution of puzzles, (g) locomotion, and (h) free cage behavior in a comparatively unstructured environment. These categories merely represent convenient ways of classifying various aspects of the interaction between organism and environment, and one should understand that they are rigorously definable in terms of specific experimental operations.

Radiation Effects

Learning and Retention. Early systematic efforts explored the success with which the animal could reproduce discriminations which had been mastered prior to exposure. For example, Kaplan and Gentry (1954) trained animals on a serial discrimination task composed of 15 pairs of

stereometric objects, then exposed them to 1000 r of whole-body radiation delivered at 15r/min. Response evocation was rare on early postexposure trials, but significant retention was demonstrated from 8 hours postexposure until 21 hours before death. Kaplan et al (1954) repeated the foregoing study with minor variations in which testing was resumed 24 hours postexposure and continued twice daily until the animals could no longer enter the transport cages. Although the radiated animals performed somewhat less well than controls after the third day, they exhibited significant degrees of retention virtually up to the point of collapse. Melching and Kaplan (1954) modified the procedure by requiring animals to discriminate objects in order to select an alley in which they could avoid electrical shock. Tests of retention conducted between 2 and 10 hours following the delivery of 1500 r at 34r/min were essentially negative. Rogers et al (1954) reported comparable results after exposures to 1295 r. Kaplan et al (1960), analyzing discrimination ability following massive doses of gamma radiation ranging from 1000 to 30000 r at 1000r/min, concluded that some animals were able to accept up to 5000 r without performing poorly, provided they were physically able to perform at all.

Harlow and Moon (1956) trained animals on a variety of tasks, including planometric discrimination and oddity problems, then exposed half of them to 100 r every 35 days until death. Formal testing was discontinued after the ninth exposure period for lack of survivors, but there was no evidence prior to death that radiation had degraded the ability to solve even the most complex learning problems, and animals on the verge of death maintained high performance levels until they

were so weak that overt response was no longer possible. Similarly, Riopelle, Grodsky, and Ades (1956) examined the effects of cumulative exposures adding to 2000 r on object quality discrimination only to find that the performance of radiated animals was equal to or better than that of controls.

When it became evident that the retention of simple discrimination habits was not seriously affected even by massive doses of radiation, efforts were made to devise more complicated problems and to examine the acquisition process, as opposed to the retention process, at generally lower levels of exposure. For example, eight months post-exposure to average doses up to 550 rem, Warren, Kaplan, and Greenwood (1955) trained animals to respond correctly to each of 108 pairs of multidimensional objects, then reversed the reinforcing operation so that the opposite member of each pair became the symbol of reward. Pre-reversal performance was not affected by the dosage levels; and post-reversal performance, although somewhat deficient, was not correlated with dose. McDowell and Brown (1959a) varied the cue reversal technique by rewarding the oddly colored of three objects during pre-reversal training, then rewarding the oddly shaped of the three objects during post-reversal training. Radiation exposure up to approximately 600 rem average dose failed to affect either phase of training in terms of errors committed. McDowell, Brown, and White (1961) used a comparable technique to assess the impact of massive focal radiation to the head, but with negative results.

Overall and Brown (1959) found no radiation effects when the task was one of learning to respond to the most recently rewarded position.

Later, however, Overall, Brown, and Gentry (1960) showed that the ability to learn size relationships between objects declined as a linear function of dosages which had been delivered three years prior to test (0 to 616 rep mixed neutron and gamma). Brown, Overall, and Blodgett (1959) presented consecutive discrimination problems in which both positive and negative cues in earlier series were selected at random to become negative when paired with new stimuli. Mixed neutron and gamma radiation up to 616 rep had no effect on the solution of this problem.

McDowell and Brown (1960b) adapted the Landoldt Ring principle to a series of eight problems ranging in difficulty from a 90° break to a 1° break in order to study the visual acuity of animals which had been exposed to as much as 616 rep three years earlier. All animals learned the easier problems readily, but they failed the more difficult ones in accordance with dosage received. Roughly comparable results were obtained following massive focal radiation to the head (McDowell and Brown, 1960b). However, neither set of results seemed decisive with respect to whether the deficit was a matter of visual acuity per se or planometric discrimination learning. The authors argued the former interpretation on the grounds that the easier problems were in fact learned.

Generalization of Habits. The ability to transfer principles acquired through experience with one set of problems to the solution of a new set of problems is generally regarded as a very high order of intellectual achievement. Such processes are studied in lower animals by presenting the training problem in such a way that reinforcement is

applied to all objects which have some particular feature in common, say triangularity, while nonreinforcement is applied to those objects which lack the feature. The critical test of transfer involves additional problems which incorporate some variant of the differentiated cue. Kaplan and Gentry (1953) explored the effects of radiation on this ability by comparing controls with animals that had received whole-body exposure to 400 r at about 16r/min. Half the exposed animals had their heads and spinal cords shielded. Transfer tests applied immediately postexposure as well as several months later gave no evidence of a deleterious effect. Comparable results were found with animals which had been exposed to whole-body doses as high as 616 rep (McDowell, 1960), and to focal head doses as high as 3000 r (McDowell and Brown, 1959c).

Manipulation. Leary and Ruch (1955) noted some decline in the ability to pull weights and manipulate mechanical puzzles shortly after the delivery of 200 r or more, but these effects appeared to be transient. On the other hand, Davis, McDowell, and Deter (1956) observed no important changes in manipulation ability after as much as 400 r.

Delayed Response. The measurement of an animal's ability to postpone its response to some reward or to some sign of reward following concealment from view was one of the earliest behavioristic approaches to the study of mental processes in lower animals. This process assumed considerable theoretical significance because of the implication that the animal, no longer able to sense the object, was responding to some internalized representation of it, thereby exhibiting implicit behavior remarkably like that found at the human level. Also, the amount of

delay attainable was generally correlated with phylogenetic sequence, ranging from about 10 seconds in the rat to much longer in the human. Davis, McDowell, and Deter (1956) were unable to degrade this response with acute whole-body exposures up to 400 r, and later studies involving up to about 1100 rem average dose found experimental animals performing about as well as (Davis, Elam, and McDowell, 1958) or better than (McDowell and Brown, 1958b) controls. Multiple exposures eventuating in total doses of 2000 r (Riopelle, 1959; Riopelle, Grodsky, and Ades, 1956) were likewise without effect, as were doses of 100 r given every 35 days until death (Harlow and Moon, 1956). McDowell, Brown, and White (1961) found no significant effect two years after their animals' heads had been exposed to 6000 r in two increments of 3000 r spaced 30 days apart. Harlow, Schiltz, and Settlage (1955) were able to degrade the response temporarily with 8000 r delivered to the head, but recovery was detectable four days later and was complete on the eighth day.

An unusual study worthy of note attempted to assess the impact of low-energy heavy nuclear components of primary cosmic radiation by exposing two Java monkeys to altitudes of 90 - 95M feet for 62 hours (Harlow, Schrier, and Simons, 1956). Delayed response, as well as other processes, was unaffected by this exposure, but the absence of track plate data precluded a determination of exposure level. About all one can say is that the animals were exposed to a hostile environment, and if they were hit, they were not measurably affected.

Attentiveness to Environmental Cues. Riopelle, Grodsky, and Ades (1956) were perhaps the first to suggest that the often superior performance of radiated animals represents a kind of tranquilizing

effect in which the animal is rendered less responsive to peripheral stimuli and consequently more attentive to the cues relevant to the problem presented for solution. Subsequent investigators confirmed this facilitative effect on oddity reversal problems (McDowell and Brown, 1959a), delayed response problems (McDowell and Brown, 1958b), discrimination problems (McDowell and Brown, 1958a; McDowell, Brown, and Wicker, 1959), and easier levels of the Landoldt Ring problem (Brown and McDowell, 1960). Further studies left no doubt that radiation narrowed the animal's scope of attention (McDowell, 1958; Overall and Brown, 1958; Brown, Carr, and Overall, 1958), producing as it were, a kind of "reduction in life space" (Davis, Elam, and McDowell, 1958). Although one might be tempted at first to rejoice over what might appear to be an unexpected bonus from an otherwise hostile environment, a more sober and insightful reflection on the reasons for these facilitative effects marks them as unwanted phenomena worthy of serious concern.

Miscellaneous Effects. Leary (1955) observed changes in the food preferences of animals which had been exposed to as little as 50 r, and Davis (1958) noted the persistence of such changes through at least 14 months postexposure. Several studies of free cage behavior have identified lower aggression (McDowell, Davis, and Steele, 1956) and exaggerated self-care (McDowell and Brown, 1958c, d) as consequences of whole-body doses as low as 400 r. At least one study has suggested an increase in reaction time as a function of dosage ranging from 0 to 670 rem (McDowell, Brown, and Wicker, 1961).

Summary

More than fifty studies of anthropoid behavior observed under various kinds, rates, and amounts of ionizing radiation have shown, on balance, that behavioral functions are highly resistant to acute whole-body doses well above those required to produce troublesome manifestations of acute radiation sickness. Despite this overwhelming evidence of resistance, however, several aspects of behavior are clearly not impregnable. Further effort, therefore, is required to relate such aspects both to the physical dimensions of the radiation environment and the visible damage produced in biological tissues, with particular emphasis on the modifying properties of other stressors.

From a practical and conservative point of view, any exposure intense enough to embarrass an individual's normal physiological mode should be regarded as behaviorally significant because it imposes constraints upon the convenience with which the individual can adapt to environmental circumstances. In terms of immediate effects, present knowledge suggests the acute radiation syndrome as the ruling factor in the specification of permissable acute exposure levels.

References

Brown, W. L., Carr, R. M., & Overall, J. E. The effect of whole-body radiation upon association of peripheral cues. USAF Sch. Aviat. Med. Rep., Rep. No. 58-47, 1958.

Brown, W. L., & McDowell, A. A. Visual acuity performance of normal and chronic irradiated monkeys. J. genet. Psychol., 1960, 96, 133-137.

Brown, W. L., Overall, J. E., & Blodgett, H. C. Novelty learning sets in rhesus monkeys. USAF Sch. Aviat. Med. Rep., Rep. No. 58-147, 1958.

Brown, W. L., Overall, J. E., & Blodgett, H. C. Novelty learning sets in rhesus monkeys. J. comp. physiol. Psychol., 1959, 52, 330-332.

Davis, R. T. Latent changes in food preferences of irradiated monkeys. J. genet. Psychol., 1958, 92, 53-59.

Davis, R. T., Elam, C. B., & McDowell, A. A. Latent effects of chronic whole-body irradiation of monkeys with mixed source radiation. USAF Sch. Aviat. Med. Rep., Rep. No. 57-59, 1958.

Davis, R. T., McDowell, A. A., & Deter, C. W. Performance of rhesus monkeys on selected laboratory tasks presented before and after a large single dose of whole-body x-radiation. J. comp. physiol. Psychol., 1956, 49, 20-26.

Frisby, C. B. A note on radiation treatment in relation to performance on certain tests. Brit. J. Psychol., 1961, 52, 65-70.

Furchtgott, E. The effects of x-irradiation on brightness discrimination. J. Psychol., 1952, 34, 37-41.

Furchtgott, E. Behavioral effects of ionizing radiations. Psychol. Bull., 1956, 53, 321-334.

Gerstner, H. B. Military and civil defense aspects of the acute radiation syndrome in man. USAF Sch. Aviat. Med. Rep., Rep. No. 58-6, 1957.

Gerstner, H. B. Acute clinical effects of penetrating nuclear radiation. Jour. Amer. Med. Assoc., 1958, 168, 381-388.

Harlow, H. F., & Moon, L. E. The effects of repeated doses of total-body x-radiation on motivation and learning rhesus monkeys. J. comp. physiol. Psychol., 1956, 49, 60-65.

Harlow, H. F., Schiltz, K. A., & Settlage, P. H. Effect of cortical implantation of radioactive cobalt on learned behavior of rhesus monkeys. J. comp. physiol. Psychol., 1955, 48, 432-436.

Harlow, H. F., Schrier, A. M., & Simons, D. G. Exposure of primates to cosmic radiation above 90,000 feet. J. comp. physiol. Psychol., 1956, 49, 195-200.

Kaplan, S. J. Radiation research in psychology; An analysis of techniques in maze experimentation. Psychol., Bull., 1962, 59, 153-160.

Kaplan, S. J., & Gentry, G. The effect of sublethal dose of x-radiation upon transfer of training in monkeys. USAF Sch. Aviat. Med. Proj. Rep., 1953, Proj. No. 21-3501-0003 (Rep. No. 4).

Kaplan, S. J., & Gentry, G. Some effects of a lethal dose of x-radiation upon memory. USAF Sch. Aviat. Med. Proj. Rep., 1954, Proj. No. 21-3501-0003 (Rep. No. 2).

Kaplan, S. J., Gentry, J., Melching, W. H. & Delit, M. Some effects of a lethal dose of x-radiation upon retention in monkeys. USAF Sch. Aviat. Med. Proj. Rep., 1954, Proj. No. 21-3501-0003 (Rep. No. 8).

Kaplan, S. J., Melching, W. H., Reid, J. B., Rothermel, S., and Johnson, O. Behavior. (In Pickering, J. E., Langham, W. H., & Rambach, W. A. (eds) The Effects from Massive Doses of High Dose Rate Gamma Radiation on Monkeys. USAF Sch. Aviat. Med. Rep., Rep. No. 60-57, 1960).

Keller, P. D. A clinical syndrome following exposure to atomic bomb explosions. Jour. Amer. Med. Assoc., 1946, 131, 504-506.

Leary, R. W. Food-preference changes of monkeys subjected to low-level irradiation. J. comp. physiol. Psychol., 1955, 48, 343-346.

Leary, R. W., & Ruch, T. C. Activity, manipulation drive, and strength in monkeys subjected to low-level irradiation. J. comp. physiol. Psychol., 1955, 48, 336-342.

Levin, W. C., Schneider, M., & Gerstner, H. B. Initial clinical reaction to therapeutic whole-body x-radiation - some civil defense considerations. USAF Sch. Aviat. Med. Rep., Rep. No. 60-1, 1959.

McDowell, A. A. Comparisons of distractibility in irradiated and non-irradiated monkeys. J. genet. Psychol., 1958, 93, 63-72.

McDowell, A. A. Transfer by normal and chronic whole-body irradiated monkeys of a single learned discrimination along a peripheral cue gradient. J. genet. Psychol., 1960, 97, 41-58.

McDowell, A. A., & Brown, W. L. Facilitative effects of irradiation on performance of monkeys on discrimination problems with reduced stimulus cues. J. genet. Psychol., 1958, 93, 73-78. (a)

McDowell, A. A., & Brown, W. L. Latent effects of chronic whole-body irradiation on the performance of monkeys on the spatial delayed-response problem. USAF Sch. Aviat. Med. Rep., Rep. No. 58-50, 1958. (b)

McDowell, A. A., & Brown, W. L. Some effects of nuclear radiation exposure on the behavior of the rhesus monkey. USAF Sch. Aviat. Med. Rep., Rep. No. 58-58, 1958. (c)

McDowell, A. A., & Brown, W. L. Some persisting effects of nuclear radiation exposure on the behavior of the rhesus monkey. USAF Sch. Aviat. Med. Rep., Rep. No. 58-63, 1958. (d)

McDowell, A. A., & Brown, W. L. Visual acuity performance of normal and chronic focal-head irradiated monkeys. USAF Sch. Aviat. Med. Rep., No. 59-5, 1958. (e)

McDowell, A. A., & Brown, W. L. A comparison of normal and irradiated monkeys on an oddity-reversal problem. J. genet. Psychol., 1959, 95, 105-110. (a)

McDowell, A. A., & Brown, W. L. Peripheral cue learning set in rhesus monkeys. USAF Sch. Aviat. Med. Rep., No. 59-4, 1959. (b)

McDowell, A. A., & Brown, W. L. Transfer by normal and chronic focal-head irradiated monkeys of a single learned discrimination along a peripheral cue gradient. USAF Sch. Aviat. Med. Rep., Rep. No. 59-18, 1959. (c)

McDowell, A. A., & Brown, W. L. Peripheral cue learning set in rhesus monkeys. J. genet. Psychol., 1960, 96, 129-132. (a)

McDowell, A. A., & Brown, W. L. Visual acuity performance of normal and chronic focal-head irradiated monkeys. J. genet. Psychol., 1960, 96, 139-143. (b)

McDowell, A. A., Brown, W. L., & White, R. K. Oddity-reversal and delayed-response performance of monkeys previously exposed to focal-head irradiation. J. genet. Psychol., 1961, 99, 75-81.

McDowell, A. A., Brown, W. L., & Wicker, J. E. Some effects of nuclear radiation exposure on preliminary WGTA training performance of rhesus monkeys. USAF Sch. Aviat. Med. Rep., Rep. No. 59-53, 1959.

McDowell, A. A., Brown, W. L., & Wicker, J. E. Effects of radiation exposure on response latencies of rhesus monkeys. USAF Sch. Aerosp. Med. Rep., Rep. No. 61-94, 1961.

McDowell, A. A., Davis, R. T., & Steele, J. P. Application of systematic direct observational methods to analysis of the radiation syndrome in monkeys. Percept. Mot. Skills, 1956, 6, 117-130.

Melching, W. H., & Kaplan, S. J. Some effects of a lethal dose of x-radiation upon retention (Studies of shock avoidance motivation). USAF Sch. Aviat. Med. Proj. Rep., 1954, Proj. No. 21-3501-0003 (Rep. No. 9).

Miller, L. S., Fletcher, G. H., & Gerstner, H. B. Systemic and clinical effects induced in 263 cancer patients by whole-body x-irradiation with nominal air doses of 15 to 200 r. USAF Sch. Aviat. Med. Rep., Rep. No. 57-92, 1957.

Overall, J. E., & Brown, W. L. Narrowing of attention in rhesus monkeys as a chronic effect of sublethal radiation. USAF Sch. Aviat. Med. Rep., Rep. No. 58-27, 1958.

Overall, J. E., & Brown, W. L. Response of rhesus monkeys to prohabilistic sequential dependencies. USAF Sch. Aviat. Med. Rep., No. 59-3, 1959.

Overall, J. E., Brown, W. L. & Gentry, G. V. Differential effects of ionizing radiation upon "absolute" and "relational" learning in the rhesus monkey. J. genet. Psychol., 1960, 97, 245-250.

Payne, R. B. Effects of ionizing radiation on human psychomotor skills. USAF Sch. Aviat. Med. Rep., Rep. No. 59-29, 1959.

Payne, R. B. Effects of ionizing radiation on human psychomotor skills. U.S. Armed Forces Med. Jour., 1959, 10, 1009-1021.

Riopelle, A. J. Performance of rhesus monkeys on spatial delayed response (indirect method). J. comp. physiol. Psychol., 1959, 52, 746-753.

Riopelle, A. J., Grodsky, M. A., & Ades, H. W. Learned performance of monkeys after single and repeated x-irradiations. J. comp. physiol. Psychol., 1956, 49, 521-524.

Rogers, C. M., Kaplan, S. J., Gentry, J., & Auxier, J. A. Some effects of cumulative doses of x-radiation upon learning and retention in the rhesus monkey. USAF Sch. Aviat. Med. Proj. Rep., 1954, Proj. No. 21-3501-0003 (Rep. No. 11).

Stone, C. P. (ed) Comparative Psychology (3d Edition) Englewood Cliffs (N. J.): Prentice-Hall, 1951.

Thoma, G. E., and Wald, N. The diagnosis and management of accidental radiation injury. J. occup. Med., 1959, I:8, 421-447.

Warren, J. M., Kaplan, S. J., and Greenwood, D. D. The solution of discrimination-reversal problems by normal and irradiated monkeys. USAF Sch. Aviat. Med. Proj. Rep., Proj. No. 21-3501-0003, Rep. No. 16, 1955.

Zellmer, R. W. Human ability to perform after acute sublethal radiation. Military Med., 1961, 126, 681-687.

Zellmer, R. W., & Pickering, J. E. Biologic effects of nuclear radiation in primates. USAF Sch. Aviat. Med. Rep., Rep. No. 60-66, 1960.

Paper C-6

THE LETHAL EFFECTIVENESS OF A SOLAR FLARE-TYPE DOSE DISTRIBUTION DELIVERED TO THE RAT

K. L. Jackson

Radiation Biology Group
Bioastronautics Section
Physics Technology Department
The Boeing Company
Seattle, Washington

Abstract

An investigation of some biological effects produced by exposure of rats to a solar flare-type depth-dose distribution has been carried out. Space proton doses to bone marrow will not be appreciably attenuated by surrounding bone and in the present study, this was simulated by use of cobalt-60 gamma radiation. Depth-dose distribution, produced in rats by a filter-rotation technique, resulted in a midline dose which was 25 per cent of the surface dose. This depth-dose is similar to that calculated for exposure of man to July 16, 1959 solar flare protons with 10 gm/cm^2 of shielding.

The 50 per cent lethal dose (LD_{50}) measured at the surface of the rat was three times greater for depth-dose exposure as compared to uniform exposure. The midline LD_{50} was less for depth-dose exposure than for uniform exposure. The depth in the body at which the depth-dose LD_{50} was equal to the uniform LD_{50} was approximately 50 per cent of the distance from the surface to the midline. The total energy absorbed at the LD_{50} was 1.5 times greater with depth-dose exposure as compared to uniform exposure. Mean survival time of decedents in the LD_{16} - LD_{84} range was significantly shorter in depth-dose exposed animals as compared to uniformly exposed animals. This suggests that depth-dose exposure produces greater injury to the intestine which was verified by measurement of intestinal weight changes.

Introduction

Interest in the biological effects resulting from whole-body exposure of mammals to a decreasing depth-dose distribution of ionizing radiation

recently has increased because space proton fields[1,2] are expected to produce this form of absorbed dose geometry[3,4]. The lethal effectiveness of decreasing depth-dose distribution down to 70 per cent of the surface dose at body-center has been discussed by Bond, et.al.[5]. However, little information is available on the lethal dose requirements for midline doses in the range of 1 to 70 per cent of the surface dose, the range expected for exposure of man to space radiation fields[4,6].

Beta irradiation of small animals has been used to produce a steep depth-dose near the body surface but this method does not produce significant doses at body-center or intermediate depths[7,8]. Interpretation of lethality and organ damage data obtained by use of low

---

1. Ney, E. P., J. R. Winckler, and P. S. Frier, Protons from the Sun, May 12, 1959. Phys. Rev. Let. 3:183-185 (1959).

2. Van Allen, J. A., and L. A. Frank, Radiation Measurements to 658,300 KM with Pioneer IV. Nature 184:219-224 (1959).

3. Dye, D. L., and J. C. Noyes, Biological Shielding for Radiation Belt Particles. J. Astronautical Sci. 7:64-70 (1960).

4. Schaefer, H. J., Further Evaluation of Tissue Depth Doses in Proton Radiation Fields in Space. U.S.N. School Aviation Medicine Research Report 17, 14 pages (May 1950).

5. Bond, V. P., E. P. Cronkite, C. A. Sondhaus, G. Imirie, J. S. Robertson, and D. C. Borg, The Influence of Exposure Geometry on the Pattern of Radiation Dose Delivered to Large Animal Phantoms. Rad. Res. 6:554-572 (1957).

6. Jackson, K. L., Influence of Solar Flare-Type Exposure Geometry on Acute Lethality: Technical Discussion and Proposed Study. Boeing Document D2-12242, 28 pages (August 1961).

7. Biological Effects of External Beta Radiation, edited by R. E. Zirkle, National Nuclear Energy Series IV-22E, McGraw-Hill Book Co., Inc., New York (1951).

8. Crook, J. C., E. V. Hulse, J. H. Mulvey, and G. J. Neary, The Acute Effects of Partial-Body Beta Irradiation of Mice. British J. Radiol. 31:477-485 (1958).

voltage X-radiation to produce a depth-dose distribution is complicated by the shielding effect of surrounding bone on marrow dose[9-12]. This appears to be an important factor in the study of biological effects produced by space proton fields since radiation doses to marrow will not be appreciably attenuated by bone[6].

In the present investigation of the effects of depth-dose irradiation of the rat, bone attenuation of marrow dose has been minimized by using cobalt-60 gamma radiation in conjunction with a filter-rotation technique. The relative depth-dose distribution studied is similar to that calculated for exposure of man to July 16, 1959, solar flare protons with 10 gm/cm^2 of shielding[6]. The advantage gained by use of gamma radiation to study depth-dose effects per se independent from RBE considerations has been discussed previously[6].

Experimental Procedure

Animals

Two-month-old, male, Sprague-Dawley rats were used in the experiments. The animals were housed four to a cage and were given water and Purina Laboratory Chow ad libitum.

---

9. Alpen, E. L., and D. M. Jones, Effects of Concomitant Superficial X-Radiation Upon the Lethal Effectiveness of 250 KVP X-Rays. Radiology 72:81-85 (1959).

10. Alpen, E. L., D. M. Jones, H. H. Hechter, and V. P. Bond, The Comparative Biological Response of Dogs to 250 KVP and 100 KVP X-Rays. Radiology 70:541-550 (1958).

11. Grahn, D., G. A. Sacher, and H. Walton, Comparative Effectiveness of Several X-Ray Qualities for Acute Lethality in Mice and Rabbits. Rad. Res. 4:228-242 (1956).

12. Report of the International Commission on Radiological Units and Measurements (ICRU) 1959, National Bureau of Standards Handbook 78, January 16, 1961.

13. Litchfield, J. T., and F. Wilcoxon, A Simplified Method of Evaluating Dose-Effect Experiments. J. Pharmacol. Exptl. Therap. 96:99-113 (1949).

Methods

A few minutes before irradiation, groups of twelve rats were anesthetized with an intraperitoneal injection of nembutal and were placed in 4.4 cm (inside diameter) cast acrylic cylinders. During irradiation the cylinders were rotated at 28 RPM about their long axes which were positioned vertically by means of the apparatus shown in Fig. 1. This technique allowed accurate positioning of the midline of the rats and caused the rats' bodies to assume a fixed cylindrical shape. In order to deliver the same midline dose to the upper, center, and lower portions of the cylinders, the long axis of a 0.5 inch diameter by 8.3 inches long (1000 C) cobalt-60 source was centered on and positioned parallel to the long axis of the cylinders.

Simultaneous exposure of six rats to a decreasing depth-dose was accomplished by rotation of the rat-containing cylinders behind wedge shaped lead filters (Fig. 1). The cross section of each filter was an isosceles triangle with an altitude of 7.5 cm and a base of 4.0 cm. The base was constructed 4 mm smaller than the diameter of the rat so that diverging rays from the source which grazed the edge of the filter at the base also grazed the surface of the rat. Because the plane of maximum thickness of the lead filter was positioned in the center of the rat (along the longitudinal axis), the midline of the rat received a low, constant dose-rate during rotation. A point on or near the surface of the rat, however, passed alternately through areas of high to low dose-rates. The net effect of such exposure geometry was to produce the depth-dose distribution shown in Fig. 2.

Simultaneous irradiation of six rats with a uniform body dose was accomplished by exposing rotating animals in the apparatus of Fig. 1 but without the use of a lead filter. In order to obtain approximately the same desired average body-surface dose-rate for the two exposure geometries, the midline to source distance for uniform and depth-dose exposure was approximately 20 inches and 10-3/4 inches, respectively. Slight adjustments of rotator positions were made to reduce the deviation of dose rate within each geometry group to less than 2 per cent of the mean.

In each series of exposures six depth-dose irradiated rats and six uniformly irradiated rats were exposed simultaneously. Because irradiation of the uniformly exposed animals required less time than was required for irradiation of the depth-dose animals, exposure of the depth-dose group was interrupted in order to remove the uniform group. The time required for removal of the uniform group was less than three minutes.

Mortality data obtained following exposure of the animals to a series of graded radiation doses were analyzed for 50 per cent lethal doses at 30 days (LD_{50}) and potency ratios by the method Litchfield and Wilcoxon[13].

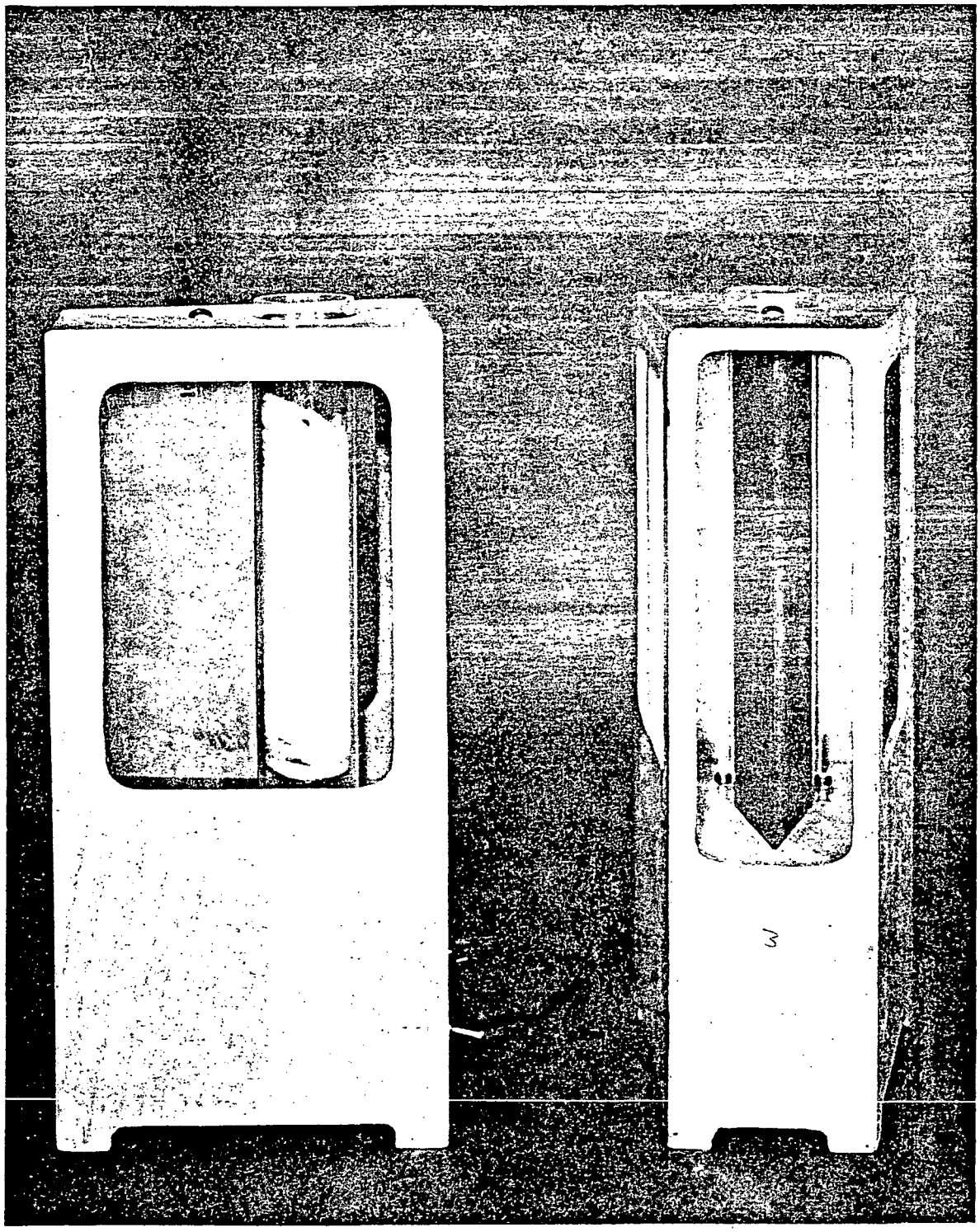

FIGURE: 1

DEPTH-DOSE FILTER-ROTATION APPARATUS

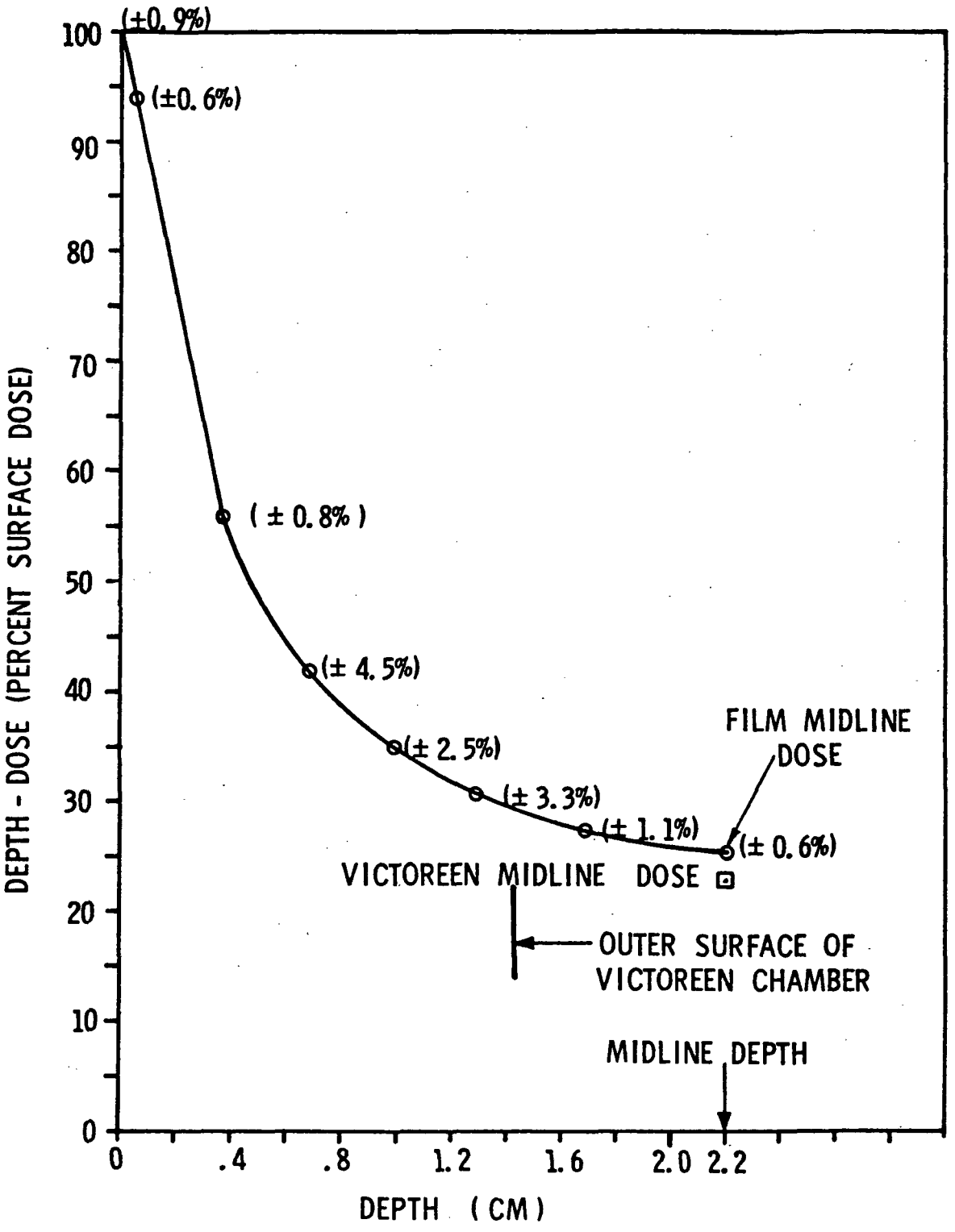

FIGURE: 2

DEPTH-DOSE PRODUCED IN RAT PHANTOM BY COBALT-60-FILTER ROTATION TECHNIQUE

In order to measure the wet weight of the small intestine, this tissue was removed under ether anesthesia and rapidly stripped free of mesenteric blood vessels, fat, and pancreas. After chilling the intestine in ice cold isotonic saline, the tissue was cut longitudinally and the luminal content was blotted away on filter paper. The intestine was rinsed in five changes of ice cold saline, reblotted on filter paper, and weighed.

Dosimetry

The primary reference for measurement of radiation doses was a #621 Victoreen 100r thimble chamber. All measurements were made with the chamber covered with a 1.3 cm thickness of pressed wood. The chamber and stem were exposed to the same radiation field. Rat phantoms were constructed from stacks of 4.4 cm diameter, 1/8 inch thick discs of pressed wood contained in the acrylic cylinders.* The tissue roentgen dose was converted to rad dose by a multiplication factor of 0.97, which is relatively constant over a considerable energy range (12).

The dose delivered to the uniformly exposed rats was determined by making a series of exposures for varying periods of time and measuring the dose with the Victoreen thimble chamber. Extrapolation of the measured dose to zero time yielded the dose delivered during the time required to raise the source to, and lower the source from, the exposure position (raise-lower-dose). Shaped lead bricks inside and below the rotators reduced the raise-lower-dose to 14.7 rad. The dose-rate with the source in the expose position was 59.6 rad/min measured at the midline of the phantom.

The dose distribution delivered to depth-dose exposed rats was measured by photographic film dosimetry using Dupont 510 film. The film loads were constructed as part of the phantom by using discs of 1/8 inch pressed wood with a circular piece of film sandwiched between the wood discs. A second strip of film was positioned in a 90 degree plane to the circular film around the outside of the wood discs. This second film was used to obtain a film density measurement near the surface of the cylinder wall. The entire film load, when sealed with black masking tape, made a tight fit in the acrylic cylinder. Micrometer measurement of masking tape, protective paper, and film thicknesses indicated the average depth of the emulsion to be 0.5 mm from the cylinder wall. The films were developed in Kodak X-Ray Developer and film densities were measured with a Macbeth-Ansco densitometer. The relationship between film density and Victoreen chamber reading was determined

*Density of the pressed wood was 1.10 gm/cm^3. The Victoreen chamber yielded the same dose in a water phantom or a pressed wood phantom when each was exposed behind a lead filter.

following simultaneous exposure of the films and thimble, each being imbedded in a pressed wood phantom and rotated in an acrylic cylinder without a lead filter. Individual standard curves relating film densities of the two films to Victoreen reading were constructed from data obtained by a series of duplicate radiation exposures.

The depth-dose distribution and dose-rate delivered to the phantom was calculated from film density measurements made at known distances from the acrylic cylinder wall following simultaneous exposure of duplicate film packs rotated behind lead filters in all depth-dose rotators. Numbers in parentheses given in Fig. 2 indicate the maximum per cent deviation from the mean of the measured dose among the six rotators. No significant buildup of the dose near the surface of the phantom was expected due to the 1/8-inch acrylic plastic wall surrounding the phantom[14]. The average dose-rate delivered to the surface of the rotating phantom, obtained by extrapolation of the depth-dose curve to the surface (Fig. 2), was determined to be 54.8 rad/min. The surface raise-lower-dose was 10.9 rad. The maximum dose-rate delivered to the surface of the phantom (measured with no rotation) was in the region of minimum lead filter thickness and this dose-rate was observed to be 189 rad/min.

Since photographic film exhibits marked energy dependence at low photon energies[15], an estimate was made of the error in dosimetry due to low energy scatter from the back of the lead filter. This error would be greatest at the center of the phantom.* Although the Victoreen chamber was too large to measure doses near the surface of the rat phantom, it could be used to determine the dose delivered to the center because in this region the dose change with depth is small over the

---

14. Burkell, C. C., T. A. Watson, H. E. Johns, and R. J. Horsley, Skin Effects of Cobalt-60 Telecurie Therapy. British J. Radiol. 27:171-176 (1954).

15. Dudley, R. A., Photographic Film Dosimetry in "Radiation Dosimetry", edited by G. J. Hine and G. L. Brownell, Academic Press, New York (1956).

* Tests made by exposure of film and Victoreen chamber behind large slabs of lead of various thicknesses indicated that the discrepancy between film and Victoreen increased with increasing thickness of lead. The discrepancy exceeded 10 per cent for slabs thicker than 5.5 cm.

dimensions of the Victoreen chamber (Fig. 2). A comparison, therefore, was made of the dose measured at the center of the phantom by the Victoreen chamber and film when these were exposed simultaneously while rotated behind a lead filter. As indicated in Fig. 2, the film registered a phantom midline dose which was 25 per cent of the surface dose and the Victoreen recorded a dose which was 23 per cent of the surface dose. Since factory calibration showed that the Victoreen chamber used reads 4.5 per cent lower for 100 KVCP X-radiation as compared to cobalt-60 gamma radiation, the error due to film energy dependence may be somewhat less than is indicated by the above test.

The total energy absorbed by a rat during depth-dose irradiation was estimated by integration of the energy delivered to a tissue cylinder by the depth-dose distribution shown in Fig. 2. The rats were assumed to be cylinders of 4.4 cm diameter with volumes equal to the body weight divided by a body density of 1.02. Graphical integration of the energy delivered was performed by summation of the mean energy delivered to a 4 mm diameter core and concentric cylinders of 2 mm wall thickness.

Results

In Experiments I and II, a total of 24 groups of six rats were exposed to graded surface doses ranging from 786 to 951 rad and 2231 to 3282 rad for uniform and depth-dose geometry, respectively. Results of analysis of mortality data obtained in these experiments are given in Table I. The surface LD_{50} values with depth-dose exposure were significantly greater than with uniform exposure and the analyses indicated the slope of dose-per cent curves in each experiment did not deviate significantly from parallelism. Therefore, potency ratios were estimated which indicate the surface LD_{50} for depth-dose exposed animals was three times greater than the LD_{50} for uniform exposure. These data also show that the midline LD_{50} for the depth-dose exposed animals was significantly lower than the midline LD_{50} of the uniformly exposed animals (Table I and Fig. 3). The LD_{50} values were numerically equal at a torso depth of 47 to 53 per cent of the distance from surface to midline (Table I and Fig. 3).

Since the dose delivered to various parts of the rat during depth-dose exposure depends upon distance of the tissue from the cylinder wall, a description of the position assumed by rats during irradiation is warranted. The trunks of the bodies made a snug fit in the cylinders and the torso was cylindrical (Fig. 1).* The end of the lower mandible was usually against the wall of the cylinder with the back of the head against the opposite cylinder wall. The fore legs were between the

*Respiration and circulation appeared normal as judged by ear color and head and thorax movements.

Table 1. Mortality Data for Rats Subjected to Uniform and Depth-Dose Exposure from Cobalt-60[a]

Experiment No.	Exposure Geometry	LD_{50} (rad)	Slope Function S	Potency Ratio at LD_{50}	Midline LD_{50} (rad)	% Depth at which Depth-Dose LD_{50} Equals Uniform LD_{50}[b]	Mean Body Weight (gm)[c]	Integral Dose (Kgrad)	Ratio of Integral Doses
I	Depth-dose	2522 (2427-2620)	1.06 (1.02-1.11)	2.99 (2.61-3.33)	631 (606-655)	47%	200	250	1.47
	Uniform	846 (831-860)	1.02 (1.01-1.04)		846 (831-860)		201	170	
II	Depth-dose	2546 (2314-2801)	1.12 (1.01-1.24)	3.21 (2.89-3.56)	636 (578-825)	54%	225	284	1.58
	Uniform	793 (763-825)	1.07 (0.71-1.59)		793 (763-825)		227	180	
III	Depth-dose	2694 (2572-2821)	1.13 (1.05-1.21)	3.18 (2.89-3.50)	673 (643-705)	53%	187	250	1.55
	Uniform	846 (833-858)	1.04 (1.02-1.06)		846 (833-858)		190	161	

[a]Values in parenthesis are 95% confidence limits.

[b]Percent of distance from surface to midline at which the LD_{50}'s for each exposure geometry were equal.

[c]Mean body weight at the time of irradiation for animals exposed within the LD_{16} to LD_{84} range.

FIGURE: 3

DOSE DISTRIBUTION AT 50% LETHALITY IN EXPERIMENT 1

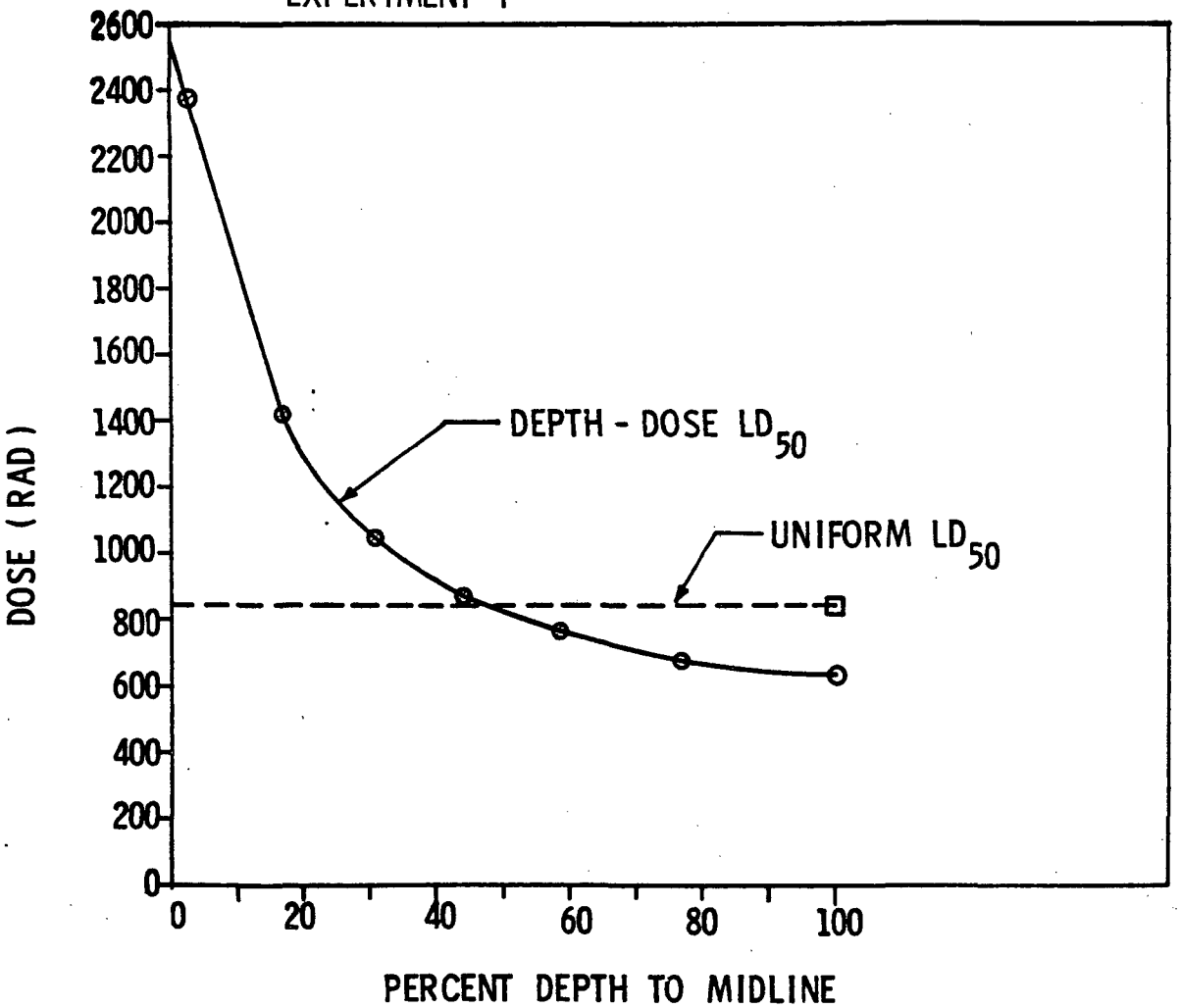

upper thorax area and the cylinder wall and the tail was coiled and generally in contact with the wall of the cylinder. The femoral portion of the hind limbs were in contact with the cylinder wall but the tibial portion varied considerably with respect to distance from the wall. Roentgenograms of a rat positioned in a cylinder showed that most of the bone structure was located near the surface of the animal but that a small amount of marrow was distributed at depths down to the midline as a result of curvature of the thoracic spine.

In order to determine if a lower dose to the tibial portion of the hind legs was responsible for any of the change in LD_{50} with depth-dose exposure, Experiment III was modified slightly. Sponge rubber pads were loosely taped between the hind legs so that in all exposures (depth-dose and uniform) the hind limbs were in contact with the cylinder walls. A total of 10 groups of twelve rats were exposed to graded surface radiation doses ranging from 820 to 897 rad and 2134 to 2910 rad. The data obtained in this experiment (Table I, Exp. III) show that positive positoning of the lower portion of the hind limbs did not decrease the depth-dose LD_{50}. The potency ratio of the LD_{50} was not significantly different from the values obtained in Experiments I and II. The estimated integral dose (Kgrad) delivered to depth-dose and uniformly exposed rats is given in Table I. At the LD_{50} the integral dose delivered to the depth-dose exposed rats was 1.5 times greater than the integ al dose delivered to the uniformly exposed rats.

All rats irradiated with depth-dose geometry in Experiments I, II, and III developed skin burns in about a 1-1/2 by 2 cm area on the thighs. This was pronounced during the third week post-exposure and epilation in the abdominal and back areas occurred during the fourth week. Body weights were followed in Experiments I and III and examination of these data revealed that mean body weight changes of animals exposed to doses within the LD_{16} to LD_{84} range did not differ significantly in the two exposure geometry groups at 1, 2, and 3 days post-irradiation. Body weights of survivors in the LD_{16} to LD_{84} range were not significantly different in the two exposure geometry groups at 30 days post-irradiation.

A difference in the mean survival times of depth-dose and uniform exposure groups, however, was detected as shown by the mean survival times given in Table II for decedents exposed to doses in the LD_{16} to LD_{84} range. These data indicate that in each experiment the mean survival time of depth-dose exposed rats was significantly less than mean survival time of the uniformly exposed rats. The median survival times were very close to the mean survival times, indicating the distributions about the means were symmetrical.

In Experiment IV intestinal weight changes as a function of time post-irradiation were measured in a group of rats irradiated with 40 per

Table 2. Mean Survival Times of Decedents Subjected to Depth-Dose and Uniform Exposures Within the LD_{16} and LD_{84} Range

Experiment No.	Exposure Geometry	Estimated Dose Range of LD_{16}-LD_{84} (rad)[a]	Range of Doses Delivered to Animals in LD_{16}-LD_{84} Range (rad)[a]	Total No. of Animals Exposed Within the LD_{16}-LD_{84} Range	No. of Decedents	Mean Survival Time (days)[b]	Probability
I	Depth-dose	2357-2658	2444-2641	12	5	10.2±0.2	$<.01$
	Uniform	829-864	837-860	12	6	11.7±0.2	
II	Depth-dose	2271-2854	2425-2668	12	4	10.3±1.1	.05
	Uniform	745-841	786-825	12	7	16.0±1.9	
III	Depth-dose	2381-3047	2522-2910	36	19	7.8±0.6	$<.001$
	Uniform	814-879	820-878	48	28	13.7±0.8	

[a]Surface doses

[b]Mean survival time ± standard error of the mean

cent of the mean surface depth-dose LD_{50} and in a second group of rats irradiated with 40 per cent of the mean uniform LD_{50} as measured in Experiments I, II and III. The doses employed were 1035 and 332 rad for depth-dose and uniform exposure, respectively. The changes observed in small intestine weight following irradiation are given in Fig. 4. These data indicate the intestinal weight loss was significantly greater in depth-dose exposed rats as compared to uniformly exposed rats on the first day ($p = .05$) and the second day ($p = .01$) following irradiation. During the recovery phase the mean intestinal weight overshoot of the non-irradiated control was greater in the depth-dose as compared to the uniformly exposed group although this difference was not significant.

Discussion

A factor which influences the magnitude of the LD_{50} in the rat is protraction of the dose due to differences in dose rate[16,17]. In the present study the time required to deliver a uniform LD_{50} was approximately 14 minutes (at 59 rad/min.) as compared to approximately 48 minutes for delivery of the depth-dose LD_{50}. An estimate of the effect of this difference in exposure time on LD_{50} can be made from data published by Logie, et. al.[17] for cobalt-60 gamma irradiation of the rat. Their data indicate that an increase in exposure time from 14 minutes (59 rad/min.) to 48 minutes would increase the LD_{50} by less than 10 per cent. In the present experiments the average surface LD_{50} and midline LD_{50} of depth-dose exposure were, respectively, 213 per cent greater and 22 per cent less than the LD_{50} of uniform exposure. Therefore, mechanisms other than dose protraction are responsible for differences observed in the lethal dose requirements of uniform and depth-dose irradiation.

It has been observed with soft X-irradiation[9-11] and confirmed in the present study that use of midline tissue dose fails to equate uniform and depth-dose LD_{50} values. The nature of the midline LD_{50} discrepancy, however, differs with cobalt-60 depth-dose and soft

---

16. Dacquisto, M. P. and E. W. Blackburn, The Influence of Delivery Rate of Whole Body 250 KV Roentgen Irradiation (30 or 3 Roentgens per Minute) on Mice, Rats, and Guinea Pigs. Am. J. Roentg. Radium Therapy Nuclear Med. 84:699-704 (1960).

17. Logie, L. C., M. D. Harris, R. E. Tatsch, and E. N. VanHooser, An Analysis of the $LD_{50(30)}$ as Related to Radiation Intensity. Rad. Res. 12:349-356 (1960).

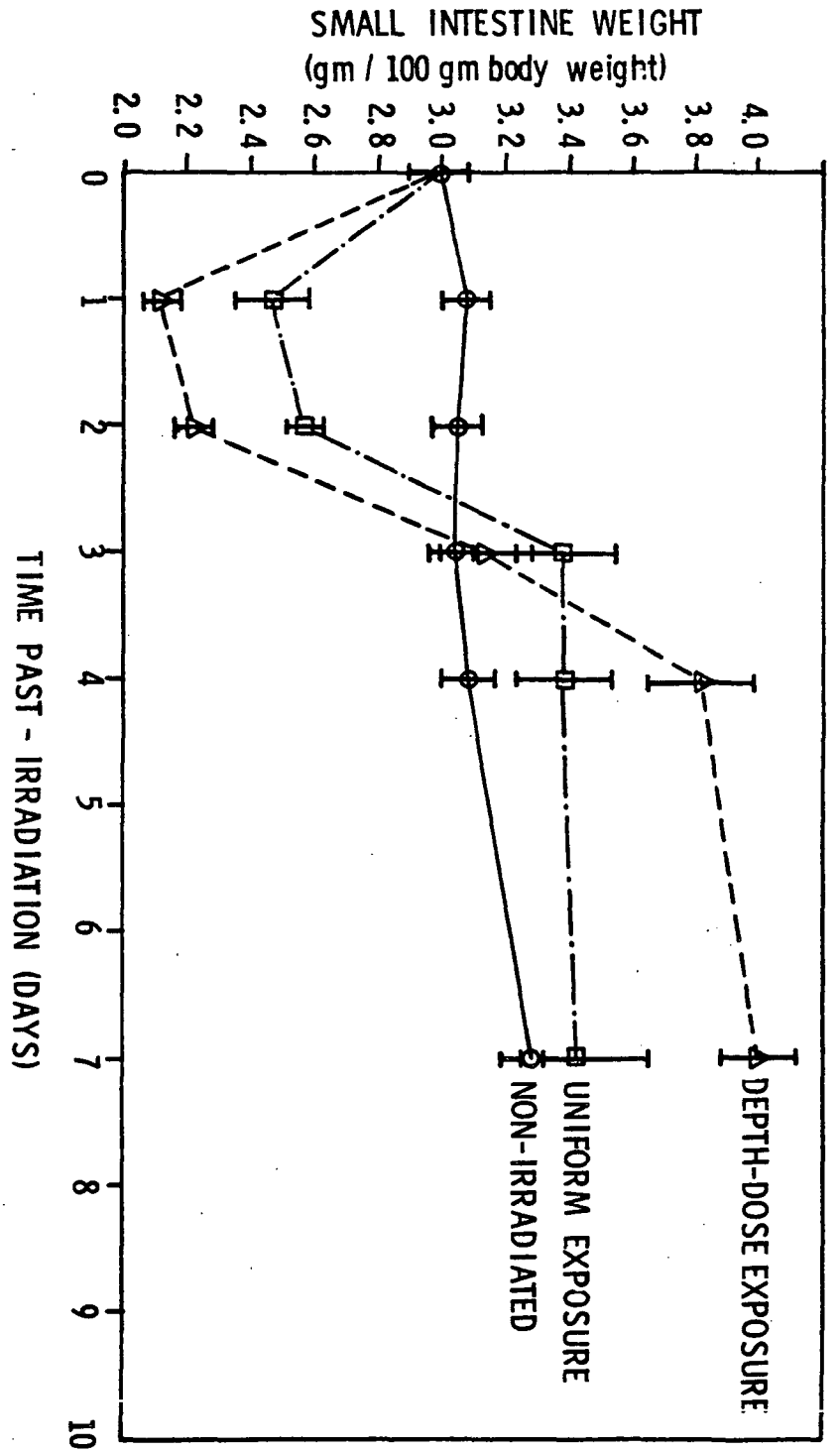

FIGURE: 4

SMALL INTESTINE WEIGHT CHANGES FOLLOWING UNIFORM AND DEPTH-DOSE IRRADIATION WITH 40% OF THE RESPECTIVE LD_{50}

X-radiation depth-dose exposure. When 80 KVP X-radiation[11], 100 KVP X-radiation[10,11] or 50 KVP X-radiation in combination with 250 KVP X-radiation[9] is used to produce depth-dose geometry, the midline LD_{50} is equal to or greater than the midline LD_{50} produced by uniform 250 KVP X-radiation. In contrast to this, in each experiment of the present study, the depth-dose midline LD_{50} was significantly lower than the uniform LD_{50} by an average of 22 per cent based on film dosimetry (and an average of 29 per cent based on Victoreen chamber measurement). The difference may be due to the marked reduction in marrow dose by surrounding bone when low voltage radiation is used[11,12] but which does not occur to an appreciable extent with high energy radiation such as cobalt-60 gamma radiation[12]. When a lethal depth-dose is produced by soft X-radiation, large soft tissue exposure as compared to uniform, hard X-ray exposure is required at marrow depths to produce sufficient injury in bone-shielded marrow. Use of soft X-radiation, therefore, results in a depth-dose midline LD_{50} which is greater than the uniform LD_{50}.

When depth-dose is produced with cobalt-60 gamma radiation, marrow receives a dose nearly equal to the soft tissue dose at the same depth in the body. As a consequence, sufficient injury to peripheral hematopoietic tissue can be produced to result in lethality without the need for a dose equal to that of uniform irradiation being delivered to the midline (Fig. 3). This is a depth-dose effect which is expected to occur with solar flare proton irradiation of man.

It is apparent from the integral dose values obtained in the present experiments (Table 1) that reduction of bone marrow shielding by use of depth-dose cobalt-60 gamma irradiation does not result in an integral dose equal to the uniform exposure integral dose. In fact, the ratio (depth-dose integral LD_{50} over uniform integral LD_{50}) of 1.5 measured in the present study is in the same range as the ratios observed for soft X-irradiation of large species where a significant depth-dose was produced; i.e., ratios of 1.3 and 2.1 for the rabbit[11] and 1.1 and 1.7 for the dog[9]. This suggests that non-uniform dose distribution, independent of bone shielding of marrow, plays an important role in the failure of the integral dose concept.

Inability of integral dose to equate uniform and depth-dose exposure is probably due to two general mechanisms: wasted energy and low doses to portions of critical organs. Some of the total absorbed energy from depth-dose exposure is wasted in tissues located closer to the surface than marrow and some energy may be wasted in critical organs maximally damaged at a lower dose than is received. Survival

of otherwise lethal gastrointestinal injury[18] or hematopoietic injury[19,20] by protection of a small portion of the critical organ system has been adequately demonstrated.

The significantly shorter survival time following depth-dose irradiation (Table 2) indicates that some factor relating to lethality is different in the two types of exposure geometry. This may result from semi-shielding of parts of the hematopoietic system during depth-dose exposure. Grahn, et.al.[11] have cited evidence, indicating that partial shielding of the hematopoietic system results in a decreased survival time. A shortened survival time, however, also suggests increased injury to the gastrointestinal tract since analyses of radiation dose-survival relationships in several mammalian species have revealed a short (3-5 day) survival time which is associated with irradiation of the intestine[21-24]. This hypothesis is strengthened by consideration of the position of the intestine in

---

18. Swift, M. N., and S. T. Taketa, Modification of Acute Intestinal Radiation Syndrome Through Shielding. Am. J. Physiol. 185:85-91 (1956).

19. Swift, M. N., S. T. Taketa and V. P. Bond, Efficacy of Hematopoietic Protective Procedures in Rats X-Irradiated with Intestine Shielded. Rad. Res. 4:186-192 (1956).

20. Alpen, E. L., and S. J. Baum, Modification of X-Radiation Lethality by Autologous Marrow Infusion in Dogs. Blood 13:1168-1175 (1958).

21. Quastler, H., Studies on Roentgen Death in Mice. I. Survival Time and Dosage. Am. J. Roentgenol. Radium Therapy 54:449-456 (1945).

22. Bond, V. P., M. N. Swift, A. C. Allen and M. C. Fishler, Sensitivity of Abdomen of Rat to X-Irradiation. Am. J. Physiol. 161:323-330 (1950).

23. Quastler, H., E. F. Lanze, M. E. Keller and J. W. Osborne, Studies on Roentgen Death in Mice. III. Acute Intestinal Radiation Death. Am. J. Physiol. 164:5456-556 (1951).

24. Cronkite, E. P., and G. Brecher, Effects of Whole-Body Irradiation. Ann. Rev. Med. 3:193-214 (1952).

the body relative to depth-dose distribution. In the peritoneal cavity the intestine is located in an approximate cylinder, which in the anterior portion is very close to the body surface. Due to this geometry a greater volume of intestine is located between the surface and half the distance to body-center than the amount of intestine located between body-center and half the distance to the surface. Calculations based on the depth-dose curve given in Fig. 2 reveal that, at the LD_{50}, the integral dose delivered to the body tissue of the rat located between the surface and half the distance to body-center was 1.7 times as great as the integral dose delivered to the same tissue by uniform irradiation. Thus, a large portion of the total intestine must have received a greater amount of energy than the same part of intestine in animals uniformly irradiated. In addition, the total body integral dose at the LD_{50} was 1.5 times as great as the uniform integral dose (Table 1) which implies that the integral dose to the total intestine was higher in depth-dose exposure as compared to uniform exposure.

Direct evidence for greater intestinal injury in depth-dose exposed rats is given by the small intestine weight changes shown in Fig. 4. The data show that when rats are subjected to the same injury as measured by mortality (i.e., 40 per cent of the respective LD_{50} for depth-dose or uniform exposure), the intestinal weight loss is significantly greater on the first two days following depth-dose exposure as compared to uniform exposure. Mean values for changes in intestine weight during the recovery phase suggest the overshoot of intestinal weight is also greater in the depth-dose exposed animals. These changes in total intestine weight are interpreted as an index of mucosa damage and recovery because previous studies with the rat have shown that total small intestine weight changes parallel mucosa weight, nitrogen, and DNA changes following irradiation(25). An overshoot of total intestine weight, mucosa weight, and mucosa nitrogen (but not DNA) is associated with the recovery phase and in the present study the overshoot in depth-dose animals is additional evidence for greater intestinal injury following depth-dose exposure.

These data suggest that greater injury to the intestine of man may occur following solar flare proton exposure as compared to uniform body exposure. Thus, sublethal space proton depth-dose exposures may cause greater early gastrointestinal illness than has been observed following uniform exposure of humans(26).

---

25. Kay, R. E., and C. Entenman, Weight, Nitrogen and DNA Content of Small Intestine Mucosa of Rats Exposed to X-Rays. Am. J. Physiol. 197:13-18 (1959).

26. Miller, L. S., G. H. Fletcher and H. B. Gerstner, Systemic and Clinical Effects Induced in 263 Cancer Patients by Whole-Body X-Irradiation with Nominal Air Doses of 15 r to 200 r. U.S. Air Force School Aviat. Med. Report 57-92, May 1957.

Paper C-7

LET SPECTRUM AND RBE OF HIGH ENERGY PROTONS*

Hermann J. Schaefer
U. S. Naval School of Aviation Medicine

Abstract

High intensity proton radiations in space temporarily superimposed upon the ordinary cosmic ray beam have energy spectra extending from a few to many hundred Mev. Analysis of the LET spectrum of a typical flare produced proton beam shows that the bulk of the energy dissipation is effected with an LET spectrum closely resembling that of standard x-rays. A basic difference exists in the spectral region beyond 10 kev/micron tissue. Though the fractional dose in that region expressed in rad remains on the level of a few per cent, it represents a significant though not a major part of the total rem dose. It is suggested that both dose fractions be treated separately in assessing the ERD (Equivalent Residual Dose) with the recovery allowance of 2.5 per cent per day applicable only to the low LET fraction .

On the RBE of protons from terrestrial sources, a large volume of experimental data is available in the literature. In two sets of classical experiments, using protons, deuterons, and alpha particles from the Berkeley cyclotron, Tobias and co-workers[1]

---

*Opinions or conclusions contained in this report are those of the author. They are not to be construed as necessarily reflecting the views or the endorsement of the Navy Department.

1. C. A. Tobias, H. O. Anger, and J. H. Lawrence, Amer. J. Roentgenol. 67, 1 (1952).

and von Sallmann, Tobias, and co-workers[2] demonstrated the basic difference in the RBE of heavy particles in the energy range of several hundred Mev where the LET is low as compared to the terminal sections of the tracks of these particles corresponding to the energy range of a few Mev where the LET is high. Because of the low penetrating power of protons of the latter type, it is experimentally much easier to produce them indirectly as recoil protons within the specimen by means of neutron irradiation. With regard to RBE values obtained with this particular method the reader is referred to the comprehensive studies of Conger, Randolph, Sheppard, and Luippold[3] on chromosomal damage in tradescantia and of Storer, Harris, Furchner, and Langham[4] on acute effects in mammalian systems.

Proton radiations in space such as the trapped protons in the inner Van Allen Belt or flare produced solar protons are a mixture of the two types mentioned above. Already the incident beams show extremely heterogeneous energy spectra extending from a few Mev to several hundred Mev and beyond. This heterogeneity is further enhanced by the spectral degradation which occurs as the beam travels in absorber material. The RBE for space radiation protons, then, can be expected to assume an intermediate value between the lower limit of 1.0 found for protons of several hundred Mev and the much higher values up to 10 reported for neutron recoil protons.

In a previous study[5] an attempt has been made to establish theoretically a mean value for the RBE of protons in space by using the RBE/LET relationship as suggested in the official recommendations of the NCRP.[6] Quite obviously this approach leaves much to be desired from a scientific standpoint. A basic objection against it derives from the

---

2. L. von Sallmann, C. A. Tobias, H. O. Anger, C. Welch, S. F. Kimura, C. M. Munoz, and A. Drungis, A.M.A. Arch. of Ophthalm. 54, 489 (1955).

3. A. D. Conger, M. L. Randolph, C. W. Sheppard, and H. J. Luippold, Radiation Res. 9, 525 (1958).

4. J. B. Storer, P. S. Harris, J. E. Furchner, and W. H. Langham, Radiation Res. 6, 188 (1957).

5. H. J. Schaefer, Dosimetry of Proton Radiation in Space, U. S. Naval School of Aviation Medicine Project MR005.13-1002 Subtask 1, Report No. 19 (1961).

6. Permissible Dose from External Sources of Ionizing Radiation, Handbook 59, National Bureau of Standards, Washington, D. C., 1954.

fact that the LET as commonly quoted for any type of ionizing radiation merely denotes the total energy dissipated per unit length of path, yet does not convey any information on the actual spacing of the ionization events in the microstructure of the irradiated tissue. Though this is a well known fact Table 1 describes it in more detail. In the first column, selected kinetic energies of protons are listed. The second column shows the corresponding LET, the third column the maximum transferable energy to electrons, and the fourth column the range in tissue for electrons of the energies of the third column.

Table 1. Energy Dissipation Characteristics of Protons

Protons		First Order Secondary Electrons	
Kinetic Energy Mev	LET Kev/Micron Tissue	Max. Transf. Energy, Mev	Range in Tissue, Micron
100	.635	.231	556
50	1.08	.113	172
10	3.95	.022	10
1	21.35	.0022	.18

It is immediately seen that the distances over which the dissipated energy is actually spread are, for higher energies, considerably larger than one micron. For a true description of the energy dissipation, therefore, it would be necessary to carry out a complete analysis of the entire chain of events tracking down all secondaries until they come to rest. This leads to an LET spectrum rather than to a single LET value. It has been generally accepted in this type of analysis to consider an energy transfer to a secondary electron as local if an energy exchange of 100 e-volts or less is involved. The range of a 100 e-volt electron in tissue equals 0.003 micron or 30 AU (1 Angstrom Unit = 10^{-7} millimeter). The computational procedures of establishing the LET spectrum for any type of radiation is very complex. So far, such computations have been carried out only for selected types of radiations and selected energies. As an introduction to the literature, the study by Burch[7] should be consulted. For the heterogeneous proton spectra encountered in space the task is further complicated because a continuum of individual LET spectra for monoenergetic protons, covering the entire energy range of

7. P. R. J. Burch, Radiation Res. 6, 289 (1957).

interest has to be set up and then has to be integrated in order to obtain the LET spectrum of the heterogeneous beam.

An important and problematic issue in the LET analysis concerns the ranges in tissue along which a proton or electron of a certain energy maintains its local LET. The upper curve in Fig. 1 shows the local LET of protons and the lower one that of electrons as a function of residual range. It is seen that a proton maintains peak values

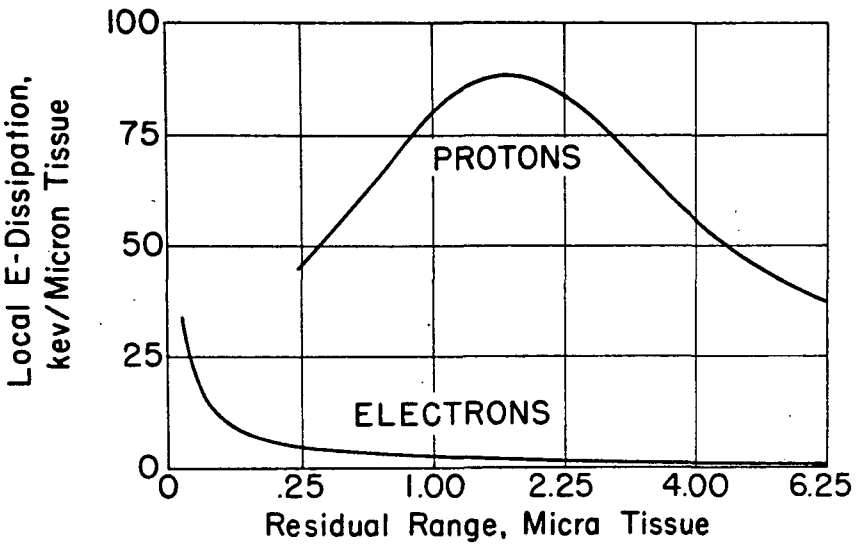

LOCAL ENERGY DISSIPATION OF PROTONS AND ELECTRONS IN THE TERMINAL SECTIONS OF THEIR TRACKS

Fig. 1

of the local LET over distances of several micra in tissue whereas an electron does so only for some 40 or 50 millimicra (400 or 500 AU). If we assume that the production of radiation damage in sensitive centers in the tissue fine structure requires penetration by an ionization column of at least several hundred AU length, the effectiveness of protons, i.e., the RBE, should be substantially greater than of electrons. This is in agreement with the experiment. It has been shown that photoelectrons of 1.3 kev are almost without effect in causing chromatid breaks due to their short range which renders them incapable of crossing the chromatid thread of about 1000 AU diameter. It is seen, then, that the concept of local energy dissipation, though it describes the microstructure of

the dose distribution much more accurately than the mean LET, has a severe limitation concerning those high LET values which are sustained only over very short distances. It is not within the scope of this treatise to discuss the microbiological significance of this difference in more detail. The reader is referred to the reviewing articles of Hutchinson,[8] Howard-Flanders,[9] and Hutchinson and Pollard.[10] In the present context, only one consequence is of importance. In establishing the LET spectra for protons in the energy interval below 1 Mev, where the local LET of the primary proton itself becomes equal to the maximum at the upper end of the LET spectrum of the electrons, the two contributions should not be added because they represent basically different types of radiation exposure for the reasons just explained. Figure 2 illustrates this

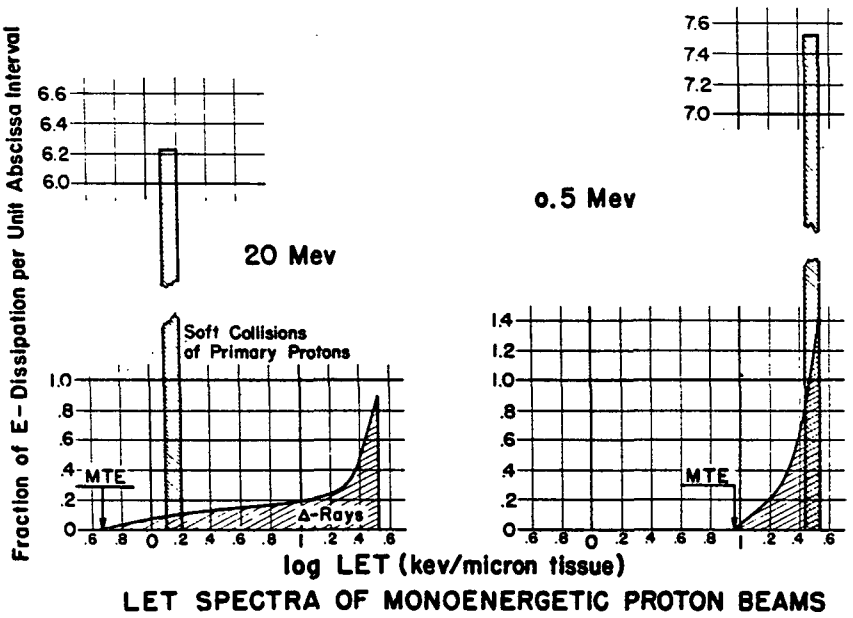

LET SPECTRA OF MONOENERGETIC PROTON BEAMS

Fig. 2

---

8. F. Hutchinson, Science 134, 533 (1961).

9. P. Howard-Flanders, "Physical and Chemical Mechanisms in the Injury of Cells by Ionizing Radiations," Advances in Biological and Medical Physics, Vol. VI, edited by C. A. Tobias and J. H. Lawrence, p. 553, Academic Press, New York, 1958.

10. F. Hutchinson and E. Pollard, "Target Theory and Radiation Effects on Biological Molecules," Mechanisms in Radiobiology, Vol. I, edited by M. Errera and A. Forssberg, Chap. 1.2, p. 71, Academic Press, New York, 1961.

graphically. Shown is at the left the LET spectrum of 20 Mev protons and at the right that of 0.5 Mev protons. The tall narrow columns represent, for both energies, the local energy dissipation of the parent proton itself, i.e., the energy imparted by the proton to electrons in so-called soft collisions in which the energy transfer does not exceed 100 e-volts. It is seen that this contribution coincides, for 0.5 Mev, with the peak LET of the secondary electrons from hard collisions. As shown above, the two contributions cannot be considered as identical nor consolidated into one spectrum.

Returning now to the original question of the RBE of a heterogeneous proton beam, we see that in integrating over the continuum of monoenergetic LET spectra for obtaining the resultant spectrum of the heterogeneous beam, only the contributions of the protons themselves should be considered. Figure 3 shows such resultant spectra for flare produced protons assuming 2 g/cm^2 (top) and 6 g/cm^2 (center) prefiltration. The bottom graph shows the LET spectrum for 220 kv x-rays as computed by Cormack and Johns.[11]

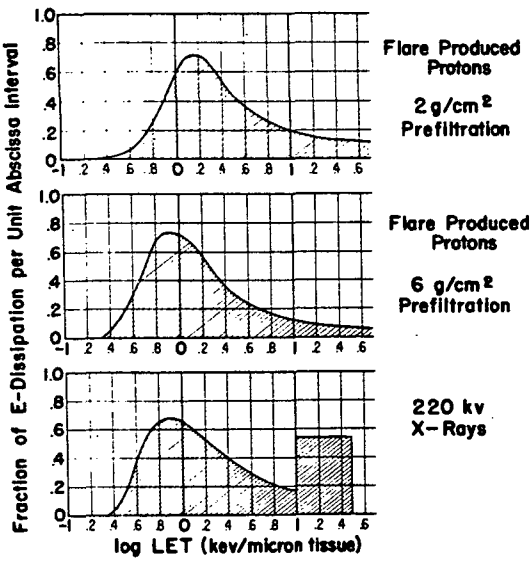

LET SPECTRA OF FLARE PRODUCED PROTONS AND OF 220 kv X-RAYS

Fig. 3

11. D. V. Cormack and H. E. Johns, Brit. J. Radiol. 25, 369 (1952).

The proton spectra, as might be expressly stated once again, show only the energy dissipation from the primary protons themselves. All secondary electrons, which receive a higher energy than 100 e-volt are disregarded. In the x-ray spectrum at the bottom, of course, all energy dissipation is due to electrons since there is no other ionizing agent present in 220 kv x-rays. The square shaped area above log LET = 1.0 is an artefact. Since the kinetics of energy dissipation below 1 kev is incompletely understood the energy dissipation in this interval is merely indicated by a square of correct total area.

As long as the comparative evaluation is limited to the LET interval below log LET = 1.0, it is interesting to note, from Fig. 3, that the two flare produced proton beams have LET spectra closely resembling that of standard x-rays. Obviously, then, this fraction representing the bulk of the total ionization dosage, should be assigned an RBE of 1.0. Beyond the point of log LET = 1.0 corresponding to an LET of 10 kev/micron tissue, however, no comparative evaluation of the proton spectra with the x-ray spectrum is allowed. This is so not just because the proton spectra in Fig. 3 do not contain the delta ray contributions, but more so for the principal reason that the high LET of the low energy delta rays are sustained over insufficient ranges for x-rays. In other words, the plateau in the x-ray spectrum beyond log LET = 1.0 represents a contribution to which an elevated RBE factor should not be assigned whereas the corresponding sections in the flare produced proton spectra represent rem doses that are substantially higher than the rad doses.

Of particular interest is a comparison of the LET spectra of flare produced protons to those of neutron produced recoil protons since the latter type radiation has been investigated by many experimenters with regard to the RBE. The center graph in Fig. 4 is identical with the center graph of Fig. 3. However, it is aligned with a lower graph showing the LET spectrum for the so-called Watt spectrum,[12] i.e., for neutron produced recoil protons from thermal fission of U-235. Again, only the energy dissipation of the protons themselves is indicated in both graphs. It is seen that, for the recoil protons, 80 per cent of the energy is dissipated at LET values in excess of the log LET = 1.0 limit in contrast to flare produced protons which dissipate more than 90 per cent of their energy at LET values below that limit. This statement pertains, of course, to the shares of the ionization dosages in rad. The rem doses of the right hand sections are substantially higher than the areas under the curves indicate.

---

12. B.E. Watt, Phys. Rev. 87, 1037 (1952).

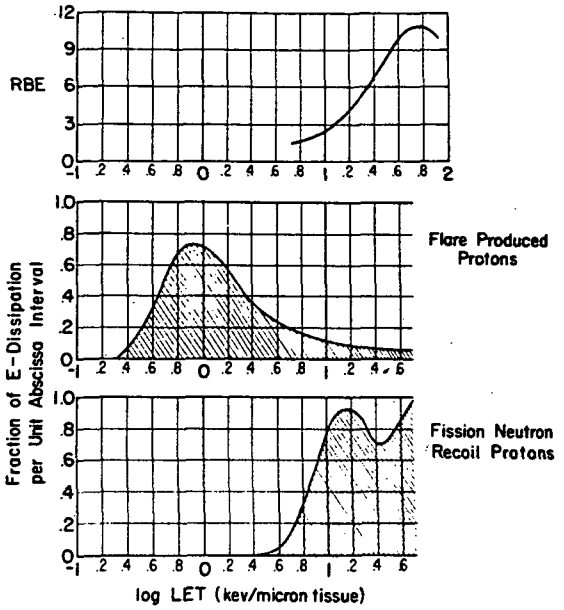

LET SPECTRA OF FLARE PRODUCED AND OF FISSION NEUTRON RECOIL PROTONS

Fig. 4

Very problematic is the question what RBE factor should be assigned to the high LET section beyond the 10 kev/micron limit. In official assessments of exposure status, it would seem proper to adhere to the Code of Federal Regulations [13] which assigns protons of the type characterized by the lower graph of Fig. 4 an RBE factor of 10. A more elaborate way, yet still using officially recommended data, would be to use the RBE/LET relationship suggested by the NCRP as mentioned above.[6] It seems of interest to point out that this latter method furnishes slightly smaller rem/r ratios if applied to the LET spectrum instead of to the mean LET value. The earlier values, therefore, and the mean values for the entire heterogeneous spectrum based thereon[5] provide a slightly larger safety margin from a radiation safety standpoint.

For reasons of scientific accuracy as well as from the practical viewpoint that the true radiation burden in a human target should be determined as closely as possible the foregoing approaches using definitions set forth in official regulations are not very

---

13. "Standards for Protection Against Radiation," Atomic Energy, Federal Regulations, Title 10, Chap. 1, Part 20, Atomic Energy Commission, 1958.

satisfactory. One has to realize, however, that a radiation which produces ionization in tissue at strictly one LET or at least at values in a narrow LET interval simply does not exist. Consequently, data on RBE factors for "monochromatic" LET values are not available. The closest approach seems to be the investigation of Conger and co-workers quoted above.[3] At least, these authors have given most careful consideration to the limitation under discussion. They arrive at an RBE/LET relationship which is shown in the upper graph of Fig. 4. It is seen that, in general agreement with the earlier estimates based on official recommendations, the critical interval of a steep rise of the RBE starts slightly below the log LET = 1.0 limit. It might also be mentioned that the data of Conger and co-workers shown in the upper graph of Fig. 4 pertain to cytological damage in tradescantia. As far as these data allow a comparison to the ones obtained by Storer and co-workers[4] on mammalian systems, the RBE for acute damage to the latter systems seems to be somewhat smaller. This again would provide for a further increase of the safety margin.

If we have arrived, in the foregoing discussion, at the conclusion that the mean LET and mean RBE furnish a total rem dose for flare produced proton radiation which closely compares to the rem dose derived from the detailed analysis of the LET spectrum, we must not lose sight of one important defect of the simplified method. We mean that it can never furnish a separate assessment of the fractional dose administered at a high LET. Though this fractional dose, assessed as ionization dose in rad, always remains on the level of a few per cent of the total ionization dose, it becomes a significant though not a major part of the total exposure after conversion into rem dose. Especially in estimates of the ERD (Equivalent Residual Dose) from repeated exposures to proton radiations in space it seems advisable to treat the two dose fractions separately allowing a recovery factor of 2.5 per cent per day only for the dose fraction whose LET spectrum closely resembles that of x-rays yet considering the high LET contribution as strictly cumulative. Another problem that comes up in this connection concerns the RBE factor that should be assigned to the high LET fraction if acute exposure or long term exposure at low dose rates is involved. Experimental evidence indicates that high LET irradiation, for the latter type of administration, shows a higher relative biological effectiveness. However, in the frame of the specific problems with which we are confronted in dealing with solar protons and the protons in the inner Van Allen Belt acute exposure seems of predominant interest. The discussion, therefore, can be terminated at this point.

Paper C-8

SOME DATA ON THE RELATIONSHIP OF RBE AND LET

W. S. Snyder
Oak Ridge National Laboratory

Abstract

The RBE of one radiation with respect to a standard radiation is usually defined as the inverse ratio of doses required to produce the same degree of a specified biological effect. It is well known that the RBE depends not only upon the quality of the radiations but also upon such conditions of exposure as dose rate, fractionation of dose, strain and condition of animals, and the biological effect studied. This paper analyzes some experimental data to obtain an indication of the dependence of RBE on LET. The cases considered include some experimental studies of effects on cells and on mice. The interpretation of such data for certain conditions of exposure in space is discussed in a preliminary way.

The relative biological effectiveness (RBE) of a radiation exposure A with respect to radiation exposure B and an end point T is usually defined as the inverse ratio of the doses $D_B(T)/D_A(T)$ required to produce the same degree of the biological effect T. The RBE of radiation dose has been found to depend upon many factors. The quality of the radiation, usually specified in terms of the rate of linear energy transfer (LET) along the tracks of the ionizing particles, is certainly one of the important factors, but it also is certain that it is not the only factor which must be considered. Many experiments have shown that dose level, dose rate, the biological end point and species used for the test, and the general situation during and after exposure may be important. Thus the RBE applicable to one exposure situation may not be applicable to another.

If we consider what the relevant conditions are likely to be for exposure during space flights of the next decade or so, it quickly becomes evident that there are a number of factors which combine to make this situation somewhat different than previous radiation exposures that man has experienced and learned to control acceptably. First of all, there is the unfamiliar nature of the radiation field -- the high-energy protons and neutrons, the mesons, and the nuclear cascade and evaporation phenomena, which are largely foreign to man's usual environment. However, there is no reason here for discouragement. Man faced a similar challenge scarcely more than 20 years ago when he had to learn to control exposure

to neutrons and exposure to a host of new radionuclides, such as Sr^{90}, Pu^{239}, etc. Then the health physicist turned to the exposure experience which had been gained with x-rays and with radium, and by judicious comparisons of the new with the old, adequate dose limits were found and a magnificent record of safety has been achieved. The concept of RBE was developed essentially for this purpose, i.e., to estimate the biological effects of the new situation in terms of previous experience with other types of radiation. There is no doubt that this is our surest course in controlling exposure in the present new situation posed by exploration of space. However, the judicious choice of RBE values for this new type of exposure will require that all factors affecting the RBE be examined and evaluated.

The RBE values appropriate for present occupational exposure may not be the same as the RBE appropriate for doses that may be incurred on certain missions in space. To use the one RBE for the other without a critical review of all the relevant factors is to betray a lack of understanding of the problem. Exposure over a working life at low dose rates may have quite different biological effects than exposure at a much higher rate for a period of a week or a month. Thus the period of exposure and the dose level must be considered as well as the LET or quality of the radiation. As a matter of fact, an Ad Hoc Committee of the ICRP on RBE has just reviewed RBE for occupational exposure and has suggested the use of other values of RBE in the case of acute accidental exposure at higher dose levels. Unfortunately, this committee did not consider the type of radiation fields likely to be encountered in space. However, those responsible for the design of the space craft and for executing the mission cannot afford to ignore the differences in exposure times and dose rates, as well as the differences in LET of the space situation as contrasted with the usual situation of occupational exposure. The success of the mission should not appear as accidental. The planning should include all fundamental aspects of the problem.

In attacking this very complicated problem, the maximum dose levels to be expected, the duration of the exposure, and the various biological effects of the exposure, all need to be taken into account. The following brief discussion of these aspects of the problem and of the bearing of LET on the problem are entirely preliminary and indicate directions of exploration rather than definitive conclusions. Although tentative, there are indications in presently available data that are quite suggestive of some conclusions. The items presented here are offered only as examples of problems where data now available suggest certain conclusions which are relevant to the problem of exposure in space and which seem to merit further study.

High energy particles, in themselves, do not seem to be a great problem. The LET is rather accurately known, and Tobias observed as long ago as 1952[1]

---

1. C. A. Tobias, H. O. Anger, and J. H. Lawrence, Am. J. Roentgenol. Ra. Therapy Nuc. Med. 67(1), 1 (1952).

that the LET on the plateau of the Bragg curve of high-energy protons, deuterons, and α particles was about that of 200 KVP x-rays and that it might be conjectured the biological effects would be similar. This has been in large part substantiated in quite a few studies of enzymes, bacteriophage, diploid yeast, and mammalian tumor cells. For example, Berry et al.,[2] in a paper now in course of publication, study the reproductive capacity of a mammalian tumor cell, P-388, irradiated in vivo by the plateau region of the tracks of 340-Mev protons or 380-Mev α particles and find a response roughly similar to that of 3-Mev x-rays, both in the oxygenated and in the anoxic condition. When the dose included sizable fractions of energy delivered from the Bragg-peak portion of the track, the effect was much more pronounced. This study is cited here mainly because a mammalian cell, irradiated in vivo, was used, but the conclusion that the biological response of very high-energy particles of low LET is, indeed, much like the response to x-rays is supported by experiments on many other biological materials.

There is also a remarkable suggestion of consistency in the biological response to the same LET from different particles. Figure 1 is adapted from a study of Fluke et al.[3] and shows phage survival cross-section as a function of LET for protons, deuterons, and ions of helium, carbon, and oxygen. It is to be recognized that the LET values used here do not include a correction for δ rays, but this should not entirely obscure the pattern that is evident. This figure illustrates also the quite common phenomenon that RBE decreases as LET increases beyond some rather high value, indicating a point beyond which energy is "wasted." The value of LET where the decrease begins to appear may vary somewhat with the type of ion and biological material, but the range does not appear to be extreme. Brustad[4] summarizes a number of such studies:

> "It has been shown that the RBE for inactivation of dry enzymes and bacteriophage (in both wet and dry states) decreases continuously with increasing LET... For all the biological systems studied thus far, however, the RBE was declining after the LET exceeded 300 kev/μ."

Another interesting pattern that is suggested relates to exposure time, i.e., to evidence, or lack of evidence, of repair processes. Andrews and Berry[5] have shown that there is no recovery between fractionated doses of fission-spectrum neutrons in their study of the mammalian tumor cells mentioned above. Berry et al. have now demonstrated that there is likewise little or no oxygen effect present in the case of fission-spectrum neutrons.[2] However, when the irradiation is by 14-Mev

---

2. R. J. Berry and J. R. Andrews, "The effect of radiation ionisation density (LET) upon the reproductive capacity of mammalian tumour cells irradiated and assayed in vivo," Unpublished.

3. D. J. Fluke, T. Brustad, and A. Birge, Rad. Res. 13, 788 (1960).

4. Tor Brustad, Rad. Res. 15, 139 (1961).

5. J. R. Andrews and R. J. Berry, Rad. Res. 16, 76 (1962).

UNCLASSIFIED
ORNL-LR-DWG. 74884

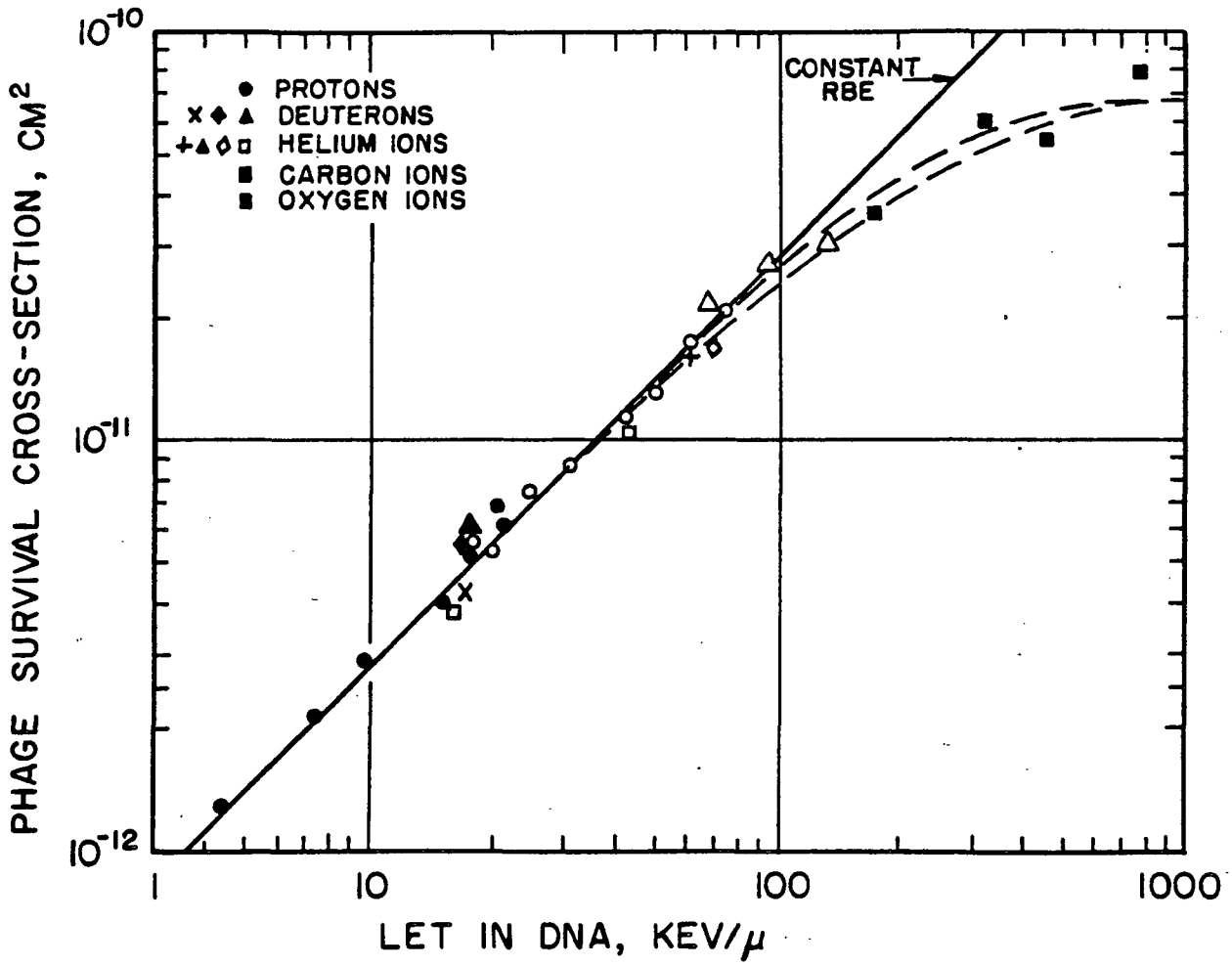

Fig. 1. RBE for Phage Survival as a Function of LET

neutrons, there is a pronounced oxygen effect, and it is probable that repair is present also. Here again the lower LET distribution of the 14-Mev neutrons seems to produce, to some extent, the type of response elicited by the classic low LET radiations. To illustrate the difference in the LET distribution of a modified-fission neutron spectrum and of monoenergetic, 14-Mev neutrons, Table 1 has been calculated using a distribution of neutron energies given by Neary[6] for a modified fission spectrum. Actually the values in Table 1 can be regarded only as qualitative since the calculation presented here represents only the first-collision dose. Nevertheless, it is apparent that there is a considerable difference in the LET distribution. The 14-Mev spectrum contains more

Table 1. Percentage of Neutron Dose in Various Ranges of LET

Neutron Source (kev/micron)	Modified-Fission-Spectrum Neutrons (% dose)	14-Mev Neutrons (% dose)
< 3.5	0.29	0.031
3.5-7	0.11	42.0
7-25	12.00	7.5
25-50	34.00	14.0
50-100	47.00	7.3
> 100	6.6	29.0

dose due to heavy-ion-recoil nuclei (range > 100 kev/μ) and less in the intermediate range of 50 to 100 kev/μ as compared with the LET spectrum of the fission neutrons. Considering the different responses reported by Berry et al., there is here, again, the suggestion that beyond a value of 100 kev/μ the RBE does not increase, but a shift of LET downward below the region of about 50 kev/μ may be significant. It should not be inferred from the above oversimplified discussion that these conclusions are firm at the present time, or that there are no problems of interpretation concerning these and other like studies. The opposite is true -- the detailed dosimetry is largely qualitative or only semi-quantitative, and there are many details and special considerations that require interpretation. Nevertheless, there is also a broad trend that is suggested by the data.

Finally, there is something that can be said concerning the influence of exposure time on the RBE. Neary[7] summarizes as follows the available data on RBE for the modified fission spectrum of neutrons as obtained using mice:

---

6. G. J. Neary, R. J. Munson and R. H. Mole, Chronic Radiation Hazards, p. 25, Pergamon Press, London, 1957.

7. Id., Ibid., p. 182.

> "Comparisons of fast neutron and gamma irradiation were made for exposure times from 24 hours to 9 months. Within this range there was no evidence that alterations in exposure time or dose rate altered the r.b.e., and published evidence to the contrary is critically examined and found wanting."

Neary also concludes that:

> "A comparison of all available information on mortality of chronically irradiated mice suggests that the r.b.e. for this effect is likely to be about 10."

The RBE he obtained for reduction of testis weight, impairment of fertility, reduction in spleen weight and in white cell count of peripheral blood were all less than 10. He concludes that:

> "Evidence was obtained that the gonads are the most sensitive organs in the mouse to chronic irradiation at very low dose rates."

Thus, there are suggestive trends in available data which offer considerable guidance in selecting RBE values appropriate for the particular conditions of exposure in space. To best interpret these trends, a more detailed knowledge of the LET spectrum obtained in the various experiments is desirable. The average LET is probably too gross a measure of radiation quality to be adequate, particularly over enormous ranges of LET. Yet much of the experimental work is reported only in terms of an average LET and needs to be reinterpreted. A more detailed knowledge of the spectrum, either by calculation along lines roughly indicated here, or by methods developed by Rossi,[8] is needed.

In summary, two conclusions have been advanced which are considered to be firmly supported by the experimental work relating to RBE:

1. The RBE to be applied for exploration in space should not be taken from currently accepted values for quite different exposure situations without a careful reassessment of all factors affecting the RBE, and LET is one, but only one, such factor. If shield weight is of critical concern, so is the question of biological effectiveness of the radiation, and the closer the design must approach critical limits of dose, the more important is the need for a careful assessment of RBE values.

2. It seems quite clear that there are many RBE values relevant to the problem and not just one value. For example, RBE's for acute effects and for long-term effects -- or for genetic damage contrasted with shortening of life -- require independent consideration.

---

8. H. H. Rossi, et al., Rad. Res. 13, 503 (1960).

The following points are not, perhaps, as firmly established, but are strongly suggested by much of the available data.

1. There is a value of LET below which the biological action of high-energy protons, α particles, etc., behave very much like x-rays. This value probably is somewhere between 25 to 50 kev/μ.

2. There is a higher range of LET values where all the heavy ions behave similarly -- lack of repair, decreasing values of RBE, etc. This value probably is about 100 kev/μ or near this value.

3. Within the exposure times, from a day to weeks or several months, as currently envisaged for space missions, the RBE probably does not vary markedly, and the values used for late effects are probably not far from those appropriate for chronic exposure. On the other hand, where acute effects are concerned, the exposure times are probably sufficiently long to allow for considerable repair of damage due to the low LET components of the dose.